

GEOLOGICAL, GEOCHEMICAL AND MINERALOGICAL
STUDIES OF SHALLOW SUBMARINE EPITHERMAL
MINERALIZATION IN AN EMERGENT VOLCANIC EDIFICE,
AT MILOS ISLAND (WESTERN SIDE), GREECE

Dissertation

zur Erlangung des Doktorgrades
der Naturwissenschaften im Department
Geowissenschaften
der Universität Hamburg

vorgelegt von

DIMITRIOS ALFIERIS

aus Athen

Hamburg
2006

**Als Dissertation angenommen vom Department Geowissenschaften der
Universität Hamburg**

**Auf Grund der Gutachten von Herrn Priv. Doz. Dr. K. Arikas
und Herrn Prof. Dr. M. Tarkian**

Hamburg, den 6. Dezember 2006

**Prof. Dr. Kay-Christian Emeis
Leiter des Department Geowissenschaften**

Acknowledgements

This dissertation has been fully supported by S&B Industrial Minerals S.A., Athens-Greece, and thus I would like to express my sincere thanks to the company and in a particular way to Mr. U. Kyriakopoulos, president of the company.

I would like to express my best and sincere thanks to Prof. Dr. M. Tarkian for the numerous kind and valuable discussion that we had along the years nonetheless his encouragement and critical reviews, and corrections of my phd thesis at various stages during this last year.

My best appreciation is given to P. D. Dr. K. Arikas for his reading and helpful discussions and comments on various issues regarding my phd thesis work, along the years.

I wish to thank very much Midas S.A., Royal Gold Inc. and Aegean Gold Inc., for permit me to publish geochemical and drill holes data from Milos island, gold project.

Dr. P. Voudouris lecturer at Athens University school of Geological sciences, has cast its critical eye over several versions of this manuscript nonetheless he had meticulous reviewed my last one and is thanked for the constructive comments and discussions that we had along the years.

I wish to thank Mrs. B. Corneliesen and Mrs. S. Heidrich for the microprobe analyses that they performed for this work.

My sincere friendly and professional thanks are addressed to J. Nethery (NEDEX Pty Ltd-Australia) for inspiring discussions on geology, tectonics, geochemistry and ore deposition, along at least a decade on the Milos field reality.

My sincere thanks also are given to Prof. Dr. Ian Plimer for the valuable discussions that we had along at least a fifteen years period on Milos geology and mineralization.

My sincere thanks are addressed to Mr. S. Tzintzos, R&D Manager-Bentonite division, at S&B Industrial minerals S.A., for his encouragement and support during my writing of the thesis.

Last but not least, I would like to express my best and sincere thanks to my wife Ute Dürubaum and my daughters Klara-Zoi and Anaïs for being so patient and to encourage me during all these years of my phd work.

Abstract

Calc-alkaline volcanic rocks in western Milos (pyroclastics and shallow subvolcanic intrusives/lava domes) were emplaced during the Upper Pliocene to Pleistocene times under transitional submarine to locally subaerial conditions, forming a series of volcanic edifices. During the eruptive phase a combination of vent clearing pyroclastic flows and water supported volcanoclastic products created a poorly consolidated pumice pile (pumice cone). Shortly after, it has been intruded by shallowly emplaced rhyolitic domes (cryptodomes). This dominantly acid explosive and intrusive activity has been followed by effusive volcanism that formed numerous dacitic-rhyodacitic-rhyolitic and andesitic domes and lava domes, emplaced shallowly underneath or on the sea-floor, creating a series of hyaloclastitic products intercalated with shallow marine sediments. Locally some of the domes gave origin to bedded pumiceous tuffs (dome-top tuff cones), while other domes and lavas raised above the sea level becoming thus subaerial. All the subvolcanic high-level intrusive and partially extrusive volcanic products represent the equivalents of a deeper magma chamber that fed the volcanic succession, and were the heat source required to drive the hydrothermal convective system responsible for the mineralization. Geochronological data, of several of these intrusions suggest that they are partially coeval with, and partially younger than the pyroclastic succession into which they were emplaced.

Methodological collection of existing information, geological mapping of surface outcrops, geochemistry, X-ray diffraction analysis, drill holes logging, air-photos and satellite imagery structural interpretation, alteration and ore mineralogical studies, were combined in order to better understand and interpret the magmatic-hydrothermal environment of ore deposition at western Milos.

The dominant structural features at western Milos are from one side a series of steep NE striking fault / lineament zones, and from the other side a series of dilational NW trending ones (fault jogs), into which, composite volcanic centers, domes and collapse calderas have been developed. They together have promoted and localized fluid upflow along steep, near vertical feeder conduits, producing in such a way zones of intense silicification, brecciation and veining. With respect to those structures, subsidiary E-W and N-S trending faults were also created and are considered to have enhanced the permeability of the volcanic and volcano-sedimentary sequences, through a further dismembering and dislocation.

Of particular interest can be characterized the quasi E-W trending lineament along the central part of western Milos (Ammoudaraki-Plakota-Rivari lineament), which subdivided it into two sectors, from a geological, hydrothermal and mineralogical point of view, the northern and southern sectors.

The tectonic structures which controlled the principal eruptive centres are the same structures which controlled and localized hydrothermal discharge that formed the various deposits and mineralization.

The alteration patterns observed at western Milos correspond at least to two distinct and partially overlapped environments, namely the volcanic-hydrothermal and geothermal environments, the first corresponding to a high sulfidation (HS) mineralizing system, and the second one to an intermediate sulfidation (IS) system. Hydrothermal alteration at the northern part of western Milos is dominated by a typical acid-sulfate submarine pool, characterized by extreme acid leaching and formation of residual quartz, grading outwards to Na-alunite, dickite/kaolinite \pm diaspore \pm pyrophyllite and then to kaolinite-illite-sericite assemblages. The observed elongated shape of the silica bodies in the northern sector of

western Milos suggests that a major structural control was exercised by E-NE striking faults.

In the southern sector the ore bearing quartz-adularia zone is flanked by an illite± smectite alteration assemblage which grades to peripheral alteration dominated by carbonates-chlorite assemblages. The abundance of quartz and adularia increases toward the upflow zone, whereas clay abundance increases toward the margin of the upflow zone with smectite dominating at <150° C and illite dominating at >200° C.

A long-lived zone of hydrothermal flow with an initial submarine to a later subaerial steam heating throughout the southern sector and partially at the northern sector (Kondaros area) occurred.

Any model for the development of the regional alteration in western Milos must account for the extent of the silicification and advanced argillic alterations, the timing of emplacement of the major mineralized veins, and the presence of late advanced argillic alteration (of steam heated nature), that obliterated some of the previous features, by overprinting them.

The development of a well framed vein system mainly at the southern sector and subordinately at the northern one, together with a well localized breccias field at the northern sector, are the principal surface manifestations of the mineralization. In a particular way precious ± base metals mineralization seems to have taken place where the N-S to NW- SE trending structures met NE-SW to ENE-WSW tectonic lineaments, thus creating feeder structures. In such a fashion it can also be considered that both veins and breccias/domes at western Milos were constrained between deep-slip and strike-slip structures. Indeed all structural elements (big lineaments, faults, fractures, joints) at western Milos display forms of the pre-, syn- and post-mineralization history (activity) as a response to the different stress regime that took place. As a whole, it is considered that strike-slip movement provided syn-mineralization mechanisms for dilatancy, which permitted to the various kinds of subvolcanic bodies to be emplaced, as well as resulted in post mineralization offsets of the various vein systems.

The Mavrovouni-Profitis Ilias-Chondro Vouno-Koumaria (southern sector) and Triades-Galana-Kondaros-Katsimoutis-Agathia-Vani (northern sector) areas, represent two large (16 Km², and 5 Km² respectively) zoned magmatic-hydrothermal systems, related to the development of the several explosive (rhyolitic/rhyodacitic) volcanic centres and associated with a postulated caldera - dome/flow dome volcanic setting. The submarine magmatic-hydrothermal systems at W. Milos produced deposits with intermediate and high sulfidation variants. The precious metals were initially introduced by hydrothermal fluids of intermediate sulfidation nature (Profitis Ilias-Chondro Vouno), and in a successive stage by intermediate/high-sulfidation states (Triades-Galana) and still later by intermediate sulfidation/high-sulfidation states (Katsimoutis-Kondaros-Vani). All the above mineralized centres are characterized by the occurrence of galena + Fe-poor sphalerite + chalcopyrite and abundance of barite, adularia, sericite and partly calcite. High sulfidation conditions prevailed at Triades-Galana-Agathia-Kondaros as indicated by the presence of enargite-tennantite-chalcopyrite-covellite in the ore assemblage. At Profitis Ilias area the bulk of gold mineralization has been deposited at the upper topographic levels, whereas base-metal and gold-silver telluride mineralization have been deposited at deeper levels, due probably to dilution of injected brines by sea water and/or local boiling processes, as the presence of second generation copper sulfides/galena and adularia respectively suggested. Based on thermodynamic calculations the values of logfS₂, logfO₂ and logfTe₂ of the mineralizing fluids were estimated.

Evidences for the W. Milos mineralization to be formed in a submarine (seafloor/sub-seafloor) environment are the abundance of framboidal pyrite, of micro-chimneys structures composed of either pyrite or various sulfide combinations including the skeletal intergrowths between sphalerite, pyrite and galena, the extreme abundance of barite and finally the seafloor deposited stratiform Mn±baryte mineralization at Vani. In this last it is also included the formation of white smokers along a NE-SW tectonic structure.

Minor and trace elements geochemical maps (As, Sb, Hg, W, Bi, Pb, Zn, Ag, Au, Mo) showed several areas of anomalous geochemical behaviour suggesting potential for epithermal precious metal mineralization. Of major importance are the elevated contents in Mo, W and Bi at the northern sector suggesting a magmatic contribution from porphyry style mineralization buried at depth. In addition magmatic-hydrothermal fluids may have played an important role in the evolution of the mineralizing system(s) at Milos, as indicated by the presence of Au-Ag tellurides (Profitis Ilias) and the high activity of sulphur evidenced by the mineralogical assemblages present. Under this aspect the close spatial relationship between the three successively emplaced intrusive/extrusive domes (Rhyda, Anda, Dado) with the three main mineralizing centers (Profitis Ilias-Chondro Vouno, Triades-Galana, Katsimoutis-Vani) respectively, probably indicates also a genetic relationship between them.

Although a number of geological, geochemical and mineralogical characteristics at western Milos mineralization show features commonly observed in submarine massive sulfide deposits, several other features are typical of subaerial epithermal ores, which suggest that the high grade intermediate/high sulfidation epithermal silver-gold mineralization took place in a shallow submarine to transitional/subaerial volcanic setting.

CONTENTS

Acknowledgements

Abstract

1. INTRODUCTION	1
1.1. Purpose of this study	1
1.2. Previous works	2
1.3. The evolution of the Hellenides	4
1.4. Geotectonic evolution of the Aegean Sea	5
1.4.1. Tectonic regime in the Aegean	5
1.4.2. Volcanic centers and tectonic setting across the Aegean region	8
1.4.2.1. The Hellenic Volcanism	8
1.4.2.2. The Southern Aegean Volcanic Arc	9
2. TECTONIC AND GEOLOGICAL SETTINGS OF MILOS ISLAND	11
2.1. Introduction	11
2.2. Tectonics	11
2.3. Geological setting of the whole Milos island	13
2.3.1. Metamorphic basement	13
2.3.2. Neogene sedimentary sequence	13
2.3.3. Volcanic sequence	13
2.3.3.1. Pliocene series	14
2.3.3.2. Transitional Lower-Middle Pleistocene series	14
2.3.3.3. Pleistocene series	15
2.3.4. Alluvial sequence	15
2.4. The other islands of Milos islands' group complex	17
2.5. Geological setting of the area under investigation	17
2.5.1. Metamorphic basement	18
2.5.2. Neogene sedimentary sequence	18
2.5.3. Volcanic sequence	18
2.5.3.1. Volcanosedimentary products in submarine environment (Lower-Middle Pliocene/~3.5 Ma)	20
2.5.3.1.1. Interbedded shallow marine tuffs/tuffites (Ismtt)	20
2.5.3.2. Acid pyroclastic products in submarine and partially subaerial environment-explosive activity (Lower/Middle -Upper Pliocene/~3.5-3.1 Ma)	21
2.5.3.2.1. Lithic / Pumice tuff subunit (Lpt)	22
2.5.3.2.2. Pumice flow subunit (Pfl)	23
2.5.3.2.3. Lower pumiceous lapilli tuff (Lmp)	23
2.5.3.2.4. Fine ash tuff (Fat)	23
2.5.3.2.5. Fine grained sediments (Fgse)	23
2.5.3.2.6. Profitis Ilias ignimbrite (PII)	24
2.5.3.3. Acid intrusive products in submarine environment-effusive activity (Upper Pliocene/~3 Ma)	25

2.5.3.3.1. High level rhyolite intrusive (Rhyda)	25
2.5.3.4. Volcanosedimentary products in submarine environment (Upper Pliocene/~3-2.7 M.a.)	27
2.5.3.4.1. Fossiliferous tuffs and tuffites (Ftt)	27
2.5.3.4.2. Reworked volcanosedimentary unit (ep)	28
2.5.3.5. Intermediate to acid subvolcanic products in submarine to sub-aerial environment -effusive activity (Upper Pliocene-Lower Pleistocene / 2.7-1.4 M.a.)	29
2.5.3.5.1. Andesitic, dacitic, rhyodacitic, rhyolitic domes and lesser lavas, dykes emplaced along NE - SW trends (Anda)	29
2.5.3.5.2. Hyaloclastitic breccias	31
2.5.3.5.3. Dacitic-rhyodacitic domes along NW - SE trends (Dado)	34
2.5.3.5.4. Autobreccias	34
2.5.3.6. The explosive unit related to the emplacement of the andesitic-dacitic -rhyodacitic-rhyolitic effusive sequence (Anda) (Upper Pliocene - Lower Pleistocene / 2.7-1.4 Ma)	34
2.5.3.6.1. Galana formation (Galf)	34
2.5.3.6.2. The upper lithic/pumice tuff unit (Ump)	35
2.5.3.6.3. The upper fine tuff unit (Uft)	35
2.5.3.7. Breccias & volcanosedimentary Units (Lower- Middle-Upper Pleistocene / 1.4-0.5 Ma)	35
2.5.3.7.1. Eruption breccias	35
2.5.3.7.2. Tectonic breccias	36
2.5.3.7.3. Pebble dyke breccias	36
2.5.3.7.4. Boulder fields breccias	36
2.5.3.7.5. Vani volcanosedimentary unit	36
2.5.3.7.6. Upper fossiliferous tuffites (Uftt)	38
2.5.3.7.7. Debris flow deposits	38
2.6. The present day topographic position of the Pliocenic- Pleistocenic volcanic/ volcanosedimentary and sedimentary products of W. Milos	38
3. PETROGRAPHY OF THE VARIOUS ROCK TYPES IN THE AREA UNDER INVESTIGATION	39
3.1. Lithic / pumice tuff (Lpt)	39
3.2. Pyroclastic Pumice flow (Pfl)	39
3.3. Lower pumiceous lapilli tuff (Lmp)	40
3.4. Fine ash tuff (Fat)	40
3.5. Profitis Ilias ignimbrite (PIi)	41
3.6. Rhyolitic intrusive bodies and dykes (Rhyda)	41
3.7. Fossiliferous tuffs and tuffites (Ftt)	42
3.8. Reworked volcanosedimentary unit (ep)	42
3.9. Andesites-dacites and rhyodacites subvolcanic bodies and lavas (Anda)	43
3.10. Dacitic – rhyodacitic subvolcanic bodies lavas and dykes (Dado)	43
3.11. Galana Formation (Galf)	45
3.12. Upper pumice tuff unit (Ump)	45

3.13. Upper fine tuff unit (Uft)	46
3.14. Upper fossiliferous fine tuff/tuffite (Ufft)	46
3.15. The Breccias	46
3.15.1. Hydrothermal eruption matrix supported breccias	46
3.15.2. Hyaloclastitic matrix supported breccias	47
3.15.3. Hyaloclastitic clast supported breccias	47
3.15.4. Tectonic breccias	48
3.16. The veins	48
3.16.1. Chalcedonic to crystalline quartz-adularia veins into pyroclastics	48
3.17. Xenoliths (magmatic inclusions) in the subvolcanic bodies and extrusive domes	49
3.17.1. Porphyritic inclusions	49
3.17.2. Cryptocrystalline inclusions	49
3.17.3. Hyalopilitic inclusions	49
3.17.4. Multi-phases inclusions	49
4. TECTONIC SETTING OF THE AREA UNDER INVESTIGATION	50
4.1. Introduction	50
4.2. The main structural features of W. Milos	51
4.3. The GIS approach to the identification and drawing of the main tectonic features	55
4.4. The linear and circular features	56
4.5. Drainage considerations	58
4.6. Conclusive remarks	59
4.7. Summary	59
5. ALTERATION FEATURES OF THE INVESTIGATED AREA	61
5.1. Introduction	61
5.2. The alteration mapping	61
5.3. The alteration zones	67
5.3.1. The Silicic alteration zone	67
5.3.1.1. Massive to Vuggy Silica	67
5.3.1.2. Silica flooding	68
5.3.2. The Advanced argillic alteration zone (AA)	69
5.3.2.1. Pre-ore advanced argillic alteration of magmatic-hydrothermal origin	70
5.3.2.2. Magmatic steam advanced argillic alteration (MS)	71
5.3.2.3. Steam-heated advanced argillic alteration (SH)	71
5.3.3. The Argillic alteration zone (A)	72
5.3.4. The Phyllic alteration zone (Phy)	72
5.3.5. The Adularia-Sericite alteration zone (Adul)	72
5.3.6. The Propylitic alteration zone (Pr)	73
5.3.7. The Oxidation patterns (Ox)	73
5.3.8. The Fresh rocks zone (Fr)	74
5.4. The alteration styles which characterize the various rock formation of W. Milos	74
5.5. Considerations on the fluid temperatures acted on Western Milos	75

5.5.1. Synthesis of the data	75
6. ON THE GEOLOGY-MINERALIZATION-ALTERATION OF WESTERN MILOS SUBAREAS	76
6.1. Introduction	76
6.2. The Northern Sector Subareas	76
6.2.1. Vani	76
6.2.2. Katsimoutis	78
6.2.3. Kondaros-Mersinia-Xerokampos	80
6.2.4. Larni - Agathia	82
6.2.5. Akrotiri - Vromolimni - Ampelakia	84
6.2.6. Galana - Favas - Tria Vouna	84
6.2.7. Triades - Agios Nikolaos	87
6.2.8. Agios Stefanos - Ralaki - Ntasifnos - Spiritou Rema - Ammoudaraki	89
6.3. The Southern Sector Subareas	90
6.3.1. Plakota - Agios Panteleimon - Petrovounia	91
6.3.2. Kirjiannoulis - Koumaria - Skiadi	91
6.3.3. Agios Ioannis - Voulismata	93
6.3.4. Chondro Vouno - Pyrgiali - Per isteria	94
6.3.5. Profitis Ilias - Livadakia - Chontri Rachi	96
6.3.6. Mavrovouni - Vathi Rema	99
7. PARAGENETIC RELATIONSHIPS AND ORE MINERALOGY	101
7.1. Triades	101
7.2. Galana	104
7.3. Agathia	105
7.4. Katsimoutis	107
7.5. Kondaros	109
7.5.1. Kondaros top	109
7.5.2. Kondaros base	109
7.6. Profitis Ilias	111
7.7. Chondro Vouno	116
8. ORE CHEMISTRY	117
8.1. Tetrahedrite-group minerals	117
8.2. Enargite	119
8.3. Sphalerite	119
8.4. Galena	120
8.5. Bornite	121
8.6. Polybasite-Pearceite	121
8.7. Tellurides	124
8.8. Native gold	124
9. GEOCHEMICAL CONDITIONS DURING ORE FORMATION AT WESTERN PART OF MILOS ISLAND	127
10. MAJOR-MINOR-TRACE ELEMENTS VARIATION AND THEIR GEOCHE-	

MICAL TRENDS	131
10.1. Major Elements Variation and their Geochemical Trends	131
10.2. The relationships between alteration zones and major elements content	131
10.3. Minor and Trace Elements Variation and their Geochemical Trends	142
10.3.1. The La pattern	144
10.3.2. The Nd pattern	144
10.3.3. The Mo pattern	144
10.3.4. The Bi pattern	144
10.3.5. The W pattern	144
10.3.6. The Cd pattern	146
10.3.7. The Ni, Cr, Co patterns	146
10.3.8. The Ce pattern	146
10.3.9. The Ga pattern	146
10.3.10. The Rb pattern	146
10.3.11. The Sr pattern	146
10.3.12. The Y, Nb patterns	148
10.3.13. The V pattern	148
10.3.14. The Zr pattern	148
10.4. The relationships between the minor and trace elements in the various alteration zones	148
10.5. The Epithermal suite of Trace Elements at W. Milos and its Variation	153
10.5.1. The Trace elements Binary diagrams	154
10.6. The distribution of the trace elements at the various western Milos subareas	157
10.6.1. Vani subarea	157
10.6.2. Katsimoutis subarea	157
10.6.3. Kondaros - Mersinia - Xerokampos subarea	158
10.6.4. Agathia - Larni subarea	158
10.6.5. Vromolimni - Akrotiri - Ampelakia subarea	158
10.6.6. Galana - Favas - Tria Vouna subarea	159
10.6.7. Triades - Agios Nikolaos subarea	159
10.6.8. Agios Stefanos - Ralaki - Ntasifnos - Spiritou Rema - Ammoudaraki subarea	159
10.6.9. Plakota - Agios Panteleimon - Petrovounia subarea	160
10.6.10. Koumaria - Kirjiannoulis - Skiadi subarea	160
10.6.11. Ag. Ioannis - Voulismata subarea	161
10.6.12. Chondro Vouno - Pyrgiali - Peristeria subarea	161
10.6.13. Profitis Ilias - Livadakia - Chondri Rachi subarea	161
10.6.14. Mavrovouni - Vathi Rema subarea	161
10.7. The geochemical distribution of the trace elements in the various subareas and their relation to the tectonics	162
10.7.1. The Au pattern	162
10.7.2. The Ag pattern	163
10.7.3. The Cu pattern	165
10.7.4. The Pb pattern	166
10.7.5. The Zn pattern	167

10.7.6. The As pattern	168
10.7.7. The Sb pattern	169
10.7.8. The Ba pattern	171
10.7.9. The Hg pattern	172
10.7.10. The Mn pattern	173
10.8. The interrelationships between the trace and the minor elements	174
10.9. Synthesis of the data	177
11. DISCUSSION	178
12. CONCLUSIONS	192
REFERENCES	197
APPENDIXES	
Appendix I	
Geological Sections	
Appendix II	
Microprobe Analyses	
Appendix III	
Equilibrium Constants Used for the Construction of the Phase Diagrams	
Appendix IV	
Trace Elements Statistical Elaboration	

1. INTRODUCTION

1.1. Purpose of this study

The primary aim of this work was focused on defining and distinguishing the two hydrothermal styles of mineralization which have been developed and acted at western Milos, in order to try to answer to the question, to which kind of processes they were related to.

Although, because of the complicated tectonic and magmatic history of the district, it has been several times explored, mainly for barite, galena and industrial minerals (bentonite, kaolinite, perlite), as well as for geothermal energy production purposes, little results have been produced until now concerning strictly the ore mineralogy and its relations to the fossil hydrothermal system which acted in the whole western Milos area.

The efforts towards geological, tectonic, mineralogical and geochemical characterization of the hydrothermal deposits at western Milos, considered as useful parameters for the specification of the ore genesis, created a detailed working frame which has included the following steps towards assigning the desired goals :

- A detailed geological mapping of the area at a scale 1:5000, against the official existing mapping 1 : 25000, through which the different rock formations have been displayed and described in detail, expressing in such a way a precise configuration related to their genesis and to the tectonism which facilitated their emplacement either destroyed them.
- A detailed air-photo interpretation, against that existing at the 1:25000 official geology map, which together with a related satellite imagery elaboration / study, resulted in a concise structural / tectonic relation to the main venting areas at the district, which at their turns are related to both volcanic activity and mineralization.
- A detailed alteration mapping, against some partial existing for the broad Vani-Katsimoutis, Triades areas, which was the result of several steps, that comprised, degree of argillization and silicification expressed as intensity (slight, moderate, strong), appropriate sampling and XRD analyses, as well as satellite imagery elaboration and interpretation, and last but not least a correlation of all these to the petrography / geochemistry of the altered rocks. Out of this work, a series of different kind of alteration maps have been produced.
- A detailed description of western Milos area, against some partial existing for the areas of Vani, Katsimoutis and Triades, after subdividing it in different subareas, on the purpose to fully localize geological, tectonic, geochemical and mineralogical “behaviours” attributed to them.
- A complete series, against some partial existing for the broad Vani-Katsimoutis, Agathia-Triades areas, of major, minor and trace elements are presented for the whole of western Milos area. On that purpose thousands of analyses are reported, explained (mineralogically, statistically), and correlated. In more, for the first time, the relation of the geochemistry to the existing tectonic network is visualized through a series of maps, and it is connected to the related vent / mineralizing areas.
- Ore microscopy and electron microprobe analyses, against some partial ones referred to Vani-Katsimoutis, Triades and Chondro Vouno-Profitis Ilias areas, of mineralized samples have been taken place in order to distinguish different types of mineralization as well as temporal and spatial relationships of the different ore paragenesis.

- A study / thermodynamic approach on the physicochemical conditions existing during ore deposition, at western Milos mineralization, following the pioneer work of Liakopoulos, 1987, who described the chemical parameters of the present geothermal field, as well as of hydrothermal alteration related to the mineralization of some areas (Vani-Triades).

It is considered that, the results achieved put another stone towards a better understanding of the style of hydrothermal mineralization, that occurred and continuous to occur in this active arc setting.

1.2. Previous works

Milos island constituted the subject of many researches and of many researchers since the eighteenth century. Savirage (1846) first, gave a description of Milos island, while little bit later Leycester (1852) will be again occupied with some aspects of the volcanism of the Milos complex island's group. Gobantz (1892) will be occupied with the silver minerals of Milos island, as will do also, one year later Huffner (1893).

Sonder (1924) recognized the importance of hydrothermal alterations on the island of Milos and created the first geological map of it. Voreadis and Mourabas (1935) have studied the silver rich baryte of Trides-Galana area (W. Milos), and through their chemical analyses had considered most probable the presence of silver chlorine minerals because of the high concentrations of these two elements. Liatsikas (1949) described the geology of Milos island and was critical on some issues related to the previous geological mapping by Sonder. Marinos (1955), did a geological reconnaissance on the kaolinitic deposits of NW Milos. At the same year Liatsikas (1955) described the ore deposits at Vani (Mn) and Triades (Pb-Ag) and other industrial minerals from western Milos. Voreadis (1956) described the kaolinite deposits at the areas of Kondaros and Agathia. Burri and Soptrajanova (1967) dealt with the petrography of the young volcanic rocks of Milos. Fytikas et al.(1976) and (1976b) presented geochronological data on the magmatism, and preliminary geological data from the first two productive geothermal wells drilled at Milos. Fytikas (1977) during his phd thesis, carried out a complete geological-geophysical survey studying principally the present day geothermal system of eastern Milos. Innocenti et al. (1981) presented geochemical data from Milos island and discussed their variations within the South Aegean Volcanic Arc context. Kalogeropoulos and Mitropoulos (1983) presented analyses of fluid inclusions, and sulfur, oxygen isotopes concerning barites from W. Milos. They concluded that the formation of the Milos baryte was related to an environment similar to that of the Kuroko barytes. Thanassoulas (1983a) applied a geoelectrical reconnaissance survey on W. Milos. Hauck (1984) studied the baryte formations on the basis of petrographic, geochemical and sulfur isotope data and concluded that their formation was due to the mixing of hot hydrothermal fluids with cold sea water. Simeakis (1985) occupied with the neotectonic evolution of Milos island complex through a geophysical approach. At the same year, Tsokas (1985), applied during his phd thesis different geophysical survey techniques in order to identify and localize, through the tectonic features of the metamorphic basement, areas showing very small resistivity values, as a direct indication of circulation of geothermal fluids. At 1996 the same author will try to interpret a well localize Bouguer anomaly at the entrance of the gulf of Milos island. Fytikas et al. (1986) presented a concise work on the volcanology and petrology of the volcanic products from the island of Milos and the neighboring islets. Liakopoulos (1987) in his phd thesis studied the hydrothermal activity and mineralization

in the areas of Vani and Triades-Galana. He concluded that the distribution of the hydrothermal minerals and the relationship between the chemical and the isotopic composition of the geothermal fluids indicate that an important process controlling the mineralization is the dilution of a K-Na-Cl rich fluid from a deeper reservoir, by a Ca-Mg rich gold water occurring at a shallower level. Niugini mining Co. (1987) first considered Milos island as a favourable place for epithermal gold mineralization. Hauk (1988) will re-introduce the concept of Kuroko-type ore deposits for the island of Milos. Fytikas (1989) and Fytikas et al. (1989), proposed an integrated model for Milos geothermal field and tried through comparison of geophysical methods to detect the presence of the hydrothermal reservoirs occurring in the island. Silver and Baryte ores mining Co. (1989) started to explore for gold and silver assisted by the French Geological survey (B.R.G.M). They located several areas hosting gold, silver and polymetallic mineralization on western Milos. Kelepertzis et al. (1990) studied the mineral and chemical composition of the kaolins from Milos island. Pflumio et al.(1991) presented further isotopic data and pointed out the importance of boiling and phase separation for the formation of the ore deposits. Silver and Baryte ores Mining Co. (1994) will create the company MIDAS S.A., as a result of the joint venture with two Australian companies (Renison Goldfields Consolidated-RGC and Niugini mining Co.), in order to look for potential deposits of gold epithermal nature. Christanis and Seymour (1995) presented a study of scale deposition as an analogue of meso- to epithermal ore formation in the volcano of Milos. Vavelidis (1995) pointed out the presence of framboidal pyrite and indicated a Kuroko-type genesis for the baryte mineralization at Katsimoutis area (NW Milos). By the autumn of 1997 the two Australian companies will be withdrawn and MIDAS S.A. will continue to exist as a daughter company of S&B. During the first months of 1998 a joint venture between an American (Royal Gold Inc.) and a Canadian (Aegean Gold Inc.) companies will be created (Milos Gold S.A.) and a financial/working agreement, on gold-silver exploration on Milos, with MIDAS S.A. will take place. Vavelidis and Melfos (1997) and (1998) will report on plumbian tetrahedrite-tennantite occurrences and on fluid inclusion evidences concerning the origin of the barite silver-gold bearing Pb-Zn mineralization at Triades (W. Milos). Constadinidou et al. (1998) will report on the mineralogy and chemistry of gold in the Profitis Ilias epithermal deposit. Hein et al. (2000) will point out the trace metal-rich, hydrothermal manganese oxide and barite, from Vani area (NW Milos).

A detailed account of the geological and mining history of the island has been presented by Plimer (2000). Dimou (2001) will indicate the presence of halogenide minerals at Profitis Ilias area (W. Milos) epithermal system. Kiliadis et al. (2001) will present fluid inclusions data on epithermal gold mineralisation in the area of Profitis Ilias (W. Milos). Liakopoulos et al. (2001) will come again across the nature and origin of the Vani manganese deposit (NW Milos). Naden et al. (2003a), (2003b) and (2005) presented fluid inclusions and isotopic data and discussed issues related to land-based geothermal systems with entrained seawater as analogues for transitional continental magmato-hydrothermal and volcanic-hosted massive sulfide mineralization. Stewart and McPhie (2003) discussed about the presence of epithermal Au deposits in a modern volcanic island arc setting, and later (2005) presented a concise work on the facies architecture of the submarine felsic volcanic island of Milos. Alfieris et al. (2004), Alfieris and Voudouris (2005) presented mineralogical, geochemical and volcanological data on the transitional submarine to subaerial magmatic-hydrothermal deposits of W. Milos. Balanti et al. 2004 reconstructed the evolution of the fossilized (Pleistocene) hydrothermal system of eastern Milos, whose activity led to the formation of large bentonite and barite deposits.

Studies on the biology and geochemistry of the hydrothermal fluids of the present geothermal system venting at submarine areas, southern and eastern offshore areas of Milos, have also been presented by several authors this last decade. In that respect it could be mentioned Valsami-Jones et al. (1998), (2005) who presented several works on the geochemistry of fluids from the present active shallow submarine hydrothermal venting system around Milos island. Dando et al. (1999), (2000) study various aspects of the hydrothermalism related to the submarine venting areas, while at the same years Sievert et al. (1999), (2000) defined bacterial populations and spatial heterogeneities of those populations at the present shallow submarine hydrothermal system of Milos. Kati et al. (2003) occupied with the hydrothermal precipitates from the active submarine vents in Paleochori Bay (E. Milos).

1.3. The evolution of the Hellenides

Greece belongs to the Hellenides, an approximately NW-SE orientated orogenic belt, which is connected to the mountain chains of Dinarides / Albanides in the northwest (Albania and former Yugoslavia) and the Taurides in the East (Turkey),(Fig. 1).



Fig. 1 : Location of the Hellenides. From U.S.G.S. modified.

The Hellenides are divided into a number of sedimentary facies belts or isopic zones (after Aubouin 1965), from the internal parts of the Hellenides (East) to the external parts (West), (Fig. 2).

These zones are separated by major NW-SE striking thrusts on the Greek mainland and the Ionian islands. The geological evolution of the Hellenides can be described as a successive stages of divergences and convergences of the African and Eurasian plates and processes related to extensional regimes in the back-arc regions (McKenzie 1970, 1972; Papazachos and Cominakis 1971; Le Pichon and Angelier 1979; Dewey and Sengor 1979).

The convergence begun during upper Jurassic / lower Cretaceous times with the closing of the Palaeo-Tethys (oceanic area), between the above mentioned plates, as evidenced by the emplacement ages of the various ophiolitic complexes in northern Greece (fig. 2). The Aegean region has been shaped as a result of a subduction process, where the Aegean

micro-plate overrides the oceanic crust of the African plate, which started at about 13 Ma ago (Angelier 1979; Le Pichon and Angelier 1979).

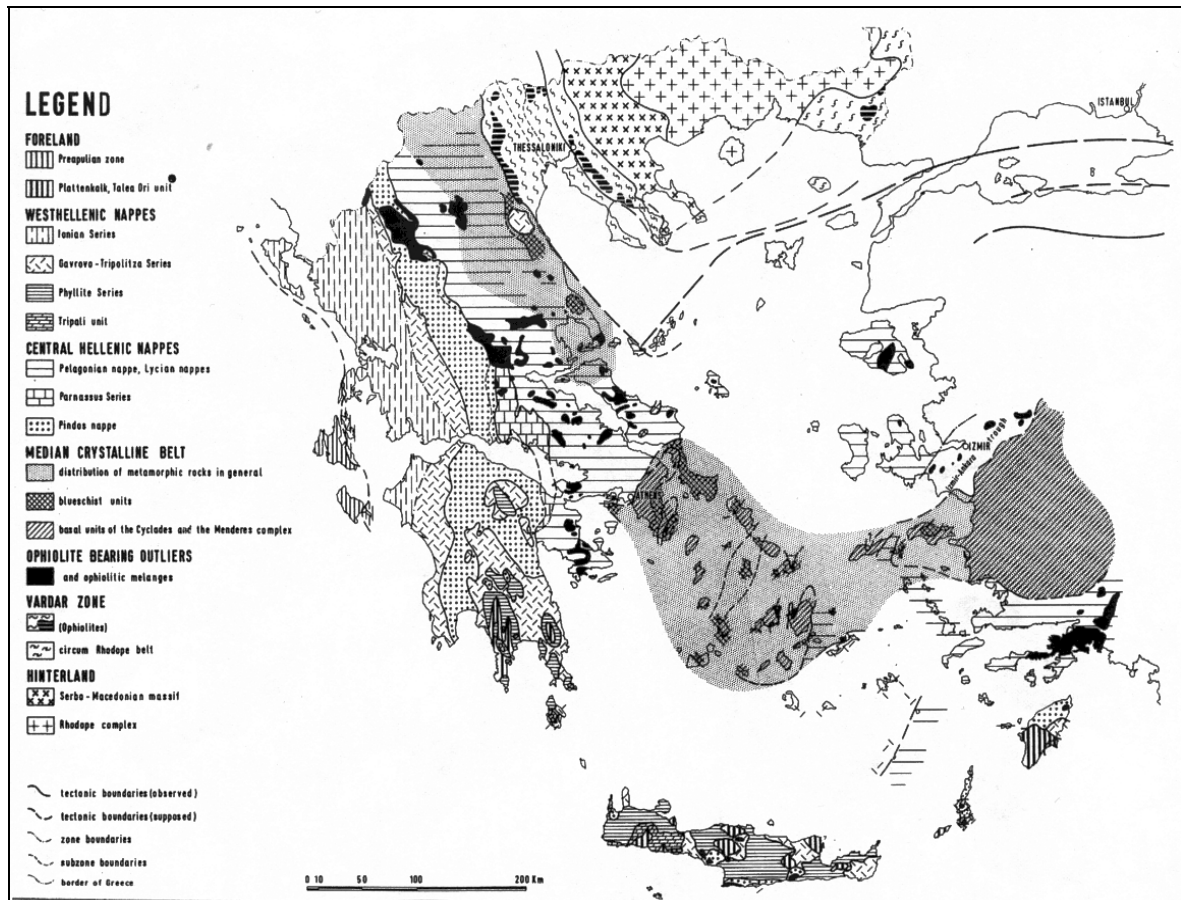


Fig. 2 : The isopic zones of the Hellenides. From Jacobshagen et al. 1978.

1.4. Geotectonic evolution of the Aegean Sea

1.4.1. Tectonic regime in the Aegean

The Aegean region is geologically a very complex area bounded in the north by the Rhodope massif, the Hellenides in the west, the Anatolian orogenic belts in the east, and the Hellenic trench in the south (fig.2, 3).

Geotectonically the region is characterized by active subduction, back-arc extension and an anticlockwise rotation along the North Anatolian Fault (McKenzie 1970; Jackson and White 1989; Papazachos and Kiratzi 1996), which is accommodated by roll-back of the slab southwards. The kinematics of the deformation are governed by two additional processes, the westward movement of Turkey relative to Europe and the continental collision between NW Greece-Albania with the Apulia-Adriatic platform in the west (fig.3). This resulted in an E-W shortening of the northern Aegean, which has been compensated by a fault block rotation and a N-S extension in the back-arc region. This area of extension was the South Aegean region.

The median Aegean crystalline belt, made up of Paleozoic basement overlain by Mesozoic carbonate sequence (Durr et al. 1978), underwent two main metamorphic phases. The older of these, late Eocene in age, took place during the subduction, in the Aegean area, where the orogenic sediments of the deep basin at that area went metamorphosed in high P - low T conditions forming the well known paragenesis of the blue schists (glaucophane-bearing paragenesis), (upper Cenozoic / 64.2 Ma); (Fytikas et al. 1976a).

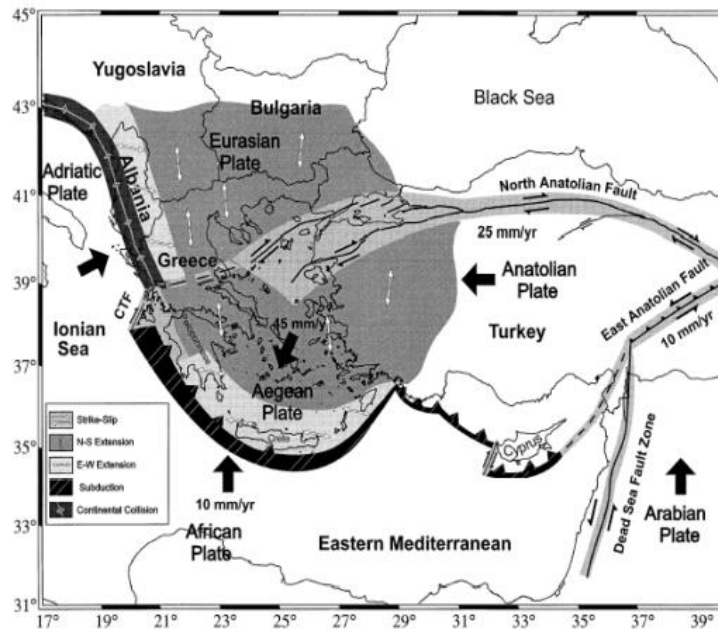


Fig. 3 : Relative motion of the Greek microplate. The arrows indicate the motions along the fault lines. CTF = Kefallonia fault zone. After Papazachos et al. 1998.

Subsequent to that episode “Milos island territory” remained submerged until the early Oligocene, when started the uprising of the metamorphic formations until to reach the surface. During this period as well as during the lower and middle Miocene the P - T conditions will be changed and as a consequence of that the blueschists facies gradually converted into the greenschist one (\pm low P and high T), quasi at 33.2 Ma (Fytikas et al. 1976a). It is considered that this age also dates the last metamorphic event that affected the Attic-Cycladic basement, connected with the Eocene-Oligocene Africa - Europe continental collision (Fytikas et al. 1976a). So it can be said that i.e. these two metamorphic episodes showed the beginning and the end of the compressive tectonism during Alpine times.

During these movements, related to the lithospheric extension, subduction has been ongoing, exercising in such a way a compressional regime in the external part of the Aegean domain.

Starting from Middle - Upper Miocene (late Serravallian-Langhian-Tortonian), the previous paleogeographic / geotectonic configuration which characterized the Aegean area until then (Pre-Apulian ridge zone followed by the Ionian, Gavrovo-Tripolitza, Pindos zones and Meso-Hellenic through, Cycladic basin; fig. 4) will be changed due to prevalently tensional tectonics, with intermittent phases of minor compressive events (Angelier et al., 1977; Le Pichon and Angelier, 1979). The effects of this tensional

tectonic activity were particularly marked in the central Aegean sector, where the crust is distinctly thinner (between 22 and 32 Km), (Makris, 1977; McKenzie, 1978a). The result of all these tensional and compressional movements, was during upper Miocene (Tortonian-Messinian, 15-10 Ma) (Bonneau, 1981), the fragmentation of the previous rigid Alpine basement units (Gautier et al. 1999) into a mosaic of relatively small-

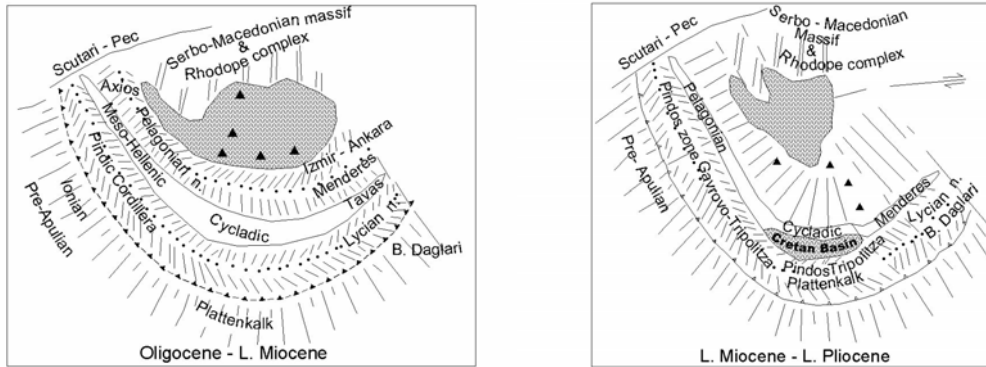


Fig. 4 : Paleo-geographic / tectonic scheme of the evolution of the Hellenides from Oligocene to L. Pliocene. From Papanikolaou and Dermitzakis 1981, modified.

sized horst and grabens (McKenzie 1978a; Le Pichon and Angelier 1979), and the creation of two new geodynamic environments (domains), the internal domain (Cyclades-Attica-Anatolia) and the external Aegean domain (Peloponnesus-Crete-Dodecanessa), (fig.2,4). At the internal domain a proto-Cretan basin started to form approximately at the area where the Cycladic back arc molassic basin was (fig.4,5), (Papanikolaou and Dermitzakis, 1981). The development of the Cretan trough, a fore-arc basin, which separates the sedimentary outer arc (central Peloponnesus, Kythera, Crete, Karpathos and Rhodes) from the present southern Aegean active volcanic arc, was of paramount importance for the tectonic development of Milos complex in the sense that it guided the tectonic architecture of it.

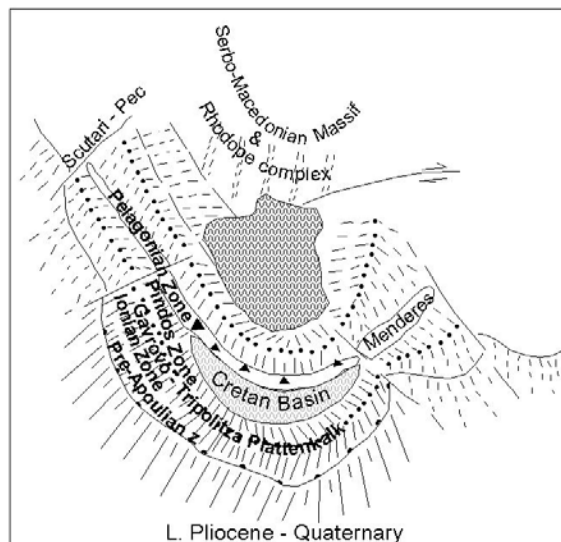


Fig. 5 : Paleo-geographic / tectonic scheme of the evolution of the Hellenides from L. Pliocene to Quaternary. From Papanikolaou and Dermitzakis 1981, modified.

Indeed the northwestern-trending faults on Milos island is interpreted to have formed contemporaneously with the opening of the Cretan basin, in response to the northeastern extensional regime which took place at the western part of it (Lyberis et al.,1981).The other principal extensional directions being NW-SE for the Eastern part of the basin of Crete and N-S for the Central part of it (fig.6).

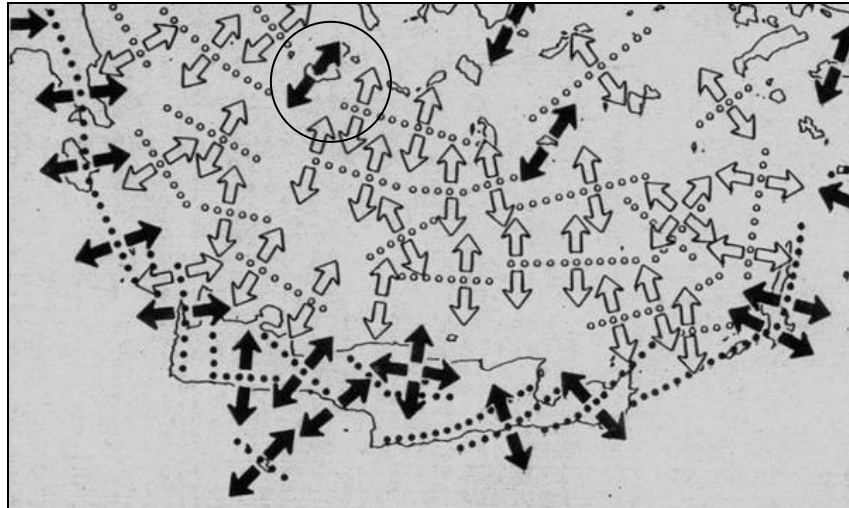


Fig. 6 : Direction of the extensions recognized on the various land domains (black arrows) and deduced on the southern Aegean sea (white arrows). Inside the circle Milos island. The southernmost island is Crete. From Lyberis et al. 1981, modified.

Finally because of the continental collision in the NW Aegean area and the subduction in the South, it is assumed that the transition from subduction to collision has been associated with a clockwise rotation of the region to the south (Duermeijer et al. 1998, 2000).

Starting from Pliocene (Serravallian) this new tectonic (neotectonic) situation which had, as mentioned above, an extensional character along NE-SW directions, and was only shortly interrupted by compressional episodes (Angelier 1976,1979;Mascle et al.,1981), created tectonically bounded sedimentary plateaus and basins.

As a whole, the variation of the tectonic regime with two extensional phases separated by a compressional one (Angelier et al. 1977) seems that directly influenced both, the rate at which the magma rose through the continental crust, as well as the composition of the magma reaching the surface.

1.4.2. Volcanic centers and tectonic setting across the Aegean region

1.4.2.1. The Hellenic Volcanism

In the Aegean area, the continuing northward subduction of the oceanic lithosphere (McKenzie 1970, 1972; Papazachos and Comninakis 1971; Le Pichon and Angelier 1979; Dewey and Sengor 1979; Papazachos and Panagiotopoulos 1993; Papazachos et al., 1993, 2000; Pavlakis 1993), which lasts until today, gave a series of magmatic arcs which ages become younger southward. Indeed, during Tertiary and Quaternary times a widespread volcanic activity occurred in the Aegean area which, variable nature of the products and time-space distribution, reflect the complicated history of the convergence between African and European plates at the eastern Mediterranean area (Fytikas et al.,1984, 1986).

Three main phases of orogenic, mainly calc-alkaline magmatic activity have been identified and described (Fytikas et al., 1984, 1986). The third phase began during lower Pliocene times forming a volcanic arc, still active, at the southern Aegean area, (Southern Aegean Volcanic Arc). The petrology and petrogenesis of the volcanic rocks of the Southern Aegean Volcanic Arc has been described by Fytikas et al., 1986; Mitropoulos et al., 1987 and Mitropoulos and Tarney 1992).

1.4.2.2. The Southern Aegean Volcanic Arc

In tectonically active settings, volcanism can generally be associated with melting due to the subduction of a hydrated lithosphere, either the extension of the lithosphere itself leads to partial melting as a result of adiabatic (extension induced) decompression.

In the Aegean region, where both subduction and extension occurred and continuous to occur simultaneously (Pe and Piper, 1972; Briquieu et al., 1986), volcanism is considered to be the result of melting associated with subduction of African lithosphere beneath the Aegean microplate (Pe-Piper and Hatzipanagiotou 1997).

The Southern Aegean volcanic arc is one of the most important geological structures of the Mediterranean area. It is a belt of volcanic centres located above an amphitheatre shaped seismic zone having the maximum depth of 180 Km, dipping 35° on the average and interpreted to represent the top of the subducting African slab (Papazachos, 1973; Makropoulos and Burton, 1984; Hatzfeld, 1994; Giuchi et al., 1996; Papazachos et al., 2000), and consist of products ranging from basaltic, andesitic, dacitic to rhyolitic in composition, all of them displaying a typical calc-alkaline chemical character (Innocenti et al., 1981).

The volcanic arc (fig.7) extends from the gulf of Saronikos in the west to the western Turkey coast to the east and includes the volcanic centers of Sousaki, Aegina, Methana, Poros, Milos, Santorini, Kos and Nisyros. The central and eastern sectors of the arc are characterized by large stratovolcanoes with caldera structures (Santorini, Kos, Nisyros) whereas the western sector is mainly characterized by small and generally monogenic in nature, eruptive centers. The volcanic activity began in the lower Pliocene (4,7 Ma at Aegina, Fytikas et al. 1984). According to Papazachos and Panagiotopoulos 1993, the more intensive volcanic activity in the eastern volcanic centres of the arc, i.e., Santorini, Nisyros compared to the western volcanic centres, i.e., Sousaki, Methana and Milos reflects the higher rate of extensional crustal deformation in the eastern part of the arc (26 mm/year) compared to the western part of it (2 mm/year).

Five normal faults trending about N59° and named after the corresponding volcanic centres (fig.7) appear to control both, the distribution of volcanic centres, and the shallow -20 km, intermediate 120–180 km depth seismicity along the arc. These seismic lineaments are interpreted as deep lithosphere rupture zones which permitted mantle-derived magma ascent.

The existing data indicate that the trench geometry leads to localised deformation and segmentation of the subducting slab, and in more, deformation within the subducted slab, is restricted to segment boundaries. The coincidence of intermediate depth seismicity and volcanic activity indicates a close link between tectonic features within the subducting slab and active magmatism above it, and suggests that melt generation is concentrated in zones above those parts of the slab that are heavily deformed, and where pore fluids from dehydration reactions are focussed to be released into the mantle wedge via hydraulic fracturing.

It is believed that these faults have had a major influence in controlling also, the distribution of the hydrothermalism along the arc generally, and in Milos particularly.

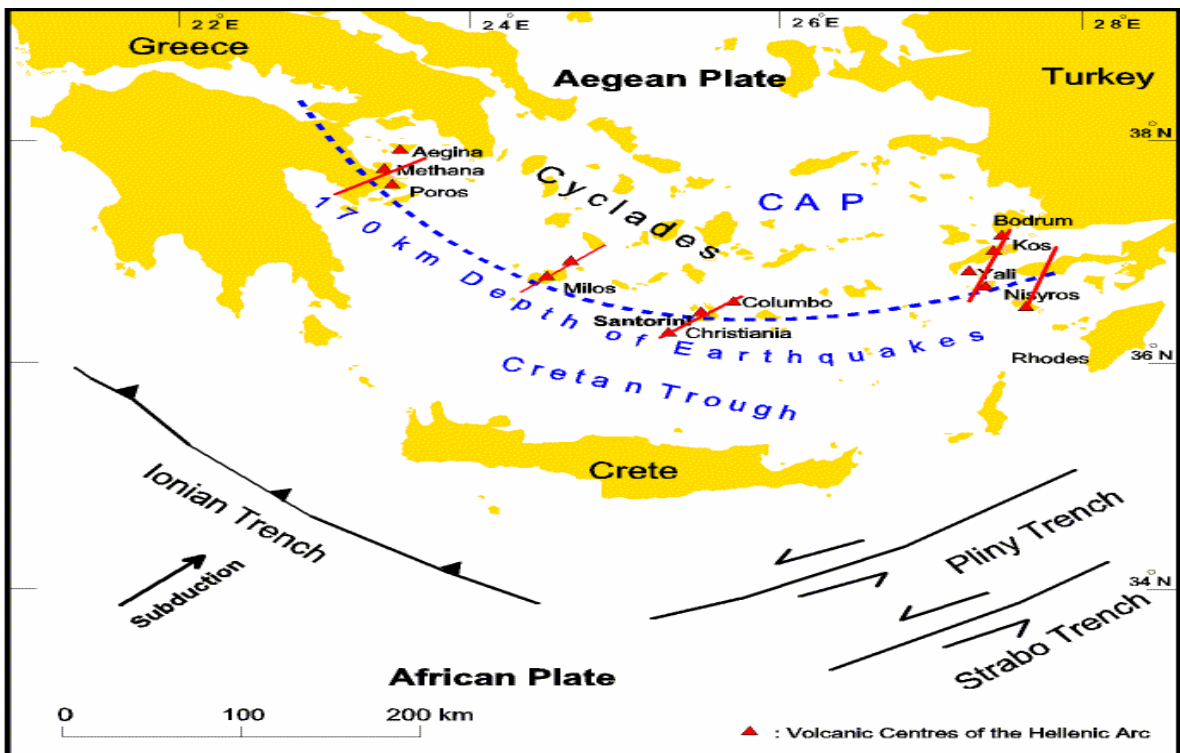


Fig. 7 : Normal faults trending about N59° and named after the corresponding volcanic centres are responsible for the distribution of the volcanic centres and the shallow, intermediate depth earthquakes along the arc. From Friedrich (2000).

2. TECTONIC AND GEOLOGICAL SETTINGS OF MILOS ISLAND

2.1. Introduction

Milos is located in the central part of the so-called south Aegean active volcanic arc (SAVA)(fig. 8), and geotectonically belongs to the central-southern Aegean crystalline sequence, known as the Attic- Cycladic massif or the median Aegean crystalline belt (fig.2) which extends eastwards into Menderes massif and westwards into the Pelagonian massif (fig. 2).

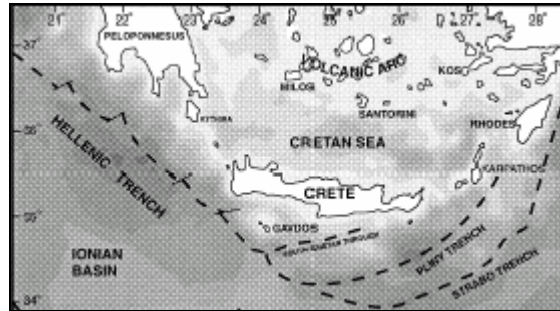


Fig. 8 : The south Aegean active volcanic arc. From Duermeijer et al. 1998.

2.2. Tectonics

Four main fault trends have been recognized in Milos island :

(1) The NW-SE, which principally influenced and tectonically determined the metamorphic basement. This trend is parallel to the south Aegean volcanic arc (arc parallel extensional fault), and it is the main marginal fault zone direction of the Neogene basins at western Cyclades and southeastern Peloponnese (Mariolakos and Papanikolaou, 1981), nonetheless the direction corresponding at the Alpine orogenesis. Finally this direction is also that one which includes the large graben of Milos gulf, the recent volcanic activity in Trachilas and Fyriplaka (E. Milos) and the corresponding horst of Profitis Ilias-Chondro Vouno area (W. Milos). Most probably, the faults of the basement which were parallel to the subduction zone were formed as steeply deeping transcurrent faults, which displayed predominantly dip-slip components of displacement.

(2) The E-W, which is considered to be the result of two chronologically different processes. An older one which took place before the starting of the volcanic activity in the island, and which is related to that series of tectonic events that affected the basement, and a later one which corresponds to the reactivation of the previous, and which is related to the emplacement of the transgressive series. The new one chronologically, corresponds to the Valachian orogenetic phase that took place during Quaternary times. This tectonique phase interested all the south Aegean Quaternary Volcanic Arc and it is characterized by big block faulting structures. At this tectonic trend belong the Ammoudaraki-Ntasifnos-Plakota-Rivari graben, at the central part of W. Milos.

This set of faults affected all the rock types at Milos.

(3) the N-S, which affected both the metamorphic basement and the overlain magmatic pile (arc normal extensional faults). It is considered to be responsible for the ascending of the magma at shallow depths and/or at the surface (Fytikas et al., 1986) and thus responsible for the emplacement of some of the domes at western Milos along this direction. It is also considered that this fault trend has an extensional character and it is related to the E-W stretching of the magmatic arc.

The N-S horst and graben structures at Milos are of smaller extent with respect to that of NW-SE and E-W, and include the Zephyria graben (E Milos), the Chalepa horst (central part of southern Milos), and a small horst that exposes basement rocks east of Profitis Ilias mountain (W. Milos).

(4) The NE-SW, which is approximately normal to the axis of the outer (southern) sedimentary arc (which is a link between the Dinaric Alps and the Turkish Taurides). This is also the trend of certain geomorphological features in the island, such as the isolines of Bouguer geophysical anomaly (Tsokas 1996) as well as of the linear clusters trending N59°E and comprising the volcanic centers (volcanoes, fumaroles and solfatara fields) and the epicentres of the shallow and intermediate depths strong earthquakes (Papazachos and Panagiotopoulos, 1993). Earthquake epicenter locations indicate that, the same major transcurrent structures facilitated oblique convergence, by reactivation during successive earthquakes.

It is also generally associated with extensional / dilational features (horstails, splays and jogs) and their linking faults mainly at W. Milos.

Generally speaking, it is considered that at Milos the E-W, ENE-WSW lineaments can be ascribed to the post Early Messinian counter clockwise ($5 \pm 14^\circ$, most probably $\sim 10^\circ$, after 4 Ma ago) rotation (Kondopoulou and Pavlides, 1990; Duermeijer et al., 2000; Van Hinsbergen et al., 2005) that affected the south western Aegean area, as a result of sinistral strike-slip movements (fig. 9).

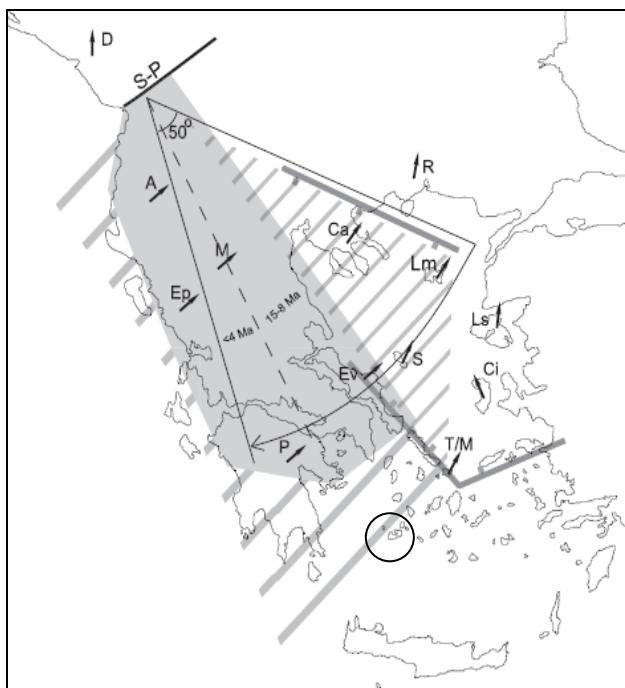


Fig. 9 : Schematic map indicating the configuration of the domain that rotated clockwise in the western Aegean region since the middle Miocene. The shaded area is inferred to rotate 50° cw. The finely hatched area has smaller finite post-Oligocene clockwise rotations of $30 - 40^\circ$. The widely hatched area doesn't contain middle Miocene sediments but it is inferred from structural observations that it belonged to the 50° cw rotating domain. Based on structural observation too, the area of Milos is considered to belong to the $\sim 10^\circ$ cw rotating domain. A= Albanides; Ca= Chalkidiki peninsula; Ci= Chios; D= Dinarides; Ep= Epirus; Ev= Evia; Lm= Limnos; Ls= Lesvos; M= Mesohellenic basin; P= Peloponnesos; R= Rhodope; S= Skyros; S-P = Scutari – Pec transform fault; T/M = Tinos and Mykonos. Into the circle Milos island. From Hinsbergen et al., 2005.

2.3. Geological setting of the whole Milos island

The island of Milos (fig.10) comprises four main geological units / sequences (Metamorphic basement, Neogene sedimentary sequence, Volcanic sequence and Alluvial cover) which were first distinguished by Sonder (1924) and then by Fytikas (1977), Fytikas et al. (1986). Recently, Stewart and McPhie (2005), gave a new approach concerning the volcanic successions, based on five main volcano types.

2.3.1. Metamorphic basement

Only limited outcrops of metamorphic rocks occur at the SW, S and SE part of the island. They consist of lawsonite-free jadeite eclogites, lawsonite eclogites, glaucophane schists, quartz-muscovite-chlorite and chlorite-amphibole schists (Fytikas and Marinelli 1976; Kornprobst et al., 1979; Fytikas et al. 1986), as well as abundant mesothermal quartz veins.

2.3.2. Neogene sedimentary sequence

This sequence represents the oldest post-orogenic autochthonous sediments of the Cycladic area (Upper Miocene (Messinian) to Lower Pliocene) (Fytikas, 1977; Altherr, 1981; Fytikas et al., 1986) and can be described as two parts sequence. The lowermost part (up to 30 m thick) consists of two basal conglomerate horizons (sub aerial red bed sediments), composed mainly of metamorphic quartz pebbles from the basement, in between of which a gray limestone horizon is situated. Minor gypsum layers outcrop locally at Provatas area (S. Milos). The upper part consists of a shallow marine carbonate sequence (limestones, only marly and arenaceous ones at its base), slightly folded with a variable thickness up to 150 m. The upper limestones at their turn are capped by a light brown to tan sandstone and sandy dolomite sequence which appears to have formed in an evaporitic environment. The total maximum thickness of the sequence is considered to be at about 185m.

2.3.3. Volcanic sequence

The volcanic rocks occupy more than 70% of the outcrops on the island (Fytikas 1977, 1986). The volcanism started during the Lower to Middle Pliocene as indicated by geological-stratigraphic observations (intercalations of tuffs into the Neogene sedimentary series), which has been dated (Fytikas 1977) to be Upper Miocene – Lower Pliocene in age. These measurements together with other radiometric ages (Fytikas et al. 1976, 1986; Angelier et al. 1977; Cantagrel and Vilminot, 1977; Bigazzi and Radi, 1981; Stewart and McPhie 2005) and paleomagnetic data (Kondopoulou and Pavlides 1990) indicate that the volcanic rocks sequence can be subdivided into four main phases between Middle to Upper Pliocene (3.5 Ma) and Pleistocene (0.08 Ma).

The description about the general geology of Milos island which follows, is based mainly on the scheme displayed by Fytikas et al. 1986, while modifications as well as relations to the newly presented work on Milos volcanology, by Stewart and McPhie 2005, are also reported.

In fig. 10, together with the generalized / schematic geological-sketch map of Milos island, as modified after Fytikas et al. 1986, are reported all the available geochronological data from the literature (Fytikas et al. 1976, 1986; Angelier et al. 1977; Cantagrel and Vilminot, 1977; Bigazzi and Radi, 1981; Stewart and McPhie 2005; Kondopoulou and

Pavlidis 1990), in order to better intergrate and locate the various volcanic / volcanosedimentary formations at Milos territory to the various geological / geochronological periods.

2.3.3.1. Pliocene series

They include acid pyroclastics followed by intrusive subvolcanics and flow dome complexes.

Phase I

The earliest volcanic episode (**Middle to Upper Pliocene 3.5-3.0 M.a.**) produced a thick (>120m) succession of felsic submarine units including pumice flows, cinerites, tuffs and pumice rich pyroclastic flows, with locally subordinate intrusive subvolcanic bodies, lavas and/or hyaloclastites with which sequence ends (Fytikas et al., 1986). It is considered that the above mentioned sequence (basal pyroclastic series-**BPS** of Fytikas et al. 1986; large submarine felsic cryptodome-pumice cone volcanoes of Stewart and McPhie 2005) has been erupted by a series of vents/volcanic centers (present work, Stewart and McPhie 2005) which today are presented partly by the sites occupied by the various subvolcanic bodies / dome complexes around the island (fig 10).

Subphase I-II

Between the end of the previous mainly explosive, partially intrusive phase (**Upper Pliocene 3.0 M.a.**), and the starting of the subsequent effusive phase (phase II), of intermediate to acid subvolcanic products in submarine to partially subaerial environment (**Upper Pliocene 2.7 M.a.**), and due to tectonic processes and reassessments, the opening of a quasi E-W directed graben structure has been established and filled by volcanosedimentary products.

Phase II

A phase of submarine volcanism (**Upper Pliocene to Lower-Middle Pleistocene 2.7-1.4 M.a.**), characterized by the emplacement of domes, plugs and lava flows (complex of Lava Flows and Domes-**LFD** of Fytikas et al. 1986 and submarine effusion and intrusion of dacitic/andesitic domes/lavas of Stewart and McPhie 2005) along a system of NNE-SSW faults mainly, and subordinately along NW-SE to E-W directions (Fytikas et al. 1986). The effusive activity was accompanied locally by explosive episodes from the domes themselves, which locally produced bedded pumiceous tuff cones (dome-top tuff cones), and/or pyroclastic flows and breccias on submarine and partially on subaerial environment.

2.3.3.2. Transitional Lower-Middle Pleistocene series

During this period (**Lower-Middle Pleistocene**) and most probably around **1.4 Ma**, due to a combine effect of tectonism and subvolcanic emplacement of phase II volcanism, the deposition of the tuffitic series (volcanosedimentary series) along an E - W direction, that initially has taken place at western Milos (subphase I-II), will continue on eastern Milos. Out of this configuration it can be deduced that, during this period a small number of islands were existed (corresponding to the various emplaced subvolcanic bodies), at the northern part of the present island while the southern Milos was a continental area.

2.3.3.3. Pleistocene series

They include acid pyroclastics followed by flow dome complexes mainly in subaerial environment.

Phase III

During **Pleistocene (1.4-0.5 Ma)** the eastern and northeastern parts of the present island were partially covered by shallow sea water (Fytikas et al. 1986). In such an environment has been developed an intense pyroclastic activity associated with rhyolitic domes (Pyroclastic series and Lava Domes-**PLD** of Fytikas et al., 1986 and rhyolitic pumice-cone volcanoes / rhyolitic lavas accompanied by phreatic activity of Stewart and McPhie 2005). The pyroclastic products mainly outcrop between Pantes and Pollonia (N-NE part of the island),(fig.10) and are made up by different ash flow tuff units locally intercalated by tuffites, pumice flow deposits, cinerites, and thick diatomite-rich ash deposits (Fytikas et al. 1986). The same pyroclastic products at the Filakopi area (N coast) are partially covered and pass laterally to a formation of hyaloclastic deposits, mainly pillow lavas, of andesitic-latic composition (Philakopi Hyaloclastites formation-**PLHF** of Fytikas et al. 1986, submarine felsic pumice breccia intruded by compositional similar cryptodomes of Stewart and McPhie 2004, 2005).

At the effusive products is attributed the large complex of domes and acid lava flows in the southern and northern middle part of the island (Halepa, Bombarda and Plakes-**HALPLA**) as well as in the eastern part (Demeneghaki) (Fytikas et al.,1986). These domes were developed mainly as extrusive subaerial domes along a N-S lineament.

In the NE part of the island (fig. 10) the submarine volcanic activity of andesitic composition was followed by a subaerial one, where dacitic mainly in composition domes and lava flows (Korakia, Kalogeros and Glaronisia) have been emplaced (Fytikas et al. 1986; Stewart and McPhie 2004,2005).

Phase IV

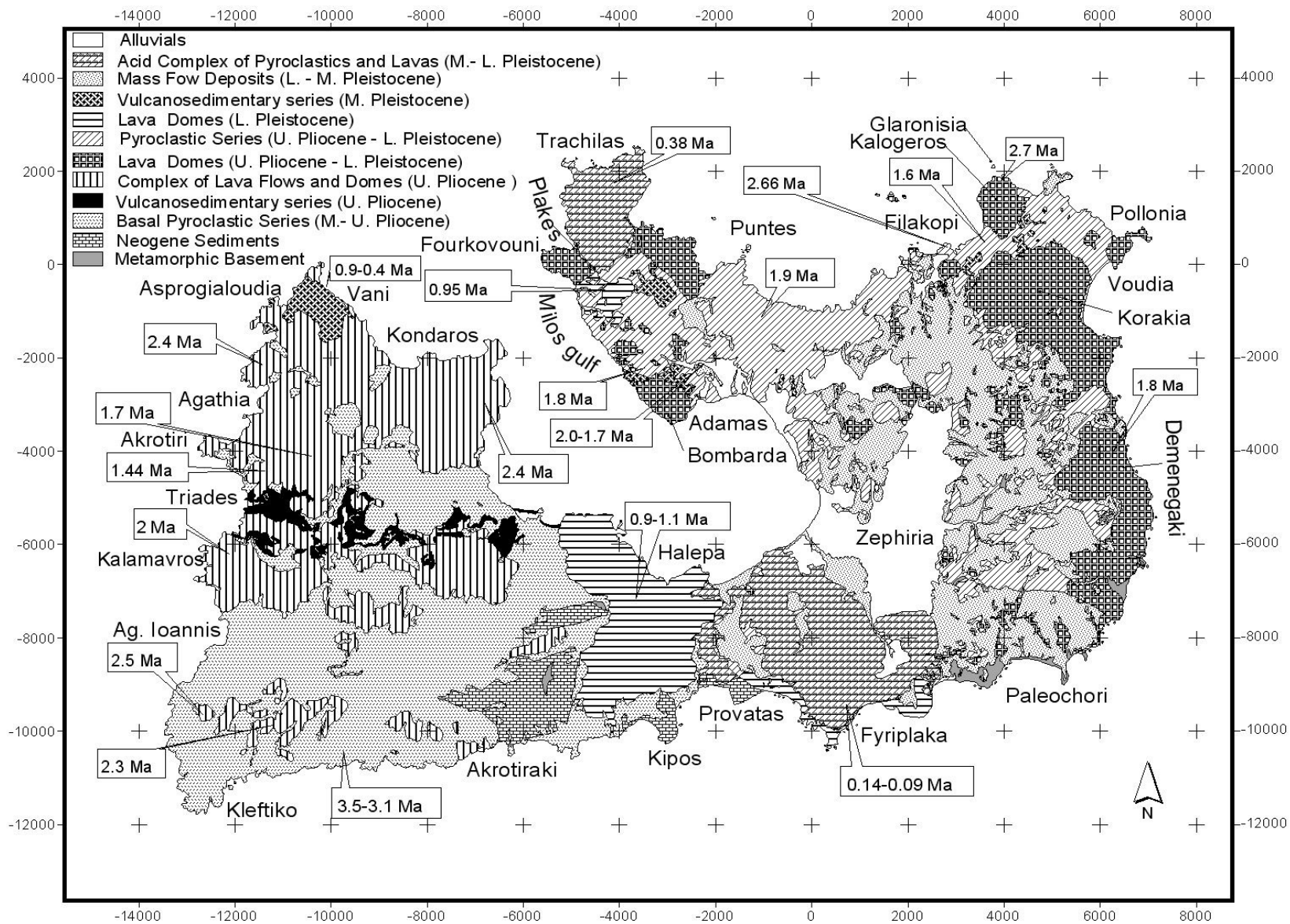
The most recent volcanic activity on Milos is concentrated in two distinct zones along the eastern coast of Milos gulf, on a well defined NW-SE striking structural lineament. They form the acid centers (subaerial explosive eruptions followed by rhyolitic lavas) of Trachilas and Firiplaka to the north and to the south respectively, with ages of 0.38 Ma and 0.14-0.08 Ma respectively (Fytikas et al. 1986; the rhyolitic complexes of Firiplaka and Trachilas of Stewart and McPhie 2005). This acid in composition activity has been accompanied by widespread phreatic activity (the “green lahar” of Fytikas 1977 and the mass flow deposits of Stewart and McPhie 2005).

2.3.4. Alluvial sequence

Recent alluvial sediments are found in the Zefiria graben indicating the presence of a lagoon-like environment. The sediments consist of clay, sand and gypsum for a total thickness of about 80 m (Fytikas et al.,1976b)

Although the last recorded volcanism was approximately 100000 years ago, Milos is still an active geothermal field. This is presently expressed by widespread surface manifestations in the form of fumaroles, hot springs, hot grounds and submarine gas escapes.

Fig. 10 : Simplified geological map of Milos island showing the distribution of the main volcanic phases and metamorphic, sedimentary units as well as the geochronological data so far available. Modified after Fytikas et al. (1986).



2.4. The other islands of Milos islands' group complex

Geological settings

Kimolos-Poliegos

These two islets (fig. 11) are, as Milos island, nearly completely built up by volcanic rocks; only few outcrops of metamorphic rocks and Neogene sediments are found and only at Kimolos, while at the same island little occurrences of granitic s.l. fragments into the pyroclastic formations testify the presence of a granitic s.l. body emplaced at shallow depths.



Fig. 11 : The Milos group of islands.

Antimilos

This small island (fig.11) represents the uppermost part of a polygenetic composite volcano (Marinos 1960; Manetti 1997) formed by lavas and minor pyroclastics. A series of flow domes have been emplaced on the southern flank of the volcano. Geochronological data (Fytikas et al., 1986) showed an age similar to that of the Trachilas volcano, on NE Milos.

Alteration settings

Argillic alteration of pyroclastic rocks on the whole of the islands' complex is widespread and seems mainly to be related to the tectonism that affected the whole of the area (tectonic control) and only for a lesser extent to the permeability of the volcanic/pyroclastic units (stratigraphic control). It is less widespread within the outcropping dacitic-andesitic sub-volcanic bodies and flow dome complexes, and it is relatively uncommon in the last volcanic products of acid dominantly composition (rhyolitic-rhyodacitic flows and domes). Silicification is regionally more restricted and generally follows specific tectonic trends.

2.5. Geological setting of the area under investigation

The volcanic successions showed in the Western part of Milos island and particularly in the investigated area (fig. 12), it is considered to be related to a feeding system located relatively deep in the crust (Fytikas et al. 1986) which sent, as a diachronous pulses, small masses of magma at shallow levels forming high level intrusions and intrusive dome/flow-dome complexes of andesitic-dacitic-rhyodacitic-rhyolitic composition and consanguineous pyroclastic products (pyroclastic flows, pyroclastic fall deposits).

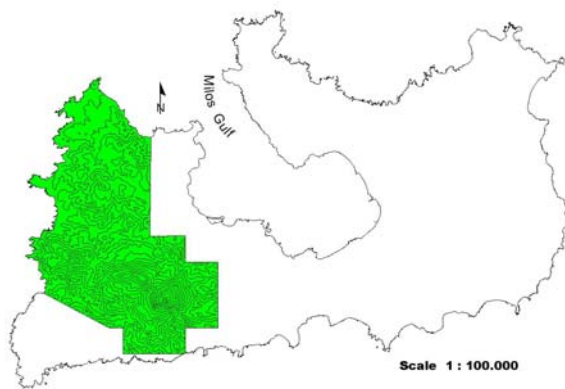


Fig.12 : The investigated area at western Milos.

The following formations are considered to constitute the geological puzzle of the investigated area at western Milos. The area under consideration has been mapped at a 1 : 5000 scale (fig. 13). There are similarities as well as differences with respect to the stratigraphy presented by the official 1:25.000 scale, geological map of the Greek geological survey (I.G.M.E), as there are with the stratigraphy presented by Stewart and McPhie (2005). There are also differences in the way that the stratigraphy is interpreted, in the present work, with respect to the above two detailed works on Milos geology / volcanology.

2.5.1. Metamorphic basement

Only limited outcrops of metamorphic rocks occur at the S and SE part of the investigated area (mainly around Profitis Ilias area). They consist of quartz-muscovite-chlorite and subordinately chlorite-amphibole schists and metamorphic quartz vein pieces.

2.5.2. Neogene sedimentary sequence

Limestones with minor interbeds of conglomerate, sandstone, siltstone outcrop at the S, SE and SW parts of the investigated area (mainly around Profitis Ilias area).

2.5.3. Volcanic sequence

Calc-alkaline volcanic activity in W. Milos spans a period from Middle-Upper Pliocene (~3.5 Ma-Fytikas et al.1986) to the present and it is originated from several centers which gave both shallow intrusive to effusive and explosive products (present work, Fytikas et al. 1986, Stewart and McPhie 2005).

In subaqueous settings magma may be extruded as lava flows and domes, or else form sills, dykes and intrusive to partly extrusive cryptodomes (McPhie et al.1993). In such an environment, initial vapour dominated conditions gave origin to explosive eruptions which generated a variety of pyroclastic products.

The diverse genetic processes involved in the formation of the different volcanic products, in subaqueous settings at western Milos, are reflected in the displayed textures.

Stratified fine ash, pumiceous lapilli tuffs and pyroclastic flow deposits, are indicative of the pyroclastic eruptions, and reflect, the first (fine ash+lapilli tuffs) an efficient sorting through a water settling of the pyroclasts according to the density, and the second (pyrocla-

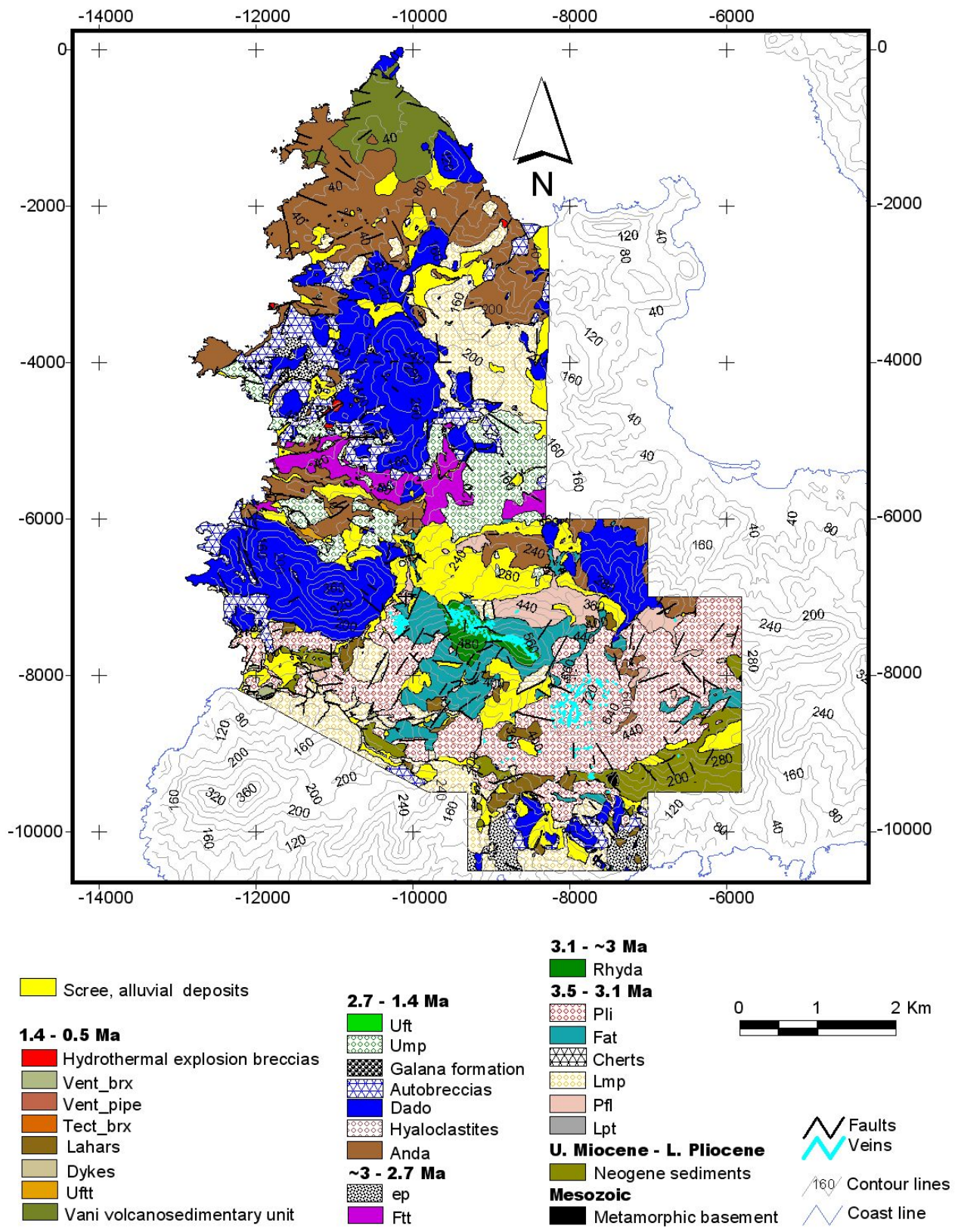


Fig. 13 : Geology map of the investigated area.

stic flows) a dynamic deposition from the active flow.

The products of the effusive activity can be classified into two main categories, the coherent and the volcanoclastic (McPhie et al. 1993). The term coherent is rather genetic, and refers to primary intrusions and lavas and gives information on the emplacement processes. The term volcanoclastic is descriptive, and refers to the presence of separate particles or fragments which generally have different shapes, types and sizes. They, respect to their genesis, take the name of in situ hyaloclastites, in the case that they remain where have been originated (primary), either can be subsequently subjected to erosion, transport, deposition, and re-deposition, and thus take the name of resedimented hyaloclastites (McPhie et al. 1993). In this last case, the redepositional process can involve only volcanic fragments or can be referred to a mixing of volcanic and sedimentary particles / fragments, and then take the name of peperite.

In both these last cases, the products are referred to as secondary volcanoclastic, or volcanogenic sedimentary (McPhie et al. 1993).

Although rapid lateral and vertical variations in rock types and textures occur at various scales throughout the investigated area, the description of the rock units below is considered to provide a representative guide to the volcanic stratigraphy encountered, and interpreted. Reconstruction of the volcanic successions was based on detailed observations on traverses along creeks and tracks with continuous outcrop exposures, as well as by detailed logging on several drilling cores belonging to chronologically different drilling campaigns that took place in the area. In both cases, textural examination of polished slabs and thin sections complemented the study. Original primary, or anyway slightly to moderately altered volcanic textures, (mainly from the domes/lavas/dykes formations), were relatively well preserved in areas where the hydrothermal alteration it was minimal, and away from lineaments / faults that disrupted severally the stratigraphic succession and altered or masked variously it.

The volcanic successions examined are considered to be directly related to the volcanic activity or contain elements derived from it.

In the fig. 14, the various locations mentioned in the following description of the different volcanic formations, are reported on a 1: 50000 topography map.

The development of a series of submarine felsic volcanic edifices at western Milos (present work, Fytikas et al. 1986, Stewart and McPhie 2005) is characterized by two main phases, principally submarine, which can be described as two main components process, the first related to an initial explosive stage and the second to an effusive one. In between these two main stages, and due to tectonic processes, an intermediate stage characterized by the deposition of volcanosedimentary products, has taken place.

2.5.3.1. Volcanosedimentary products in submarine environment (Lower-Middle Pliocene/ ~3.5 Ma)

2.5.3.1.1. Interbedded shallow marine tuffs/tuffites (Ismtt)

Shallow marine pumiceous tuffs/tuffites of acid composition are found to be interbedded with the upper Miocene lower Pliocene sediments (mainly limestones, mudstones unconformably lying on the already uprised metamorphic basement). Their presence indicates that the sedimentary deposition continued, at least locally, following the onset of volcanism. In that sense they can be characterized as re-sedimented syn-eruptive volcanoclastic

deposits. Most probably the emission center was some where at the SW part of W. Milos, most probably on Katsibardos / Topakas dome area.



Fig. 14: Western Milos' location names map

This unit is typified at the southern part of Profitis Ilias area at contact with limestones/marly limestones, and has also been intersected, during the Midas S.A. 1999-2000 drilling campaign.

This magmatic-sedimentary activity corresponds to the phase I of the generalized description of volcanism on Milos island.

2.5.3.2. Acid pyroclastic products in submarine and partially subaerial environment - explosive activity (Lower/Middle-Upper Pliocene/~3.5-3.1 Ma)

This complex of pyroclastic products is relatively consistent throughout the investigated area at western Milos. K-Ar dating, placed this sequence in the range of 3.5 to 3.1 Ma (Fytikas et al., 1986). This explosive magmatic activity corresponds to the phase I of the generalized description of volcanism on Milos island, the basal pyroclastic series of Fytikas et al. 1986, and to the felsic cryptodome-pumice cone volcanoes of Stewart and McPhie 2005.

The following described pyroclastic formations, are considered partly to be the products of settlement, through the water column (present work, Stewart and McPhie 2005), which

resulted in an efficient sorting according to the density (hydraulic sorting), during and after eruption and transport. In such a way stratification developed in response to rapidly repeated explosions and consequent settlement after the created water turbulences. For the remaining part of the pyroclastic formations, it is considered that, they are related to the deposition generated by active pyroclastic flows (ignimbrites).

Debris-flow deposits, generally in marginal positions with respect to the main centers, were produced by downslope slumping and mass-flow resedimentation events during, but mainly after the pyroclastic eruptions, and most probably are related to the phreatomagmatic eruptions.

As a whole the interpreted stratigraphy exhibits subaqueous textural features consistent with a combination of a subaqueous stratified pyroclastic fall deposit (the upper stratigraphic part : Lmp-Fat units), on a pyroclastic (volcaniclastic) flow deposit (the lower stratigraphic part : Lpt-Pfl units)-(fig.15).

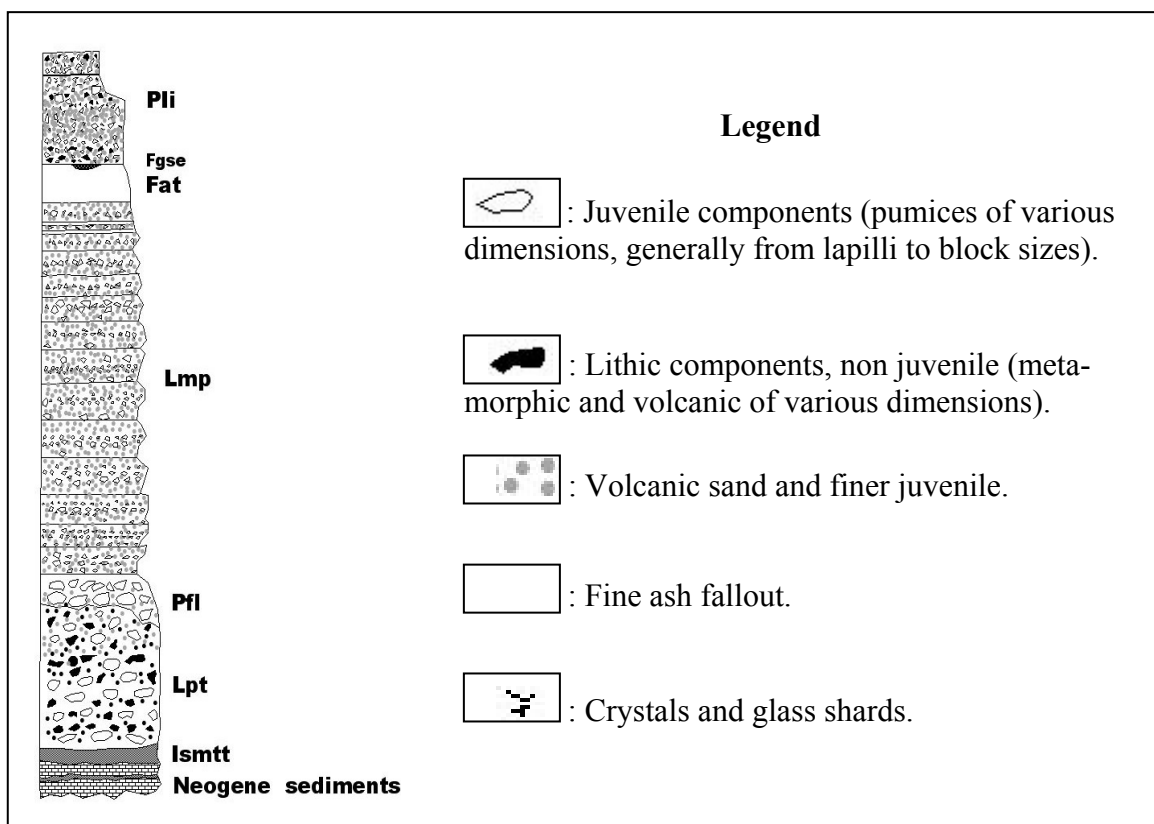


Fig. 15 : Stratigraphic column representing the explosive pyroclastic activity from 3.5-3.1 Ma.

2.5.3.2.1. Lithic / Pumice tuff subunit (Lpt)

It is made up by a medium sized submarine lithic fraction, subangular to subrounded generally unsorted either presenting a smoothly normal grading, and a coarse sized pumice also submarine fraction, generally clay altered and locally welded (fig.16a).The lithic clast fraction is dominated by subvolcanic (mainly dacitic porphyry) clasts, minor sedimentary (dark) pyritic ones, and subordinately by metamorphic fragments. Locally the metamorphic fragment's fraction is dominant. The lithic clasts are considered to be vent/conduit derived accessory pyroclasts generated by the explosive disintegration/clearing of it.The pumice

fraction represents the explosive component of the eruption. The Lpt subunit represents the basal layer of a pyroclastic flow deposit, depleted in coarse clasts, and showing better sorted and reversely graded. The boundary with the overlying (upper) part of the flow unit can be characterized from transitional to sharp.

The max thickness is considered to be in the order of 50 m.

It is typified at the northern slope of Koumaria and in Fragovigla areas, and it is interbedded with several pumice flow subunits (see next).

2.5.3.2.2. Pumice flow subunit (Pfl)

The distinctive characteristic of the unit is its well defined coarse pumice clast concentration at the top (fragments up to 0.50 m length and prismatic to ovoid in shape),(fig.16b). As a whole it is characterized by medium to coarse pumice fragments, unlayered and cemented by a glassy (shard rich) matrix. It is presented moderately to strongly argillized and it has a creamish, greyish to locally reddish colour. It is considered that several pumice flow units, each one containing the Lpt+Pfl subunits (i.e., a stratified pyroclastic flow deposit), outcrop in the area between Mavrovouni and eastern Profitis Ilias, reflecting the different dynamic processes operated during flow emplacement.

It is typified at Profitis Ilias, Koumaria areas. The max thickness is considered to be in the order of 35 m.

2.5.3.2.3. Lower pumiceous lapilli tuff (Lmp)

A pumiceous lapilli tuff, generally white in colour, locally dark grey. The pumice fragments are included in a variety of sand sized to fine ash/glassy matrix. The unit lacks of compaction and welding. At the interface with the underlain pumice flow subunit it is characterized by medium to coarse sized pumice fragments and it is presented lithic rich (fine grained lava / subvolcanic fragments of similar composition and subordinately sedimentary ones), while at the interface with the overlain fine ash unit is presented considerably finer.

Crystal rich well compacted tuffs are also presented locally, in between the different pumiceous lapilli tuff subunits.

The unit is typified at the Chondro Vouno saddle. Its max thickness is considered to be in the order of 60 m.

2.5.3.2.4. Fine ash tuff (Fat)

It is a fine grained, thinly laminated to massive ash tuff unit white in colour and strongly clay altered. In the area between Koumaria and the Chondro Vouno saddle several outcrops of the unit occur. It seems to have a very variable thickness (from cm to tens of meters) around Chondro Vouno-Koumaria-Skiadi-Peristeria-Pyrgiali areas. In more it seems that there is a close relationship with the underlying lapilli sized pumice tuff unit where locally it is interlayered and generally defines an upward somehow finishing sequence. Its max thickness is considered to be in the order of 80 m.

The unit is typified at Koumaria.

2.5.3.2.5. Fine grained sediments (Fgse)

Fine grained sediments(cherts), strongly silicified and grey-black in color occur at several places at western Milos in the near of vent areas(e.g. Mavrovouni, Koumaria, Favas).Their occurrence has been linked to hydrothermal (feeder) conduits, which produced an exhalative activity affecting shallow water mud pools. They are located at the top of the fine ash tuff (Fat) unit.

The unit is typified at Koumaria.

2.5.3.2.6. Profitis Ilias ignimbrite (PII)

A submarine to subaerial (at the upper part, above ~ 650m), shallowly dipping, medium to coarse pyroclastic flow unit (ignimbrite), poorly to locally moderately welded, consisting mainly of pumiceous(75%), locally flattened clasts, and subordinately by sub-angular to sub-rounded fine tuff fragments. Locally, at the upper parts, it is presented very rich in basement shists (chloritic schists-20%), while several thin horizons of crystal tuffs and/or of fine ash are also displayed (fig. 16c). At the lower parts of the sequence an enrichment in porphyritic fragments (dacite-5%) has been observed to occur (e.g. Mavrovouni-Tsouvala area). The unit is beige to greyish to brownish in colour and it is widespread, and generally cap the fine ash tuff unit (e.g. Koumaria area), either it is lying directly on the Neogene sedimentary sequence (e.g. Tsouvala area). In the area between Profitis Ilias and Koumaria the ignimbrite unit has undergone much disruption and because of that it is only locally preserved with exposures documented at NNW of Chondro Vouno.

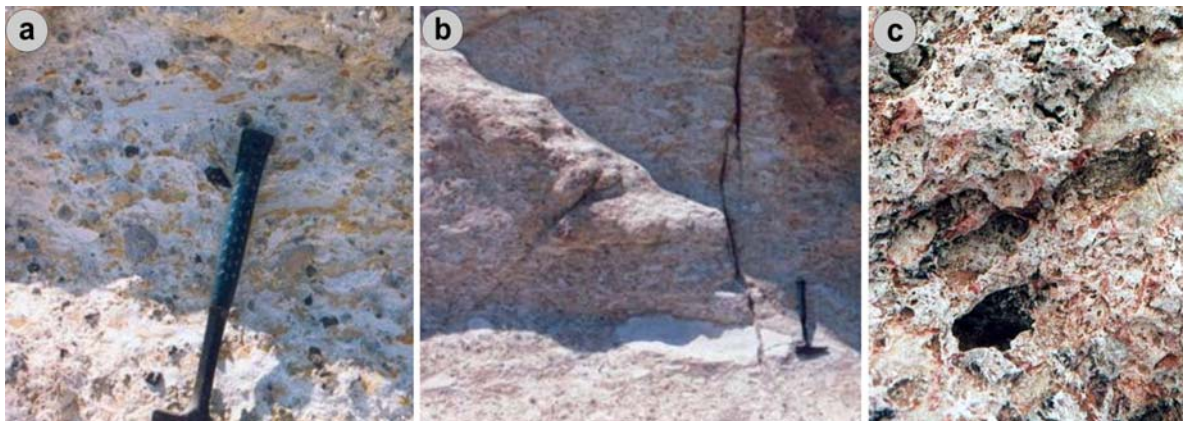


Fig.16 : (a) The lithic/pumice tuff subunit (Lpt).Are very well visible all the constituent components of it, as described in the text; (b) The pumice flow subunit (Pfl). Are well visible big pumiceous fragments (~50 cm); (c) Silicified Profitis Ilias ignimbrite at the top quasi of Profitis Ilias mountain.

At places (e.g Ag. Ioannis, Profitis ilias) the ignimbrites are showed to be denser toward their source, where welding was possible due to higher temperatures, despite they generally present reduced thicknesses at those places.

Fossiliferous layers indicative of shallow waters (-10 up to -50m), mostly including molluscs and echinoids, of Middle-Upper Pliocene age (Fytikas,1977) are relatively abundant in the lowermost part of the exposed sequence.

As a whole it can be said that the lower part of the formation is undifferentiated being pumice-rich to lithic rich.

It is typified at Profitis Ilias mountain where preserves its max thickness of 275 m on the western flank of it. Its thickness is considered to vary between the various places from 1 to 120 m.

Most probably this ignimbrite unit corresponds to a rebuilding of the Profitis Ilias volcanic edifice, related to a new magma pulse/high level emplacement of an intrusive/subvolcanic body.

2.5.3.3. Acid intrusive products in submarine environment-effusive activity (Upper Pliocene/ ~3 Ma)

2.5.3.3.1. High level rhyolite intrusive (Rhyda)

The genesis of the whole pile of the previously mentioned pyroclastic series, was due to the emplacement and extrusion of several felsic magmas in a subaqueous setting, that through magmatic-volatile driven eruptions, resulted in the creation of several volcanic submarine felsic cryptodome - pumice cone volcanoes (Stewart and McPhie 2005). Indeed in subaqueous settings, as those on Milos archipelago, magmas can be extruded as lava flows and domes, either as sills, dykes and intrusive to partly extrusive cryptodomes (McPhie et al. 1993). The main characteristic of these volcanic centres, except the thick intervals of the submarine felsic pumice breccia (Stewart and McPhie 2005), is that this pyroclastic pile is intruded by compositionally similar rhyolitic and dacitic cryptodomes and sills (Stewart and McPhie 2005).

On that respect and logic, it is considered, that one time degassed, the felsic cryptodome (Rhyda), ascended and intruded the above described pyroclastic pile, as well as partially covered it. It is considered that this happened immediately or quasi, after the cease of the explosive activity, along a principal NNW - SSE direction, and before the emplacement of the andesitic-dacitic-rhyodacitic (Anda and Dado) subvolcanic dome/flow dome complexes of the next volcanic effusive phase. Based on that, as well as on the reported geochronological data (Fytikas et al. 1986, Stewart and McPhie 2005) it is suggested that the intrusion/emplacement of the rhyolite body has occurred during the time period between 3.1 and 2.7 M.a., and most probably around 3 M.a. (fig.10, fig.13, fig. 17b).

It is also considered, and it is suggested by Stewart and McPhie 2005, the (Rhyda) intrusion had the form of a series of small volume cryptodomes and sills. Field and drill hole data suggest that the rhyolite (Rhyda) intruded through the whole thickness of the pyroclastic pile, after passing through the underlying limestones and part of the metamorphic basement, until it reached the Profitis Ilias ignimbrite unit, where it has been expanded laterally (e.g. Chondro Vouno), at the interface between the fine ash tuff formation (Fat) and the Profitis Ilias ignimbrite (PIi),(see also stratigraphy column fig.17b). That is, it presented a strong tendency to produce flat lying to shallow dipping lobes extending longitudinally from the main intrusive feeder, thus following the bedding of the surrounding tuff units. This last suggestion it could be also compatible to what it has been said for the ignimbrite of Profitis Ilias, previously. Fluidal dykes crossing at various areas the Profitis Ilias ignimbrite formation (PIi), have been encountered at several areas on both north (fig.18a) and southern flanks of the mountain (fig.18b).

It corresponds to the submarine felsic cryptodome, of the felsic cryptodome-pumice cone volcanoes of Stewart and McPhie 2005, and to the basal pyroclastic series of Fytikas et al. 1986.

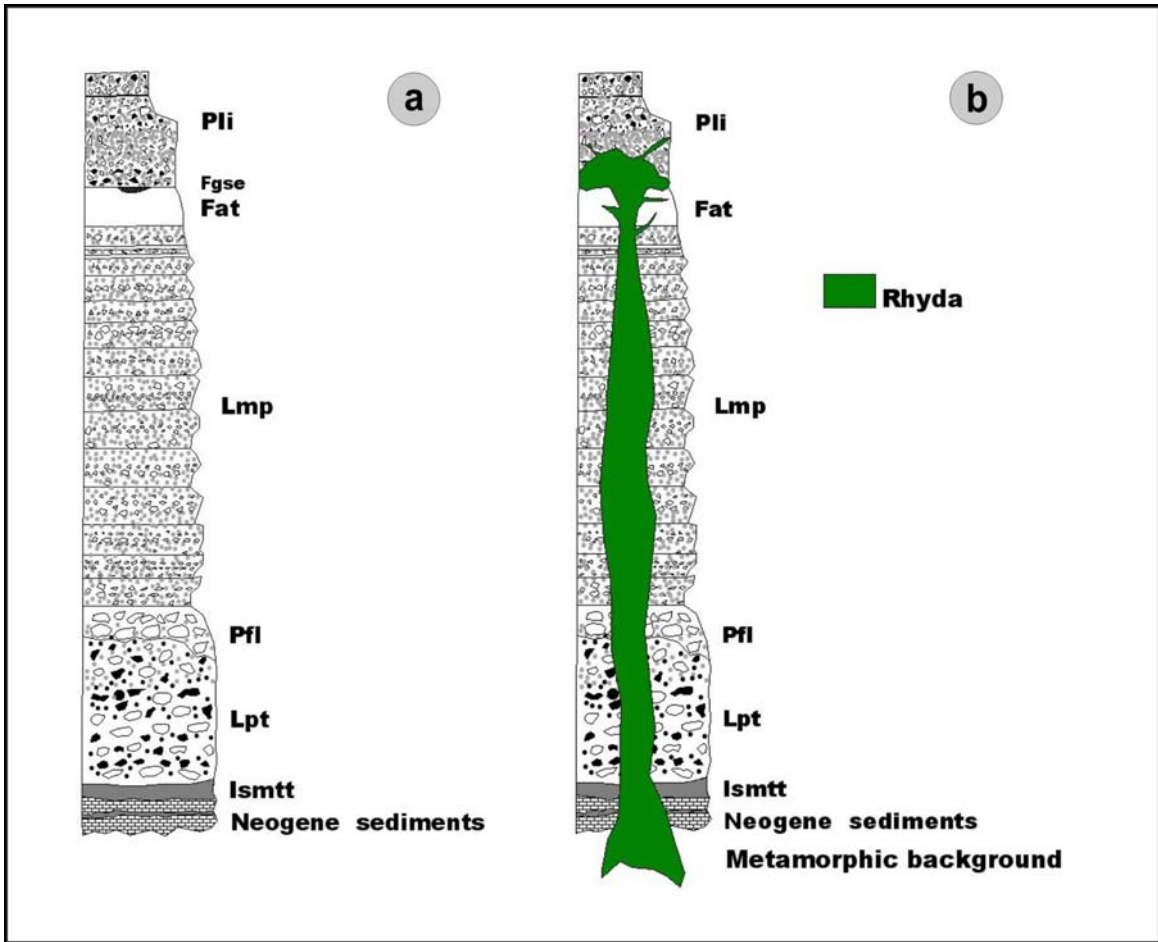


Fig. 17 : Stratigraphic columns showing the relationships between the various units (a), and (b) after the previously formed pyroclastic pile has been intruded by the shallow (high level) rhyolitic intrusive body (Rhyda) at about 3 Ma.



Fig. 18 : Fluidal dykes of acid composition belonging to the Ryda unit, encountered at the northern (a) and southern (b) flanks of Profitis Ilias mountain, running in between sheeted veins.

2.5.3.4. Volcanosedimentary products in submarine environment (Upper Pliocene/~3-2.7 Ma)

Between the end of the previous explosive phase and the intrusive (cryptodome) one, (~3 M.a.), and the subsequent effusive phase, of intermediate to acid subvolcanic products in submarine to subaerial environment at (2.7 M.a), and due to tectonic processes and reassessments, the opening of a quasi E-W directed graben structure has been established and constituted the “recipient” of the surrounding area, which in the mean time was also subjected to relative uplift movements. This sedimentation/activity period corresponds to an intermediate phase(subphase), that has been considered and interpreted during this work, as one that took place between the phase I of the generalized description of volcanism on Milos island, (the basal pyroclastic series of Fytikas et al. 1986 / the felsic cryptodome-pumice cone volcanoes of Stewart and McPhie 2005), and the next phase II (complex of Lava Flows and Domes of Fytikas et al. 1986 / and submarine effusion and intrusion of dacitic/andesitic domes/lavas of Stewart and McPhie 2005).

It can be described as two components unit, the first nearly for the whole of its thickness more or less homogeneous-sand to silt sized, and fossiliferous, and the second more variously clastic and reworked (resedimented and affected by hydrothermal processes). Their interpreted stratigraphy it is shown at (fig. 21 a), together with that related to effusive activity.

2.5.3.4.1. Fossiliferous tuffs and tuffites (Ftt)

Shallow marine deposited tuffaceous sandstones and siltstones with abundant fossils. The unit is developed more or less across the center of western Milos and it is characterized by the presence of many macro- and micro-fossils (Lamellibranches, echinoids, brachiopods) indicative of a shallow sea (Fytikas 1977),(fig. 19 a, b).

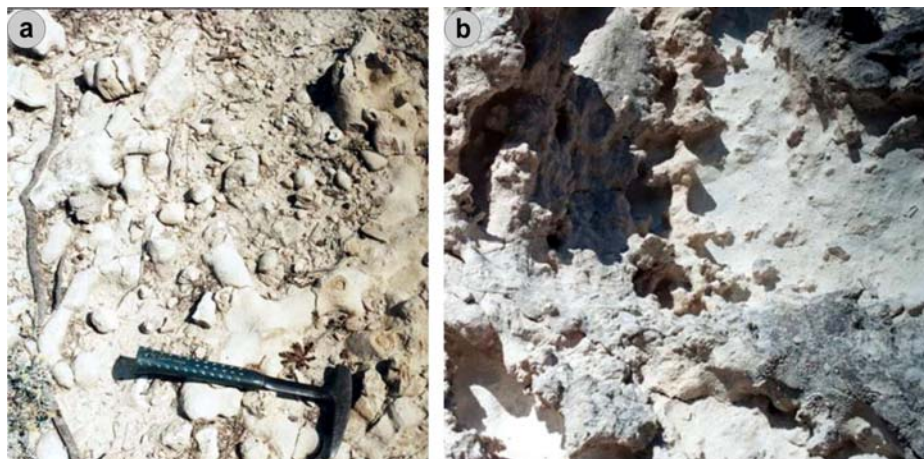


Fig. 19 : (a),(b) Fossiliferous tuffites at Triades area. At the center-right part of the picture (b) partially fragmented parts of echinoids are visible.

Locally (e.g., Triades), interbedded lavas and volcanic conglomerates (Anda, see next) indicate that their deposition started little bit before the emplacement of the Anda unit (domes and flow-domes complexes) and probably continued along with, and at any case the whole process has taken place at a shallow sea water environment, and while they were

still unconsolidated. Without doubt they are older than the development of the Dado (see next) dacite volcanism.

Thin horizons of cinerites, tuff sand, tuffaceous siltstones have been also encountered. At the upper parts they show alternations/interbedding with the ep unit (reworked volcanosedimentary unit, see next), and a lateral facies relation with the brecciated (hyaloclastitic) portions of the dacitic-rhyodacitic domes (Anda). They are white in colour and locally yellowish.

The lack of the tuffaceous sediments at Agathia to the north, and at Koumaria to the south, demonstrates very clearly that these areas were topographically high terrains, at that period, thus lying above sea level in a subaerial environment.

The average thickness of the unit is considered to be between 5 and 10 m.

This unit it is typified at Triades – Ntasifnos – Ag. Stefanos areas.

2.5.3.4.2. Reworked volcanosedimentary unit (ep)

This unit is strongly related and correlated to the emplacement of the subvolcanic bodies (Anda) and of the various kinds of the breccias (hyaloclastites) affected or involved by/in hydrothermal processes, at the northern sector, and thus, it is considered, it constitutes the marker horizon of these lasts. In this sense it is a unit sedimented contemporaneously with the emplacement of the various acid shallowly emplaced domes (Anda) and thus formed and reworked contemporaneously with them as a mixture of previously existing sediments (Ftt) and newly generated (hyaloclastites of various dimensions) ones. So in this sense they can be considered as peperites (following the terminology of McPhie et al. 1993).

They are presented as reworked volcanosedimentary horizons, moderately stratified and containing, for a part, small fragments of lithics (acid subvolcanics-Anda), pumice tuffs, and for the rest crystal fragments (mainly quartz and subordinately feldspars), in a coarse sandy and locally sandy + silty matrix (fig. 20a,b,c).

Locally, (e.g., Pyrgaki area) it is presented moderately to strongly silicified, made up nearly by pure quartz crystal fragments (crystal-rich sandstones).

The volcanoclastic sandstones, as a whole, are yellowish to yellow-reddish in colour and sandy in size, and locally are presented brecciated.

The average thickness of this unit is considered to be between 5 and 10 m.

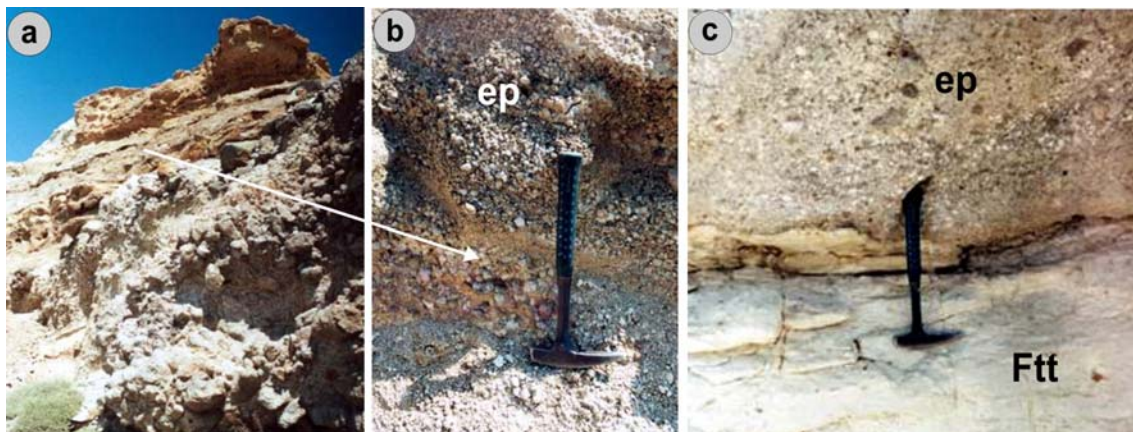


Fig. 20 : Reworked volcanosedimentary horizon (ep) at contact (a) with in situ hyaloclastite from a subvolcanic dacitic body (Anda) and (c) with the fossiliferous tuff/tuffite unit (Ftt), at Triades area. In (b) a zooming in the locus of the photo (a) where the ep unit is located.

At Triades the presence of graded sandstone beds intercalated with the talus breccia indicates that the breccias were deposited in shallow marine environments adjacent to emergent domes (partly subaerial environment).

2.5.3.5. Intermediate to acid subvolcanic products in submarine to subaerial environment -effusive activity (Upper Pliocene-Lower Pleistocene / 2.7 – 1.4 Ma)

Widespread effusive, intermediate to acid volcanism, on western Milos will succeed the previous dominantly explosive and acid one, under form of numerous dacitic, rhyodacitic, rhyolitic and andesitic domes and flow dome complexes. This new volcanic phase will intrude and disrupt the still wet and unconsolidated volcanosedimentary unit, (constituting the sea floor), formed in the mean time between the current and the initial one, and will be accommodated on it. Quenched (hyaloclastitic) margins partly pumiceous and partly obsidian, talus breccias will be the “trade marks” of this subvolcanic emplacement into sediments, in a submarine to partially subaerial environment.

2.5.3.5.1. Andesitic, dacitic, rhyodacitic, rhyolitic domes and lesser lavas, dykes emplaced along NE-SW trends (Anda)

Generally andesitic to dacitic in composition and locally only of rhyodacitic to rhyolitic one, with a compositional trend (andesitic to dacitic-rhyolitic) going from SW to NE at the southern part of W. Milos and from ENE to WSW at the central-northern part of it. Locally lavas, dyke and sill like features follow the orientation of the bedding in the surrounding tuff and tuffitic country rocks. They vary considerably in texture but seem that their characteristic “code” is the presence of amphibole (hornblende) and ilmenite. Another important characteristic is the presence of elongate voids (cavities), in quartz porphyry bodies, which have also an important hydrothermal/mineralization implication /significance.

They are typified at Triades-Pyrgaki-Galana and relatively at the area between Profitis Ilias and Mavrovouni.

Their interpreted stratigraphy, at three different places at western Milos, it is shown at fig.21a (for Triades-Galana-Ag. Stefanos-Ralaki areas), 21b (for Profitis Ilias-Chondro Vouno- Mavrovouni areas) and at 21c (for Koumaria- Ag. Panteleimon areas).

It is considered that the subvolcanic domes were partly exogenous, and that successive pulses of magma have created several, more or less coalescing domes, in a submarine environment. Some of them reached the sea surface and raised above sea level becoming subaerial and thus forming small volcanic islands.

As it is shown in fig.10,14, except for some locations of the area enclosed between Triades-Galana-Favas, where geochronological data (Fytikas et al. 1976,1986; Angelier et al. 1977; Cantagrel and Vilminot,1977; Bigazzi and Radi,1981; Stewart and McPhie 2005) show ages between 2.1 and 1.4 M.a., the age distribution of the rest of western Milos, concerning domes/flow dome complexes, is presented very uniform being at the south around 2.5 M.a., at the north around 2.4 M.a. and in the middle around 2 M.a.. Similar results, about consistency / location of dome emplacement, have been achieved considering the domes having a zonal distribution. In this case the outer zone has domes emplaced at ~2.4 M.a., the next (inner) zone at ~2 M.a. and the last one (more internal) contain domes showing the younger ages, between 1.7-1.4 M.a.(Favas, Galana areas). This fact shows, at least into the context of the geochronological knowledge so far, that at these

places the effusive activity persisted at least 1 million years after the emplacement of the first domes (which started at the southern part of western Milos).

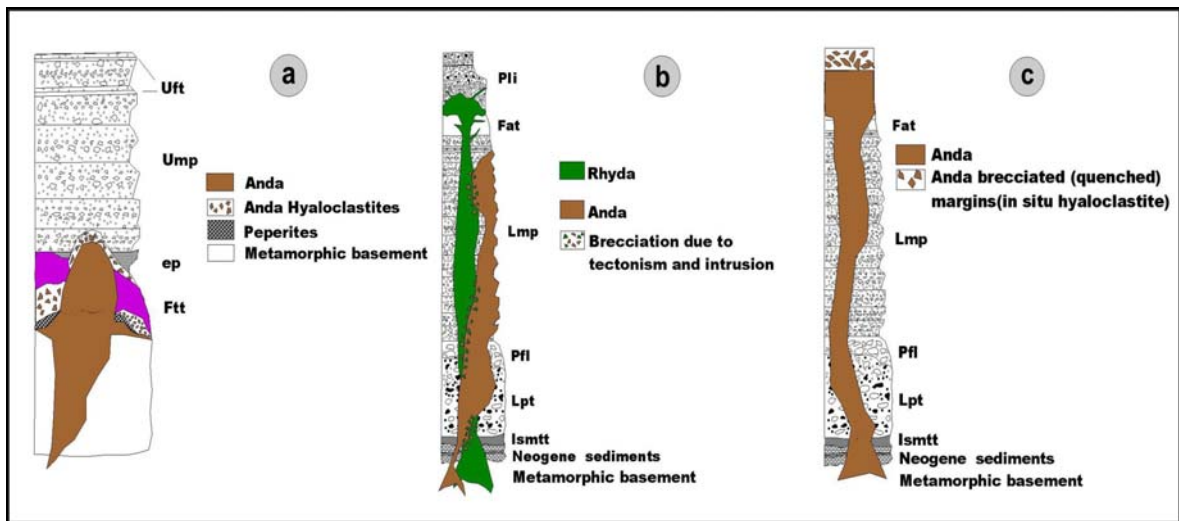


Fig. 21 : Stratigraphic column showing the shallow intrusive/partially extrusive Anda domes/lava domes at three different districts, (a) Triades-Galana-Ag. Stefanos-Ralaki, (b) Profitis Ilias-Chondro Vouno-Mavrovouni, and (c) Koumaria-Ag. Panteleimon, between 2.7-1.4 Ma.

A last consideration which has been developed and it is very important, is that related to the trend of emplacement of the domes. As field work has shown, some of the domes have been emplaced along NE-SW trends and others along NW-SE ones, in both cases following specific lineaments (see next about tectonics), related to the extensional tectonics that has characterized Milos during Pliocene-Pleistocene times.

This last consideration has important implications to the mineralization (see next, about tectonics, ore mineralogy, description of subareas), and for this reason it has been chosen as the base concept on which, this effusive volcanic phase, is described.

This dome/flow dome unit (Anda), together with the next described dacitic-rhyodacitic one (Dado), are considered to be shallow to very shallow entities, with respect to the earlier rhyolite intrusives(Rhyda), and most probably this is another distinctive characteristic regarded them and their relations to the alterations /mineralization.

The characteristic brecciation, as integral part of the Anda suite, which has been formed in a submarine environment, is essentially a monomictic andesitic or dacitic-rhyodacitic breccia (precisely a hyaloclastite, formed after quenched-margins fragmentation) around a crackled external surface,(generally showing jigsaw-fit texture), which constitutes the “membrane” to a massive core. Further away, and because of the fact that the subvolcanic bodies have been intrusive to the sedimentary terrain lying on the sea floor, clasts from different parts of the dacite or andesite bodies have been transported in shorter or longer distances and sedimented locally together with parts of the existing sediments. This sedimentation process formed mixed volcanic and sedimentary formations (volcanosedimentary formation), presenting bedding further away from the intrusion area, and peperites (mixing of coherent lava or magma with unconsolidated sediment-McPhie et al.1993) in the near of it. This configuration (concerning the emplacement of the domes), is recently described in very details by Stewart and McPhie 2005, as a facies association comprising three principal segments, (1) a central coherent core, (2) a monomictic breccia which can

be either clast supported and stratified or non stratified, and (3) a sediment-matrix breccia at the lateral-end part.

These above mentioned configurations and facies, are typified at Triades, Galana areas where several small coalescing dacitic domes intruded poorly consolidated fossiliferous tuffites and sandy-silty sediments (sandstones, siltstones) in a shallow marine environment and then accommodated by them. The margin of the dome were rapidly cooled and thus quenched margins (hyaloclastites) were formed, due to contact with the sediment/sea water.

All these brecciated formations, (brecciated andesites, dacites, rhyodacites, rhyolites) which have, as already mentioned, important implications to the mineralization are described in the next paragraph as they have been seen in the field, i.e., as segments of a physically disintegrated subvolcanic body, which has been truncated and displaced by a diachronous tectonic activity along different directions which, in the most of the cases, dismembered further them. This consideration together with the fact that acid lava dome eruptions, at shallow water vents, typically involve complex combinations of phreato-magmatic, explosive magmatic and effusive activity (McPhie et al. 1993), further complicated their shapes and aspects/attitudes while contemporaneously opened new spaces for the incoming hydrothermal solutions.

2.5.3.5.2. Hyaloclastitic breccias

As it has been mentioned previously, in subaqueous settings magma may be extruded as lava flows and domes. In a broader sense subaqueous eruption settings are considered special, because of the importance of quench fragmentation on contact with water or wet sediments (McPhie et al. 1993). In fig. 22 extrusive domes (flow domes) are displayed and show the distribution of the massive and/or flow banded (coherent) core and of the laterally, variously fragmented (in situ and deposited) parts.

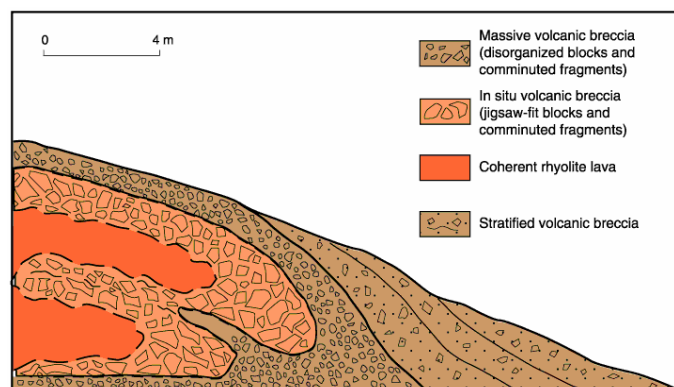


Fig. 22 : The coherent and the fragmented (hyaloclastitic) components of extrusive domes. From McPhie et al. 1993.

In this sense, definitely, quenched (hyaloclastitic) margins (fig. 23a,b,c) partly pumiceous (fig. 23e) and partly obsidian (fig. 23f) constitute the essential elements of what is described here as hyaloclastitic breccias.

As a matter of fact several breccias outcropping especially at the northern sector, are not breccia pipes (i.e., breccias directed related to feeder structures), but rather the brecciated segments (hyaloclastic parts) of intrusive domes/flow-dome complexes, in a submarine

environment. In such a way, the breccias (e.g., Triades-Galana), can be classified as irregular bodies outcropping in a dome field setting, where the most of them are the products

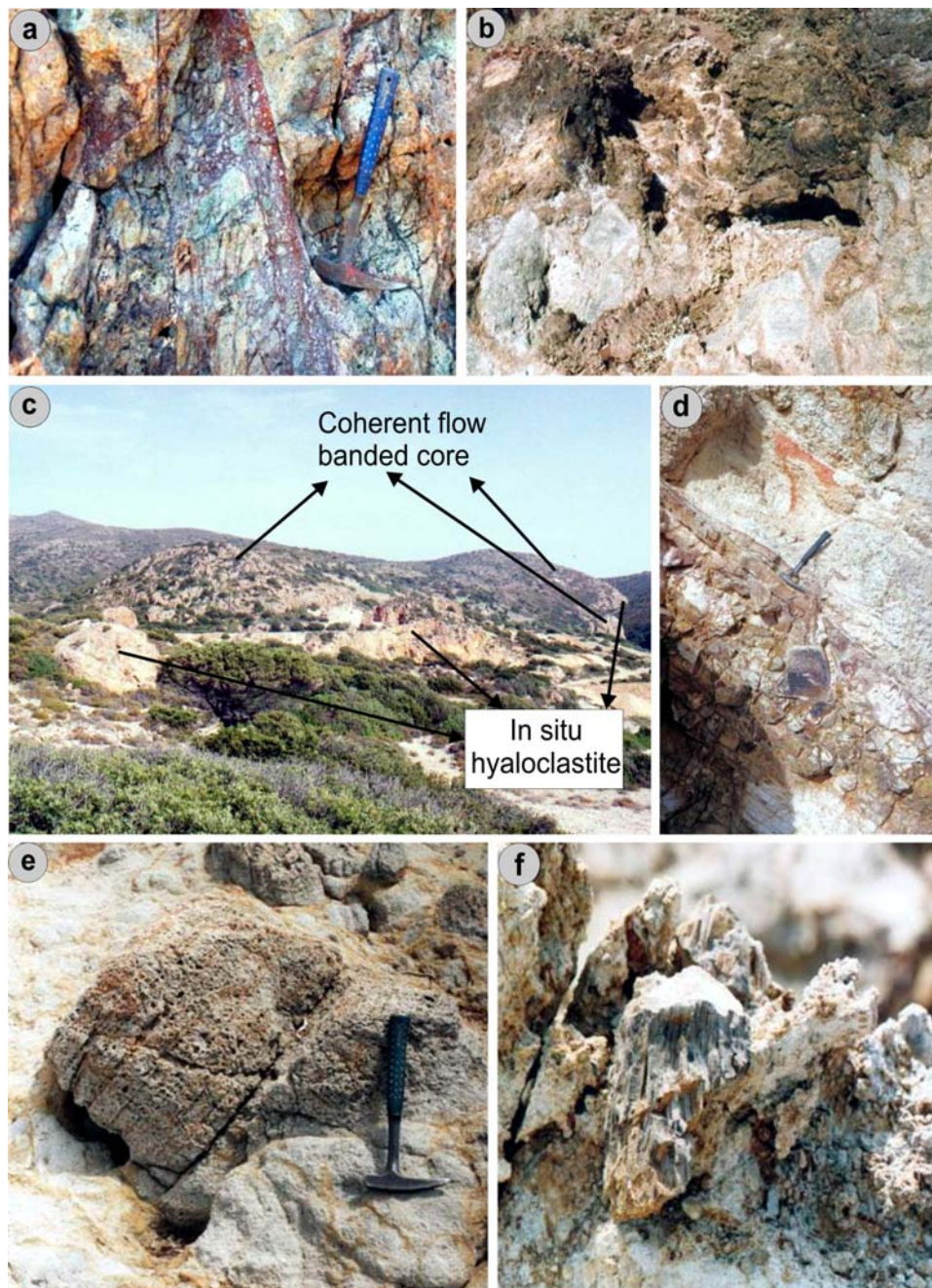


Fig. 23 : In situ hyaloclastites(quenched margins), from various areas of W. Milos: (a) Plakota; (b) Vani; (c) Triades-Ag. Nikolaos domes emplaced along NE-SW to ENE-WSW directions; (d) Triades; (e) Triades-partly pumiceous (f) Vromolimni- partly obsidian.

of quenching (quenched margins), of the (Anda) domes. They have more or less a similar age to the host submarine fossiliferous tuff / tuffites (Ftt), and to the reworked vulcanosedimentary unit (ep), which they intruded (fig. 24), and are slightly older than the less altered to unaltered, dacitic-rhyodacitic dome sequence (Dado) and their autobreccias.



Fig. 24 : Dacitic-rhyodacitic (Anda) dome intrusive after fossiliferous tuffites and sandstones at Ntasifnos-Ag. Athanasios area.

In the area of Triades-Galana-Vromolimni the matrix of the resedimented hyaloclastites present the whole range of deposits, from resedimented fine hyaloclastites (<1/16 mm) to resedimented hyaloclastite sandstones (1/16-2mm), to resedimented granular hyaloclastites (2-4 mm), to resedimented hyaloclastite breccias (4-64 mm), to resedimented coarse hyaloclastite breccias (>64 mm).

Mass-flow redeposition of in situ hyaloclastite, in response to over-steepening of flow or dome surfaces, generated stratified resedimented hyaloclastites at the flow margins and along the tops and flanks of the domes. In many cases, parts of lava flows and domes in direct contact with submarine sediments mixed with them, producing texturally complex lava-sediment breccias (peperites), which is common at lower and side contacts (i.e., along the intrusive margins) of domes, and at all contacts of locally burrowing parts of lava flows (McPhie et al. 1993). Finally, in addition to massive lava flows and domes, subaqueous silicic lavas form lobes, i.e., pillow-like bodies associated with hyaloclastites (McPhie et al. 1993). This last is an important figure, met on both SW and NE parts of western Milos, and it is considered to be related to important vent and mineralized areas (e.g. Vani area).

For all the above mentioned reasons, it is considered that the contact relationships and the distribution of the massive (coherent) dome/lava with respect to in situ fragmented part of it (hyaloclastites) and/or resedimented hyaloclastites, and eventually to the “basal” peperites, are of crucial importance concerning not only the mode of their emplacement but also concerning mineralization. Indeed because of the fact that, around vent areas significant amounts of the volcanic products are reworked, eroded and resedimented laterally, the final record of dome related, shallow water volcanism, is expected to include a wide range of volcanic and volcanosedimentary products.

In Triades-Pyrgaki area a series of “mixed” (as mentioned above) breccias (fig. 23c), whose dimensions vary from 5x5 m up to 100x50 m, and show a clear spatial relation to the volcanoclastic sandstone subunit of the reworked volcanosedimentary unit (ep), are the products of what has taken place in a slightly later stage with respect to the time of emplacement of the Anda domes. They have been affected, in various degrees, by hydrothermal solutions which deposited in the open spaces mostly silica- (crystalline and amorphous) and barite. In such a fashion, part of the breccias are presented strongly

silicified, baritized and locally also argillized, and part are truncated by quartz-chalcedony-baryte veins and minor base metal sulphide veins (see next-ore mineralogy chapter).

2.5.3.5.3. Dacitic-rhyodacitic domes along NW - SE trends (Dado)

Dacitic, rhyodacitic generally massive feldspar-biotite-amphibolite porphyritic domes/flow dome complexes from vents situated generally along NW-SE lineaments, (e.g., Mavrovouni -Ammoudaraki, Rivari-Vani). Several dykes related to feeder zones also belong to the Dado group. Generally they are flow banded around a massive/coherent core, while externally are “collared” by an autobrecciated carapace (autobreccia) consisting of coarse angular clasts, which is considered to be the main characteristic feature of the Dado domes, and it is related to their partial emplacement into a subaerial environment. The mafic inclusions are another common feature of these subvolcanic bodies.

Locally, they present lateral minor jig-saw fit breccias and Mn-hematite alterations. Their autobrecciated carapace, cover older pyroclastic formations, such as the lower pumiceous tuff unit (Lmp) at the southern sector and the slightly older andesite/dacite unit (Anda) and other pyroclastic formations (Lmp, Ump) at the northern sector.

Their interpreted stratigraphy at western Milos, it is shown at fig. 25

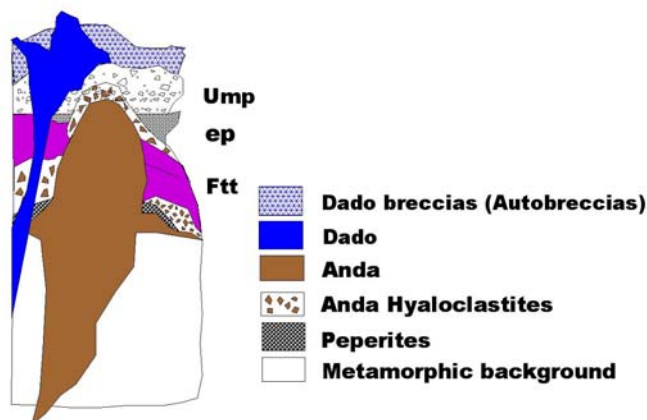


Fig. 25 : Stratigraphic column representing the shallow intrusive/partially extrusive Dado domes / lava-domes.

2.5.3.5.4. Autobreccias

They are related to the Dado domes emplacement, as it has been explained previously.

2.5.3.6. The explosive unit related to the emplacement of the andesitic-dacitic-rhyodacitic-rhyolitic effusive sequence (Anda) (Upper Pliocene-Lower Pleistocene / 2.7 – 1.4 Ma)

The explosive activity related to the emplacement of the andesite-dacite-rhyodacite-rhyolite effusive sequence (Anda) is represented by a series of minor and major pyroclastic activity products (subaqueous rhyolitic dome-top tuff succession of Cas et al. 1990).

2.5.3.6.1. Galana formation (Galf)

It is a pyroclastic formation with a dominant lithic component (exclusively metamorphic ones from the basement), and subordinately pumiceous ones. The explosive event that generated it cleared up the conduit which was located into the metamorphic basement, laying shallowly underneath Galana, and above the intruded in it subvolcanic body.

2.5.3.6.2. The upper lithic/pumice tuff unit (Ump)

The pyroclastic sequence consist of lithic-rich fragments (acid block sized volcanics), at its base, overlying coherent dacites-rhyodacites and their associated marginal breccias (hyaloclastites), to mixed volcanic and pumiceous ones, at intermediate positions, to lapilli sized pumice tuffs at the main body, in a fine to coarse ash matrix into which varying amounts of crystal fragments (quartz, feldspars and biotite) are also included.

Along the Triades-Ammoudaraki beach area, it is mainly composed of perlitic pumices to pumiceous - perlitic dome clasts that are identical to the source lava dome (fig. 26a).

These outcropping tuffs are associated with a rather localized dacitic volcanism, the most pronounced one being developed in the central part (Ralaki-Ag Stefanos and Triades coast, areas) of western Milos. It caps the dacitic-rhyodacitic sequence (Anda) from which it took origin. At Ralaki old kaolin quarry area it is very well visible that the Ump unit stays on a totally silicified horizon which constituted the silica cap on a lake or shallow sea environment. The pumices at this basal interface have dimensions up to 50 cm and include many silica cap fragments.

2.5.3.6.3. The upper fine tuff unit (Uft)

It is transitional to the upper part of the Ump unit and it is presented moderately to strongly silicified with barite veins and stockworks, abundant sulphur incrustations. Except the norm, i.e., to be located above the Ump unit, it is locally also intercalated to the upper parts of it, where it presents a granular aspect.

2.5.3.7. Breccias & volcanosedimentary Units (Lower-Middle-Upper Pleistocene/ 1.4-0.5 Ma)

2.5.3.7.1. Eruption breccias

Several feeder structures, at both sectors, are preserved as hydrothermal breccia zones and/or as phreatomagmatic breccia zones, and are showed to be aligned and continuous along NE structures, (i.e., along the same structures that host the systems of the veins). In a lesser extent they are aligned also along E-W directions. These zones are expressed superficially by hydrothermal eruption breccias which include in their bodies ejected mineralized fragments formed at various depths. These last include crustiform-colloform banded silica (chalcedonic/crystalline quartz)-adularia veins and minor quartz-baryte-alunite veins, cemented generally in a strongly silicified and/or argillized matrix. It seems that the most of these feeder structures before the brecciation stage were locus of a hot spring environment (e.g. Mersinia, Xerokampos, Mavrovouni and Ag. Ioannis stream area).

Eruption deposits (Hydrothermal eruption breccias and phreatomagmatic breccias) rim the eruption pipes/craters and vary from clast to matrix supported with silica, sulfides, sulfosalts, sulfates, oxides and carbonate infill. When poorly sorted matrix supported breccias, they are presented loosy to strongly cemented, and contain clasts of various

dimensions, from granule (2-4 mm), to boulder (>64 mm) sized. The clasts are locally derived (fine ash, pumiceous tuffs and lava/dome fragments of rhyolitic, rhyodacitic, dacitic composition) in a silt to sand sized argillized and moderately to strongly oxidized and/or strongly silicified matrix (fig. 27d).

Locally they present re-brecciated textures (polymictic, phreatomagmatic, peperite breccias) (fig. 27a,b,c), enclosing subangular to subrounded (locally mosaic style), clasts of lapilli (2-64 mm) to block (>64 mm) sized. They grade out into zones of microbrecciated country rocks. They are typified at the old barite mine area at Triades where are considered to be large bodies that came out (formed) from pipe like structures, which have disrupted previous formations (hyaloclastites and tuffs) and then have been accommodated on the paleo-seafloor forming lobate structures at the vent area and tabular to massflow bodies laterally. Of course these configurations are in function to the stratigraphic level to which they reached (e.g., at Galana they intersected lower stratigraphic units than at Triades).

2.5.3.7.2. Tectonic breccias

Tectonic breccias are developed by deformational processes and include fault breccias which vary from milled puggy fault zones, to open space to jigsaw fit ones lying on a major or minor fault segment. These breccias are usually distinguished by their planar fault surfaces. They are generally presented propylitized to moderately argillized (kaolinized, smectitized).

They are typified at Triades, Kalamavros, Ammoudaraki.

2.5.3.7.3. Pebble dyke breccias

This kind of breccias contain mainly rounded to subordinately angular clasts, from a variety of rock types, in a sand to silt size rock flour matrix. It is slightly altered and it is considered to be emplaced in close association with poorly mineralized and fracture intrusive dacitic dome, after much of the associated hydrothermal alteration had ceased.

The pebble dike breccias are also taken as indicators of decompressive events (Sillitoe, 1985) and thus as related to phreatic / phreatomagmatic diatremes.

It is typified at Vani area.

2.5.3.7.4. Boulder fields breccias

The boulder fields are interpreted as representing eruptive centers, where the ignimbritic products form loose accumulations analogous to cinder cones, rather than sheets. Their characteristic architecture is that of re-brecciated and re-silicified banded veins and tuff fragments in an also strongly silicified matrix.

It is typified at Mavrovouni.

2.5.3.7.5. Vani volcanosedimentary unit

The Vani volcanosedimentary sequence overly the Anda dome setting and consists of tuffaceous clastic and volcanoclastic deposits (fig.26b), which are lower to middle Pleistocene in age and were deposited sometime in the period 0.9–0.4 Ma (Papanikolaou et al.1990). This statement is in agreement with the graben formation along the center of Milos (Milos gulf), which started between volcanism phase III and IV of the generalized

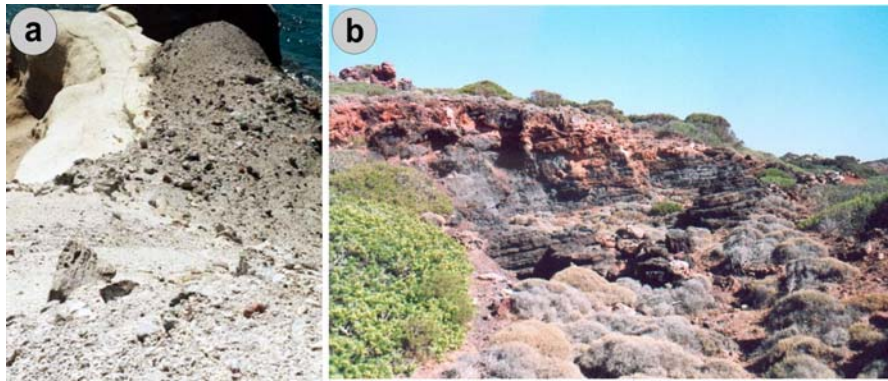


Fig. 26 : (a) The base of the Ump unit outcropping at several places along the seaside, between Triades and Ammoudaraki; (b) the manganiferous and partially oxidized (iron oxi-hydroxides). Vani volcanosedimentary unit.

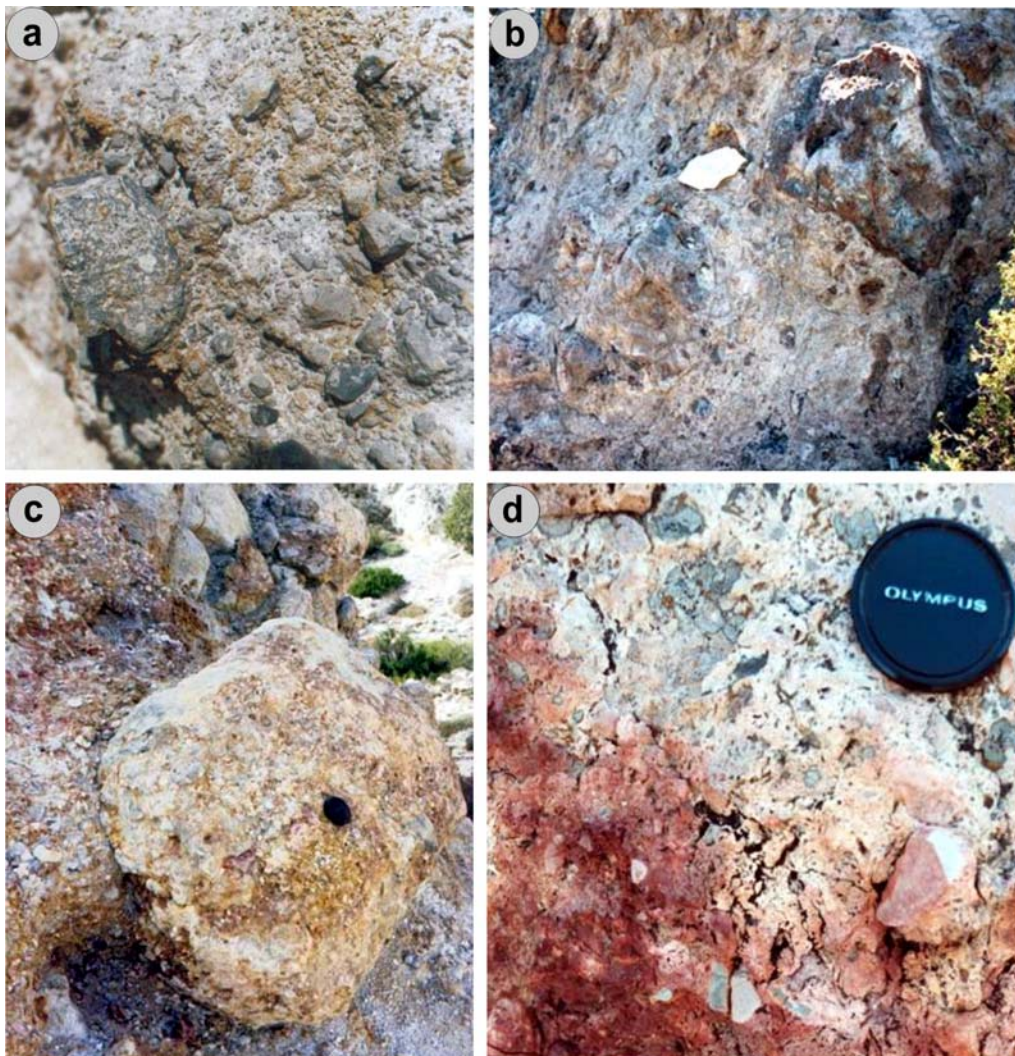


Fig. 27 : (a) Polymictic hydrothermal explosion breccia at Ag. Nikolaos; (b) phreatomagmatic breccia at Ag. Ioannis; (c) re-brecciated and re-sedimented peperite breccia at Triades; (d) strongly cemented by silica and oxidized hydrothermal explosion breccia at Ag. Ioannis.

description, i.e., at about 0.95 Ma.

The volcanoclastic sandstone at Vani it is an altered pyroclastic material coming from the tuffs of Upper Pliocene age. It consist of two subunits, a lower and an upper, separated by a thin layer (~ 20-30cm) of conglomerates, composed of volcanoclastic sandstone and dacitic pebbles.

The underlying volcanoclastic sandstone (the lower subunit) is strongly silicified and impregnated by manganese oxides. It is composed mainly of K-feldspar, chlorite and sericite crystals.

2.5.3.7.6. Upper fossiliferous tuffites (Uftt)

The upper fossiliferous (brachiopods, echinoids) tuffites are brownish in colour and contain various thin carbonate horizons. They stay on transgressive conglomerates and are related to another (younger) phase of subsidence due to tectonic causes, along the well known E-W directed Ammoudaraki - Plakota - Rivari lineament, which caused their deposition.

2.5.3.7.7. Debris flow deposits

Landslide and debris flow/avalanche deposits (lahars), lobate to sheet like, showed to be unconsolidated and chaotically arranged containing angular block-boulder to clast sized fragments (argillized, silicified tuff fragments and silicified epithermal vein pieces) included into a silt to sand size matrix. Partly at least, are considered to be related to a phreatic-, phreato- magmatic activity.

Are typified at Mavrovouni, Chondri Rachi, Pyrgiali areas.

2.6. The present day topographic position of the Pliocenic-Pleistocenic volcanic/volcanosedimentary and sedimentary products of W. Milos

The conglomerates and beach rocks formed at various places around western Milos indicate the existence in the past of emergent volcanic islands in the environs of a major basin system.

There are many evidences at western Milos that it has risen from place to place more than 150 m, as for ex., at Triades where the fossiliferous marine tuffs and tuffites are at 150 m a.s.l, the marly bedded marine tuffs at Tsouvala at 200 m a.s.l, manganiferous marine silica caps at Agathia at 120 m a.s.l., unconsolidated gravels at Ralaki at 180m a.s.l and at Profitis Ilias (wave action cliff face), at 500m a.s.l.

In **Appendix I**, a series of geological sections after drill hole (DDH and RC) data have been created using the Interdex software programme (developed by the Australian company Visidata Pty Ltd and now acquired by Gemcom software International Inc.-Canada). The aim of doing that was to get also along the third dimension (depth) and thus to have some insights about geology, along it, as well as to better described and confirm regional stratigraphy.

3. PETROGRAPHY OF THE VARIOUS ROCK TYPES IN THE AREA UNDER INVESTIGATION

Detailed field macroscopic observations on the various rock types have been supplemented by microscopic studies in thin sections, of the variously altered rocks, and in some polished sections, in order to identify the opaque minerals into the specimens. X-ray identification of alteration minerals has been utilized where it was necessary.

Seventy-six samples were collected from W. Milos over a large area with varying degrees of alteration. Out of these specimens, twenty-eight thin sections were prepared for petrographic analysis at Hamburg University and together with 35 thin sections prepared at earlier times from Silver and Baryte Ores mining Co.(now S&B Industrial Minerals S.A.), and from Midas Joint Venture (an American-Australian-Greek joint venture), the whole of the rock type occurrences has been petrographically investigated.

The results are summarized and categorized following the previously used volcanic description for western Milos.

3.1. Lithic /pumice tuff (Lpt)

Macroscopic Texture:

- Medium-coarse pyroclasts, and fine to medium sized lithic clasts (subvolcanic >metamorphic) poorly sorted and with a massive aspect.

Microscopic Texture:

Volcaniclasts:

- The pumice clasts are made up by plagioclases (smectitized ± kaolinized, sericitized, opacitized), K-feldspars (mainly sericitized sanidine), quartz (magmatically corroded), biotite (chloritized, sericitized), clinopyroxene (oxidized) and totally altered amphiboles (opacitized, smectitized) in a vitrophyric matrix showing eutaxitic structures. Glomeroporphyric intergrowths are present between quartz and clinopyroxene crystals.

- The lithic subvolcanic fragments are of dacitic, rhyodacitic and andesitic composition. In the generally slightly altered lithic (dacite, metamorphic basement schists) component of the pyroclastic formation, the volcanic fragments are made up by plagioclase (slightly kaolinized or sericitized), K-feldspars, amphibole, biotite, a few clinopyroxene (slightly chloritized), and opaque minerals (magnetite, hematite) in a groundmass made up by microcrystalline quartz and plagioclase locally argillized.

- A few partially degassed and strongly kaolinized lava fragments, showing the same dacitic composition as the fresh lithic components, are also present subordinately into the pyroclastic formation.

Matrix:

- It is made up by a clast component, of the same kind as the pyroclasts, but considerably finer, and by a crystal component which because of the advanced alteration is presented as ghosts of plagioclases and clinopyroxenes.

Type areas: Fragovigla, koumaria.

3.2. Pyroclastic Pumice flow (Pfl)

Macroscopic Texture:

- Medium to coarse, prismatic to subrounded pumice fragments cemented by a glassy matrix.

Microscopic Texture:**Pyroclasts:**

- Prismatic felsic pumices made up by plagioclases (smectitized \pm kaolinized), K-feldspars (sericitized), biotite (sericitized) and in a lesser extent quartz.

Matrix:

- Quartz, K-feldspars, plagioclase crystals in a sericitized and locally oxidized fine matrix. Locally shard-rich components are present.

Type areas: Mavrovouni, Spyritou Rema.

3.3. Lower pumiceous lapilli tuff (Lmp)**Macroscopic Texture:**

- Generally fine to medium sized pyroclastic formation, in a sand sized to fine ash/glassy matrix.

Microscopic Texture:**Pyroclasts:**

- Lapilli sized pumices, at the southern sector generally slightly to moderately argillized and/or silicified, and at the northern sector quasi everywhere strongly argillized (kaolinized) and/or silica flooded (chalcedony, cristobalite, opal), as well as in several places barytized, alunited. The pumices are made up by plagioclase (smectitized \pm kaolinized, sericitized, opalitized), K-feldspars (mainly sericitized, adularized sanidine), quartz magnetically corroded), biotite (sericitized), clinopyroxene (oxidized) and totally altered amphiboles (opacitized, smectitized, silica replaced).

- The coarser, block-sized, andesite/dacite are opalized and sericitized and made up by plagioclase (sericitized, kaolinized, albitized, smectitized), clinopyroxene (sericitized), amphibole (opalized, oxidized), quartz, K-feldspar phenocrysts, in a moderately argillized groundmass made up by sericitized and subordinately smectitized plagioclase, clinopyroxene and orthopyroxene.

Matrix:

- It is either microcrystalline or vitrophyric. In the first case it is made up by sanidine and albite microlites, with alteration minerals such as silica, sericite, Fe-hydroxides and locally barite, jarosite, kaolinite, quartz, calcite either it is quasi totally silicified (opalized) with ghosts of plagioclase and clinopyroxene. In the second case the vitrophyric matrix shows eutaxitic structures, and locally it is presented alunited. The alunition has the form of filling cracks in plagioclases, either it is presented as veins. In this last case, coarse crystals of alunite after magma degassing, occur at northern sector (e.g. Kondaros).

Quartz and/or adularia veinlets cutting through the matrix are also present on both sectors.

Type areas : Kondaros, Kondaros - Anemophysima, Larni - Vani, Favas - Mersinia, Triavouna, Agathia, Triades old barite mine, Chondro Vouno, Agios Ioannis, Mavrovouni.

3.4. Fine ash tuff (Fat)**Macroscopic Texture:**

- Very fine white to creamish and locally reddish in color fine tuff.

Microscopic Texture:

- As a whole it is presented either moderately to strongly argillized, or sericitized and patchy silicified. The principal constituents are quartz, K-feldspars (kaolinized, sericitized orthoclase, sanidine). Iron oxides (mainly hematite) are locally present. Quartz generally is

present in small amounts, as well as ferromagnesian minerals, which are completely replaced by microcrystalline quartz. Smaller Fe-Ti oxide crystals have been completely replaced by very small leucoxene crystals, while rutile and rare zircon are also present.

It locally exhibits typical ignimbritic textures (eutaxitic) and it is composed mainly of a micro- to crypto-crystalline mat of quartz-feldspathic and locally glassy material.

Kaolinite, up to a maximum of 30%, occurs as fine patchy aggregates with a very finely matted fabric interlocked with the chalcedonic phase.

Type areas: Koumaria, Ralaki, Favas, Larni.

3.5. Profitis Ilias ignimbrite (PII)

Macroscopic Texture:

- Medium-coarse ignimbrite.

Microscopic Texture:

Pyroclasts:

- Pumiceous and subvolcanic clasts, as well as metamorphic fragments from the basement, are the principal ones, while some tabular crystal clasts (K-feldspars) and angular to subrounded (quartz) ones, also occur.

Concerning the subvolcanic fragments it is important to note that there are two kinds of porphyritic dacitic fragments, one generally slightly to moderately altered made up by quartz (as angular to subrounded crystals, often magmatically corroded), amphiboles (chloritized/sericitized/silicified/oxidized), plagioclase (kaolinized) in a silicified groundmass where devitrification structures (spherulitic structures) are also observed. The second kind it is presented more altered, and possibly more important, concerning the probable existence of mineralized subsurface areas. It is made up by quartz, plagioclase (sericitized+smectitized), K-feldspar (adularia), clinopyroxene (sericitized), augite in a sericitized and partially smectitized groundmass. The sericitization overprints the chronologically earlier adularization event.

- The pumice fraction is made up by plagioclase (kaolinized, calcitized, adularized) in a kaolinized, sericitized, adularized and calcitized matrix.

“Fiamme” (collapse pumices) structures with agglutinated fragments of glass and pumice are typical at Agios Ioannis subarea, which corresponds to the lower parts of the formation.

Matrix:

- When argillized, there are Illite, sericite, the principal clay minerals to be found, while locally it is stained by goethite and/or jarosite. Kaolinite and smectite are also subordinately present. When silicified, it presents a cryptocrystalline mosaic texture, and usually it is truncated by colloform-crustiform quartz-adularia veins/veinlets. Quartz-adularia occur in quasi equal amounts, generally as chalcedonic to microcrystalline and crystalline mosaic textured quartz-adularia aggregates. Fine bands of hematite after pyrite, marcasite paralleling the colloform-crustiform trend of the quartz-adularia veins are locally present.

Type areas: Profitis Ilias, Livadakia, Tsouvala.

3.6. Rhyolitic intrusive bodies and dykes (Rhyda)

Macroscopic Texture:

- Strongly kaolinized and locally silicified intrusive, with quartz and locally some strongly altered feldspars observable, and strongly silicified flow dykes are the two principal macroscopic expressions.

Microscopic Texture:

They present a porphyritic texture.

Phenocrysts:

- Plagioclases (generally kaolinized \pm sericitized \pm smectitized, but also locally strongly silicified and adularized), amphiboles, \pm K-feldspar (sanidine), \pm biotite, subrounded quartz.

As a whole can be assigned to them a 10 vol. % quartz, and a 5-10 vol.% plagioclase, \pm biotite phenocrysts.

Groundmass:

- Crypto- to micro- crystalline kaolinized \pm sericitized \pm silicified and/or quartz \pm albite with plagioclases (opalitized, kaolinized, sericitized), ghosts of amphiboles.

Quartz veinlets and oxidized veinlets after sulphides cutting through the ground mass and/or through plagioclases are also present. Locally spherulitic devitrification structures occur.

Type areas: Chondro Vouno, Profitis Ilias.

3.7. Fossiliferous tuffs and tuffites (Ftt)

Macroscopic Texture:

- Shallow marine deposited tuff sand and tuffaceous sandstone and siltstone with abundant macro- and micro- fossils.

Microscopic texture:

- They present a general microcrystalline texture with partially sericitized, smectitized plagioclase, K-feldspars. Locally barite, jarosite, Fe- hydroxides are also present.

Type areas: Triades, Pyrgaki, Galana.

3.8. Reworked volcanosedimentary unit (ep)

Macroscopic Texture:

- Very uniform sand sized quartz, K-feldspar crystal fragments and/or very fine lithic fragments of intermediate/acid subvolcanics and crystal fragments, immersed in a fine matrix.

Microscopic Texture:

Volcaniclasts:

- They belong to different lithological types which can be described as follows:

- a) porphyritic andesite made up by plagioclase and amphibole immerse in a cryptocrystalline groundmass.
- b) porphyritic andesite-dacite made up by plagioclase and amphibole immerse in a microcrystalline groundmass constituted by quartz, plagioclase microlites.
- c) porphyritic dacite made up by plagioclase, quartz and amphibole immerse in a microcrystalline groundmass constituted by quartz, plagioclase microlites.
- d) porphyritic dacite made up by plagioclase, quartz and amphibole immerse in a hyalopilitic groundmass constituted by plagioclase microlites.

- e) Pyritized, sericitized porphyritic rhyolite with a silicified and locally devitrified (spherulitic textured) groundmass.

- The crystal fragments are quartz, K-feldspars (sericitized, adularized).

Matrix:

- Silicified micro- to cryptocrystalline matrix. Barite, jarosite, Fe-hydroxides are also present.

Type areas: Triades, Pyrgaki, Galana.

3.9. Andesites-dacites and rhyodacites subvolcanic bodies and lavas (Anda)

Macroscopic texture:

- Generally altered (kaolinized, silicified) and brecciated (hyaloclastites). Locally lavas, dykes are concordant to the tuffs, tuffites surrounding them.

From surface samples:

When fresh:

Microscopic Texture:

They present a porphyritic texture.

Phenocrysts:

- Quartz, magmatically corroded (dacites, rhyodacites, rhyolites). The plagioclases are presented generally zoned and magmatically corroded. Hornblende (partially or sometimes completely converted to opaque minerals), K-feldspars (sanidine) minor clinopyroxene (andesites, dacites), biotite (dacites, rhyodacites, rhyolites), minor quartz (dacites-rhyodacites/subrounded, magmatically corroded), minor and not always present orthopyroxene, zircon, and ilmenite (rhyodacites).

Both orthopyroxene and biotite, when present frequently show reaction relations with the amphibole (reaction rims).

Some times the phenocrysts have a more or less equal size (equigranular) and thus they have an aspect of a grainy phaneritic rock matrix.

As a whole can be assigned at the plagioclase a 10-15 vol. %, and a 5-8 vol. % for hornblende and minor pyroxene phenocrysts.

Groundmass:

- It is microcrystalline to cryptocrystalline-aphanitic (andesites) groundmass made up by microlites of plagioclases, K-feldspars (dacites, rhyodacites) and subordinately clinopyroxene, hornblende. The amphiboles here are either absorbed by the groundmass or totally replaced by hematite or jarosite.

The rhyodacites present a more vitreous (glassy) groundmass showing often perlitic cracks and devitrification structures (spherulites)

When altered:

Phenocrysts:

- The plagioclases are presented sericitized, smectitized, kaolinized, alunitized, albitized, adularized, opalitized and at depths calcitized); the K-feldspars (sericitized, adularized), biotite (chloritized, oxidized), clinopyroxene (smectitized), amphibole (sericitized, smectitized, chloritized, opacitized).

In the lava bodies and/or subvolcanics sometimes are observed xenolithic inclusions having an intermediate composition.

Groundmass:

- Micro- to cryptocrystalline groundmass made up by quartz and argillic minerals (sericite, smectite, kaolinite, ± zeolites) is encountered. Strongly silicified to glassy or cryptocrystalline varieties, with perlitic cracks and spherulitic structures are also encountered.

In detail, the sericitized groundmass is made up by plagioclase and quartz. Locally it is cut by microcrystalline quartz and/or oxidized veinlets, or it is hematite stained. Locally and especially when brecciated, abundant barite is present. In places, some acicular barite is also present together with opaque minerals (magnetite, hematite).

Ultra-thin veinlets and cataclases are filled by jarosite, barite and Fe-oxides/ hydroxides and very fine opaque minerals (either disseminated and/or in veinlets) locally oxidized.

Adularia in form of veinlets is found to be together with secondary quartz, accompanying metallic mineral aggregates. Locally the matrix is recrystallized in adularia.

- Sparsely dykes of dacitic composition are encountered and are presented slightly altered and relatively adularized, made up by plagioclase (kaolinized, sericitized, adularized), clinopyroxene (sericitized) in a groundmass made up by plagioclase. Some oxidized veinlets are also present, cutting them along NE directions.

- Locally, propylitized lava fragments in a volcanic agglomerate formation, present a porphyritic texture made up by K-feldspars (adularia), amphiboles (oxidized) in a cryptocrystalline groundmass cut by micro-crystalline quartz and stockwork of adularia veinlets.

From subsurface samples (after drillhole data – 1992 Triades drilling campaign):

Macroscopic Texture:

- Physical cores

Microscopic Texture:

Phenocrysts:

- Porphyritic subvolcanic dacitic body made up by quartz (magmatically corroded), plagioclase (partially argillized and/or replaced by calcite, ankerite), biotite and amphibole (replaced by calcite, either partially argillized, chloritized with FeOx patches).

Groundmass:

- In a microcrystalline (quartz, feldspars) groundmass. Calcite, ankerite and opaque minerals, fill also all the cracks in the groundmass. Locally Fe-oxide veinlets are present.

- Xenoliths of subvolcanic bodies of more basic composition are also present. This slight alteration, at quasi 200m from the present surface, show a clear propylitic environment of alteration.

- Locally at depths of ~ 100m, the same metallic paragenesis found and described (see next) for the surface outcropping matrix supported breccias (hyaloclastites), has also been encountered here at the coherent dacitic body. It would be two different metallic paragenesis, disseminated or in veinlets form, made up by marcasite-pyrite the first (marcasite being the dominant component), and a sphalerite-galena the second (sphalerite being the dominant one). It seems that the second paragenesis is later chronologically with respect the first one, as Zn-Pb minerals are developed peripherally and inglobe the marcasite-pyrite compounds.

Type areas: Vani, Larni, Mersinia, Kondaros-Anemophysima, Galana, Agathia, Triades, Spyritou Rema, Plakota, Ag. Panteleimon, Chondro Vouno.

3.10. Dacitic-rhyodacitic subvolcanic bodies lavas and dykes (Dado)

When fresh:

Microscopic Texture:

- They present a porphyritic texture, made up by plagioclase, amphibole, clinopyroxene, K-feldspars, biotite, minor and not always present orthopyroxene.

Phenocrysts:

- Quartz is presented magmatically corroded. Plagioclases (andesine-labradorite) show complex zoning patterns and generally present resorption textures (dusty mantles, sieved cores, reaction rims and rounded shapes). They are also observed in glomeroporphyric intergrowths. Amphibole is sometimes completely converted to opaque minerals. Clinopyroxene is rather of small dimensions, while orthopyroxene is rare.

As a whole can be assigned to them a 5 vol. % quartz, and a 10-15 vol.% plagioclase, biotite phenocrysts.

Groundmass:

- It is microcrystalline to glassy containing various amounts of acicular and tabular plagioclase, clinopyroxene, rarely orthopyroxene, subordinate amphibole and opaque minerals. Glomeroporphyric intergrowths of plagioclase, amphibole, clinopyroxene and/or of clinopyroxene (some of them totally hematitized), are also locally observed. Titanium-magnetite is also present.

When altered:

Phenocrysts:

- Plagioclases (sericitized, slightly kaolinized), biotite (chloritized,oxidized), amphibole (chloritized, sericitized, opacitized), K-feldspars (slightly kaolinized, smectitized in cracks), clinopyroxene (smectitized).

Groundmass:

- Opalitized or sericitized ± kaolinized ± smectitized, where locally several open spaces (cracks) are filled by alunite and cut by hematitic veinlets. Locally glomeroporphyric intergrowths of plagioclases are present.

Type areas: Bouloubasi -Katsimoutis, Kondaros.

3.11. Galana Formation (Galf)

Macroscopic Texture:

Volcaniclasts:

- Lithic (metamorphic) rich / pumice bedded tuff.

Microscopic Texture

- The lithic components (exclusively metamorphic schists from the basement) are quite fresh.

- The pumice clasts are made up by plagioclases (kaolinized, sericitized, opalitized), K-feldspars (sericitized), quartz, biotite (sericitized, chloritized) and totally altered amphiboles (smectitized) in a vitrophyric matrix showing eutaxitic structures.

Matrix:

- It is made up by a finer clast component of the same kind as the pyroclasts and by a crystal (mainly plagioclase) component.

Type areas: Galana.

3.12. Upper pumice tuff unit (Ump)

Microscopic Texture:

Pyroclasts:

- The pumice component is made up by porphyritic dacitic-rhyodacitic, andesitic fragments constituted by K-feldspars (sanidine, generally sericitized, smectitized), plagioclases, quartz, biotite (chloritized, sericitized), and ghosts of amphiboles and clinopyroxenes in a microcrystalline groundmass made up by plagioclase and quartz microlites.

In the dacites, clinopyroxene (chloritized), orthopyroxene (chloritized) are encountered.

Some lithics encountered at the base and top of the unit are of the same composition and constitution as the pumices.

Matrix:

- Sand sized matrix including some quartz and feldspar crystals and pumices of very small dimensions. At places it is presented strongly argillized and/or overprinted by silica (silica flooding).

Type areas: Triades, Ralaki, Ammoudaraki

3.13. Upper fine tuff unit (Uft)

Macroscopic Texture:

Moderately to strongly silicified fine tuffs located above the Ump unit but also intercalated to the upper parts of it.

Microscopic Texture:

- As a whole it is presented either moderately to strongly argillized, and / or patchy silicified. The principal constituents are quartz, K-feldspars (kaolinized sanidine). Iron oxides (mainly hematite) are locally present. Quartz generally is present in small amounts, as well as ferromagnesian minerals, which are completely replaced by microcrystalline quartz.

It locally exhibits typical ignimbritic textures (eutaxitic) and it is composed mainly of a micro- to crypto- crystalline mat of quartz - feldspathic and locally glassy material. Kaolinite occurs locally strongly interlocked with chalcedonic silica.

Type areas: Ralaki, Ag. Stefanos.

3.14. Upper fossiliferous fine tuff/tuffite (Uftt)

Macroscopic Texture:

- Shallow marine deposited fossiliferous tuffites and carbonate - tuffite horizons.

Microscopic Texture:

- Microcrystalline texture with smectitized feldspars and carbonate concretions.

Type areas: Ntasifnos, Spyritou Rema, Ralaki.

3.15. The Breccias

3.15.1. Hydrothermal eruption matrix supported breccias

Macroscopic Texture:

- Matrix supported polymictic breccias made up by volcanic (rhyolitic, rhyodacitic/dacitic), and fine tuff fragments in a fine to sand sized argillized, and moderately to strongly silicified and / or strongly oxidized matrix.

Microscopic Texture:

The clasts:

- The fine tuff part is totally silicified. The generally strongly altered rhyolitic intrusive fragments are characterized by rounded and magmatically corroded quartz crystals in between hematitic veinlets and opaque minerals (metalics). The dacitic-rhyodacitic subvolcanic part is made up by quartz, plagioclase (sericitized, smectitized partially), biotite (\pm chloritized), amphibole (totally argillized \pm FeOx patches) in a microcrystalline feldspar-like (sanidine, albite), partially kaolinized and/or partially zeolitized vitrophyric matrix. Pyrite of hypogene origin occurs as scattered, interstitial euhedral and subhedral grains and clusters.

Ultra-thin veinlets and cataclases are filled by jarosite, barite and Fe-oxides/hydroxides as well as by very fine opaque minerals (marcasite, pyrite) locally oxidized.

Locally the clasts are argillized and alunitized, these last occurring as patchy matted and micaceous aggregates into a chalcedonic silica phase, thus depicting a previous (before the brecciation) alteration style.

The matrix:

- The lithic, and where exist the tuff clasts (angular to subangular in shape) are cemented by barite, chalcedonic and adularia aggregates, and at several places by minor dusty pyrite. As constituents together with the previous mentioned, there are microlites of feldspars (kaolinized, albitized) and quartz, generally where a moderate to strongly argillized and/or locally strongly silicified matrix is present.

- A pyritic \pm marcasitic matrix and related stockwork micro-veining is common in this kind of breccia matrix. The marcasite here is found enclosed into the mass of pyrite as monograins and/or forming glomerophyric structures.

- Silica-barite matrix, including disseminated (<3%) framboidal pyrite, low-Fe sphalerite is also present locally.

Type areas: Triades, Favas, Pyrgaki.

3.15.2. Hyaloclastitic matrix supported breccias

Macroscopic Texture :

- Resedimented subangular clasts from the shallow emplaced subvolcanic/lava dome complexes.

Microscopic Texture :

The Clasts :

- Their fragments present the same mineralogy as the coherent subvolcanic facies mentioned before for the Anda (andesitic, dacitic, rhyodacitic, rhyolitic) subvolcanics.

The Matrix :

- It constitutes a major component of the breccia, and it is generally of silt to sand sized. Microscopically it is showed argillized with patchy silicified and oxidized parts.

3.15.3. Hyaloclastitic clast supported breccias

Macroscopic Texture:

- They are made up mainly by volcanic or by pumiceous fragments in a scarce, fine silt to sand sized argillized and moderately oxidized matrix.

Microscopic Texture:

The clasts:

- They constitute the main component of an essentially in situ breccia (in situ hyaloclastites) where the clasts present a jig saw fit texture and are either completely silici-

fied (mainly the subvolcanics) or completely kaolinized (mainly the pumiceous ones, which essentially derive from the same subvolcanic bodies). Their mineralogy under the microscope is the same with that of the coherent subvolcanic facies mentioned before for the Anda (andesitic, dacitic, rhyodacitic and rhyolitic subvolcanics).

- Locally at depths (>150 m), the clasts are sericitized and contain pyrite, either disseminated or in ultra-thin veinlets.

The matrix:

- The matrix constitutes a minor component of the breccia, and it is very fine. When altered it is presented argillized and/or silicified, either moderately oxidized.

Opaque minerals (galena, sphalerite) occur as interstitial and intergranular grains and clusters together with pyrite.

- Locally at intermediate depths (~80 m), the matrix is mineralized made up by pyrite, marcasite into a silica-argillic-carbonate gangue.

Type areas: Triades, Galana, Ag. Nikolaos.

3.15.4. Tectonic breccias

Macroscopic Texture:

- Jigsaw-fit mainly and subordinately clast supported breccia.

Microscopic Texture :

The fragments:

- Porphyritic dacitic-rhyodacitic, rhyolitic subvolcanic lava fragment made up by quartz (magmatically corroded and generally zoned), plagioclase, biotite and amphibole (moderately argillized (kaolinized), smectitized, chloritized with FeOx patches) in a microcrystalline (quartz, feldspars) groundmass.

The matrix:

It constitutes a minor component which is the product mainly of the relative friction movements of the clasts, and thus presents the same mineralogy with them.

3.16. The veins

3.16.1. Chalcedonic to crystalline quartz-adularia veins into pyroclastics

Microscopic Texture:

- Quartz and adularia occur from 20% to 50% as fine colloform-crustiform banded chalcedonic, microcrystalline and crystalline mosaic textured aggregates. Locally, scattered hypogene sphalerite, galena, chalcopyrite and supergene chalcocite, covellite (residual chalcopyrite occluded by covellite) as well as fine bands of hematite after pyrite paralleling the colloform-crustiform trend of the veins, are present.

A few (<2%), anhedral to subordinately euhedral hypogene acanthite, electrum grains are occluded in the chalcedonic phase of the quartz-adularia veins (Triades, Chondro Vouno, Mavrovouni).

Type occurrences: Profitis Ilias ignimbrites.

3.16.2. Chalcedonic silica - baryte veins into dacite dome/ flow dome complexes

Microscopic Texture:

- Fine pyrite +/-covellite +/-sphalerite of hypogene origin, are occluded into the chalcedo-

nic phase, while the barytized phase constitutes more than the 90% of their mass.
Type occurrences : Triades.

3.17. Xenoliths (magmatic inclusions) in the subvolcanic bodies and extrusive domes

The mineral species in the xenoliths are the same as in the rocks that host them, but in different proportions and generally of smaller grain size. This similarity in mineral species is indicative of a magma composition and of a pressure of crystallization more or less stable on a large regional scale. The more mafic compositionally, magmatic inclusions, are considered to be similar to the parent magma, i.e., segregated from it (cognate xenolith), which gave the genesis to the host rock.

The generally finer to very fine grain size of the xenoliths indicates that the crystals grew with a fast cooling rate.

Several kinds of inclusions have been observed and can be subdivided as follows:

3.17.1. Porphyritic inclusions

The most, if not all of these inclusions are of dacitic composition, and the encountered minerals are plagioclase + clinopyroxene + orthopyroxene + magnetite in a microcrystalline groundmass made up predominantly by quartz + plagioclase ± K-feldspars microlites.

3.17.2. Cryptocrystalline inclusions

As revealed by XRD analysis, they are mineralogically similar to the host. The only difference which could be ascribed, is related to a slight differences in colour, which some times is darker and other times lighter with respect to that of the hosts. Their groundmass is from glassy to cryptocrystalline.

These kinds of inclusions generally are characterized by sharp boundaries to the host.

3.17.3. Hyalopilitic inclusions

They are made up by acicular crystals and/or microlites, crystallites of feldspars (mainly plagioclases) and amphiboles sparse in a glassy groundmass.

3.17.4. Multi-phases inclusions

In this kind of inclusions textural relations indicate that intermediate composition inclusions made up by plagioclase, orthopyroxene, clinopyroxene are included in other inclusions made up by plagioclases and amphiboles, and show interlocking arrangements with them, most probably due to exsolution of one phase from another.

4. TECTONIC SETTING OF THE AREA UNDER INVESTIGATION

4.1. Introduction

Although during the late Messinian, the Messinian salinity crisis occurred throughout the Mediterranean region (Krijgsman et al., 1999), no geological evidence was found at Milos island for the accompanying drastic sea level drop and subsequent rise (present work, Van Hinsbergen et al, 2004). Instead of that what is important to take in consideration is a considerable sea level rise (~900 m) which occurred between 5 and 4,4 m.y. on Milos (Van Hinsbergen et al, 2004), i.e. approximately 300k years after the Pliocene flooding, which ended the Messinian salinity crisis (Krijgsman et al., 1999; Van Hinsbergen et al, 2004).

This relative sea level rise at Milos is not considered as a local phenomenon of tectonic subsidence but rather is interpreted as a large-scale extension in the central-southern Aegean area which had as a consequence the creation from Saronic Gulf to the sea of Crete of a complex pattern of E-W, N-S and WNW-ESE trending normal faults, along which the WNW-ESE trending subsided between 900 and 1000m in the Plio-Quaternary (Wright 1978; Papanikolaou et al.1988; Van Hinsbergen et al, 2004).

The dominant structural features at western Milos are from one side a series of steep NE striking fault/lineament zones which appears to have been characterized by left lateral strike-slip and dip-slip motion, and from the other side a series of dilational NW trending ones,(fig. 28) into which, composite volcanic centers, domes and collapse calderas have been developed. They together have promoted and localised fluid flow producing zones of

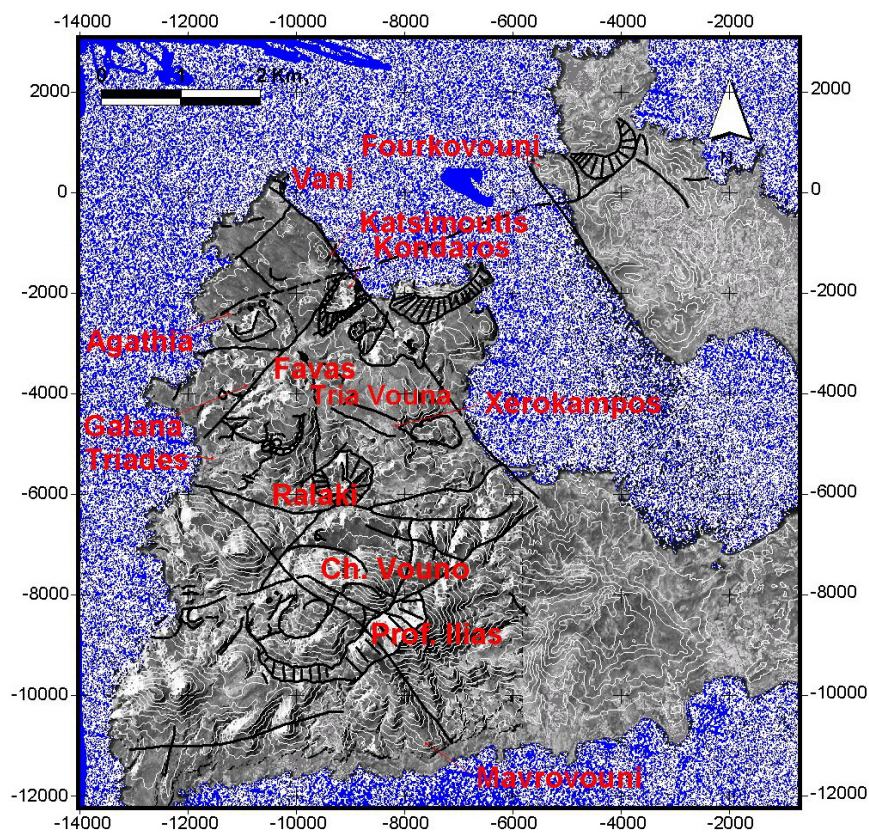


Fig. 28 : The dominant structural features of western and partly eastern Milos

intense silicification, brecciation and veining. With respect to those structures, subsidiary E-W and N-S trending faults were also created and are considered to have enhanced the permeability of the volcanic and volcanosedimentary sequences, through a further dismembering and dislocation, which took place.

4.2. The main structural features of W. Milos

An oblique convergence, as that which took and still takes place in this part of the eastern Mediterranean sea (fig.3), is characterized by dilation formed in association with major strike-slip faults. It is considered that this dilation facilitates from one part the emplacement of intrusions into extensional settings as well as promotes the formation of epithermal and/or epithermal/porphyry related gold-silver systems (Corbett G.J. and Leach T.M.,1998).

During Oligocene times (Sonder 1924, Liatsikas 1949, Wetzenstein 1975), NW-SE trending faults related to the orogenic Alpine phase, affected exclusively the metamorphic background of Milos island (as it was the only rock formation existed at that time). This system created a series of step-like configurations, towards the NE and SW with respect to a NW-SE trending core, at least concerning the southern part of western Milos (e.g., Profitis Ilias, Chondro Vouno areas which constituted the central core/horst area). This resulted in a fragmentation of the basement with the creation of different graben and horst blocks (fault bounded blocks).

During upper Pliocene times (Fytikas 1989) the reactivation of the previous tectonic lines of the Pelagonian metamorphic basement (fig.2) and the creation of new transcurrent faults along NE directions, created a new tectonic setting on both the metamorphic and the Neogenic sedimentary cover through which took place the calc-alkaline volcanism of the island. On that respect the principal faults / lineaments were displayed along ENE-WSW up to E-W and NNW-SSE up to N-S directions (precisely between the azimuth values of 100° - 90° and 350° - 360° respectively), and subordinately along a NW-SE one, as it is evidenced by the alignment of the various domes occurring at W. Milos.

At a final stage, during Upper Pliocene - Pleistocene times, the reactivation once again of NW trending faults created the Milos gulf and reshaped the previously created "puzzle" forming a new and better defined polygonal pattern. The main and immediate salient view on this final tectonic configuration is, that one, made up by two main NW trending lineaments linked by an arcuate fault, trending approximately E-W, and another series of NE trending and steeply deeping faults (fig. 37).

The above mentioned, successive tectonic regimes created a series of horst and graben blocks trending NW-SE and E-W (Fytikas 1977,1989; Papanikolaou et al.1989, 2003).

The today's NE-SW and NW-SE visible tectonic lineaments and faults, which affected during upper Pliocene-Pleistocene times (Fytikas 1977,1989; Papanikolaou et al.,1989, 2003) also the volcanic cover, it is clearly related with the neotectonic movements of the different horst and graben areas / blocks (Fytikas 1977,1989; Papanikolaou et al.,1989, 2003) which determined and drew the today's shape of Milos.

Out of several E-W trending faults present at western Milos, there is one which has an arcuate shape and presents a north to northwest dipping slickensides, along its escarpment, indicating essentially both normal and sinistral slip vectors. This is the Ammoudaraki-Plakota-Rivari lineament, which dips 40° to the north and it is considered of a particular interest. This dip-slip and sinistral strike-slip structure subdivides the western Milos area in two sectors (northern and southern),(fig. 29a) concerning both, age of volcanism and

secondary alteration/sulfidation state (see next), as well as from a tectonic point of view. Indeed, this arcuate structure constitutes the southern margin of a graben structure trending quasi E-W which has been filled with fossiliferous tuffitic siltstone and sandstone material and at a period corresponding at the end of the first phase of explosive and at a lesser extent localised effusive volcanic activity (3.5-3 Ma) and before the starting of the main effusive volcanic activity (2.7 Ma).

Along the margins of the graben, andesitic, dacitic and rhyodacitic subvolcanic bodies have been intruded and created also some small volcanic edifices (e.g. Ralaki)-(fig. 29b), thus creating favourable conditions for mineralization through the localisation of fluid flows.

Based on all these considerations and facts (field observations), it seems that this escarpment can be considered as a structural margin of a caldera collapse structure (fig.30).

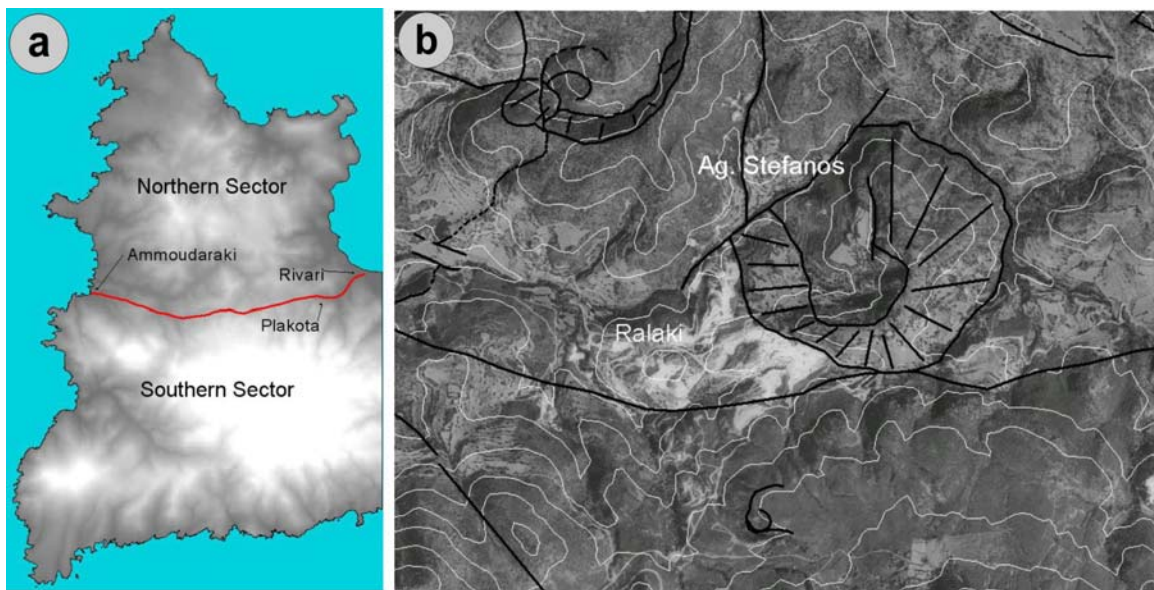


Fig. 29 : (a) The Ammoudaraki-Plakota-Rivari lineament at western Milos. In white, the higher topographically areas; (b) air photo depicting clearly the Ralaki volcanic edifice.

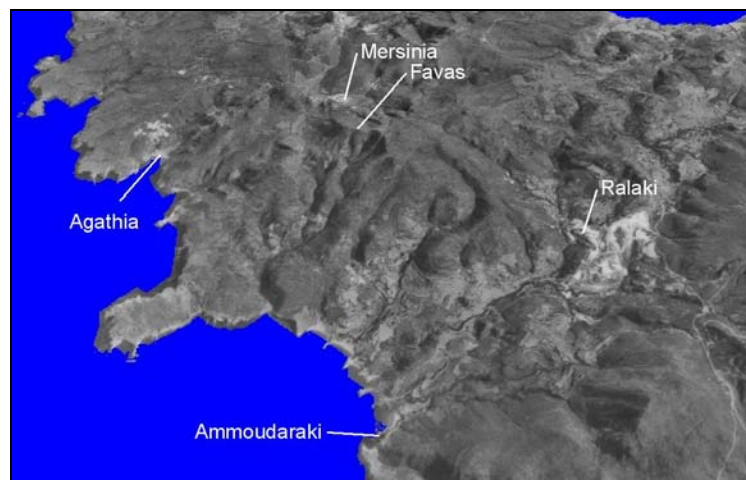


Fig. 30 : Probable caldera margin as deduced from airphotos interpretation. It is postulated that the limits of it are well framed through the areas depicted through names.

The today's picture along the Ammoudaraki – Plakota lineament, is that of a steep scarp, juxtaposing high elevation intermediate to acid composition flows, subvolcanic intrusions and pyroclastic lithologies of the northern sector, to low elevation acid in composition subvolcanic intrusives (rhyolite, dacites- rhyodacites) and pyroclastics of the southern sector. It presents an approximate downthrown in the range of 70 - 90m to the north, which contrasts with the present at the southern part E-W lineament, which affected the Neogene sedimentary cover, and dips to the south.

Out of the above mentioned main (“generalized”) tectonic lines configuration, there are some prominent structural directions, which are very characteristic and appear to reflect the regional tectonics on the island as well as the major control on the emplacement of the magmas. These directions are the N20°E (20°), N80°E (80°), the N40°W (140°) and the N65°W (115°). Between them the N40°W structure defines Milos bay and has been a major control for the emplacement of the Dado magmas. The N80°E structures are mainly exposed, at the southern sector, in the Neogene sediments, as a series of faults stepping the section down to the south, while to the East creates a graben structure inside the basement unit which is filled by pyroclastics (Profitis Ilias ignimbrite). The N65°W structural zone steps down to the N in a series of parallel faults which separate the Profitis Ilias ignimbrites in a serie of segments dipping to the S and SW.

The N20°E together with N-S striking directions seems that favoured the upwelling of the magmas as many of the domes and hydrothermal vents / craters are aligned along these trends (fig.31).

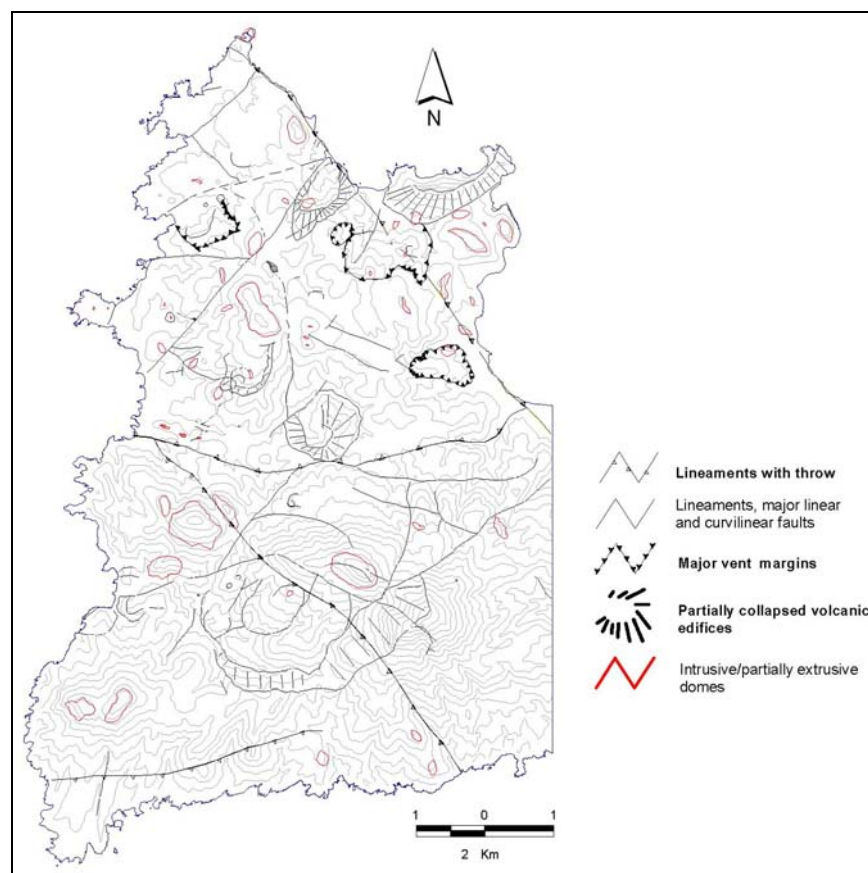


Fig. 31 : The distribution of the intrusive/partially extrusive dome bodies in between the lineament and major vent/crater structures at W. Milos.

The N20°E structures the most characteristic of which cut across the collapsed Kondaros volcano, confirms the above mentioned consideration (fig. 31a).

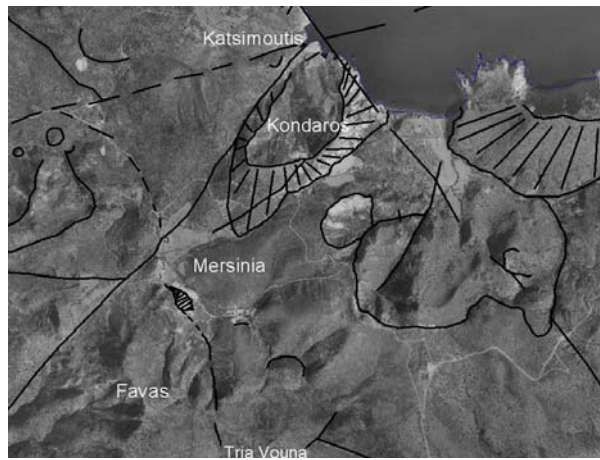


Fig. 31a : A zoom on the Kondaros collapsed volcano which is truncated by the N20°E lineament (Triades-Katsimoutis lineament).

As a final consideration, in the above mentioned tectonic configuration, it would be also worth to show the exact location of the two main magmatic-hydrothermal outflow domains, the breccias one (at the northern sector) and the veins domain (at the southern one). These domains represent the expression of the “driving through tectonics” of the hydrothermal mineralizing solutions at western Milos (fig. 32).

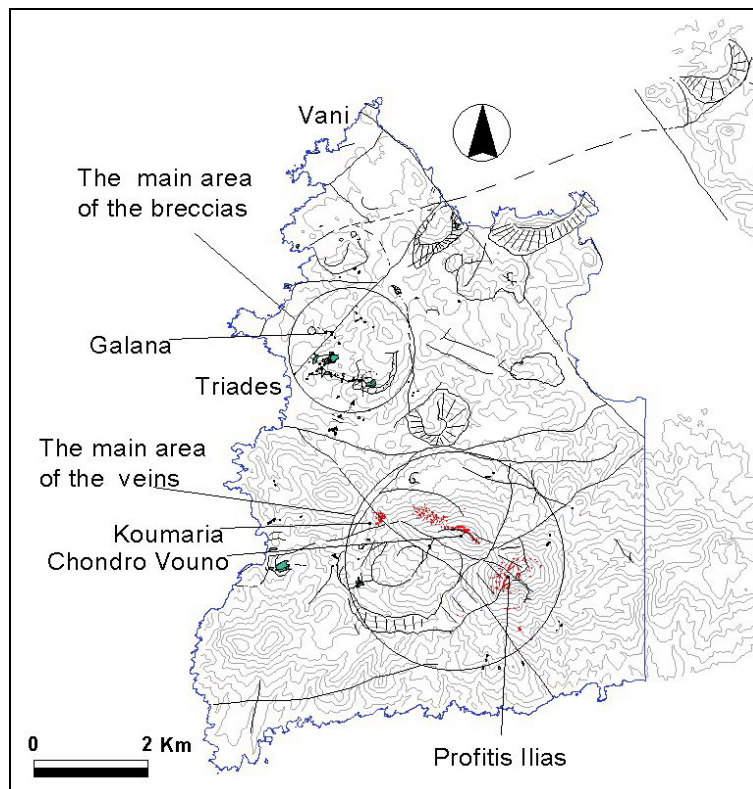


Fig. 32 The two main magmatic-hydrothermal outflow domains at W. Milos.

4.3. The GIS approach to the identification and drawing of the main tectonic features

A 3D Digital Elevation Model (DEM) based terrain modelling (fig. 33a) constructed after digitizing 1:12.500 scale topography maps 'contour lines (4m contour intervals), of S&B property, was the base for to create a shaded relief model using the Arcview software programme (v. 3.2) with its extensions 3D Analyst and Spatial Analyst (ESRI corporation-USA),(fig. 33b).

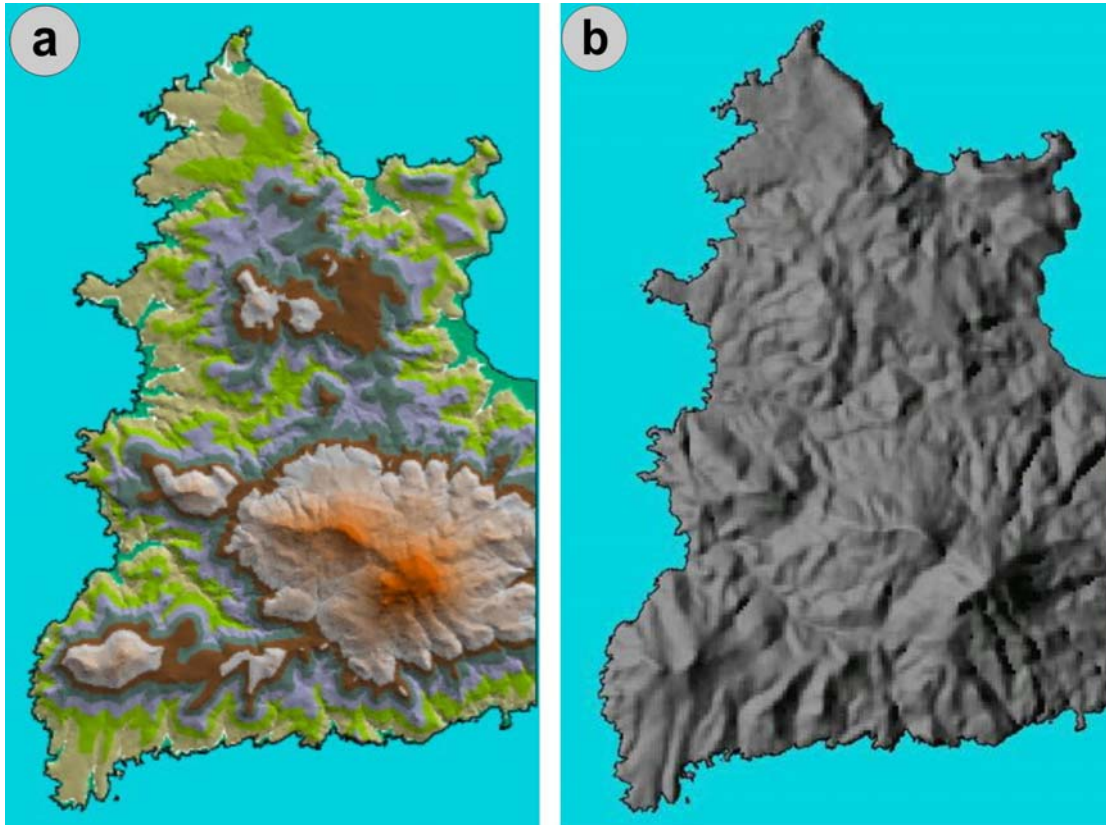


Fig. 33 : (a) 3D digital elevation model (DEM) based terrain modelling; (b) shaded relief model after the DEM using computational techniques.

This (shaded relief) model, which shows the terrain under a user-defined light source direction artificial illumination (in this case with azimuth : 290° , height : 45m) is nothing else than a 3D solid picture emphasizing (fig. 33b) the bright sides and shadows and thus depicting very well the big linear discontinuities as well as the circular and arcuate structures. The comparison of the DEM model with that of the shaded relief gave the first tectonic output through a series of selfmade observations and computational techniques, always using the Arcview software. In a second step a georeferenced Spot satellite image of W. Milos (fig. 34a -of S&B/MIDAS property) together with a series of 1:12,5k scale airphotos (of S&B property), which have been scanned and georeferenced first, have been then dropped on the DEM model becoming thus 3D images (fig. 34b).Through this combination was possible to localize once more very well the linear and circular features corresponding to important big fault lines, and to vent areas/collapse structures, as well as to resurgent or collapsed dome areas, respectively. As a final step, the comparison and

putting together of all of the 3D models produced in different ways, has given the final, linear and circular features, pattern (fig. 37).

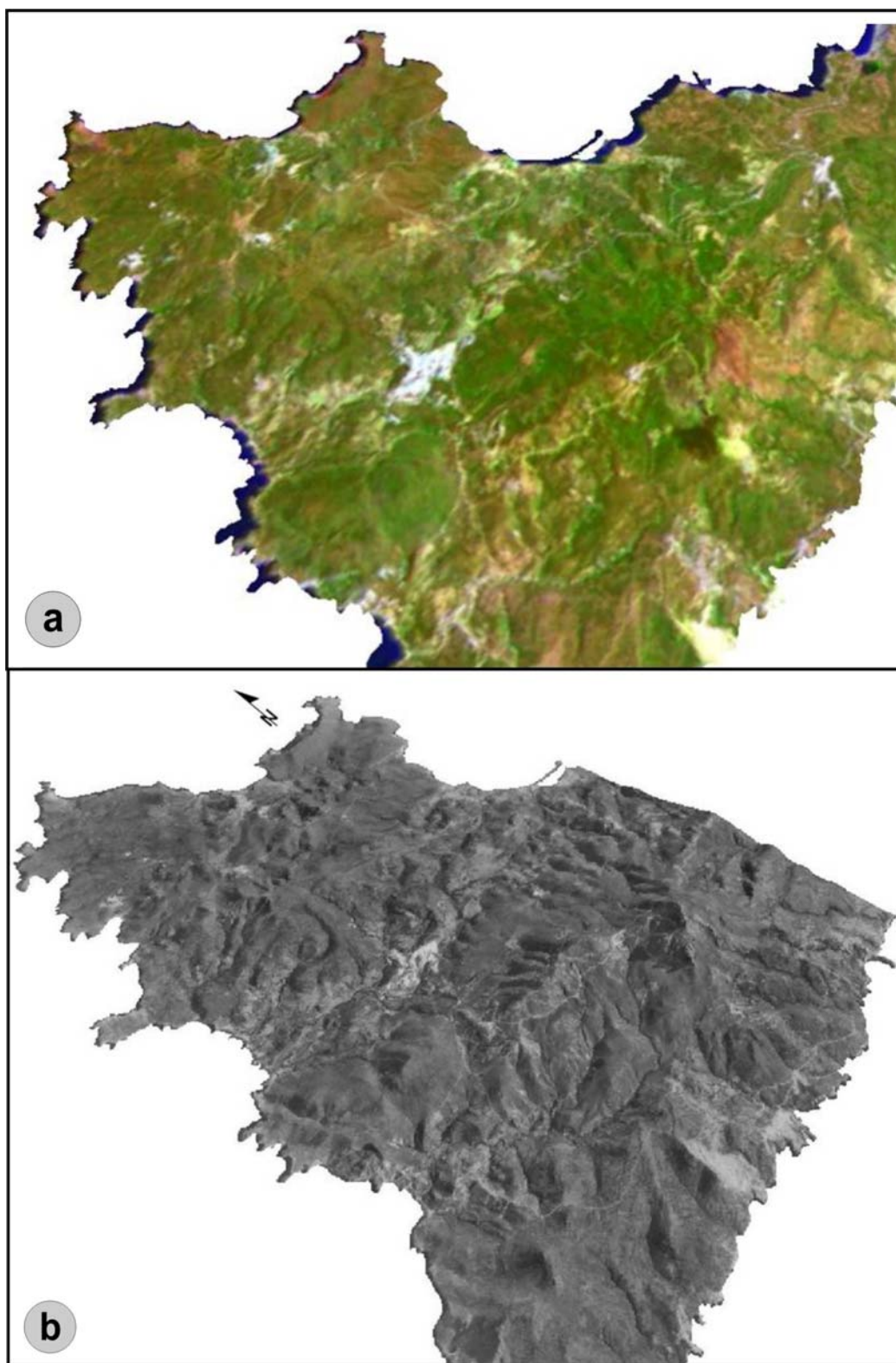


Fig. 34 : (a) a 3D satellite Spot image of western Milos (b) 3D image of W. Milos after 1:12,5k scale air photos.

4.4. The linear and circular features

As it was said previously, through the elaboration of a satellite Spot imagery and a series of 1:12,5k scale resolution airphotos of the area, was possible to reconstruct some how the paleo-tectonic and paleo-volcanic environments.

Circular structures of various diameters, from 0.5 to ~1,5 Km are considered to be related to volcanism. Of course no any visible circular feature at the air photos was a caldera or a vent because it is well known that also volcanic doming either flow breccias of various nature are also arcuate and reproduce this “circular effect”.

In the previously seen fig. 34a,b, it is possible for anybody to look and distinguish a series of linear and circular features which correspond, the firsts to major important faults, generally of regional significance, and the seconds to phreatic/phreatomagmatic eruption craters, either to volcanic edifices as well as to volcanic doming(e.g., that one at Ralaki, in the near of Triades, where these volcanic structures were important centers of both pyroclastic submarine emission after subvolcanic domes, and of a later gas venting).In the volcanic terrains arcuate collapse structures and nested venting areas, after phreatic / phreatomagmatic activity, are very common, as well as andesitic to dacitic-rhyodacitic flow-dome complexes aligned along arcuate, generally collapse structures (e.g. Triades).

There have been also other smaller structures, at W. milos, which are considered to be common features of shallow submarine hot spring lake systems, as that ones identified at Agathia and Mersinia.

For two major circular to semicircular/arcuate structures, and/or arcuate fragments composing them, very well visible on all of the available imagery seen so far, one caldera collapse feature (already mentioned before), is postulated for that one shown at the northern (upper) part of the image(fig. 35), and a partially collapsed (lower part), volcanic edifice (the Profitis Ilias edifice) structure, is assumed for the other, into which a series of domes, breccias have been emplaced.

These features except the fact that were situated mainly in tectonically “disturbed” zones

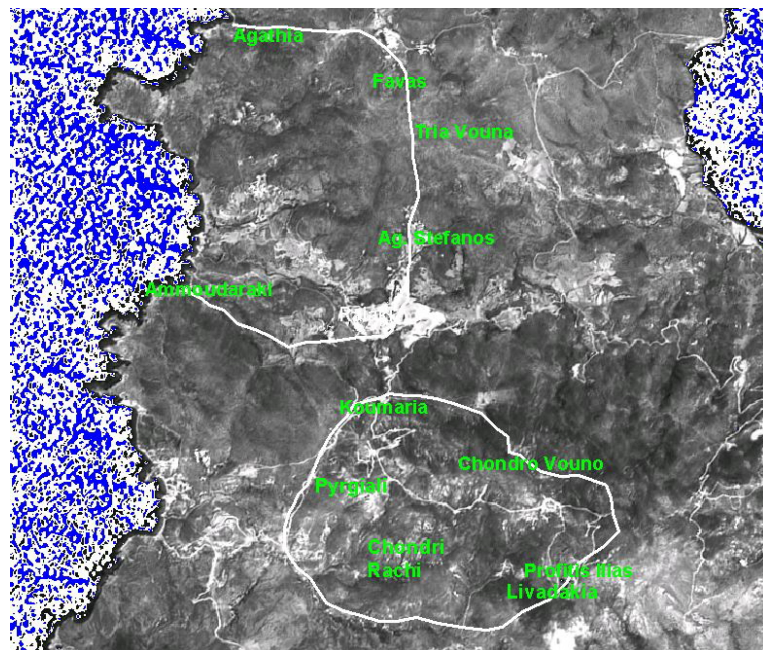


Fig. 35 : Two very well visible circular features at W. Milos (for details see text).

(key structural zones), conceptually provided also very valuable criteria in exploring for mineralized zones.

After the air-photos interpretation and field checking of the designed structures it has been produced a “structural frame” which it is considered to reconstruct and reproduce very accurately the paleo-tectonism and related volcanic activity.

4.5. Drainage considerations

In the fig. 36, it is very well depicted the relationship between the main volcanic and tectonic features from one side, and the drainage network system from the other. Indeed as it can be seen in the fig. 36, classical radial drainage pattern normally associated with the volcanic vent areas is present around the main volcanoes/vent areas of W. Milos (e.g., Profitis Ilias volcano (main circular feature at the southern sector), either around large domes (e.g., Favas dome, at the Northern sector (for location names see fig. 14) . Locally parallel running streams could indicate a tilted block, and thus the presence of a listric normal fault, orientated perpendicular to the flow direction of these streams, while strike-slip fault zones show commonly up-lining of depressions.

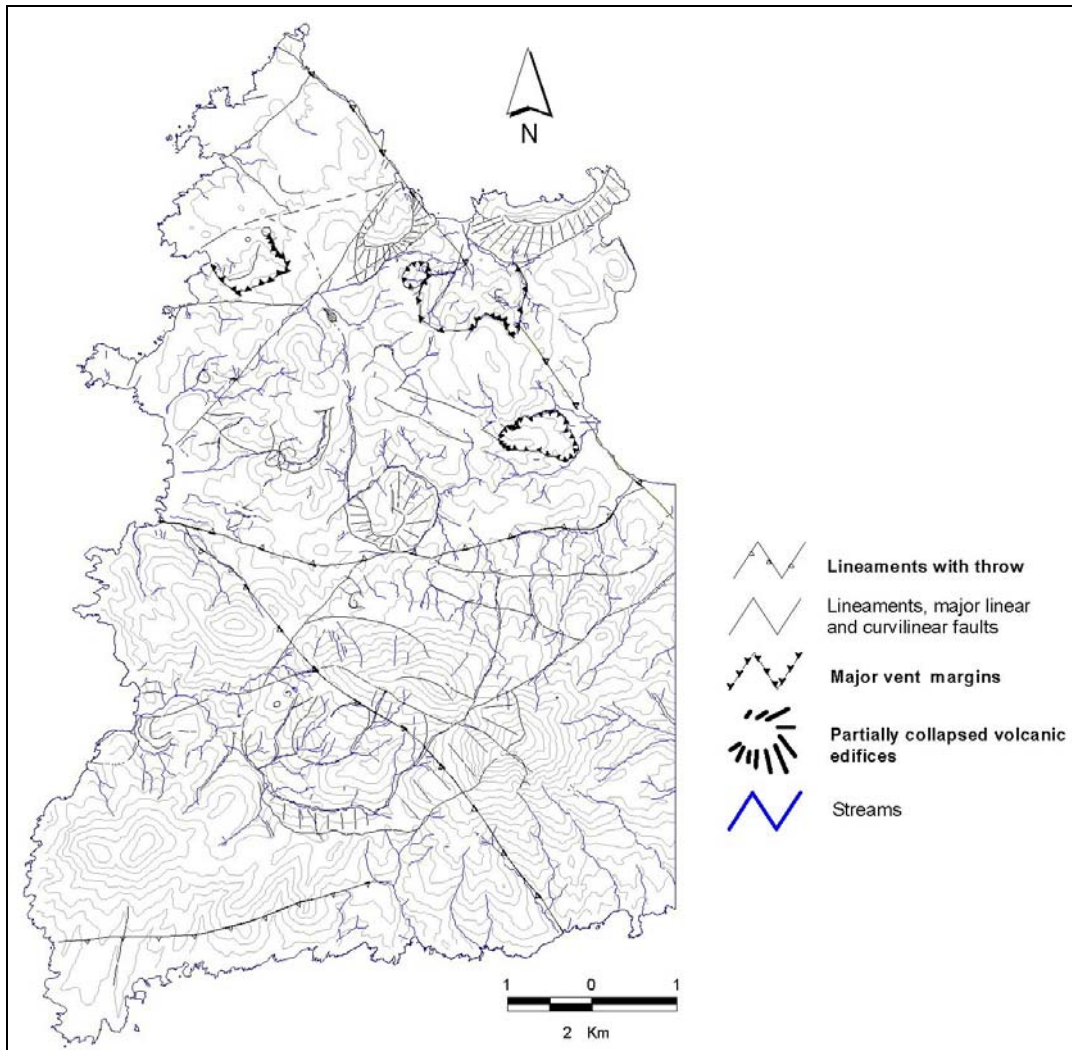


Fig. 36 : Relationships between tectonic elements and drainage patterns at western Milos.

4.6. Conclusive remarks

The multitude of NE-trending lineaments at western Milos is suggestive of directed extension/strike-slip movements. From the other side the NW-trending lineaments cross-cut the NE-trending ones. Possibly all these lineaments initially formed in response to extensional movements and were later reactivated by strike-slip movements.

In a particular manner, the NW normal faults (arc parallel normal faults) constitute prominent features in the western part of the island, and some of them, as for example that one which extends along the edge of Milos gulf, cross it for its entire length, and focus the sites of several subvolcanic dome structures the most of which are also mineralized (e.g. Kondaros, Vani).

In any case, it is postulated that minor but repeated movements on the lineaments would have provided recurring pathways for circulating geothermal waters above and adjacent to active subvolcanic domes.

Such tectonic elaboration, as that one in this work, was also helpful in better identify and study the relationships between the big lineaments and the subvolcanic/breccia bodies, in order to possibly reconstruct the volcano-tectonic processes which have taken place as well as the stratigraphic position and the spatial distribution of the various pyroclastic sequences which characterized western Milos.

As it is very well known, major linear features have long been used as guides to the regional search for ore deposits as some of them represent zones of weakness through which mineralizing fluids may be directed and deposited.

4.7. Summary

An intense extensional faulting is the dominant feature on the whole Milos and thus, on the whole western Milos area (Fytikas 1977, 1989). It is believed that two approximately orthogonal fault sets (the first one with NW-SE and NE-SW directions and the second one with N-S and E-W directions) have influenced rock distribution (by localizing rising magmas), (fig. 37) and hydrothermal mineralization. In such a tectonic regime the most "open" structures correspond to those whose planes show the same direction as that of the maximum stress.

The structural elements interpreted and designed from the satellite Spot image and the air-photos, together with the main geological elements related to explosive volcanism and doming resulted in an effective final representation of the whole western Milos, where a very good compatibility between the geological/volcanic and tectonic/volcanic elements has been achieved.

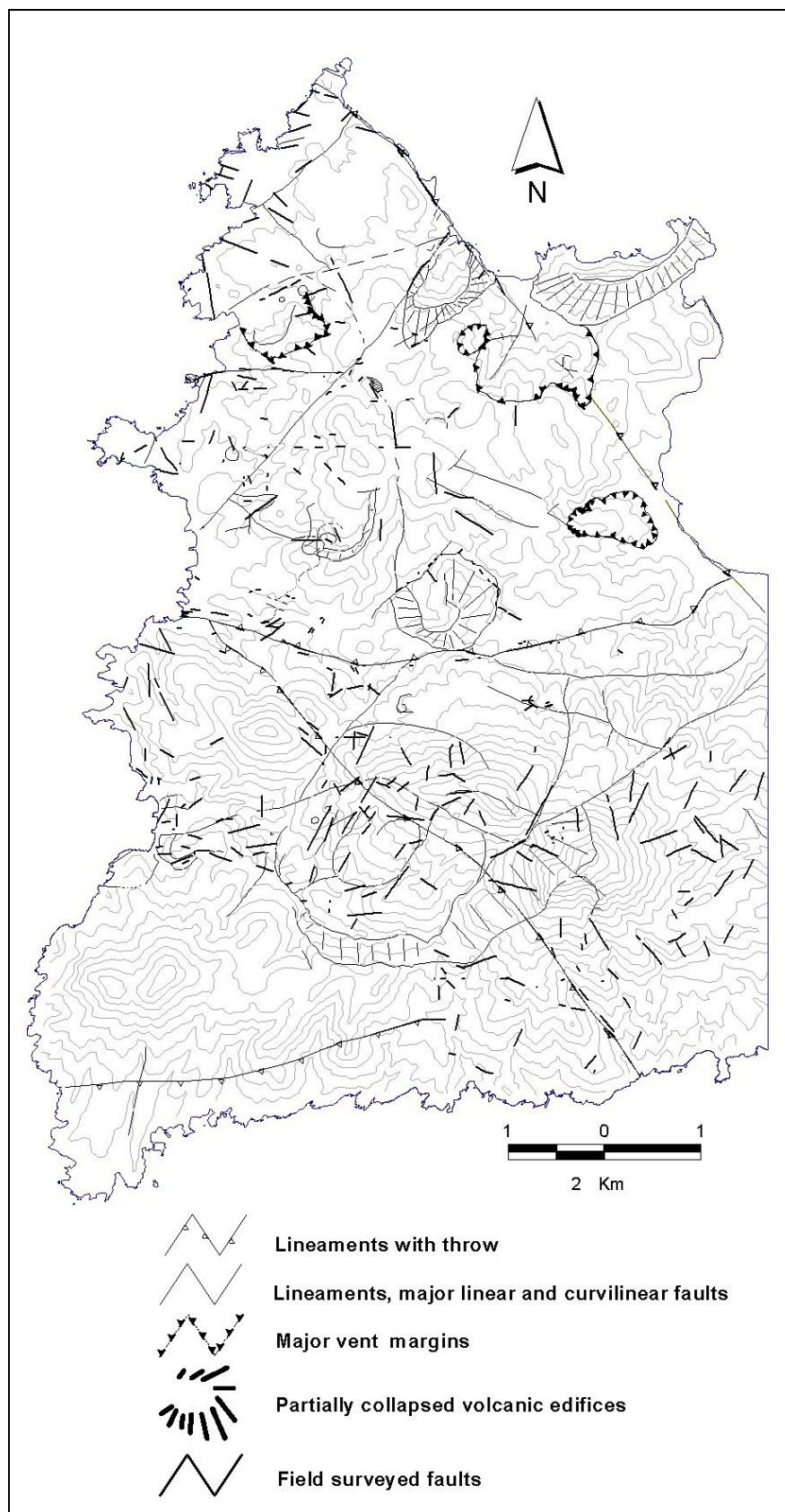


Fig. 37 : The dominant structural features of western Milos as deduced from airborne imagery interpretation and field surveying.

5. ALTERATION FEATURES OF THE INVESTIGATED AREA

5.1. Introduction

The alteration patterns observed at western Milos correspond at least to two distinct and overlapped environments, namely the volcanic-hydrothermal and geothermal environments as described by Henley & Ellis (1983) and Hedenquist & Lowenstern (1994).

The first environment corresponds to the so-called high sulfidation (HS) mineralizing system, and the second one to the intermediate sulfidation (IS) system. The two systems are well described through the alteration maps of figs. 38 to 41.

The purpose in constructing maps of the alteration mineralogy was (1) to characterize the clays in terms of their mineralogy, (2) to determine their spatial and geologic distribution within the various formations, and especially within the mineralized areas (breccias/veins) and (3) to use their characterization and distribution to gain information about the physico-chemical conditions of argillic alteration at W. Milos.

Alteration minerals are stable over limited temperature and/or pH ranges (Reyes 1990), and thus they provide information to reconstruct the thermal and geochemical structure, as well as the hydrology of the extinct (fossilized) hydrothermal system.

A continuous magma supply and storage in relatively shallow magma reservoirs, as those in Milos Island (Fytikas et al. 1986), provided the required heat for the development of a convective hydrothermal (geothermal) system. Ascending fluids changed the initial chemistry of the primary magmatic minerals and undergone themselves too, important physico-chemical changes that affected their capacity to transport metals.

It is world-wide recognized, that acid sulfate fluids related to the degassing of magma and condensation or disproportionation of volatiles (Giggenbach et al. 1990), predominate in early vapour-dominated regimes in stratovolcano edifices, and they produce hypogene acid-leached mineral assemblages at the so-called magmatic-hydrothermal environment.

5.2. The alteration mapping

In order to better understand and localize/delineate the various alteration zones at western Milos, a series of successive approaches in creating, more detailed at each step, alteration maps has taken place. The first approach has been implemented through mapping the different degrees of alteration intensities for argillization and silicification patterns.

At fig.38 an argillic alteration pattern, expressed as “degree of argillization” has been created.

What it has been seen first, was two intense argillic alteration areas (green colour), having somehow an arcuate shape and trending along ENE to NE directions. They are surrounded by a moderate to strong argillic alteration (magenta colour), which as a whole gives the impression of two “corridor”- like structures, one at the central part of western Milos and the other at the southern part, into which several coalescing and generally fresh to slightly altered domes have been emplaced. Although that, it should be said that some kind of zonation has also been observed, one at the northern and the other at the southern geographic areas of western Milos, which seems also to be somehow independent from each other.

In a successive step, in order to better match any vent/outflow center to the previously mapped argillic alteration, the degree of silicification has been introduced (fig. 39). As it can be seen from figure 39, except the previously recognized NE trend for the argillization degree, and now also seen for the silicification one (which also has somehow an arcuate shape),

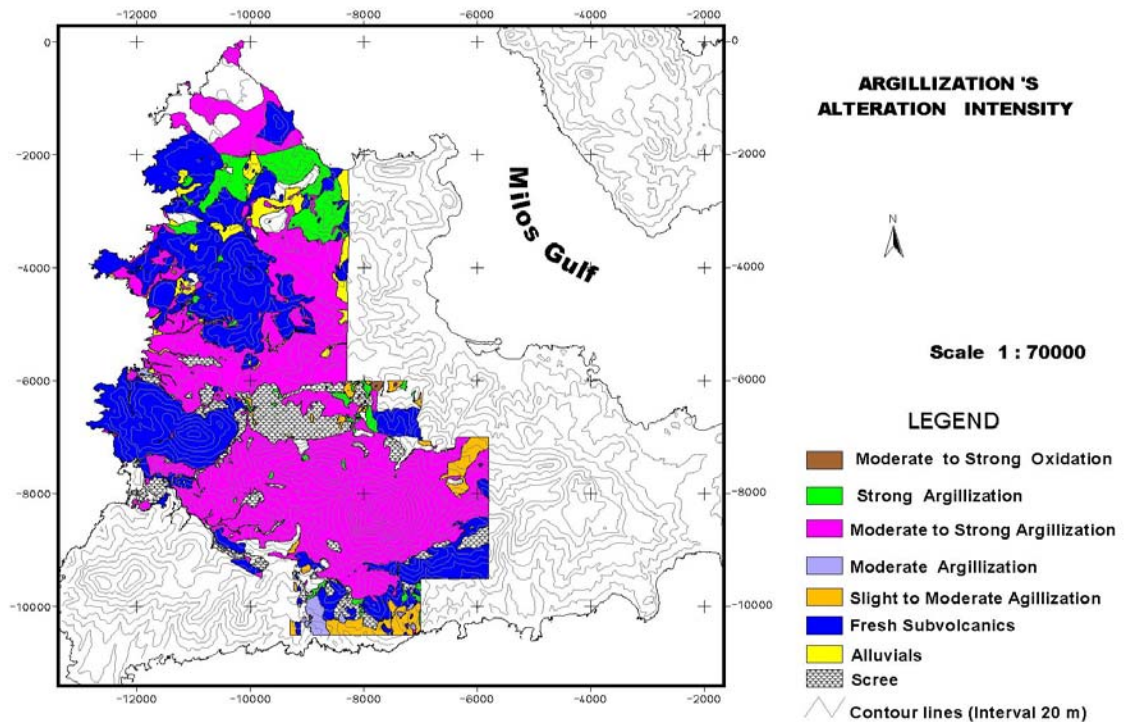


Fig. 38 : The argillization intensity patterns of the investigated area at W. Milos.

there are visible another two sites which present a strong degree of silicification, and strike along E-W to NE directions. It seems that these trends are most probably related to important faults/lineaments, which cross throughout western Milos and are somehow subparallel to each other.

The second approach towards identifying the alteration zones in detail has been implemented through sampling the previous defined zones, and identifying their mineralogical composition by X-ray diffraction analysis (XRD) in the Institute of Mineralogy and Petrology Hamburg University, S&B Industrial Minerals S.A.-Athens), and by optical microscopy as well as by electron microprobe analyses in the Institute of Mineralogy and Petrology, Hamburg University.

Based on that, an initial alteration location map (fig. 40), and a well-drawn alteration zonation map (fig. 41), after 320 X-ray diffraction analysis, have been created, showing the trend and the shape of the various alteration zones (massive to vuggy silica, advanced argillic, argillic, phyllic, adularia-sericite, propylitic, steam-heated advanced argillic), as defined based on their relative content in specific minerals. Under this point of view it seems that there is a well-defined concentric attitude of the alteration zones, grading from a massive to vuggy silica center, to an advanced argillic alteration zone (alunite-kaolinite-quartz± dickite± pyrophyllite± diaspore± amorphous clay, halite), to an argillic alteration zone (illite+kaolinite ± smectite± sericite), then to a phyllic zone (quartz-sericite-pyrite) at the northern part of W. Milos, while adularia-sericite centres surrounded by argillic and then by propylitic (quartz, albite, chlorite, smectite, pyrite, carbonates) alteration zones, are located on both southern and northern parts of W. Milos.

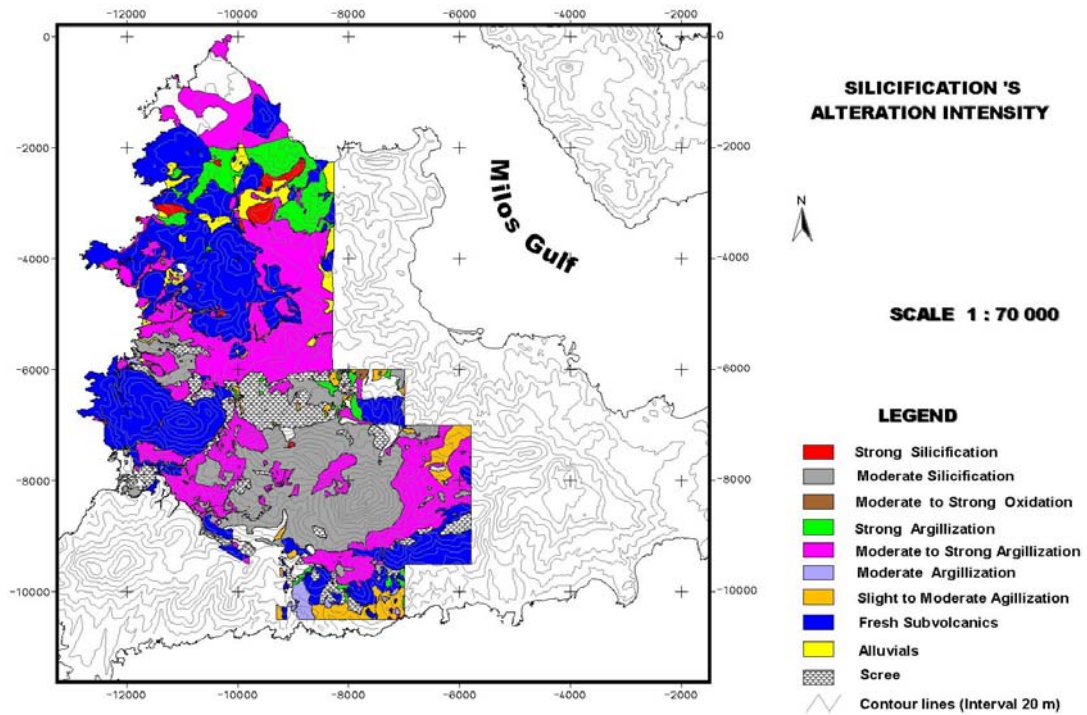


Fig. 39 : The silicification intensity patterns of the investigated area at western Milos

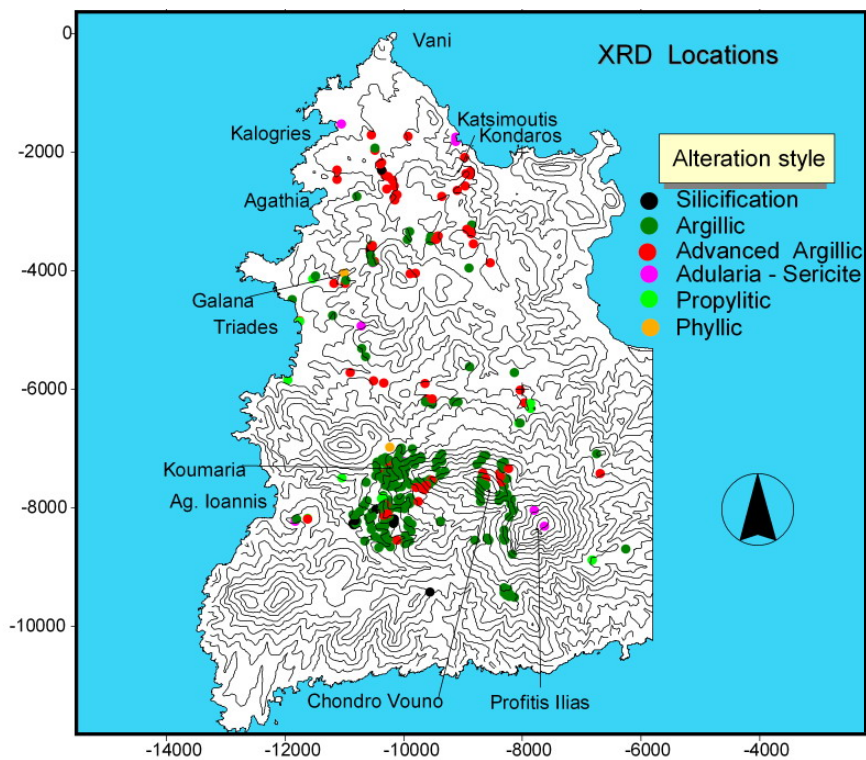


Fig. 40 : Alteration style as obtained after XRD analysis of the samples taken at W. Milos

The alteration pattern observed at Fourkovouni area on the eastern part of Milos (fig. 41), it is considered to be the continuation to the E-NE of the well framed and strongly altered area at the N part of western Milos.

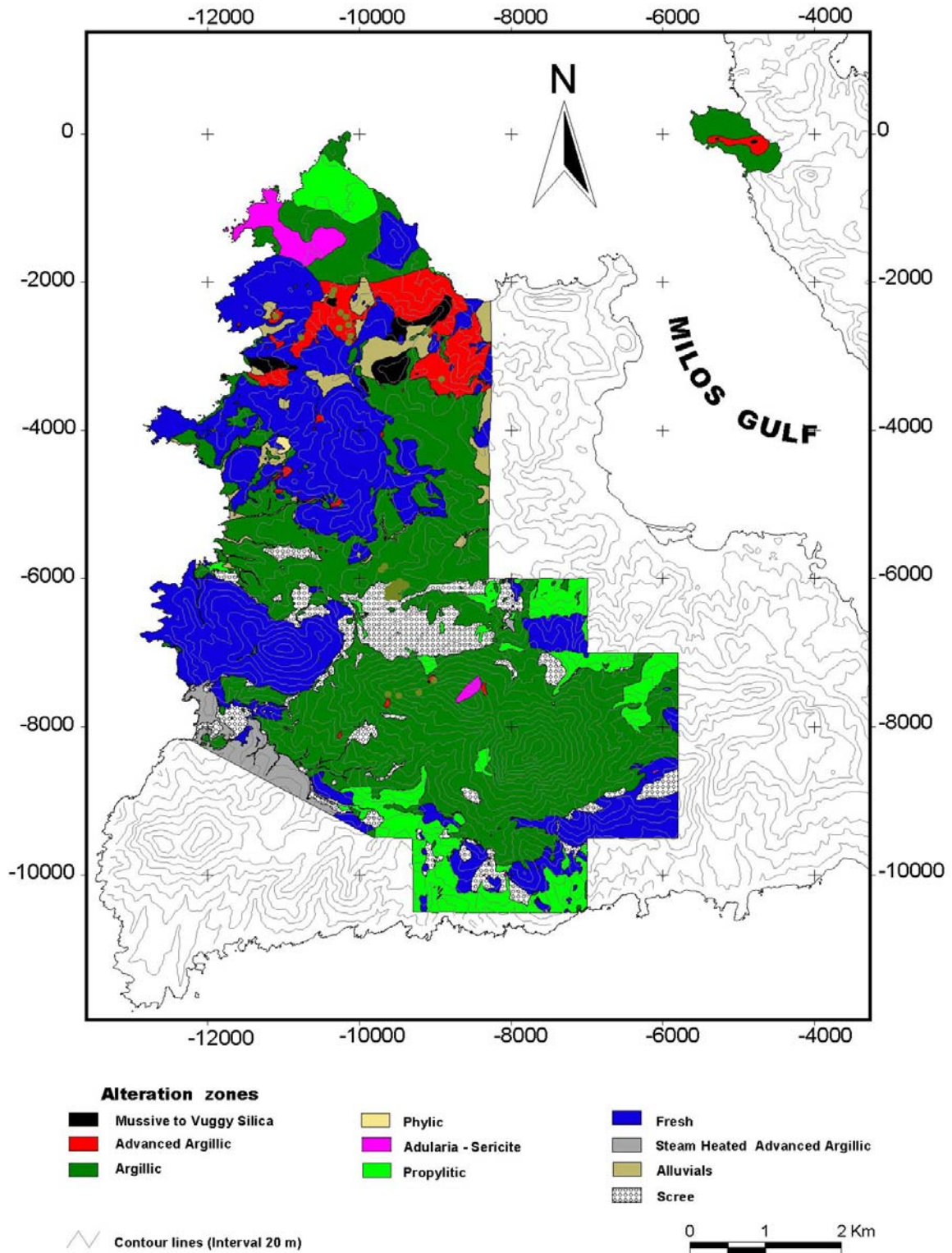


Fig. 41 : Surface distribution of alterations zones at western Milos area.

The third approach undertaken was related to the recognition and identification of spatial alteration patterns by applying remote sensing techniques. In that sense, remote sensing provided information on the surface properties of several exploration targets and helped in mapping alteration zonations. Especially through the use of broadband sensors available, such as the Landsat Thematic Mapper (TM) and the SPOT ones, it was possible to discriminate between silicified and clay altered lithologies.

On this purpose several satellite images, e.g. Landsat5 TM (multispectral bands 1-5, thermal infrared band 6), Landsat7 TM (multispectral bands 1-5,7, thermal infrared bands 6 and 9, and panchromatic band 8) with different acquisition dates (during 1987, 1999 and 2001) have been downloaded from the internet, while a Spot type image was acquired from the French Geological survey (BRGM) through an initial joint venture that took place between Silver and Baryte ores mining Co (S&B) and BRGM. All of them have been processed through appropriate image processing softwares (Imagine software of the ERDAS Corporation-USA, and Image Analysis software of the ESRI-ERDAS joint Corporations). The objective of this work was to define areas of anomalous spectral compositions and associate them with mineralizing centres. Indeed some specific ratio bands are worldwide used for to distinguish the various alteration minerals present. In that sense, the TM ratio 5/7 distinguishes altered rocks containing clays and alunite from unaltered rocks. Both rocks have similar values in band 5, the reflectance of unaltered rocks in band 7 is similar to that in band 5, therefore the 5/7 ratio for unaltered rocks is unity. The iron minerals have low blue reflectance TM band 1 and high red reflectance TM band 3. Iron-stained hydrothermally altered rocks therefore have high values in a 3/1 ratio image. Colour composite ratio images are produced by combining three ratio images in blue, green, and red (ratios L3/L5, L3/L1, and L5/L7 in red, green, and blue, respect tively). An advantage of the colour ratio image is that it combines the distribution patterns of both iron minerals and hydrothermal clays.

Although manual image interpretation was valuable and provided highly detailed and accurate information, some automatic interpretations using computer algorithms, took also place.

In the above sense, samples collected in the field and analysed by XRD, have been located through the use of their reference coordinates on the satellite image. Multispectral classification is a computer routine for information extraction that assigns pixels into classes based on similar spectral properties. In a supervised multispectral classification, the operator specifies the classes that will be used. In an unsupervised multispectral classification, the computer specifies the classes that will be used. Through the so called "supervised classification" the computer algorithm examined the properties of these areas and then seeked for similar regions throughout the image. In such a way the identification of the alteration areas has been aided with in situ data and by manual image interpretation.

In terms of digital spectral analysis, image classifications was possible to be performed because of the resolution of the images (between 15 and 30m), which essentially permitted to pinpoint alteration anomalies as small as 30 meters.

Both "guided" and "unguided" ways of processing of the satellite imagery was performed and the results can be visualized at the fig. 42 a,b,c,d.

In the first Landsat processed satellite image (Fig.42a), the hydrothermal composite image has been obtained using the band ratios L5/L7, L3/L1, L4/L3. In this image in orange + light green are well defined the argillic and advanced argillic zone, which also are well visible and defined in white colour at the Spot image (fig.42b) and in pink at the "guided" through the use of XRD field data Landsat image (fig.42d). Furthermore it is interesting to

note that in the “guided” image (Fig.42d) the light green colour defines silicified zones, while the yellow colour defines mixed silicified and argillized zones. Similarly, in the “guided” image (fig.42c) the green colour defines all the degrees of the argillic alteration, from the slight one to the strong argillization. Finally it is interesting to note how in the first Landsat image (fig.42a), the argillization patterns delineate very well the various tectonic lineaments and other fault related features (fig. 43).

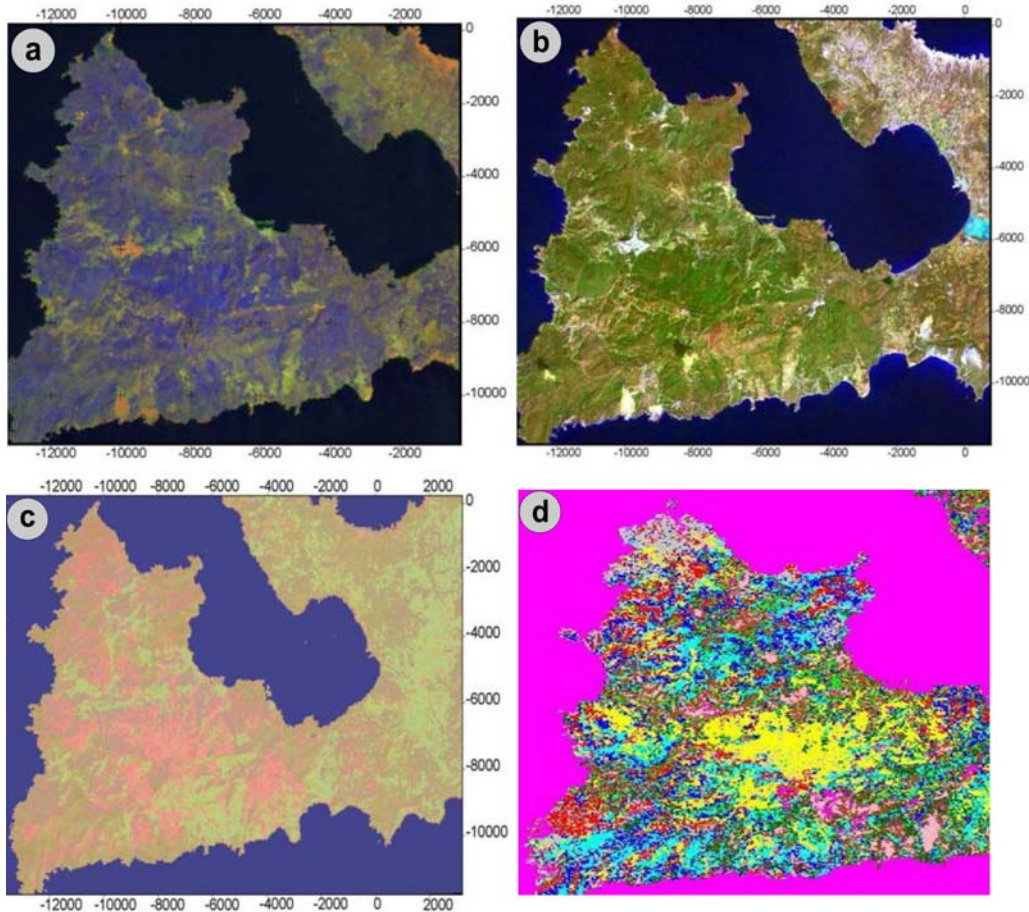


Fig. 42 : Satellite images, from left to right : (a) Landsat hydrothermal composite product; (b) Spot pseudocolours; (c) and (d) ”Guided” Landsat after Xrd field data, using two different algorithms.

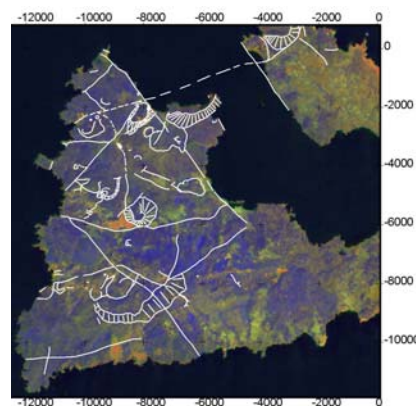


Fig. 43 : The spatial and genetic relationships between main tectonic lineaments and alteration patterns at W. Milos as shown through a processed Landsat image.

5.3. The alteration zones

As previously mentioned, alteration mapping (fig. 41) and XRD qualification (fig. 40), have established a sequence of specific alteration zones, which are the recipients of intense hydrothermal alteration and are also considered to host ore deposits and mineralization across the area.

The various alteration zones belong, to two different environments/systems which are also mineralized. The first one (high sulfidation system) is related to highly oxidized hydrothermal fluids (magmatic-hydrothermal environment), while the second one (inter-mediate sulfidation system) to slightly acid-alkaline ones (geothermal environment).

The high sulfidation system (HS)

Acid-sulfate alteration can be produced in three different environments: a magmatic-steam environment, which is dominated by a rapidly ascending vapor phase of magmatic origin; a magmatic-hydrothermal environment, characterized by condensation and disproportionation of magmatic gases, and displays significant magmatic components in the hydrothermal fluids; and a steam-heated environment, which occurs in the upper portions of hydrothermal (geothermal) systems (Rye et al., 1992). As a whole, high sulfidation systems can result from fluids rapidly channelled directly from a hot magma along faults and can produce all three types of acid-sulfate alteration during their lifespan.

The intermediate sulfidation system (IS)

An intermediate sulfidation system is characterized by alteration styles, which correspond to those from a geothermal system(s) and contain fluids reacting slowly and repetitively with the host rocks after being mixed and diluted in various degrees with meteoric-, connate- and/or sea-waters (Bogie et al. 2006). They generally have a layered configuration reflecting zones of different chemistry. The shallowest zone is frequently acid, steam-heated, and connected to the source fluid at depths.

The various alteration zones are described and commented below:

5.3.1. The Silicic alteration zone

The silicic alteration occurs in two distinct styles, i.e., as a residual and massive silicification, which resulted through acid-leaching of pre-existing rocks, silicate destruction and ion depletion (vuggy silica), and as a silicification caused by the deposition of mobilized silica where takes the form of crusts and impregnations (silica flooding).

5.3.1.1. Massive to Vuggy Silica

In this alteration zone fine-grained quartz is the principal and quasi the unique constituent of the rock (massive silica rock). The vuggy silica consists of porous masses with a spongy appearance (see next chapter 6). In the vuggy silica variety quartz replaces the groundmass of the original rock and the vugs belong to the original phenocrysts of the volcanics or of the clasts into the pyroclastic rocks. In this style of silicification, locally relict rutile grains have been identified. Euhedral to subhedral pyrite grains are disseminated locally and/or oxidized into the vuggy and massive quartz rocks.

Generally speaking, within the large silicified masses, the vuggy quartz areas occur as irregular local masses either centrally located or near the margins of the quartz-alunite zone. From the other side, it seems that the massive silica bodies, which are the products of local quartz/silica introduction, form somehow discontinuous silica caps above quartz-alunite and/or vuggy quartz zones (see next chapter 6). Locally, the massive nature of the silica may in part reflect the massive nature of the original rock, as well as in part, the late-stage deposition of hydrothermal silica that filled initial voids and fractures (e.g. Kondaros, Agathia). Massive silicification may form in an environment dominated by acid fluids in the case that these fluids become saturated with silica as a result of acid leaching, and deposit silica during cooling or neutralization (Fournier 1985). Cooling or neutralization may occur at a water table or aquifer.

In a broader sense intense silicification in the area is associated and occurs mainly in brecciated zones, adjacent to linear and/or circular structures (fig.44a), around veins and stockworks, as well as lenses within pervasively replaced tuffs or tuffaceous units. The peripheral part of the silicified zone tends to be weakly silicified and is marked by various colors of white, reddish-purple, yellowish-brown. The rock is porous to compact and is mineralogically similar to the highly silicified part.

5.3.1.2. Silica flooding

Silicification is also manifested as erosion-resistant hills (Galana, Skiadi, Chondro Vouno, Profitis Ilias) associated with structurally controlled quartz veinlets and veins. Silicification occurred as numerous events, the earliest possibly being small quartz veinlets followed by several silica flooding events, along with at least two quartz-barite veining stages.

The layered silica, like that occurring in the area of Favas (see next chapter 6), at Mavrovouni and in Koumaria is different from siliceous sinters and most probably corresponds to a deposition around outflow venting zones (on the bottom), located into submarine acid lakes.

Several subaerial and submarine sinters (silica cap styles of silicification) have been recognized at the northern and southern parts of western Milos (Agathia-Vani, Kondaros-Mersinia-Anemophysima-Xerokampos, Agathia, Ralaki and Koumaria-Gournes-Agios Ioannis) (fig.44b). The presence of this late stage (and upper level) deposition of hydrothermal silica, has contributed substantially to the reconstruction of the paleo-environment of these sectors, as well as to the better understanding the dynamics of the fossil geothermal system(s) and the mineralizing processes in western Milos. At Kondaros-Anemophysima-Xerokampos the sinter is siliceous and locally subaerial as evidenced by locally preserved desiccation cracks (see next chapter 6), (fossilized mud pool), while at Kondaros-Mersinia it is siliceous, submarine and mineralized (As, Sb). At Agathia the sinters are silica-manganiferous and considered to be deposited in a submarine environment. In other areas (e.g. Ralaki) the sinter include yellow-orange chalcedonic silica and show locally thin horizontal banding with desiccation cracks (suggesting temporary emergence), being interlayered with strongly argillized (kaolinized mainly) tuffs overlain advanced argillic altered (kaolinite-alunite-dickite-diaspore-halite) dacitic-rhyolitic dome/flow dome complexes.

Concerning the big boulders in the area of Pyrgiali they are considered to be the remnants of a silicified cap that has been truncated by a later explosive event of phreatic or phreatomagmatic nature.

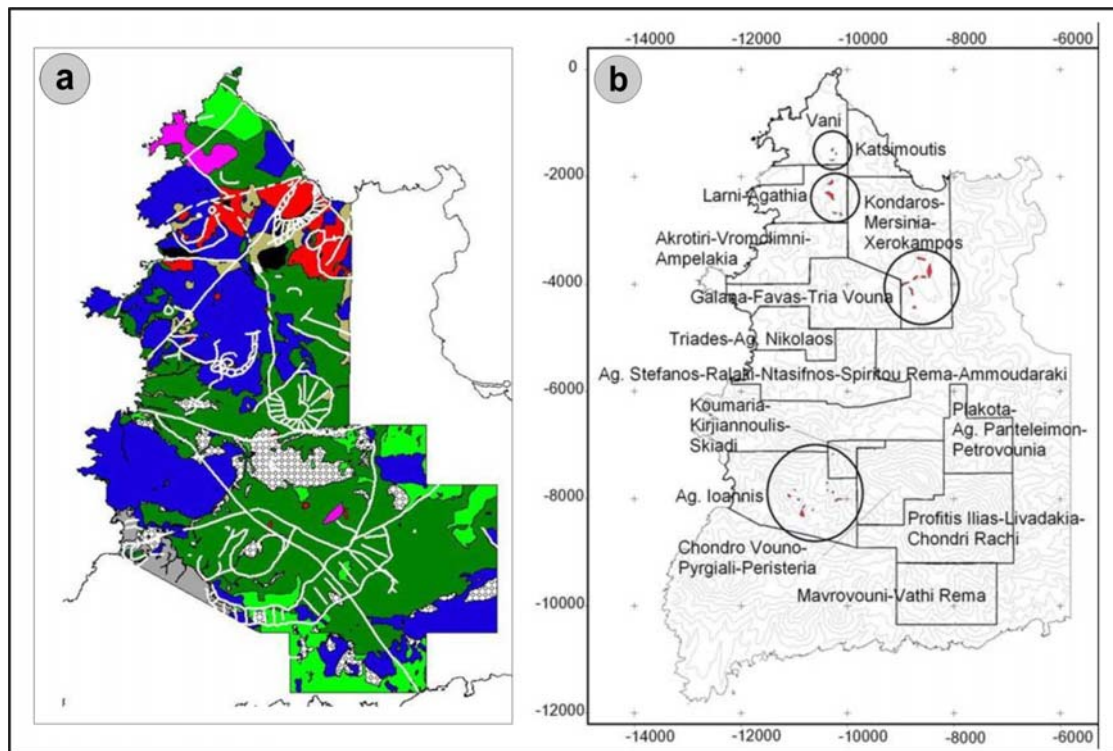


Fig. 44 : (a) Spatial relation between tectonics and hydrothermal alteration zonation, legend as in fig.41; (b) Surface distribution of the silica caps/sinters at western Milos.

Through a virtual connecting of different areas, i.e., that of Pyrgiali, the area above Ralaki (west of Kalamavros dome) and the area above Ntasifnos it is possible to reconstruct an old silica cap area and thus it is possible to postulate that Kalamavros dome has been intruded through this silica cap.

As a whole, all these above mentioned sinter/silica cap areas are associated with faults and this shows clearly that they were silica-rich fluids pathways. In any place where silica caps/sinters have been observed, it should be emphasized that they stay, in the most of the cases, on the lower pumiceous tuff unit (Lmp) and some times only on the fine ash tuff unit (Fat).

In more it seems that locally, (e.g. silica sinter deposits at Kondaros-Anemophysima), they are aligned along main graben structures, as in this case along the main NW-SE trending graben structure of Milos gulf.

Concerning submarine sinters, it is considered that they have been created either after the mixing of hydrothermal fluids and sea water, or after steaming in submarine environment. At any case it was a rather dynamic process as it can be observed in the places where several thin opaline sinter horizons alternate with fine ash kaolinized material (e.g. Ralaki area, old kaolin mining area).

5.3.2. The Advanced argillic alteration zone (AA)

Advanced argillic alteration in western Milos, produced after acid-leaching of the volcanic rocks due to reaction with acid-sulfate and and/or chloride rich fluids, was formed in two distinct environments: the magmatic-hydrothermal or high-sulfidation environment and the steam-heated one. Minerals diagnostic of high sulfidation epithermal gold mineralization,

in areas of advanced argillic alteration, can be used to distinguish alteration produced by oxidized steam condensates from that one produced by acid magmatic volatiles in active systems. Pyrophyllite coexisting with dickite, diaspore, kaolinite and alunite at several areas in western Milos, confirms that most of the alunite is primary.

5.3.2.1. Pre-ore advanced argillic alteration of magmatic-hydrothermal origin

The earliest recognized advanced argillic alteration in western Milos is characterized by intergrowths of alunite \pm quartz \pm cristobalite, kaolinite \pm dickite \pm pyrophyllite \pm diaspore, halite and pyrite surrounding vuggy and massive silica rocks. This assemblage is considered to be of hypogene magmatic-hydrothermal origin (Rye et al. 1992; Arribas et al. 1995) and was formed prior to the brecciation of the felsic subvolcanics, i.e. before the event of their intrusion within the early acid pyroclastic series and the later sediments. It also predates the main mineralizing, (intermediate sulfidation style) event. Outcrops of hypogene advanced argillic alteration have been recognized at the northern and southern parts of western Milos (Kondaros, Agathia, Vromolimni, Favas, Ralaki and Chondro Vouno - fig. 44a, see also next chapter 6).

In the advanced argillic alteration zone quartz is found in places, replacing the original groundmass/matrix of the rock (andesite/dacite/rhyodacite or pumice tuffs), and the alunite as pseudomorphs after feldspar phenocrysts. More in detail, the groundmass/matrix of the original rocks have been changed to variable mixtures of quartz and alunite and local to opaline silica \pm rutile. Weathered quartz-alunite rocks also contain in addition jarosite and \pm limonite, as well as allophane. In thin sections irregularly interlocking quartz grains are also present. Alunite is intimately intergrown with quartz granules in the groundmass, as well as rectangular laths irregularly placed within a mosaic of quartz grains. Rarely alunite is present as irregular veinlets and stringers. Among the former phenocrysts, only the rounded and embayed quartz grains have “resisted” the hydrothermal “attach” without any apparent change. The feldspar, amphibole and biotite phenocrysts have been altered to alunite and quartz (Fig.45a,b). Within the former amphibole crystals lacy skeletons of rutile, leucoxene, and pyrite were detected. Original biotite has been altered largely to alunite, pyrite, rutile and quartz. Alunite found in veinlets generally is associated with jarosite (probably after pyrite) and dickite, kaolinite, pyrophyllite, diaspore (e.g., Kondaros

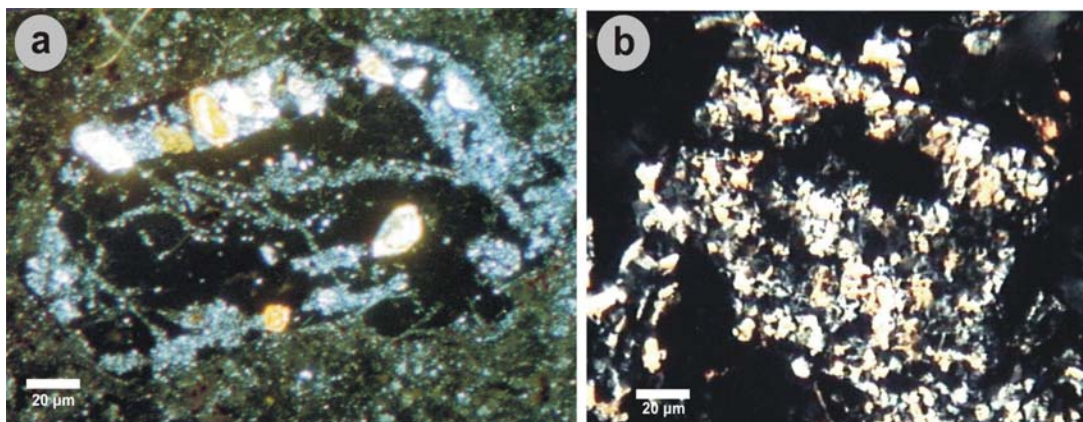


Fig. 45 : (a) Alunite and quartz, cristobalite; (b) alunite pseudomorph after feldspar phenocrysts where it is also found disseminated in the matrix (sample U36, Favas-Tria Vouna).

and Chondro Vouno), while locally it is also associated with scorodite (e.g., Profitis Ilias area-Dimou 2001). This paragenesis reinforces its hypogene magmatic-hydrothermal origin. Microprobe analyses of alunite (Table I) suggested that they represent members of the solid solutions series alunite-natroalunite. Elevated contents in Ba, Sr and Ca substituting for Na, K and P₂O₅ substituting for SO₃ are consistent with their hypogene magmatic-hydrothermal origin.

Table 1 : Representative microprobe analyses of alunite from western Milos

wt %	1	2	3	4	5	6	7	8	9
K ₂ O	4.81	7.25	4.39	1.98	0.34	1.07	0.90	1.12	8.23
Na ₂ O	3.28	1.80	3.72	4.93	6.90	6.43	6.30	6.33	0.57
FeO	0.00	0.00	0.00	0.00	0.40	0.00	0.26	0.00	0.00
Ce ₂ O ₃	0.03	0.04	0.00	0.00	0.01	0.03	0.08	0.05	0.23
CaO	0.12	0.11	0.10	0.07	0.03	0.03	0.05	0.16	0.22
BaO	0.58	0.59	0.35	0.09	0.03	0.02	0.02	0.00	2.04
SrO	0.04	0.02	0.09	0.00	0.05	0.00	0.00	0.05	0.08
Al ₂ O ₃	36.11	35.83	35.94	33.58	37.60	36.98	37.41	37.14	35.00
SO ₃	38.04	38.02	39.02	36.34	40.08	40.35	40.52	40.06	37.11
P ₂ O ₅	0.70	0.56	0.43	0.14	0.11	0.06	0.08	0.11	1.54
Total	83.77	84.27	84.09	78.30	85.60	85.24	86.19	85.04	85.14
Cations on the basis of 11 (O)									
K	0.428	0.648	0.387	0.186	0.029	0.092	0.076	0.096	0.741
Na	0.444	0.245	0.499	0.702	0.895	0.837	0.811	0.826	0.078
Ca	0.009	0.008	0.008	0.005	0.002	0.002	0.004	0.011	0.017
Ba	0.016	0.016	0.009	0.002	0.001	0.001	0.001	0.000	0.057
Sr	0.001	0.001	0.003	0.000	0.002	0.000	0.000	0.002	0.003
Ce	0.001	0.001	0.000	0.000	0.000	0.001	0.002	0.001	0.006
Al	2.970	2.960	2.930	2.901	2.966	2.927	2.928	2.950	2.913
Fe	0.000	0.000	0.000	0.000	0.022	0.000	0.015	0.000	0.000
S	1.992	2.000	2.026	2.001	2.014	2.034	2.020	2.026	1.967
P	0.041	0.033	0.025	0.009	0.006	0.004	0.004	0.006	0.092

5.3.2.2. Magmatic steam advanced argillic alteration (MS)

Another style of alunite deposition has been recognized in isolated surface exposures of cavities and vein-filling cracks at Kondaros area. This alunite is very coarse-grained (crystals up to 5cm) and clear white to pink in colour. Rare inclusions of barite and jarosite are present. The coarse-grained nature of this alunite and lack of coeval sulfides is consistent with a magmatic steam origin, as initially defined by Rye et al. (1992) on the basis of data for veins of coarsely crystalline alunite at Marysvale, Utah (Cunningham et al. 1984).

5.3.2.3. Steam-heated advanced argillic alteration (SH)

Blanket-like zones of silica minerals (cristobalite, opal, chalcedony) ± kaolinite, alunite, and native sulfur occur at the present-day surface. This alteration extends to greater depths along structures, locally crosscutting pre-ore advanced argillic and peripheral argillic as-

semblages. The tabular, near-surface distribution of this assemblage, in addition to the alteration mineralogy, is consistent with the steam-heated environment (Rye et al. 1992). Alteration is typically pervasive (e.g. Agios Ioannis area, see next chapter 6), occurring as powdery, friable masses, having substituted the original textures, which only locally are preserved. Fine-grained jarosite occurs locally as overgrowths on alunite. Textural relationships suggest that steam-heated assemblages formed after pre-ore advanced argillic alteration, are never observed in contact with alunite-pyrite-enargite bearing mineralization. Based on field observations, steam-heated alteration may have been considered, at least in part, to be coeval with intermediate-sulfidation type mineralization.

5.3.3. The Argillic alteration zone (A)

This alteration zone is mainly characterized by the presence of illite + kaolinite \pm smectite \pm sericite in weakly to moderately silicified rocks (mainly as secondary quartz in the groundmass). All of the primary phases, except for the quartz phenocrysts, are completely replaced by clay minerals. The groundmass consists of illite, kaolinite, montmorillonite and quartz, while sometimes rutile (leucoxene) is also present. From the northern side of Chondro Vouno towards Koumaria, fine ash tuffs are intensely clay altered (illitized), and seem to be a transitional phase to the silicified and gold mineralized tuffs at depth as well as above. The argillic alteration zone is marginal with respect to the hypogene quartz-alunite zone, or it occurs without any spatial relationship to advanced argillic alteration, within strongly fractured fault zones (see next chapter 6). Generally speaking, the rocks affected by argillic alteration resemble in their hardness the quartz-alunite ones, and the only difference is the clay minerals content (illite-kaolinite) occurring essentially in the place of alunite. In addition to kaolinite and illite the argillic envelopes contain abundant quartz and montmorillonite as well as minor leucoxene. Within this alteration zone, kaolinite is generally more widely distributed towards the transition to quartz-alunite zone (for ex. Triades-Galana-Kondaros, see next chapter 6) while the illite is more common in the middle part of the zone and towards the contact area with the propylitic zone (for ex. Koumaria-Chondro Vouno-Profitis Ilias).

5.3.4. The Phyllic alteration zone (Phy)

This alteration style is strongly present at Galana area and is characterized by the assemblage sericite, quartz and pyrite on both phenocrysts and groundmass. It is considered that this zone represents a transitional zone between an advanced argillic lithocap and an underlying buried porphyry system, at the northern part of western Milos.

5.3.5. The Adularia-Sericite alteration zone (Adul)

Adularia occurs in the principal upflow zones, caused by boiling (e.g. Chondro Vouno), as well as together with sericite (fig.46) bordering silicified zones near the veins (e.g. Profitis Ilias, Katsimoutis, Galana, Triades). In this last case it is surrounded by illite alteration, illite-montmorillonite (argillic alteration) and then by propylitic alteration mineral assemblages, expressing thus a progressive zonation outwards, and reflecting the concentric nature of the isotherms, as well as a progressive cooling.

In this zone plagioclase is altered to adularia and minor albite, which are variably replaced by calcite + illite. Clays are illite with minor illite-smectite. Secondary quartz is abundant

in the groundmass. Chlorite and calcite occur also in variable amounts. The presence of adularia in several places at western Milos is related to boiling processes, while adularia also represents the dominant mineralizing gangue mineral. Indeed, much of the gangue mineralogy comprising quartz and adularia formed in response to the boiling of fluids upon periodic, structurally controlled pressure release and consequently developed the characteristic banded fissure vein ores. In this respect it is important to mention that it hasn't been observed platy calcite with the characteristic bladed texture related to boiling, in the highest temperature upflow zones, neither carbonate replacement structures.

In a general way, it has been observed that the abundance of quartz and adularia increases toward the center of the upflow zone, whereas clay abundance increases toward the margin of the upflow zone.

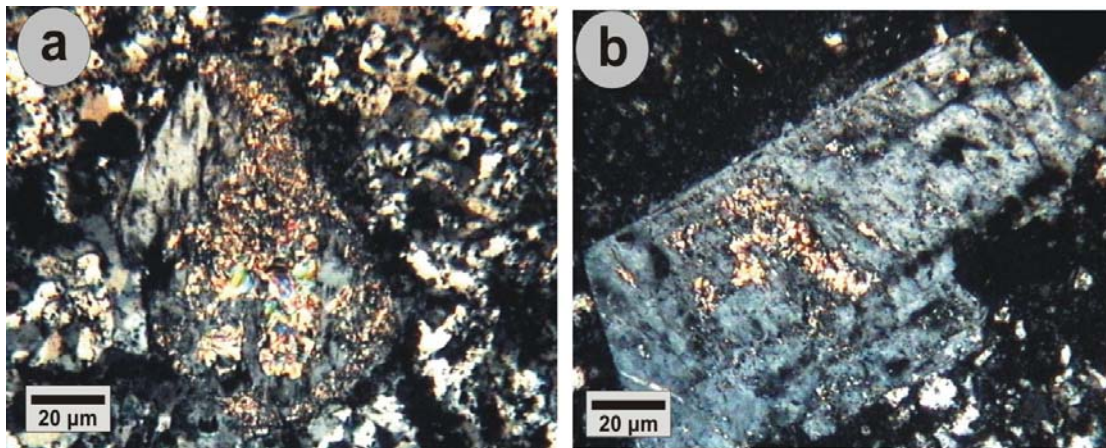


Fig. 46 : Adularia and sericite from Galana (a) and Profitis Ilias (b)

5.3.6. The Propylitic alteration zone (Pr)

Argillic alteration grades into narrow or wide areas of propylitized rocks which consist of quartz, albite, chlorite, smectite, pyrite, carbonates \pm sericite \pm pyrite \pm Fe-oxides \pm zeolites (see next chapter 6). The mafic minerals (pyroxenes and green hornblende, biotite) are replaced by chlorite \pm carbonate \pm albite \pm leucosene ($\text{TiO}_2 + \text{Fe}_2\text{O}_3$). During this alteration style plagioclase was altered to albite and/or calcite. The groundmass consists of feldspars with chlorite microaggregates, carbonate and fine-grained impregnated pyrite, while locally it is presented variably stained due to the pyrite weathering. At deeper levels the propylitic alteration envelopes the adularia bearing zones.

5.3.7. The Oxidation patterns (Ox)

Oxidation was formed in both subaerial and submarine settings, the second one due to weathering after mixing with seawater.

In the near-surface environment the sulphide minerals are oxidized and minerals such as jarosite, gypsum and other sulfates, arsenates and Fe-hydroxides are typical. The oxidation profile is highly irregular, reflecting both the distribution of structural discontinuities and the degree of permeability of the host rocks.

In the area between Agathia and Vani supergene gossans are found because of a weathering process in which an iron oxide cap is formed above a probable deposit at depth.

This is considered to be a submarine oxidation process. Pyrite within the altered wall rock is oxidized to limonite, goethite and hematite.

The base of wallrock oxidation is as shallow as 100 to 130m at western Milos.

5.3.8. The Fresh rocks zone (Fr)

The mineral assemblages of the relatively unaltered rocks (mainly dacitic-rhyodacitic subvolcanic bodies and flow domes) include quartz, sanidine plagioclase and biotite. The groundmass makes up about 50% of the rock and is mainly composed of quartz and alkali feldspar. Accessory minerals are rutile and zircon.

5.4. The alteration styles which characterize the various rock formation of W. Milos

The alteration styles that have characterized the various geological formations (units/subunits) at western Milos, can be summarized as follows :

- Argillic alteration (illite, smectite, sericite) and locally propylitic (chlorite, ankerite, pyrite) have characterized the lithic/pumice tuff subunit (**Lpt**).
- An argillic and moderate to strong silicic (chalcedonic, opaline flooding) alteration have characterized the pumice flow subunit (**Pfl**).
- Argillic alteration and in several places advanced argillic (dickite/kaolinite, pyrophyllite, diaspore, Na-alunite, APS (aluminum phosphate sulfate)-alunite, halite, cristobalite, tridimite) have characterized the lower pumiceous tuff unit (**Lmp**).
- An argillic, a moderate to strong silicic (chalcedonic, opaline flooding), advanced argillic alteration (quartz, illite, nacrite, APS-alunite, sericite, jarosite at the northern sector), quartz-adularia (quartz-adularia together with the low temperature minerals cristobalite-mordenite at the southern sector locally) alteration styles have characterized the fine ash tuff unit (**Fat**).
- An argillic together with a moderate to strong silicic and adularia-sericite alteration, have characterized the Profitis Ilias ignimbrites (**PIi**).
- A propylitic (albite, montmorillonite, ankerite) to argillic with the whole range of silicification intensities, from slight to strong and only locally with advanced argillic alteration (quartz-kaolinite, APS-alunite, halite, opal-CT) at the northern sector, have characterized the coherent intrusive/extrusive domes (**Anda**) and related hyaloclastites (**Anda-brx**).
- A propylitic to a slight-moderate silicification have characterized the slightly younger dome/flow dome complexes (**Dado, Dado-brx**).
- A patchy (partial alteration) argillic alteration characterized the upper lithic/pumice tuff unit (**Ump**) and the upper fine ash tuff unit (**Uft**).
- The hydrothermal eruption/explosion breccias (**Hbx**) are characterized by moderate to strong argillic and/or silicic and locally by advanced argillic (APS-alunite, nacrite, illite) alteration.
- The submarine **silica caps** at Mersinia is characterized by quartz, Na-alunite, anatase included/enveloped in an amorphous silica, and at Agathia by chalcedony.
- The subaerial **silica sinter** at Kondaros-Xerokampos is characterized by quartz, cristobalite, kaolinite.
- The various volcanosedimentary units (**ep, Ftt, Uftt**) are characterized by slight to moderate argillic alteration and locally by strong oxidation alteration patterns.

5.5. Considerations on the fluid temperatures acted on Western Milos

5.5.1. Synthesis of the data

At western Milos the suite of temperature sensitive hydrothermal minerals (alteration minerals) have been used in order to understand the paleosetting of the existing hydrothermal/geothermal system. The presence of cristobalite or tridymite (e.g. Kondaros, Mersinia) derived by seafloor acid-sulfate alteration suggests temperatures below about 110°C (White & Hedenquist 1994).

Zones of progressively higher paleo-temperatures were mapped based on the presence of kaolinite, smectite, and interstratified clays, with the highest paleotemperature indicated by chlorite clays. This is the pattern one would expect to result from the water ascending along fractures. Alteration zones are temperature dependent, changing from kaolinite to dickite + kaolinite (at about 120°C – part of Mersinia, Kondaros-Anemophysima, Ralaki, northern flank of Profitis Ilias) to dickite (at about 180°C) – part of Mersinia-Agathia, and to pyrophyllite (at about 240-250°C-Kondaros main volcanic edifice). Based on the previous suggestions as well as on experimental and thermodynamic data (Hemley et al. 1980; Hurst & Kunkle 1985), the occurrence of pyrophyllite and coexisting dickite, kaolinite (e.g. at Kondaros-Mersinia area) suggests temperatures of formation close to 250°C under quartz saturated conditions, where magmatic vapors are absorbed by ground water to produce acid water at the base of the high-sulfidation epithermal environment (Hedenquist et al 1998).

Pyrophyllite implies an acid fluid saturated with respect to quartz, with a temperature at about 250°C or little bit below and shows depths greater than 800m, something that is compatible with the presence at Kondaros, of the big lineament striking NW-SE and having a vertical displacement of over 400m as referred by Papanikolaou et al. (1990).

It is also considered to indicate a position beneath the quartz-alunite lithocap.

The sericite in the area of Koumaria-Chondro Vouno-Profitis Ilias indicate a near neutral to slightly acid pH for the fluid and a temperature above 220°C. Smectite (stable at temperatures lower than 160°C) gives way to interstratified illite-smectite (Chondro Vouno saddle), whereas illite by itself (NW-W Koumaria, Profitis Ilias) is generally stable at temperatures greater than 220°C.

The ore zone contains minerals indicating the highest pH, such as adularia and calcite (Prof. Ilias, Chondro Vouno, Kondaros-Katsimoutis), as boiling in the conduits causes CO₂ and H₂S loss, and consequent increase in pH; however these minerals are relatively temperature insensitive.

Finally, the chalcedonic silicification observed in massive silica bodies at Agathia, Vromolimni and Kondaros, implies local silica saturation and temperatures between 190° and 100°C as suggested by White & Hedenquist (1994) for this kind of environments.

6. ON THE GEOLOGY-MINERALIZATION-ALTERATION OF WESTERN MILOS SUBAREAS

6.1. Introduction

A zoned hydrothermal alteration system with associated epithermal high sulfidation (HS) type hydrothermal breccias and intermediate sulfidation (IS) type mineralization, dominated by veins and veinlets, has been developed at a shallow submarine to locally subaerial environment at western Milos. It is considered to be related to the development of shallow emplaced intrusive to extrusive domes / lava domes, at an area as large as 65km², representing the whole vertical interval from the transitional environment between deep epithermal (high-intermediate sulfidation), to near surface or seafloor deposition of mineralized silica caps/sinters.

In this chapter the most important characteristics of the most relevant areas, are exposed and documented. As mentioned above, they represent separate events or different levels of exposure of the same hydrothermal system.

Because of an important lineament, the Ammoudaraki-Plakota one, which subdivides Western Milos in two sector areas, the Northern and Southern sector, not only geographically, but also concerning their hydrothermally development, it has been decided to be followed a description related to the above concept through the following map (Fig.47).

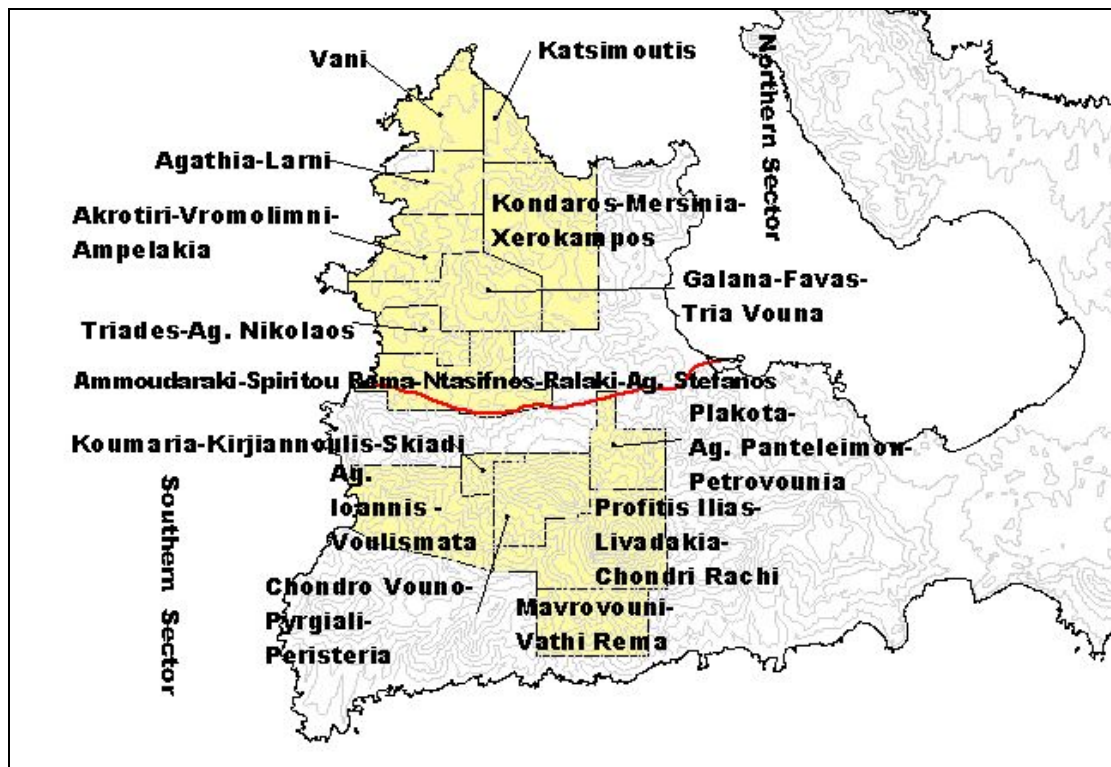


Fig. 47 : The various subareas of Western Milos as described in the text. In red is the important Ammoudaraki-Plakota lineament subdividing it in two different sectors.

6.2. The Northern Sector Subareas

6.2.1. Vani

The Vani subarea can be described as made up by two main subunits, the upper one which

is essentially a manganese - bearing volcanosedimentary unit, consisting of volcanoclastic sandstones, conglomerates and tuffs (Fig.48b), which is underlied by variously altered (mainly argillized and locally propylitized) andesitic-dacitic domes (the lower subunit), (Fig.48c). At the northernmost cape zone (Troulos cape), a late dacite dome (Dado) has intruded the above mentioned, and mostly reworked volcanosedimentary unit, updoming and brecciating it. The dacitic dome is strongly altered (silicified, argillized and locally adulari-



Fig. 48 : (a) The propylitic and K-feldspar (adularia) altered, and veined dacitic dome (Dado), at the northernmost part of cape Vani; (b) volcanoclastic unit with NW-dipping stratiform manganese and manganese-iron horizons, which overly dacitic (Anda) domes; (c to e) Asprogioloudia area, W. Vani: propylitized pillow lavas venting area with stockworks of chalcidony-Mn (sub-seafloor/seafloor deposition), covered by Mn-oxide concretions, representing Mn-chimneys (white smokers) and by tuffitic sandstones; (f to g) bioturbated volcanoclastic sediments including barite-rich micro-chimney edifices, overly Mn-oxide concretions.

zed) (Fig. 48a). Mineralization at Vani is spatially and temporally related to both NE-SW and NW-SE trending tectonic lineaments, the later related to the development of the Western Milos' gulf big lineament (i.e., the same system which is further described for the areas of Katsimoutis and Kondaros base) and of course to the development of the subvolcanic domes all around it (Trouslos cape being one of them). Manganese mineralization at Vani took place in two principal phases (Liakopoulos, 1987; Liakopoulos et al. 2001; Hein et al. 2000; Glasby et al. 2005). The first one deposited a generation of manganese oxides (pyrolusite and ramsdellite), which is the product of a hydrothermal system channelled along a NE-SW direction and venting at seafloor (white smoker). The second generation of manganese oxides (including the isostructural series cryptomelane-hollandite-coronadite and the hydro-haeterolite characterized by high contents of K, Ba, Pb and Zn, respectively) is paragenetically related with baryte and arsenosiderite, and is considered to be the product of another fluid channelled along the NW-SE direction and enriched in Zn, Pb, Ba, W, Ag, Sb and As. It represents a low temperature seawater-dominated convective system. This enrichment, at least for a part, it was due to the interaction of this later fluid with the first generation manganese oxides and is probably related to sulphide mineralization at depth (Liakopoulos et al. 2001; Glasby et al. 2005). In other words the second generation of manganese was derived not only from the hydrothermal solution, but also from the dissolution of the previous generation of manganese oxides (pyrolusite and ramsdellite), and thus re-mineralized the original manganese oxides and re-deposited sulphides. Two stages of sinter formation have been recognized in the area. The first it is submarine and it is considered the older one, related to the NE-SW trending fault system. It lies underneath the volcanosedimentary fossiliferous cover. The other one, the younger, is related to the NW-SE trending lineament, which is the one which was responsible for the uplifting of the whole NW area of western Milos, and at which corresponds also the subaerial sinter further south at Kondaros area.

Fieldwork evidences indicated the occurrence of epithermal banded quartz-chalcedony-baryte-Mn±Fe veinlets and veins, within the dacitic pillow lavas, domes and into the overlying volcano-sedimentary sequence, (Trouslos cape-N.Vani). It is considered that these veins probably represent feeder zones of the stratiform Mn-Pb-Zn-Cu mineralization. Similar features in the broad Vani area are the crustiform banded (epithermal) amethystine-chalcedony veins (Kalogria area-SW Vani) and quartz-chalcedony-baryte-Mn-Fe stockwork veinlets hosted within propylitized andesitic dacite subvolcanics (Anda) (Asprogiouloudia area -W.Vani). At Asprogiouloudia area the above mentioned feeder zones are overlain by bioturbated manganese and barite rich sediments (fig. 48). It is considered that these veins at Asprogiouloudia, similarly to Trouslos area, represent feeder zones of Mn-Baryte low temperature (< 200° C) seafloor discharges ("white smoker"). It is suggested that the second Vani manganese mineralization represents the final hydrothermal manifestation of the major Ag-Pb-Zn Katsimoutis-Kondaros epithermal intermediate sulphidation style system (see below).

6.2.2. Katsimoutis

Two crosscutting mineralized striking directions (NE-SW and NW-SE, i.e. a stockwork texture) is the main feature of the area. Starting from the big NW-SE lineament (Fig. 49a,b) passing through Katsimoutis and Vani areas, along the shore, there are several smaller faults and fissures crosscutting the underlying dacites (Dado) subvolcanics and the overlying tuffs. They are filled mainly by quartz-baryte-Mn veins and veinlets. The NE

(N30°) - trending mineralized veins dip from 65° to 75° somewhere to the East and in other places to the West. The NE-SW trending veins already described by Liakopoulos (1987) consist of base metal sulfides with chalcedony-baryte-Mn and/or Mn-baryte veins (fig. 49c,e,g) and are developed along, and in between, the main Katsimoutis-Triades lineament and the Vani outflow (“white smoker”) zone. The dominant alteration style is that of adularia-sericite. The later NW-SE mineralized fault/lineament system (the western bounding fault of the Milos gulf (graben), consists of sheeted and banded veins and stockworks



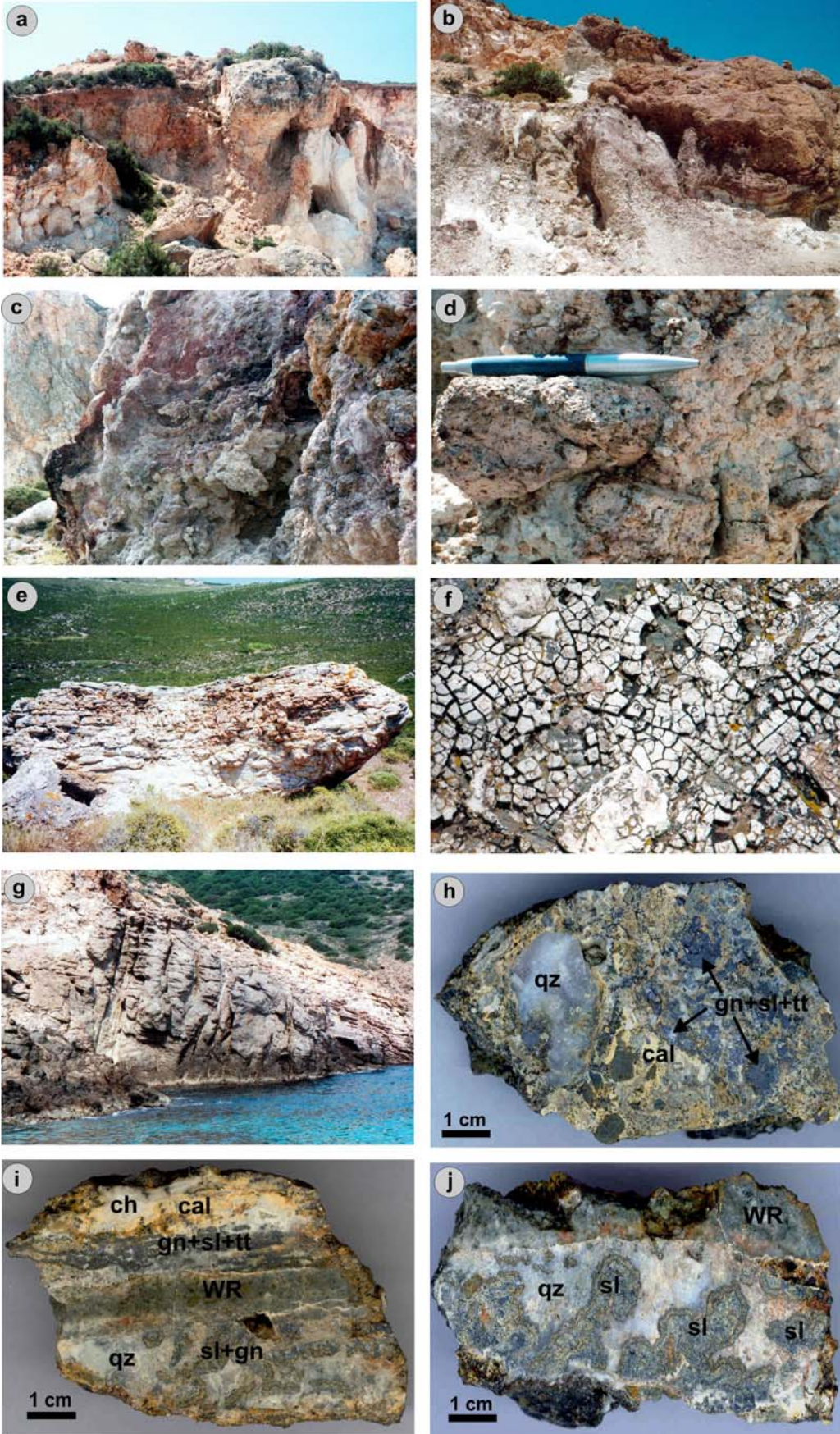
Fig. 49 : (a) The NW-SE mineralized fault along the Western Milos gulf. View from Kondaros through Katsimoutis to Vani; (b to d) chalcedony-baryte-Manganese veins cutting through propylitized dacitic dome lavas; (e) NE-trending quartz-barite base metal-rich veins at Katsimoutis; (f) colloform banded chalcedonic silica (ch) and late calcite after aragonite (cal) postdate early brecciated galena (gn) + sphalerite (sl) + tetrahedrite (tt) + polybasite mineralization; Propylitic wallrock alteration (WR) and late manganese (Mn) is also present; (g) quartz-barite (bar) and galena (gn) from Katsimoutis mine (NE-trending veins).

which have a width between 0.5-1 m, and are at least 50 to 100m long (fig. 49b,d,f). The characteristic alteration style of the subvolcanic domes is propylitic to argillic and hosts the above mentioned NW-SE trending mineralization, which is an epithermal Ag-bearing intermediate sulphidation (IS) type. It shows features like cockade structures, colloform banding and consists of carbonate, adularia and chalcedony gangue (fig.49f). At the south-eastern end of Katsimoutis bay, quartz-baryte-Mn veinlets in a stockwork configuration have been developed. Further away toward Kondaros an early deposition of base metals sulphides and Ag-sulphosalts on both matrix and including fragments, on a brecciated wallrock, was followed by colloform chalcedonic banded veinlets and late Mn oxides and calcite pseudomorph after aragonite and final zeolite (Fig. 49f). Very similar structures with chalcedony, aragonite and galena-sphalerite, manganese in a propylitized host (dacite subvolcanic), are encountered in veins situated along the main NW lineament, at mid way to Kondaros.

6.2.3 Kondaros-Mersinia-Xerokampos

Andesite/dacite flow dome complexes (Anda) overlain by submarine lower pumiceous lapilli tuffs (Lmp), and locally dacitic flow domes (Dado) are the main geological units in the area. Several relict structures of probable monogenic volcanic activities (necks and coarse pyroclastic breccias) are important features of the area (fig. 50a). There exist also other, vent like structures present in the area (Fig. 50b), placed in a lake environment (as the presence of a thin diatomite horizon testifies), which reminds at an intense phreatomagmatic activity in a strongly alkaline lake environment. As it is evident from field observations the vent like breccia structures are post Andesite/dacite dome emplacement. The Kondaros-Mersinia area is characterized by leached silica caps (including spongy porous rock with chalcedony after opal, massive silica and subordinate vuggy quartz), which constituted the flank of an important volcanic edifice (Kondaros edif.). The main alteration features in the area are hypogene high sulphidation (HS) style silicic caps and strong advanced argillic alteration (quartz, alunite, dickite, \pm pyrophyllite, \pm diaspore) which pass laterally to intermediate argillic, argillic alteration (Fig. 50c and d). The alunite occurs as vein filling, as well as massive replacement alunite hosted within ash flow tuffs and breccias. The silica and clay alteration assemblages are coincident with the lower pumiceous lapilli tuff unit (Lmp), roughly trending N-S in the area. Locally, up to 10cm thick, banded alunite veins cut the totally altered pumice rich pyroclastic unit (Lmp). Strongly silicified, lapilli pumice tuff is cut locally by thin, grey silica veinlets (up to 0.5 cm wide), having NE (30°) and NW (300°) crosscutting strike directions. Vuggy silica pieces belonging to the andesite/dacite unit (Anda), have been also found at vein breccia structures below the silica cap at Mersinia (Fig. 50d). An initial vuggy silica zone, at the

Fig. 50 : (a) Coarse pyroclastic breccias capping vent/neck areas at Mersinia; (b) explosion breccia pipes cutting through the lapilli pumice tuffs and volcanic agglomerates; (c) coarse mineralized and advanced argillic altered breccias at Kondaros old kaolinite-alunite mine at the sea side; (d) vuggy silica fragment included into the explosion breccia at Mersinia; (e) silica sinter horizon at Mersinia; (f) subaerial sinters with the characteristics dessication cracks at Mersinia; (g) quartz-base metal veins cutting through propylitic altered lavas at the Kondaros beach; (h) hydrothermal breccia with milky quartz + galena (gn) + sphalerite (sl) + tetrahedrite (tt) + polybasite fragments in an chalcedonic-calcite (cal)-barite matrix; (i) Propylitic altered lava (WR) surrounded by galena (gn), sphalerite (sl), tetrahedrite (tt) and polybasite mineralization in a quartz (qz), calcite (cal) and chalcedony (ch) gangue; (j) quartz-vein with sphalerite showing colloform structure. The wallrock alteration (WR) of the dacitic lava is propylitic.



main Kondaros Hill (Santoriniou), has been later totally flooded and steam - heated by silica which obliterated nearly all the previous characteristic HS alteration style features.

A number of subaerial silica sinters occur at the Kondaros-Anemophysima subarea (Fig. 50e and f) scattered along a NW trending zone (i.e., parallel to the structure controlling the emplacement of the Vani and Kondaros subvolcanic bodies). They lie on the lower pumiceous lapilli tuffs (Lmp) (here strongly silicified and/or kaolinized). A Zn-Pb-Ag±Cu±Mn vein type mineralization (quite similar to that described above from Katsimoutis), containing base metal sulphides and Ag-sulphosalts along the western lineament (NW-SE) of Milos gulf (Fig. 28), and most probably another precious metal rich vein style mineralization at depths below the sinters (as supported by the presence of banded veins at Xerokampos, see below), are the main features of the area. The main NW fault related to the Ag-bearing ore at Kondaros, dip approximately 80°W.

At Kondaros, base-precious metal mineralization is hosted within a propylitic and intermediate argillic altered dacitic flow dome (Anda) which constitute the lowest outcropping trending formation. At higher elevations the NW-SE mineralized veins are strongly oxidized and crosscut advanced argillic altered rocks of the lower pumiceous lapilli tuff unit (Lmp). Baryte is strongly present as void fillings and as disseminated replacements. Finally it is important to mention a series of pure calcite veinlets (<2cm) running along NE-SW directions through the Kondaros andesitic/dacitic dome's flank, at the sea side.

Xerokampos area is characterized by sparse silica sinters and float colloform-crustiform quartz veins. The silica sinters overly mainly the lower pumiceous pyroclastic unit (Lmp), while the vein floating overly the younger upper pumiceous lapilli tuff unit (Ump) both of submarine character. The main feature of the area is a vent located in the midway between Tria Vouna and Xerokampos, inside the younger lapilli tuff unit (Ump) and also covered by it, which includes sericitized and propylitized fragments of andesitic/dacitic (Anda) composition, truncated by quartz veinlets. This important vent area belongs to the various features related to the major fault/Lineament described at the Tria Vouna-Favas area (see below). Obviously the vein floating is related to this vent area and thus it is supposed that there is a blind vein type mineralization occurring underneath.

6.2.4. Larni-Agathia

It seems that the most interesting feature at Larni is an important NE to E trending lineament, which delineates the volcanosedimentary area of Vani from that of Agathia-Kondaros. Evidence on that are the overturned fine and lower pumiceous lapilli tuffs (Fat and Lmp respectively; fig. 51a). The whole area is strongly altered, argillized (kaolinized, smectitized), silicified (along the fault traces and the veins), alunitized locally. Along the main NE to E trending lineament a swarm of quartz-baryte veins (fig. 51a), cut through the strongly altered (kaolinized) tuffs. In addition, at the N, NW and NE of Larni, i.e., towards Vani and Katsimoutis, outcrop strongly silicified and barytized lava flows of dacitic composition (Dado).

The Agathia area can be described as a strongly altered lower pumiceous lapilli tuff (Lmp) area, where a series of dacite domes (Anda) mainly, and subordinately subvolcanics lavas of dacitic composition (Dado), massive to in situ brecciated, have been emplaced. An ignimbrite sheet (Agathia ignimbrite) of local extent, related to a younger dacite (Dado) emplacement, is intercalated between the lavas. Other interesting features of the area include the presence of explosion craters and lag breccia masses (Fig. 51b), these last most

probably from a volcanic edifice situated somewhere into the sea at the coast area between Agathia and Kalogries. The dominant alteration features in the Agathia area are the presence of a silica cap (massive and vuggy silica) (fig. 51d,e) and a strong advanced argillic alteration underneath the silica cap (fig. 51c), generally outcropping along NE-SW trending faults. The presence of vuggy silica within the silicic alteration, as well as the presence of structures resembling conduits (microlayered black silica) within the vuggy silica (fig. 51e), remind common structures further south at Favas area, especially in the area where the hyaloclastites/explosion breccias are situated (see below). At Agathia two different styles of mineralization have been distinguished. A pyrite-chalcopyrite one, associated to the high-sulfidation system silicified (chalcedonic silica) areas (fig. 51f), and an intermediate sulfidation type characterized by submarine silica-manganiferous sinters and Mn-Fe oxides related to chimneys (vent zones) similar to the Vani-Katsimoutis ones.

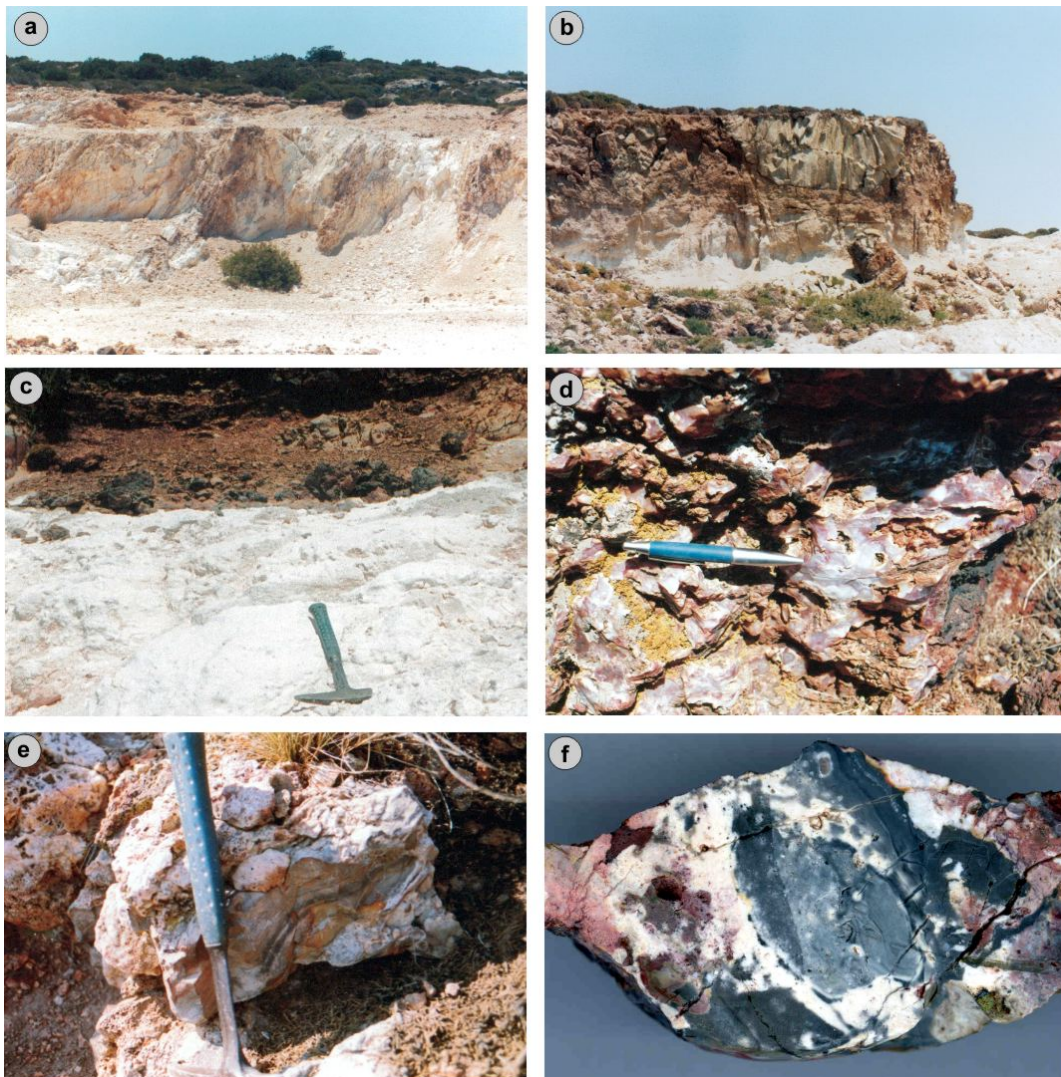


Fig. 51 : (a) Overturned lapilli pumiceous tuffs cut by quartz-baryte veins; (b) coignimbrite lag breccia overlying strongly argillized pumiceous lapilli tuffs (Lpm), the length of the included volcanic fragments is about 4m; (c) advanced argillic zone underlying the silica flooded area; (d) opaline-chalcedonic silica rich in Fe-oxides/hydroxides; (e) vuggy silica and massive silica with chalcedonic microlayering probably suggesting a conduit (outflow) zone; (f) sulfide-rich black chalcedony, in the chalcedonic silica area at Agathia.

Red to brown opal/chalcedony veins striking E – W, with some bladed barite and abundant disseminated pyrite locally, are also present.

6.2.5. Akrotiri - Vromolimni - Ampelakia

A series of NE-SW trending faults along which several small dacitic domes (Anda, Dado) have been emplaced, is the main geological-tectonic feature in the area. In the midway between Vromolimni and Akrotiri, a hydrothermal explosion breccia, the only one which show some “roots” on the whole western Milos, rised through a fault alongside a totally argillized (kaolinized-illitized) subvolcanic rhyolitic body (Anda),(fig. 52a,b). The breccia is a polymict, matrix supported, made up by strongly argillized and silicified volcanic, metamorphic and re-brecciated fragments, in a strongly argillized and locally silicified matrix (fig. 52a,b). This breccia contains oxidized base metal sulphide mineralization.

The main alteration-mineralization feature in the Vromolimni-Ampelakia area is a massive to vuggy silica cap (fig. 52c) which extents from the sea side at Vromolimni(to the west), to Ampelakia flat ground(to the east), terminating at an oxidized-base metals rich hydrothermal breccia, which outcrops over there. Underneath the silica cap, as it is observed at Vromolimni, along the coast, (fig. 52d), the argillic s.l. alteration style is the dominant one. This alteration is a part of a more extensive argillic alteration zone encountered in all over Vromolimni, Agathia and Ampelakia areas. Dominant NE-SW trending faults/lineaments outline the silica cap and the hydrothermal breccias in the area.



Fig. 52 : (a) A hydrothermal explosion breccia at the sea side between Akrotiri and Vromolimni; (b) argillized, silicified subangular to subrounded subvolcanic fragments in the previous breccia; (c) massive to vuggy silica in the mid way between Vromolimni (to the east) and Ampelakia (to the west-looking up); (d) argillic s.l. alteration at Vromolimni, in the back side Agathia area.

6.2.6. Galana - Favas - Tria Vouna

At Galana area submarine to locally transitional lithic/pumice tuffs (Galana formation) and tuff breccias were put in place (dome-top tuff succession) by a rhyolitic-rhyodacitic dome (Anda). Later the whole rock complex has been intruded by a new generation of dacite flow dome (Dado) which has covered quasi the total of the area under the lavas and the autobrecciated carapace that created. Around Galana area, a dominant phyllic alteration (quartz-sericite-pyrite) grades upward (toward Favas-Kondaros) into an advanced argillic alteration including sparse massive to vuggy silica minor zones (fig. 53a).

The mineralization is related to two different events. An early one, related to a NE-SW extensional lineament (Triades-Katsimoutis lineament), along which have been emplaced the Anda domes of rhyolitic-rhyodacitic composition, and a later one, related to the subvolcanic emplacement of the dacitic flow dome (Dado) along a NW-SE direction. In the first case mineralization (very fine grained pyrite and subordinately sphalerite and galena) occurs in hyaloclastites (in situ and resedimented of the Anda subvolcanic formation). In the second case the dacitic intrusion produced a new breccia containing relicts from the previous event (old breccia fragments) in a matrix containing sulphides and sulfosalts (sphalerite, galena, chalcopyrite, bornite, tetrahedrite-tennantite, enargite (fig. 53b). The polymetallic mineralization occurs in a gangue made up by barite, kaolinite, sericite, adularia and quartz/chalcedony. The mineralization, considered to be of intermediate sulfidation type, is expressed as multistage breccia zones and barite-galena veins, crosscutting previously strongly silicified massive to vuggy silica, quartz-sericite and quartz-kaolinite alteration zones. Galena, which gave also the name at the place (Galana), occurs in different forms, i.e., as coarse grained euhedra in disseminated form, intergrown with barite, as well as in quartz veins. At Galana, just at the edge of the fresh overlying volcanic carapace (NW from the main subvolcanic intrusion area), a part of the overturned silica cap, along the main NE trending lineament as well as brecciated sinter pieces, testify the presence previously of a submarine lake, at the lower part of the lower pumiceous tuff unit (Lmp) and very near to the interface with the older rhyolitic-rhyodacitic (Anda) subvolcanic body.

The most dominant feature at Favas area is a series of breccia pipes and flow breccias surrounding in a ring fashion (ring-fault controlled breccia pipes) the dacitic subvolcanic (Dado) Favas dome, and cutting through the submarine fine tuff (Fat) and lower pumiceous lapilli tuff (Lmp) (Fig.53c and d). They are presented mainly strongly silicified, oxidized and subordinately argillized. At the contact with the breccias the Favas dacitic dome is alunitized (fig.53e). The tuffs, which host the breccias are strongly silicified and alunitized (Fig.53f) and dip toward the Favas dome itself, showing essentially the pre-existence of a feature related to a vent or small crater. The breccia pipes are strongly oxidized and mineralized showing a gold, copper, and molybdenum enrichment. The next dominant feature in Favas mountain is the presence of black-grey microlayered chalcedonic silica, considered to be fluid conduits which configure outflow venting (upwelling) zones of high-sulfidation hydrothermal fluids (Fig.53f and g). Another dominant feature it is a series of

Fig. 53 (a) massive to vuggy silica at the area between Galana and Favas; (b) sericitic altered dacite wallrock fragments (WR) cemented by galena (gn) - sphalerite rich ore and quartz (qz) gangue (Galana); (c) the SW part of the ring-fashion breccia field at Favas area, looking NNW; (d) polymictic breccia including rounded fragments in an Fe-oxide rich matrix (Favas-Tria Vouna); (e) alunitic (alu) altered dacite at the contact with the breccia. Chalcedonic silica (ch) is also present (Favas); (f) layered chalcedonic silica in the ring breccia structure (Favas); (g) hand-specimen of microlayered black chalcedony from the ring breccia (Favas); (h to j) Cu-bearing veins and stockworks cutting through the flow breccias, looking ENE (Favas).



intermediate sulfidation type sheeted chalcedonic quartz-Ba and subordinately chalcedonic quartz-Ba±Mn±Cu veins and veinlets, vein-breccias running NE-SW (fig.53 h to j).

The position of the Tria Vouna seems to be marginal with respect to the vent/crater area (Favas dome), and just at the crossing of two important linear structures (faults/lineaments), the one coming along N-S direction (from Agios Stefanos to Mersinia) and the other along NE direction (from Agios Nikolaos to Xerokampos). The dominant features at Tria Vouna are three coalescent dacitic domes (Dado), which intruded through the altered (kaolinized and locally silicified lower pumiceous lapilli tuffs (Lmp).

6.2.7. Triades - Agios Nikolaos

The mineralized area at Triades extends between the southern end of the Katsimoutis-Triades lineament and the northern normal fault of the small graben of Ntasifnos. In Triades a shallowly dipping volcanosedimentary sequence of fossiliferous tuffs (Ftt), tuffites and epiclastics (mainly sandstones-(ep), is intruded by flow-banded andesitic-dacitic-rhyodacitic subvolcanic bodies (Anda, Dado).

The mineralization is considered to be genetically related to the older andesitic-dacitic-rhyodacitic domes (Anda). The occurrence of tuffites, tuff sand (Ftt), and local medium-coarse epiclastic units (ep) indicate weak periods of pyroclastic activity alternating with terrigenous source of basin infilling in a submarine to transitional submarine to subaerial environment. Dominant alteration style in the area is argillic (kaolinite-sericite) with spotty advanced argillic and/or silicic alteration. The main feature of Triades is its breccias s.l., landscape. There are different kind of breccias, such as hyaloclastitic breccias related to the Anda domes, fault related breccias and breccia pipes, which are difficult sometimes to differentiate each other (fig. 54b to e) due to intense alteration and overlapping/ coalescing of them. It is considered that structural doming in the area, above subvolcanic intrusives, whether or not spatially related to volcanic vent areas, created dilatant fractures which controlled the hydrothermal brecciation and epithermal mineralization (Triades classics). The distribution of the breccias is associated with the combining action of the subvolcanic intrusives and the faults cutting through NE-SW to E-W directions. All the breccias have been deposited in a shallow submarine to transitional environment, as evidenced by the fossiliferous tuffites and epiclastic sandstones which host them. The breccias are more or less similar in age to the above mentioned formations and clearly older than the slightly younger dacitic domes (Dado). The various kinds of alterations encountered at the breccias can be classified as strongly silicified hydrothermal breccias, strongly argillized polymictic matrix supported breccias (Fig. 54d), strongly to moderately silicified and moderate argillized clast supported breccias (Fig. 54c). The tectonic, and jig jaw subvolcanic (insitu hyaloclastites), intrusive breccias contain silica, kaolinite and barite as part of an advanced argillic alteration zone, while locally some of them are sericitized. A part of the Triades breccias is interpreted to be a debris flow /talus-landslide breccia, deposited by avalanching of material down fault scarps generated most probably by the emplacement of the various slightly younger Dado domes that produced an updoming of the surrounding area (Fig. 54a and b). This resurgent doming produced a collapsing of several of the in situ breccias situated at higher topographic levels (e.g. at Favas), as well as to some of them located in the surrounding areas (i.e., in between Favas, Galana and Triades) (fig. 54a), with the deposition of thick wedges of avalanched breccias at the base of the scarps.

The younger subvolcanics (Dado) are generally mantled by a carapace of autobrecciated deposits, while their original conical or domal shape is remarkably well preserved. The

autobrecciated carapace cover in several places the older alteration and hydrothermal brecciation features. The mineralization, as well as the hydrothermal alteration, is linked with N30° E and E–W (present work, Liakopoulos 1987), trending faults and are expressed

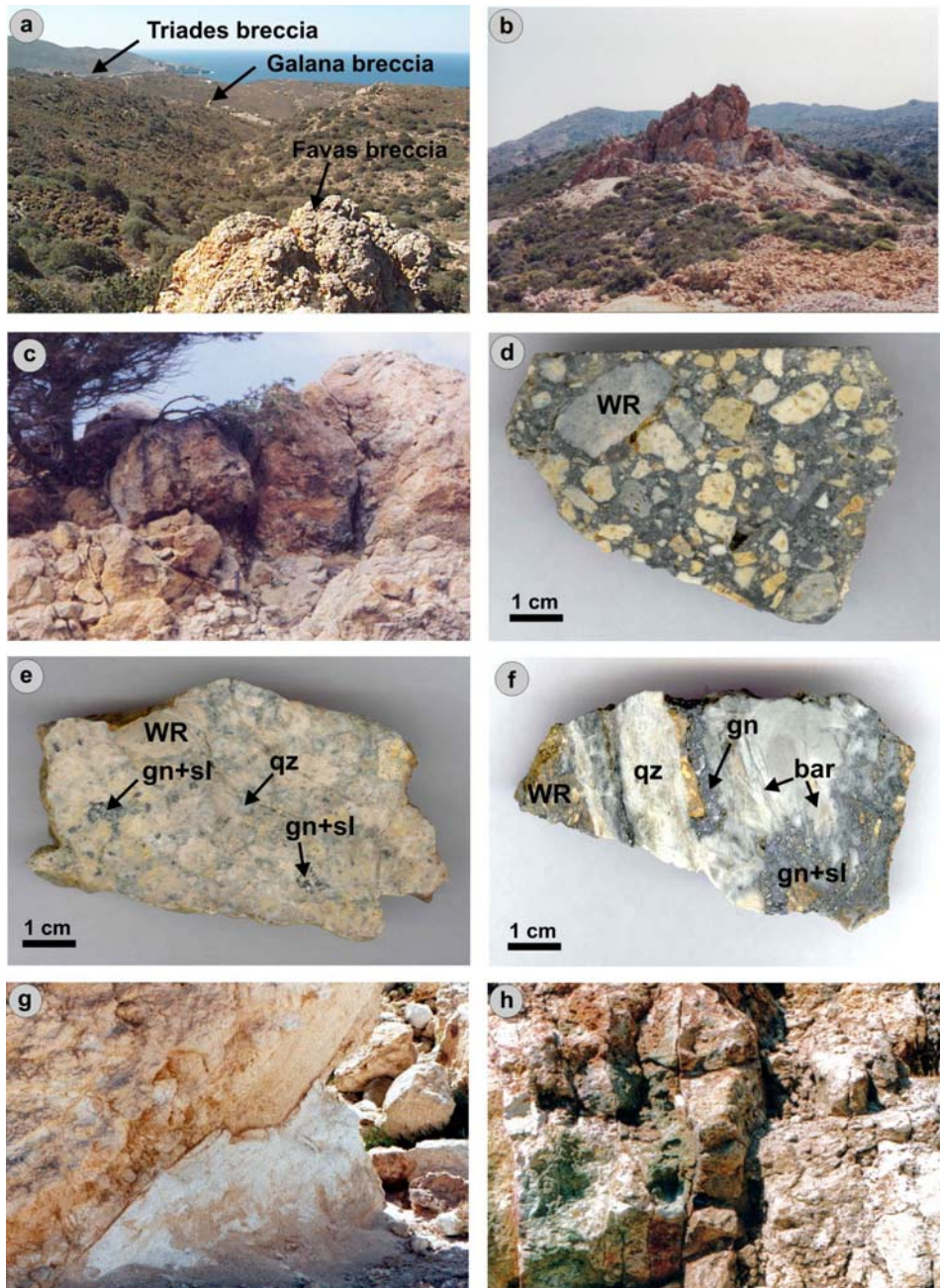


Fig. 54 : (a) In situ hyaloclastitic breccias at Favas and redeposited hyaloclastitic avalanched breccias at Triades and Galana; (b) Redepleted hyaloclastitic breccia at Triades; (c) silicic alteration cap above a hyaloclastitic breccia at Triades; (d) Breccia pipe hand specimen with sericitized wallrock (WR) fragments in a quartz-sphalerite-galena matrix; (e) Breccia pipe hand specimen with alunitic altered wallrock (WR) fragments in a silica-galena-sphalerite matrix; (f) Quartz-baryte vein with galena (gn) and sphalerite (sl), wallrock alteration (WR) is sericitic; (g) Argillitically (Advanced argillic), altered tuff overlain by mineralized flow (redeposited hyaloclastite) breccia (Triades); (h) Quartz-baryte veins, within an argillic alteration halo, with locally malachite staining through a flow banded coherent dacitic core -Anda dome-(Agios Nikolaos).

as multistage breccia zones (different oval shaped mineralized breccia bodies, ranging in size from 150x50m to 5x5 m) and quartz-barite-galena veins/stockworks related to quartz-kaolinite-sericite alteration. The sulfide assemblages occur either in the matrix of silicified and hydrothermally brecciated tuffs and volcanosedimentary units or as fractures filling material. The porous and permeable texture of the breccias allowed the influx and passage of mineralizing solutions filling open spaces, either as early chalcedonic or kaolinitic matrix, mainly in open space expansion breccias (dilatant structural environments), or as later sulphide matrix in syn-mineralization fluid transport breccias. The silicification and the mineralization events were clearly controlled by both structure and rock permeability. At the surface sulfide mineralization is intimately associated with the silicified alteration zones. At deeper levels, it occurs as sulfide veinlets and as lens-shaped bodies of barite (Liatsikas 1955). Geochemical evidences suggest that gold is mostly related to the breccias (fig.54d).

Parts of the main Triades body, exposed in the open pit area (old barite mine) reveal the presence of disseminated pyrite, sphalerite, galena and chalcopyrite partly coated by enargite and covellite. Azurite, malachite and anglesite have been considered to represent supergene alteration mineralization. Barite, kaolinite, sericite and quartz are the gangue minerals.

The presence of enargite is a strong indication that Triades mineralization is of high-sulfidation style. Triades has been formed in a shallow submarine setting, in a sub-seafloor to seafloor environment where the volcanoclastic sequence was unconsolidated and saturated with seawater. This is in accordance to Plimer (2000) statement, that Triades represent a subseafloor stockwork zone.

The Agios Nikolaos area is characterized by several unmineralized and fresh to slightly altered dacitic domes (Dado), while their hyaloclastite breccias form carapaces which cover previously altered and mineralized volcanics. The mineralization in the area it is related to massive-vuggy silica and quartz-kaolinite alteration zones and it is hosted in hydrothermal breccias (large siliceous and/or siliceous-argillic breccias) with abundant barite and locally malachite staining, and in quartz-baryte veins (Fig. 54h). Mineralized black chalcedonic silica fragments are also present into the hydrothermal breccias thus showing earlier styles of mineralization.

6.2.8. Agios Stefanos-Ralaki-Ntasifnos-Spiritou Rema-Ammoudaraki

The Agios Stefanos area is situated between the Favas-Tria Vouna and the Ralaki subareas (Fig. 47). It is dominated by barytized fossiliferous tuffite, lapilli pumiceous tuffs (Ump) and totally altered (kaolinized) dacitic lavas (Anda). It lies near a major volcanic structure. Due to a complex tectonic configuration the mineralization potential of the area is poorly exposed.

At the Ralaki area, fine ash tuffs (Fat), locally pumiceous lapilli tuffs (Ump) and fossiliferous tuffs and tuffites (two different generations) overly strongly altered (kaolinized) shallow submarine subvolcanic bodies of rhyolitic, dacitic, andesitic composition (Anda), to which are genetically and spatially related. Alunite, dickite, diaspore, kaolinite, chalcedony, opal (advanced argillic alteration) are the main alteration minerals in Ralaki. Black chalcedonic silica veinlets with pyrite in kaolinized-alunitized tuffs, and subvolcanic dacites - rhyolites along NE-SW to quasi E-W striking directions are the most important mineralization features. Hydrothermal conduits situated inside the pumiceous lapilli tuffs (Lmp) at old Ralaki kaolin mine indicates a submarine silica feeder zone and a seafloor silica deposition (fig. 55b).

Jarosite as a supergene mineral, and barite and/or chalcedonic silica-barite veinlets with minor sulphides, are also another characteristic feature of the area. Finally, chalcedony after

opaline silica, as well as variably opalized seams or thin beds in coarse kaolinized lower pumice tuffs (Lmp) is another evidence of acid leached rocks in the area.

At the upper side of Ralaki towards Kalamavros (left side of Kalamavros looking SW), there is a field of strongly silicified and barytized boulders (belonging to the lower pumiceous lapilli tuffs (Lmp), which are interpreted to be remnants of an ancient silica cap. Geologically the Ntasifnos-Spiritou Rema is made up by strongly altered (kaolinized and locally silicified) subvolcanic dacite (Anda) underlying also strongly altered tuffs and fossiliferous tuffites. A structurally down-dropped (graben) zone cuts off the central part of Ntasifnos area (Spyritou Rema), and is expressed on the southern edge by a major quasi curvilinear fault (the Ammoudaraki-Plakota-Rivari fault). This fault is expressed on the surface by silicified brecciated zones (fig. 55a). A quasi vertical fault (N-S) to the graben direction is marked by intense clay alteration and oxidized sulfide mineralization.

The presence of a silicified quartz porphyry body (Anda), with jarosite and alunite veinlets (probably of supergene or steam-heated origin), in the back side of Ntasifnos (Spiritou Rema) and in the front of Agios Athanasios hyaloclastitic breccia is another characteristic of this area.

At Ammoudaraki, the presence of strongly silicified and locally oxidized dacitic subvolcanics (Anda) overlain partly by fossiliferous tuffs and by lower pumiceous lapilli tuffs (Lmp) and locally by grey-coloured pumiceous lapilli tuff (Ump), are the main geological features of the area. Locally slumping structures suggest a west dipping inclined paleorelief, onto which wet tuffs have been slid down. The alteration “spectrum” varies from strongly silicified (silica flooding) to strongly argillized varieties along a quasi W-E direction.

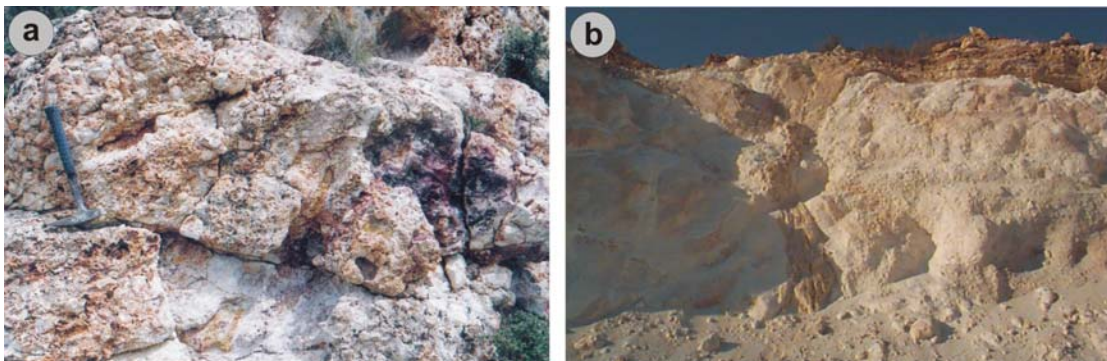


Fig. 55 : (a) strongly silicified breccia at Ntasifnos along the Amoudaraki/Plakota lineament; (b) hydrothermal conduit at the old Ralaki kaolin mine: submarine silica feeder zone and seafloor silica deposition.

The major E-W trending and N dipping slightly arcuate fault system (lineament) outcropping from Ammoudaraki to Plakota has the aspect of an escarpment and seems to separate the Koumaria-Chondro Vouno-Prof. Ilias horst block from that of Triades-Galana-Kondaros-Agathia-Vani. This escarpment has facilitated and controlled, the emplacement of several domes, but also controlled the passage of the various hydrothermal fluids which have been responsible for both the alteration and mineralization that occurred along this stripe.

6.3. The Southern Sector Subareas

This sector represents a large 14Km² zoned hydrothermal alteration system with associated epithermal intermediate sulfidation-type quartz veins and stockworks related to the development of major NE-SW to E-W extensional structures. This system is hosted within fine (Fat) and composite tuff units (PIi, Lpt, Lmp) and subordinately into subvolcanic intrusive dome structures (Rhyda, Anda). Relict high sulfidation alteration assemblages are locally observed, and suggest the presence of a previous HS alteration system, which most probably represents the southern extension of the HS system already described for the northern sector subareas.

6.3.1. Plakota - Agios Panteleimon - Petrovounia

The main characteristics of the Plakota area are the strongly altered (silicified and/or argillized) subvolcanic dacites (Anda), the fossiliferous tuff and tuffites (Ftt) and the sediments containing many floated colloform-crustiform banded silica and quartz-baryte vein fragments. Along the E-W trending Ammoudaraki-Plakota lineament, strong silicification, oxidation and quartz-pyrite, quartz-baryte veinlets occur.

The main geological feature of the Agios Panteleimon area is the presence of several dacitic domes of both types (Anda, Dado), emplaced into kaolinized-illitized lower pumiceous lapilli tuff (Lmp) along two main fault trends. The strongly argillized (kaolinized, illitized) small coalescing domes of first generation were controlled by a fault zone, striking N30°E and dipping to ESE, and the second generation porphyritic domes have been emplaced along NNW-SSE and ENE dipping fault zone.

The second generation of the flow domes are presented strongly silicified and hematitized, and show a jig-saw style of brecciation. Locally pyrite stringers fill the cracks. Banded chalcidonic to massive manganiferous quartz veins are found inside the andesites and rhyodacites (Anda) of the area and are locally associated with silicified breccias, shearing many characteristics with the Katsimoutis area vein occurrences. Brecciated silica-barite veins trending WNW to NW (285°- 300°) is another feature of the area.

The Petrovounia area is a plateau like area situated on the N-NE flanks of Profitis Ilias, and it is characterized by a series of subvolcanic dome and flow-dome complexes (Anda) which are silicified and oxidized. A series of NW-SE (300°) parallel running and down to the NNE dipping faults, created tectonic corridors which controlled the mineralization in the area. The mineralization consists of scattered pyrite along N60°W parallel running faults, with strong hematite staining.

6.3.2. Kirjiannoulis - Koumaria - Skiadi

The geology of Kirjiannoulis area is characterized by bedded fine tuffs (Fat) and pumiceous felsic ones (Lmp), intruded by a dacite porphyry (Anda). The porphyry body is presented slightly silicified. Two main mineralizing features characterize the area. The first is the quartz-sulphide veins and veinlets with a strong attitude to be parallel to the bedding, and the second is some thin quartz and/or quartz-baryte, opaline veinlets (striking N75°W) and impregnations of barite and opal in the porphyry body. A high proportion of quartz vein floats in the surroundings are attributed to belong to this area.

Koumaria-Skiadi lies on the western end of the Chondro Vouno ridge and seems to be controlled by both NW (N 300°-320° W) and NNE trending faults. The NNE faults (N10° to 25°E), which constitute the principal tectonic feature of the area, dip moderately to

steeply to the W (~60° - 75°) and appear to have sustained dip-slip normal movement, as testified by the slicken-sided structures occurring in the area. The NW trending fault is considered to be a strike-slip dilational fault jog. The outcropping stratigraphy of Koumaria-Skiadi comprises, a lower lithic/pumice tuff (Lpt), pumice flow (Pfl) subunits, overlying by pumiceous tuff (Lmp), fine ash tuff (Fat) units, and locally at the uppermost part, by the poorly welded, argillized to locally oxidized and silicified, Profitis Ilias ignimbrites (PIi). Locally between the two illitized and moderately sericitized lowermost formations, there are intercalated thin and discontinuous horizons of silicified fine grained (fine cherty) sedimentary rocks of black-grey colour, which are interpreted to be the product of deposition on a small lake bottom of upwelling silica fluids through a hydrothermal pipe structure.

Mineralization (pyrite, marcasite, chalcopyrite, bornite, sphalerite, galena and native gold) is associated mainly with steeply dipping ENE to NE up to E-W trending, thin crystalline sheeted quartz, quartz±barite and quartz-barite-Mn veins (average 10cm, max. thickness 25cm),(fig.56a,b,c), forming parallel sets, as a series of parallel running corridors averaging a width of 10m (max 25m) and running at a max length of 150m, within the silicified ignimbritic cap (PIi). At a lesser extend, another series of more or less isolated veinlets are encountered in the underlying the PIi unit, lower formations (Fat, Lmp). The veins thin out laterally and vertically towards the fine tuff unit which underlain it. Banded quartz veins are also subordinately present within the uppermost unit (PIi), as well as chalcedony veinlets in pervasively hematitized sites. At any case and independently of whether argillized or silicified, the uppermost Profitis Ilias ignimbrites (PIi) have a higher (1-5%) quartz and/or quartz-baryte veinlets content than the lower units, and the quartz-veins appear to be confined at the limits of the pumiceous tuff unit(Lmp). The intermediate stratigraphically fine tuff unit is truncated by hematite/jarosite and pyrite, marcasite (<1%) veinlets. Locally, hydrothermal explosion breccias into silicified Profitis Ilias ignimbrites, including 1 - 2% quartz veinlets is common, either with pyrite and local presence of Fe-oxides, or with baryte, galena, sphalerite, quartz and quartz-baryte veinlets together with Jarosite.

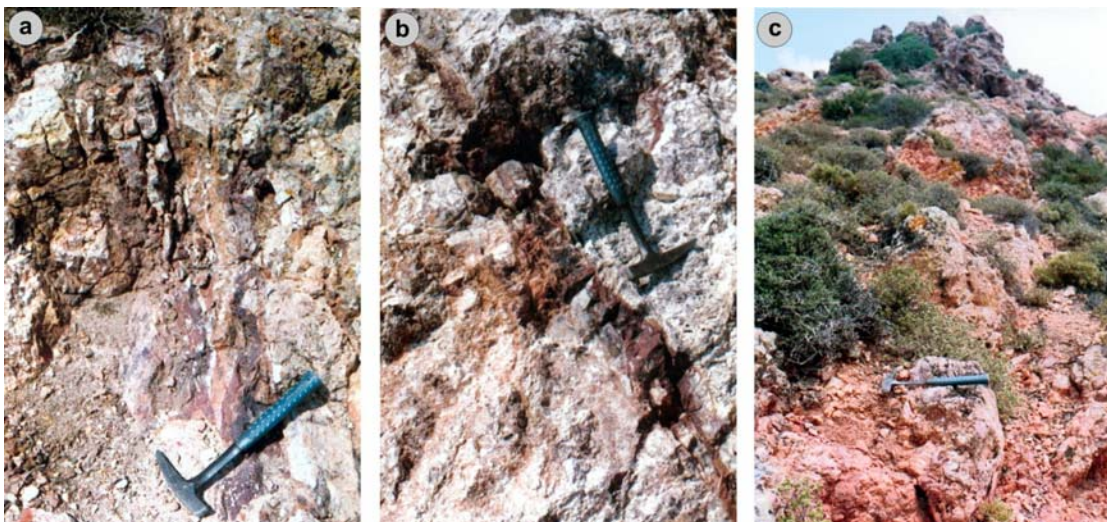


Fig. 56 : (a to c). Crystalline quartz and quartz-baryte-Mn veins in silicified and oxidized Profitis Ilias ignimbrite at Koumaria – Skiadi subarea.

Quartz-baryte±alunite veinlets in generally oxidized wallrocks, are also another dominant characteristic of the area's system and could belong to a high sulfidation mineralizing event.

At Skiadi, the veins have a direction NE -SW, i.e. parallel to the strike of the Profitis Ilias ignimbrites (PIi) and crosscutting the main tectonic trend direction NW - SE, running from Ammoudaraki to Mavrovouni.

In the area between Skiadi and Pyrgiali (see next), iron-stained lower pumiceous lapilli tuffs (Lmp) with spotty adularia and spongy silica constitute a localized feature.

6.3.3. Agios Ioannis - Voulismata

The main rock formation in the area is the lower pumiceous lapilli tuff unit (Lmp) which is presented strongly argillized, with locally overprinted strong silicification. Another dominant feature of the area is its steam heated character (fig.57a), recognized by the presence of friable aggregates of alunite+kaolinite+quartz occurring sparsely in the area. West-northwest of the Agios Ioannis monastery, a phreato- magmatic vent structure associated with a strongly iron stained argillized breccia up to 5m thick, cuts the Profitis Ilias ignimbrite (PIi).

Other series of vents are located along two major trends. The first trend, along a NE-SW direction is the same trend that characterizes the system of the veins/veinlets of Profitis Ilias and Chondro Vouno, Koumaria, as well as of the eruptive centers and smaller pipes that have been localized in the area between Agios Ioannis, Gournes, Pyrgiali and Skiadi. The second trend is along an E-W direction and localizes important volcanic emission centers and tectonic-stratigraphic contacts, as well as hydrothermal pipe structures.

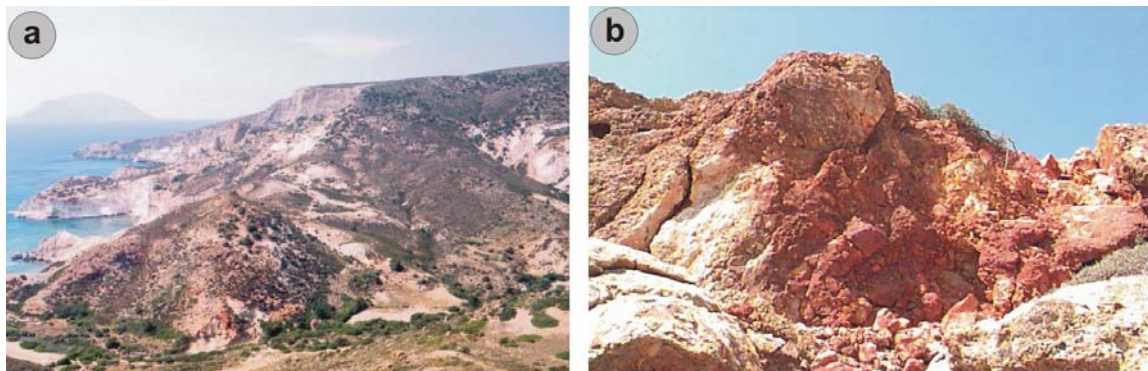


Fig. 57 : (a) Steam-heated Agios Ioannis area: (b) Strongly oxidized pipe-neck area above Agios Ioannis beach.

As a whole, the vent configurations that have been recognized in the area of Agios Ioannis, can be described as a strongly oxidized apron breccias disconformably blanketing strongly argillized lower pumiceous lapilli tuff formations (Lmp), into which also strongly iron stained coarse brecciated pipes occur (fig.57b). Here also as in Koumaria, Mavrovouni and Favas has been recognized the presence of thin and discontinuous horizons of silicified fine-grained sedimentary rocks (fine cherty silicified) of black-grey color, at which have been given the same interpretation as previously, i.e., of a hydrothermal pipe area, where

upwelling of silica fluid one time reached the surface and has been deposited as an exhalite.

At Voulismata area, north of Agios Ioannis, a series of mineralized vents running NE-SW constitute the main feature of the area.

6.3.4. Chondro Vouno - Pyrgiali - Peristeria

The Chondro Vouno ridge is a rhyolitic intrusive (Rhyda) which constitutes (Fig.58a) a horst, bounded by NW and NE trending normal faults. One of the NW normal faults extends further to southeast intersecting at the area of Mavrovouni other sets of faults.

The stratigraphy towards the NW-W parts of Chondro Vouno is well correlated with that of the Koumaria-Skiadi area, including, (starting from the surface), the fine ash tuff unit (Fat), the lower pumiceous lapilli tuff unit (Lmp), the pumice flow unit (Pfl), and the lithic/pumice tuff unit (Lpt). Scattered outcrops of Profitis Ilias ignimbrite (PIi) also occur in the area. The various tuff units outcropping in the area are presented strongly altered, generally argillized (kaolinized, illitized) and silicified, and to a lesser extent sericitized and adularized. At the crest of the mountain and along the veins, the silicification is stronger, while laterally the pumice flow unit is presented argillized and only locally flooded by silica. It seems that before the silicification event there was an extensive and pervasive kaolinitic alteration most probably related to a high sulphidation (HS) system.

At Chondro Vouno the picture of the veins' development is complicated being influenced by the various tectonic trends (NE, NW) as well as by their nature, being chalcedonic, amethystine, saccharoidal and milky. Without doubt their distinctive features are the colloform-crustiform banding generally with barite. Two main sets of veins have been encountered at Chondro Vouno, the weakly mineralized one being along NW-SE (30°-50°W) direction (along the crest of the mountain) (Fig.58a to c) and the mainly mineralized along NE striking directions (from N-NE (35°) to NE-E (65°-80°). The various kinds of silica veins vary in width from hairline to 5cm crystalline quartz, drusy quartz veins with locally strong associated limonite after sulfides, to finely colloform-crustiform quartz veins up to 1m in width. It has been observed that from the highest middle crest point of Chondro Vouno to the saddle zone, going towards Profitis Ilias, NE-SW trending colloform banded chalcedonic quartz-baryte veins are mineralized with chalcopyrite, low-Fe sphalerite, galena and malachite staining (Fig. 58e). Electrum and acanthite as anhedral interstitial grains have been observed microscopically to be included into chalcedonic quartz veins. Generally it could be said that the colloform banded chalcedonic- adularia veins are associated with minor sphalerite, galena and acanthite.

At the NNW part of the ridge the veins trend NE and have a massive to saccharoidal and amethystine aspect containing some sulfides, while at the NW to N end, the NE trending veins become more E-W trending and steeply (70° - 90°) dipping to the S, and have a drusy character. They seem to predate NW-trending colloform chalcedonic-barite veins. Downhill to the N and NNW, the colloform-crustiform veins become amethystine (in the so called Amethyst area) (fig.58f). At the base of the amethyst ridge area the veins strike sub-horizontally from E-W to NE-SW, while above them, on the crest, the veins, as mentioned previously although have the same striking direction (NE-SW), dip steeply to the south. At the veins intersection areas, brecciation is encountered including fragments of earlier vein material. The most of these intersection points present a colloform-crustiform quartz growth locally mixed with amethystine/sugary quartz veins which at their turn are

cut at low angles by amethystine/ milky quartz veinlets which strike at NE (~60°) and dip to SE.

As a general observation, it seems that there are special relations that govern the strike of the different kind of veins in between the various lithological units. Indeed at the higher topographic levels, the fine tuff unit (Fat) which strikes from ENE to ESE (60°-110°) and dip from NW to W, hosts crystalline amethystine quartz veinlets/veins which have a direction about ENE (70° – 80°) and dip from SE to S, (i.e., parallel to quasi parallel to the strike of the lithological unit but dipping exactly to the opposite side). At lower topographic levels, where the intrusive rhyolite body (Rhyda) outcrops, having a strike of ENE-WSW (60°) and dipping to NW (i.e., parallel to the overlying intruded fine tuff unit), the amethystine quartz veinlets strike from NNE - SSW (10°- 40°), NE - SW (45°) to ENE-

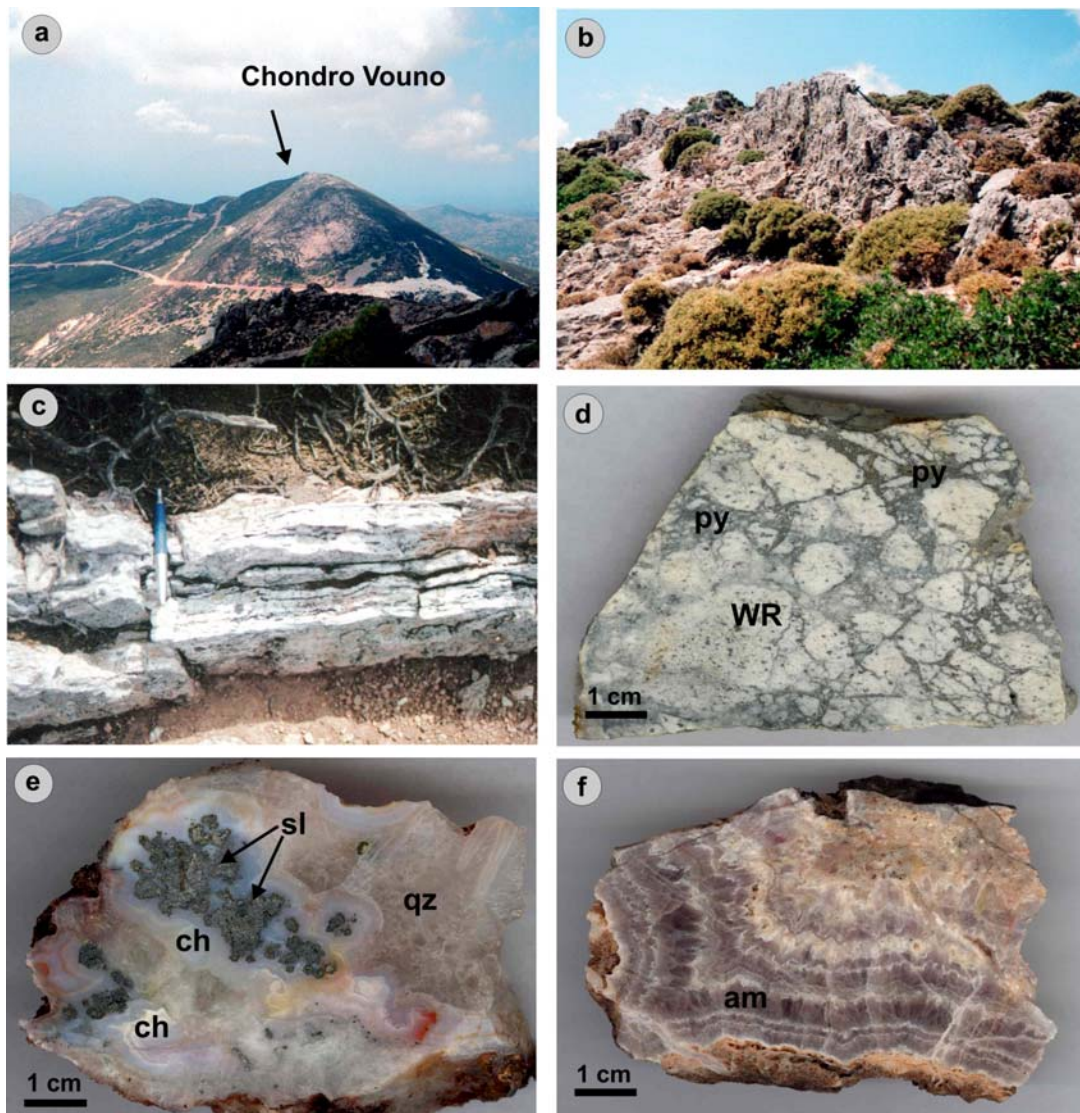


Fig. 58 : (a) The Chondro Vouno ridge, shown from Profitis Ilias; (b and c) Quartz-chalcedony-barite veins running along the crest of the mountain at a NNW-SSE direction; (d) adularized wallrock fragments (WR) of pumiceous tuff in an quartz-pyrite (py) matrix; (e) Colloform sphalerite (sl) and galena surrounded by chalcedony (ch) and quartz (qz) from a NE-SW trending vein at the saddle between Chondro Vouno-Profitis Ilias; (f) Hand specimen of amethystine quartz vein from the NE-SW trending vein system at Amethyst area.

WSW (58° - 85°) and WNW - ESE (105°-120°), NNW - SSE (150°-160°) and dip from subvertically to the ESE up to SE - SSE, the SE being the dominant dip.

At the Western part of Chondro Vouno toward Peristeria, NNE to E-W trending vein sets locally contain appreciable limonite after base metals. The E-W set appears to be younger than the NNE one, and it is vuggy and locally contains baryte or amethystine quartz. It seems that the above scheme, in this last part it is further complicated by a series of N-S running faults, related to mineralized veins, veinlets and breccias crosscutting the previous mineralized NE-SW to E-W trending system. It is considered that the N-S mineralized strike direction belongs to the N-S trend of the subvolcanic bodies (Rhyda, Anda). The breccias contain silicified subvolcanic and tuff angular fragments in a silicified (locally black chalcedony) - pyritized (with subordinately low-Fe sphalerite, galena, chalcopryrite and covellite, < 2 %) matrix. Drusy quartz veins crosscutting the breccia body are locally limonitized after sulphides, indicating that the breccia predates significant gold mineralization.

Locally Mn microlayers with minor barite are intercalated into the lower pumiceous lapilli tuff unit (Lmp), striking from E -W to WNW- ESE and dipping from N to NE, following also a general silicified trend. In the area, Mn-Fe oxides bearing micro- crystalline quartz/barite veinlets strike at WNW - ESE (290°) directions and dip sub- vertically. The supergene profile of the area is expressed by Fe-oxides, jarosite and alunite stockwork veinlets.

Laterally with respect to Koumaria-Skiadi area, going toward S-SW, a field of small boulders (<2 m) of drusy quartz, quartz-baryte veins are situated between larger silicified, adularized and barytized ignimbritic (PIi) boulders (Pyrgiali). These are interpreted to be the remnants of an intermediate sulphidation (IS) silicified area that has been truncated by a later explosive event most probably of phreatic/phreato- magmatic nature. Below the silicified boulders, a moderately to strongly argillized lower pumiceous lapilli tuff unit (Lmp) with some local spotty strong hematization is the predominant outcropping formation. Base metal veinlets (bornite, pyrite) trending N60°E and dipping to SE also outcrop. Crustiform/colloform quartz veinlets striking N70°E and dipping to the N is another feature of the area.

At topographically lower levels, towards the footwall of Pyrgiali and along the same NE trending and SE dipping trends, fault/fractures filled by crystalline baryte and fine sulfides are also present. Little bit further to the West, at Trakoniates, hydrothermal explosion breccias are present and dominate the whole sub-zone over there.

At Peristeria area a set of NE-SW (40°-60°) striking and steeply to 70° NW dipping faults, expressed through a series of breccias and stockworks, are cutting through a quartz-sericite-illite altered and barite impregnated fine tuffs (Fat). Two types of breccias are distinguished, the first being a vein-breccia type made up by quartz vein clasts (~50%) and subordinately altered tuffs, either in a silicified and partially oxidized matrix with disseminated (up to 2%) sphalerite, galena, pyrite and Cu-staining, or just in a smectitized/illitized and locally oxidized matrix. The second type is a very fine silica-pyrite matrix supported breccia. Thin quartz stockworks and chalcedonic/crystalline quartz-baryte veinlets, showing partially colloform-crustiform banding with sphalerite, galena and pyrite disseminated grains, is another feature of the area.

6.3.5. Profitis Ilias - Livadakia - Chontri Rachi

The Profitis Ilias ignimbrite (PIi) dominates the surface geologic picture and overlies fine

tuffs (Fat), pumice flow tuffs (Pfl) and the older lithic/ pumice tuff (Lpt), while at the southern-southeastern parts covers interbedded conglomerate, marls, limestones and basement schists. At the upper parts of Profitis Ilias mountain, various flow dykes (Rhyda) which intruded the Profitis Ilias ignimbrite are presented deformed and folded during flow, which implies that the cooling rates were low (i.e. subaerial environment) and the material had a sufficiently ductile behaviour.

The Profitis Ilias ignimbrite (PIi) is characterized mainly by felsic pumices and schist fragments. In a more general sense it can be described as a sequence consisting of products ranging from coarse-grained lithic, pumice airfall and pumice flow deposits (central facies eruptive area of Profitis Ilias) to distal facies with increasing proportion of laharcic/block (volcanic avalanches) and ash-sized airfall material. The Profitis Ilias ignimbrite strikes NNE -SSW (10° - 15°) and dip to the WNW. Locally it is presented crystalline, with the crystalline fragments, in order of decreasing abundance being K-feldspars (orthoclase and sanidine), quartz, volcanic glass, mafic Fe-Mg minerals, leucoxene, rutile and rare zircon. Silicification is intense along the crest of Profitis Ilias, while in other parts, where veins and stockworks are located, can be assigned as moderate to intense. Towards the outer limits of the silicification, vein density decreases and veins become thinner and finally disappear. Laterally away from the veins, the degree of argillization increases.

Profitis Ilias is bounded by a trapezoidal set of faults some of which are normal and forms a horst like block similar to Chondro Vouno. Tectonic structures and veins form a pattern suggestive of a dominant N-S trending and west dipping normal faults with associated east dipping extension fractures in the hanging wall area to the main horst structure. Furthermore, structures appear to have developed discrete major vein zones rather than a more broadly distributed stockwork of veins.

The mineralization is related to quartz-sericite-adularia veins and stockworks, hosted in the acid lower pumiceous lapilli (Lmp), fine tuffs (Fat) and ignimbrites (PIi) as a series of steeply dipping, N-S to NE-SW, up to ENE (45° - 80°) trending epithermal quartz veins along N to NE striking faults. There is also another set of veins trending N 30° W. The veins vary from drusy quartz with base metals and telurides, to colloform banded chalcedony-crystalline quartz-barite-base metals \pm Au, quartz-adularia-Ag \pm Au, barite-Manganese, amethystine quartz-Ag \pm Au.

At the upper stratigraphic levels, sheeted, crustiform-colloform banded chalcedonic-quartz-barite veins, consist of marginal fine-grained quartz to chalcedony, followed by coarse-grained barite, chalcedony-quartz with base metal sulfides, and by an internal part occupied by coarse-grained comb-quartz with final barite. Carbonate replacement textures also exist. Lower in the sequence, drusy quartz veins with base metal sulfides and telurides, may represent feeder zones to the near-surface crustiform-colloform banded chalcedonic-quartz veins. The vein thickness and continuity of the individual veins vary along strike (up to 3m), although structural zones containing the veins remain continuous along strike and down-dip. Locally, vein-breccia structures including veinlet fragments and some silicified tuff fragments (up to 30cm) into a silicified matrix, are observed.

Ore metallic paragenesis at the upper levels occur mainly into the colloform-crustiform chalcedony-crystalline quartz phase (Fig. 59f), and consist of base metal sulphides (galena, sphalerite, chalcopyrite) and sulphosalts, gold (native and electrum), silver halogenides (chlorargyrite, iodargyrite) and native silver (Constantinidou et al. 1998; Dimou 2001; Kiliyas et al. 2001). Generally the early and late barite generation lack quasi of any metallic mineral as is the case for the late comb quartz crystal veins. However late amethystine qu-

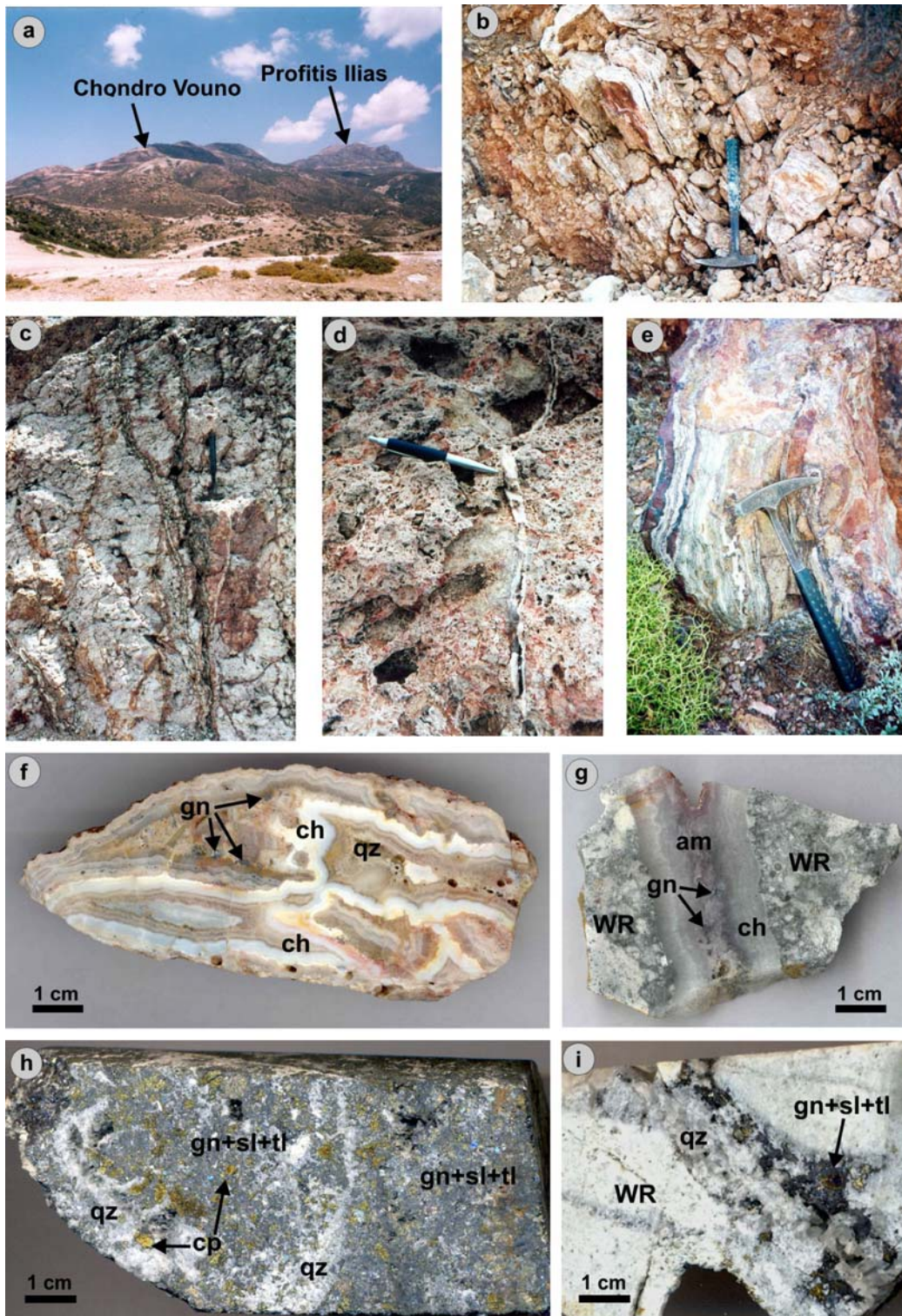


Fig. 59 : (a) Panoramic view of Profitis Ilias and Chondro Vouno, from N to S; (b) Vein-breccia structure; (c) Quartz-Barite-Mn and oxidized based metals veins crosscutting argillic altered tuffs; (d) Silicified and vuggy Profitis Ilias ignimbrite at the top of the mountain, cut by quartz-chalcedony veinlets; (e) crustiform-colloform chalcidonic banded vein; (f) Hand specimen of colloform banded chalcedony (ch) - quartz (qz) vein with galena; (g) Banded chalcedonic (ch) - quartz vein with late amethyst (am) and galena (gn), Wallrock (WR) alteration is quartz-adularia; (h and i) Drillhole specimens with galena (gn), sphalerite (sl), chalcopyrite (cp) and Au-Ag-tellurides (tl) in a quartz gangue. Wallrock (WR) alteration is quartz-adularia.

artz is hosting base metal sulphides (Fig. 59g). It is important to mention that at depths base metals, native gold and Au-Ag-tellurides are abundant and described for the first time during this study (Fig. 59h,i). In addition bornite, chalcocite and covellite replacing chalcopyrite are interpreted to be the result of combined action of sea water oxidation and renewed hydrothermal pulses and not as previously thought of supergene oxidation (see next chapter 7-ore mineralogy). The gangue paragenesis consists of quartz, barite, adularia mainly under form of small veinlets and subordinately disseminated. The supergene mineralization at Profitis Ilias contains goethite/lepidocrosite after pyrite, cerussite, Fe-Mn-Al oxides and hydroxides, jarosite, alunite and malachite.

Livadakia is an area located between the Chondro Vouno-Profitis Ilias saddle at north, the Chondri Rachi at west and Profitis Ilias-Kampanas Gremna area at east. Along this area a crossing of several important lineaments/faults is verified (NE trending fault which drops down to the north the Chondro Vouno subarea, the NW trending and west bounding Chondro Vouno fault, as well as another series of faults which have a radial disposition with respect to the Profitis Ilias- Kampanas Gremna subareas). Moderate to intense argillic alteration is the main feature of the area. At Chondri Rachi, the outcropping stratigraphy comprises a dacitic flow dome (Dado) intruded within a lower lithic/pumice tuff unit (Lmp), overlain by a fine ash tuff (Fat), and at the uppermost part by the poor welded Profitis Ilias ignimbrite. In between the Profitis Ilias ignimbrite boulder field in the broader area, there are a minor number of boulders containing either colloform-crustiform quartz veins or vein-breccia fragments, so suggesting for a relation to a shallow submarine phreatomagmatic vent, venting at the place where now it is situated the Chondri Rachi dome.

At Tsouvala area the Profitis Ilias ignimbrites (PLi) unit lies unconformably on the underlying limestone/sediments and dip from horizontal to slightly 5° to the Est. At their base a rich coarse (boulder size) lithic (subvolcanic, sedimentary, metamorphic) fragment layer, dominate the landscape. In this layer the dacitic subvolcanic fragments reach quasi metric dimensions.

6.3.6. Mavrovouni - Vathi Rema

The main feature at Mavrovouni is a large area of highly milled and silicified multiple stage breccia boulders (1-3m length) composed of fragments of older breccias, country rocks and colloform banded quartz and quartz - chalcedony vein ones, hosted within clay-rich (kaolinite-illite) pumice flow unit (Pfl) and moderately to strongly argillized and locally strongly silicified lithic/pumiceous tuffs (Lpt). These boulders form a large complex of phreatomagmatic-phreatic eruption breccia occurring in a localized hot spring area, most probably associated with the emplacement at shallow depths of several subvolcanic dacitic bodies (Anda, Dado) in the area between Profitis Ilias and Mavrovouni. Indeed the pumice flow unit (Pfl) and the lithic pumice tuff unit (Lpt) outcropping in the area, seem to reproduce the palaeo- seafloor topography as it resulted after a shallow intrusion emplacement. The spectacular boulders of multi episode vein breccias seen at Mavrovouni reflect multi episodes of mineral deposition and hydraulic fracturing followed by explosive pressure release. Little bit further down with respect to the boulders fields, younger cross-cutting dikes and sills of dacitic/andesitic composition (Dado) also outcrop. The andesite/dacite is fresh with only locally some propylitic alteration. Locally cherty silicified mudstones are also present.

The major tectonic lineaments that controlled through their intersection the Phreatomagma-

tic-phreatic eruption breccias at Mavrovouni are considered to be an important normal fault (trending NW-SE) starting from Ammoudaraki going through Koumaria and extending towards SE to the vicinity of Mavrovouni where intersects E-W running structures, and another set of N-NE trending faults which seem to be the same as that “acted” at Profitis Ilias. The NW striking fault (N 320° W) is considered to be a strike-slip dilational fault jog. The mineralization style of Mavrovouni area can be described taking into consideration the two main formations which host it, i.e., a) the hydrothermal multistage breccias and b) the silicified volcanics. The first are essentially a matrix supported breccias with different relative contents in older breccia fragments, metamorphic ones from the basement, older silicified lithic tuffs, volcanics and colloform-crustiform banded crystalline quartz and crystalline quartz-chalcedony vein fragments immersed in a strongly silicified milled matrix. The content in vein clasts into the silicified boulders is variable from place to place, being around 20 vol. %, in some zones, and around 50 vol. % and 80 vol. % in others. The silicified lithic/pumiceous tuffs are characterized by the presence of quartz and sphalerite, galena, chalcopryrite bearing veins/stockworks and Cu, Fe-oxides staining. The pumice flow tuff is intensely clay altered and associated with pyrite. The including fragments into the big breccia boulders can be described in more details through a subdivision as follows: silicified and alunited quartz veined acid lithic tuffs showing open space filling colloform-crustiform chalcedonic to microcrystalline quartz-alunite veinlets and veins including acanthite (interstitial euhedral to anhedral grains). Alunite occurs as fine flakes and aggregates surrounded by crystalline quartz. Most probably this indicates an earlier high sulfidation event, which is postdated by banded epithermal quartz veins containing hypogene pyrite and supergene covellite, chalcocite after chalcopryrite (similar to those described from deeper levels at Profitis Ilias). Strongly silicified ignimbrite (PIi) truncated by thin colloform-crustiform banded quartz-adularia veinlets containing mainly anhedral to subordinately euhedral hypogene acanthite grains, pyrite, chalcocite, covellite after chalcopryrite, is another local feature. The Vathi Rema area is located W-NW from Mavrovouni. It is another field of multi-breccia boulders mainly made up by quartz-veined Profitis Ilias ignimbrites (PIi). This style of boulders is totally different from that one of the silicified breccia boulders seen at Mavrovouni, and because of their elongate shape and configuration it appears rather as a debris slide coming from the southern flank of Profitis Ilias mountain.

7. PARAGENETIC RELATIONSHIPS AND ORE MINERALOGY

Textural and paragenetic studies from western Milos sulphide mineralization provide important information about its formation and evolution from a sub-seafloor/seafloor to a transitional shallow submarine to subaerial setting. Comparison can be made with active and extinct volcanic-hosted massive sulphide (VHMS) or transitional VMS to epithermal deposits such as Lahanos and Kizilkaya deposits in northeastern Turkey (Leitch 1981, 1990), the Hellyer/Tasmania deposit (Solomon & Gaspar 2001), the Neves-Corvo ores/Portugal (Gaspar 2002), Conical Seamount/offshore Lihir islands, Papua New Guinea (Petersen et al. 2002; Gemmel et al. 2004), Rainbow field/Mid-Atlantic Ridge (Marques et al. 2006), Rodrigues Tripple Junction/Indian Ocean (Halbach et al. 1998), TAG hydrothermal mound/Mid-Atlantic Ridge (Petersen et al. 2000), the Brothers and Rumble II West volcanoes/offshore New Zealand (Wright et al. 1998; De Ronde et al. 2003, 2005), North Fiji Basin (Kim et al. 2006), White Church and Hine Hina/Lau back-arc (Herzig et al. 1998), East Pacific Rise (Haymon & Kastner 1981), Endeavour Segment/Juan de Fuca Ridge (Tivey & Delaney 1986), the Bransfield Strait/Antarctica (Petersen et al. 2004), the Lerokis and Kali Kuning deposits on Wetar island/Indonesia (Scotney et al. 2005), the Lucky Strike, Rainbow and Logatshev fields/Mid-Atlantic Ridge (Rouxel et al. 2004), Pueblo Viejo/Dominican Republic (Kesler et al. 1981, 2005). It follows a description of sulphide textures and paragenesis of each subarea under study. The results are summarized in Tables 2.

7.1. Triades

The sub-seafloor/seafloor Triades mineralization contains mainly galena, sphalerite, tetrahedrite-group minerals and pyrite and it is enriched in Ag (up to 855 ppm) and Au (up to 4.1 ppm) (Liakopoulos 1987; Vavelidis & Melfos 1998). A re-examination of ore material from Triades during this study recognized for the first time the abundance of enargite in the mineralization (Alfieri et al. 2004). The textural features of the ore, indicate an early deposition of pyrite followed by galena with tetrahedrite inclusions plus minor chalcopyrite, at which follows a high-sulfidation ore assemblage composed of enargite, tennantite, hypogene covellite and late pyrite (Figs. 60 and 61, Table 2). The ores are accompanied by barite, sericite, kaolinite and quartz gangue.

Early **pyrite** occurs as euhedral crystals (Fig. 60 a, e, f, g, h), whereas late pyrite occurs as colloform banded pyrite, framboids and spherulites (Vavelidis & Melfos 1998; this study, Fig. 61d). A feature observed in some early Triades pyrite shows a concentric growing around a hole considered to represent a micro-chimney structure. **Sphalerite** occurs throughout the whole paragenetic sequence. It includes tetrahedrite/tennantite (Fig. 60c) while it is also surrounded by tennantite (Fig. 60d). Sphalerite displays mutual relationships and thus it is considered to be contemporaneous with galena (Fig.60g). **Galena** is closely associated to Ag-bearing tetrahedrite. Indeed it contains small inclusions and it is crosscut by tetrahedrite (Fig. 60h). Galena is also observed as inclusion in tennantite (Fig. 60a, e) or in contact to tennantite included in sphalerite (Fig.61a). According to Vavelidis & Melfos (1998) the Triades sphalerite and galena display colloform, banded or atoll-shaped textures, however these are not observed during the present study. **Chalcopyrite** is included and also surrounds galena. **Tennantite** is closely related to enargite and both are probably deposited contemporaneously during late introduction of As-bearing solutions in the mineralization, or the Enargite has been deposited immediately after tennantite.

Tennantite surrounds galena (Fig. 60a, b, g), sphalerite (Fig. 60d) and pyrite (Fig. 60e, g) while it is also included in sphalerite (Figs 60c and 61 a, b).

Enargite, a minor but important constituent in the mineralization, occurs either as inclusions in tennantite (Fig. 60 a, g) or clearly postdates tennantite (Figs. 61b, c). A silver-rich enargite surrounds sphalerite and seems to predate tennantite (Fig. 60b). Enargite is closely associated with covellite and an unknown silver sulfosalt (probably proustite) (Fig. 61b, c).

Covellite is intergrown with enargite (Fig. 61c) indicating its hypogene origin.

An **unknown silver sulfosalt** (probably proustite) accompanies tennantite and enargite in the mineralization (Fig. 61a, b). This phase together with Ag-bearing tetrahedrite and the Ag-bearing enargite are carriers of silver in the mineralization.

The presence of enargite in Triades mineralization is a definitive criterion for its classification into the high-sulfidation category (Arribas 1995; Hedenquist et al. 2000). Similarly to the subaerial epithermal settings, where enargite forms either early or late in the paragenetic sequence (Einaudi et al. 2003; Sillitoe & Hedenquist 2003), in submarine settings (Brothers Volcano / Offshore New Zealand, Wetar island/Indonesia, etc) enargite is

Table 2 : Paragenetic sequence of vein mineralization in western Milos Island

Location	TRIA	GAL	PI-CV	KONDB	KONDT	KATM	AGA
Mineral							
Quartz	-----	-----	-----	-----	----	-----	----
Amethyst			-----				
Chalcedony			-----	----		-----	
Sericite	-----	-----	-----				
Adularia	-----	-----	-----	-----		-----	
Calcite				---		---	
Barite	-----	-----	-----	-----		-----	
Pyrite	-----	-----	-----	----	----	----	----
Bornite			---				
Enargite	----	----					
Covellite	----	----	---		----		----
Chalcocite			---				
Galena	----	----	-- ---	-----	-----	-----	-----
Chalcopyrite	----	----	-----		--		--
Sphalerite	-----	-----	--- ---	-----		-----	
Marcasite							
Hematite				----		----	
Pyrrhotite							
Native Gold			---- --				
Electrum			-----				
Tetrahedrite	----	----	-----	----		----	
Tennantite	----	----					
Polybasite				----		----	
Pearceite				----		----	
Hessite			-----				
Petzite			-----				
Altaite			-----				

Abbreviations : TRIA = Triades, GAL = Galana, PI-CV = Profitis Ilias – Chondro Vouno, KONDB = Kondaros base, KONDT = Kondaros top, KATM = Katsimoutis, AGA = Agathia.

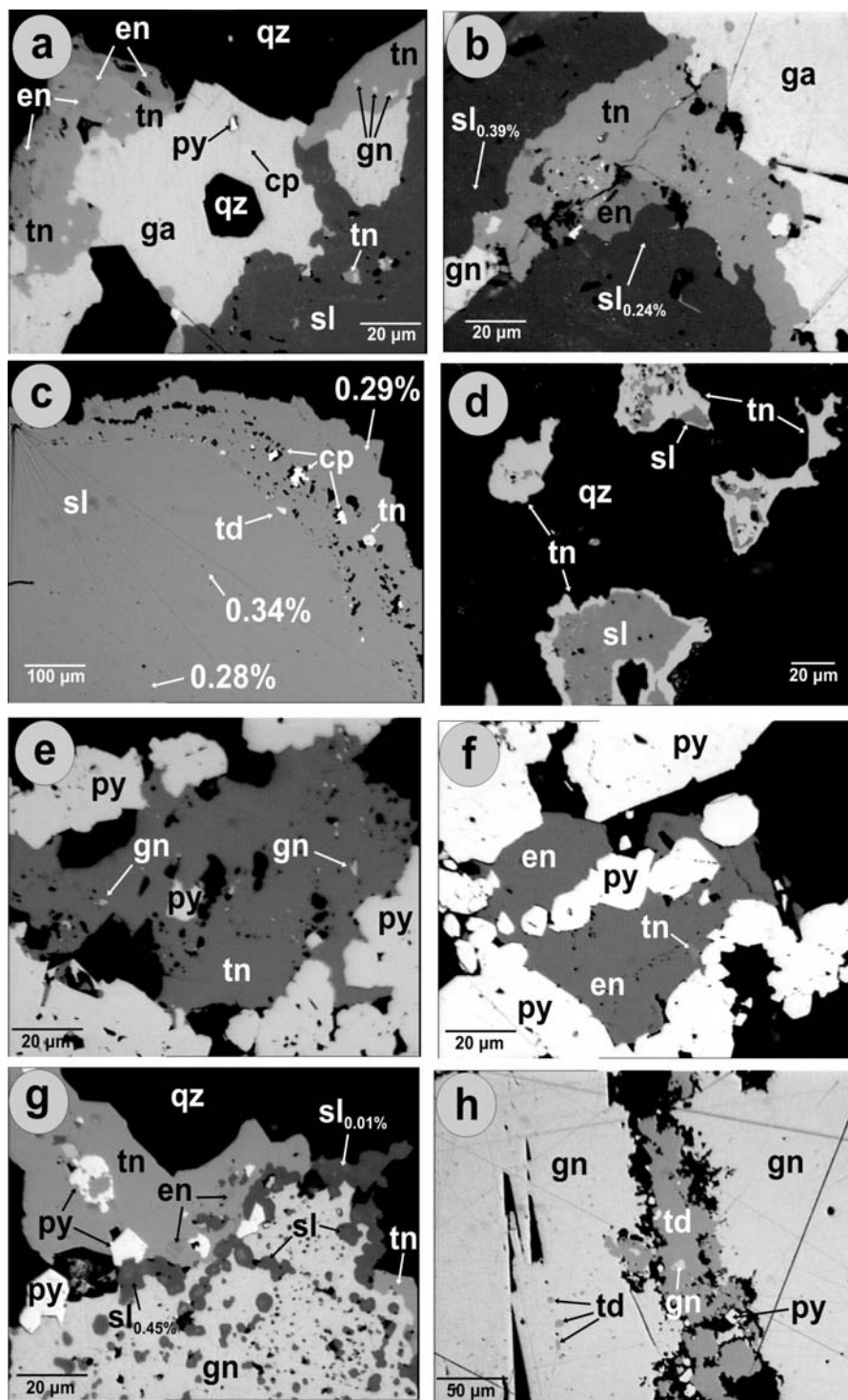


Fig 60 : Microphotographs (Reflected light) of Triades ores (a) pyrite (py) and chalcopyrite (cp) enclosed within galena (gn). The later is enclosed and also surrounded by tennantite (tn) and enargite (en). Late sphalerite (sl) surrounds tennantite. Quartz (qz) is gangue. (VA31); (b) Tennantite (tn), and enargite (en) associated with galena (gn) and sphalerite (sl). (VA50); (c) Sphalerite (sl) with tennantite (tn) and tetrahedrite (td) inclusions. (VA31); (d) Sphalerite (sl) surrounded by tennantite (tn). (VA31B); (e) Tennantite (tn) with galena (gn) inclusions surround pyrite (py). (VA31B); (f) Enargite (en) and tennantite (tn) surround pyrite (py). (VA31B); (g) pyrite (py) surrounded by galena (gn) – sphalerite (sl) intergrowth and late enargite (en) – tennantite (tn). Quartz (qz) is gangue. (VA31B); (h) Galena (gn) included and also encloses tetrahedrite (td). Pyrite (py) also enclosed in tetrahedrite. (VA50).

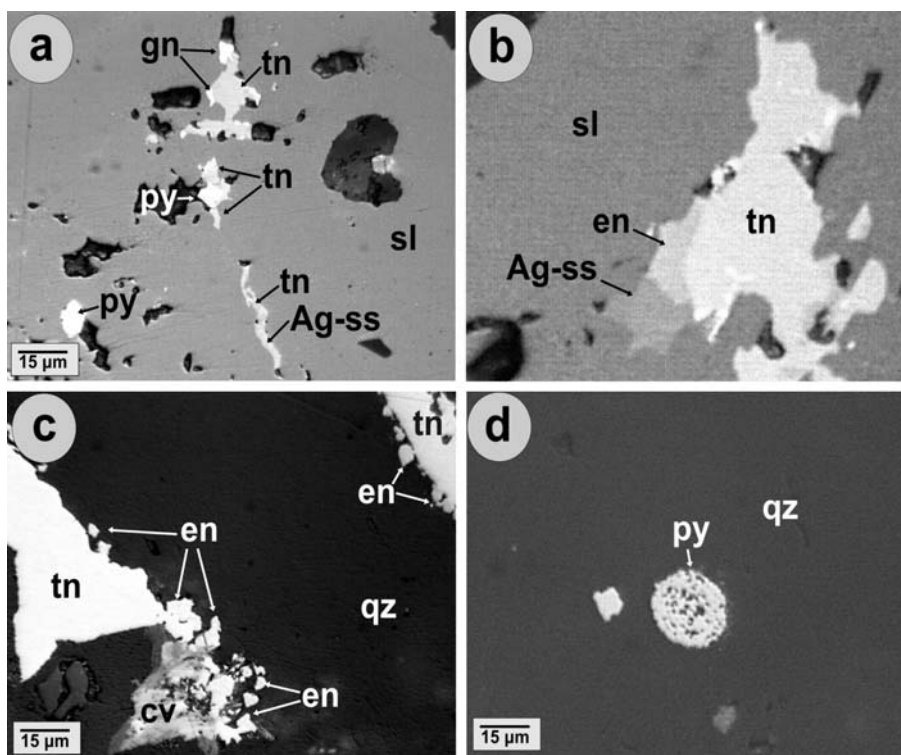


Fig.61 : Microphotographs (Reflected light) of Triades ores (a) Galena (gn), tennantite (tn), pyrite (py) and unknown silver sulfosalt (Ag-ss) included in sphalerite (sl) (VA31); (b) Tennantite (tn), enargite (en) and unknown silver sulfosalt (Ag-ss) included in sphalerite (sl) (VA31); (c) Enargite (en) and covellite (cv) surround tennantite (tn) (VA31B), (d) Framboidal pyrite (py) included in quartz (qz) (VA31B).

reported either as an early or late mineral (Sillitoe et al. 1996; de Ronde et al. 2005; Scotney et al. 2005).

7.2. Galana

Galana mineralization (Liakopoulos 1987) is similar to that described from Triades. Paragenetic relationships (this study) suggest early pyrite, followed by chalcopyrite, galena, tetrahedrite and Fe-poor sphalerite and then by an As-Cu-bearing assemblage including tennantite and enargite (Fig. 62, Tables 2).

Pyrite is euhedral and coarse-grained and contains small inclusions of bornite/digenite and sphalerite (Fig. 62a, c, f). Framboidal pyrite has not been observed here.

Galena is very abundant at Galana. It surrounds pyrite, occurs as small inclusions in enargite, tennantite and sphalerite and is deposited contemporaneous with chalcopyrite and tetrahedrite (Fig. 62 a to e).

Sphalerite similarly to Triades is deposited throughout the ore assemblage. It was introduced after pyrite and also surrounds tennantite and enargite late in the paragenetic sequence.

Tennantite is abundant at Galana and postdates chalcopyrite, galena and sphalerite (Fig. 62a, b, c, e).

Enargite is associated to tennantite (Fig. 62a, b), similarly to Triades. Overgrowths of enargite on tennantite and vice versa, suggest that they have grown simultaneously. It should be mentioned that this is the first reported occurrence of enargite at Galana similarly to Triades. The presence of enargite and tennantite in Galana mineralization is of

metallogenic significance, since both minerals help classifying this mineralization into the high sulfidation category (Einaudi et al. 2003). The ores are accompanied by quartz, sericite and barite gangues.

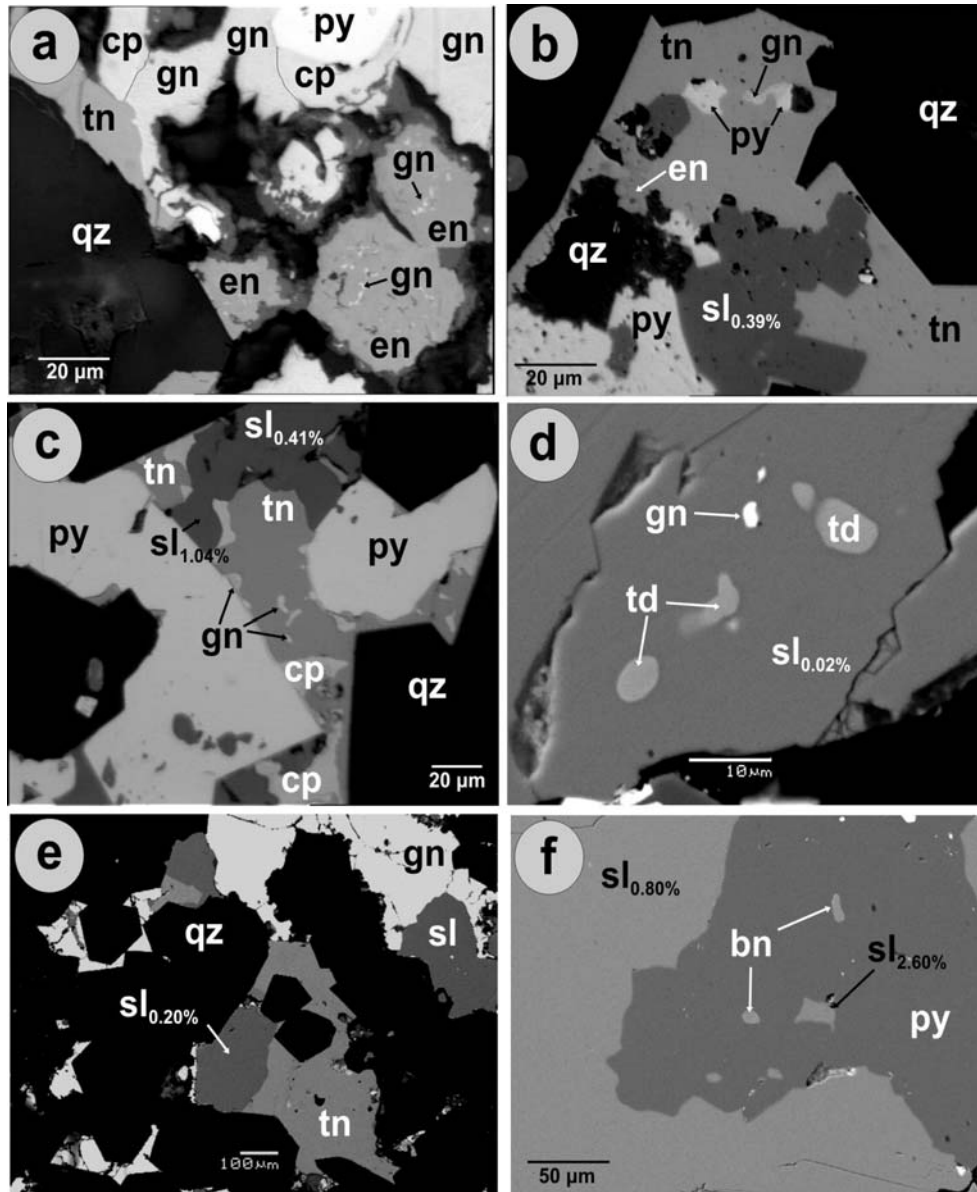


Fig 62 : Microphotographs (Reflected light) of Galana ores (a) pyrite (py) surrounded by chalcopyrite (cp) and galena (gn) and then by tennantite (tn) and enargite (en). Galena (gn) is also enclosed within enargite. Quartz (qz) is gangue. (VA51); (b) Pyrite (py), sphalerite (sl) galena (gn) and enargite (en) surrounded by tennantite. Quartz (qz) is gangue. (VA51); (c) Sphalerite (sl), galena (gn) chalcopyrite (cp) and tennantite (tn) surround pyrite (py). Quartz (qz) is gangue. (VA51); (d) Tetrahedrite (td) and galena (gn) included in sphalerite (sl). (GAL1); (e) tennantite (tn), galena (gn) and sphalerite (sl) surround pyrite (py). Quartz (qz) is gangue (GAL2); (f) Pyrite (py) with inclusions of bornite (bn) and sphalerite (sl) enclosed within Fe-poor sphalerite (sl). (GAL1).

7.3. Agathia

Sulfide mineralization at Agathia is restricted within the vuggy- and massive silica zones, especially in the microlayered black silica structures crosscutting massive silica. A com-

mon feature at Agathia is the presence of a concentric zonation of early collomorphic melnikovite pyrite overgrown, recrystallized and overprinted by euhedral, coarser grained pyrite and marcasite. Late iron sulfides are intergrown with natroalunite (Fig. 63a to e). The whole texture is very similar to “round layered shelly pyrite balls” described from the Lahanos massive sulfide deposit in Turkey, which probably formed by filling in or growing around a tube-worm hole, and overgrown by later euhedral pyrite (Leitch 1990). Similar structures are characteristic of sulfides on recent seafloor e.g., Axial Seamount/Mid-Atlantic Ridge, Juan de Fuca ridge, the Galapagos ridge, the East Pacific Rise and the Guayamas basin in the Gulf of California (Hannington & Scott 1988; Normark et al. 1983; Law et al., 1983; Hekinian et al., 1980; Peter & Scott 1988), at fossil spreading ridges, e.g.

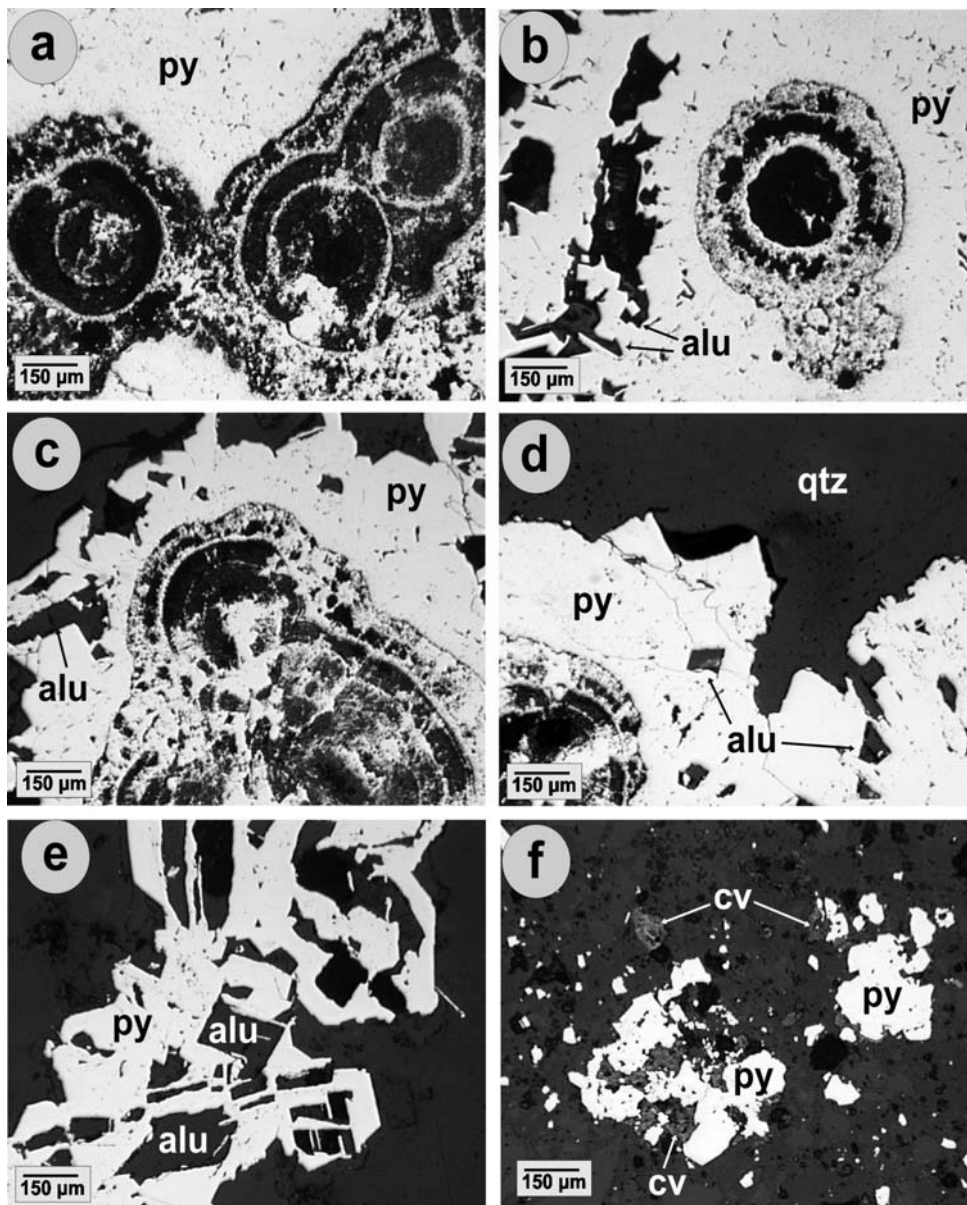


Fig 63 : Microphotographs (Reflected light) of Agathia ores (a to d) Micro-chimneys composed of early colloidal “melnikovite” pyrite recrystallized to coarse-grained pyrite (py) and by late marcasite (mr). Alunite (alu) is included in marcasite. Quartz (qz) is the gangue, (Agathia, VA13); (e) Alunite (alu) intergrown with marcasite (mr) (VA13); (f) covellite (cv) postdates and surrounds pyrite (py), (VA13).

Samail ophiolite/Oman, Troodos complex/Cyprus (Haymon et al., 1984; Oudin & Constantinou 1984, 1994), as well as at the fossil VHMS deposits at Neves-Corvo/Portugal (Gaspar 2002).

At Agathia late coarse-grained pyrite-marcasite are overgrown by sphalerite, galena and covellite of hypogene origin (Fig.63f). The overprinting of the primary depositional textures by recrystallization and precipitation of later coarse-grained pyrite-marcasite, sphalerite, galena and covellite at Agathia it is considered to be the result of an intensification in the hydrothermal activity which most probably have taken place immediately after initial precipitation as suggested by Leitch 1990. Ore and gangue mineralogy clearly indicate Agathia mineralization as of a high-sulfidation type.

7.4. Katsimoutis

At Katsimoutis area the NE-SW trending vein-type base-metal mineralization has already been described by Liakopoulos (1987) and Vavelidis (1995). These authors demonstrate early deposition of framboidal, spherical or atoll-shaped As-bearing pyrite, succeeded by galena, sphalerite and second generation of, this time, As-free pyrite. According to Vavelidis (1995) the presence of colloform and framboidal pyrite at Katsimoutis is an evidence of a submarine depositional environment.

Recently, Alfieris & Voudouris (2005) described a previously unrecognized Ag-rich base-metal bearing mineralization developed along the major NW-SE Kondaros-Katsimoutis fault which crosscut the above mentioned NE-SW trending Katsimoutis occurrence. Carbonate, barite, adularia and quartz are the gangues. Mineralization took place under several (at least three) substages each of them characterized by the same paragenetic sequence. In general, paragenetic studies indicate early deposition of pyrite and sphalerite followed by galena including polybasite-pearceite solid solutions and Ag-tetrahedrite, and then by pyrite plus hematite, chalcopyrite and marcasite (Fig. 64).

Pyrite is closely associated with galena, tetrahedrite, silver sulfosalts and hematite. It occurs as small inclusions in galena (Fig. 64a, d), in sphalerite, where it accompanies galena, tetrahedrite, silver sulfosalts and hematite (Fig. 64f), and also surrounds galena (Fig. 64h). Framboidal pyrite has not been observed in the studied Katsimoutis mineralization. **Sphalerite** is coarse grained and occurs throughout the paragenetic sequence displaying a weak chemical zoning. Sphalerite cores include pyrite, galena, tetrahedrite, silver sulfosalts and hematite and are Fe-richer than sphalerite rims, which are deficient in the above minerals (Fig. 64e, f). **Chalcopyrite** and **bornite** are minor phases and occur as inclusions in sphalerite in association with galena and pyrite. **Galena** is coarse-grained and abundant in the mineralization. It is replaced by sphalerite (Fig. 64g) and pyrite (Fig. 64h) and it is considered to be the main carrier of silver as it contains exsolved grains of argentian tetrahedrite and polybasite-pearceite solid solutions. **Hematite** is ubiquitous in the mineralization. It accompanies early phases (pyrite, galena, tetrahedrite, silver sulfosalts) included in sphalerite and also occurs as isolated laths in the silicified matrix (Fig. 64g).

Argentian tetrahedrite forms either small blebs exsolved from galena or occurs in association with pyrite, galena, silver sulfosalts and hematite in sphalerite cores.

Polybasite-pearceite solid solutions were deposited contemporaneously with argentian tetrahedrite and occur as exsolved grains within galena, or in association with pyrite, galena, tetrahedrite and hematite in sphalerite cores.

The Katsimoutis base metal assemblage grades into sulfide-poor colloform banded chalcidony and finally into very coarse-grained calcite pseudomorphs after aragonite.

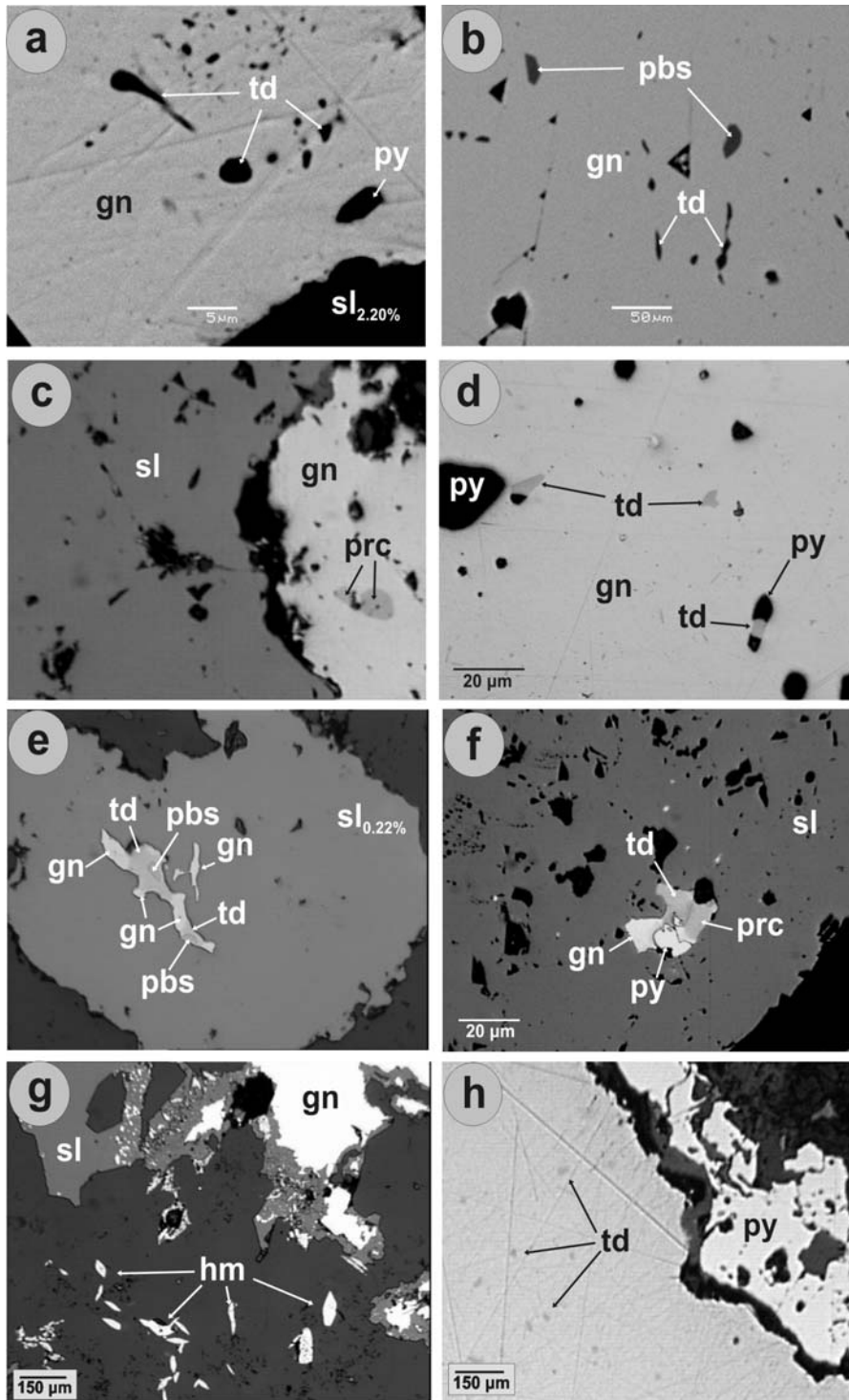


Fig 64 : Microphotographs of Katsimoutis ores (a) tetrahedrite (td) and pyrite (py) enclosed within galena (gn) in association with sphalerite (sl), (KAT1, SEM-BSE image); (b) Polybasite (pbs) and tetrahedrite (td) grains included in galena (gn), (KAT2, SEM-BSE image); (c) Galena (gn) including pearceite (prc) in association to sphalerite (sl), (KAT1a, reflected light); (d) Pyrite (py) and tetrahedrite (td) included in galena (gn), (KAT9, reflected light); (e) intergrowth of tetrahedrite (td), galena (gn) and polybasite (pbs) within sphalerite (sl), (KAT1b, reflected light); (f) Intergrowth of tetrahedrite (td), galena (gn), pyrite (py) and pearceite (prc) in sphalerite (sl), (KAT1a, reflected light); (g) Galena (gn) replaced by sphalerite (sl), hematite (hm) is also present (VA20, reflected light); (h) Galena (gn) with argentic tetrahedrite (td) exsolutions surrounded by pyrite (py), (KAT2, reflected light).

Manganese oxides accompany late carbonates in the veins. The precipitation of aragonite from a hydrothermal fluid-seawater mixture and by CO₂ degassing has been reported from inactive chimneys at Guayamas basin (Hannington et al. 1986) and from shallow-water hydrothermal fluids at Tutum Bay, Ambitle Island/Papua New Guinea (Pichler & Veizer 2004).

7.5. Kondaros

In Kondaros area two mineralization styles have been distinguished:

7.5.1. Kondaros top

At higher topographic elevations (Kondaros top), sulfide mineralization is entirely hosted within brecciated massive silica bodies of high-sulfidation style. Sulfides show concentric zoning and the textures are quite similar to those reported from Agathia. They consist of inner framboidal pyrite, recrystallized and surrounded by euhedral, coarse-grained pyrite and late marcasite. Barite and natroalunite are intergrown with the iron sulfides (Fig. 65a to c). Late **chalcopyrite** and **covellite** replace alunite, crosscut and surround marcasite and pyrite (Fig. 65a to c).

Chalcopyrite and covellite also occur in sulfide veinlets crosscutting the silicified matrix (Fig. 65c). This mineralization can be considered to represent seafloor deposition of a shallow submarine high-sulfidation system. Type examples are the Lerokis and Kali Kuning deposits on Wetar island/Indonesia (Sewell & Wheatley 1994; Scotney et al. 2005). The upper Kondaros mineralization could be analogous to the recent sea-floor magmatic-hydrothermal system of Desmos caldera in the eastern Manus back-arc basin off Papua New Guinea, where basaltic andesite have been altered to pyrophyllite and alunite and mineralized with iron sulfides, enargite and covellite (Gamo et al. 1997; Gena et al. 1998; Sillitoe 1999).

7.5.2. Kondaros base

At lower elevations (Kondaros base), the Kondaros mineralization is quite similar to the NW-SE trending Katsimoutis one, since it represents its SE continuation.

The paragenetic sequence, similar to that from Katsimoutis, indicate early deposition of pyrite and sphalerite followed by galena including polybasite-pearceite solid solutions and Ag-tetrahedrite, and then by pyrite together with hematite, chalcopyrite, minor bornite and finally by late sphalerite (Figs. 65 d to f and 66, Table 2).

The Kondaros-base mineralization shows some textural evidences which is believed to represent mineral precipitation within fluid conduits (Tivey et al. 1995). Indeed often the sulfides form concentric structures with a core composed of galena, pyrite and minor sphalerite, rimmed mainly by sphalerite and then by pyrite (Fig. 65e, f). Very fine-grained skeletal intergrowths of galena, pyrite and sphalerite at the core, and intergrowths of needle-shaped pyrite with sphalerite at the inner rim, are characteristic features of this assemblage. These skeletal intergrowths are suggestive of alternative precipitation from separate Pb-rich and Zn-rich fluids rather than replacement, i.e., similar to those from Pacmanus hydrothermal field, where sphalerite forms colloform growths and overgrowths with tennantite and chalcopyrite at the central conduit. It is believed that these intergrowths are suggestive of very rapid precipitation from mineralized plumes discharging immediately below, or on the seafloor.

There is a close relationship between galena and silver-bearing phases like polybasite, pearceite and Ag-tetrahedrite, as already described for Katsimoutis mineralization. The

silver-bearing sulfosalts occur either in association with galena enclosed within sphalerite (Fig. 66a), or in the form of small exsolved grains in galena (Fig. 66b). Microscopic observations and electron microprobe data indicate zoning in sphalerite, where Fe-richer cores are closely related to the deposition of galena and silver-bearing phases, similarly to the Katsimoutis mineralization (Fig. 66a). Spherulitic hematite and pyrite, as well as colloidal, atoll-like pyrite is a ubiquitous constituent of late-stage mineralization.

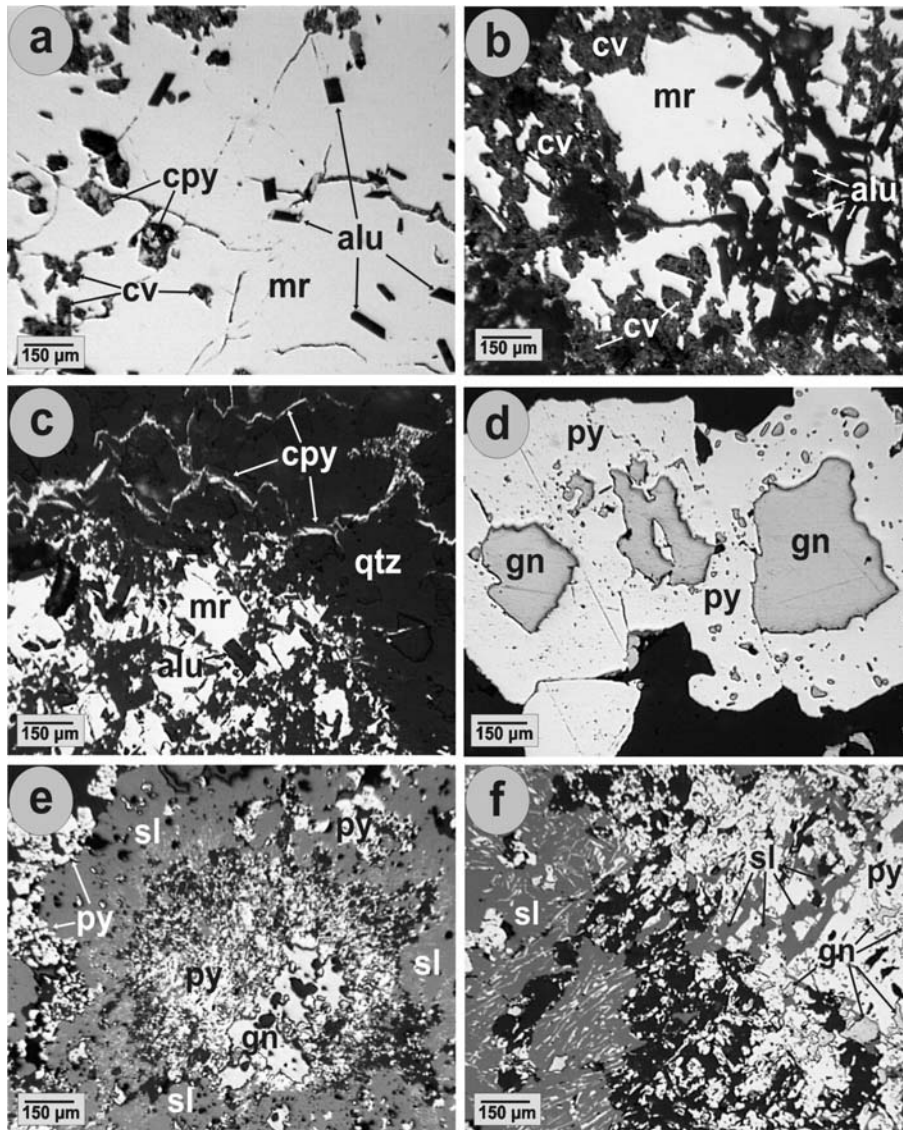


Fig. 65 : Microphotographs of Kondaros ores (a to c) Marcasite (mr) with alunite (alu) inclusions. Chalcopyrite (cpy) and covellite (cv) replaces alunite and also occur in veinlets within massive silica (qtz) gangue (VA16, reflected light); (d) Galena (gn) surrounded by pyrite (py) (KONT4, reflected light); (e) microchimney consisting of early pyrite (py) and galena (gn), late sphalerite (sl) and latest pyrite (py) (KONT4, reflected light); (f) Skeletal intergrowth between pyrite (py), galena (gn) and sphalerite (sl) in the previously shown microchimney, (KONT4, reflected light).

The mineralization is accompanied by quartz, calcite (after aragonite), barite, and adularia gangue. Vugs are filled by late unknown zeolite spherulites.

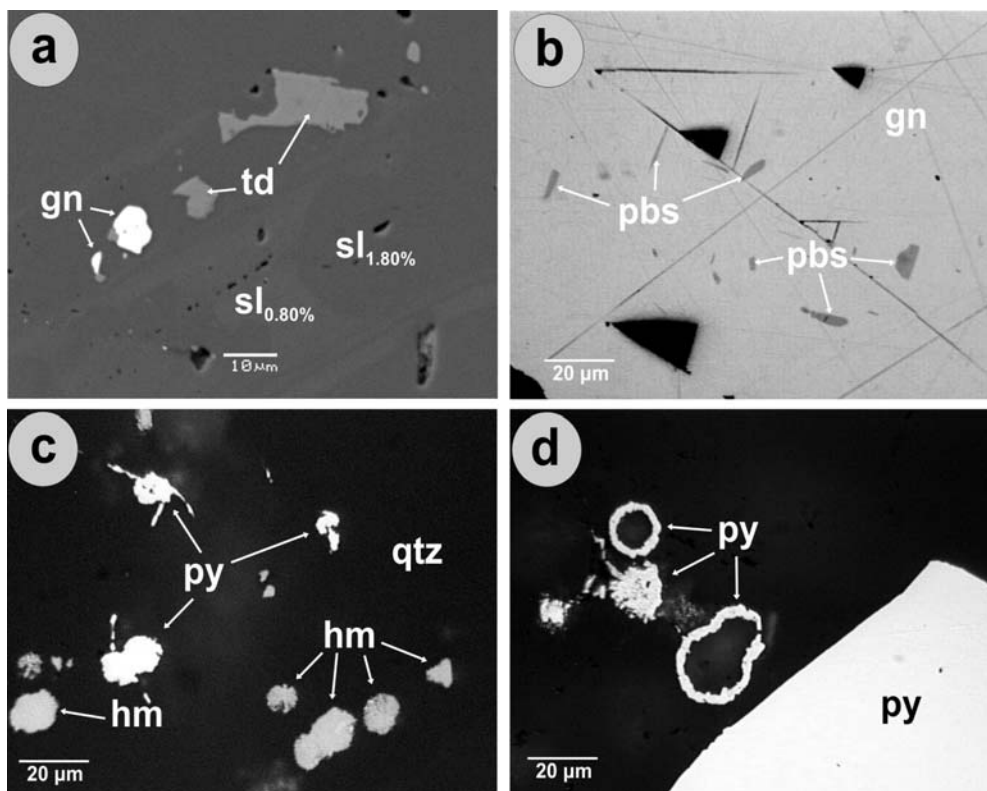


Fig. 66 : Microphotographs of Kandaros ores (a) Tetrahedrite (td) and galena (gn) enclosed in sphalerite (sl), (KON2, SEM-BSE image); (b) polybasite (pbs) exsolutions in galena (gn), (KON13, reflected light); (c) Framboidal pyrite and hematite in quartz gangue (KONT14, reflected light); (d) Framboidal and atoll-like pyrite (py) postdating coarse-grained pyrite (KONT4, reflected light).

7.6. Profitis Ilias

Mineralization at Profitis Ilias comprises mainly pyrite, chalcocopyrite, galena, Fe-poor sphalerite, native gold and electrum (Constadinidou et al. 1998, Kiliyas et al. 2001). Native gold and electrum were described by the above authors only from oxidized samples and not in contact with the sulfide assemblage. In addition, Dimou (2001) described silver halogenides from the upper parts of the deposit, and she considered a substantial amount of silver to be hosted within these secondary phases.

Surface material sampled during this study, indicate deposition of base metal sulfides (galena, sphalerite and chalcocopyrite) and tetrahedrite with both, the chalcedonic and the late comb amethystine quartz. Galena includes chalcocopyrite, tetrahedrite and sphalerite. Pyrite is the most abundant sulfide among the surface samples and was deposited early in the paragenetic sequence. Surface samples from Profitis Ilias are characterized by the presence of atacamite. In some drillhole samples from the upper levels of the deposit, atacamite and native copper comprise more than 70 vol. % of the silicified rock. The presence of atacamite at Profitis Ilias and its mineralogical significance for the ore forming conditions (involvement of seawater), is already discussed by Dimou (2001).

Of major importance for the genetic interpretation of Profitis Ilias deposit, is the recognition of a previously unknown precious metal mineralization in drillhole material coming from the deeper levels of the deposit (elevation 320m above sea level). This mineralization is characterized by an early deposition of pyrite followed by an assemblage composed of the tellurides hessite, altaite and petzite and by native gold, chalcocite, galena, chalcocopyrite and finally by sphalerite (Figs. 67, 68a, b, c and Tables 2). A second

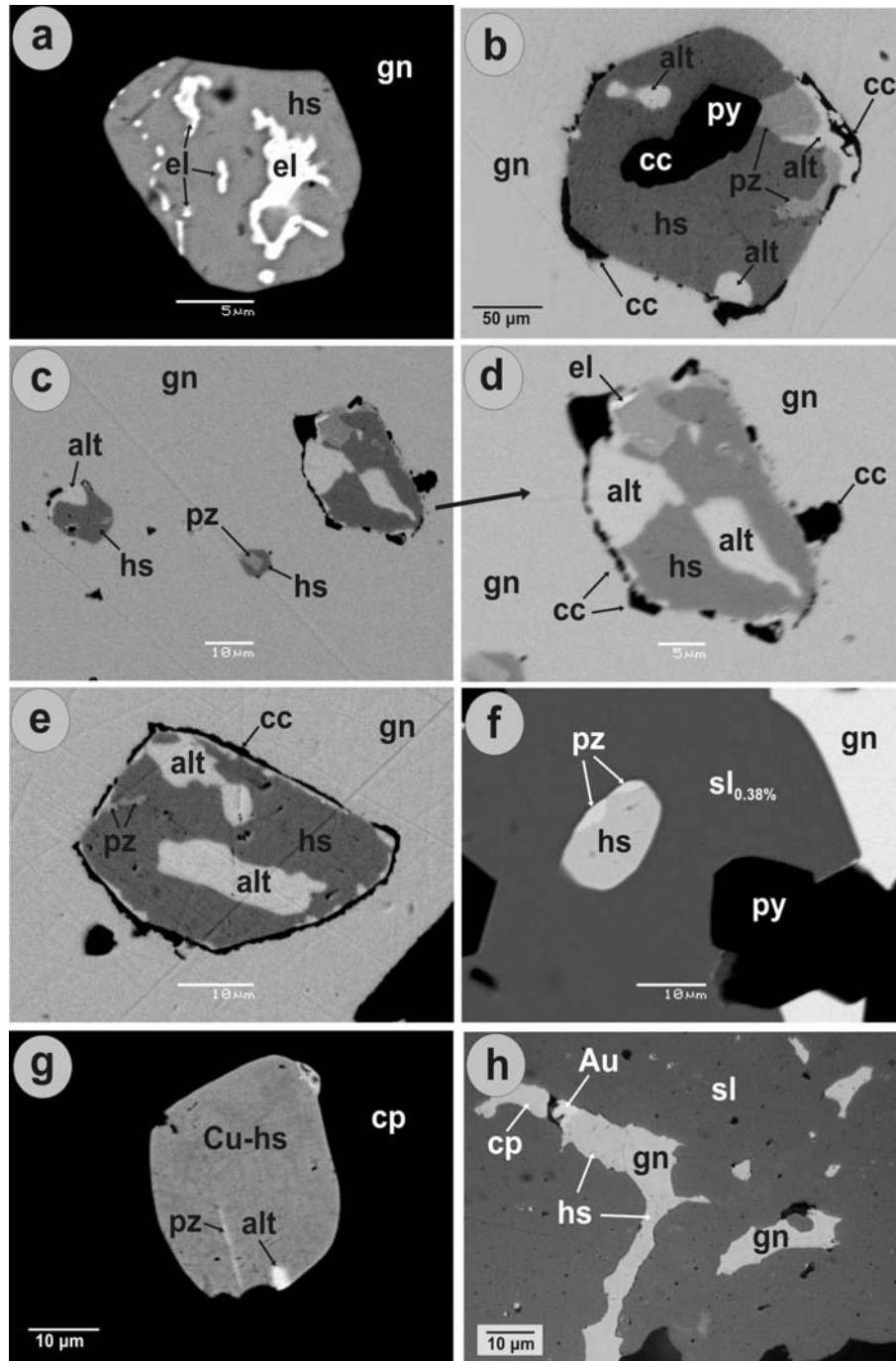


Fig. 67 : Microphotographs (Scanning electron microscope-back scattered electron image, SEM-BSE) of Profitis Ilias ores (a) Hessite (hs) with electrum (el) exsolutions enclosed within galena (gn). (PD12-318); (b) Petzite (pz) at the grain boundaries between hessite (hs) and sphalerite. Galena (gn) and pyrite (py) is also present. (PD12-318); (c) altaite (alt), hessite (hs) and petzite (pz) enclosed within galena (gn). (PD12-318); (d) Enlargement of fig. 3c: Altaite (alt), hessite (hs), petzite (pz) and electrum (el) separated from galena (gn) by a chalcocite (cc) rim. (PD12-318); (e) Hessite (hs), altaite (alt) and petzite (pz) rimmed by chalcocite (cc) and enclosed within galena (gn). (PD12-318); (f) chalcocite (cc) enclosed and also rimming the tellurides hessite (hs), petzite (pz) and altaite (alt). Pyrite (py) accompanies chalcocite. Galena (gn) is also present. (PD12-318); (g) Unknown sulfotelluride, probable Cu-bearing hessite (Cu-hs), petzite (pz) and altaite (alt) included in chalcopyrite (cp) (PI1c); (h) chalcopyrite (cp), galena (gn), hessite (hs) and native gold (Au) included in sphalerite (sl), (PI2A-2, reflected light).

mineralizing event which introduced copper sulfides and a second generation of galena overprints both the tellurides and the earlier sulfides.

The tellurides are included either in galena, chalcopyrite and sphalerite, or they occur at the grain boundaries between sphalerite and galena. In a broader sense the telluride assemblage is separated from galena by synchronous growth of chalcocite.

The following contact assemblages of gold-, silver- and tellurium-bearing phases have been observed: hessite-petzite, altaite-petzite, altaite-hessite, native gold-petzite and native gold-hessite.

Hessite mainly occurs as composite blebs within galena (Figs. 67a to e and 68c), within sphalerite (Figs. 67f, h and 68a) and chalcopyrite (Fig. 67g). Hessite also occurs along grain boundaries between early pyrite and galena. Most hessite contain exsolved petzite, and/or Au, altaite.

Native gold occurs as filaments in blebs of hessite (Fig.67a), as isolated inclusions in chalcopyrite, or at grain boundaries between hessite and chalcopyrite.

Petzite is present as minute grains within blebs of hessite or as coarser inclusions surrounded by hessite. The round shape of some petzite inclusions, suggests co-crystallization of hessite-petzite. Petzite occurs also as skeletal flakes in hessite or as inclusions with square cross-section.

Altaite occurs in the form of exsolved grains in hessite, where it is closely associated with petzite.

Galena is a major constituent of Profitis Ilias mineralization. It is present in two generations. Early galena form subhedral to anhedral grains, which accompany chalcopyrite, sphalerite and the precious metals in the ore. Late galena occurs in veinlets and vugs, crosscutting earlier sulfides and being closely associated to the late copper sulfides. It is euhedral forming small cubes up to 150µm in length.

Chalcopyrite similarly to galena was introduced from both early and late stage fluids. Early coarse-grained chalcopyrite accompanies sphalerite and is precious metal carrier in the ore. Late chalcopyrite occurs either in veinlets, closely related with the second generation galena, or replaces late bornite.

Sphalerite of both first and second generation it is also present in the deep Profitis Ilias ore. Early sphalerite is a major carrier of precious metal tellurides, whereas late-stage sphalerite forms small subhedral grains associated with copper sulfides.

Pyrite was also introduced during early and late hydrothermal events in the mineralization. It occurs either as coarse-grained euhedral crystals, or as small subrounded grains in an atoll-like configuration accompanying galena and chalcopyrite (Fig. 68d).

The copper sulfides **bornite**, **covellite**, **digenite** and **chalcocite** replace chalcopyrite and sphalerite and mimic the copper-rich assemblages of the zones showing a supergene enrichment. The copper sulfides replace chalcopyrite initially along fractures within grains, and subsequently around its margins. Indeed chalcopyrite is partly to completely altered and replaced by fine-grained covellite, bornite, chalcocite or by digenite with inclusions of bornite. Copper is released from primary chalcopyrite and redeposited within the copper sulfides by chemical migration to the margins of altered primary sulphide grains. Locally covellite, bornite and digenite tend to be completely pseudomorphous after chalcopyrite. Covellite also occurs as inclusions in sphalerite.

Chimney-like structures are locally observed either around a tube-like hole, probably a central conduit, where the outer walls are occupied by early bornite and the inner walls by covellite (Figs. 68g and 69b), or in the form of concentric bands around a central sulphide assemblage (Fig. 69h). In the second case an inner bornite±chalcocite±digenite assemblage

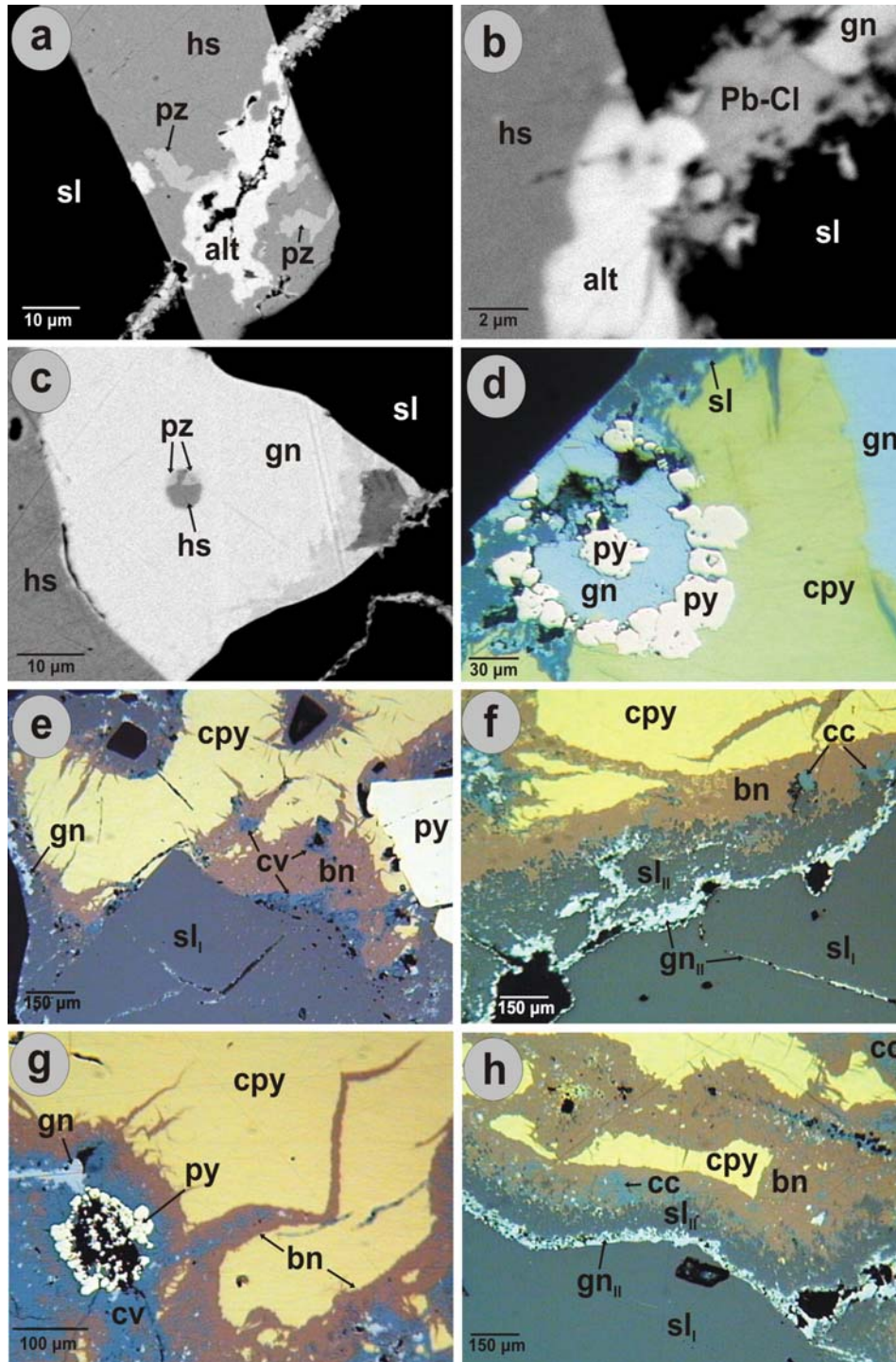


Fig.68 : Back scattered electron (a-c) and reflected light (d-h) images demonstrating the ore paragenesis of Profitis Ilias (a) Hessite (hs) with Altaite (alt) and petzite (pz) inclusions surrounded by sphalerite (sl) and crosscut by second generation galena (gn) (PI1c); (b) Altaite (alt), hessite (hs), and sphalerite (sl) succeeded by second generation galena (gn) and unknown Pb-Cl compound (PI1c); (c) Petzite (pz)-hessite (hs) bleb included within galena (gn). Galena is also in contact to hessite and sphalerite (sl) (PI1c); (d) Atoll-like pyrite (py) surrounds galena (gn) and it is surrounded by chalcopyrite (cpy) (PI1a); (e to h) chalcopyrite (cpy) and galena (gn) replaced by a Cu-rich assemblage composed of bornite (bn), digenite (dg), chalcocite (cc) and covellite (cv) as well as by a second generation galena (gn_{II}), sphalerite (sl_{II}) and probably pyrite (py), in (g).

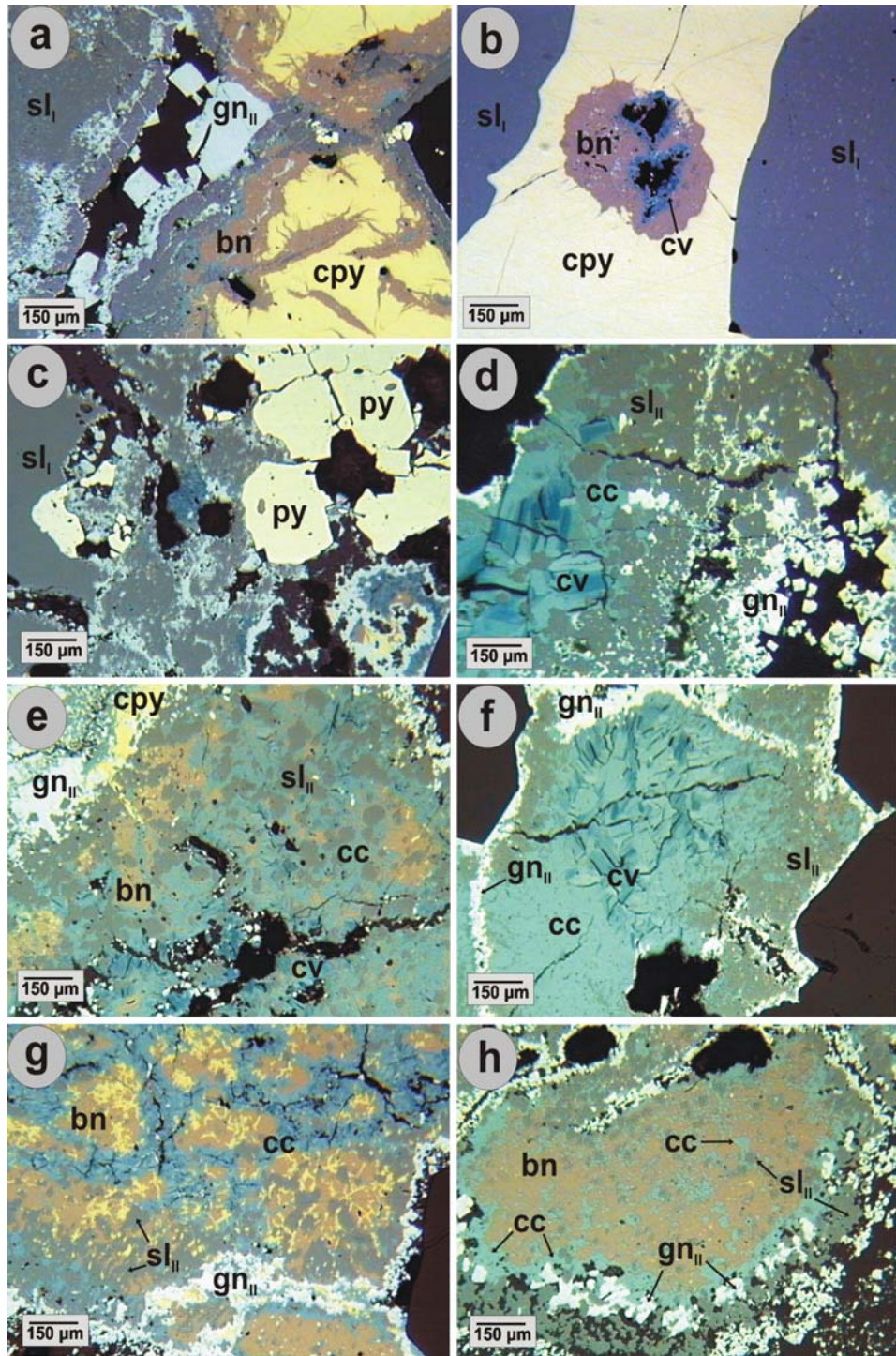


Fig. 69 : Reflected light images demonstrating ore paragenesis of Profitis Ilias ores (a) Coarse-grained second generation galena (gn_{II}) in cavities postdating bornite (bn) and early chalcopyrite (cpy) and sphalerite (sl_I); (b) micro-chimney within chalcopyrite (cpy) composed of bornite (bn) and covellite (cv); (c) Sphalerite (sl) replaced by covellite (cv) and second generation galena (gn_{II}). Pyrite (py) remains fresh; (d to g) Various textures between bornite (bn), digenite (dg), chalcocite (cc), covellite (cv), second generation galena (gn_{II}) and sphalerite (sl_{II}). Chalcopyrite (cpy) in e and g probably belong to the late Cu-rich association (PI2a, PI6c); (h) Cu-rich assemblage in a chimney-like structure: bornite (bn), digenite (dg) and remobilized sphalerite (sl_{II}) surrounded by second generation galena (gn_{II}) and sphalerite (sl_{II}), (PI6c).

is progressively surrounded by sulphide bands composed of digenite, second generation galena, sphalerite and again galena. These copper sulfides are similar of alteration assemblages found in the outer walls of black smoker chimneys, where the oxidation of chalcopyrite by seawater produces a supergene secondary assemblage of Cu-sulfides, Cu-chlorine phases (atacamite) and rare native Cu (Haymon et al. 1984; Hannington et al. 1988). The textures described from Profitis Ilias resemble those observed from inactive deposits and external rims of active black smoker chimneys at Lucky Strike, Rainbow and Logatchev/Mid-Atlantic Ridge seafloor hydrothermal fields, exhibiting varying degrees of replacement of chalcopyrite by a Cu-rich assemblage of bornite, covellite and digenite (Rouxel et al. 2004). These authors suggest a formation either by hydrothermal reworking of copper sulfides below seafloor by hydrothermal vents, or by late-stage processes at low temperature.

Rather than believing in previous works about a supergene origin of bornite and covellite in Profitis Ilias deposit (Constantinidou et al. 1998; Kiliass et al. 2001), the presence of second generation galena, sphalerite and chalcopyrite together with bornite, covellite and digenite at Profitis Ilias strongly suggest a hydrothermal origin of copper sulfides. These are lower temperature phases formed probably by the combined action of seawater oxidation of chalcopyrite and by late-stage hydrothermal pulses. A hydrothermal origin of copper sulfides associated with late pyrite from inactive chimneys at Rodrigues Triple Junction/Indian Ocean has also been proposed by Halbach et al. (1998). Under this aspect the formation of Profitis Ilias (at least the lower telluride-bearing parts) is a typical sub-seafloor precipitation of sulfides forming stockwork zones as proposed by Hannington et al. (1995). Later low-temperature circulation of seawater and a renewed hydrothermal pulse led to the formation of second generation phases, including copper sulfides, galena and sphalerite. Atacamite and native copper in the upper parts of Profitis Ilias may result from direct oxidation of the sulfides by seawater.

7.7. Chondro Vouno

Surface material from Chondro Vouno contains sphalerite with abundant inclusions of galena, chalcopyrite and Ag-tetrahedrite (Fig. 70a), similarly to that from Profitis Ilias. Fine-grained colloform and spheroidal pyrite forms a tubular porous foundation, which is overgrown by coarse-grained pyrite, sphalerite or chalcopyrite, and probably represent fluid chimneys (Fig. 70b).

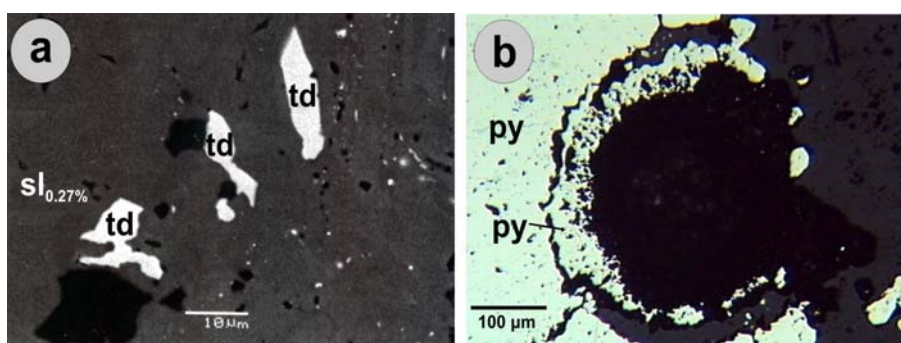


Fig. 70 : Microphotographs demonstrating ore paragenesis of Chondro Vouno ores (a) Tetrahedrite (td) included in sphalerite (sl) (SEM-BSE); (b) Micro-chimney composed of pyrite (py), (Reflected light, VA25).

8. ORE CHEMISTRY

Microprobe analysis was an important tool in order to better quantify the mineralizing processes in the island. The chemical variations of most ore minerals were investigated using a Cameca-SX 100 wavelength-dispersive electron microprobe at the Department of Mineralogy and Petrology, University of Hamburg. Operating conditions were 20kV and 20nA. The following X-ray lines were used: AgL α , AsL α , AuM α , BiM β , CuK α , FeK α , HgM α , PbM α , SK α , SbL α , SeL α , TeL α , ZnK α . Pure elements (for Ag, Au, Bi, Se, Te), pyrite and chalcopyrite (for Fe, Cu and S), galena (for Pb), sphalerite (for Zn), HgS (for Hg), Sb₂S₃ (for Sb) and synthetic GaAs (for As) were used as standards. Corrections were applied using the PAP online programme (Pouchou and Pichoir 1991).

8.1. Tetrahedrite-group minerals

Tetrahedrite-group minerals represent a minor but important constituent of all studied mineralization. Representative microprobe analyses of tetrahedrite-group minerals are given in Table 3 while all EPMA (Electron Probe MicroAnalysis) data are plotted in Fig. 71. Two types of tetrahedrite-group minerals are distinguished: a) A zincian tetrahedrite/tennantite, and b) An argentian (plumbian) tetrahedrite/tennantite type.

Tetrahedrite-group minerals from Triades represent members of the tetrahedrite/tennantite solid solution series, characterized by coupled substitution of Sb by As with As/(As+Sb) ratios ranging between < 0.1 and 1.0 (Fig. 71a). Both As- and Sb-rich members coexist in one sample, but there is a dominance of tennantite over tetrahedrite especially during late-stage ore deposition (see above). All the analyzed tetrahedrite-group minerals show high contents in Zn (between 6.3 and 10.9 wt %) and are classified as zincian tennantites/tetrahedrites. Silver substituting for Cu show a broad compositional range (Fig. 71b) and reach values up to 9.98 wt% (in Sb-rich members).

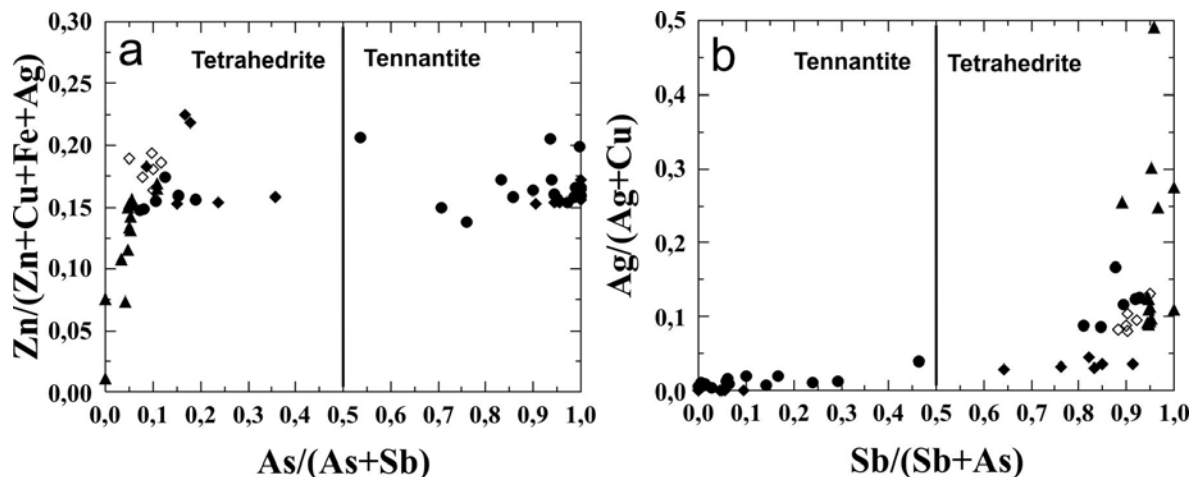


Fig. 71 : Chemical variation of tetrahedrite-group minerals (a) Zn/(Zn+Cu+Fe+Ag) vs As/(As+Sb) diagram and (b) Ag/(Ag+Cu) vs Sb/(Sb+As) diagram. Triades (filled circles); Galana (filled diamonds); Chondro Vouno-Profitis Ilias (open diamonds); Kastimoutis-Kondaros (triangles).

Table 3 : Representative microprobe analyses of tetrahedrite-group minerals (1-13) and enargite (14-16) from Western Milos

wt%	1	2	3	4	5	6	7	8	9	10	11	12	13	14	15	16
Cu	32.77	29.71	31.09	32.16	29.51	42.06	41.63	33.71	35.08	31.38	26.07	17.93	23.95	41.09	47.44	46.89
Ag	4.87	7.60	6.15	7.19	9.98	0.38	0.06	2.75	1.81	7.61	15.18	29.39	17.54	7.13	0.04	0.23
Fe	1.56	1.31	1.45	0.08	2.36	0.34	1.01	0.33	1.32	0.51	1.22	0.70	1.26	0.25	0.81	0.13
Zn	7.51	8.56	8.95	6.87	8.26	8.31	9.16	10.23	7.29	6.76	7.38	2.91	4.76	1.60	0.00	0.52
Sb	27.21	28.69	27.04	26.80	25.63	0.02	0.02	25.22	20.99	28.34	26.30	26.16	27.55	5.34	0.12	0.03
As	1.84	0.92	1.79	1.94	2.23	20.86	20.92	3.36	7.19	1.02	1.97	0.71	0.86	14.05	19.27	18.94
Hg	n.a.	n.a.	n.a.	n.d.	n.d.	n.d.	n.d.	n.d.	n.d.	0.00	0.00	n.a.	n.a.	0.04	n.d.	n.d.
Pb	n.a.	n.a.	n.a.	n.d.	n.d.	0.02	n.d.	n.d.	n.d.	0.24	0.00	n.a.	n.a.			
S	23.39	23.11	23.51	24.18	24.05	28.67	28.46	24.35	25.53	23.30	22.41	21.49	22.57	29.85	32.67	32.77
	99.14	99.91	99.98	99.21	102.02	100.66	101.25	99.96	99.46	99.19	100.52	99.29	98.48	99.35	100.35	99.50
atoms	29	29	29	29	29	29	29	29	29	29	29	29	29	8	8	8
Cu	8.897	8.161	8.404	8.740	7.848	9.736	9.592	8.894	9.042	8.673	7.314	5.434	6.933	2.717	2.930	2.914
Ag	0.777	1.230	0.980	1.150	1.563	0.051	0.008	0.426	0.276	1.240	2.506	5.245	2.991	0.278	0.002	0.008
Fe	0.481	0.409	0.447	0.025	0.714	0.090	0.263	0.099	0.386	0.160	0.389	0.240	0.414	0.019	0.057	0.009
Zn	1.984	2.288	2.352	1.815	2.136	1.869	2.052	2.625	1.827	1.815	2.012	0.857	1.339	0.103	0.000	0.031
Sb	3.857	4.112	3.814	3.801	3.557	0.002	0.002	3.474	2.822	4.088	3.851	4.138	4.163	0.184	0.004	0.001
As	0.423	0.215	0.409	0.446	0.503	4.094	4.088	0.751	1.572	0.240	0.468	0.182	0.210	0.788	1.009	0.998
Hg	n.a.	n.a.	n.a.	0.000	0.000	0.000	0.000	0.000	0.000	0.000	0.000	0.000	0.000	0.001	0.000	0.000
Pb	n.a.	n.a.	n.a.	0.000	0.000	0.000	0.000	0.000	0.000	0.021	0.000	0.000	0.000			
S	12.583	12.583	12.592	13.022	12.678	13.154	12.995	12.731	13.038	12.765	12.459	12.903	12.950	3.911	3.998	4.037

1-3: Chondro Vouno-Profitis Ilias; 4-6: Triades; 7-9: Galana; 10-13: Katsimoutis-Kondaros; 14-15: Triades; 16: Galana

Vavelidis & Melfos (1997) reported in their work Ag-values in tetrahedrites from Triades in the order of 11.8-12.6 wt %. In the same area the silver content in tennantites (As <1.0 apfu) is low and varies between 0.03 and 1.4 wt%. The Bi, Te and Pb contents in measured tetrahedrite-group minerals are below detection limit while Hg reaches values up to 0.29 wt%. At Galana, similarly to Triades, zincian tetrahedrite-group minerals represent members of the tetrahedrite/tennantite solid solution series, with As/(As+Sb) ratios ranging between < 0.1 and 1.0 (Fig. 71a). They show high contents in Zn (6.8 to 10.9 wt %) and Fe (< 1.5 wt %). Silver substituting for copper varies between 0.02 - 2.5 wt% Ag, with Ag/(Ag+Cu) ratios < 0.05. The Kontaros-Katsimoutis system contains almost pure tetrahedrites with As/(As+Sb) ratios < 0.15 (Sb-content varies between 26.1 and 29.5 wt %). Their Ag-content is the highest measured at western Milos reaching values up to 29.4 wt%. The Ag/(Ag+Cu) ratios range widely between <0.1 to 0.5 (Fig. 71b). The Zn-content is lower compared to that from Triades-Galana ranging between 0.5 and 7.6 wt %, with Zn/(Zn+Cu+Fe+Ag) ratios varying between 0.01 and 0.17 (Fig. 71a). In addition a plumbian variety is detected in this area containing up to 7.5 wt % Pb and 6.7 wt % Ag. Plumbian tetrahedrite-tennantite with up to 2.3 wt % Pb is already reported for Triades mineralization by Vavelidis & Melfos (1997). The Chondro Vouno-Profitis Ilias tetrahedrite-group minerals are almost pure tetrahedrite with Zn/(Zn+Cu+Fe+Ag) ratios varying between 0.15 and 0.20 (Fig. 71a). The Ag-content varies between 4.9 and 7.6 wt% Ag (Table 3).

The compositional gap between 0.4 and 0.7 atomic ratios of As/(As+Sb) in Triades-Galana tetrahedrite-tennantite, as demonstrated in figure 71a, could be an indication for the involvement of two distinct fluids in the mineralization. In addition the Kondaros-Katsimoutis tetrahedrites display a trend in the Zn/(Zn+Cu+Fe+Ag) vs As/(As+Sb) diagram (Fig. 71a), which supports the idea of a distinct hydrothermal system which acted most probably separately from that which produced the Triades-Galana and Chondro Vouno-Profitis Ilias deposits. Finally it is clearly demonstrated (Fig. 71b) that the highest Ag-content in tetrahedrite-group minerals occurs in Sb-rich members in accordance to observations of Johnson et al. (1986).

8.2. Enargite

Enargite (Cu₃AsS₄) is a common ore constituent in Triades and Galana mineralization but it is not observed in Katsimoutis-Kondaros and Profitis Ilias-Chondro Vouno one. Microprobe analysis indicated an almost ideal chemical formula (Table 3, 4). It usually contains small amounts of Ag (< 0.25 wt %), Fe (< 1.2 wt %), Zn (< 2.4 wt %), Sb (< 0.35 wt %) and Hg (< 0.07 wt %). An exception to that it is represented by an Ag-rich enargite surrounding sphalerite and coexisting with zincian tennantites in Triades mineralization (Analysis 14-Tab.3); this enargite is Ag-rich (7.1 wt %), Zn-poor (1.6 wt %) and contains 5.3 wt % Sb substituting for As.

8.3. Sphalerite

Sphalerite, a useful mineral in order to place limits on the various fluid sulfidation states when coexisting with pyrite (Chamanske 1974, Barton & Skinner 1979), it is a common constituent in the mineralization studied. More than 85% of the sphalerites analyzed are of the very low-Fe variety with no more than 0.5 wt % Fe (Table 5). The Triades sphalerite contain 0.01 to 0.7 wt. % Fe (0.03 to 1.2 moles % FeS). At Galana, early sphalerites, which occur together with bornite as inclusions in pyrite contain 2.6 wt % Fe (corresponding to 4.6 moles % FeS). Late sphalerite from the same locality are Fe-poor (Fe-content 0.02 - 0.8

wt %), corresponding to 0.04 - 1.4 moles percent FeS, thus being quite similar to those from Triades. The EPMA data on sphalerite from Kondaros-Katsimoutis coexisting with the Ag-rich assemblage, revealed Fe contents between 0.2 and 2.5 wt. % (0.4 - 4.3 moles % FeS).

Table 4 : Representative microprobe analyses of Enargite

wt%	1	2	3	4	5
Cu	47.12	45.70	47.42	46.25	46.76
Ag	0.01	0.16	0.03	0.10	0.14
Fe	1.22	0.11	0.02	0.05	0.04
Zn	0.00	2.38	n.d.	1.02	0.04
Sb	0.34	0.34	n.d.	n.d.	n.d.
As	19.48	18.99	19.34	19.01	19.29
Hg	n.d.	0.05	0.04	0.07	0.01
S	32.95	31.91	33.28	32.75	32.56
	101.12	99.63	100.13	99.29	98.84
atoms	8	8	8	8	8
Cu	2.888	2.861	2.921	2.883	2.926
Ag	0.000	0.006	0.001	0.004	0.005
Fe	0.085	0.008	0.001	0.003	0.002
Zn	0.000	0.145	0.000	0.062	0.003
Sb	0.011	0.011	0.000	0.000	0.000
As	1.012	1.008	1.010	1.004	1.024
Hg	0.000	0.001	0.001	0.001	0.000
S	4.003	3.960	4.065	4.042	4.039

Triades: 1: (VA50), 2 : (VA31/1); Galana: 3- 5 :(VA51).

Finally the Chondro Vouno- Profitis Ilias sphalerites contain <0.5 wt% Fe (0.5 to 0.9 moles % FeS). The sphalerites analyzed during this study are quite similar in composition to the sphalerites from Profitis Ilias epithermal deposit reported by Constadinidou et al. (1998) (Fe-content varies between 0.2 and 1.2 wt %, corresponding to 0.35-2.09 mole % FeS). All analyzed sphalerites contain Mn (< 0.7 wt. %) and Cd (0.2 – 0.8 wt. %), (Table 4). According to recent distinction on sulfidation states with respect to sphalerite composition, as proposed by Einaudi et al. (2003), it is considered that most mineralization at Triades-Galana took place under high- to very high-sulfidation states (although at Galana some intermediate-sulfidation pulses are recorded), and at Katsimoutis-Kondaros at intermediate sulfidation state (the boundary between high- and intermediate sulfidation states is at 1 mole % FeS). Profitis Ilias deposit was formed at intermediate to high-sulfidation states.

8.4. Galena

Galena, the most common mineral in Milos mineralization was traditionally considered to represent together with barite the main silver-hosting mineral. EPMA data from Triades-Galana, Katsimoutis-Kondaros and Profitis Ilias-Chondro Vouno deposits indicated no Ag- and Bi contents and minor content (<0.09 wt %) for Sb in galena. This suggests clearly that the high silver content of western Milos mineralization is accounted to inclusions in Ag-bearing tetrahedrite and Ag-bearing sulfosalts in galena as discussed by Sharp & Buseck (1993).

8.5. Bornite

Bornite is detected as small inclusions within early pyrite at Galana and as inclusions in sphalerite at Katsimoutis areas. It also occurs as a product of seawater oxidation of chalcopyrite in Profitis Ilias deposit. It contains up to 0.6 wt % Ag.

Table 5 : Representative microprobe analyses of sphalerite

wt%	1	2	3	4	5	6	7	8	9	10	11
Zn	65.89	65.83	64.40	67.85	67.36	65.77	64.32	65.60	66.46	67.73	66.08
Fe	0.39	0.68	1.04	0.19	0.79	1.79	2.47	0.68	0.22	0.48	0.52
Mn	0.05	0.10	0.49	0.00	0.13	0.18	0.11	0.03	0.02	0.06	0.37
Cd	0.51	0.62	0.31	0.09	0.77	0.81	0.20	0.09	0.15	0.23	0.24
S	33.07	32.68	32.63	33.82	32.05	31.02	31.89	33.08	32.68	33.18	32.86
Total	99.91	99.90	98.87	101.8	101.1	99.58	99.03	99.49	99.53	100.41	100.1
atoms	2	2	2	2	2	2	2	2	2	2	2
Zn	0.982	0.984	0.969	0.991	1.004	0.998	0.971	0.979	0.995	1.003	0.984
Fe	0.007	0.012	0.018	0.003	0.014	0.032	0.044	0.012	0.004	0.008	0.009
Mn	0.001	0.002	0.009	0.000	0.002	0.003	0.002	0.001	0.000	0.001	0.007
Cd	0.004	0.005	0.003	0.001	0.007	0.007	0.002	0.001	0.001	0.002	0.002
S	1.006	0.997	1.001	1.006	0.974	0.960	0.981	1.006	0.998	1.001	0.998
mole%											
FeS	0.70	1.20	1.80	0.30	1.36	3.08	4.32	1.21	0.40	0.79	0.90

Triades: 1:(VA50),2:(VA31); Galana: 3:(VA51),4:(GAL2); Kondaros: 5,6: (KONT2); Katsimoutis: 7: (KAT1) / 8,9: (Kat1b); Chondro Vouno: 10: (CV); Profitis Ilias: 11: (PI2-1b).

8.6. Polybasite-Pearceite

Several authors have reported on the presence of Ag-Cu-Sb-sulfosalts in western Milos mineralization, however without any documentation (e.g., Vavelidis & Melfos 1997, 1998 and Liakopoulos et al. 2001) reported the presence of pyrargyrite, argentite, proustite and polybasite at Triades-Galana. In addition Ag-Cu-Sb-sulfosalts have also been reported at Profitis Ilias by Constandinidou et al. (1998). During the present study no Ag-Cu-Sb-sulfosalts have been recognized being present in the above occurrences. The presence of polybasite (together with argentian tetrahedrite) as main Ag-carriers in Katsimoutis-Kondaros mineralization was first described by Alfieris & Voudouris (2005). Table 6 presents EPMA results from Ag-Cu-Sb-sulfosalts analyzed during this study. They contains up to 71.7 wt% Ag, up to 8.3 wt % Cu and up to 11.9 wt % Sb. Two grains (analyses 16 and 17) contain 2.5 to 3.1 wt% As and can be considered as polybasite-pearceite solid solutions. The chemical variation of Ag-Cu-Sb-As-sulfosalts and of the analyzed tetrahedrite-group minerals, in terms of $CuS_2-Ag_2S-(Sb_2S_3+As_2S_3)$, is demonstrated in Fig.72.

The assemblage fahlore + polybasite-pearceite solid solution + sphalerite at Kondaros-Katsimoutis is usefull to estimate temperatures during the mineralization event. For this purpose it has been used the geothermometer of coexisting polybasite-pearceite and tetrahedrite-group minerals (Sack 2005), which represents a minor modification to Sack's (2000) model which at its turn reproduces the composition of fahlores produced in experiments on this assemblage for the subsystem $Ag_2S-Cu_2S-ZnS-Sb_2S_3$.

Table 6 : Representative microprobe analyses of polybasite (1-15), pearceite (16, 17)

	1	2	3	4	5	6	7	8	9	10	11	12	13	14	15	16	17
Ag	68.41	67.62	70.01	68.11	70.00	69.75	70.92	67.17	71.71	69.65	69.90	71.00	66.85	64.11	64.49	71.57	70.49
Cu	5.33	6.39	5.50	7.46	5.88	6.82	2.73	2.83	2.99	2.51	2.70	3.28	6.62	8.33	7.74	4.67	4.80
Sb	10.73	9.89	10.25	9.98	10.25	10.07	11.61	11.95	10.79	11.64	11.27	10.32	11.00	10.84	10.85	5.50	6.01
As	0.00	0.29	0.29	0.16	0.22	0.49	0.19	0.17	0.24	0.20	0.18	0.18	0.17	0.00	0.41	3.13	2.48
S	15.36	15.58	14.80	15.58	15.14	14.95	15.84	14.85	15.34	15.34	16.07	14.63	15.17	16.17	15.93	15.36	14.78
Total	99.83	99.77	100.85	101.29	101.49	102.08	101.30	97.00	101.07	99.41	100.19	99.48	99.83	99.45	99.42	100.24	98.69
Atoms	29	29	29	29	29	29	29	29	29	29	29	29	29	29	29	29	29
Ag	14.308	13.901	14.635	13.884	14.466	14.323	14.751	14.665	15.035	14.825	14.590	15.218	13.931	13.070	13.228	14.765	14.867
Cu	1.896	2.239	1.962	2.574	2.073	2.369	0.964	1.048	1.065	0.906	0.981	1.194	2.343	2.882	2.699	1.634	1.718
Sb	1.986	1.796	1.894	1.804	1.872	1.837	2.139	2.312	2.004	2.195	2.084	1.960	2.031	1.958	1.969	1.006	1.123
As	0.000	0.089	0.090	0.044	0.067	0.155	0.057	0.053	0.072	0.061	0.054	0.055	0.050	0.000	0.111	0.931	0.742
S	10.810	10.975	10.418	10.693	10.521	10.316	11.083	10.908	10.824	10.984	11.288	10.548	10.639	11.089	10.994	10.663	10.490

Kondaros: 1-3: (KONT4) / 4-6: (KONT2) / 7-12: (Kont13); Katsimoutis: 13: (kat9) / 14,15: (KAT2) / 16,17: (kat1a).

Fahlore and polybasite-pearceite compositions from Kondaros-Katsimoutis area are plotted in terms of Cu/(Cu+Ag) vs. As/(As+Sb) and represented in Fig. 73.

Temperatures indicated by fahlore coexisting with polybasite-pearceite solid solution at Kondaros-Katsimoutis mineralization vary from above 300° to below 200 °C, but most of them cluster at about 200-225 °C. This is in accordance to the fluid inclusion measurements from Katsimoutis (Vavelidis 1999), who suggested a range in mineralization tempe-

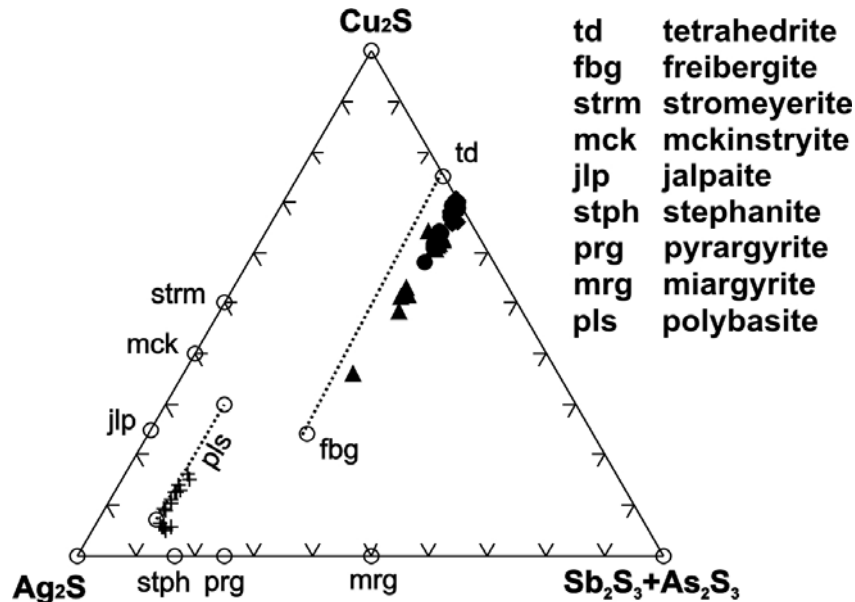
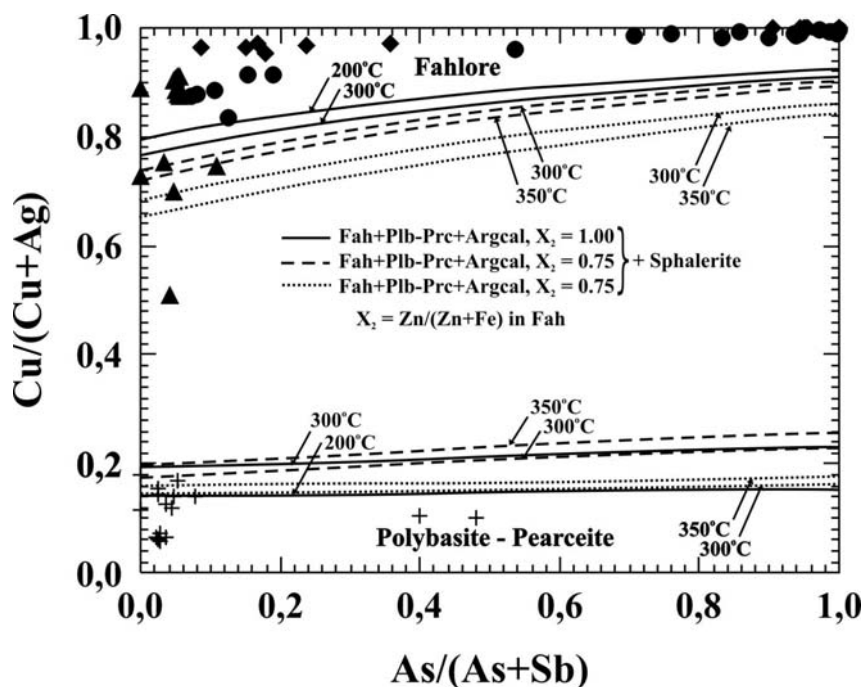


Fig. 72 : Ternary diagram of Ag-Cu-(Sb+As) sulfosalts. Theoretical compositions are shown as open circles. Filled circles (Triades), triangles (Kondaros-Katsimoutis) and diamonds (Galana) represent composition of tetrahedrite-group minerals analyzed in the present work. Crosses are compositions of polybasite-pearceite from Kontaros-Katsimoutis. Compositional ranges of tetrahedrite-freibergite and polybasite solid solution are shown by dashed lines for reference.

ratures from 320°C to about 160°-180°C. Alternatively the lowest temperatures (<180 °C) predicted for coexisting sulfosalts in Kondaros-Katsimoutis could represent equilibration temperatures after cooling.

Fig. 73 : Fahlore (triangles) and polybasite-pearceite (crosses) compositions from Katsimoutis samples plotted in the Cu/(Cu+Ag) vs As/(As+Sb) diagram (after Sack 2005). For comparison other western Milos fahlores (circles and polygons) are also plotted. The Katsimoutis assemblages are saturated with respect to sphalerite. Some tetrahedrite-polybasite seems to be re-equilibrated to lower temperatures (<180° C). Darkest and lightest curves represent compositions of Fahlore (Fah) and Polybasite-Pearceite (Plb-Prc) calculated for the assemblage Fah + Plb-Plc + (Ag,Cu)₂S solid solution (Argcal) + ZnS Sphalerite (Sph) at 200 and 300 ° C using the updated parameters by Sack (2000). Dashed curves for 300 and 350 ° C are plotted for this assemblage and for the Fah + Plb-Prc + pyrargyrite-proustite (Prg-Prs) + Sph assemblage considering molar Zn/(Zn+Fe) in Fah of 0.75.



8.7. Tellurides

The tellurides hessite, petzite and altaite in addition to native gold, are identified for the first time during this study and representative microprobe analyses are given in Table 7. They occur in the following contact assemblages: hessite-petzite, altaite-petzite, altaite-hessite, native gold-petzite and native gold-hessite. Contact assemblages of gold, silver and tellurium-bearing minerals are plot on a ternary diagram in terms of Au-Ag-Te (Fig. 74).

Hessite (Ag_2Te), the most abundant telluride, has Au content below 0.1 wt %, and a Ag-content in the range 62.5 to 66.5 wt%. Petzite (Ag_3AuTe_2) is closely associated with hessite. EPMA revealed Au contents between 24.7 and 26.2 wt %. A phase similar to petzite, with a composition between end-member petzite and x-phase, forms small grains surrounding hessite and small grains of gold. Its Au content is 18.4 wt%.

This phase it is probable petzite related to melt phenomena as reported by Rucklidge & Stumfl (1968). Altaite (PbTe) is a common telluride spatially associated with hessite and petzite but not observed in contact to galena. It is almost stoichiometric altaite.

8.8. Native gold

Native gold in association with tellurides contains 13.8 to 14.5 wt % Ag. No electrum has been detected in the studied mineralization of Profitis Ilias. Constantinidou et al. (1998) reported a wide compositional range for native gold/electrum in oxidized Profitis Ilias samples varying from 0.0 to about 35 wt% Ag.

Mineralogical data on the tellurides presented during this study from the deeper levels of Profitis Ilias deposit are quite similar to those described from the western Thrace and Limnos Island porphyry-epithermal deposits (Voudouris & Alfieris 2004, 2005), as well as the Rosia Montana epithermal deposit (Ciobanu et al. 2004a,b). In submarine settings there are mainly the copper-gold enriched VMS-epithermal deposits (Eskay Creek and Boliden) where gold occurs in the presence of native metal and tellurides (Hannington et al. 1999). Telluride enrichment has also been mentioned in the Iberian Pyrite Belt (Marcoux et al. 1996; Pinto et al. 2005) and in the Urals province, for both pyrite-chalcopyrite ("black

smoker”) and sphalerite-quartz-barite (“white smoker”) ore assemblages (Vikentyev 2004; Maslennikov & Maslennikova 2005). At Profitis Ilias deposit there is a close affinity between galena and hessite quite similar to Rosia Montana (Ciobanu et al. 2004a,b). As they suggested, galena incorporates significant amounts of other metals in solid solution, exsolving those elements to form discrete minerals during cooling, and may therefore play an important role in the distribution and enrichment of precious metals, in base metal ores.

Table 7 : Representative microprobe analyses of hessite (1-4), petzite (5-10) and Native gold (11,12) from Profitis Ilias area.

	1	2	3	4	5	6	7	8	9	10	11	12
Au	0.05	n.a.	0.05	n.d.	26.17	24.84	18.35	24.99	25.45	24.68	85.15	81.08
Ag	62.86	66.27	64.86	63.75	44.02	41.31	47.97	42.41	40.95	41.35	13.79	14.37
Te	36.55	38.42	36.17	36.37	33.73	32.73	33.08	32.77	33.84	32.94	n.a.	5.07
	99.58	104.69	101.09	100.10	103.38	98.53	99.41	99.68	100.18	98.68	100.35	99.94
Atoms	3	3	3	3	6	6	6	6	6	6	1	1
Au	0.001	0.000	0.001	0.000	1.008	1.000	0.701	0.994	1.003	0.992	0.738	0.727
Ag	1.997	2.013	2.004	2.024	3.095	3.037	3.347	3.082	2.945	3.037	0.218	0.235
Te	0.982	0.987	0.945	0.976	2.005	2.034	1.952	2.013	2.057	2.045	0.000	0.070

1, 2: (PI2-3); 3, 4: (PI2b-1); 5-7: (PI2-3); 8: (PI2-1); 9: (PI2-1b); 10: (PI2-2); 11: (PI2b-1); 12: Gold (PI2-1b).

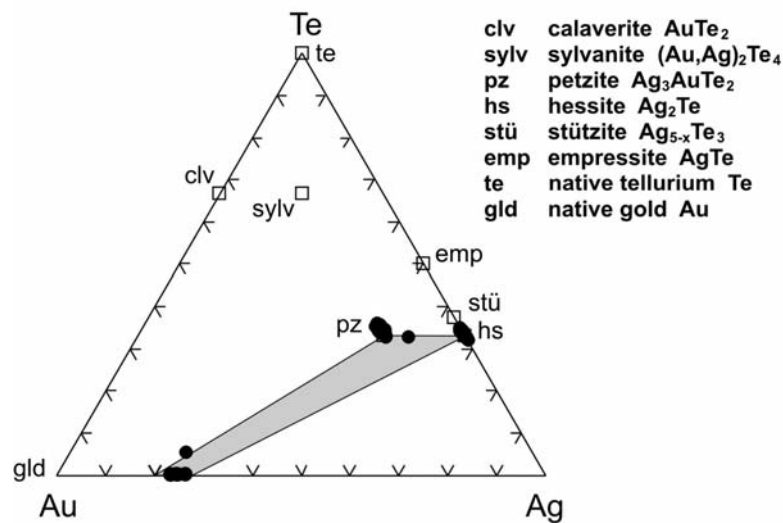


Fig. 74 : Ternary Au-Ag-Te diagram (atomic proportions) for mineral compositions analyzed in the present study. Theoretical compositions are shown as open squares, whereas solid lines indicate compositions of coexisting phases.

In the Au-telluride-base metal association of Profitis Ilias, the main telluride is hessite displaying a morphology and mineral association that, following Ciobanu et al. (2004b), may be suggestive of formation as droplets from a liquid (melt), at temperatures above the melting point of the respective minerals. Indeed following them in their saying: “the key mineral is hessite and its ability to act as gold carrier in base metal sulfides extracted from fluids above their melting points”, comes obvious that this seems to be the case also here.

The concept of precious metals precipitating from melts it is also proposed for metamorphic deposits (Tomkins & Mavrogenes 2002) as well as for Au scars (Meinert 2000). Thus at Profitis Ilias, gold which is present as native element as well as petzite, it is considered to be concentrated from the higher-temperature base metal precipitates within the blebs that crystallized to form hessite and included phases. From the other side the presence of altaite, pyrite and chalcocite indicates that the hessite-forming droplets originally contained Pb, Fe, Cu and S. Temperatures of initial entrapment of hessite-forming droplets in galena, are constrained by the measured fluid inclusion data to vary between 250° and 300°C (Kiliyas et al. 2001). The petzite-hessite equilibrium assemblages described in the present study could represent the product of the breakdown of the γ -phase or χ -phase below 120°C from the following assemblages: stützite + γ -phase, γ -phase or χ -phase, or stützite + sylvanite + γ -phase (Cabri 1965, Kracek et al. 1966). Both the “ γ ” and “ χ ” phases are important in interpreting natural telluride assemblages because they can explain fields of exsolution (representing eutectic decompositions) among hessite and stützite from one side, and petzite and sylvanite from the other, at temperatures <50° or <120 °C respectively. At Profitis Ilias some of the hessite-petzite blebs might have originated from compositions in the range of the “ χ ” phase. Skeletal inclusions or separations of petzite from the hessite bleb, are evidences that petzite exsolved from the “ χ ” phase at temperatures below 120°C. However, as proposed by Ciobanu et al. (2004a) for Rosia Montana, crystallization of the Au-Ag-tellurides could be initiated from Au-rich centres instead of eutectic decomposition, since neither curvilinear boundaries nor exsolutions are present. From the observed relationship at Profitis Ilias it is proposed two steps of evolution: galena-hessite solid solution, followed by a hessite-petzite-Au one.

In the **Appendix II** are reported representative microprobe analyses of Tetrahedrite-group minerals, Enargite, Sphalerite, Polybasite-Pearceite solid solution, Tellurides and Native gold from various subareas of western Milos.

9. GEOCHEMICAL CONDITIONS DURING ORE FORMATION AT WESTERN PART OF MILOS ISLAND

The aim of this chapter is to study the physicochemical conditions during ore deposition of western Milos mineralization. Following the pioneer work of Liakopoulos (1987), who described for the first time the chemical parameters of the present geothermal field, as well as of part of hydrothermal alteration related to western Milos mineralization, a thermodynamic approach for the ore depositing processes in western Milos is presented below. Phase diagrams of coexistent minerals were constructed using the methods described by Barnes & Kullerud (1961), Garrels & Christ (1965), Ohmoto (1972), Henley et al. (1984) after the equilibrium relationships presented in the **Appendix III**. The theoretical framework for the construction of phase diagrams, as well as the thermodynamic data of minerals, gases and ions in standard state (298.15°K, 1bar) are derived from Helgeson (1969), Helgeson & Kirkham (1974), Helgeson et al. (1978, 1981).

The sulfide and telluride mineralogy, the composition of sphalerite, as well as the published fluid inclusion data were used to constrain fS_2 , fO_2 and fTe_2 values of the hydrothermal solutions in western Milos mineralization (Figs. 75 and 76). The phase diagrams were constructed for both $T = 275^\circ C$ and $225^\circ C$ and vapour pressure. Thermodynamic data for sulfides and tellurides used for calculating fS_2 , fO_2 and fTe_2 were derived from Mills (1974), Barton and Skinner (1979) and Afifi et al. (1988). Equilibrium constants used for the construction of the phase diagrams are listed also in the **Appendix III**.

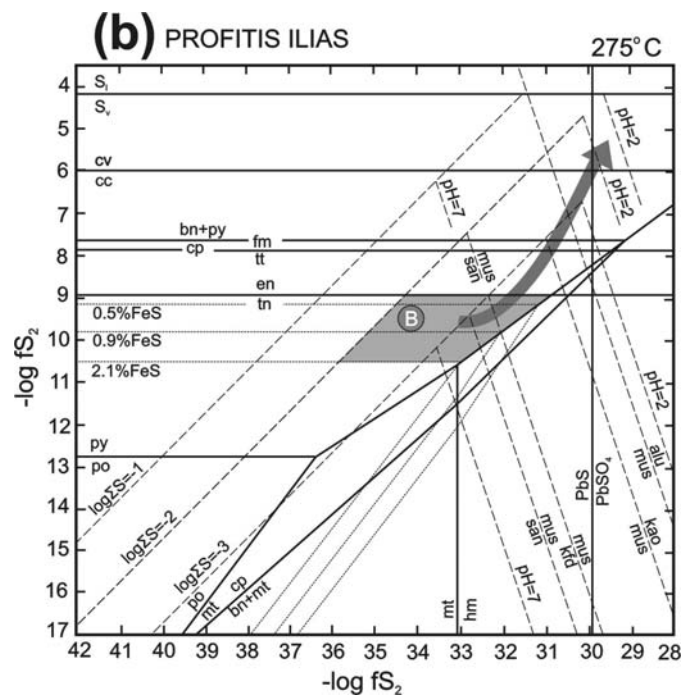
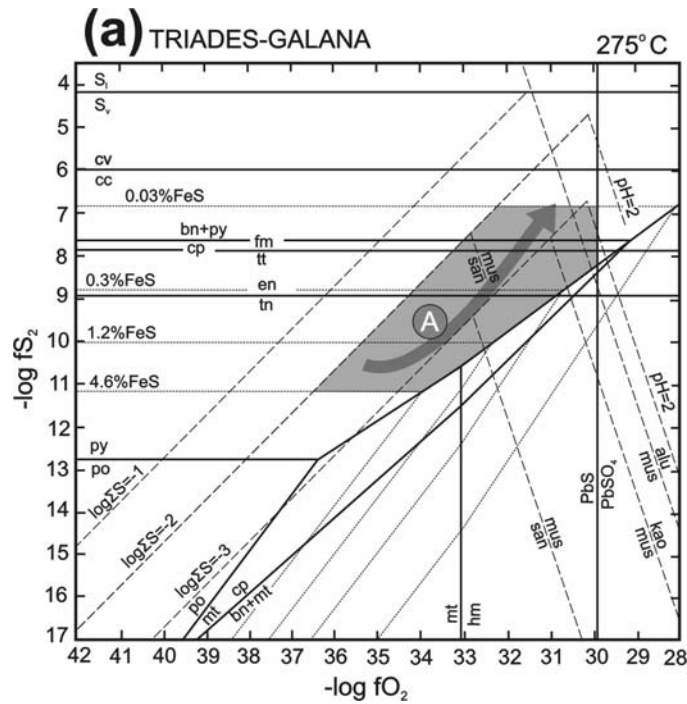
The shaded areas in Figures 75a and b represent the hypothetical ore forming conditions of the Triades-Galana and the deep telluride-bearing Profitis Ilias- (Chondro Vouno) mineralization respectively. The fS_2 values of the mineralizing solutions were calculated using the iron contents of the analyzed sphalerites in equilibrium with pyrite, according to the relationship $\log X_{FeS} = 7.16 - 7340/T - 0.5 \log fS_2$ (Barton & Skinner 1979).

The $\log fS_2$ values calculated from Triades-Galana sphalerite ($m_{FeS} = 4.6$ to 0.03 in early and late sphalerite respectively) vary between -11.2 and -6.84 , and suggest a trend towards higher sulfidation states of the fluids with time (Fig. 75a; $T = 275^\circ C$). The bulk of ore deposition took place under $\log fS_2$ values in the range -10.04 to -8.84 as indicated by the iron content of most sphalerite analyzed ($m_{FeS} = 0.3 - 1.2$). The calculated $\log fS_2$ and the sulfidation-oxidation trend proposed for Triades-Galana are in accordance to the late occurrence of tennantite and enargite in the mineralization.

For the deep Profitis Ilias-Chondro Vouno mineralization (Fig. 75b; $T = 275^\circ C$) the $\log fS_2$ values calculated from sphalerite ($m_{FeS} = 0.5 - 0.9$) vary between -9.78 to -9.28 . The sulfidation-oxidation trend shown is quite similar to that from Triades-Galana and corresponds to the late formation of low-temperature bornite+covellite+ chalcocite due to the combined action of hydrothermal reworking and seawater oxidation.

For the Triades-Galana mineralization an upper limit for the $\log fO_2$ values can be fixed by galena/anglesite boundary, while for Profitis Ilias-Chondro Vouno by the intersection of the pyrite/hematite and enargite/tennantite boundaries. Estimated upper $\log fO_2$ values range between -29.92 and -31 respectively. These values coincide with the presence of adularia and/or sericite in the vein assemblages. The lower limits for the $\log fO_2$ values can only be approximated for a maximum total sulfur value of 0.01 considered to be characteristic for intermediate sulfidation epithermal deposits (Heald et al. 1987). Taking into consideration the maximum iron content in the sphalerites, it has been estimated a lower fO_2 values of about -37 and -36 for Triades-Galana and Profitis Ilias-Chondro Vouno respectively.

The Kondaros-Katsimoutis mineralization (Fig. 75c; $T = 225^{\circ}\text{C}$) was formed under $\log f_{\text{S}_2}$ values in the range between -13.98 to -11.92, based on iron content of sphalerite analyzed ($m_{\text{FeS}} = 0.4 - 4.3$). For the lower temperature ($T = 225^{\circ}\text{C}$) constructed diagrams the upper part of Profitis Ilias-Chondro Vouno deposits $\log f_{\text{S}_2}$ values fall within this range and vary between -12.61 and -12.12 ($m_{\text{FeS}} = 0.5 - 0.9$). The occurrence of calcite, pyrite and the absence of anhydrite in Kondaros-Katsimoutis indicate an upper limit for the $\log f_{\text{O}_2}$ values fixed by the intersection of the pyrite/hematite and calcite/anhydrite boundaries and estimated to be at about -36.



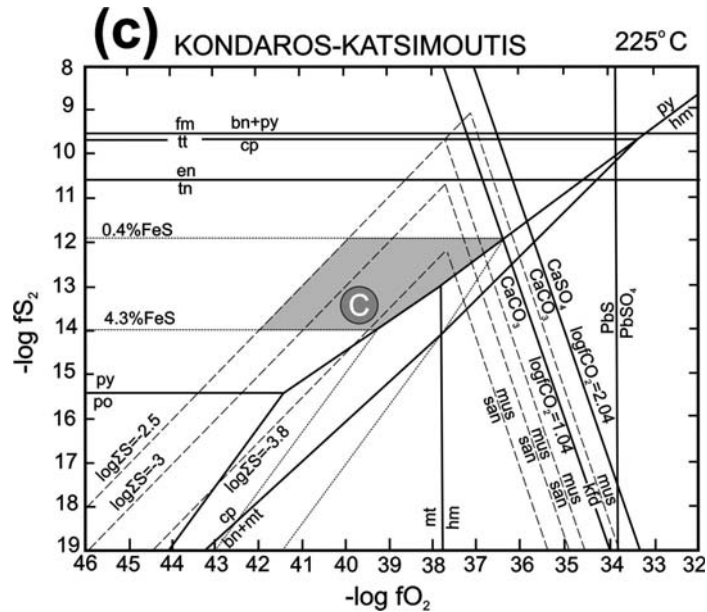


Figure 75 : (a to c): $\text{Log}f\text{S}_2 - \text{log}f\text{O}_2$ diagrams constructed for $T=275^\circ$ and 225°C and vapour saturation pressure. Hypothetical ore forming conditions of the Triades-Galana (a), Profitis Ilias (b) and Kondaros-Katsimoutis (c) mineralization are limited by the marked areas A, B and C respectively. Thick solid lines: mineral stability field in the system Fe-O-S; thin solid lines: stability limits of Cu-Fe sulfides and sulfosalts; short strippled lines: Fe-content in sphalerite (in moles % FeS); long strippled lines: ΣS^- concentration contours and pH related stability limits of silicates, alunite (for $\log a_K = -1.89$ and $I = 0.30$). The calcite/anhydrite stability limits (thin solid lines) are constructed for $\Sigma\text{C} = 0.1$ and 1.0 . The sulfide/sulfate dominance limit is constructed for a pH value of 5.81. The stability fields of silicates, sulfates and carbonate are constructed for stoichiometric phases ($a=1$). Equilibrium constants and source of thermodynamic data used for the construction of the diagrams are listed in the Appendix III. Abbreviations: alu = alunite; bn = bornite; cc = chalcosine; cv = covellite; kao = kaolinite; kfd = K-feldspar; cp = chalcopyrite; en = enargite; fm = farnatinite; hm = hematite; mt = magnetite; po = pyrrhotite; mus = muscovite; py = pyrite; san = sanidine; tn = tennantite; td = tetrahedrite; S_l = sulfur liquid; S_v = sulfur vapour.

The telluride mineralogy, the composition of sphalerite, as well as the published fluid inclusion data were used to constrain $f\text{Te}_2$ and $f\text{S}_2$ values of the hydrothermal solutions in the Te-bearing deep Profitis Ilias mineralization. Telluride stabilities were calculated for 275°C and presented in Fig. 76. The telluride deposition occurred under $\log f\text{S}_2$ values between -10.4 and -9.3 as indicated by the range of sphalerite compositions ($m_{\text{FeS}} = 0.5 - 2.1$). Maximum $\log f\text{Te}_2$ values can be defined by the stützite/ γ boundary at about -7.3 . Most telluride deposition took place at $\log f\text{Te}_2$ values close to the galena-altaite boundary with a lower limit at about -8.5 (calaverite/native gold boundary). It is proposed that the telluride deposition took place under intermediate sulfidation states, as defined by Einaudi et al. (2003).

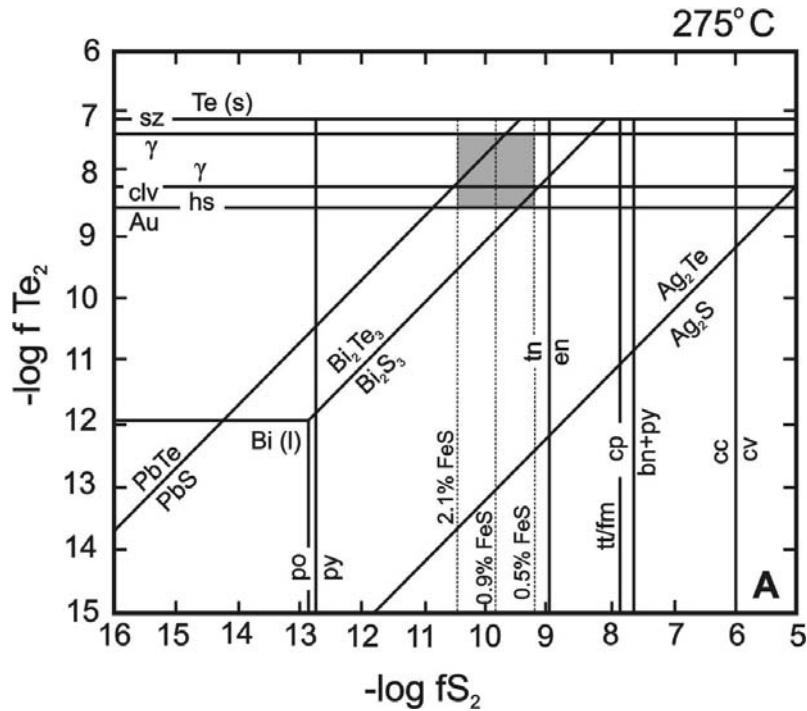


Fig. 76 Log f_{Te_2} - log f_{S_2} diagram indicating equilibria between tellurides and sulfides at 275°C. The shaded area indicates approximate conditions of telluride deposition at Profitis Ilias deposit, calculated from the composition of sphalerite and observed mineral assemblages. Abbreviations: clv = calaverite, hs = hessite, sz = stützite, γ = gamma-phase, tn = tennantite, tt = tetrahedrite, fm = famatinitite, en = enargite, cp = chalcopyrite, bn = bornite, py = pyrite, po = pyrrotite, cc = chalcocite, cv = covellite.

Note : The meaning of **x-** and **γ -** phases in the diagrams

- During Cabri's (1965a,b) experiments on phase relations in the Au-Ag-Te system, a new **phase**, designated as "**x**" has been found to be stable along the AuAg₃Te₂-Ag₂Te (petzite-hessite) join, between 50° ± 20 °C and its incongruent breakdown above 415° ± 20 °C to petzite-hessite solid solution and intermediate Ag₂Te. The gold content of this phase ("**x**" **phase**), extends from about 2.5 to 14.5 wt% Au on the join.
- The **gamma("γ")-phase** is a phase intermediate in composition between Ag_{5-x}Te₃ (stützite) and Ag₂Te (hessite), which first has been reported by Kiukkola and Wagner (1957) and then confirmed by Cabri (1965a).

10. MAJOR-MINOR-TRACE ELEMENTS VARIATION AND THEIR GEOCHEMICAL TRENDS

10.1. Major Elements Variation and their Geochemical Trends

A series of 137 surface samples, representing various types of alteration and alteration degrees, have been analyzed by XRF method, (42 at Hamburg University, 5 at X-RAL labs Canada for Midas S.A. and 95 during various periods at the labs of Silver and Baryte ores mining company [S&B]), for their major elements content. The aim was to obtain a first impression on the losses and gains during hydrothermal alteration processes that occurred at western Milos. Furthermore in order to understand their variation and the related geochemical trends, a series of fresh samples reported in the literature (Burri and Soptrajanova 1967, Innocenti et al. 1981, Bol and Hasselman 1985, Fytikas et al. 1986, Liakopoulos 1987) have been used for comparison. Through a series of binary diagrams of the major elements against silica dioxide (fig. 77), have been, from one side, configured their distribution patterns, and from the other side have been emphasized their relative variations. Indeed as it is observed from the fig. 77, some of the major elements show an enrichment (Al_2O_3), other are depleted (TiO_2 , Na_2O , Fe_2O_3 , MgO , CaO , MnO) and other display a mixed behavior (K_2O , P_2O_5). However, apparent minor enrichment and depletion may reflect addition or removal of other components as well. In general, the amounts of TiO_2 , Na_2O , CaO , MgO , Fe_2O_3 and MnO decrease with increasing SiO_2 content.

A further step towards understanding the interrelationships between the major oxides has been approached through a multivariate correlation analysis, the results of which are tabulated on Table 8, and visualized as a scatterplot matrix in fig. 78. In this figure the correlation of the variables is shown by an ellipse (along the diagonal axis), which is a function of the means and standard deviations of the X and Y variables and the correlation between them. If the ellipse is fairly round and is not diagonally oriented, the variables are uncorrelated. Well, as it is shown from both fig. 78 and the major elements Pearson's correlation coefficients in Table 8, there exist a major positive correlation between Al_2O_3 and P_2O_5 (0.60) as well as between Al_2O_3 and the degree of alteration, i.e., LOI - loss on ignition (0.66). Fe_2O_3 correlates somehow with CaO (0.50). MnO is very strongly correlated with CaO (0.88) and MgO (0.75). The CaO and MgO are also very well correlated (0.69), and both of them present an affinity with Na_2O (0.59). Finally, a positive correlation between LOI (i.e., the degree of alteration) and the content of SO_3 (0.65), which essentially is related to the acid alteration style and the presence of alunite, is observed. Concerning negative correlations, the most pronounced is that between SiO_2 and Al_2O_3 (-0.65), degree of alteration, i.e., LOI (-0.73) and the content of SO_3 (-0.58).

10.2. The relationships between alteration zones and major elements content

One of the aims in examining the major elements "behavior" was to define patterns related to various alteration styles as a possible exploration tool, and as an indication of the processes involved in the creation of the various mineralization and alteration styles. Based on that, it is considered that the distribution patterns of Al, Na, K, S define specific targets of interest related to the alteration zones (Argillic and Advanced Argillic zones), and on the other hand the distribution of Ca is related to generally barren areas.

As a whole, it is suggested that the variation in the SiO_2 content observed, it is mainly re-

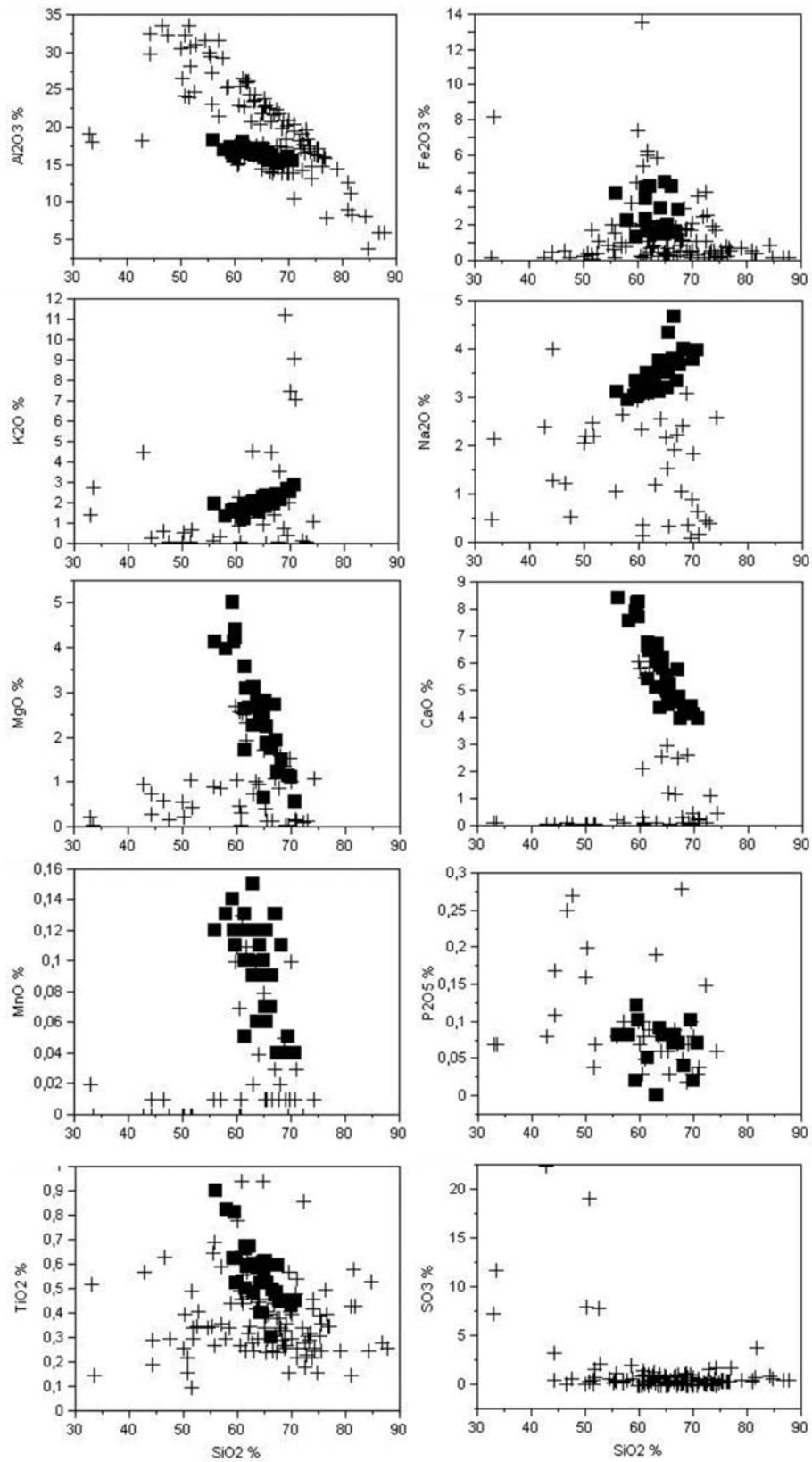


Fig. 77 : Binary diagrams of variation of the major elements (Al_2O_3 , TiO_2 , Fe_2O_3 , K_2O , Na_2O , MgO) vs. SiO_2 for the altered volcanic rocks of western Milos (crosses) and the fresh ones reported in the literature (solid square).

lated to the argillic alteration zone at southern sector and to the advanced argillic at the northern one.

Table 8: Major elements Pearson's correlation coefficients.

	SiO2 %	Al2O3 %	Fe2O3 %	MnO %	MgO %	CaO %	Na2O %	K2O %	TiO2 %	P2O5 %	SO3 %	LOI
SiO2 %	1	-0,65159	0,050636	0,2298	0,1656	0,1817	-0,1232	0,301	0,168	-0,2817	-0,585	-0,7344
Al2O3 %	-0,6516	1	-0,38635	-0,4032	-0,3215	-0,334	-0,0535	-0,465	-0,1801	0,6012	0,087	0,66016
Fe2O3 %	0,0506	-0,38635	1	0,4586	0,1883	0,5055	0,15105	0,019	0,4139	-0,2311	-0,047	-0,327
MnO %	0,2298	-0,40318	0,458629	1	0,7504	0,8899	0,52661	0,073	0,1984	-0,2662	-0,253	-0,6334
MgO %	0,1656	-0,32153	0,188265	0,7504	1	0,6973	0,59768	-0,112	-0,0336	-0,2718	-0,19	-0,39
CaO %	0,1817	-0,33408	0,505469	0,8899	0,6973	1	0,58939	-0,109	0,2879	-0,2241	-0,224	-0,5653
Na2O %	-0,1232	-0,05354	0,151049	0,5266	0,5977	0,5894	1	-0,203	-0,1535	-0,1401	0,011	-0,0268
K2O %	0,3014	-0,46479	0,01924	0,0732	-0,1124	-0,109	-0,2031	1	-0,1315	-0,2778	0,086	-0,3289
TiO2 %	0,168	-0,18007	0,413877	0,1984	-0,0336	0,2879	-0,1535	-0,132	1	-0,0467	-0,06	-0,2162
P2O5 %	-0,2817	0,601203	-0,23109	-0,2662	-0,2718	-0,224	-0,1401	-0,278	-0,0467	1	0,023	0,35829
SO3 %	-0,585	0,086751	-0,04704	-0,253	-0,1903	-0,224	0,01087	0,086	-0,0602	0,02269	1	0,65243
LOI	-0,7344	0,66016	-0,32701	-0,6334	-0,39	-0,565	-0,0268	-0,329	-0,2162	0,35829	0,652	1

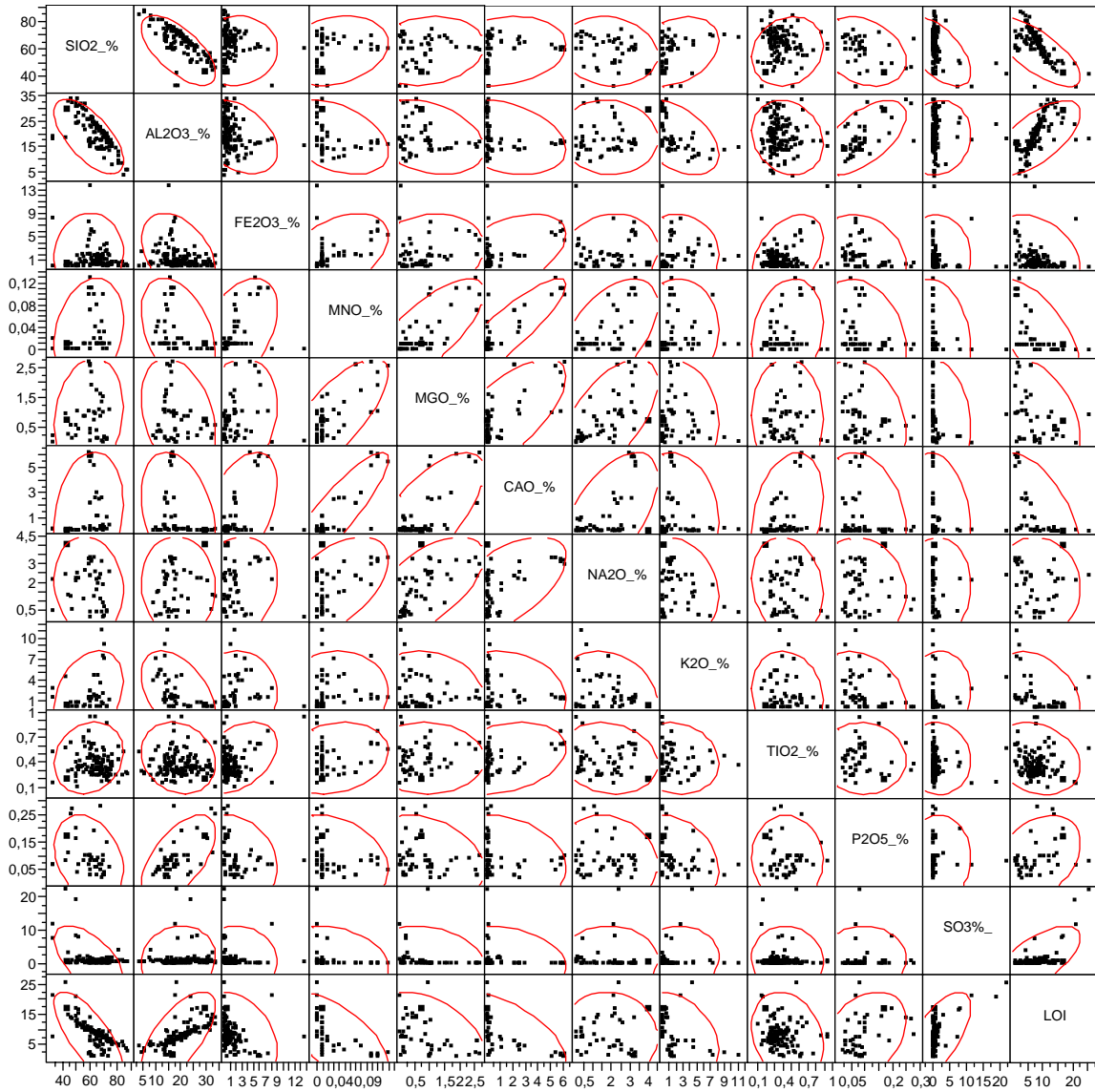


Fig. 78 : Scatterplot matrix of western Milos major elements

The Al_2O_3 presents the higher values in relation to the advanced argillic alteration zone of the northern sector (fig.79), where indeed it delineates a major area over there. The other area (more south), presenting high alumina values also, belongs as well to the northern sector and is related to the former Ralaki kaolin mine.

The TiO_2 although it is considered an immobile element, under advanced argillic and/or silicic alteration in high sulphidation environments, has been locally remobilised.

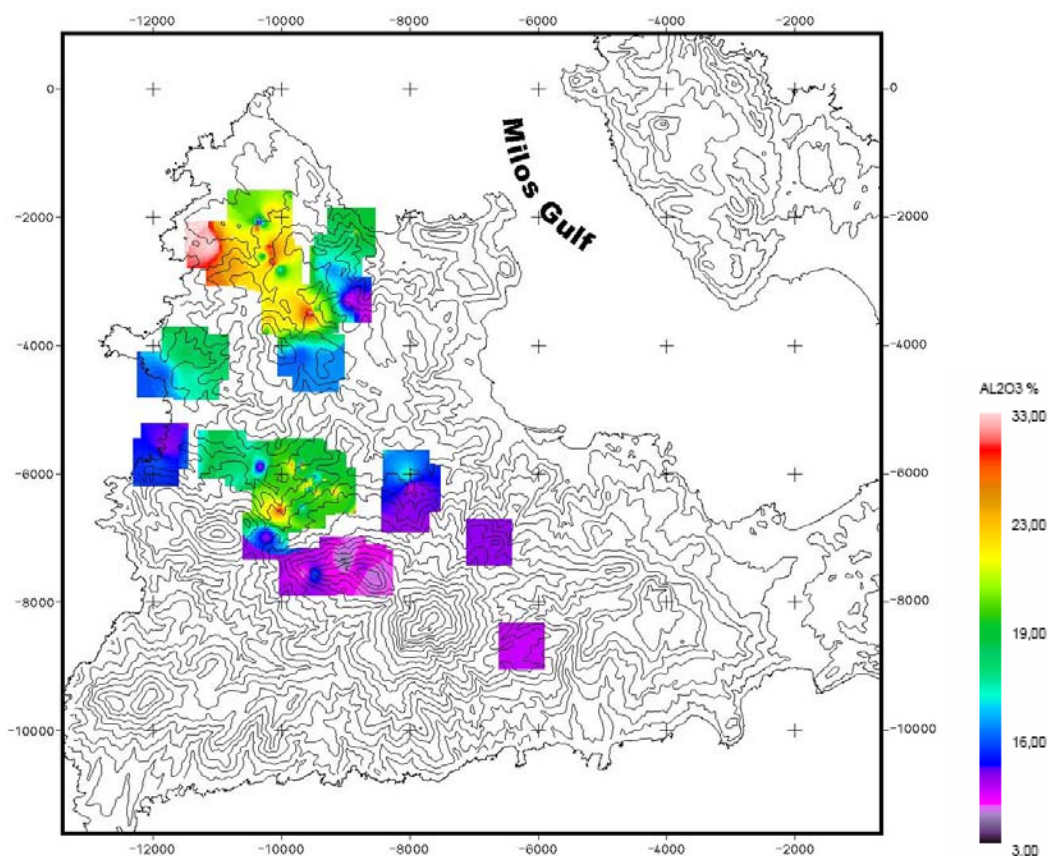


Fig. 79 : Lithochemical map of Al_2O_3 . Colours correspond to wt % Al_2O_3 .

The Fe_2O_3 shows high values at both sectors, assuming to be related to a pyrite enrichment in the alteration zones. In the lithochemical map (fig.80) are displayed some high values (enriched areas), which correspond to specific subareas, namely, the broad Koumaria subarea (southern sector), and some ones from the northern sector, as for instance Galana subarea, the segment between Ag. Athanasios and SE part of Favas mountain and the contact zone between the subvolcanic Tria Vouna coalescing domes and the pyroclastics of the lower tuffaceous lapilli tuff unit (Lmp), (Favas-Tria Vouna subarea). As it has been mentioned before, it is considered that the high ferric iron concentrations mainly correspond to areas where pyrite is a dominant alteration mineral, and thus can be accounted for by the common presence of limonite, goethite.

The MgO is considered to be related to the argillic and propylitic alteration zones, where it is a constituent of the smectite, sericite and chlorite inside the slightly to moderately altered rocks. It seems to be completely leached away in the strongly altered rocks.

The higher concentration of CaO is assumed to be related to the fresh and in a lesser extend to propylitic (due to the presence of calcite) altered rocks at western Milos. From

the other side, in a general more arbitrary way, it can be said that the progressive destruction of plagioclase in more intensely altered rocks can be followed by the progressive decrease in CaO content. In addition, the predominance of illite, kaolinite and alunite in the more intensely altered rocks accounts for the decrease in CaO.

The Na_2O content is related to the advanced argillic alteration zone, due to the presence of natroalunite and halite, (e.g., at the subareas of Favas-Tria Vouna and Ralaki), and to the propylitic zone (presence of albite), mainly at the southern sector. In a more generalized way, the variations in Na_2O content reflect the destruction of plagioclase in the advanced argillic and argillic altered rocks, as well as the sodium content of alunite in the alunitized rocks.

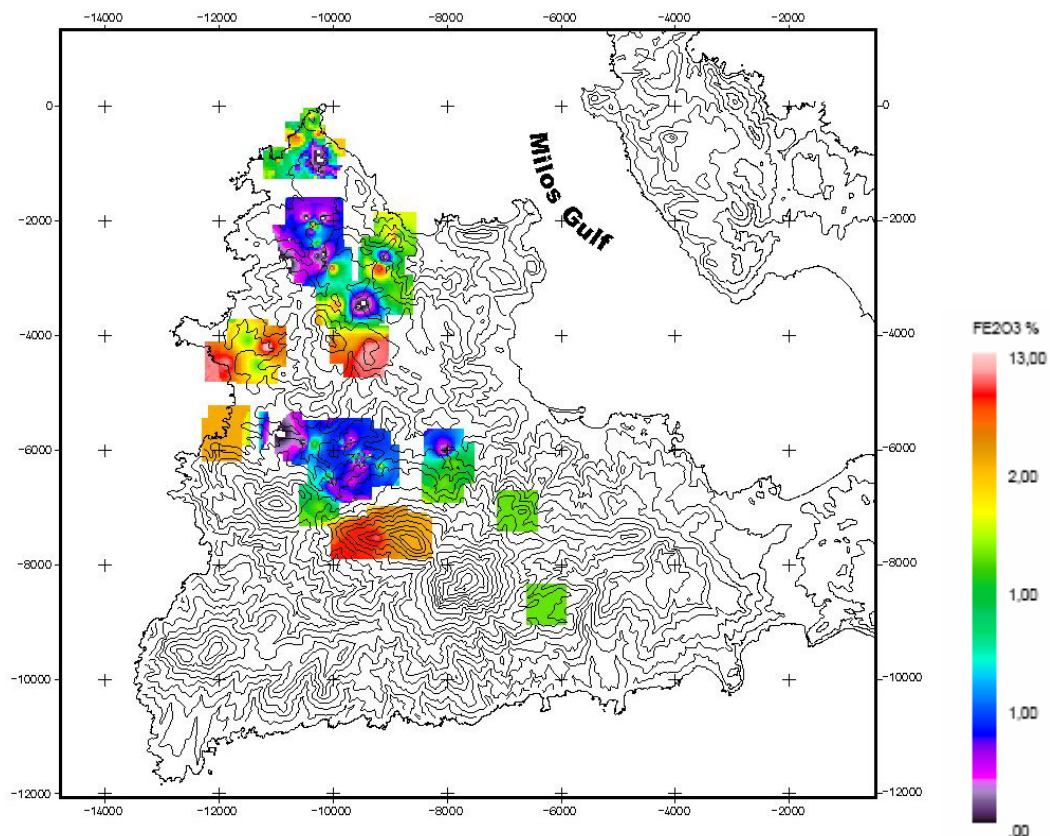


Fig. 80 : Lithochemochemical map of Fe_2O_3 . Colours correspond to wt % Fe_2O_3

The K_2O at western Milos is related to the argillic and adularia-sericite alteration zones. In the lithochemochemical map (fig. 81) high values are displayed at Agios Panteleimon subarea and along all the crests between Chondro Vouno and Koumaria. In a more generalized way it can be said that K_2O is more variable and on average higher in mineralized than in poorly mineralized rocks where, in this last case its stability is related to the stability of sanidine. Indeed some more or less fresh sanidine is present in the less argillized rocks occurring in the outer parts of the illite-kaolinite (argillic alteration) zone. The relative increase in K_2O in the adularia-sericite zone is attributed to the substitution of plagioclase by adularia and sericite. In the illitic rocks probably indicates the sum of potassium contained in residual sanidine plus the additional potassium held largely in the illite. The relationships between K_2O content and Na_2O , CaO in the various alteration zones at

western Milos can also be seen through a ternary plot diagram (fig. 83), where the initial enrichment in sodium occurred relative to calcium, followed by major increases in potassium contents towards the veins and brecciated areas where alteration also intensifies.

The P_2O_5 is considered to be related to the advanced argillic alteration zone of the northern sector. It is probably incorporated to the structure of alunino-phosphate-sulfate (APS) minerals detected through XRD studies in this zone.

Concerning SO_3 , it is considered to be related to the presence of pyrite and/or alunite in the advanced argillic alteration zone, and to the presence of jarosite either in the argillic, advanced argillic alteration zones, or as supergene mineral after the oxidation of pyrite.

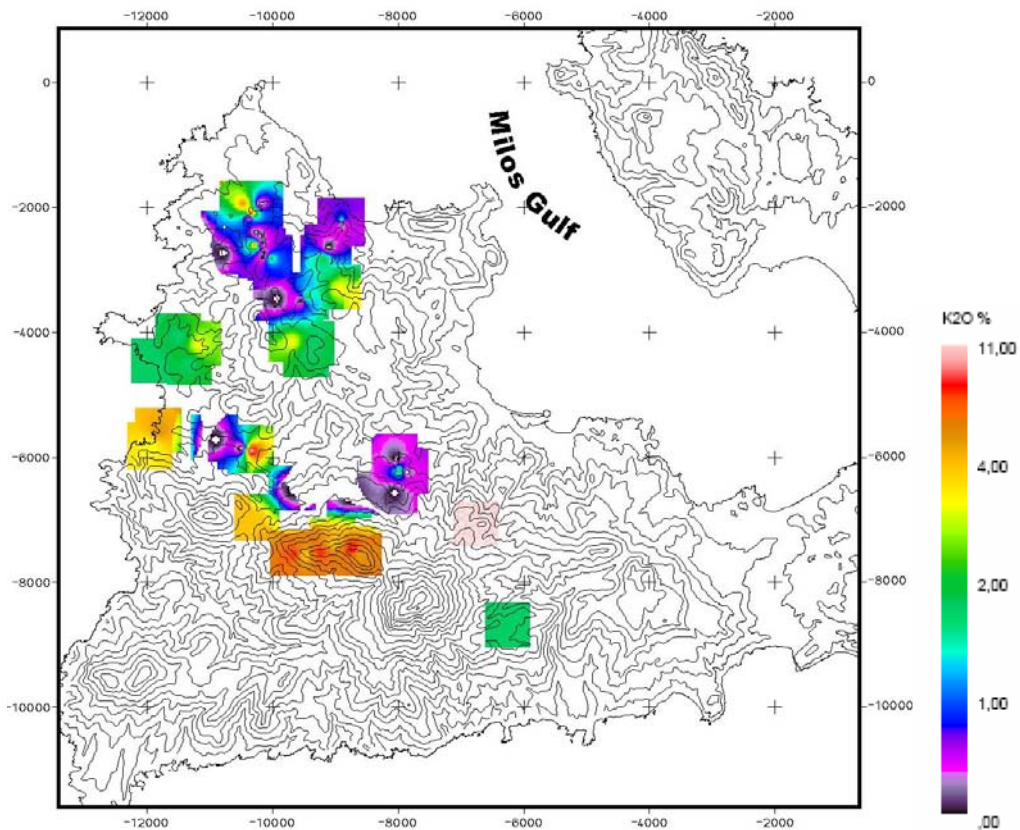


Fig. 81 : Lithochemical map of K_2O . Colours correspond to wt % K_2O .

A even more detailed approach toward correlating the distribution of the major elements and the various alteration zones on W. Milos, has been achieved through a series of XRD analyses performed at Hamburg University for 32 surface samples (fig. 82), and 23 subsurface ones (fig. 84) coming from reverse circulation drill holes (RC holes/MIDAS S.A.), which have been connected to the chemistry of the altered rocks. The results are tabulated (Tab. 9, 10 respectively) and shown through the ternary K-Na-Ca diagrams (fig. 83, 85 respectively).

The table 9 describes the chemical variation, of the generally moderate to strongly altered surface rock types, for their major elements content related to the alteration zones which they belong as revealed after XRD analysis.

The ternary diagram (fig. 83) shows a distribution of the samples belonging to the argillic, advanced argillic, phyllic(sericitic), propylitic (sericitic-chloritic), adularia alteration zones

toward both K- and Na- terms which is explained through the presence of the adularia, K-alunite and sericite for the K-terms, and natroalunite, halite for the Na-terms. The samples towards Ca- terms share characteristics of calcite/ankerite presence (propylitic zone) and plagioclase relics (rests) in the argillic zone.

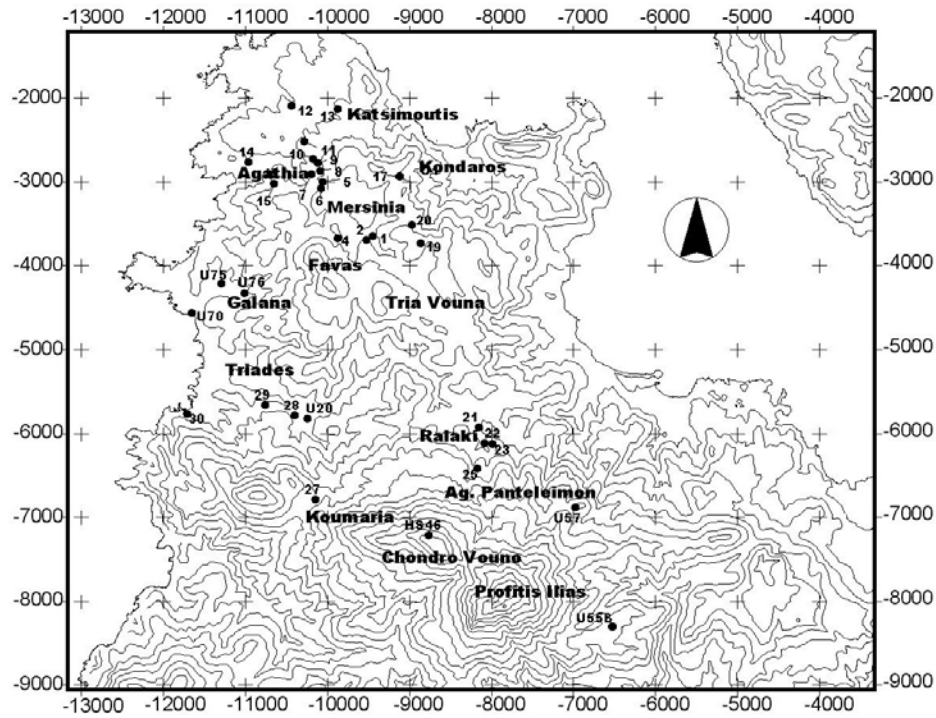


Fig. 82 : Location map of the samples analyzed chemically and by XRD.

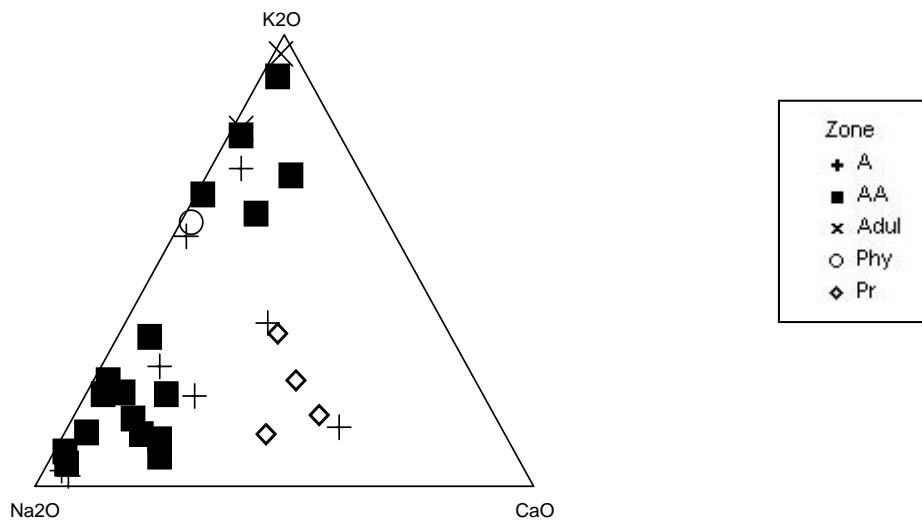


Fig. 83. Ternary plot of K_2O , Na_2O and CaO (wt. %) of moderate to strongly altered surface volcanic rocks at western Milos.

The table 10 describes the variation of the major elements content in the RC holes samples related to the alteration zones which they belong as revealed after XRD analysis.

Table 9 : Chemical variation of the major elements of some surface altered samples and related alteration minerals after XRD analysis.

Sample	SiO2 %	Al2O3 %	Fe2O3 %	MnO %	MgO %	CaO %	Na2O %	K2O %	TiO2 %	P2O5 %	SO3 %	H2O+	XRD	Zone
1	32,98	19,16	0,18	0,02	0,24	0,11	0,48	1,41	0,52	0,07	7,33	7,55	kaol,ser,hal,q	A
2	44,16	32,51	0,05	0,00	0,30	0,07	1,30	0,03	0,29	0,11	3,32	14,68	kaol,hal,q	A
4	60,67	22,99	2,10	0,01	0,33	0,14	0,38	0,13	0,46	0,10	1,46	10,46	kaol,q	A
15	51,31	24,00	0,37	0,00	1,05	0,08	2,49	0,09	0,49	0,04	0,04	13,00	kaol,hal	A
U55B	74,13	13,25	1,77	0,01	1,08	0,48	2,60	1,10	0,25	0,06	0,00	3,11	q,hal,kaol	A
U70	60,82	15,94	5,38	0,13	2,55	5,48	3,36	1,32	0,56	0,05	0,01	2,51	q,kaol	A
U75	65,13	18,02	1,26	0,01	0,40	1,21	1,55	1,56	0,54	0,06	0,00	6,74	q,hal,kaol	A
U76	33,34	18,19	8,21	0,00	0,04	0,11	2,15	2,79	0,15	0,07	11,76	21,19	q,al,kaol,hal	A
5	47,34	32,44	0,17	0,00	0,17	0,09	0,55	0,11	0,30	0,27	0,67	13,57	Kaol,q,hal,al	AA
6	65,39	22,89	0,30	0,01	0,14	0,10	0,36	0,05	0,41	0,03	0,03	9,22	kaol,q,hal,al	AA
7	42,72	18,28	0,16	0,00	0,96	0,07	2,41	4,47	0,57	0,08	22,43	25,63	al,q	AA
8	51,64	28,24	0,06	0,00	0,44	0,08	2,21	0,68	0,30	0,07	0,74	15,27	kaol,al,q	AA
9	49,96	30,64	0,24	0,00	0,58	0,08	2,07	0,10	0,26	0,16	0,09	14,24	kaol,hal,al	AA
10	56,94	21,58	1,03	0,01	0,86	0,13	2,65	0,36	0,59	0,10	0,18	12,35	kaol,hal,al	AA
11	44,06	29,85	0,53	0,01	0,74	0,09	4,02	0,32	0,19	0,17	0,51	16,92	kaol,hal,al,q	AA
12	62,88	20,74	0,91	0,02	0,76	0,13	1,20	4,56	0,25	0,19	0,17	6,14	q,ser,al	AA
13	55,52	23,23	0,19	0,01	0,89	0,22	1,07	0,16	0,69	0,08	0,34	12,08	Kaol,q,hal,al	AA
14	46,42	33,70	0,61	0,01	0,60	0,13	1,24	0,66	0,63	0,25	0,13	13,99	kaol,hal,al,q	AA
17	72,20	17,27	0,20	0,00	0,12	0,11	0,45	0,14	0,86	0,15	0,07	7,88	q,kaol,al,hal	AA
19	50,12	26,65	0,06	0,00	0,24	0,09	2,21	0,57	0,40	0,20	8,05	17,11	kaol,q,al,hal	AA
20	69,56	13,95	1,73	0,01	1,53	0,47	0,90	2,05	0,43	0,03	0,11	5,15	cris,mont,q,al,kaol	AA
21	67,70	17,53	0,87	0,01	0,86	0,32	1,08	0,09	0,38	0,28	0,08	8,18	cris,kaol,mont,al,hal	AA
28	60,26	18,03	0,27	0,00	0,46	0,32	3,27	0,91	0,49	0,10	0,95	14,16	kaol,al,hal,trid,cris	AA
29	69,39	18,50	0,50	0,00	0,04	0,10	0,09	0,41	0,57	0,10	1,03	9,08	cris,kaol,al,hal	AA
U20	70,66	13,98	1,15	0,01	0,18	0,30	0,66	9,07	0,48	0,03	0,00	2,23	cris,mont,q,al,kaol	AA
HS46	69,80	14,00	2,16	0,10	1,02	0,15	1,86	7,48	0,40	0,08	0,00	1,61	q,adul	Adul
U57	68,86	14,92	1,80	0,01	0,05	0,13	0,38	11,21	0,36	0,07	0,00	1,60	adul,q	Adul
27	67,83	14,60	1,16	0,02	1,59	0,12	2,42	3,56	0,34	0,05	0,15	6,02	q,ser	Phy
22	66,98	13,94	1,87	0,03	1,09	2,51	2,24	1,45	0,31	0,07	0,00	4,70	alb,mont	Pr
23	64,76	14,47	1,77	0,08	1,74	3,00	2,17	0,95	0,38	0,08	0,00	4,45	alb,mont	Pr
25	68,53	14,01	1,77	0,05	1,37	2,61	3,11	0,75	0,33	0,02	0,00	3,11	mont,alb	Pr
30	60,41	15,04	2,00	0,07	2,58	2,14	2,36	2,28	0,27	0,03	0,00	6,16	alb,mont	Pr

Abbreviations : (A : argillic zone, AA : advanced argillic zone, Adul : adularia zone, Phy : sericitic zone, Pr : propylitic zone. q : quartz, kaol : kaolinite, ser : sericite, hal : halite, al : alunite, mont : montmorillonite, alb : albite, cris : cristobalite, adul : adularia, trid : tridymite.

The subsurface samples belong to two different areas (Chondro Vouno and Mavrovouni)- (fig. 84), which are considered very important from a mineralization point of view.

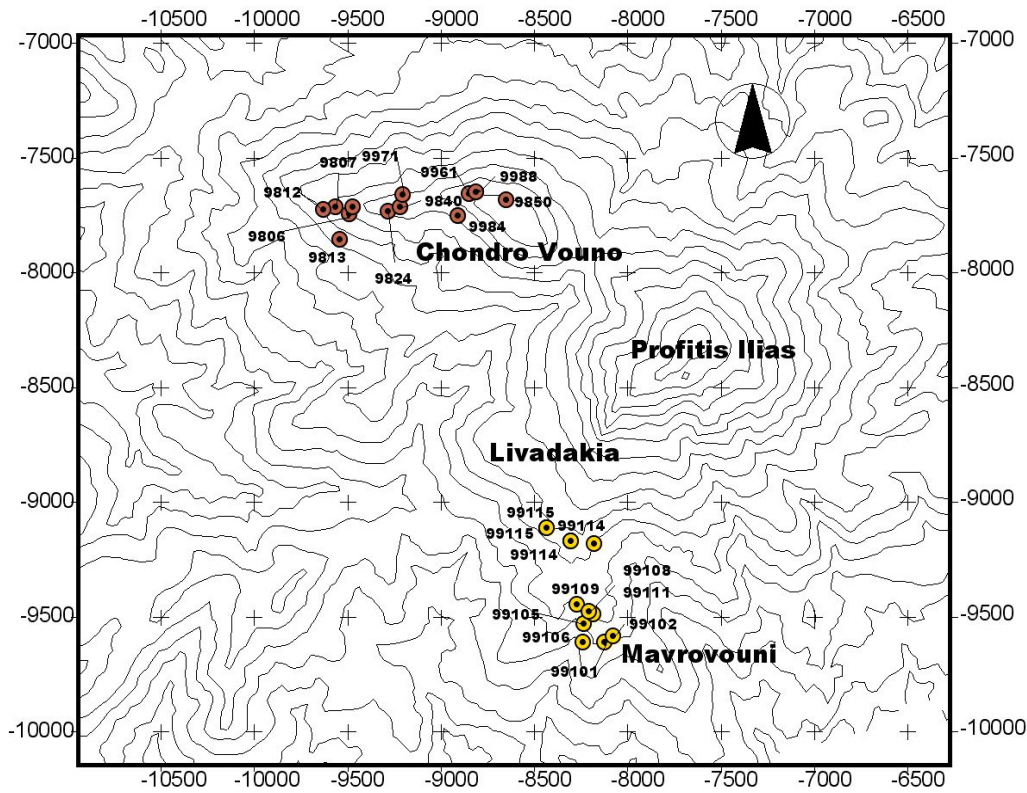


Fig. 84 : RC drill holes location map of the subsurface samples analysed chemically and by XRD.

The K-Na-Ca digram (fig. 85), shows a distribution of the samples belonging to the argillic, advanced argillic, phyllic (sericitic), propylitic (sericitic-chloritic), and steam heated advanced argillic alteration zones. The K, Na and Ca compositions expressed through the ternary diagram explain very well the existence of an argillic, advanced argil-

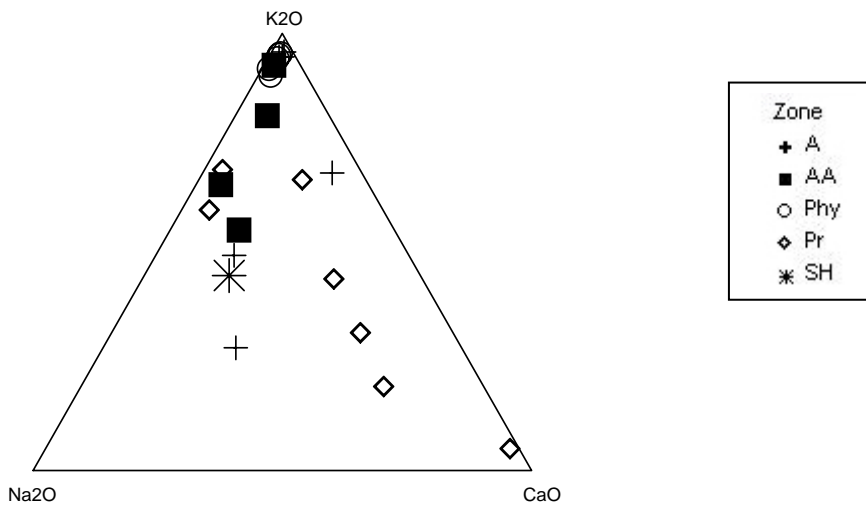


Fig. 85 : Ternary plot of K_2O , Na_2O and CaO (wt. %) of moderate to strongly altered volcanic subsurface rocks at western Milos.

Table 10 : Chemical variation of the major elements of some subsurface altered samples and related alteration minerals after XRD analysis.

Hole	Sample	SiO ₂ %	Al ₂ O ₃ %	Fe ₂ O ₃ %	MnO %	MgO %	CaO %	Na ₂ O %	K ₂ O %	TiO ₂ %	P ₂ O ₅ %	SO ₃ %	H ₂ O+	H ₂ O-	Total	XRD	Zone
9806	AF 6	74,7	12,57	1,83	0,02	0,47	0,06	0,15	3,7	0,17	0,03	0,15	4,29	0,43	98,56	q,ser,kaol	A
9807	AF 7	76,03	13,1	1,3	0,02	0,91	0,07	0,07	3,32	0,17	0,02	0,11	3,72	0,52	99,35	q,ser,kaol	A
9813	AF 13	72,67	12,85	2,33	0,02	1,05	0,98	0,25	2,62	0,21	0,02	0,32	4,79	1,17	99,29	q,ser,kaol	A
9850	AF 50	73,82	12,86	1,43	0,07	1,8	0,1	0,15	4,49	0,18	0,04	0,01	2,92	0,47	98,34	q,ser,kaol	A
99102	AF 102	75,31	10,18	2,06	0,03	0,42	0,65	1,52	2,1	0,28	0,02	0,19	5,63	0,98	99,37	q,kaol	A
99108	AF 108	68,74	13,22	2,64	0,01	1,96	0,25	0,44	0,27	0,2	0,03	0,25	7,4	4,99	100,39	mont,crist	A
9984	AF 84	73,29	13,88	2,12	0,02	0,61	0,06	0,25	3,83	0,3	0,05	0,14	4,31	0,44	99,3	q,ser,kaol,al	AA
99105	AF 105	72,67	11,38	2,65	0,01	0,47	0,13	0,29	1,78	0,31	0,03	0,65	7,1	0,81	98,28	q,kaol,al,ser	AA
99106	AF 106	71,09	12,59	2,73	0,03	0,61	0,62	1,44	2,48	0,27	0,03	0,17	6,13	1,4	99,6	q,al,kaol,ser	AA
99109	AF 109	68,96	15,1	3,09	0,01	1,05	0,11	0,72	1,55	0,4	0,04	0,23	6,4	1,64	99,29	q,mont,kaol,al,ser	AA
99101	AF 101	69,69	13,21	1,66	0,05	0,33	1,22	2,78	3,21	0,18	0,03	0,02	5,94	0,63	98,95	Amorphous silica	SH
9812	AF 12	77,07	12,78	1,23	0,03	0,38	0,06	0,09	3,1	0,18	0,02	0,12	3,32	0,37	98,74	q,ser	Phy
9824	AF 24	76,22	11,97	1,64	0,02	0,5	0,06	0,4	5,28	0,16	0,02	0,11	2,63	0,43	99,44	q,ser	Phy
9840	AF 40	76,3	11,67	1,92	0,04	0,91	0,11	0,36	4,48	0,16	0,03	0,06	2,54	0,44	99,01	q,ser	Phy
9843	AF 43	79,56	10,33	1,93	0,02	0,27	0,05	0,11	2,7	0,14	0,03	0,25	3,78	0,2	99,36	q,ser	Phy
9971	AF 71	75,99	13,04	1,36	0,01	0,79	0,06	0,12	3,52	0,17	0,02	0,1	3,52	0,27	98,97	q,ser	Phy
9961	AF 61	72,98	12,22	2,38	0,01	0,35	0,17	1,45	3,62	0,33	0,09	0,18	3,77	0,46	98,01	q,alb	Pr
9988	AF 88	76,13	10,97	2,04	0,18	1,61	0,17	1,14	1,95	0,16	0,03	0,01	2,96	1,04	98,39	q,ser,kaol,mont,alb	Pr
99111	AF 111	62,42	12,37	2,21	0,07	3,24	4,3	1,44	1,36	0,23	0,05	0,06	7,99	3,49	99,23	alb,dol,ank,mont,crist,q	Pr
99113	AF 113	68,24	12,71	2,08	0,05	2,1	3,07	1,14	1,95	0,23	0,04	0,12	6,26	0,5	98,5	q,ser,alb,dol,ank	Pr
99114	AF 0	72,84	11,89	1,53	0,06	1,4	2,13	0,99	2,44	0,19	0,02	0,2	4,52	0,79	98,99	q,ser,alb,dol,ank	Pr
99115	AF 115	72,85	13,19	1,87	0,04	1,53	0,84	0,53	2,73	0,24	0,02	0,07	4,38	0,84	99,13	q,ser,alb,dol,ank,kaol	Pr
99115	AF 1	27,77	6,57	3,62	0,13	6,06	25,61	0,6	1,31	0,33	0,13	0,53	25,65	0,47	98,79	q,ser,dol,ank	Pr

Abbreviations: (A : argillic zone, AA : advanced argillic zone, SH : steam heated advanced argillic, Phy : phyllic, Pr : propylitic zone. / q : quartz, ser : sericite, kaol : kaolinite, al : alunite, mont : montmorillonite, alb : albite, cris : cristobalite, dol : dolomite, ank : ankerite.

lic and sericitic alteration zones, through K-alunite and sericite alteration mineralogy. The samples towards Ca- and K- terms are compatible with the presence of calcite/ankerite/sericite (propylitic zone) and sericite (argillic zone). As a final step, all the available analyzed samples (137) have been “dropped” on the alteration zonation map (Fig. 41) and thus the rest of the samples that were not analysed through XRD have been classified with respect to those zones. The results, as a mean values, for all the concerning zones are tabulated in the table 11, together with the mean of the available subsurface samples from the RC holes reported above, and a series of samples taken from the literature and considered fresh, as reported by Burri et Soprajanova 1968, Innocenti et al. 1981, Bol and Hasselman 1985, Fytikas et al. 1986, Liakopoulos 1987. The results after comparing them have indicated :

Table 11 : The mean values of the major oxides chemistry at the various alteration zones.

	A (Surf)	A (Sub)	AA (Surf)	AA (Sub)	Adul(Surf)	Phy (Surf)	Phy (Sub)
SiO ₂ %	66,4204	73,54	65,8429	71,5	68	67,83	77,08
Al ₂ O ₃ %	19,1253	12,46	18,8632	13,23	16,43	14,6	11,95
Fe ₂ O ₃ %	1,34267	1,93	1,10723	2,64	2,41	1,16	1,61
MnO %	4,50E-02	0,02	1,18E-02	0,01	0,04	2,00E-02	0,02
MgO %	0,81642	1,1	0,58687	0,68	0,46	1,59	0,57
CaO %	1,45786	0,35	0,11687	0,23	0,08	0,12	0,06
Na ₂ O %	1,63643	0,43	1,34125	0,67	1,46	2,42	0,21
K ₂ O %	2,12964	2,75	2,16438	2,41	6,58	3,56	3,81
TiO ₂ %	0,37326	0,2	0,36191	0,32	0,25	0,34	0,16
P ₂ O ₅ %	9,16E-02	0,02	0,10062	0,03	0,05	0,05	0,02
SO ₃ %	0,909	0,17	1,65256	0,29	0	0,15	0,12
LOI	7,29352	4,79	8,85651	5,98	2	6,02	3,15

(**Abbreviations** as in Tab. 10 / Surf : surface – Sub : subsurface)

	Pr (Surf)	Pr (Sub)	SH (Surf)	SH (Sub)	Fr
SiO ₂ %	60,41	64,74	68,53	69,69	64,41
Al ₂ O ₃ %	15,04	11,41	14,01	13,21	16,60
Fe ₂ O ₃ %	2,00	2,24	1,77	1,66	2,71
MnO %	0,07	0,07	0,05	0,05	0,10
MgO %	2,58	2,32	1,37	0,33	2,27
CaO %	2,14	5,18	2,61	1,22	4,69
Na ₂ O %	2,36	1,04	3,11	2,78	2,94
K ₂ O %	2,28	2,19	0,75	3,21	3,35
TiO ₂ %	0,27	0,24	0,33	0,18	0,56
P ₂ O ₅ %	0,03	0,05	0,02	0,03	0,06
SO ₃ %	0,00	0,16	0,00	0,02	0,00
LOI	6,16	7,93	3,11	5,94	1,43

- A net **gain** of **SiO₂** for all the alteration zones with respect to the fresh mean composition.
- A **gain** for the **Al₂O₃** for the surface samples of the argillic and advanced argillic alteration zones, and a **loss** for all the others.
- A net **loss** for the **Fe₂O₃** for all the alteration zones.
- A net **loss** for the **MnO** for all the alteration zones.
- A net **loss** for the **MgO** for all the alteration zones except the propylitic zone.
- A net **loss** for the **CaO** for all the alteration zones except the subsurface propylitic zone.

- A net **loss** for the **Na₂O** for all the alteration zones except the steam heated surface zone.
- A net **gain** for the **K₂O** for the adularia and phyllic zones and a loss for all the others.
- A net **loss** for the **TiO₂** for all the alteration zones.
- A net **loss** for the **P₂O₅** for all the alteration zones except the surface expression of the advanced argillic zone.

All these relative variations are compatible to the alteration minerals which have been identified at western Milos and characterize the various alteration zones.

10.3. Minor and Trace Elements Variation and their Geochemical Trends

An initial series of 77 samples have been measured (23 by I.C.P [Inductively coupled plasma-atomic emission spectrometry] carried out at the laboratory of French Geological Survey [B.R.G.M] at Orleans, under the former joint venture between Silver and Baryte Ores Mining Company S.A.[S&B] and B.R.G.M from 1989 to 1992; 6 by XRF at X-RAL labs (Australia, Canada) for Midas S.A. Joint Venture and 48 by XRF at Hamburg university) in order to further approach, see and understand their variation and their related geochemical trends.

The following elements (Ce, Co, Cr, Ga, La, Nb, Nd, Ni, Rb, Sr, V, Y, Zr, W, Bi, Mo, Cd) examined, showed grades which are considered anomalous, with respect the fresh ones, suggesting that the hydrothermal processes, which occurred at western Milos, affected also the relative concentrations of the minor and trace elements. In table 12 the Pearson's correlation coefficients for Ce, Co, Cr, Ga, La, Nb, Nd, Ni, Rb, Sr, V, Y, Zr, for the 77 measured altered samples towards their silica content, as well as to each other (W, Bi, Mo, Cd excluded because missing for the major number of samples), are reported .

Table 12 : Pearson's Correlation coefficient between minor/trace elements at western Milos

	SiO ₂ %	Ce_ppm	Co_ppm	Cr_ppm	Ga_ppm	La_ppm	Nb_ppm	Nd_ppm	Ni_ppm	Rb_ppm	Sr_ppm	V_ppm	Y_ppm	Zr_ppm
SiO ₂ %	1	-0,30522	0,25328	-0,13028	-0,13734	-0,20596	0,61409	-0,00874	-0,07626	0,45107	-0,28283	0,07296	0,20796	0,5581
Ce_ppm	-0,30522	1	-0,18401	0,58518	0,68689	-0,14856	-0,37401	0,80944	0,13002	-0,03721	0,43114	-0,10156	0,07672	-0,27672
Co_ppm	0,25328	-0,18401	1	0,02852	0,10144	-0,11816	0,63151	0,11458	-0,06267	0,30574	-0,28032	0,37494	0,21723	0,23953
Cr_ppm	-0,13028	0,58518	0,02852	1	0,5985	0,51084	-0,12651	0,52486	0,12894	0,11498	0,40736	0,31451	0,12164	-0,18655
Ga_ppm	-0,13734	0,68689	0,10144	0,5985	1	-0,31227	-0,0674	0,82286	-0,01465	0,06779	0,28374	0,2986	0,12645	0,08628
La_ppm	-0,20596	-0,14856	-0,11816	0,51084	-0,31227	1	-0,20086	-0,25546	-0,12158	-0,04948	0,18785	0,07305	0,03834	0,00099
Nb_ppm	0,61409	-0,37401	0,63151	-0,12651	-0,0674	-0,20086	1	0,05486	-0,17767	0,53195	-0,53321	0,21739	0,3104	0,5254
Nd_ppm	-0,00874	0,80944	0,11458	0,52486	0,82286	-0,25546	0,05486	1	-0,08004	0,08749	0,37444	0,11051	0,28232	0,11436
Ni_ppm	-0,07626	0,13002	-0,06267	0,12894	-0,01465	-0,12158	-0,17767	-0,08004	1	-0,11322	0,37176	0,07952	0,03638	0,14053
Rb_ppm	0,45107	-0,03721	0,30574	0,11498	0,06779	-0,04948	0,53195	0,08749	-0,11322	1	-0,05294	-0,03985	-0,0651	0,06418
Sr_ppm	-0,28283	0,43114	-0,28032	0,40736	0,28374	0,18785	-0,53321	0,37444	0,37176	-0,05294	1	-0,25952	0,02997	-0,3968
V_ppm	0,07296	-0,10156	0,37494	0,31451	0,2986	0,07305	0,21739	0,11051	0,07952	-0,03985	-0,25952	1	0,22394	0,35525
Y_ppm	0,20796	0,07672	0,21723	0,12164	0,12645	0,03834	0,3104	0,28232	0,03638	-0,0651	0,02997	0,22394	1	0,37354
Zr_ppm	0,5581	-0,27672	0,23953	-0,18655	0,08628	0,00099	0,5254	0,11436	0,14053	0,06418	-0,3968	0,35525	0,37354	1

As it can be seen from the table 12, there is only a positive intermediate affinity between SiO₂ and Nb (0.61), Zr (0.55), while the correlations between silica and the other minor elements can be considered of none importance. Concerning their interrelations, the most important are those expressed between Ce-Ga-Nd (Table 12, fig.86), being (0.68 and 0.80 respectively). Another correlation coefficient matrix is presented in Table 13 and in fig. 87, and it is referred to Ce, Co, Sr, W, Bi, Mo and Cd. As it can be observed, a very strong correlation exist between bismuth and cadmium (0.91), between tungsten and cobalt (0.93) and a strong one between molybdenum and strontium (0.79). In the fig. 87, as it has been said in the previous paragraph, the correlation of the variables is shown by an ellipse

(along the diagonal axis), which is a function of the means and standard deviations of the X and Y variables and the correlation between them. If the ellipse is fairly round and

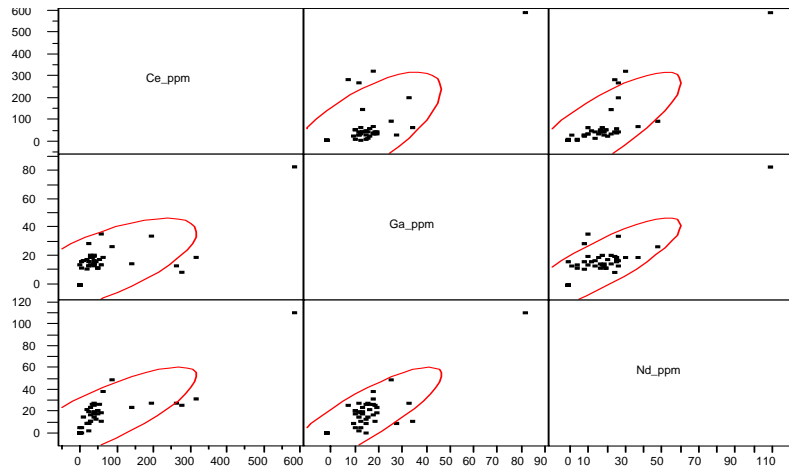


Fig. 86 : Scatterplot multivariate correlation matrix between Cerium, Gallium and Neodymium.

Table 13 : Correlation coefficient of some of the minor/trace elements at western Milos

	Ce ppm	Co ppm	Sr ppm	W ppm	Bi ppm	Mo ppm	Cd ppm
Ce ppm	1	-0,34976	-0,378497	-0,366851	-0,084179	-0,457706	0,001265
Co ppm	-0,34976	1	-0,20413	0,934714	-0,155945	-0,157705	-0,211
Sr ppm	-0,378497	-0,20413	1	-0,165422	-0,021485	0,792795	0,060943
W ppm	-0,366851	0,934714	-0,165422	1	0,023862	-0,07787	-0,0425
Bi ppm	-0,084179	-0,155945	-0,021485	0,023862	1	0,368791	0,913112
Mo ppm	-0,457706	-0,157705	0,792795	-0,07787	0,368791	1	0,384801
Cd ppm	0,001265	-0,211	0,060943	-0,0425	0,913112	0,384801	1

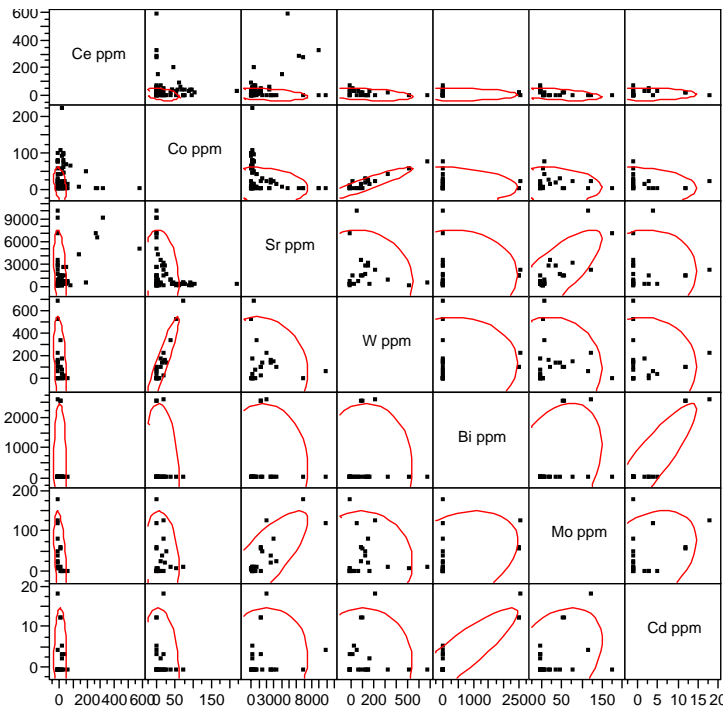


Fig. 87 : Scatterplot multivariate correlation matrix between Ce, Co, Sr, W, Bi, Mo and Cd.

is not diagonally oriented, the variables are uncorrelated. So, the various correlations between the analyzed elements are well visible and clearly shown.

In a further attempt to better understand the genetic relationships between those elements and the various tectonic lineaments and/or volcanic centres of western Milos, a series of geochemical maps have been created. Through these maps it has been possible to relate tectonics with alteration and mineralizing processes. The results are presented below :

10.3.1. The La pattern

This anomaly (Fig. 88) is related to the argillic, advanced argillic and phyllic zones and it seems to be the key to the relation between Galana and Mersinia subareas (constituting the higher part of an acid hot spring system). Indeed Mersinia being a former sea bottom, later has been lifted up due to tectonic processes and constituted a subaerial hot spring environment, today represented by a massive silica cap, similar to that of Agathia.

10.3.2. The Nd pattern

It is shown (Fig. 88) as a N-S trending anomaly displayed in two different subareas and mainly inside the argillic alteration zone. The anomaly is very well delineated at Chondro Vouno subarea. It is also present in anomalous concentrations at Ntasifnos subarea, where it is considered to be the surface expression of the fluids circulating along the adges of a small but important graben.

10.3.3. The Mo pattern

As it can be observed from the fig. 88, Mo is related to a complex geotectonic environment on both Agathia area and Pyrgaki, depicted by a combination of a major lineament structure and an associated volcanic centre. In such a fashion in the first case a major structure going from Agathia bay to Fourkovouni-Fyropotamos area (eastern Milos), delimits to the north the Vromolimni-Ampelakia silica cap, as well as the well located volcanic centre at the area of Pyrgaki. Most probably anomalous Mo incidates the presence of molybdenite in the Agathia-Galana-Triades mineralization. The Mo anomalous patterns are displayed inside the argillic and advanced argillic alteration zones.

It could be also possible that the previous mentioned Agathia - Fyropotamos lineament together with that one of Kalogries - Vani, running parallel to each other, are the margins of a horst structure related to an uprised magma body underneath. The above mentioned concept related to the Mo behaviour is reinforced by the Bi anomaly located at the same area of the former volcanic centre of Pyrgaki.

10.3.4. The Bi pattern

It is developed in the area between Triades - Galana (Fig. 88) as a major anomaly bisected by the Triades - Katsimoutis lineament and clearly related to the previously mentioned molybdenum (Mo) anomaly. Of course Bi is related to the presence of sulfosalts as well as to the presence of galena and pyrite/chalcopyrite. The Bi anomaly is displayed inside the argillic alteration zone.

10.3.5. The W pattern

The tungsten anomaly is related to a major quasi N-S running lineament, which passes from the well known breccia field and vent area of Mersinia (Fig. 88). It is worth to mention also that a large W anomaly (up to 2420 ppm) has been reported by Glasby et al. (2005) from the Vani deposit, but not considered during this study. In the present work it is

considered that W together with other trace elements (Au, Ag, As, Sb, Hg), document, through the present fossil extinct system, the analogy between epithermal precious metal depo sits and active geothermal systems. The W anomalous patterns are displayed inside

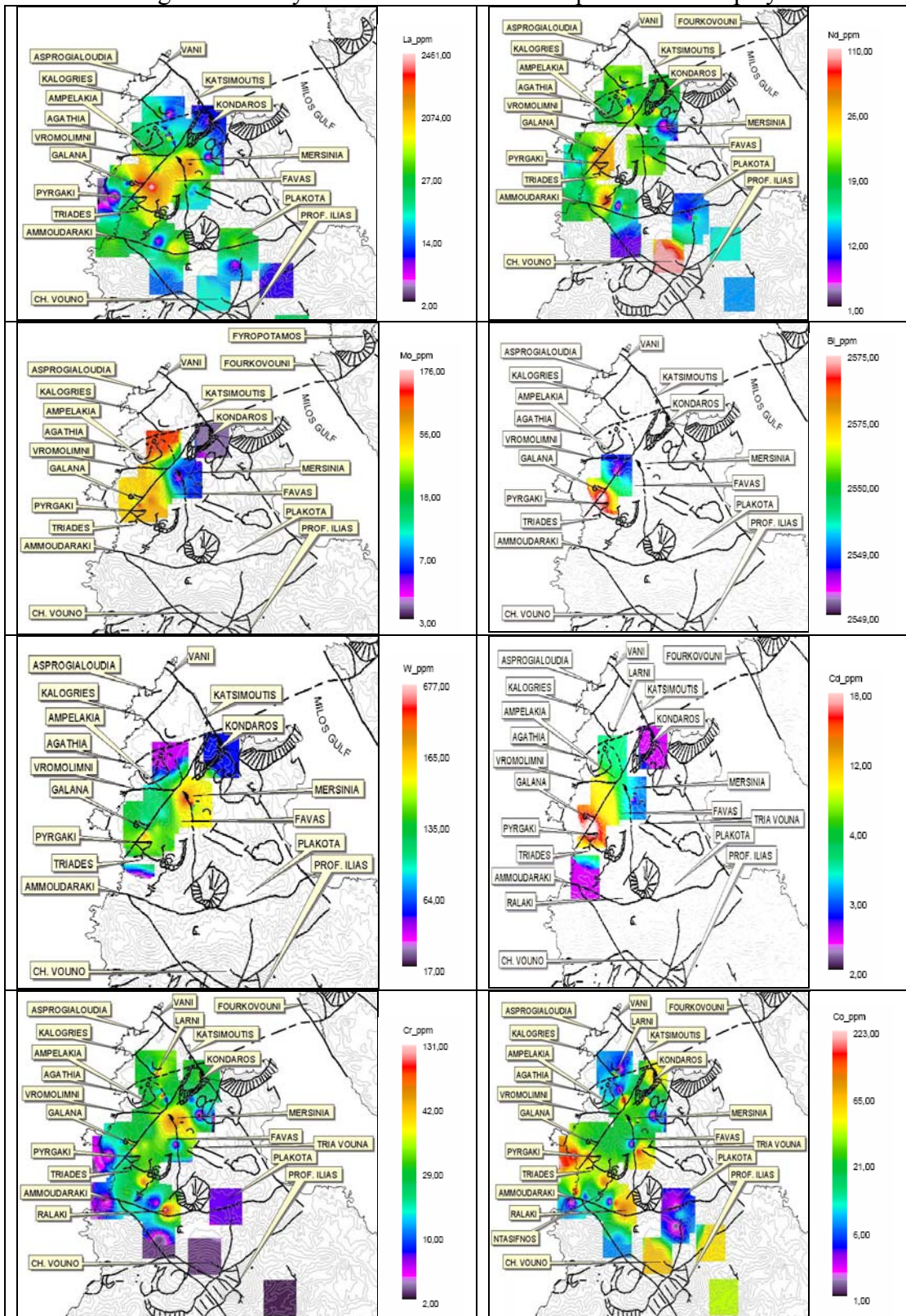


Fig. 88 : Distribution patterns of La, Nd, Mo, Bi, W, Cd Cr and Co at W. Milos. Values in ppm

the argillic and advanced argillic alteration zones.

10.3.6. The Cd pattern

It has exactly the same “behaviour” (Fig. 88), as that of Bi in Pyrgaki (between Triades - Galana subareas), and it is considered to be related to the sphalerite presence in the base metal assemblage of the area, and without doubt indicates a lower (deeper) position in the system. As an anomaly it is related to the argillic alteration zone.

10.3.7. The Ni, Cr, Co patterns

Ni concentrations are low (at about 25 ppm max) and are considered not anomalous. Chromium delineates a big circular feature (fig. 88), segments of which are visible through the air-photos. This feature passes through Ralaki to Triades and then to Mersinia area and is related to the argillic and advanced argillic alteration zones.

Cobalt is presented in anomalous concentrations and seems to delineate very well all the main lineament structures (fig. 88), i.e., Ammoudaraki-Plakota, Triades-Katsimoutis, Ralaki-Pyrgaki-Akrotiri and the smaller ones of the Tria Vouna-Xerokampos grabben. It is related to the presence of pyrite and marcasite and its geochemical behaviour is also locally related to that of Cr. As an anomaly it is displayed mainly inside the argillic alteration zone.

10.3.8. The Ce pattern

It pictures out very clear the inferred Pyrgaki/Galana intrusive body, “described” also previously through the Mo, Bi and La anomalies. As an anomaly it is related to the argillic, advanced argillic and adularia alteration zones (fig. 89).

10.3.9. The Ga pattern

It shows a clear relation to the main Triades - Katsimoutis lineament with two anomalous areas located the first around Pyrgaki-Galana volcanic centre and the second at the oxidized silica cap at Agathia area. It also reinforces the meaning of the well known site at Tria Vouna area, along the micrograben margins of Tria Vouna - Xerokampos. It is also encountered at Chondro Vouno area, related to the local vent area, and having a position in between an open angle tectonic configuration. It is related to the argillic and advanced argillic alteration zones (fig. 89).

10.3.10. The Rb pattern

Rb follows the trend of K, which means essentially it is in relation to the adularia and sericite alteration minerals, i.e., to the adularia and argillic alteration zones. It is presented anomalous at the Agios Panteleimon, Chondro Vouno (southern sector) and Larni at (Northern sector) subareas (fig. 89).

10.3.11. The Sr pattern

It seems to be very well developed, as an anomaly, at the area between Triades-Galana-Favas-Agathia-Larni picturing out essentially the quartz-alunite zone (advanced argillic zone) and the geochemical behaviour of Ba (on both argillic and advanced argillic zones), as an indicator of the hydrothermal solutions’ outflow areas. It is also related to the presence of alunite (advanced argillic zone). It seems also to be somehow related to the adularia alteration zone (fig. 89).

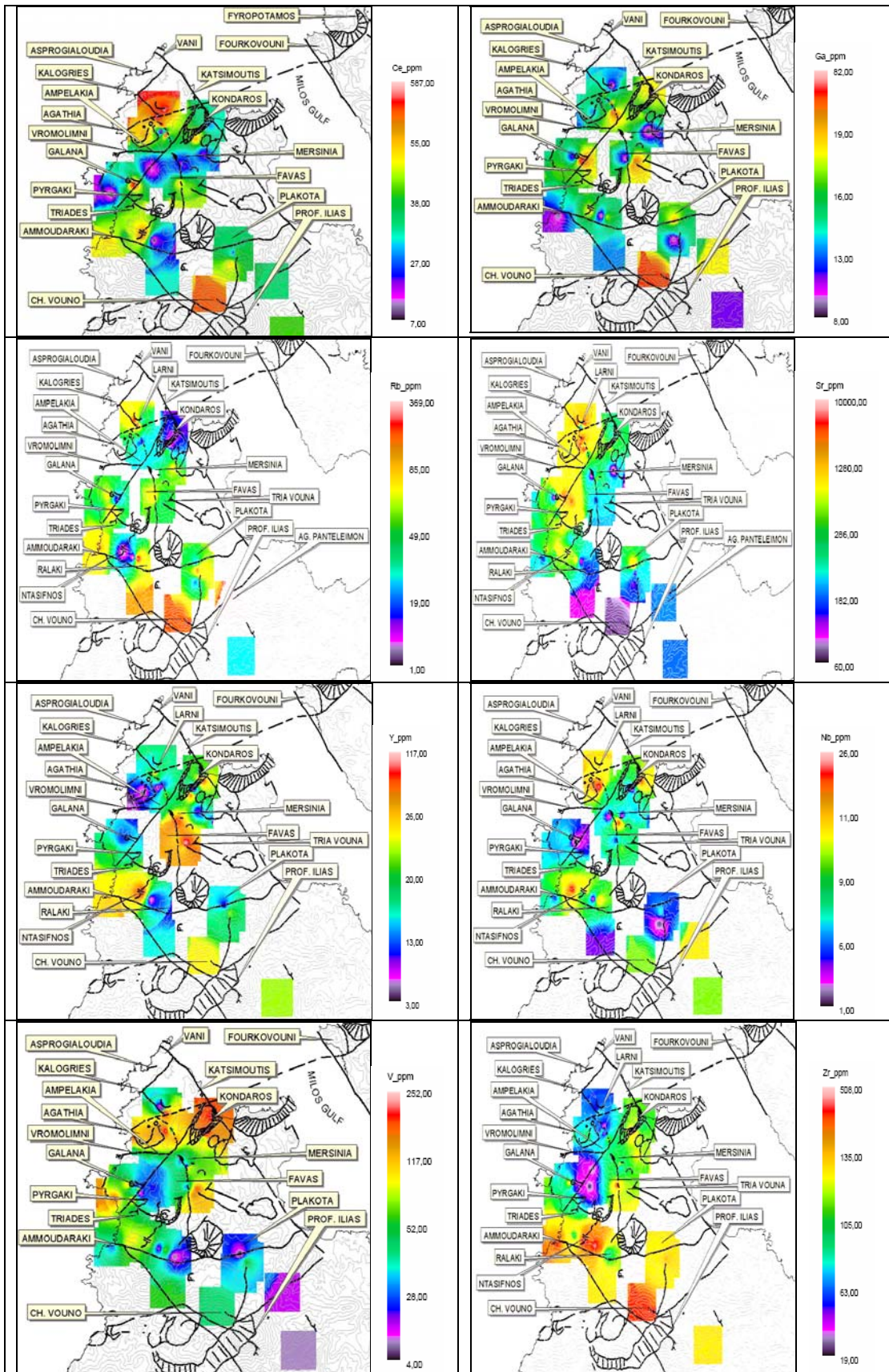


Fig. 89 : Distribution patterns of Ce, Ga, Rb, Sr, Y, Nb, V and Zr at W Milos. Values in ppm.

10.3.12. The Y, Nb patterns

The Nb, Y anomalous patterns are related to the argillic and advanced argillic alteration zones. It is considered that both of them essentially indicate the existence of two slightly different magma types existed in the chamber that fed this segment of the magmatic sequence. Their anomalies are very well developed along the micro-graben structures of Ntasifnos, Tria Vouna - Xerokampos and along the small graben at the southern footwall of Kondaros volcano (fig. 89).

10.3.13. The V pattern

It is very well developed, as an anomaly, at Kondaros area and clearly related to the quartz-alunite lithocap of the area (advanced argillic zone), as well as to the oxidized silica cap of Agathia subarea. Anomalous values are also encountered at the well known areas of Tria Vouna and Pyrgaki, the first related to a micro-graben structure and the second to a small volcanic edifice (fig. 89).

10.3.14. The Zr pattern

Zr although considered an immobile element shows considerable mobility along trends related to outflow zones, as for ex. Chondro Vouno vent area and other two vent areas along the Ammoudaraki-Plakota lineament (fig. 89). The shown anomalies are related to the argillic alteration zone.

10.4. The relationships between the minor and trace elements in the various alteration zones

A further approach toward correlating the distribution of the above mentioned elements within the various alteration zones on W. Milos, has been achieved through a series of XRD analyses performed at Hamburg University for 32 surface samples (fig. 82), and 23 sub surface ones (fig. 84) coming from reverse circulation drill holes (RC holes), which have been connected to the chemistry of the altered rocks. The results are tabulated (Tab. 14, 15 respectively) and shown through the ternary Rb-Sr-Ba diagrams (fig. 90, 91 respectively).

The table 14 describes the variation of the generally moderate to strongly altered surface rock types, for their minor elements content related to the alteration zones which they belong as revealed after XRD analysis.

The ternary diagramme (fig. 90a) shows the distribution of Rb-Sr-Ba samples belonging to the argillic, advanced argillic, phyllic (sericitic), propylitic (sericitic-chloritic), adularia alteration zones. The behaviour of Rb is directly related with that of K which essentially reflects the presence of adularia and sericite and which is clearly distinct from that expressed by Ba, Sr which are related with the presence of alunite and barite. A strong correlation exist between Rb and Ba, Sr in the advanced argillic alteration zone as well as a correlation between Rb and Ba in the adularia and partially in the phyllic alteration zones.

The binary diagram of the fig. 90b reflects the substitution of K by Rb in the lattice of k-feldspars substituted at their turn by adularia in the adularia alteration zone and by sericite in the advanced argillic zone.

The ternary diagram Rb-Ba-Sr for the subsurface samples at fig. 91a shows rather a strong correlation for Ba of all the alteration zones, and partially the propylitic zone for Sr.

Table : 14 Chemical variation of the minor elements of some surface altered samples and related alteration minerals after XRD analysis.

Sample	Ba ppm	Ce ppm	Co ppm	Cr ppm	Ga ppm	La ppm	Nb ppm	Nd ppm	Ni ppm	Rb ppm	Sr ppm	V ppm	Y ppm	Zr ppm	XRD	Zone
1	100000	n.d.	n.d.	n.d.	n.d.	n.d.	n.d.	n.d.	n.d.	n.d.	n.d.	n.d.	n.d.	n.d.	kaol,ser,hal,q	A
2	37736	n.d.	n.d.	n.d.	n.d.	n.d.	n.d.	n.d.	n.d.	n.d.	n.d.	n.d.	n.d.	n.d.	kaol,hal,q	A
4	8954	n.d.	n.d.	n.d.	n.d.	n.d.	4	n.d.	n.d.	n.d.	n.d.	n.d.	n.d.	n.d.	kaol,q	A
15	35	58	n.d.	n.d.	13	27	n.d.	18	1	n.d.	361	132	4	104	kaol,hal	A
U55B	117	39	42	3	12	24	9	14	3	28	182	14	22	135	q,hal,kaol	A
U70	2294	11	104	4	16	2	7	14	1	41	298	141	20	105	q,kaol	A
U75	286	28	18	13	12	12	8	19	n.d.	68	87	100	12	118	q,hal,kaol	A
U76	643	195	46	8	33	79	1	27	5	14	329	98	n.d.	57	q,al,kaol,hal	A
5	17699	587	n.d.	100	82	203	n.d.	110	n.d.	42	4848	112	18	44	Kaol,q,hal,al	AA
6	3126	n.d.	n.d.	n.d.	n.d.	n.d.	n.d.	n.d.	n.d.	n.d.	n.d.	n.d.	n.d.	n.d.	kaol,q,hal,al	AA
7	249	7	6	16	15	2	n.d.	n.d.	7	19	796	153	3	109	al,q	AA
8	172	28	1	9	12	2	n.d.	1	9	11	1220	52	7	64	kaol,al,q	AA
9	1020	58	n.d.	33	35	30	n.d.	10	4	15	2502	n.d.	12	19	kaol,hal,al	AA
10	1478	265	n.d.	30	12	9	n.d.	27	7	58	6966	n.d.	21	60	kaol,hal,al	AA
11	288	317	2	19	18	16	n.d.	31	9	58	9100	n.d.	28	n.d.	kaol;hal,al,q	AA
12	559	145	5	12	14	33	n.d.	23	6	184	4099	7	13	43	q,ser,al	AA
13	28385	280	1	35	8	4	n.d.	25	8	39	6442	n.d.	19	n.d.	Kaol,q,hal,al	AA
14	4334	n.d.	n.d.	n.d.	n.d.	n.d.	n.d.	n.d.	n.d.	n.d.	n.d.	n.d.	n.d.	n.d.	kaol,hal,al,q	AA
17	638	44	3	n.d.	15	20	3	12	5	1	671	245	5	156	q,kaol,al,hal	AA
19	1106	25	n.d.	21	28	16	n.d.	8	4	10	1368	252	8	100	kaol,q,al,hal	AA
20	328	19	2	2	10	5	7	8	5	63	60	57	10	117	cris,mont,q,al,kaol	AA
21	1404	33	2	7	19	39	n.d.	10	4	23	2457	4	10	133	cris,kaol,mont,al,hal	AA
28	180	8	2	7	11	7	4	4	7	8	950	18	5	176	kaol,al,hal,trid,cris	AA
29	271	65	11	6	18	28	8	37	n.d.	8	362	70	32	185	cris,kaol,al,hal	AA
U20	924	22	91	5	17	n.d.	13	21	2	272	105	57	12	157	cris,mont,q,al,kaol	AA
HS46	1108	91	61	4	26	20	9	48	n.d.	175	62	42	23	161	q,adul	Adul
U57	784	30	57	n.d.	18	13	11	16	n.d.	369	184	18	n.d.	n.d.	san,q	Adul
27	239	29	7	4	13	14	5	10	5	149	121	56	16	135	q,ser	Phy
22	431	27	8	n.d.	15	28	8	8	2	171	151	37	19	135	alb,mont	Pr
23	307	40	10	n.d.	14	23	5	19	2	85	205	54	22	138	alb,mont	Pr
25	313	48	2	n.d.	11	6	3	17	6	21	152	37	19	125	mont,alb	Pr
30	593	50	2	5	11	33	6	20	7	72	171	33	26	161	alb,mont	Pr

Table : 15 Chemical variation of the minor elements of some subsurface altered samples and related alteration minerals after XRD analysis.

Hole	Sample	Ba ppm	Ce ppm	Co ppm	Cr ppm	Ga ppm	La ppm	Nb ppm	Nd ppm	Ni ppm	Rb ppm	Sr ppm	V ppm	Y ppm	Zr ppm	XRD	Zone
	9806 AF 6	1186	25	24	11	15	9	6	14	11	120	31	22	14	113	q,ser,kaol	A
	9807 AF 7	749	50	0	17	8	15	9	15	4	135	28	12	20	109	q,ser,kaol	A
	9813 AF 13	601	33	8	3	10	38	8	4	5	82	19	15	19	131	q,ser,kaol	A
	9850 AF 50	654	38	16	1	15	31	5	22	1	166	36	11	20	134	q,ser,kaol	A
	99102 AF 102	3845	0	0	0	0	0	0	0	0	0	0	0	0	0	q,kaol	A
	99108 AF 108	858	9	0	7	7	0	7	6	6	6	80	20	11	132	mont,crist	A
	9984 AF 84	702	33	10	7	15	14	3	15	6	112	23	38	12	150	q,ser,kaol,ε	AA
	99105 AF 105	12373	0	0	0	0	0	0	0	0	0	0	0	0	0	q,kaol,al,σε	AA
	99106 AF 106	1913	31	6	85	18	22	7	10	14	92	228	49	15	124	q,al,kaol,σε	AA
	99109 AF 109	1984	29	3	35	11	23	6	14	7	45	142	72	17	141	q,mont,kac	AA
	99101 AF 101	651	31	0	46	12	28	8	9	16	103	87	14	20	128	Amorphou	SH
	9812 AF 12	319	36	10	5	10	10	8	11	7	106	28	19	19	119	q,ser	Phy
	9824 AF 24	989	30	11	7	11	23	6	13	4	162	29	17	13	109	q,ser	Phy
	9840 AF 40	789	33	1	5	11	36	9	13	2	138	55	10	16	110	q,ser	Phy
	9843 AF 43	652	33	0	5	11	11	7	3	6	84	23	14	14	100	q,ser	Phy
	9971 AF 71	672	36	2	2	10	38	6	13	4	131	17	11	20	115	q,ser	Phy
	9961 AF 61	10919	0	0	0	0	0	0	0	0	0	0	0	0	0	q,alb	Pr
	9988 AF 88	184	60	11	4	27	20	4	20	3	65	18	6	11	121	q,ser,kaol,r	Pr
	99111 AF 111	759	35	3	27	9	15	7	12	10	39	128	25	19	130	alb,dol,ank	Pr
	99113 AF 113	965	44	20	14	8	32	10	14	9	61	66	35	23	120	q,ser,alb,d	Pr
	99114 AF 0	622	35	21	7	9	29	8	9	7	84	39	11	19	135	q,ser,alb,d	Pr
	99115 AF 115	611	24	4	6	7	31	8	8	6	90	29	21	22	136	q,ser,alb,d	Pr
	99115 AF 1	221	9	15	130	11	11	4	9	89	50	405	99	22	61	q,ser,dol,ar	Pr

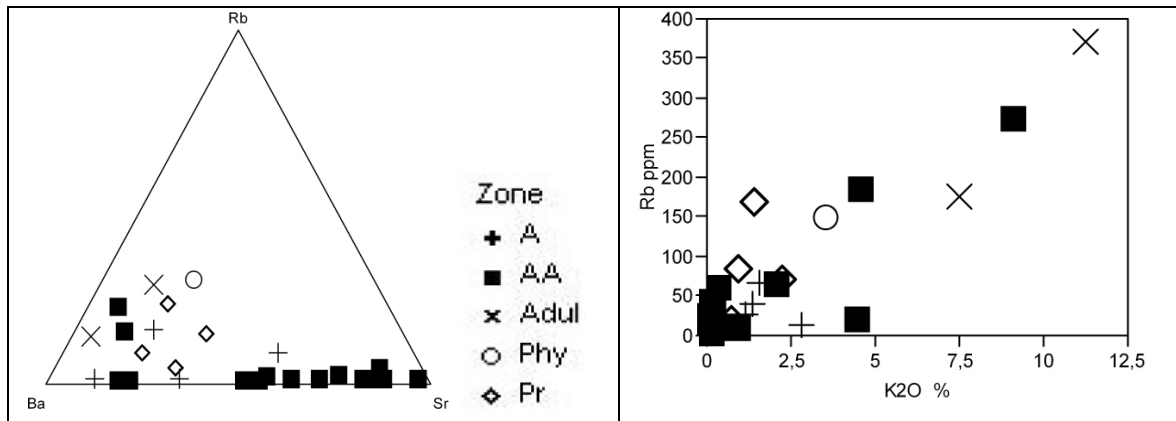


Fig. 90 : Surface samples (a) along a Rb-Ba-Sr ternary diagram [Left]; (b) the Rb-K2O binary diagram [Right], for W. Milos altered rocks.

In the fig. 90b the relationship between Rb and K shows three trends, one where the K increases while the Rb remains quasi constant for the argillic, advanced argillic alteration zones, one that Rb increases with the increasing of K for argillic, advanced argillic and phyllic alteration zones, and one which Rb increases in the advanced argillic zone, while K remains quasi constant. The relationships are more clear for the subsurface samples, where exist two trends, one with an increasing of K while Rb remains constant and another where Rb follows the increasing of K.

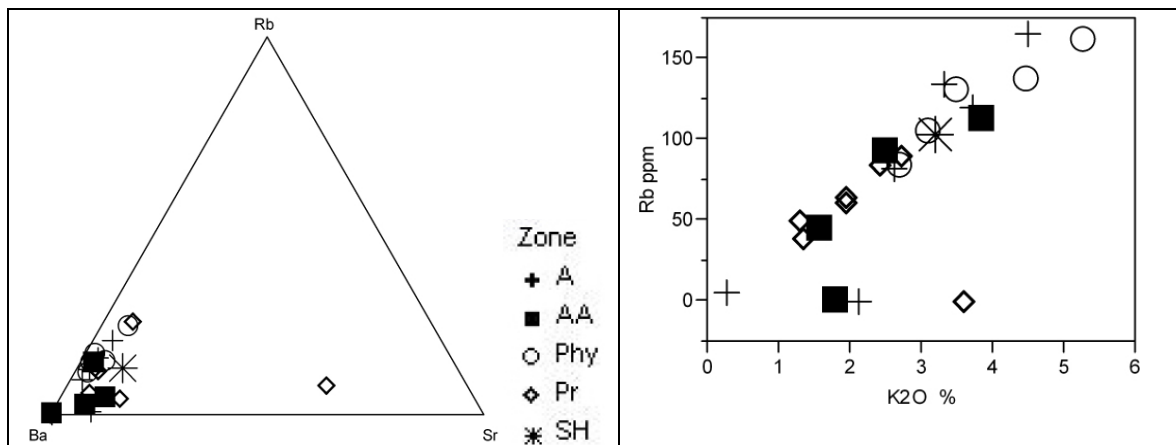


Fig. 91 : Subsurface samples (a) along a Rb-Ba-Sr ternary diagram [Left] ; (b) the Rb-K2O binary diagram [Right], for W. Milos altered rocks.

As a final step, all the available analyzed (137) samples have been “dropped” on the alteration zonation map (fig. 41) and thus have been classified with respect to those zones. The results, as a mean values, for all the concerning zones are tabulated in the table 16 together with the mean of the available subsurface samples from the RC holes reported above, and a series of samples considered fresh, as reported in the literature (Burri et Soprajanova 1968; Innocenti et al. 1981; Bol and Hasselman 1985; Fytikas et al. 1986; Liakopoulos 1987). The results after comparing them showed :

Table 16 : The mean values for some minor and trace elements chemistry at the various alteration zones (Surf : surface - Sub : subsurface, samples / Abbreviations as in Tab. 10).

	A (Surf)	A (Sub)	AA (Surf)	AA (Sub)	Adul (Surf)	Adul (Sub)	
Ce ppm	58,31	25,83	116,63	23,25	60,5		
Co ppm	49,39	8	6,02	4,75	59		
Cr ppm	9,19	6,5	18,6	31,75	4		
Ga ppm	15,52	9,16	19,2	11	22		
La ppm	21,37	15,5	29,6	14,75	16,5		
Nb ppm	6,14	5,83	3,6	4	10		
Nd ppm	19,34	10,16	20,82	9,75	32		
Ni ppm	2,47	4,5	4,71	6,75			
Rb ppm	59,21	84,83	37,33	62,25	272		
Sr ppm	484,95	32,34	2269,3	98,25	123		
V ppm	68,95	13,34	84,03	39,75	30		
Y ppm	20,61	14	10,67	11	23		
Zr ppm	97,28	103,16	85,97	103,75	161		
W ppm			134,5				
Bi			2558				
Mo			54,5				

	Phy (Surf)	Phy (Sub)	Pr (Surf)	Pr (Sub)	SH (Surf)	SH (Sub)	Fr
Ce ppm	30	33,6	41,25	29,57		31	33
Co ppm	13,35	4,8	5,5	10,57			24
Cr ppm	20,83	4,8	5	26,85		46	14
Ga ppm	15	10,6	12,75	10,14		12	22
La ppm	880,5	23,6	22,5	19,71		28	20
Nb ppm	5	23,6	5,5	5,85		8	7
Nd ppm	10	23,6	16	10,28		9	20
Ni ppm	5	23,6	2,62	17,71		16	21
Rb ppm	150	23,6	87,25	55,57		103	165
Sr ppm	1288,5	23,6	169,75	97,85		87	208
V ppm	37,17	23,6	40,25	28,14		14	100
Y ppm	16	23,6	21,5	16,57		20	23
Zr ppm	86,25	23,6	139,75	100,42		128	142
W ppm							154
Bi							no data
Mo							no data

-First of all there is a **relative enrichment** of the surface samples with respect to the subsurface ones.

-A net **gain** for **Ce** for the argillic, advanced argillic, propylitic and adularia surface alteration zones and a loss for the others, while the phyllic subsurface zone remains constant.

-A net **loss** for the **Co** for quasi all samples for all the zones except for the adularia and argillic surface zones.

-A net **loss** for the **Cr** for quasi all the alteration zones except the advanced argillic, steam heated advanced argillic and phyllic surface alteration zones and the propylitic and advanced argillic subsurface zones.

-A net **loss** for the **Ga** for all the alteration zones.

- A net **loss** for the **La** for the propylitic, argillic and advanced argillic subsurface zones, and a gain for all the others zones.
- A net **loss** for the **Nb** for all the alteration zones except for the phyllic subsurface and the adularia surface zones.
- A net **loss** for the **Nd** for all the alteration zones except for the phyllic subsurface and the adularia surface zones, while the advanced argillic surface alteration zone remain essentially constant.
- A net **loss** for the **Ni** for all the alteration zones except for the phyllic subsurface alteration zone.
- A net **loss** for the **Rb** for all the alteration zones except the surface expression of the adularia zone.
- A net **loss** for the **Sr** for all the alteration zones except the subsurface expression of the phyllic zone and the surface expression of the argillic and advanced argillic surface alteration zones.
- A net **loss** for the **V** for all the alteration zones.
- A net **loss** for the **Y** for all the alteration zones except the surface expression of the adularia zone. The subsurface phyllic alteration zone remains constant.
- A net **loss** for the **Zr** for all the alteration zones except the surface expression of the adularia zone.
- A net **loss** for the **W** for the surface expression of the advanced argillic zone. There are no data for comparison concerning the other alteration zones.
- For the **Bi** and **Mo** there are no data for to compare the various alteration areas of western Milos, except what is reported for the surface expression of the advanced argillic alteration zone.

All these relative variations are compatible to the alteration minerals which have been identified at western Milos and characterize the various alteration zones.

10.5. The Epithermal suite of Trace Elements at W. Milos and its Variation

A total of 2546 surface samples have been collected and analyzed at various periods, for their content in trace elements. All of them are altered and mineralized to various degrees. For the most of the samples, the measurements were carried out at the former Bondar Clegg, Vancouver based laboratories (later acquired by ALS Chemex), on behalf of Silver and Baryte Ores mining Co.(S&B) and the former MIDAS* and Milos Gold* joint Ventures during various periods (*J.V. between S&B - Renison Goldfields Consolidated (RGC) - Niugini mining - Royal Gold Inc.-Aegean Gold Inc.). The rest for a part was carried out at the XRAL labs in Australia and for 42 samples the measurements took place simultaneously with the major and minor elements by XRF at Hamburg University. The detection limit for gold (Au) was 5 ppb, for silver (Ag) 0.1 ppm, for Copper (Cu) and zinc (Zn) 1 ppm, for lead (Pb) 2 ppm, and for arsenic (As), antimony (Sb) 5 ppm. The total of the above mentioned samples has been shared between the two principal sectors that define western Milos, i.e., the northern and southern one, and their main descriptive statistical parameters are tabulated (Tables 17, 18).

Table 17 : Descriptive statistics of the northern sector trace elements

	Au ppm	Ag ppm	Cu ppm	Pb ppm	Zn ppm	As ppm	Sb ppm	Ba ppm	Hg ppm	Mn ppm
Cases	180	257	653	660	768	689	551	595	220	85
Mean	0,44434	45,9588	49,2291	510,23	300,219	80,7186	46,3247	2051,9	1,51545	4715,94
Std.error	4,18E-02	3,82667	5,35969	78,4951	46,9357	7,59704	4,52256	139,186	0,20791	571,392
Std.deviation	0,56136	61,3463	136,961	2016,57	1300,72	199,413	106,16	3395,11	3,08381	5267,98
Minimum	1,00E-02	1	0,4	0,4	1	0,1	0,1	35	0,4	8
Maximum	2,41	323	1714	17900	16578	1780	788	21634	24	12000
Median	0,155	19,2	14	24	50	9	6	860	0,4	1435

Table 18 : Descriptive statistics of the southern sector trace elements

	Au ppm	Ag ppm	Cu ppm	Pb ppm	Zn ppm	As ppm	Sb ppm	Ba ppm
Cases	1409	1206	182	181	181	175	182	180
Mean	1,28769	23,6322	47,3187	874,674	216,79	26,716	50,1082	11174,3
Std.error	8,00E-02	1,26769	2,68049	59,1345	39,1008	2,66473	2,67771	506,25
Std.deviation	3,00107	44,0237	36,1618	795,574	526,048	35,2511	36,1242	6792,06
Minimum	8,00E-03	0,2	8	5	8	1	1	303
Maximum	32,468	377,9	187	5449	5360	291	247	25000
Median	0,207	7,6	35	630	98	17	44,95	9650

10.5.1. The Trace elements Binary diagrams

A series of binary (Harker) diagrams representing the whole epithermal suite of trace elements (Au, Ag, Cu, Pb, Zn, As, Sb, Ba, Hg) and Mn against silver (Ag) are reported and explained in the following figures 92 and 93. The reason for which all the trace elements have been plotted against silver is that the mineralizing magmas at western Milos are enriched in silver/base metals and that silver is a widespread element in all western Milos mineralization. The following binary diagrams express the correlation of the various trace elements against silver in the various subareas. Their patterns express a multi sourcing, most probably due to successive metalliferous magmatic pulses that have taken place.

In a further attempt to better describe the subareas and their content in the epithermal suite of elements, individual statistical correlations (referred to each of the subareas), have been performed in order to emphasize their characteristics and potential.

The following diagrams expose very well the importance of silver as a main ore constituent and its relation to quasi all the elements of the epithermal suite. The displaying of the various trace elements has been based on a classification by subareas, giving so the possibility at a glance, to have an idea about the relative contents of the elements per se, as well as to be able to observe the mutual relations between those areas.

Although there are concentrations of silver more than the limit of the 400 ppm set (Midas S.A. archives), it is considered that values up to this level reflects better the real range of the values encountered around western Milos.

It is obvious, after looking at the binary diagrams that for some of the subareas there are more than one trends which reflect the different ore mineralogy and paragenesis, as well as it is obvious that for some other areas the increasing of the concentration of the individual metals was independent from the presence of silver. Nevertheless for some areas (e.g. Triades) the role of silver was determinative concerning the increasing of the metal concentrations after being “guided” by the silver.

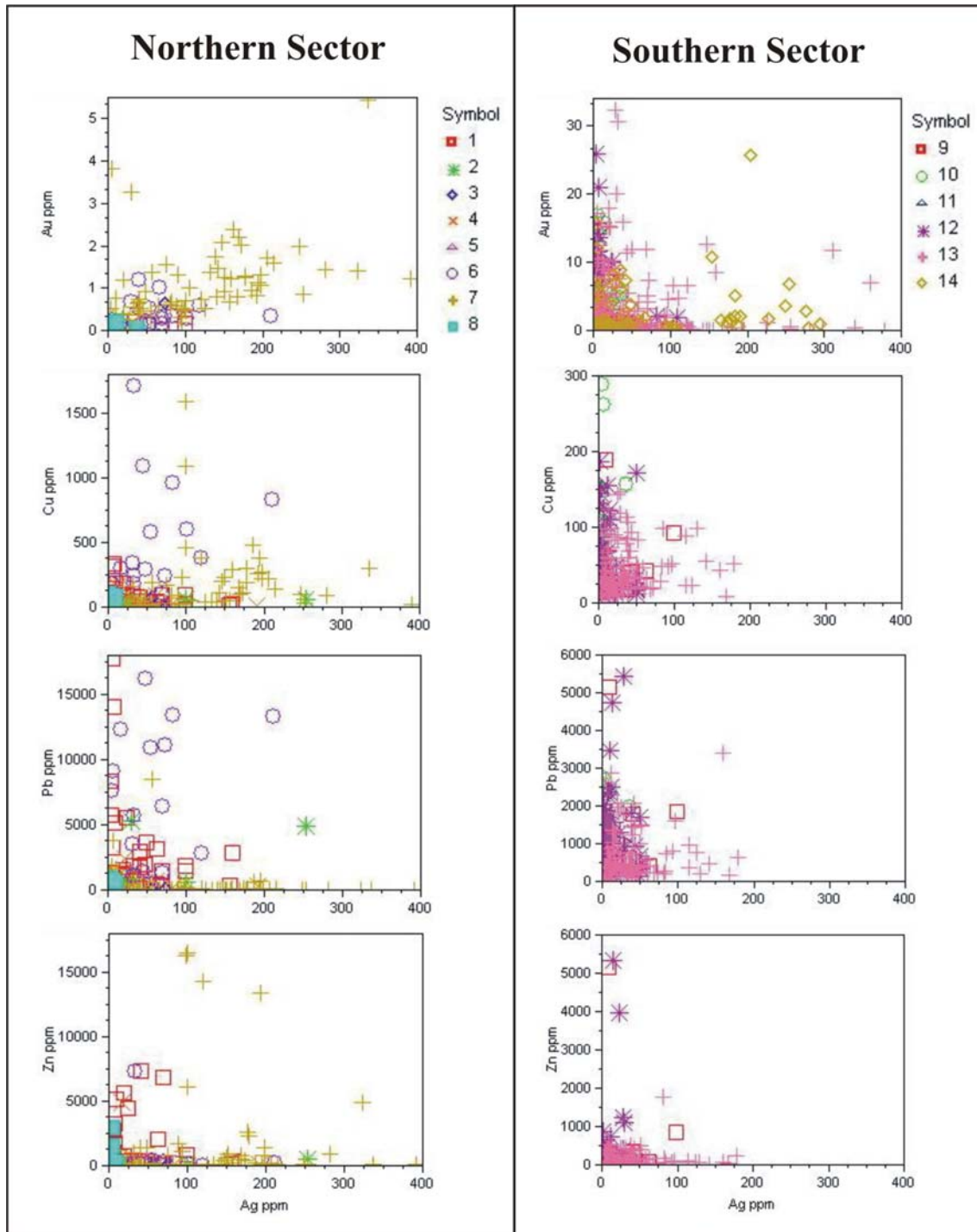


Fig. 92 : Binary diagrams of Au, Cu, Pb, Zn vs. Ag for the Northern and Southern Sectors. Symbols as: 1: Vani, 2: Katsimoutis, 3: Kondaros-Mersinia-Xerokampos, 4: Agathia-Larni, 5: Vromolimni-Akrotiri-Ampelakia, 6: Galana-Favas-Tria Vouna, 7: Triades – Ag. Nikolaos, 8: Ag. Stefanos-Ralaki-Ntasifnos-Spiritou Rema-Ammoudaraki, 9: Plakota-Ag. Panteleimon-Petrovounia, 10: Koumaria-Kirjiannoulis-Skiadi, 11: Ag. Ioannis-Voulismata, 12: Chondro Vouno-Pyrgiali-Peristeria, 13: Profitis Ilias-Livadakia-Chontri Rachi, 14: Mavrovouni-Vathi Rema.

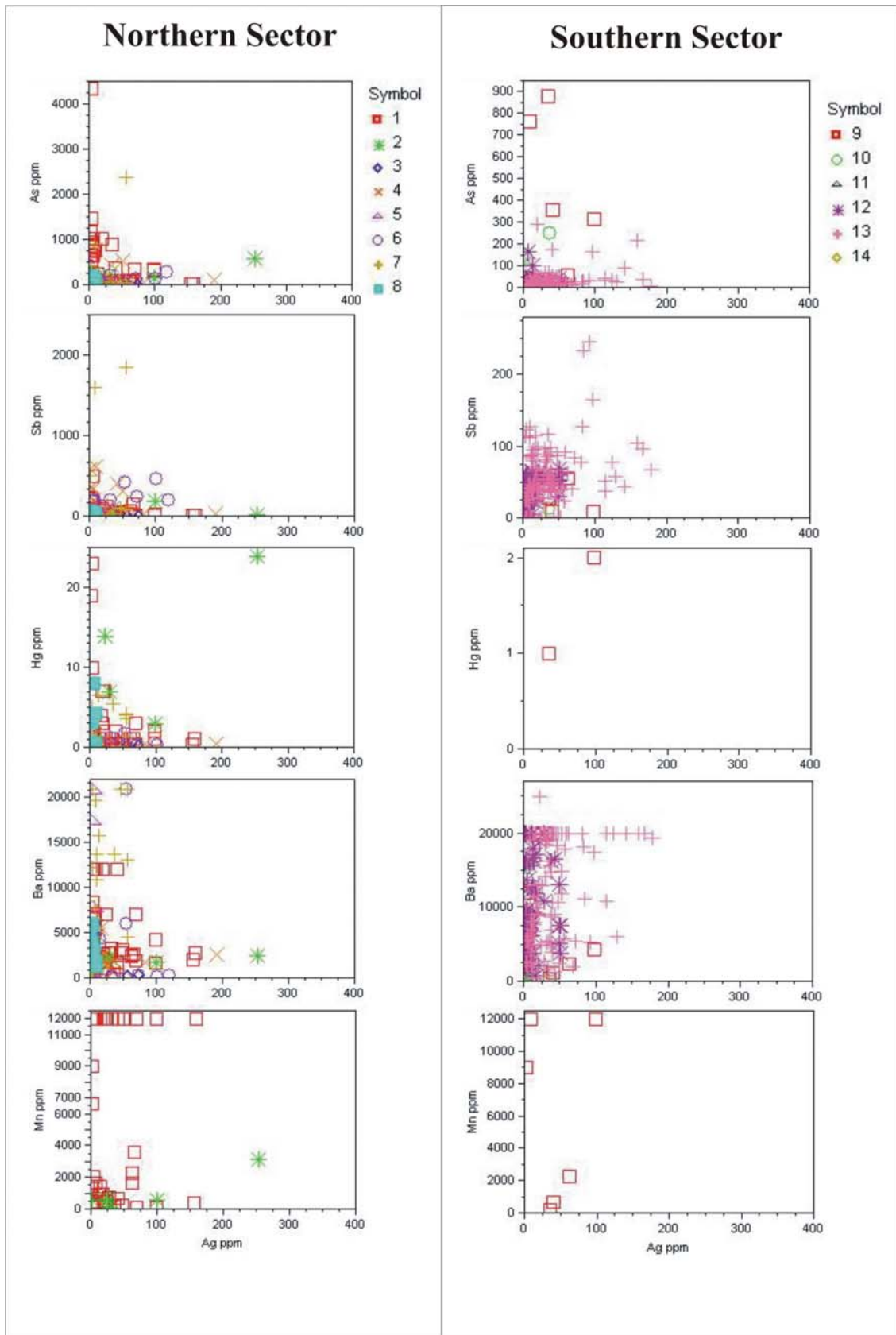


Fig. 93 : Binary diagrams of As, Sb, Hg, Ba, Mn vs. Ag for the Northern and Southern Sectors. Symbols and localities (subareas) as in fig. 92.

10.6. The distribution of the trace elements at the various western Milos subareas

Concerning the distribution of the trace elements, has been followed a description related to the various subareas of western Milos. The reason of doing that was to emphasize the link between geochemistry and mineralization. Contemporaneously it comes more obvious for anybody to follow this kind of description and relate it to the binary diagrams to the geochemical maps and to the geochemical - tectonic ones shown at the present chapter.

10.6.1. Vani subarea

At the Vani subarea it has been observed a relatively strong positive correlation (0.63) between gold and silver and a negative correlation between the last one (i.e., silver) and with all of the three zinc (-0.54), barium (-0.54) and manganese (-0.61) elements. Vice versa, zinc has a very strong positive correlation with arsenic (0.80), copper (0.79), lead (0.79) and quasi perfect with barium (0.98). This last correlates also very strongly with arsenic (0.83), lead (0.72), copper (0.72) and quasi perfectly with manganese (0.96). Copper shows a perfect correlation with lead (0.99). Arsenic shows quasi a strong correlation with mercury (0.70).

Last but not least is the quasi perfect correlation expressed by manganese with respect to zinc (0.95), arsenic (0.90) and the intermediate correlation exhibited with copper (0.57), lead (0.57) and mercury (0.58).

Although through the Pearson correlation there is not shown any correlation between silver and lead, in the Partial correlation (**see Appendix IV**) it is shown one enough strong (0.74) between them. The same tendency to be correlated these two elements, although a weak one, it is presented through both non parametric correlations, Spearman's Rho and Kendall's Tau b (**see Appendix IV**).

The principal components analysis (PCA) at the area of Vani shows that the first component (Au), accounts for the 53,94 % of the variation, while the cumulative percent shows that the first three principal components (Au,Ag,Cu) account for the 89,06 % of the variation (**see Appendix IV**).

All the parametric and no parametric correlation tests fully supports each other as well as the above mentioned results (**see Appendix IV**).

10.6.2. Katsimoutis subarea

At Katsimoutis subarea, silver shows a very strong correlation with manganese (0.93), zinc (0.90), arsenic (0.85), mercury (0.75) and copper (0.72). Its relationship with barium (0.58) and lead (0.47) can be characterized rather as intermediate to weak respectively. Zinc correlates quasi perfectly with arsenic (0.95) and very strongly with mercury (0.89), while it shows an intermediate correlation to barium (0.56) and lead (0.51). In the same manner copper shows a slight correlation with zinc (0.44), barium (0.40), antimony (0.38) and an intermediate correlation with lead (0.56) and arsenic (0.54). The same is valid between lead and mercury (0.52), arsenic (0.60). Arsenic, at its turn is strongly correlated with mercury (0.75). Interesting is the slightly negative correlation exhibited between antimony and lead (-0.42), arsenic (-0.37), mercury (-0.37). Barium is strongly correlated with mercury (0.77) and lead (0.72). Finally manganese presents a nearly perfect correlation with zinc (0.98), arsenic (0.95) and a strong one with mercury (0.80) while its relation to copper (0.51), lead (0.41) and barium can be characterized as intermediate to slight.

The principal components analysis (PCA) at the area of Katsimoutis show that the first component (Ag), accounts for the 63,62 % of the variation, while the cumulative percent shows that the first three principal components (Ag,Cu,Pb) account for the 92,57 % of the variation (see **Appendix IV**).

All the parametric and no parametric correlation tests fully supports each other as well as the above mentioned results (see **Appendix IV**).

10.6.3. Kondaros - Mersinia - Xerokampos subarea

In this subarea the emphasis is given to the perfect correlation between arsenic and antimony (0.99) and the quasi perfect one between zinc and arsenic (0.95), antimony (0.95) from one part, and copper and zinc (0.93), arsenic (0.93) and antimony (0.93) from the other. Gold is negatively correlated with zinc (-0.47), barium (-0.40), arsenic (-0.33) and antimony (-0.32). Barium shows a negative correlation with silver (-0.65) and a strong correlation with arsenic (0.72) and antimony (0.72), while exhibits an intermediate correlation with zinc (0.58).

The principal components analysis (PCA) at the area of Kondaros - Mersinia - Xerokampos shows that the first component (Au), accounts for the 58,24 % of the variation, while the cumulative percent shows that the first three principal components (Au,Cu,Pb) account for the 88,43 % of the variation (see **Appendix IV**).

All the parametric and no parametric correlation tests fully supports each other as well as the above mentioned results (see **Appendix IV**).

10.6.4. Agathia - Larni subarea

In this subarea arsenic, antimony and mercury correlate strongly to each other (correlation coefficient 0.81 for all of them). Zinc shows an intermediate correlation with copper (0.58) and barium (0.60), as does barium with antimony (0.49) and mercury (0.45). Lead is slightly correlated with copper (0.32) and negatively with barium (-0.33).

Through the Inverse correlation (see **Appendix IV**) it is observed a positive (1,07) correlation between barium and arsenic. Pairwise correlations (see **Appendix IV**) show an intermediate correlation between zinc and copper (0.58) as well as a strong one between manganese and zinc (0.92), copper (0.90). These last correlations are also confirmed by the non parametric tests, (Spearman's Rho, Kendall's Tau b correlations), (see **Appendix IV**).

The principal components analysis (PCA) at the area of Agathia – Larni shows that the first component (Ag), accounts for the 37,57 % of the variation, while the cumulative percent shows that the first three principal components (Ag,Cu,Pb) account for the 76,19 % of the variation (see **Appendix IV**).

All the parametric and no parametric correlation tests fully supports each other as well as the above mentioned results (see **Appendix IV**).

10.6.5. Vromolimni - Akrotiri - Ampelakia subarea

Two quasi perfect correlations exhibited between arsenic and antimony (0.99) and copper and silver (0.96) are the main characteristics of this subarea. From the other side copper exhibits a negative correlation with zinc (-0.81), arsenic (-0.36), antimony (-0.34), barium (-0.35) and mercury (-0.45). Negatively also correlates silver with zinc (-0.74) and mercury (-0.64), as well as barium with mercury (-0.62) and mercury with lead (-0.97). Zinc

correlates strongly with arsenic (0.82) and antimony (0.82) and slightly with barium (0.42) and mercury (0.42). Barium exhibits an intermediate correlation with lead (0.54), arsenic (0.52) and antimony (0.47). Finally lead shows an intermediate correlation with silver (0.58), and a slight correlation with copper (0.41).

The principal components analysis (PCA) at the area of Vromolimni - Akrotiri - Ampelakia shows that the first component (Ag), accounts for the 53,55 % of the variation, while the cumulative percent shows that the first three principal components (Ag,Cu,Pb) account for the 100 % of the variation (see **Appendix IV**).

All the parametric and no parametric correlation tests fully supports each other as well as the above mentioned results (see **Appendix IV**).

10.6.6. Galana - Favas - Tria Vouna subarea

Two main correlations are exhibited in this subarea. The first is the strong correlation between gold and silver (0.84), and the second the strong correlation between copper and antimony (0.91), lead (0.78) and zinc (0.72), and of course between themselves (i.e., lead-antimony (0.84), zinc-antimony (0.74)). Gold is moderately correlated with arsenic (0.52) and negatively correlated with mercury (-0.57). Silver, is moderately to strongly correlated with arsenic (0.64).

A correlation between antimony and arsenic is also evident through the non parametric Kendall's Tau b correlation (0.53)- (see **Appendix IV**).

The principal components analysis (PCA) at the area of Galana – Favas - Tria Vouna shows that the first component (Au), accounts for the 40,09 % of the variation, while the cumulative percent shows that the first three principal components (Au,Ag,Cu) account for the 83,97 % of the variation (see **Appendix IV**).

All the parametric and no parametric correlation tests fully supports each other as well as the above mentioned results (see **Appendix IV**).

10.6.7. Triades - Agios Nikolaos subarea

The strong correlation between arsenic and antimony (0.83) is the main characteristic of the subarea, while silver also exhibits a positive correlation with barium (0.63) and mercury (0.63). The correlation between gold and silver is rather slight (0.34), as it is that one with mercury (0.32), while with barium (0.47) it reaches an intermediate correlation. Copper shows an intermediate correlation with zinc (0.50) and less than that with antimony (0.45) and arsenic (0.37). Finally mercury shows an intermediate correlation with zinc (0.52) and barium (0.54).

The principal components analysis (PCA) at the area of Triades - Agios Nikolaos shows that the first component (Au), accounts for the 30 % of the variation, while the cumulative percent shows that the first three principal components (Au,Ag,Cu) account for the 73,63 % of the variation (see **Appendix IV**).

All the parametric and no parametric correlation tests fully supports each other as well as the above mentioned results (see **Appendix IV**).

10.6.8. Agios Stefanos - Ralaki - Ntasifnos - Spiritou Rema - Ammoudaraki subarea

This subarea essentially is the area across the Ammoudaraki – Plakota fault, which is the limit between northern and southern sector of western Milos, subdividing it not only

geographically but also mineralogically. The main characteristic of the area is the quasi perfect correlation between gold and mercury (0.98) as well as the strong positive correlations between copper - antimony (0.83), zinc - antimony (0.81) and the negative ones between barium - silver (-0.84) and barium - gold (-0.53). Gold is also positive correlated with silver (0.61) and slightly with copper (0.45) and antimony (0.43), while exhibits a negative correlation with barium (-0.53). Copper exhibits a slight to moderate correlation with mercury (0.33), lead (0.40) and zinc (0.53). Lead is correlated strongly with barium (0.78) and negatively with gold (-0.41), silver (-0.49) and mercury (-0.53). It exhibits also a slight to moderate correlation with arsenic (0.44) and zinc (0.56). Arsenic is moderately to strongly correlated with copper (0.60), zinc (0.61), antimony (0.62) and slightly to lead (0.44).

The principal components analysis (PCA) at the area of Agios Stefanos - Ralaki - Ntasifnos - Spiritou Rema - Ammoudaraki shows that the first component (Au), accounts for the 43,25 % of the variation, while the cumulative percent shows that the first three principal components (Au,Ag,Cu) account for the 89,26 % of the variation (see **Appendix IV**).

All the parametric and no parametric correlation tests fully supports each other as well as the above mentioned results (see **Appendix IV**).

10.6.9. Plakota - Agios Panteleimon - Petrovounia subarea

In this area there is a quasi perfect correlation and thus interrelation between copper-lead-zinc-barium, (copper-lead: 0.96; copper-zinc: 0.93; lead-zinc: 0.94; barium-copper: 0.96; barium-lead: 0.92; barium-zinc: 0.97). Arsenic shows an intermediate to slight correlation with lead (0.52), zinc (0.48) and copper (0.41).

The principal components analysis (PCA) at the area of Plakota - Agios Panteleimon - Petrovounia shows that the first component (Ag), accounts for the 59,93 % of the variation, while the cumulative percent shows that the first three principal components (Ag,Cu,Pb) account for the 92,75 % of the variation (see **Appendix IV**).

All the parametric and no parametric correlation tests fully supports each other as well as the above mentioned results (see **Appendix IV**).

10.6.10. Koumaria - Kirjiannoulis - Skiadi subarea

A strong positive correlation is exhibited in this subarea between silver and arsenic (0.80). Antimony shows a moderate correlation with lead (0.58) and barium (0.57), while copper is slightly correlated with arsenic (0.35) and antimony (0.38).

The Spearman's Rho correlation shows an intermediate correlation between lead and gold (0.55).

The principal components analysis (PCA) at the area of Koumaria - Kirjiannoulis - Skiadi shows that the first component (Au), accounts for the 38,51 % of the variation, while the cumulative percent shows that the first three principal components (Au,Ag,Cu) account for the 69,58 % of the variation (see **Appendix IV**).

All the parametric and no parametric correlation tests fully supports each other as well as the above mentioned results (see **Appendix IV**).

10.6.11. Ag. Ioannis - Voulismata subarea

The available data show no correlations in this subarea (the gold - silver correlation is 0.07).

10.6.12. Chondro Vouno - Pyrgiali - Peristeria subarea

Slight generally correlations are exhibited between silver - antimony (0.49), copper - zinc (0.43) and antimony - barium (0.39).

The principal components analysis (PCA) at the area of Chondro Vouno - Pyrgiali - Peristeria shows that the first component (Au), accounts for the 24,39 % of the variation, while the cumulative percent shows that the first three principal components (Au,Ag,Cu) account for the 58,10 % of the variation (**see Appendix IV**).

All the parametric and no parametric correlation tests fully supports each other as well as the above mentioned results (**see Appendix IV**).

10.6.13. Profitis Ilias - Livadakia - Chondri Rachi subarea

A slight correlation is exhibited here between copper - lead (0.45) and silver - antimony (0.31).

The Spearman's Rho non parametric correlation shows a positive correlation between zinc and copper, lead (0.50, 0.53 respectively), as well as between lead and gold (0.47), (**see Appendix IV**).

The principal components analysis (PCA) at the area of Profitis Ilias - Livadakia - Chondri Rachi shows that the first component (Au), accounts for the 22,67 % of the variation, while the cumulative percent shows that the first three principal components (Au,Ag,Cu) account for the 57,16 % of the variation (**see Appendix IV**).

All the parametric and no parametric correlation tests fully supports each other as well as the above mentioned results (**see Appendix IV**).

10.6.14. Mavrovouni - Vathi Rema subarea

A very slight correlation between gold and silver (0.25) it is shown in this subarea.

The principal components analysis (PCA) at the area of Profitis Ilias - Livadakia - Chondri Rachi shows that the first component (Au), accounts for the 62,57 % of the variation, while the cumulative percent shows that the first two principal components (Au,Ag) account for the 100 % of the variation (**see Appendix IV**).

10.7. The geochemical distribution of the trace elements in the various subareas and their relation to the tectonics

A series of geochemical maps in this paragraph show the distribution of the epithermal suite of trace elements (Au, Ag, Cu, Pb, Zn, As, Sb, Ba, Hg) at western Milos, as well as their relation to the main tectonic features of the area.

As a whole it is considered that the patterns of the trace elements displayed below, are the reflection of the various tectonic trends that “dominated” from period to period resulting to the various mineralization styles in western Milos.

There are many compatibilities between trace element patterns and tectonic lineaments, as well as a relationship between trace element patterns and ore mineralogy.

10.7.1. The Au pattern

As it is well visible from the figure 94, Au anomalies at the southern sector show a series of parallel running and NE trending patterns, which essentially correspond to the auriferous quartz-chalcedony-base metals-Au-Ag veins at that district. From the other side, at the northern sector the anomalies are well “closed” and are related to the multi breccia pipes and flow breccias occurring in the area.

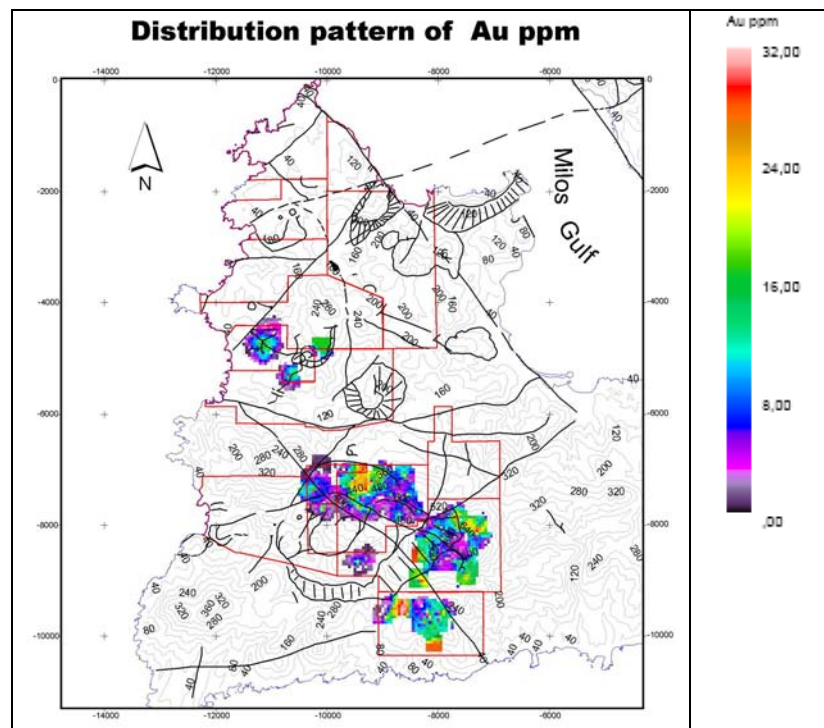


Fig. 94 : Distribution pattern of gold at western Milos.

Although the observations related to the NE trend is coming mainly from field data, it is also important to say that there is at least one more trend which is “visible” through the map configurations, and this is the NW one, which is considered to correspond to an overprinting of a later auriferous tectonic event to the previous NE one. Indeed, as it is observed from the figures 94 and 95, all the anomalies are somehow disposed in a semicircular/arcuate manner around a postulated volcanic edifice, subjected to a partial

calderic collapse or subsidence, attributed to a combination of volcanological and tectonic elaborations. In more, it is well visible from the figures 94 and 95 that this “circular continuity” is “interrupted” by the Ammoudaraki - Mavrovouni lineament, which runs along NW – SE directions and seems post dating the NE – SW trending mineralized vein structures.

As a general observation, it comes also clear, except the fact that the gold anomalies are very localized, the content in gold which is strongly different between the northern and southern sectors as well as the fact that along E – W trends no gold anomalies have been observed.

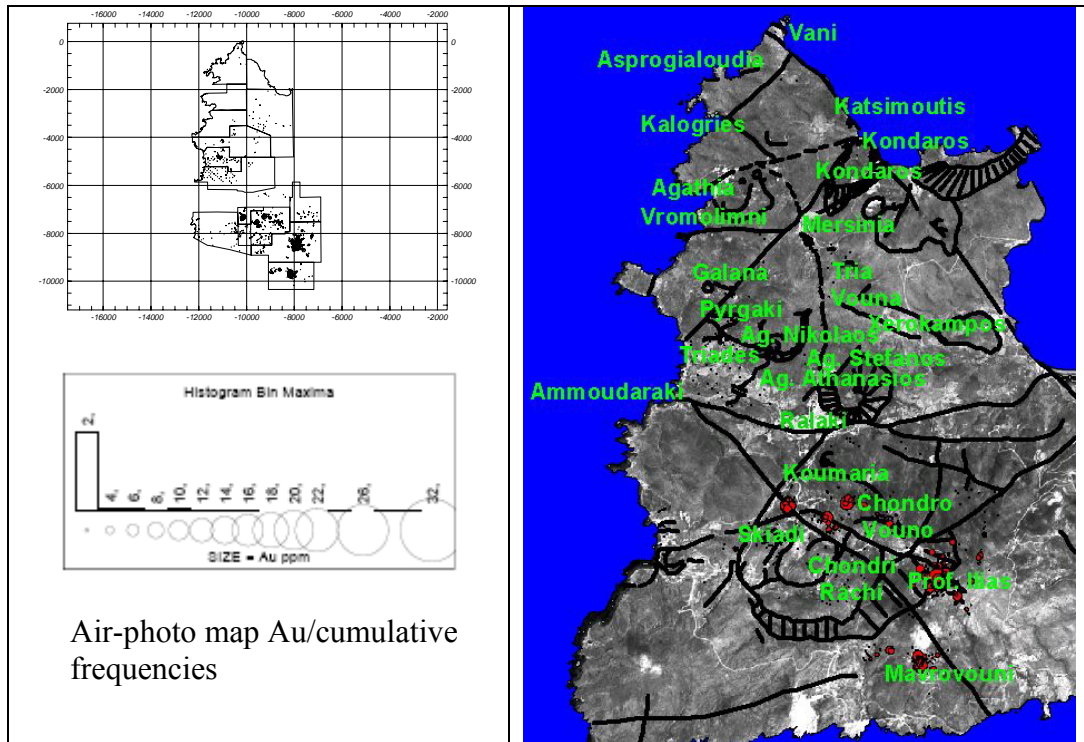


Fig. 95 : Cumulative distribution of gold related to the regional tectonics at western Milos.

10.7.2. The Ag pattern

The silver geochemical pattern (fig.96) is very widespread on both sectors (northern and southern) and especially at the areas of Triades - Pyrgaki and at the northernmost Katsimoutis - Vani subareas.

Concerning the dominant trend directions of the Ag anomalies it seems that here also there is an overprinting of both the NE and NW striking directions with a predominance of the last one (fig. 97).

At Triades – Galana (northern sector) the anomaly is much wider with respect to that of the Au previously seen. Here also it seems that some, probably more localized trends, “influenced” the final configuration of the element’s pattern. These localized trends are considered to be the N-S and the E-W ones.

Definitely a more similar pattern for both silver and gold, it seems to be valid at the southern sector where a strong relation to the volcanic edifice configuration, is assumed.

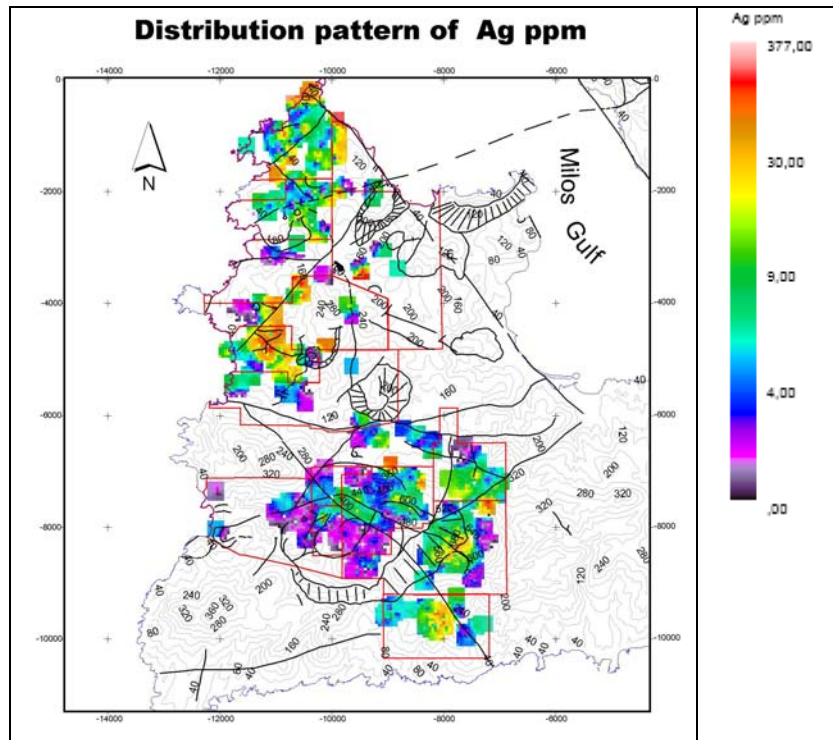


Fig. 96 : Distribution pattern of silver at western Milos.

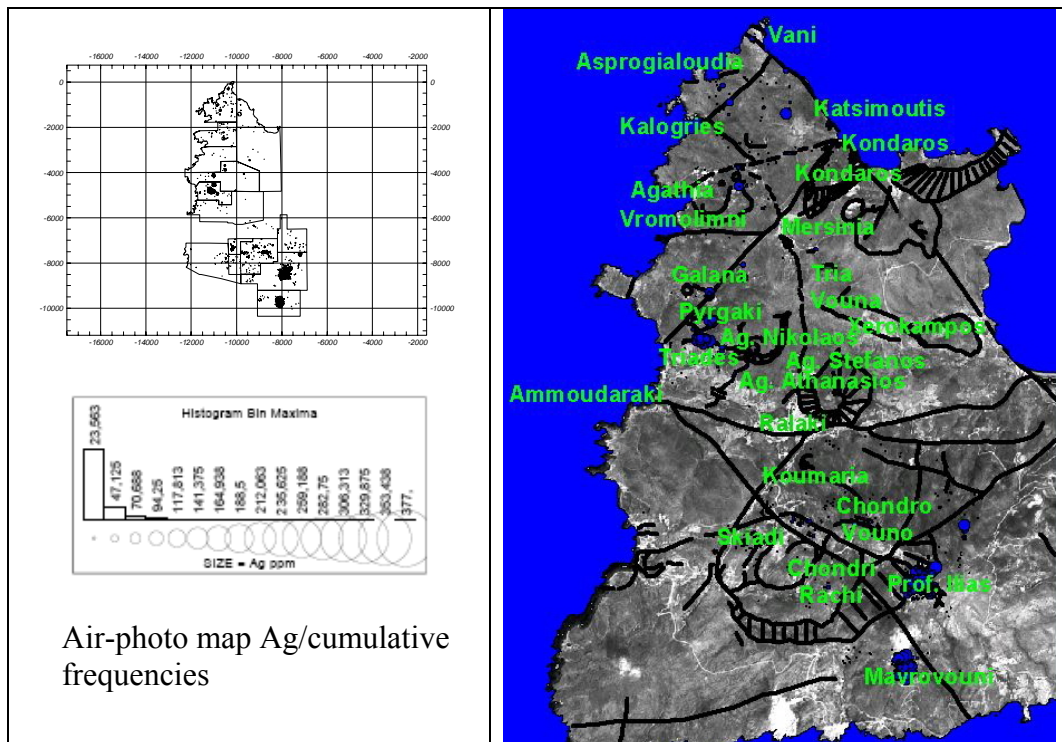


Fig. 97 : Cumulative distribution of silver related to the regional tectonics at western Milos.

10.7.3. The Cu pattern

The Copper trend is much more “isolated” and well outlined at the southern sector, with

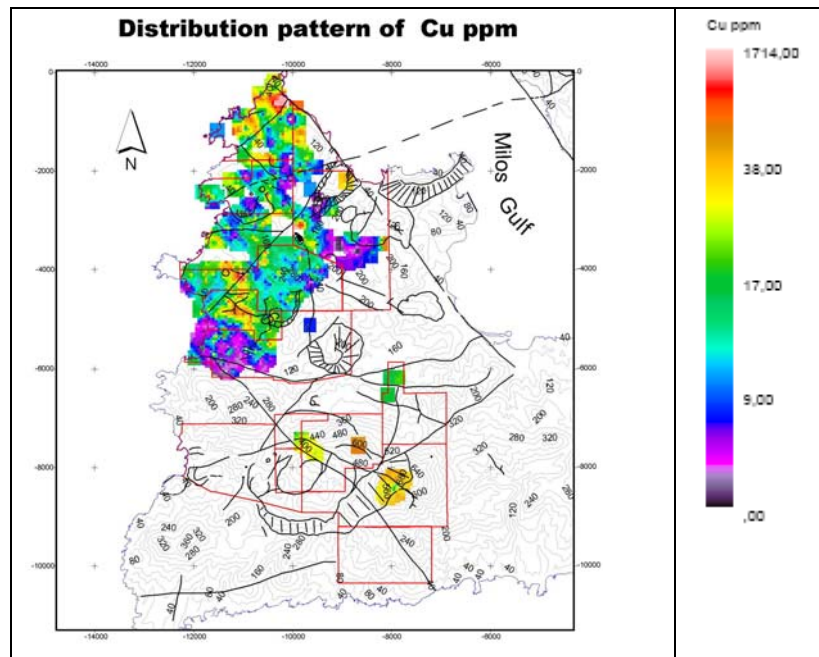


Fig. 98 : Distribution pattern of copper at western Milos.

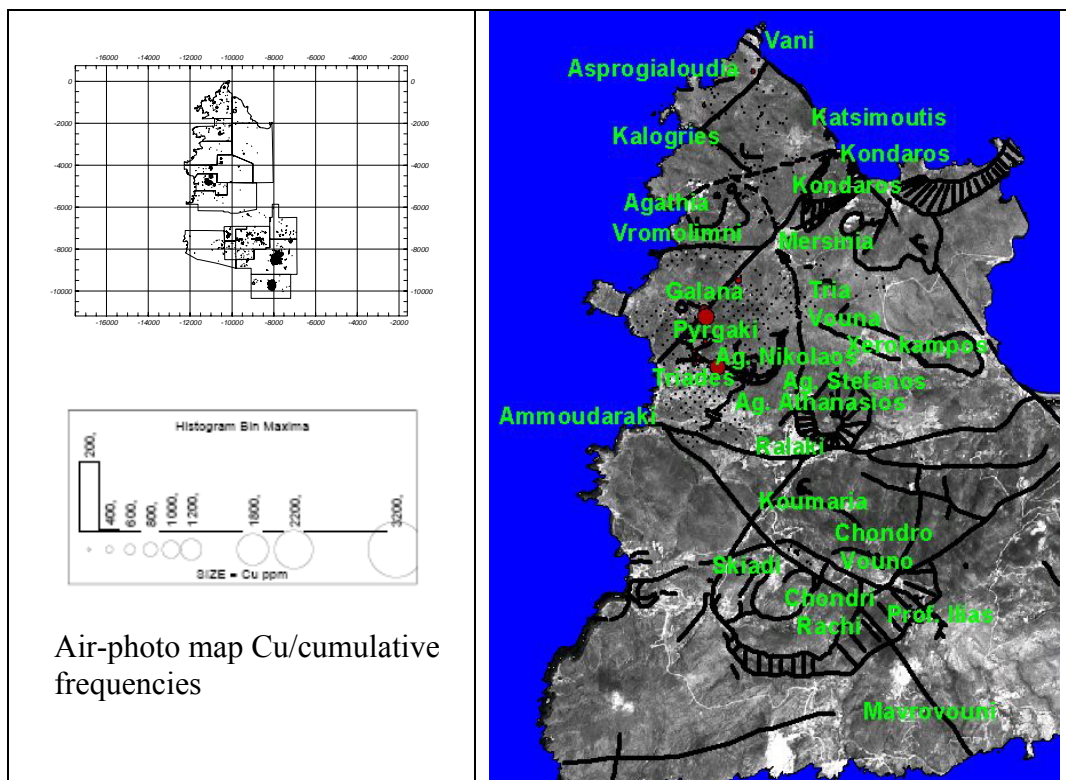


Fig. 99 : Cumulative distribution of copper related to the regional tectonics at western Milos.

respect to the Au and Ag anomalies previously seen. The areas that host this anomaly are Chondro Vouno and Profitis Ilias (fig. 98,99). At the northern sector, and especially for the areas of Triades, Galana and Favas it seems that the copper anomalies are rather localized along a NE-SW tectonic lineament. For the area of Vani, also located at the northern sector, it seems that the copper anomaly is a consequence of a quasi vertical crossing of the main two lineaments that characterize Milos island, i.e., the NE-SW and the NW-SE ones (fig. 99).

10.7.4. The Pb pattern

The pattern of lead is very well outlined at the broad area of Vani, along a NE- SW direction (Asprogioloudia-main Vani areas) as well as in the southern sector along a NW-SE direction (Profitis Ilias, Chondro Vouno, Koumaria). In the area of Galana-Favas-Mersinia it seems that there is another clear pattern for the lead along the well established NE- SW Triades-Katsimoutis lineament. At the northern sector, the lead anomaly towards Katsimoutis area it is rather open (fig. 100), while that of Agathia rather closed and related to a localized volcanic structure (fig. 100,101). As a whole, it is well visible that the bulk of the anomalies are related to the Triades-Katsimoutis lineament and to the Kalogries-Vani one, i.e. two NE parallel running lineaments along the margins of a paleo-horst area (fig. 101).

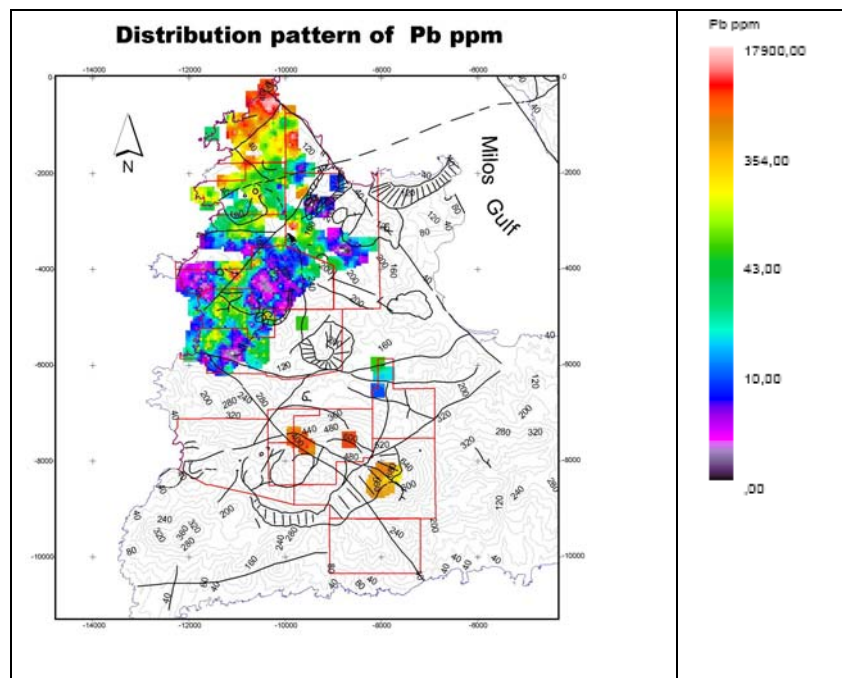


Fig. 100 : Distribution pattern of lead at western Milos.

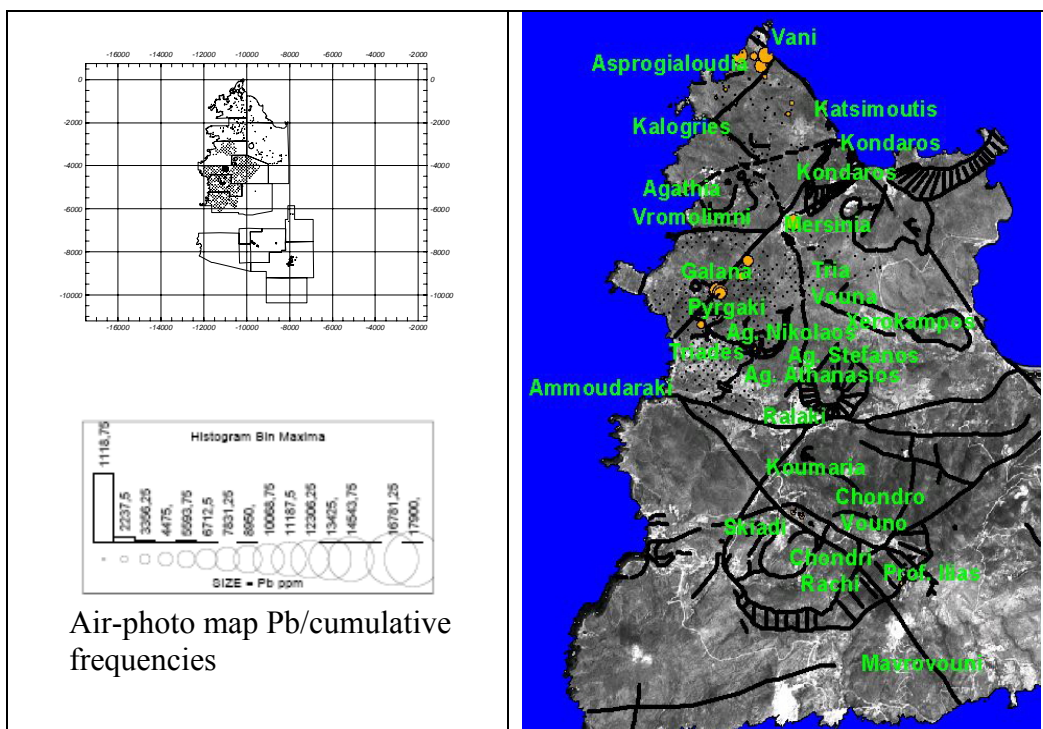


Fig. 101 : Cumulative distribution of lead related to the regional tectonics at western Milos.

10.7.5. The Zn pattern

The Zn anomaly is very pronounced at Vani and at Agathia subareas (northern sector), as well as at Triades-Galana subareas (fig. 102), where it seems to delineate a big circular fea-

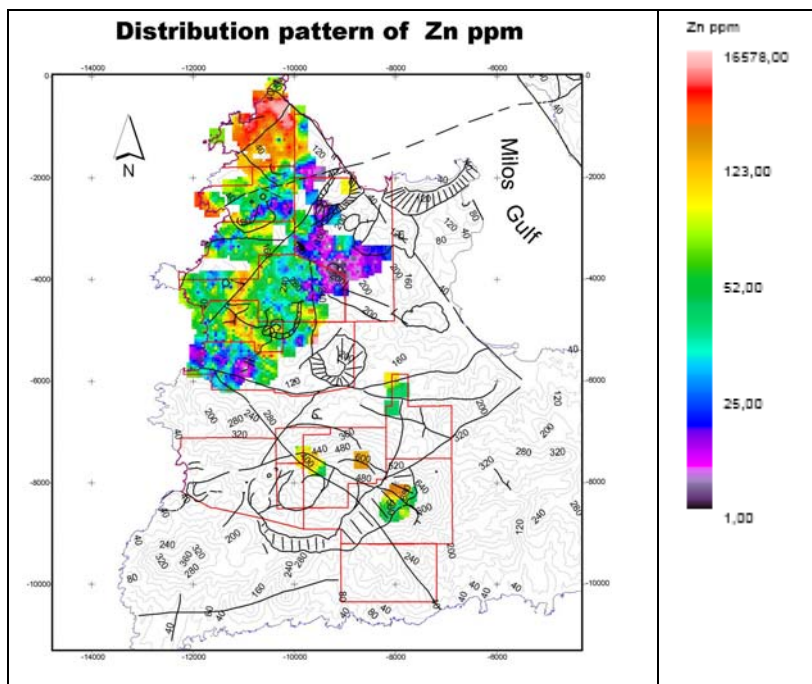


Fig.102 : Distribution pattern of zinc at western Milos.

ture which extends in an arcuate form, from the area of Ntasifnos up to the area of Favas, and seems also to occlude smaller circular features (minor volcanic structures). It could be related to a caldera or an important crossing of tectonic lineaments at this sector, either to a major multi-vent feature (fig. 103). At Profitis Ilias and Chondro Vouno subareas, the zinc anomaly is less pronounced, both as grades and extension.

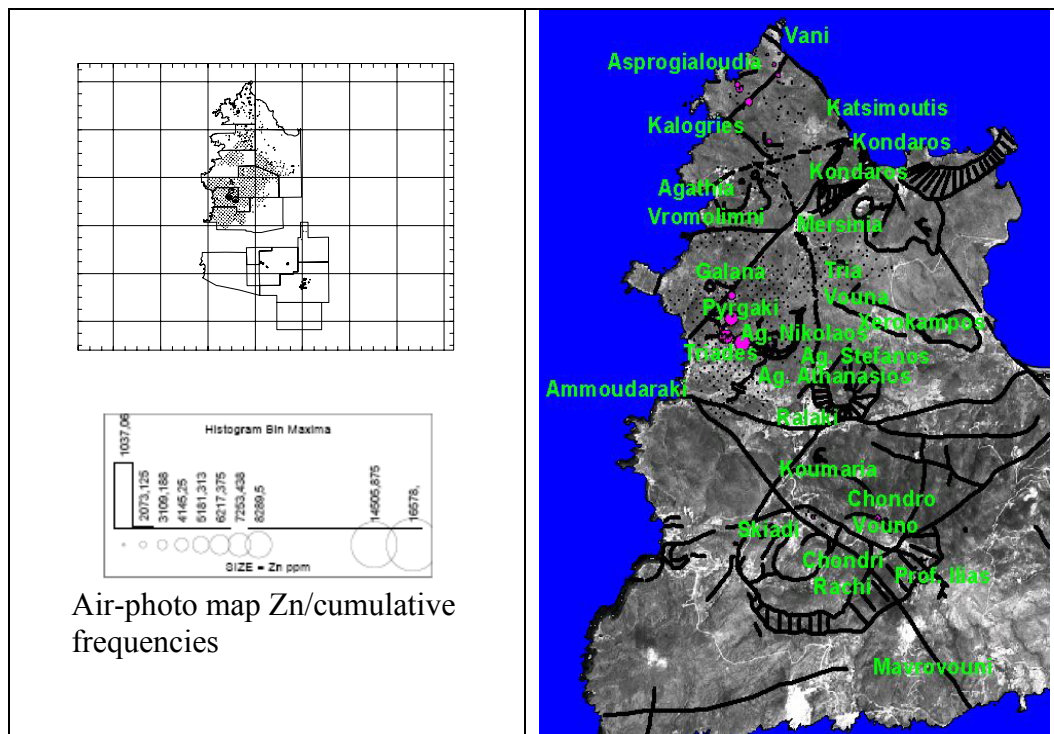


Fig. 103 : Cumulative distribution of zinc related to the regional tectonics at western Milos

10.7.6. The As pattern

The arsenic pattern shows very high values (more than 0.4%) at the areas of Vani, Kondaros, Mersinia and Xerokampos, as well as at the areas of Galana, Triades and Ntasifnos (fig. 104). For this element it seems to be in front of two enough well visible mineralizing trends, the NE-SW and the N-S ones. It also seems that the central part of the major NE-SW Triades-Katsimoutis lineament lacks of any arsenic anomaly, due to the presence of unaltered post mineralization volcanic products (fig. 105), which cover the below occurring mineralized ones.

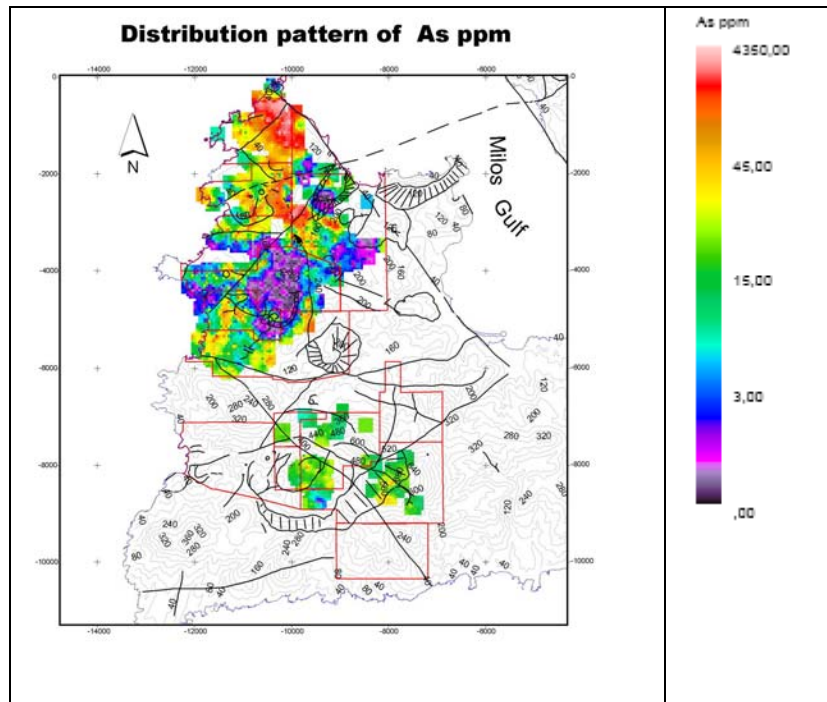


Fig.104 : Distribution pattern of arsenic at western Milos.

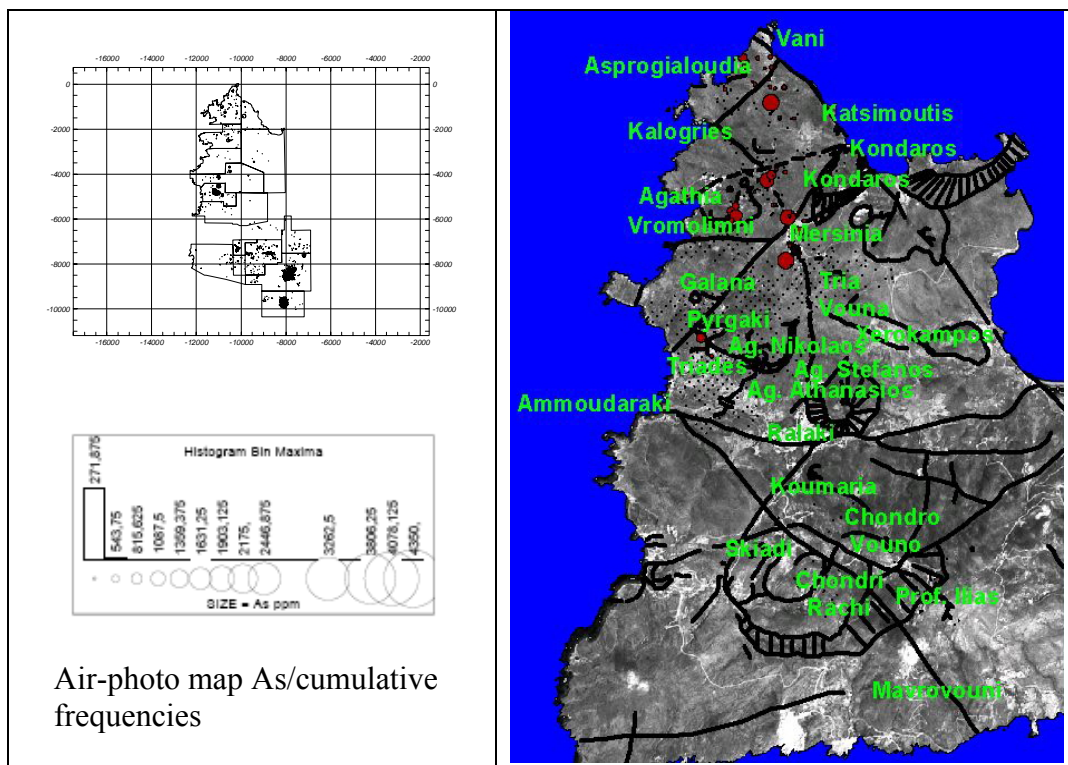


Fig. 105 : Cumulative distribution of arsenic related to the regional tectonics at western Milos

10.7.7. The Sb pattern

The antimony pattern has a configuration (fig. 106) as that of “filling” a gap space, at the

northern sector, getting wider toward Mersinia-Larni-Vani subareas. Most probably it depicts a crossing of two different tectonic trends, the NE – SW and the N – S. At Triades – Galana it seems that the anomaly has a circular distribution (fig. 106) around a main multi-vent area, analog to that for arsenic. The Larni subarea shows also a remarkable anomaly, which seems to be related to a NE-SW trending lineament (Agathia-Kondaros

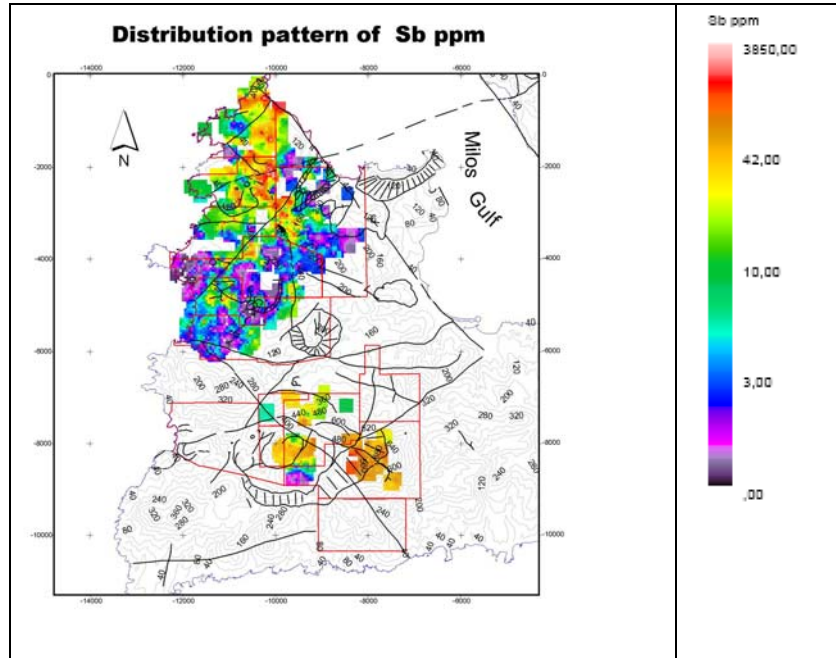


Fig.106 : Distribution pattern of antimony at western Milos

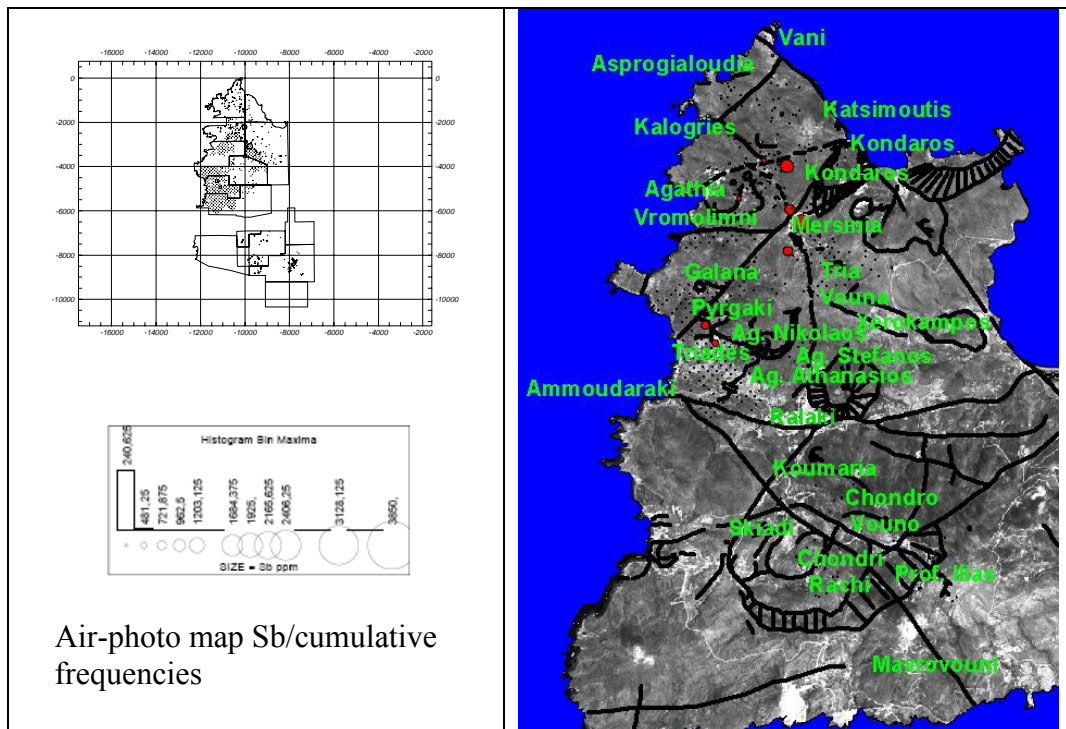


Fig. 107 : Cumulative distribution of antimony related to the regional tectonics at W. Milos.

lineament) which meets a NNW trending fault line coming from Mersinia area. At Profitis Ilias the dominant trend is the NE-SW, but here also it seems that a most probably secondary (fig. 107) trend along N-S direction played also some role in configuring the antimony anomaly. Finally in the area of Koumaria a different trend seems to prevail, and this is the NNW-SSE one.

10.7.8. The Ba pattern

For the southern sector barium shows a clear NW - SE pattern, while for the northern sector it is more specifically concentrated (fig. 108) around Pyrgaki-Triades-Agios Nikolaos, along an E-W trending lineament at Vromolimni (Vromolimni-Mersinia lineament) and at Larni, where the Mersinia-Kalogries fault line intersects the Agathia-Kondaros one. At Asprogi Loudia - Vani areas the exhibited anomaly is related to NE trending faults/lineaments structures (e.g. Kalogries - Vani lineament, white smoker area at Asprogi Loudia)-(fig. 109).

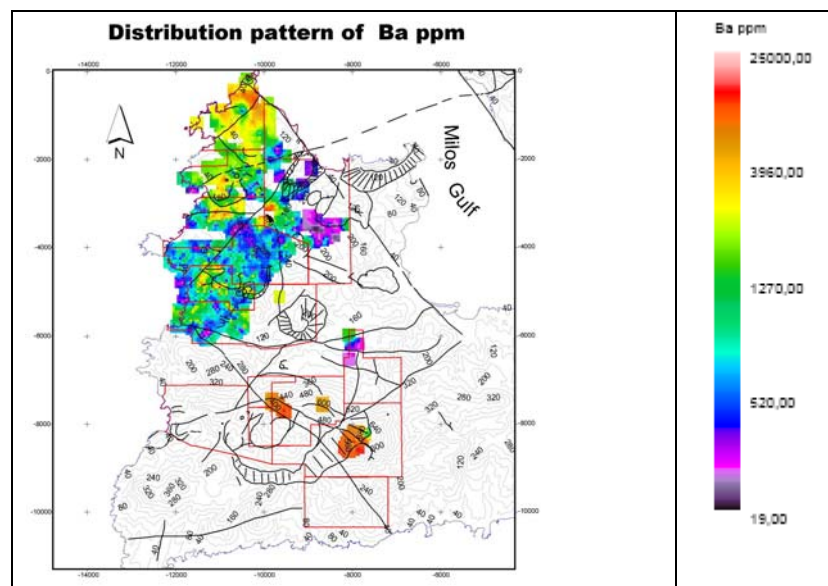


Fig.108 : Distribution pattern of barium at western Milos.

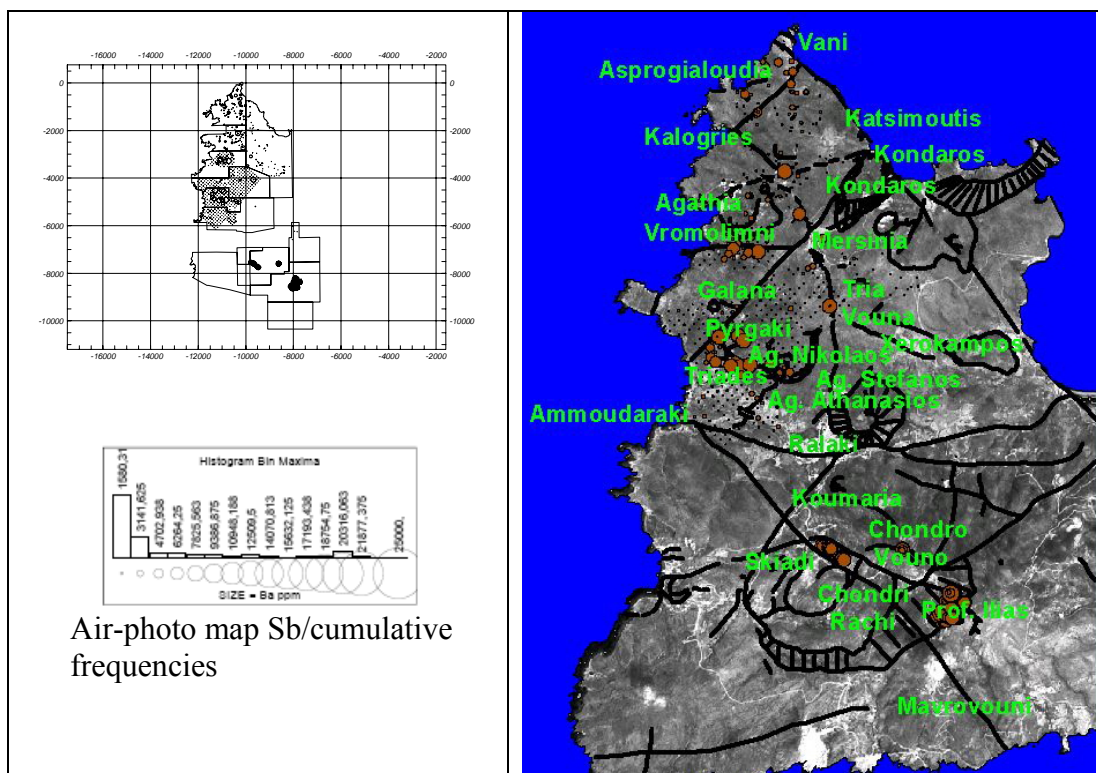


Fig. 109 : Cumulative distribution of barium related to the regional tectonics at western Milos.

10.7.9. The Hg pattern

Concerning mercury, it seems that it displays very well outlined anomalies (fig. 110) related at important fault patterns, i.e., along N-S directions in the areas of Larni-Vani and along E-W directions at Vromolimni area. Another crosssection of tectonic trends, this time

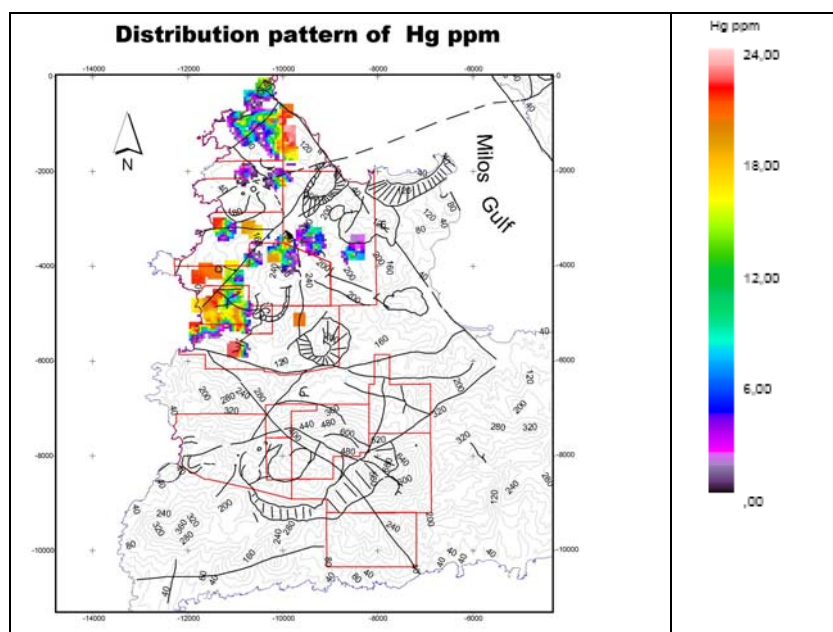


Fig.110 : Distribution pattern of mercury at western Milos.

along NE-SW and N-S directions are those which determine the anomalous pattern of mercury at Triades - Galana (fig. 111).

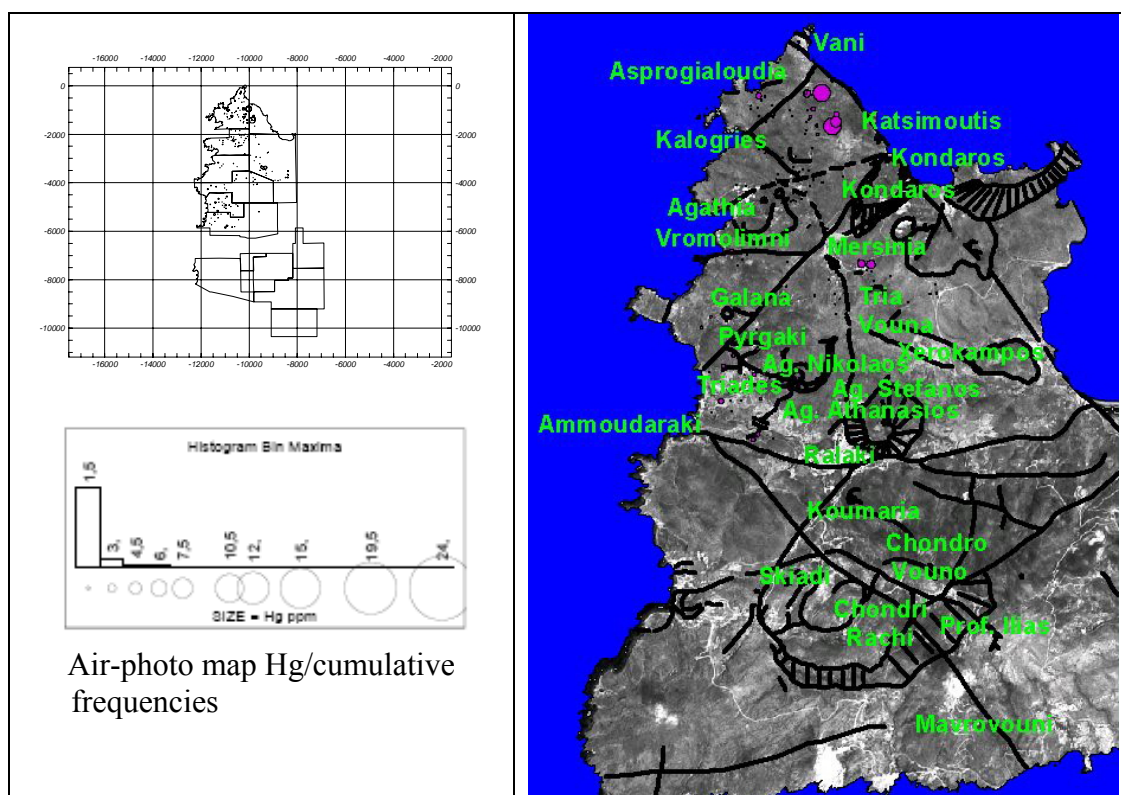


Fig. 111 : Cumulative distribution of mercury related to the regional tectonics at western Milos.

10.7.10 The Mn pattern

The anomalous patterns shown are referred essentially to the areas of Vani-Larni-Asprogioudia where the former manganese mine operated since the end of eighteenth century. The anomaly is very well localized at this part of northern sector area and in part, as it is well visible at the fig. 112, it is related to the white smoker vent area, located along a NE-SW trend, and for another part to a NW-SE anomaly related to the main lineament delimiting the western margin of Milos gulf (graben) structure (fig. 113).

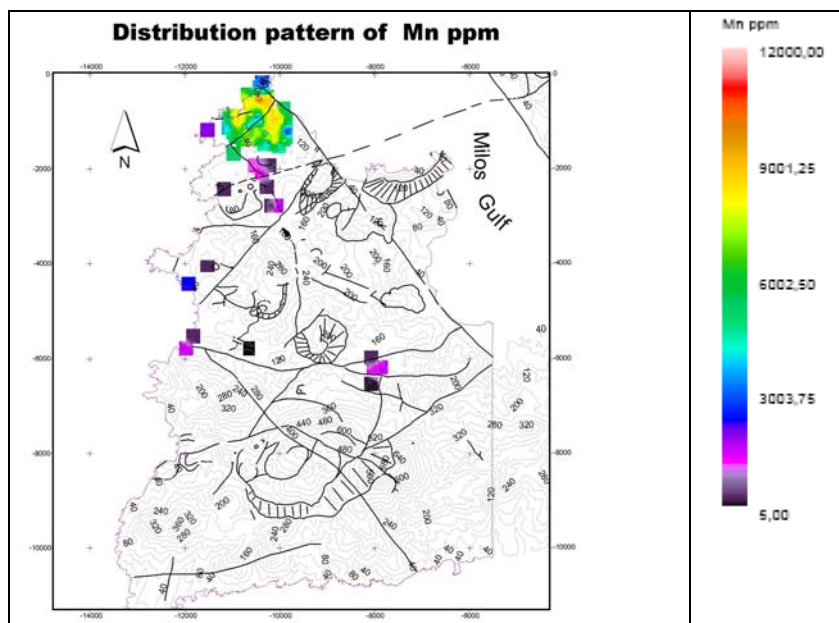


Fig.112 : Distribution pattern of manganese at western Milos.

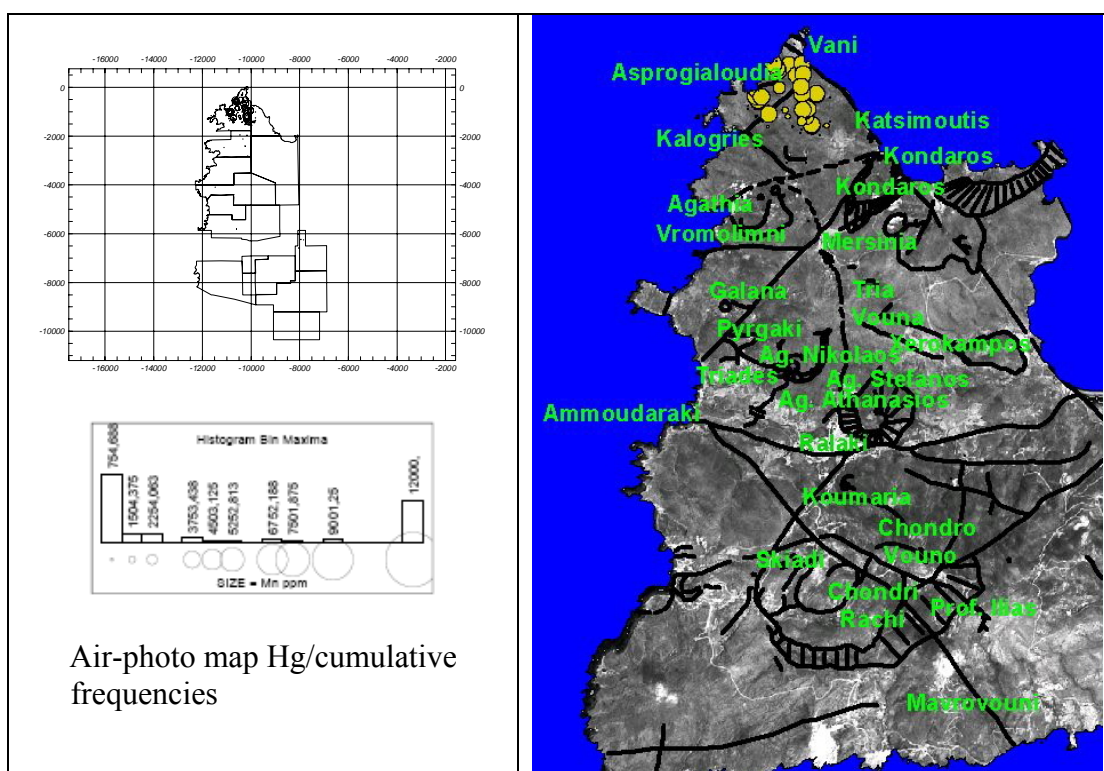


Fig. 113 : Cumulative distribution of manganese related to the regional tectonics at W. Milos.

10.8. The interrelationships between the trace and the minor elements

Through a series of airphoto images on which are reported the main tectonic features of western Milos, as well as minor and trace element anomalies (coloured cumulative frequencies circles), it was possible to show and demonstrate some relationships between

the various trace and minor elements at western Milos. As it is well seen at figure 114, demonstrating the relationships between gold (Au), silver (Ag) and copper (Cu), it is possible to see that silver is very strongly correlated with the copper on both southern and northern sectors of western Milos. This relationship suggests a magmatic contribution of silver in the mineralization most probably related to the existence of a porphyry Cu mineralization underneath. In the same way, i.e., as related to a buried porphyry style mineralization, could be interpreted the composite distributions shown in figure 116, where bismuth-molybdenum-copper-tungsten (Bi-Mo-Cu-W) are inferred to be related to a buried porphyry mineralization at depth. On the other hand the arsenic-antimony-mercury-gallium-lanthanum (As-Sb-Hg-Ga-La) anomalies shown in figure 115 could express overlapping of an epithermal style mineralization on the previous, above mentioned one.

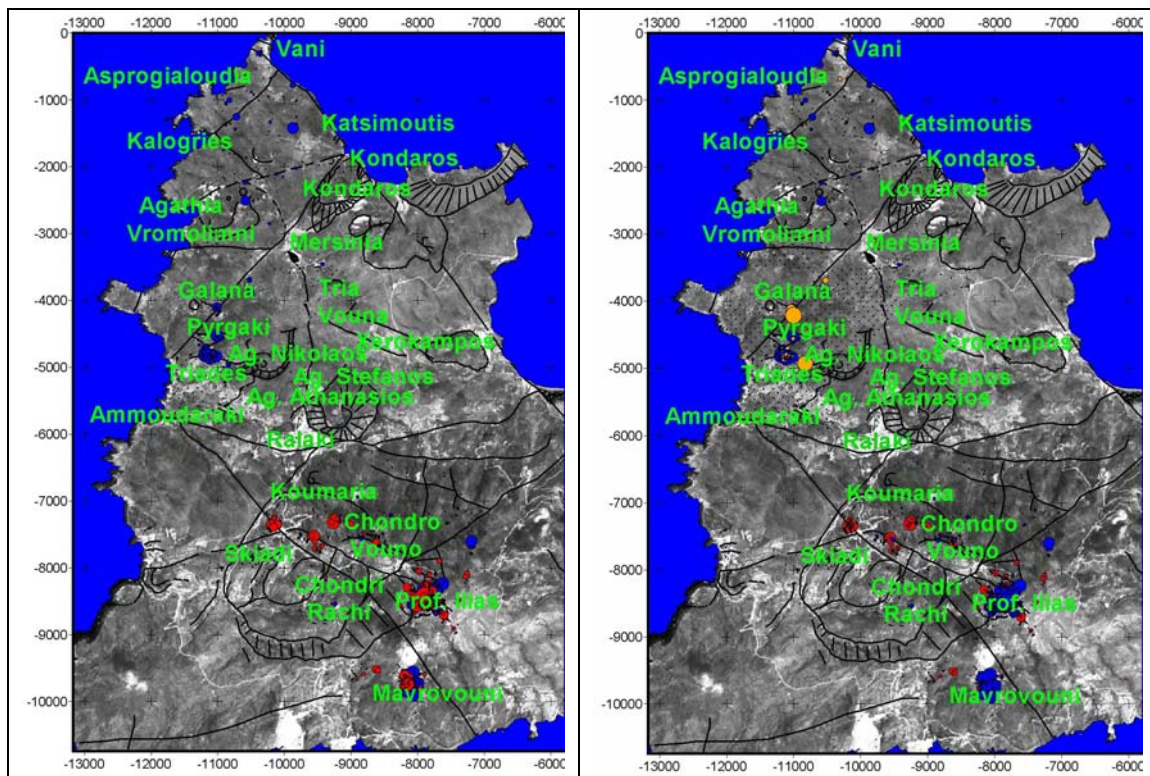


Fig. 114 : Composite distribution of Au (red circles)-Ag (blue circles) [Left], Au (red circles)-Ag (blue circles)-Cu (orange circles) [Right] at western Milos.

Through these maps comes obvious that on western Milos the relationships between the trace and minor elements it was a function, from one side of the tectonic causes that opened the ways to the incoming magmas/fluids, and from the other side of the well established structures (volcanic edifices and hot-spring lakes), which hosted and reproduced, through mutual interactions, the right physico-chemical environments for ore deposition. The strong “guidance” of the metallics by the tectonic lineaments is ubiquitous, as is ubiquitous the fact that the geochemical anomalies delineate structures which some times are not any more visible either on the ground or through using airborne imagery.

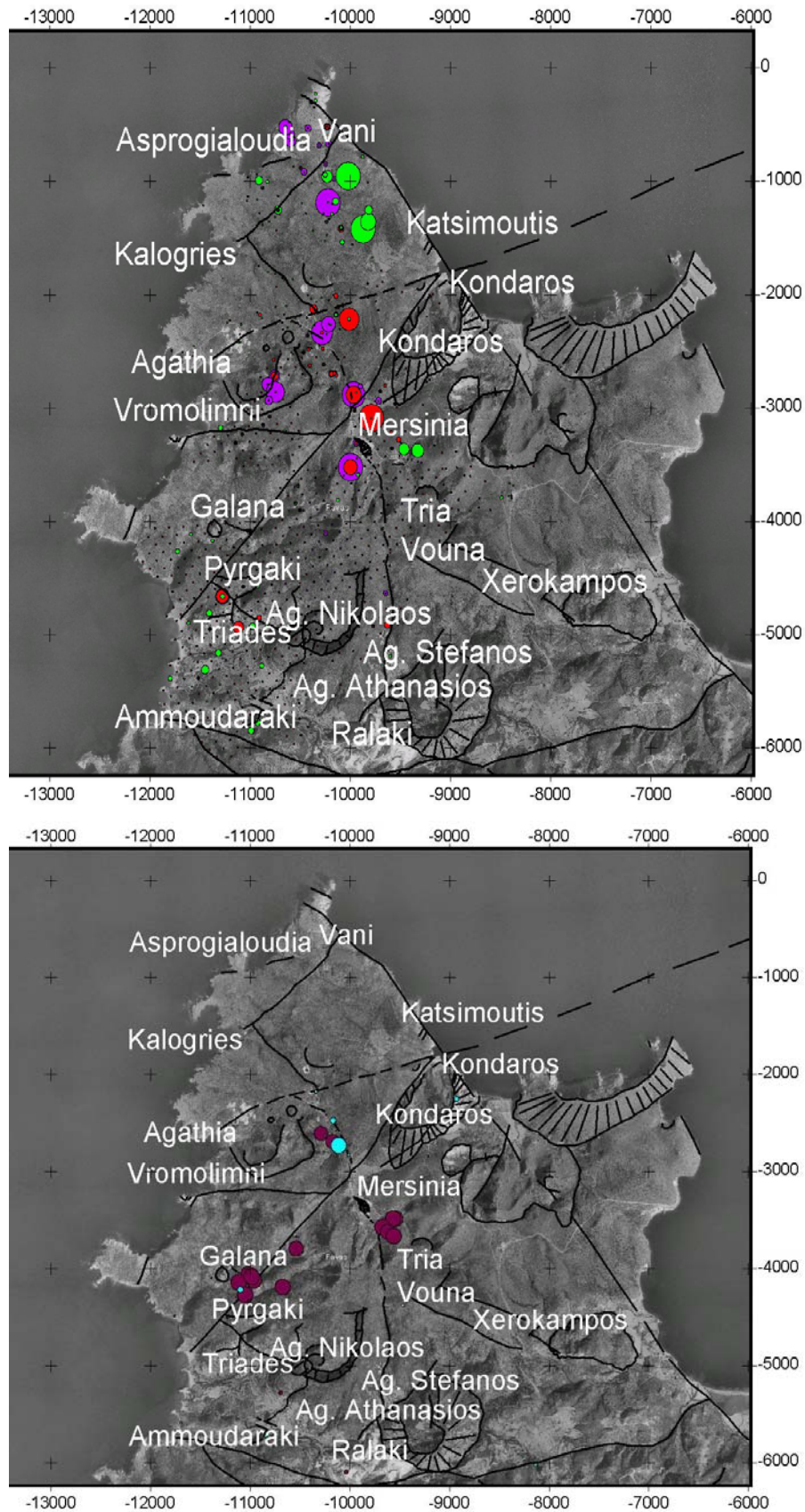


Fig. 115 : Composite distribution of As (lilac circles), Sb (red circles), Hg (green circles)[above] and Ga (magenta circles), La (cyan circles) [below], at the northern sector of western Milos.

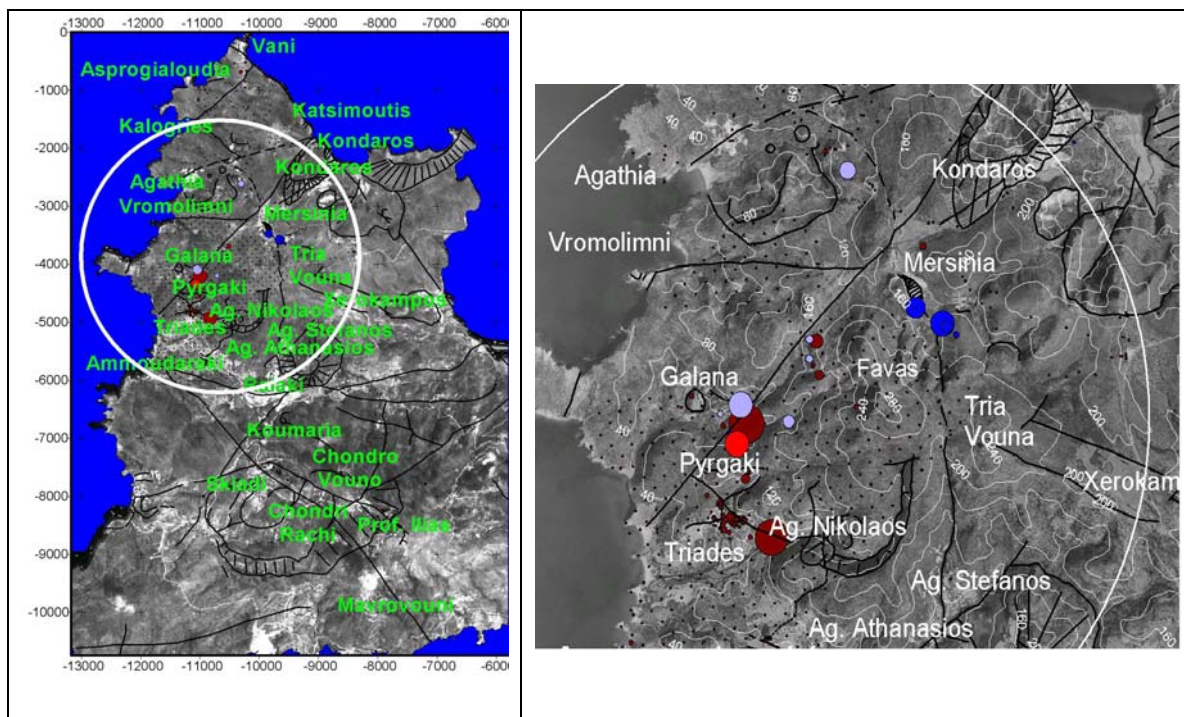


Fig. 116 : Composite distribution of Bi (red circles), Mo (lilac circles), Cu (brown circles) W (blue circles) at the northern sector of western Milos.

10.9. Synthesis of the data

Through the elaboration of a series of geochemical maps and air-photos imagery, using ArcView v.3.2 software system (ESRI corporation, USA), was possible to identify relationships between the minor and trace metallic elements, and to reconstruct the limits of the mineralized areas as emphasized by putting together geochemistry and tectonics.

11. DISCUSSION

An epithermal ore deposit represents only a small part of the magmatic-hydrothermal system responsible for its formation. Every element of the epithermal model is crucial in locating and defining an epithermal target: the structural setting, evidence of a mineralizing system, a heat center (temperature zonation from fluid inclusion data and clay mineralogy), geochemical anomalies showing target halos, and geophysical anomalies showing alteration and structure.

Transitional shallow submarine to subaerial subduction-related volcanic arc environments are characterized by a wide range of precious and base metal deposits which have been recognized as transitional in character between submarine massive sulphides and volcanogenic deposits in the epithermal environment and have been named VMS-epithermal transitional deposits (Hannington et al. 1999; Hannington & Herzig 2000; Huston 2000).

Methodological collection of existing information, geological mapping of surface outcrops, geochemical sampling and analysis, drill logging, structural interpretation, alteration and ore mineralogical studies, were combined in order to better understand and interpret the magmatic-hydrothermal environment of ore deposition at western Milos.

The western Milos deposits display a number of geological, mineralogical and geochemical characteristics that are in part typical of VMS deposits and in part resemble volcanogenic epithermal gold deposits. More specifically shallow sub-marine, and transitional to sub-aerial, arc-volcanic rocks of western Milos (Fytikas et al. 1986; Stewart and McPhie 2003, 2005; Alfieris et al. 2004) contain epithermal deposits such as the Mavrovouni Au-Ag, Profitis Ilias Pb-Zn-Cu \pm Ag-Au-Te (Constandinidou et al. 1998; Kiliyas et al. 2001; Alfieris et al. 2004; Alfieris and Voudouris 2005, 2006), Chondro Vouno Au-Ag \pm Pb-Zn, Triades-Galana Pb-Zn-Cu-As \pm Ag-Au deposits (Hauck 1984, 1988; Liakopoulos 1987; Vavelidis & Melfos 1998; Alfieris et al. 2004; Alfieris and Voudouris 2005) and Katsimoutis-Kondaros Zn-Pb-Ag (Liakopoulos 1987; Alfieris and Voudouris 2005) and Vani Mn-Pb-Zn (Liakopoulos 1987; Hein et al. 2000; Liakopoulos et al. 2001; Glasby et al. 2005). The fluid inclusion and stable isotopic data (Hauck 1984, 1988; Vavelidis & Melfos 1998; Kiliyas et al. 2001; Naden et al. 2003a, b; Ballanti et al. 2004; Naden et al. 2005) suggest a strong involvement of seawater in the mineralizing solutions. These are closely linked to a mineralized active geothermal system that is characterized by three-component mixing between seawater, meteoric water and a minor magmatic component (Liakopoulos 1987; Pflumio et al. 1991; Kiliyas et al. 2001; Naden et al. 2002, 2003a, b, 2005).

All the deposits are genetically related to shallow submarine subvolcanic intrusive/partially extrusive domes-flow dome complexes, and are encountered mainly in form of veins and stockworks, hosted, either in shallow submarine acid pyroclastic products (fine ash tuffs and coarse ignimbrites) at Profitis Ilias, Chondro Vouno, and Koumaria, or in syn-volcanic intrusions and their autoclastic facies (hyaloclastites) at Profitis Ilias, Chondro Vouno, Koumaria, Triades, Galana, Kondaros-Katsimoutis, Vani, in form of breccias (hydrothermal, phreatomagmatic) at Triades-Galana, Ag. Ioannis, Mavrovouni, and as stratiform horizons at Vani.

Under this aspect Milos deposits can be considered as hybrid, transitional VMS-epithermal one (Naden et al. 2005), or shallow submarine to subaerial epithermal (Stewart & Mc Phie 2003, 2004, 2005; Alfieris & Voudouris 2005). The paleogeography at the time of mineralization comprised scattered islands (mainly volcanic domes and subordinately parts of the metamorphic basement) flanked by shallow marine areas. A modern analog for the

setting of epithermal-style mineralization of western Milos is according to Stewart & Mc Phie (2004) the shallow submarine to subaerial volcanic complex of the island of Panarea (Tyrrhenian sea, Aeolian volcanic arc- Italy / Minniti and Bonavia 1984).

A common feature of western Milos mineralization is the development of a pre-ore hypogene advanced argillic alteration in a submarine environment, related to the various volcanic centers/vent areas. At Milos island early endogenous and exogenous domes/flow domes (Rhyda, Anda) were emplaced into and on precursor tuffs. The domes field was intensely altered within less than 1Ma of domes emplacement, mainly at the northern sector, where acid-sulfate alteration is spatially and genetically related to the above domes. Late dacitic to rhyolitic dome, flow-dome complexes (Dado), typically represent late-stage devolatilized magma emplaced in either eroded stratovolcanoes or resurgent calderas, are not genetically related to the advanced argillic alteration.

The advanced argillic alteration is zoned from a central massive to vuggy silica core, succeeded outwards by silica-alunite, silica-kaolinite (\pm alunite) and mixed layer clays (kaolinite-illite). The residual silicic alteration is structurally and lithologically controlled. The observed elongated shape of the silica bodies in the northern sector of western Milos suggests that major structural controls were ENE-WSW striking faults. The zoned alteration pattern is the result of the process of neutralization and cooling within permeable lithologies and away from the major fluid feeder tectonic structures. An initial lithological control is evidenced by the localization of silicification in permeable host rocks near intersections with NE trending structures. The identification in the southern sector (similarly to the northern one) of relict minerals indicating hypogene acid conditions (diaspore-dickite-alunite), most probably suggest widespread development of advanced argillic alteration at the whole of western Milos island.

Although advanced argillic alteration has been widely recognized as typical of subaerial high sulphidation (HS) systems, increasing discoveries during the last years, indicate the role that it can also play in submarine environments. The role of magmatic volatiles in creating acid sulfate alteration and/or metallic high sulfidation minerals is already proved in different submarine environments of the world, e.g. Lau and Manus back arc basins/Papua New Guinea, Tyrrhenian sea, Aeolian volcanic arc/Italy (Minniti & Bonavia 1984; Sarano et al. 1989; Sakai et al. 1991; Herzig et al. 1993; Herzig & Hannington 1995; Herzig et al. 1997; Gamo et al. 1997). The pyrophyllite-sericite-alunite alteration described from the Basin Lake prospect/western Tasmania is also considered to be of submarine origin (Williams & Davidson 2004). Without doubt a critical factor in the development of high sulphidation conditions in submarine settings is the relatively shallow depth of emplacement of associated subvolcanic intrusive/extrusive acid (mainly dacitic) dome(s), while deeper subvolcanic heat source/s will result in large-scale convection and dilution by seawater, making thus direct contributions from the subvolcanic magma more difficult and/or impossible (Hannington et al. 1999).

No stable isotope systematics are available for advanced argillic alteration, but a magmatic-hydrothermal origin with a dominantly magmatic fluid source is suggested, based on field, petrographic and mineralogical data. Alunite, dickite/kaolinite, halite, diaspore and pyrophyllite in the advanced argillic alteration zones of Kondaros-Ralaki-Agathia and partly Chondro Vouno, Mavrovouni, are interpreted to have formed from acidic fluids generated by absorption of magmatic vapour by seawater, as documented at the active Conical Seamount/Lihir island (Herzig et al. 1999; Petersen et al. 2002), and the transitional subaerial to submarine high-sulfidation epithermal Pueblo Viejo deposit/Dominican Republic (Kesler et al. 1981, Muntean et al. 1990, Kesler et al. 2005). Coarsely crystalline

magmatic-steam alunite is restricted to the near-surface portion of Kondaros area mainly. Fluid mixing likely accounts for the formation of sericite/muscovite instead of alunite in the Basin Lake prospect, owing to the decrease in acidity and sulfate content of the fluids (Williams & Davidson 2004), as it is believed to be the case in some high sulfidation prospects at Milos (e.g. Triades-Galana). Alternatively the presence of sericite, kaolinite at Triades-Galana represents a deeper level of the high sulfidation alteration system.

Ore-stage alunite hasn't been observed, but the acidic alteration characterized by granular, colloform and fine-grained disseminated and framboidal pyrite in association with alunite at Agathia and Kondaros is considered to be of hypogene origin and may represent high-level features of the high-sulfidation system.

Barren acid-leached zones formed in the steam-heated submarine to subaerial environment below seafloor or above paleowater tables, may be preserved above or alongside the shallow high sulphidation alteration (e.g. Agios Ioannis, partially Kondaros-Agathia-Vromolimni areas, Profitis Ilias). Steam-heated alteration zones were formed from oxidation of H₂S during boiling of the magmatic-hydrothermal ore fluids.

The deposition of the ore minerals wasn't simultaneous to the process of the high-sulfidation advanced argillic alteration at western Milos, but it was attributed to later fluids of both intermediate and high sulphidation character. The fluids/vapors responsible for the initial period of acid sulfate alteration, were evolved to late intermediate sulfidation fluids and still later overprinted by high-sulfidation ones. Whereas the advanced argillic alteration zones seem to have formed in a hypogene acidic environment, the ore minerals were deposited under more reduced conditions as evidenced by the sericitic and adularia alteration zones. The change from a strong acid leaching and silicification towards the deposition of the ore minerals delineates a change from very strongly oxidizing conditions to a less oxidizing environment favorable for the deposition of the sulfides and barite. Fluctuating sulfidation and oxidation conditions during ore deposition were suggested by the presence of hematite in Kondaros-Katsimoutis, of covellite-bornite at Profitis Ilias and of enargite, adularia at Triades-Galana.

As a whole, mineral deposition at western Milos took place in an open-space system along segments of faults striking in two different directions (NE-SW and NW-SE). The ore bodies cover areas of a few km², and extend tens of metres vertically and hundreds of metres laterally, typically occupying steeply dipping veins (0.1-10m wide), stockworks, and breccias.

Geological, mineralogical and geochemical signatures strongly suggest that western Milos deposits form parts of a porphyry-epithermal system considered to have been formed in a shallow submarine setting. It seems that the Cu-Mo-Bi-W mineralization exposed at Triades-Galana-Favas is formed at a shallow submarine epithermal setting. The deep epithermal Au-Ag-Te-base metal mineralization at Profitis Ilias underlies and preceded the typical shallow epithermal crystalline sheeted to chalcedony colloform banded and vuggy milky to amethystine quartz veins at Profitis Ilias higher levels, also exposed at Chondro Vouno. At Koumaria similar epithermal mineralization has been also encountered.

At Profitis Ilias it seems that these two above mentioned mineralization are intrusion-related in the scheme proposed by Gorrbet and Leach (1998): The Au-Ag-Te-base metal mineralization can be classified as transitional between quartz-sulfide Au-Cu and carbonate-base metal Au, with the notable exception the absence of carbonates most probably due to the seawater involvement. On the other hand the banded quartz-

chalcedony veins overprint the previous ones, and can be classified as shallower epithermal quartz Au-Ag. It is important to mention that both styles of mineralization are regarded as intermediate sulfidation type according to Sillitoe & Hedenquist (2003).

Both Triades-Galana and Profitis Ilias systems have been developed along a NE-SW direction and at their turn are cut by a NW-SE mineralized system, best exposed at Kondaros-Katsimoutis-Vani. The last one is considered to represent upper epithermal levels similar to those exposed at the upper part of Profitis Ilias, but belonging to another mineralizing hydrothermal event.

There are several mineralogical evidences that seawater was involved in all studied mineralization and that these were probably formed in a submarine (and eventually in a partly subaerial) environment. These evidences are:

a) The presence of atacamite and silver halogenides (Dimou 2001) quasi at the summit of the Profitis Ilias mountain, and the presence of secondary copper sulfides (at about 300m asl). Seafloor oxidation is considered as the principal mechanism resulting in the formation of atacamite in the Conical Seamount and several other submarine mineralization (Petersen et al. 2002). Similarly secondary copper sulfides replacing chalcopyrite from the Logatchev hydrothermal field on the Middle Atlantic Ridge are interpreted, by Petersen et al. (2002, 2005), as to have been formed under supergene conditions at ambient temperatures during interaction of primary sulphides with oxidized seawater.

The mineralization in the deeper parts of Profitis Ilias is a typical sub-seafloor precipitation of sulfides forming stockwork zones as proposed by Hannington et al. (1995). Cu-rich stockwork telluride mineralization may form during seawater-hydrothermal fluid mixing either during conductive cooling or boiling of the hydrothermal fluids. Later, low-temperature circulation of seawater resulted in the formation of low-temperature secondary phases, including secondary copper sulfides (bornite, covellite, digenite, chalcocite). The interplay between seawater oxidation and a new hydrothermal pulse gave way to the deposition of a second generation galena and sphalerite.

b) The presence of framboidal pyrite at Triades, Galana, Kondaros and Katsimoutis is attributed according to (Vavelidis & Melfos 1998; Vavelidis 1995) to represent mineral deposition in a submarine environment. In this study, these features are considered to be the product of fluid venting at near sea-bottom. Their formation was triggered by bacterial activity.

c) The presence of micro-chimney similar structures in several locations (e.g. Chondro Vouno, Profitis Ilias, Agathia, Triades, Kondaros-Katsimoutis) composed of either pyrite or various sulfide combinations including the skeletal intergrowths between sphalerite, pyrite and galena.

d) Extreme abundance of barite (both stratiform and vein-type) in all Milos mineralization.

e) The presence of stratiform manganese±baryte mineralization at Vani considered to represent a seafloor deposition (Plimer 2000).

f) The presence of aragonite at Kondaros-Katsimoutis is usually attributed to rapid precipitation rates and stabilizing effects of Ba, Sr and possibly Mg on the orthorhombic crystal structure in a shallow submarine environment (Browne 1973; Folk 1994; Pichler 2006).

There is controversy about the classification of western Milos mineralization. This mineralization has been considered either as Kuroko-type, transitional VMS to epithermal, or as shallow submarine, epithermal (Hauck 1984, 1988; Vavelidis & Melfos 1998;

Stewart & Mc Phie 2003; Naden et al. 2005). The formation of western Milos deposits partially fit to the model presented by Hannington et al. (1999) in relation to the formation of high-and low-sulfidation VMS-epithermal deposits in a submarine felsic dome complex. The high-sulfidation VMS deposits occupy a position which is closest to the volcanic vent. If the sea water is sufficiently shallow near the top of the dome to allow boiling of ascending fluids, this results in much of the sulfide being deposited as stockwork mineralization beneath the seafloor. High-sulfidation (HS) deposits are most closely associated with high-level degassing magmas (extrusive felsic domes) and this is probably the case for western Milos. In submarine settings, most of the hydrothermal discharge will be concentrated in the summit region of the volcano rather than on the flanks resulting in superposition of different styles of mineralization (Hannington et al. 1999). Where magmatic volatiles are involved, the acidic nature of hydrothermal solutions promotes advanced argillic alteration, and the formation of a unique assemblage of Cu-Fe sulphides (e.g. enargite, luzonite, tennantite, bornite-pyrite, covellite), similar to that associated with high-sulfidation epithermal Au-Cu deposits (Hannington et al. 1999). This way of thinking gave rise to the application of a 'high-sulfidation' model to some gold rich, shallow-water VMS deposits (Sillitoe et al. 1996).

Boiling is well documented at Profitis Ilias deposit (Kilias et al. 2001). This is in accordance to the statement of Hannington et al. (1999) that "shallow submarine and partially emergent conditions may lead to widespread boiling and the development of extensive stockwork mineralization". At Profitis Ilias the bulk of gold mineralization has been deposited at the upper levels under boiling conditions, whereas base metal, telluride mineralization at deeper levels most likely deposited, at least for a part, due to dilution, during periodic injection of brines and/or local boiling processes (as the adularia presence suggests). The subaqueous adularia-sericite epithermal deposit at Bay of Plenty along the offshore extension of the Taupo Volcanic Zone in New Zealand (Stoffers et al. 1999), could be another active analog of Profitis Ilias-Chondro Vouno deposits.

Although no massive sulfides were found at Milos (this is probable the result of shallow water conditions which promoted boiling), stratiform manganese as well as subaqueous silica horizons (Cape Vani, Agathia respectively) clearly demonstrate submarine conditions. The stratiform Mn-Ba deposit at cape Vani, considered to be the final hydrothermal manifestation of the epithermal Kondaros-Katsimoutis system (Alfieris & Voudouris 2005), is regarded to be deposited on the seafloor (Plimer 2000).

There are evidences (mostly empirical), suggesting that magmatic fluids and gases may have played a role in the evolution of the hydrothermal system(s) at Milos Island, in a matter similar to both Conical Seamount and Ladolam gold deposits at Papua New Guinea (Gemmel et al. 2004) and also in comparison to volcanogenic gold deposits in the epithermal environment (Sillitoe & Hedenquist 2003):

- A) The elevated contents in Mo, W and Bi at Galana and Favas are a strong evidence of a magmatic contribution from a buried porphyry-type deposit at depth below the Triades-Galana-Kondaros system.
- B) The presence of precious metal tellurides in the Profitis Ilias deposit is another indication of a magmatic contribution at least of tellurium in the system. A magmatic origin of tellurium in the form of magmatic vapors is suggested for terrestrial systems by Afifi et al. (1988) and Jensen & Barton (2000). According to Cooke & McPhail (2001) deposition of precious metal tellurides in epithermal deposits could be the result of

interaction between tellurium-enriched magmatic vapour and precious metal bearing hydrothermal solutions. The elevated Te content in the sulfide chimneys at the Pacmanus hydrothermal field (Bismarck sea-NE of Papua New Guinea) is considered to be a signature of a magmatic contribution (Parr et al. 1996, Yang & Scott 2002). Under this aspect another buried porphyry-type deposit, contributing through magmatic gases and possibly metals is postulated beneath the Profitis Ilias and Chondro Vouno deposits.

Common features with copper-gold enriched VMS-epithermal deposits of Eskay Creek and Boliden, where gold mainly occurs in the presence of native metal and tellurides (Hannington et al. 1999), presents the tellurium-enriched segment of the Profitis Ilias deposit. Telluride enrichment has also been mentioned in the Iberian Pyrite Belt (Marcoux et al. 1996, Pinto et al. 2005) and in the Urals province. In the fossil Uralian VHMS deposits several tellurides are reported in both pyrite-chalcopyrite (“black smoker”) and sphalerite-quartz-barite (“white smoker”) ore assemblages (Vikentyev 2004, Maslennikov & Maslennikova 2005). It should be mentioned that telluride-rich VHMS deposits such as those in the Urals have not yet been found on the modern seafloor.

- C) A magmatic contribution to the mineralizing fluids is also supported by fluid inclusion data on quartz and sphalerite (Kilias et al. 2001) from the telluride bearing mineralization indicating temperatures in the range of 230° to 290 °C (average 270 °C) and salinities in the range of 4.5 to 14 wt % NaCl equiv. (average ~ 9 wt% NaCl equiv.).
- D) The high activity of sulfur, as indicated by the mineralogical assemblages, suggests that part of the precious metal might have been sourced by a direct magmatic contribution (Yang & Scott 2002, 2005; Ulrich et al. 2002). It should be mentioned that the Fe-content in sphalerite from Milos is very low (<1wt% Fe) rather unusual for the intermediate sulfidation state of ore fluids described from Conical Seamount and several other submarine epithermal deposits. Recently, Ihle et al. (2005) described very low-Fe content in sphalerite associated with gold from Pacmanus massive sulfide deposit, eastern Manus basin (PNG) and considered high activities of sulfur and oxygen during formation in accordance to Hannington et al. (1995).
- E) The present worked out model implies that, metals were contributed to a large proportion by a magmatic vapour phase. Metal transport, including As, Mo, W, Bi in the vapour phase has been described from condensates and sublimates of fumarolic gases in a manner as described by Gemmell (1987), Symonds (1993), Yudovskaya et al. (2006), and was also analytically revealed in fluid inclusions (Yang & Scott 2002, 2005). The high Arsenic concentrations “capture” by the geochemistry prospecting and revealed in the chemistry of the sulfides, give permission to conclude that As had escaped from the magma in a vapour phase.
- F) Based on sulfur isotope evidence, Hauck (1984) and Balanti et al. (2004), suggested a magmatic contribution at Triades mineralization.

At Milos it is considered that magmatic volatiles, which probably contributed to the mineralization, represent fumarolic emissions from the intrusives/domes, vented into a shallow water environment, where fluid conduits were fissures generated by seismic shocks.

The close spatial relationship between the three successively emplaced intrusive/extrusive domes (Rhyda, Anda, Dado) with respect to the three main mineralizing centers (Profitis

Ilias-Chondro Vouno, Triades-Galana, Katsimoutis-Vani) probably indicates also a genetic relation between them.

This work reinterprets previous results and presents new data suggesting that precious metal deposits in western Milos are rather of intermediate sulfidation (IS) than of low sulfidation (LS) type (according to the scheme proposed by Hedenquist et al. 2000; John 2001; Einaudi et al. 2003). Mineralogical data presented in this study indicate common features between the Profitis Ilias-Chondro Vouno, Kondaros-Katsimoutis-Vani and Triades-Galana mineralized centers, all of them characterized by the occurrence of galena + Fe-poor sphalerite + chalcopyrite and abundance of barite, adularia, sericite and partly calcite, i.e., features typical of intermediate sulfidation epithermal type deposits. Locally high sulfidation conditions prevailed at Triades-Galana-Agathia-Kondaros as indicated by the presence of enargite-tennantite-chalcopyrite-covellite in ore assemblages. Precious metals were introduced by hydrothermal fluids of both intermediate sulfidation (Profitis Ilias-Chondro Vouno, Kondaros - Katsimoutis) and high-sulfidation (Triades-Galana) states.

Following Alldrick (1995) it's possible to deduced a lot of similarities between western Milos and subaqueous hot Spring Au-Ag deposits (Synonyms: subaqueous-hydrothermal deposits; Eskay-type; Osorezan-type) found in several parts of the world, so far (e.g., Eskay Creek, Lulu in Canada; Osorezan, Volcano Islands and Jade hydrothermal field in Japan; Mendeleev Volcano in Kurile Islands, Russia; Rabaul in Papua New Guinea; White Island in New Zealand; Bacon-Manito and Surigao del Norte in Phillippines). As reported by Alldrich (1995) the characteristics of these deposits (fine clastic sulfides and "framoid"-like chemical precipitates to very coarse grained sulfide aggregates in breccia veins; stringer-style vein networks, finely laminated stratiform sulphide layers, epithermal-style breccia veins with large vugs, coarse sulfides and chalcedonic silica), their ore mineralogy (sphalerite, tetrahedrite, native gold, galena, chalcopyrite, enargite, pyrite, stibnite, realgar, native arsenic, cinnabar, marcasite, magnetite, scorodite, jarosite, limonite, anglesite, native sulfur), their gangue mineralogy (sericite, chalcedonic silica, amorphous silica, calcite, barite, potassium feldspar, alunite, halite and cristobalite) and their alteration mineralogy (illite-quartz-gypsum-barite or quartz-sericite-pyrite associated with the near-footwall stockwork zones, and chlorite-pyrite alteration associated with the deep-footwall stockwork zones where alteration minerals are restricted to fractures), remind a lot to the features encountered at the western part of Milos island.

In addition the style of alteration and sulfide mineralization at Milos it is similar to the active Conical Seamount and Desmos Caldera system at Papua New Guinea (Herzig et al. 1999, Petersen et al. 2002, Gemmel et al 2004). However in Conical Seamount, base and precious metals were introduced in a later stage from near neutral pH fluids under lower sulfidation state conditions, following an early high-sulfidation mineralizing event, that contrasts to Milos style of mineralization (intermediate towards high sulfidation). Additional comparisons can be made between Milos and Ladolam porphyry-epithermal style Au deposit (Plimer et al. 1987; Müller et al., 2002). If Profitis Ilias-Chondro Vouno system is underlain by a buried porphyry system similarly to Landolam gold deposit, remains to be proved in the future. Under this aspect Milos mineralization could be also comparable to the magmatic-hydrothermal system at Nisyros volcano at the eastern edge of the south Aegean volcanic arc (Brombach et al. 2003), where a deep porphyry-type

potassic alteration overprinted by porphyry-related anhydrite veins, grades upwards to epithermal quartz-adularia veins with base metal sulfides.

It is considered that the faults of the basement, which were parallel to the subduction zone (i.e., trending NW-SE) were formed as steeply deeping transcurrent faults, which at the surface displayed strike-slip components of displacement. This point of view is also reinforced by the fact that settings of oblique convergence are characterized by dilation formed in association with major strike-slip or transcurrent faults (Corbett & Leach 1998). This dilation facilitates from one part the emplacement of intrusion into extensional settings as well as promotes the formation of low, intermediate and high sulfidation porphyry-related gold-silver systems (Corbett & Leach 1998). In such a fashion it can also be considered that both veins and breccias/domes at western Milos were constrained between deep-slip and strike-slip structures. Indeed all structural elements (big lineaments, faults, fractures, joints) at western Milos display forms of the pre-, syn- and post-mineralization history (activity) as a response to the different stress regime that took place. As a whole, it is considered that strike-slip movements provided syn-mineralization mechanisms for dilatancy, which permitted to the various kinds of subvolcanic bodies to be emplaced, as well as resulted in post mineralization offsets of the various vein systems.

Milos island is one of the few places in the world, where submarine hydrothermal vents have been described at shallow depths (Fitzsimons et al. 1997). Other well described places are Bay of Plenty- New Zealand (Pichler et al. 1999a), Ambitle and Lihir, Papua New Guinea (Stoffers et al. 1999; Pichler et al. 1999), Bahia Concepcion, Mexico (Canet et al. 2005). The active submarine hydrothermal system on Milos discharges gas and brines from the sea bottom at a depth of 10m having temperatures higher than 90°C, in common with Lihir (60° to 96°C), the Ambitle system (89° to 98°C) and the Bahia Concepcion (62° to 87°C). The Bay of Plenty occurs at a depth of 200m with a maximum temperature of 200°C.

At Milos the brine discharged by the system at seafloor is enriched in Na, K, Ca, Cl, SiO₂, and dissolved CO₂ and H₂S with respect to seawater (Valsami et al. 2005).

As stable isotope studies (Botz et al. 1996; Nagao et al. 1991) demonstrated for the recent hydrothermal submarine activity at southeastern and eastern parts of Milos (Dando et al. 2000) there is a magmatic source/contribution for the released gases, indicated by the presence of a mantle-derived He component together with other fluid sources, showing seawater/rock interactions at the deeper crust, with highly saline brines and low saline vapour phases. The hydrothermal fluids mixed with entrained sea water at different ratios, led to differences in the composition of the mineralized fluids. The main mineral phases which precipitate are Fe/Mn sulfides, arsenian sulfides, elemental sulfur, baryte and gypsum (Dando et al. 2000).

A similar situation to that described for Milos occur at Kimolos, Poliegos, where the NE-SW trending manganese system is overprinted by a NW-SE silver-bearing mineralization equivalent to the Kondaros – Katsimoutis mineralizing fault system.

Evolution of western Milos volcanism and mineralization

The following hypothetical model (fig. 117) attempts to interpret the volcanological and

metallogenetic processes that occurred during the time span between the Middle-Upper Pliocene to Upper Pleistocene (3.5 - 0.5 Ma), at western Milos:

Phase I (3.5 – 3.1 Ma)

The beginning of felsic volcanism at Milos, and particularly at the western part of the island, dated at 3.50 ± 0.14 Ma by Fytikas et al. (1986), gave origin to thick (500-600m) intervals of pyroclastic products (the basal pyroclastic series of Fytikas et al. 1986 / the pumice breccia of Stewart & McPhie (2005). Tuffitic horizons (locally fossiliferous; **Ismtt**) interbedded in the Neogene sedimentary unit as well as within the pyroclastic pile (mainly at its base), indicate a shallow submarine depositional setting (present work; Fytikas et al. 1986; Stewart & McPhie 2005).

The submarine explosive activity was characterized by magmatic volatile driven eruptions (exsolving of magmatic gases), highly degassed (vesiculated) material (pumiceous clasts), and by vent clearing and conduit erosion. The clearing of the conduit(s) resulted in the deposition of the vent(s)-derived clasts (mainly from the rhyolitic/rhyodacitic porphyry and subordinately from the metamorphic basement and/or from the overlying Neogene sediments) and juvenile pumice fragments immediately at the seafloor. A small part of the emitted pumiceous material had been settled from suspension in between the spaces left by the lithic fragments as well as above them (lithic pumice tuffs-**Lpt**).

The main pumice rich fraction from the eruption plume has been collapsed in different time spans, after being transported in longer or shorter distances, as a function of their sizes and the dynamics of the various kinds of currents created. The settling down of pumice and ash components from the buoyant plume, made up by coarse pumice rich clasts into a fine pumiceous matrix (pumice flow tuffs-**Pfl**), covered the previous lithic/pumice tuff unit and filled the spaces in between the clasts. Followed the pumiceous lapilli tuff unit (**Lmp**), commonly without any specific internal structure, but generally showing, mainly medium sized pumice concentrations parallel to bedding, and a relative decrease in size from bottom to top, finishing with a very fine ash tuff unit (**Fat**). Locally alternations of Lmp and Fat units took place. Successive pyroclastic flow accumulations resulted in a partial emergence of the Profitis Ilias volcanic edifice and thus in a deposition in subaerial environment of part of the Profitis Ilias ignimbrite (**Pli**).

Phase II (3.1 – 1.4 Ma)

Rhyolitic-rhyodacitic cryptodomes (**Rhyda**), shortly after the pyroclastic cone creation (3.0 Ma, Fytikas et al. 1986; Nethery 1998; Stewart & McPhie 2005), intruded the above mentioned thick and poorly consolidated pyroclastic pile. Because of the functioning of these cryptodomes as mineralizing sources, beyond being a heating ones, the circulating hydrothermal solutions will fill the gaps and fractures in the area all around them (pyroclastic pile/cryptodome interface) as well as the fractures inside them cryptodomes with Ag, Au \pm Pb-Zn crystalline/chalcedonic quartz veins, Pb-Zn-Cu \pm Ag-Au-Te veins and stockworks, respectively.

After a period of tectonic re-assessments, during which a series of volcanosedimentary products (sandstones, fossiliferous mudstones-**ep**, **Ftt**) have been deposited (mainly at the central part of western Milos), widespread effusive volcanic activity took place (2.7-1.4 Ma,) with numerous dacitic-rhyodacitic-andesitic domes and lavas (**Anda**). Some local

pyroclastic cones (dome-top tuff cones of Cas et al. 1990) have also been created, above these domes, at the northern part of W. Milos (the upper lithic / pumice tuff unit-**Ump**), (e.g. Ralaki volcanic cone).

In detail, dacitic-andesitic magma injected into the still unconsolidated wet pumiceous pile of the previous explosive activity at the southern sector, as well as into the volcanosedimentary (fossiliferous tuffs-tuffites, epiclastic units; **Ftt, ep**) units of the northern sector, was subjected to a quench fragmentation of the margins. The creation of a fragmental carapace (hyaloclastite breccia) showing a range of features, from jigsaw fit textures to intensely fractured and brecciated domains and interactions with the sediments (peperite), was of paramount importance for at least a part of the mineralizing stage at the northern sector (Pb-Zn-Cu-As \pm Ag-Au veins / quartz-barite \pm Pb veins, breccias).

Quasi contemporaneously at the end, or short time later, with respect to the emplacement of the Anda domes, injection of dacitic-rhyodacitic magmas (**Dado**) took place, due mainly to a change in the tectonic activity from NE – SW to NW – SE directions, (reactivation of the NW-SE lineaments). These domes have been emplaced partly in a subaerial environment, and in that case show a characteristic carapace of in situ autobreccia enveloping them.

During this period part of the pyroclastics as well as some of the subvolcanics intruded, will be altered to HS (dickite, alunite/APS-alunite \pm diaspore, pyrophyllite) due to the venting exercised by these shallow emplaced subvolcanic bodies (Anda). This alteration occurred extensively at Vromolimni-Agathia-Kondaros as well as at Profitis Ilias areas. The weak presence of this alteration style at Triades, Galana it could be due to a probable erosion that has occurred, either, if it is combined with the presence of adularia, can be explained by fast neutralization of the fluids by sea water or by subsurface boiling of the fluids. It seems that hydrothermal pulses which took place at Profitis Ilias (IS,HS) acted in the same way also here in a subseafloor environment, although the different metal signature (Mo,Bi,W,As-Ag-Au) occurring suggests the possibility to be in presence of a distinct magma source as well.

In the areas of Vromolimni, Agathia, Kondaros and along a NE-SW tectonic trend will be created massive to vuggy silica bodies related to a HS submarine hot-spring system. This system is considered to be the NE extension of the Triades-Galana hydrothermal corridor, where massive silica with alunite, pyrite and marcasite developed at the seafloor.

High sulfidation (HS) mineralization (chalcopyrite+covellite) is considered to be contemporaneous to the enargite+covellite mineralization at Triades-Galana and overprints the previous silicic bodies (with alunite+ pyrite, marcasite).

At the end of this phase (II), tectonic uplift along the major NW-SE directed western Milos bay lineament, created subaerial domains (<1.8 m.y, most probably around 1.6-1.7 Ma) at the northern sector, and focused new hydrothermal and mineralizing activity.

This tectonic system(NW-SE) was a principal conduit along which IS hydrothermal solutions partly recharged in a shallow submarine environment and partly in a subaerial setting where they created the sinters at Mersinia-Kondaros Anemophysima/Xerokampos.

As it happened with the Rhyda cryptodomes initially at the phase II, has also taken place with the Anda, Dado domes, which functioned as mineralizing and heating sources too. The filling of the open spaces by the circulating hydrothermal solutions created a series of quartz-barite \pm base metals and base metals \pm precious metals veins, while partially filled the cracks of the hyaloclastites forming thus a mineralized matrix cementing them.

During this upper limit of the phase II has also started to be developed the mineralization at Vani area, related to both NE-SW and NW-SE mineralization trends.

Phase III (1.4 - 0.5 Ma)

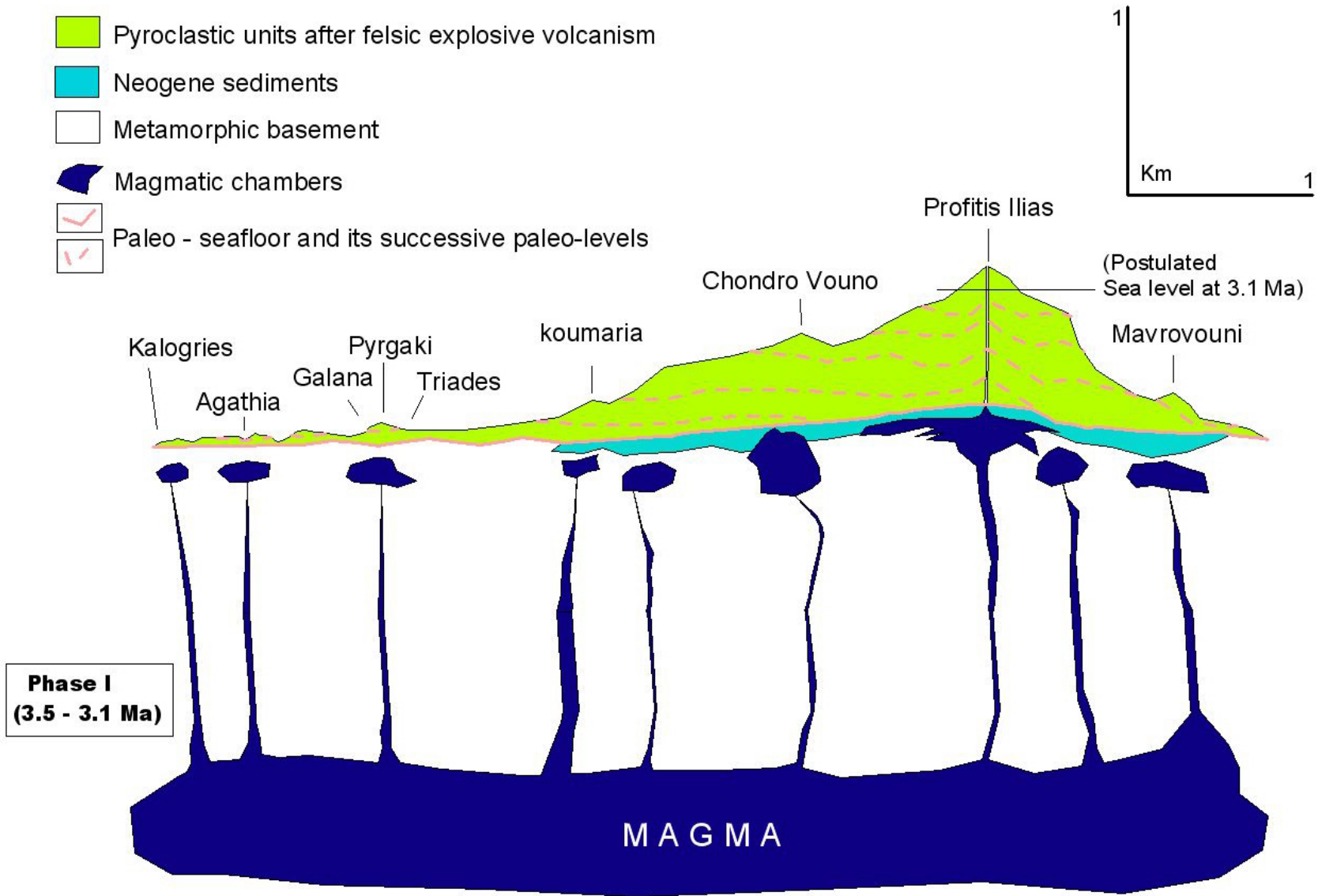
In such a hydrothermalized and mineralized environment (geothermal system), created after the emplacement of the Anda and Dado domes, further surface manifestations will take place and will express the dynamics of that system, thus completing the picture of the western Milos alteration and mineralization. Some of these manifestations at the northern and partially at the southern sectors will be expressed as a series of submarine and partially (at the NW part of W. Milos) subaerial hot springs related to the outflow of hydrothermal solutions along zones of weaknesses. Some others as hydrothermal breccias related to explosive injections of hydrothermal solutions along intensely fractured zones and some others as phreatic breccias / aprons related to phreatic / phreatomagmatic explosions.

During this phase argillic alteration will persist due to a continuous circulation of the hydrothermal fluids, as will do the steam heated advanced argillic alteration, which in several areas will obliterate locally the previous alteration style/s.

During this phase III, will also be continued the development of the mineralization at Vani area.

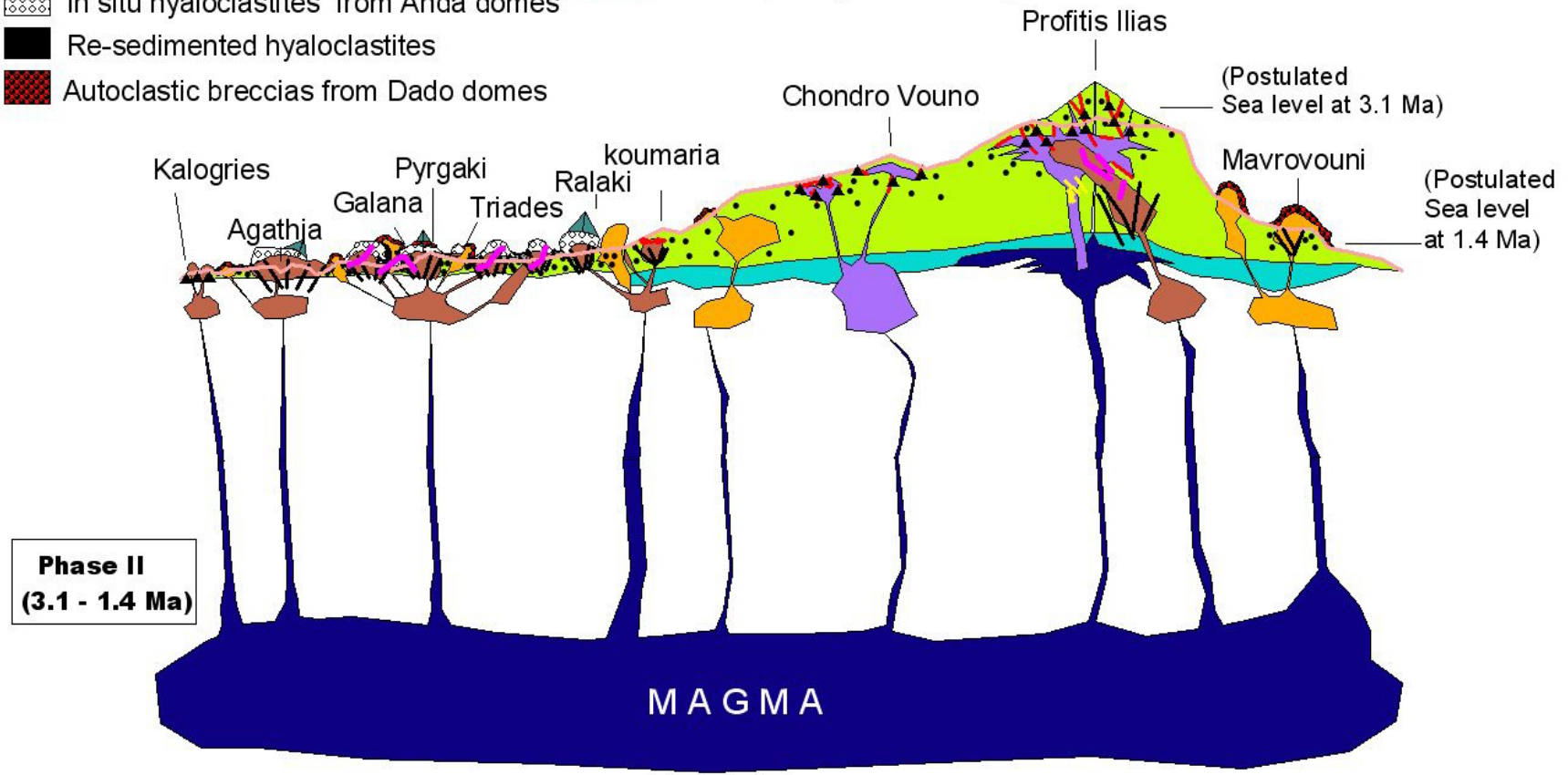
The persisted tectonic activity and contemporaneous erosion during Quaternary times was resulted in the final shape of the island.






Fig. 117 : Draining of magma into satellite chambers, linked with a major, shallow-level (1-2km deep) magma chamber below Milos island, drove the magmatic evolution, alteration and mineralization during the three (I, II, III) postulated phases.



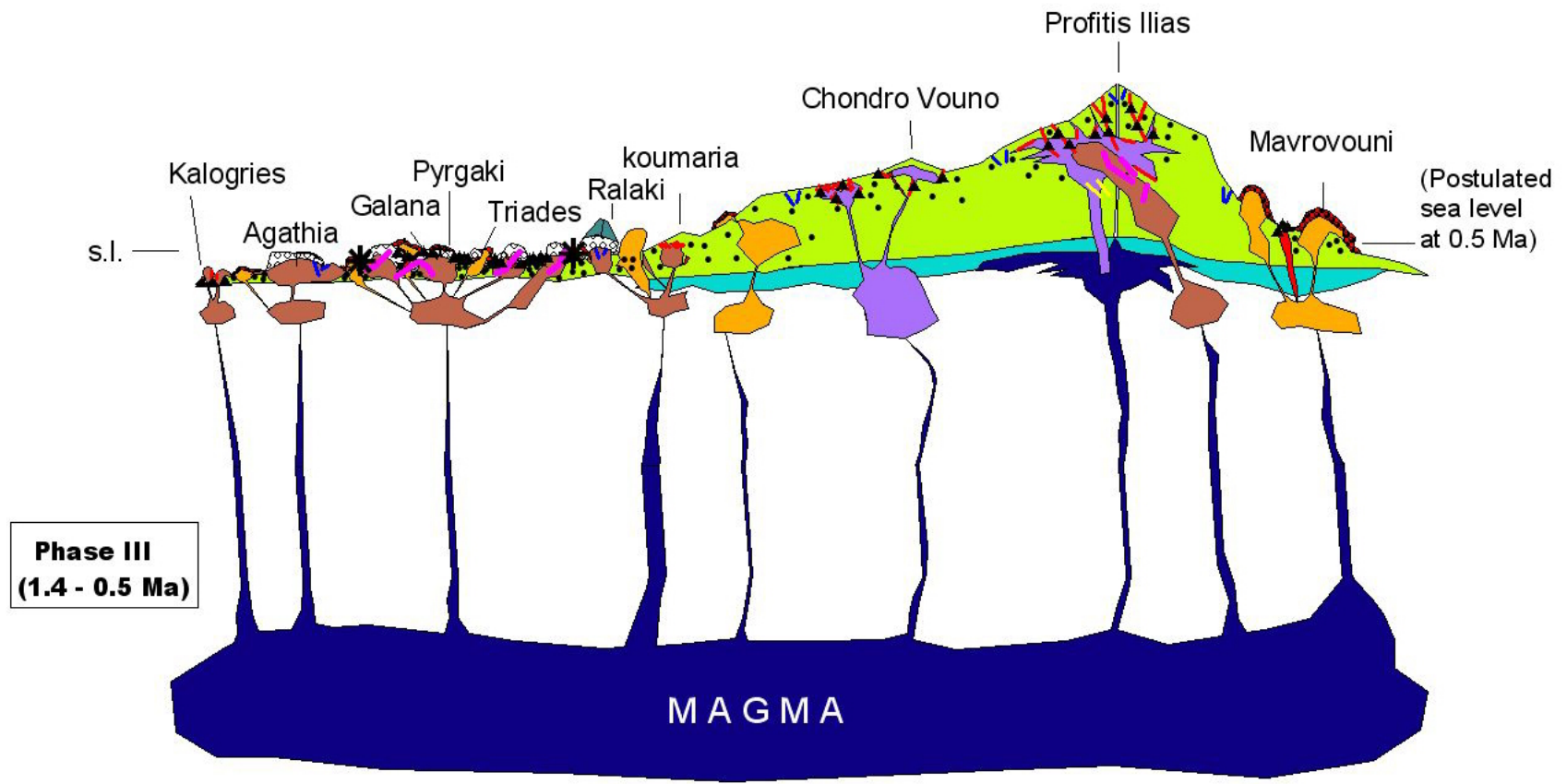
- Rhyda intrusive domes
- Anda domes / flow domes
- Dado domes / flow domes
- Ftt / ep volcanosedimentary units
- In situ hyaloclastites from Anda domes
- Re-sedimented hyaloclastites
- Autoclastic breccias from Dado domes
- Advanced Argillic alteration
- Argillic alteration
- Adularia - sericite alteration
- Postulated paleo - seafloor
- Dome top tuff (pumice cone)
- Base metals -Au -Te Veins
- Ag - Au crystalline/chalcedonic quartz veins
- Quartz-barite-base metals-Ag veins

190



-  Breccia pipes / hydrothermal explosion breccias
-  Steam heated advanced argillic alteration
-  Submarine to subaerial hot springs
-  Argillic alteration
-  Adularia - sericite alteration

161



12. CONCLUSIONS

1. Calc-alkaline volcanic rocks in western Milos were emplaced during the Upper Pliocene to Lower Pleistocene times under submarine to subaerial conditions in an emergent volcanic edifice constrained by tectonic lineaments. The shallow submarine to subaerial arc-volcanic rocks contain epithermal deposits such as the Mavrovouni Au-Ag, Profitis Ilias Pb-Zn-Ag-Au-Te-Cu, Chondro Vouno Au-Ag \pm Pb-Zn, Triades-Galana Pb-Zn-Ag-Bi-W-Mo \pm Cu-Au, and Katsimoutis-Kondaros-Vani Zn-Pb-Ag-W-Mn. As a whole, western Milos is an example of an entire hydrothermal system with exhalative (Vani-Asprogioudia-Kalogries), seafloor/sub-seafloor to subaerial epithermal (Triades, Galana, Kondaros), and sub-seafloor epithermal mineralization (Profitis Ilias, Chondro Vouno). These are closely linked to a mineralized active geothermal system that is characterized by mixing between seawater, meteoric water and a minor magmatic component.
2. Faulting played an important role in localizing rising magmas and consequent volcanism and mineralization. Indeed the western Milos mineralization occur over a strike length of ~10km (from Vani to Mavrovouni) along a NW-SE trending frame/panel, where three fault-delimited corridors (a. Agios Ioannis - Mavrovouni - Profitis Ilias - Chondro Vouno - Koutsounorachi - Agios Panteleimon, b. Ralaki - Triades - Galana - Xerokampos - Tria Vouna - Favas - Vromolimni - Agathia - Kondaros - Katsimoutis, c. Kalogries - Asprogioudia - Vani) meet the two NW-SE trending lineaments (Mavrovouni - Ammoudaraki and Rivari - Vani) paralleling in such a way the most pronounced graben trend (the gulf of Milos). The mineralization is spatially and genetically related to the emplacement of andesites-dacites-rhyodacites and rhyolites along NE-SW and NW-SE trends. In such an open space system with main faults striking along NE-SW and NW-SE directions, E-W, N-S trending faults, helped further the architecture of the nested areas.

The extent and continuity of the major lineaments, those mineralized with precious metals (Au, Ag) along NE-SW directions, those striking NW-SE and mineralized with silver and base metals (Ag, Zn, Pb) and those at ESE-WSW to E-W directions, dividing the two differently mineralized sectors, are related to deep basement structures. In more, the intersection of the above mentioned lineaments with circular features evidenced by the airphoto and satellite imagery interpretation, suggests that these features may have controlled both volcanism and subsequent mineralization. What created the sites of the potential mineralization were the intersection points between the graben's borders aligned NW-SE and the extensional lineaments along NE-SW trends, where vents/pipes, breccias and extrusive domes have been formed and/or intruded. Vein orientations as well as configurations, such as sigmoidal veins, various offsets and slickensides, indicate lateral movements (mainly sinistral). Probably this is in agreement with the fact that sinistral movement on the NW-SE graben bounding structures has dilated ESE-SE fractures which are interpreted to form a fluid upflow feature. In a more precise way it could be said that, mineralization is controlled by NE striking faults with dextral separation, linking major E-W left lateral and N-S to NNW-SSE steeply dipping extensional structures (duplex like structures).

3. Initial magma degassing along permeable vent structures (NE-SW to E-W trending faults) resulted in the development of a hypogene advanced argillic alteration in a submarine environment. Pyroclastics, rhyolitic-rhyodacitic cryptodomes and dacitic-andesitic domes were subjected locally to an advanced argillic alteration of high sulfidation-style (dickite, alunite/APS, \pm diaspore, pyrophyllite, halite). Magmatic gases were probably derived from both rhyolitic-rhyodacitic and dacitic-andesitic intrusives (Rhyda, Anda). Massive to vuggy silica bodies with alunite, pyrite, marcasite, related to the HS (high sulfidation) system were developed at the seafloor/sub-seafloor. The role of the vent structures in localizing the ascending magmatic volatiles has been recognized during this study. Advanced argillic alteration present at Vromolimni-Agathia-Kondaros and as relics at Profitis Ilias, is probably equivalent to deeper kaolinite-sericite alteration at Triades-Galana.
4. Following the early stage of acid leaching, base and precious metal mineralization were formed under intermediate to high sulfidation fluid states in the three main mineralized centers: the Profitis Ilias-Chondro Vouno, the Triades-Galana and the Agathia-Kondaros-Katsimoutis-Vani. Mineralization at western Milos was developed either within the intrusives, or at their fractured carapaces, at their interfaces to the overlying pyroclastics and/or volcanosedimentary units, or within these last. The ore bodies typically occupying steeply dipping veins (e.g. Profitis Ilias, Chondro Vouno, Katsimoutis, Kondaros), stockworks (e.g. Koumaria, Chondro Vouno), breccias (e.g. Triades, Galana) and stratiform occurrences (e.g. Cape Vani). The lack of an extensive vein system in the northern sector area is mainly the result of different lithologies between the two sectors. In the northern sector mineralization is mostly confined to areas of siliceous alteration related to NE-SW, E-W trending faults and eventually to previous not any more outcropping caldera structures. On the other hand at the southern sector the fluid flow was mainly driven by rock permeability.
5. Precious/base metals vein mineralization at Profitis Ilias-Chondro Vouno (southern sector) is strongly developed mainly within and immediately overlying domes and sill-like intrusives, which have been emplaced along NW to WNW trending structural zones after intruding a thick pile of pyroclastic rocks. The intrusives have a rather elongate dome shape and/or sill like form, and have been emplaced longitudinally with respect to the intrusive centers. The polymetallic mineralization which accompanied the emplacement of the domes/sills, and especially the drusy veinlet variety, has been mainly developed at the uppermost portions of the domes: the characteristic intersections at Profitis Ilias of base metals-telluride mineralization at RL levels between 260m and 330m, i.e. below to the postulated boiling zone at 420m are base metal sulfides, tellurides and native gold together with fine acicular drusy crystalline quartz veinlets. Gold-rich mineralization is confined to silica-rich zones of the pyroclastics and subvolcanic/intrusive bodies above the 420m zone. The typology there is of crustiform-colloform quartz-adularia veins. These include banded, vuggy quartz, chalcedony veins and silica-cemented breccias as well as brecciated quartz and chalcedony veins, which show evidence of several episodes of breaking and re-cementing. It seems that these two different ore parageneses are both zoned and intermixed in time and space and also the shallower one overprint the deeper one and consequently the metal contents of

these two zones vary, showing a higher Cu+Au+Ag at depth while Ag and Au are dominant in elevated crustal settings (classified with decreasing crustal level as: deeper quartz-sulphide gold+copper/polymetallic base metal-gold -silver veins and shallowest epithermal quartz gold-silver).

At Profitis Ilias precious and base-metal vein mineralization at higher topographic levels and precious metal tellurides at lower levels, most likely deposited during periodic injection of magmatic volatiles and dilution of brines by sea- and meteoric water. It could be possible that late stage hydrothermal pulses were either of high sulfidation nature, or alternatively their HS affinity was the result of seawater oxidation. The lower telluride bearing parts of Profitis Ilias mineralization is a typical sub-seafloor precipitation of sulfides forming stockwork zones.

The vein systems at Koumaria, Amethyst and Chondro Vouno occur near the contact between the fine rhyolitic tuff (Fat), the overlying Profitis Ilias ignimbrite and the intruded domes (Rhyda) at a similar stratigraphic level to the upper part of Profitis Ilias mineralization. In the transitional shallow submarine to partially emergent (Profitis Ilias) environment the development of stockwork mineralization of intermediate sulfidation type along the NE-direction was the result of boiling as evidenced by the widespread presence of adularia.

6. The Triades-Galana-Agathia-Kondaros hydrothermal system is associated with the emplacement of shallow marine intrusive to extrusive dome complexes that may represent late-stage devolatilized magma emplaced into an eroded pumice cone volcano (as that of the southern sector) or a resurgent caldera structure. The crackled and brecciated carapaces of the domes, emplaced into a volcanosedimentary (sandstones and conglomerates) environment, have been filled by ore fluids, which disseminated precious and base metals mineralization into the matrix and the crackled jigsaw open spaces (hyaloclastite of various kinds). Another part of the mineralized fluids was more focused along NE-SW trending faults, which truncated the coherent and partially flow banded mass of the above mentioned domes, and filled those open spaces. Except the above mentioned volcanic (hyaloclastic) breccias, another kind of breccias are present in the area (hydrothermal breccias) and resulted from a series of explosive events with a concomitant hydrothermal circulation of mineralized fluids, which dominantly re-mineralized parts of the previous occurrences. Triades-Galana-Kondaros correspond to a seafloor/sub-seafloor depositional environment and to a high-intermediate sulfidation states of ore fluids. Enargite is a common constituent of Triades and Galana and it is not observed in other parts of W. Milos. Its late deposition together with covellite suggests possibly a reactivation of the hydrothermal system and introduction of precious metals with As-bearing solutions under high/very high sulphidation states. A silver sulfosalt, most probably proustite, accompanies tennantite and enargite in the mineralization and together with Ag-bearing tetrahedrite and Ag-bearing enargite are considered the carriers of silver in the mineralization.
7. The area of Kondaros-Mersinia-Agathia it is considered to represent a submarine to locally subaerial hot volcanic lake at the top of a volcanic-hydrothermal system which was fed directly by degassing magma at shallow levels. Indeed, the geochemical anomaly around Mersinia it is related to the exposure of a silica cap,

sinter, Fe/Mn hot-spring deposits, advanced argillic alteration, sulfates, sulfides, and it is associated with anomalous As, Sb, Ba and Hg geochemistry. These facts together with the development of steam-heated zones at Kondaros area constitute an evidence of boiling mineralized centers underneath. Mineralization at Agathia-Kondaros-Mersinia is restricted within the vuggy and massive silica zones. Silica flooding at the sea floor corresponding to a submarine acid lake environment resulted in the deposition of the more volatile metals (As, Sb, Hg). The high sulfidation mineralization (chalcopyrite+covellite) at Agathia-Kondaros, overprinting the previous mentioned silicic bodies (with alunite+pyrite+marcasite), it is considered to be contemporaneous to the enargite+covellite mineralization at Triades-Galana.

8. At a chronologically later period with respect the dominancy of the NE-SW faults, the reactivation of NW-SE faults created a new Ag-generation mineralization. This mineralization has been localized by structural intersections of these younger NW-SE trending faults and fractures with pre-existing NE-SW trending quartz-adularia/quartz-baryte veins, locally creating brecciated vein structures. The NW-SE tectonic system, which followed the NE-SW extensional regime, was a principal conduit which channelled intermediate sulfidation hydrothermal solutions partly recharged in a shallow submarine environment and partly in a subaerial setting where they created the silica caps/sinters at Mersinia-Kondaros-Anemophysima/Xerokampos and partly at Vani. Both sub-seafloor (Kondaros base-Katsimoutis) and seafloor (Vani) ore deposition took place in the submarine domain of this system. The hydrothermal solutions responsible for the sub-seafloor silver-bearing IS (intermediate sulfidation) mineralization were strongly oxidizing as suggested by the abundance of hematite. As indicated by the presence of adularia and carbonates, at Kondaros-Katsimoutis area, boiling has taken place under sub-seafloor conditions. The hydrothermal activity ended with manganese+aragonite. Mineralization at Vani has been fed by both NE-SW and NW-SE mineralized fault systems. Along NE directions, colloform banded veins of the Kalogries-Asprogioloudia-Vani system hosted into propylitized dacites (Anda) and feeding manganese-barite chimneys (white smokers) on the sea floor are related to the stratiform emplacement of manganese-barite horizons into overlying shallow marine tuff/tuffites. It is considered that this mineralized system is equivalent to the final manganese bearing stage along NE direction of the IS system of Profitis Ilias - Chondro Vouno - Koumaria. Along NW directions, a steep faulting associated with hydrothermal brecciation and quartz-base metal- silver sulfosalts and late Mn oxides, has occurred at Vani.
9. Present works data's revealed that the high silver content of western Milos galena mineralization is accounted to inclusions of Ag-bearing tetrahedrite, Ag-bearing sulfosalts and tellurides. Tetrahedrite-tennantite minerals represent a minor but important constituent of all studied mineralization. At Triades, Galana there is a dominance of tennantite over tetrahedrite. The Kondaros-Katsimoutis and Chondro Vouno-Profitis Ilias systems contain almost pure tetrahedrites with variable Ag-contents. More than the 85% of the sphalerites analyzed are of the very low-Fe variety with no more than 0.5 wt % Fe. Higher Fe-contents, up to around 2.5 wt%, are encountered at Kondaros-Katsimoutis and at Triades-Galana areas and coexist

with Ag-rich assemblages. Gold at Profitis Ilias, (both native and in tellurides), is considered to be concentrated from the higher temperature base metal precipitates within the blebs, that crystallized to form hessite and included phases. With respect to that a 2-steps evolution it is proposed; an initial galena-hessite solid solution followed by a hessite-petzite-Au one. Native gold in association with tellurides contain around 14 wt% Ag. The sulfidation-oxidation trend showed for the deep Profitis Ilias-Chondro Vouno mineralization is quite similar to that from Triades-Galana, and corresponds to the late formation of low temperature bornite+covelite+chalcocite, due to the combined action of hydrothermal reworking and seawater oxidation.

10. The different metal signature at Triades-Galana and at Agathia-Favas-Kondaros (Mo-Bi-W-As-Hg-Ag-Au) compared to Profitis Ilias (Te-Au-Ag) one, suggest probably distinct magma sources (most probably andesitic- dacitic - rhyodacitic for Profitis Ilias, rhyolitic-rhyodacitic for Triades-Galana, and dacitic-andesitic for Kondaros-Katsimoutis). The enrichment of the deposits in Te, Mo, W and Bi is a strong indication of either a direct magmatic contribution of these metals, or of a remobilization of them from an earlier magmatic-hydrothermal porphyry style mineralization at depth.
11. Although the high- and intermediate sulfidation styles of mineralization in western Milos are regarded as typical epithermal, with colloform banded and comb textured quartz veins, banded chalcedony veins and vein breccias, jigsaw breccias cemented with quartz and chalcedony, drusy cavities in veins and breccias which are lined with crystalline quartz and silica sinter deposits, the hydrothermal solution is thought to be mainly a solution of seawater origin, which would have occasionally mixed with a fluid of magmatic origin. In such a way and related to tectonic movements, the style of circulation of hydrothermal solution changed from an initial vapour dominated hydrothermal system (related to the pre-ore advanced argillic alteration) to a later sea-water dominant hydrothermal system with minor contribution of magmatic waters and to a final meteoric water predominance of the hydrothermal solution related to decline in activity of dacitic-rhyodacitic magmatism and to the emerging, (transitional to subaerial context), of the volcanic edifice.

References

- Afifi, A.M., Kelly, W.C. and Essene, E.J. (1988) Phase relations among tellurides, sulfides and oxides, I. Thermochemical data and calculated equilibria. *Econ. Geol.* 83, p.377-394.
- Alfieris, D., Kiliyas, S., Naden, J. and Voudouris, P. (2004) Spatially coincident low- and high-sulphidation epithermal mineralization in an emerging volcanic edifice, W. Milos, Greece. 5th Int. Symp. Eastern Mediterranean Geology, 4pp.
- Alfieris, D. and Voudouris, P. (2005) Ore mineralogy of transitional submarine to subaerial magmatic-hydrothermal deposits in W. Milos, Greece. Cook N. and Bonev I. (eds), Au-Ag-Te-Se deposits, *Geoch. Miner. Petrol.*, 43, p.1-6.
- Alfieris, D. and Voudouris, P. (2006) First occurrence of tellurides in the epithermal Profitis Ilias deposit, Milos Island, Greece. 12th Quadrennial IAGOD Symposium, Moscow, 4pp.
- Alldrick, D.J. (1995) Shallow Subaqueous Hot Spring Au-Ag; in Selected British Columbia Mineral Deposit Profiles, Volume 1, D.V. Lefebure and G.E. Ray, (Eds), British Columbia Ministry of Energy, Mines and Petroleum Resources, Open File 1995-20, p. 55-57.
- Allen RL. (1992) Reconstruction of the tectonic, volcanic and sedimentary setting of strongly deformed Zn-Cu massive sulfide deposits at Benambra, Victoria. *Econ. Geol.* 87, p. 825-854.
- Altherr R. (1981) Zur Petrologie der Miozaenen Granitoide der Zentralaegaeis (Griechenland). *Habil. Schrift Univ. Braunschweig*, 218 pp.
- Andriessen, P.A.M., Boelrijk, N.A.I.M., Hebeda E.H., Priem H.N.A., Verdurmen E.A.Th. and Verschure, R.H. (1979) Dating the events of metamorphism in the Alpine orogen of Naxos (Cyclades, Greece). *Contrib. Mineral. Petrol.*, 69, p. 215-225.
- Angelier, J. (1976) La neotectonique cassante et sa place dans un arc insulaire, l'arc egeen meridional. *Bull. Soc. Geol. France*, (7), t. XVIII, n 5, p. 1257-1265.
- Angelier, J., Cantagrel, J.M., and Vilminot, J.C. (1977) Neotectonique cassante et volcanisme plioquaternaire dans l' arc egeen interne, l' ile de Milos (Grece) . *Bull. Soc. Geol. De France*, (7) t XIX No 1, p.119-194.
- Angelier, J. (1979) - Neotectonique de l' arc Egeen. *Soc. Geol. Du Nord, Lille*, 3, p.418.
- Angelier, J. (1979) Recent Quaternary tectonics in the Hellenic Arc, examples of geological observations on lands. *Tectonophysics*, 52, p.267-275.
- Arribas A.Jr. (1995) Characteristics of high sulphidation epithermal deposits, and their relation to magmatic fluid. *Mineralogical Association of Canada Short Course Notes*, 23, p.419-454.
- Aribas A.Jr., Cunningham C.G., Rytuba J.J., Rye R.O., Kelly W.C., Podwysocki M.H., McKee E.H., and Tosdal R.M. (1995) Geology, Geochronology, fluid inclusions, and stable isotope geochemistry of the Rodalquilar gold alunite deposit, Spain. *Econ. Geol.*, 90, p. 795-822.
- Aubouin J. (1965) Geosynclines. *Developments in geotectonics* 1, pp. 335. Amsterdam New York-Elsevier.
- Ballanti D., Dietrich V. J. and Gartzos E. (2004) Genesis of the bentonite and barite deposits on Milos island, Greece. *Mineral Wealth*, 130, p. 7-32.
- Baltatzis E., Valsami-Jones E., Magganas A., and Kati M. (2001), Tamarugite from Milos island, Greece. *N. Jb. Miner. Mh., H.* 8, p.371-377.

- Barnes, H.L., and Kullerud, G. (1961) Equilibria in sulfur-containing aqueous solutions in the system Fe-S-O and their correlation during ore deposition. *Econ. Geol.*, 56, p.648-688.
- Barton PB Jr, Skinner BJ (1979) Sulfide mineral stabilities. In: Barnes HL (ed.) *Geochemistry of hydrothermal ore deposits*. Wiley Interscience, New York, p 278-403.
- Bigazzi G. and Radi G. (1981) Datazione con le tracce di fissione per l'identificazione della provenienza dei manufatti di ossidiana. *Riv. Sci. Preistor.*, 36, p.223-250.
- Boggie I., Lawless J.V., Rychagov S. and Belousov V. (2006) Magmatic related hydrothermal systems. Classification of the types of geothermal systems and their ore mineralization. *Symposium, Moscow 2006*, p.51-73.
- Bol G. M. and Hasselman J.F. (1985) The petrology and geochemistry of volcanic rocks from Milos (Aegean sea, Greece). Thesis, Utrecht.
- Bonneau M. (1981) Evolution Tectonique de l'arc Egeen depuis le Jurassique Superieur jusqu'au Miocene. *International Symposium On The Hellenic Arc And trench (H.E.A.T) vol. 1, Athens 1981*, p. 62-88.
- Botz R., Stuben D., Winckler G., Bayer R., Scmitt M., and Faber E. (1996) Hydrothermal gases from offshore Milos island, Greece. *Chem. Geol.*, 130, 161-173.
- Briqueu, L., Javoy, M., Lancelot, J.R., Tatsumoto, M. (1986) Isotope geochemistry of recent magmatism in the Aegean arc: Sr, Nd, Hf, and O isotopic ratios in the lavas of Milos and Santorini. Geodynamic implications. *Earth Planet. Sci. Lett.* 80, p.41-54.
- Brombach T, Caliro S, Chiodini G, Fiebig J, Hunziker JC, Raco B. (2003) Geochemical evidence for mixing of magmatic fluids with seawater, Nisyros hydrothermal system, Greece. *Bull Volcanol*, 65, p.505-516.
- Burri, C. and Soptrajanova, G. (1967) Petrochemie der jungen vulcanite der inselgruppe von Milos (Griechenland) und deren stellung im Rahmen der Kykladenprovinz. *Vierteljahresschr. Naturforsch. Ges. Zuerich*, 112, p. 1-27.
- Cabri L.J. (1965a) Discussion on "Empressite and stützite redefined" by R.M. Henea. *Am. Mineralogist*, 50, p. 795-801.
- Cabri L.J. (1965b) Phase relations in the Au-Ag-Te system and their mineralogical significance. *Econ. Geol.* 60, p.1569-1606.
- Canet C., Prol-Ledesma R-M., Proenza J.A., Rubio-Ramos M. A., Forrest M.J., Torres Vera M.A., Rodriguez-Diaz A.A. (2005) Mn-Ba-Hg mineralization at shallow submarine hydrothermal vents in Bahia Concepcion, Baja California Sur, Mexico. *Chem. Geol.* 224, p. 96-112.
- Cas RAF, Allen RL, Bull SW, Clifford BA, Wright JV (1990) Subaqueous rhyolitic dome-top tuff cones: a model based on the Devonian Bunga Beds, southeastern Australia and a modern analogue. *Bull Volcanol* 52, p.159-174.
- Chamanske GK. (1974) The FeS content of sphalerite along the chalcopyrite-pyrite-bornite sulfur fugacity buffer. *Econ. Geol.* 69, p. 1328-1334.
- Christanis K. & Seymour ST. K. (1995) A study of scale deposition. An analogue of meso-to epithermal ore formation in the volcano of Milos, aegean arc, Greece. *Geothermics Vol. 24, No 4*, pp. 541-552.
- Ciobanu CL, Cook NJ, Damian G, Damian F. (2004a) Telluride and sulfosalt associations at Săcărîmb. In: Cook N, Ciobanu CL (eds) *Au-Ag-telluride deposits of the Golden Quadrilateral, Apuseni Mts., Romania, IAGOD Guidebook Ser 12*, p.145-186.
- Ciobanu CL, Cook NJ, Tămaş C, Leary S, Manske S, O'Connor G, Minuţ A. (2004b) Tellurides-gold-base metal associations at Roşia Montană: the role of hessite as gold

- carrier. In: Cook N, Ciobanu CL (eds) Au-Ag-telluride deposits of the Golden Quadrilateral, Apuseni Mts., Romania, IAGOD Guidebook Ser 12, p.187-202.
- Constadinidou, H., Kiliyas, S., Cheliotis I., Naden, J., Shepherd, J., Simos, I., E. Crossing (1998) Mineralogy and chemistry of gold in the Profitis Ilias epithermal deposit, Milos island, Aegean sea, Greece. Bull. Geol. Soc. Greece, 32, p.157-164.
- Cooke D.R., McPhail D.C. (2001) Epithermal Au-Ag-Te mineralization, Acupan, Baguio District, Philippines: numerical simulations of mineral deposition, Econ. Geol. 96, p.109-131.
- Cook N.J, Ciobanu CL, Damian G, Damian F. (2003) The mineralogy of two Neogene ore provinces in Romania: review and additional data. In: Eliopoulos et al. (eds) Mineral exploration and sustainable development. Millpress, Rotterdam p.1157-1160.
- Cook N.J, Ciobanu CL, Damian G, Damian F (2004) Tellurides and sulfosalts from deposits in the Golden Quadrilateral. In: Cook N, Ciobanu CL (eds) Au-Ag-telluride deposits of the Golden Quadrilateral, Apuseni Mts., Romania, IAGOD Guidebook Ser 12, p.111-144
- Cook N.J, Ciobanu CL (2004b) Telluride metallogeny in the 'Golden Quadrilateral' and beyond: Quo Vadis? In: Cook N, Ciobanu CL (eds) Au-Ag-telluride deposits of the Golden Quadrilateral, Apuseni Mts., Romania, IAGOD Guidebook Ser 12, p.203-210.
- Cook N.J, Ciobanu CL (2005) Tellurides in gold deposits: Implication for modelling. In: Mao J. and Bierlein F.P. (eds), Mineral deposit research. Meeting the global challenge, Springer, Berlin, p.1387-1391.
- Corbett, G.J., and Leach, T.M. (1998) Southwest Pacific rim gold-copper systems: Structure, alteration and mineralization. Econ. Geol., Special Publication 6, 238 p., Society of Economic Geologists.
- Cunningham C.G., Rye R.O., Steven, T.A., Mehnert, HH. (1984) Origins and exploration significance of replacement and vein-type alunite deposits in the Mrysvale volcanic field, west-central Utah. Econ.Geol. 79, p. 50-71.
- Dando, P.R., Stuben, D., Varnavas, S.P. (1999) Hydrothermalism in the Mediterranean Sea. Proc. Oceanogr. 44, p.333-367.
- Dando P.R., Aliani S., Arab H., Bianchi C.N., Brehmer M., Cocito S., Fowler S.W., Gundersen J., Hooper L.E., Kolbl R., Kuever J., Linke P., Makropoulos K.C., Meloni R., Miquel J.C., Morri C., Muller S., Robinson C., Schlesner H., Sievert S., Stohr R., Stuben D., Thomm M., Varnavas S.P. and Ziebis W. (2000) Hydrothermal studies in the Aegean sea. Phys. Chem. Earth, vol. 25, No. 1, p. 1-8.
- De Ronde C.E.J., Faure K., Bray C.J., Chappell D.A., Wright I.C. (2003) Hydrothermal fluids associated with seafloor mineralization at two southern Kermadec arc volcanoes, offshore New Zealand. Miner. Deposita 38, p. 217-233
- De Ronde C.E.J., Hannington M.D., Stoffers P., Wright I.C., Ditchburn R.G., Reyes A.G., Baker E.T., Massoth G.J., Lupton J.E., Walker S.L., Greene R.R., Soong C.W.R., Ishibashi J., Lebon G.T., Bray C.J., Resing J.A. (2005) Evolution of a submarine magmatic-hydrothermal system: Brothers Volcano, Southern Kermadec Arc, New Zealand. Econ. Geol. 100, p.1097-1133.
- Dewey J.F. & Sengor C. A.M. (1979) Aegean and surrounding regions. Complex multiplate and continuum tectonics in a convergent zone. Geol. Soc. Am. Bull., 90, p. 84-92.
- Dimou, E. (2001) The halogenide minerals atacamite, iodargyrite, chlorargyrite in the epithermal gold mineralization of Profitis Ilias at Milos and their significance. Bull. Geol. Soc. Greece. 34: p.835-844.

- Duermeijer, C.E., Krijgsman, W., Meijer, P.T., Langereis, C.G., Ten Veen, J.H. (1998) Post-early Messinian counterclockwise rotations on Crete: implications for Late Miocene to Recent kinematics of the southern Hellenic arc. *Tectonophysics* 298, p. 177-189.
- Duermeijer, C.E., Nyst, M., Meijer, P.T., Langereis, C.G., Spakman, W. (2000) Neogene evolution of the Aegean arc: paleomagnetic and geodetic evidence for a rapid and young rotation phase. *Earth Planet. Sci. Lett.* 176, p. 509– 525.
- Duerr, St., Altherr, R., Keller, J., Okrusch, M., Seidel, E. (1978) : “The median Aegean crystalline belt. Stratigraphy, structure, metamorphism, magmatism”. In : Closs, H., Roeder, D., Schmidt, K., (Eds.) “Alps, Apennines, Hellenides”. IUGG Sc. Rep. 38, p. 455 – 477.
- Einaudi, M.T., Hedenquist, J.W., E.E. Inan. (2003). Sulfidation state of hydrothermal fluids : the porphyry-epithermal transition and beyond. In : S.F. Simmons, I.J. Graham (Eds). *Volcanic, geothermal and ore-forming fluids : Rulers and witnesses of processes within the Earth. Soc Econ Geol Spec Publ* 10, p. 285-313.
- Fitzsimons, M.F., Dando, P.R., Hughes, J.A., Thiermann, F., Akoumianaki, I. and Pratt, S.M. (1997) Submarine hydrothermal brine seeps off Milos, Greece: observations and geochemistry. *Marine Chemistry* 57, 325-340.
- Fournier R.O. (1985) The behaviour of silica in hydrothermal solutions, in Berger B.R. & Bethke P.M. (eds). *Geology and geochemistry of epithermal systems. Rev Econ Geology*. 2, p. 45-61.
- Friedrich, W.L. (2000) *Fire in the Sea. Volcanism and the Natural History of Santorini*, Cambridge Univ Pr., Cambridge, 256 p.
- Fytikas, M., Giuliani, O., Innocenti, F., Marinelli, G., Mazzuoli, R. (1976a) “Geochronological data on recent magmatism of the Aegean sea”. *Tectonophysics*, 31, p.29-34.
- Fytikas M., Kouris D., Marinelli G., and Surcin J. (1976b) : Preliminary geological data from the first two productive geothermal wells drilled at the island of Milos. In : proceedings of Inter. Congress on thermal waters, geothermal energy and volcanism of the Mediterranean area. Athens Oct. 1976. Expanded abstracts p. 511 - 515.
- Fytikas M. (1977) Geological and geothermal study of Milos island (Greece). Phd thesis University of Thessaloniki. Geological and geophysical research vol. XVIII, No 1, (IGME) p.1-228.
- Fytikas, M., Innocenti, F., Kolios, N., Manetti, P., Mazzuoli, R., Poli, G., Rita, F., Villari, L. (1983): “The island of Milos. Volcanological evolution within the south Aegean active volcanic arc” XVIII IVGG General Assembly, IAVCEI symp. A, Hamburg, 15 – 27 August 1983. Abstract p.15.
- Fytikas M, Innocenti F, Mannetti P, Mazzuoli R, Peccerillo A, Villari L. (1984) Tertiary to Quaternary evolution of volcanism in the Aegean region, In: Dixon JE, Robertson AHF (eds). *The geological evolution of the eastern Mediterranean: Oxford, Geol Soc Spec Publ* 17, p. 687-699
- Fytikas, M., Innocenti, F., Kolios, N., Manetti, P., Mazzuoli, R., Poli, G., Rita, F. & Villari, L. (1986) -Volcanology and petrology of volcanic products from the island of Milos and neighbouring islets. *J. Volcan. Geoth. Res.* 28, p.297-317.
- Fytikas, M., Garnish, J.D., Hutton, V.R.S., Staroste, E., Wohlenberg, J. (1989) An integrated model for the geothermal field of Milos from geophysical experiments. *Geothermics* 18, p.611–621.

- Fytikas, M. (1989) Updating of the geological and geothermal research on Milos Island. *Geothermics* 18, p.485–496.
- Fytikas M. & Marinelli G. (1976) Geology and geothermics of the island of Milos (Greece). Institute of Geology and Mineral Exploration (IGME), p. 1-58.
- Fytikas M. and Vougioukalakis G.(1993) Volcanic structure and evolution of Kimolos and Polyegos (Milos island group). *Bull. Geol. Soc. Greece*, vol. XXVIII/2, p. 221-237.
- Gamo T., Okamura K., Charlou J.L., Urabe T., Auzende J.M., Ishibashi J., Shitashima K., Chiba H., and Shipboard Scientific Party (1997) Acidic and sulfate rich hydrothermal fluids from the Manus back-arc basin, Papua NEW Guinea. *Geology*, v.25, p. 139-142.
- Garrels, R.M. and Christ, C.L. (1965) Solutions, minerals, and equilibria. New York, Harper and Row, 450p.
- Gaspar O.C. (2002) Mineralogy and sulfid mineral chemistry of the Neves-Corvo ores, Portugal: insight into their genesis. *Can. Mineral.* 40, p. 611-636.
- Gautier, P., Brun, J.-P., Moriceau, R., Sokoutis, D., Martinod, J., Jolivet, L. (1999) Timing, kinematics and cause of Aegean extension: a scenario based on a comparison with simple analogue experiments. *Tectonophysics* 315, p.31– 72.
- Gammel BJ, SharpeR, Jonasson IR, Herzig PM. (2004) Sulfur isotope evidence for magmatic contributions to submarine and subaerial gold mineralization. Conical Seamount and the Ladolam gold deposit, Papua New Guinea. *Econ. Geol.* 99, p. 1711-1725.
- Gena, K. Mizuta T. Ishiyama D. Matsubaya O. & Urabe T. (1998) Mobility of major, minor and trace elements in basaltic-andesite from a high sulphidation type of advanced argillic alteration in DESMOS caldera, Manus Basin, Papua New Guinea. *Geol. Assoc. America, Abstracts with Programs*, 30: A-127.
- Giggenbach, W.F., Garcia, P.N., Londono, C.A., Rodriguez, V.L., Rojas, G.N. and Calvache, V.M.L. (1990) The chemistry of fumarolic vapor and thermal spring discharges from the Nevaldo del Ruiz volcanic-magmatic-hydrothermal system, Colombia. *Jour. of volcan. and geoth. Res.*, v. 42, p. 13-39.
- Glasby G.P., Papavassiliou C.T., Liakopoulos A., and Galanopoulos V. (2000) Past mining of the Vani manganese deposit, Milos island, Greece.
- Glasby GP, Papavassiliou CT, Mitsis J, Valsami-Jones E, Liakopoulos A, Renner RM. (2005) The Vani manganese deposit, Milos island, Greece. A fossil stratabound Mn-Ba-Pb-Zn-As-Sb-W-rich hydrothermal deposit. In: Fytikas M, Vougioukalakis GE (eds) *The South Aegean Active Volcanic Arc. Present knowledge and future perspectives, Developments in Volcanology*, Elsevier, 7, p. 255-291.
- Giuchi, C., Kiratzi, A., Sabadini, R., Louvari, E. (1996) A numerical model of the Hellenic subduction zone: active stress field and sea-level changes. *Geophys. Res. Lett.* 23, p.2485– 2488
- Gobantz, A. (1892) Die silberhaeltigen mineralien auf der insel Milos. *Oester. Z. Berg. u. Huettenwesen*, 18, Jg.XL, p.213-216, Wien.
- Halbach, P., Blum, N., Münch U., Plüger, W., Garbe-Schönberg, D. and Zimmer, M. (1998) Formation and decay of a modern massive sulphide deposit in the Indian Ocean. *Mineral. Deposita* 33, p.302-309.
- Hannington M.D., Peter J.M., Scott S.D. (1986) Gold in sea floor polymetallic sulphide deposits. *Econ. Geol.* V. 81, p. 1867-1883.
- Hannington M.D., Scott S.D. (1988) Mineralogy and geochemistry of a hydrothermal silica-sulfide-sulfate spire in the caldera of axial seamount, Juan de fuca Ridge. *Can Miner.*, 26, p. 603-626.

- Hannington M.D. and Herzig P.M. (2000) Submarine epithermal deposits and the VMS-epithermal transition: a new exploration target. Volcanic Environments and Massive Sulfides Conference, November 2000: Centre for Ore Deposit Research, University of Tasmania.
- Hannington M.D. and Scott S.D. (1989) Sulfidation equilibria as guides to gold mineralization in volcanogenic massive sulfides. Evidence from sulphide mineralogy and the composition of sphalerite. *Econ. Geol.*, vol. 84, p.1978-1995.
- Hannington MD, Tivey MK, Larocque AC, Petersen S, Rona P (1995) The occurrence of gold in sulfide deposits of the TAG hydrothermal field, Mid-Atlantic Ridge. *Can Mineral.* 33, p. 1285-1310
- Hannington, M.D., Poulsen, K.H., Thompson, J.F.H., and Sillitoe, R.H. (1999) Volcanogenic gold in the massive sulphide environment. In: Barrie C.T. and Hannington M.D. (eds), *Volcanic associated Massive Sulphide Deposits: Processes and Examples in Modern and Ancient Settings*. *Rev. Econ. Geol.* 8, p.325-356.
- Hauck M. (1984) Die Barytlagerstaetten der Inselgruppe Milos, Aegaeis (Griechenland). Ph. D. thesis, Univ. Karlsruhe, 241 pp.
- Hauck M. (1988) Kuroko-type ore deposits on the Aegean Islands, Greece. In: Friedrich GM, Herzig PM (eds). *Base metal sulfide deposits*. Springer Verlag, Berlin, p. 216–228.
- Haymon R.M. and Kastner M. (1981) Hot spring deposits on the East Pacific Rise at 21°N: preliminary description of mineralogy and genesis. *Earth Plan Sci Letters.* 53, p.363-381.
- Haymon R.M., Koski R.A. and Singlair C. (1984) Fossils of hydrothermal vent worms from Cretaceous sulfide ores of the Samail ophiolite, Oman, *Science*, 223, p.1407-1409.
- Hatzfeld, D. (1994) On the shape of the subducting slab beneath the Peloponnese, Greece. *Geophys. Res. Lett.* 21, p.173-176.
- Heald, P., Foley, N.K., and Hayba, D.O. (1987) Comparative anatomy of volcanic hosted epithermal deposits: acid-sulphate and adularia-sericite types. *Econ. Geol.*, v. 82, p.1-26.
- Hedenquist, J.W., Simmons, S.F., Giggenbach, W.F., and Eldridge, C.S. (1993) White Island, New Zealand, volcanic-hydrothermal system represents the geochemical environment of high-sulphidation Cu and Au ore deposition: *Geology*, v. 21, p. 731-734.
- Hedenquist J.W. (1995) The ascent of magmatic fluid: discharge versus mineralization. In: J.F.H. Thompson, ed., *Magmas, Fluids and Ore Deposits*. Mineralogical association of Canada Short Courses series, v., 23, p. 263-290.
- Hedenquist J.W. and Lowenstern, J.B. (1994) The role of magmas in the formation of hydrothermal ore deposits. *Nature*, v.370, p.519-527.
- Hedenquist, J. W., Arribas, A., and Reynolds, T. J. (1998) Evolution of an intrusion-centered hydrothermal system: Far Southeast-Lepanto porphyry and epithermal Cu-Au deposits, Philippines: *Economic Geology*, v. 93, p. 373-404.
- Hedenquist, J.W., Arribas, A.Jr., and Gonzalez-Urien, E. (2000) Exploration for epithermal gold deposits. *Reviews in Economic Geology*, v.13, p.245-277.
- Henley, R.W. and Ellis A.J. (1983) Geothermal systems, ancient and modern. *Earth science Reviews*, v.19, p.1-50.
- Henley, R.W., Truesdell, A.H., Barton, P.B.Jr., and Whitney, J.A. (1984) Fluid-mineral equilibria in hydrothermal systems. *Rev. Econ. Geol.*, 1, 267p.

- Hein, J.R., Stamatakis, M.G., J.S. Dowling (2000) Trace metal-rich Quaternary hydrothermal manganese oxide and barite deposit, Milos Island, Greece, *Trans. Inst. Min. Metall.*, 109, p.67-76.
- Hekinian R., Fevrier M., Bischoff J.L., Pikot P. and Shanks W.C. (1980) Sulphide deposits from the East Pacific Rise near 21° N, *Science*, 207, p.1433-1444.
- Helgeson, H.C. (1969) Thermodynamics of hydrothermal systems at elevated temperatures and pressures. *Am. Jour. Sci.* 267, p.729-804.
- Helgeson, H.C., and Kirkham, D.H. (1974) Theoretical prediction of the thermodynamic behaviour of aqueous electrolytes at high pressures and temperatures: I. Summary of the thermodynamic/electrostatic properties of the solvent. *Am. Jour. Sci.* 274, p.1089-1198.
- Helgeson, H.C., Delany, J.M., Nesbitt, H.W., and Bird, D.K. (1978) Summary and critique of the thermodynamic properties of rock-forming minerals. *Am. Jour. Sci.* 278-A, p.1-229.
- Helgeson, H.C., and Kirkham, D.H., and Flowers, G. (1981) Theoretical prediction of the thermodynamic behaviour of aqueous electrolytes at high pressures and temperatures: IV. Calculation of activity coefficients, osmotic coefficients, and apparent molal and standard and relative partial molal properties to 600°C and 5kb. *Am. Jour. Sci.* 281, p.1249-1561.
- Hemley, J.J., Montoya, J.W., Marinenko, J.W., and Luce, R.W. (1980) Equilibria in the system Al₂O₃- SiO₂-H₂O and some general implications for alteration/mineralisation processes. *Econ. Geol.*, 75, p. 210-228.
- Henley, R.W. and Ellis A.J.(1983) Geothermal systems, ancient and modern. *Earth science Reviews*, v.19, p.1-50.
- Herzig, P.A., Hannington M.D., Fouquet Y., Von Stackelberg U., and Petersen S. (1993) Gold rich polymetallic sulfides from the Lau back arc and implications for the geochemistry of gold in sea-floor hydrothermal systems of the southwest Pacific. *Econ. Geol.*, v.88, p.2182-2209.
- Herzig, P.M., Hannington, M.D., Arribas, A..Jr. (1995) Sulfur isotopic composition of hydrothermal precipitates from the Lau back-arc. Implications for magmatic contributions to seafloor hydrothermal systems. *Mineral. Depos.* 33, p.226-237.
- Herzig, P.M. and Hannington M.D. (1995a) Polymetallic massive sulfides at the modern sea floor : A review. *Ore Geology Reviews*, v.10, p. 95-115.
- Herzig, P.M., Hannington, M.D., Arribas, A..Jr. (1998) Sulfur isotope composition of hydrothermal precipitates from the Lau back-arc: Implications for magmatic contributions to seafloor hydrothermal systems. *Min. Depos.* 33, p. 226-237.
- Herzig P.M., Petersen S and Hannington M.D. (1999) Epithermal-type gold mineralization at Conical Seamount. A shallow submarine volcano south of Lihir Island, Papua New Guinea. In: Stanley et al., eds, *Mineral deposits: Processes to processing*. Rotterdam, Balkema, p. 527-530.
- Hoffman C. and Keller J. (1979) Xenoliths of lawsonite-ferroglaucophane rocks from a Quaternary volcano of Milos (Aegean sea, Greece). *Lithos*, vol. 12, p. 209-219.
- Huffner Th. (1893) Ueber den berg und huettenmaennischen Wert der auf der Griechischen insel Milos vorkommenden silbererze.
- Huston D.L. (2000) Gold in volcanic-hosted massive sulfide deposits: distribution, genesis, and exploration, In: Hagemann S.G. & Brown P.E. (eds), *Gold in 2000, Reviews in Economic Geology*, 13, p. 401-426.
- Jackson JA, White Nj (1989) Normal faulting in the upper continental crust. Observations from regions of active extension. *J. Struct. Geol.* 11, p. 15.

- Jacobshagen V, Durr S, Kockel F., Kopp K.O., Kowalczyk G. (1978) Structure and geodynamic evolution of the Aegean region. In : Closs, Roeder et Schmidt (eds). Alps, Apennines, Hellenides, p. 537-564, Stuttgart.
- Jensen, E.P., Barton, M.D. (2000) Gold deposits related to alkaline magmatism. *Rev. Econ. Geol.* 13, p.279-314.
- John, D. A. (2001) Miocene and early Pliocene epithermal gold-silver deposits in the northern Great Basin, western USA. Characteristics, distribution, and relationship to magmatism. *Econ. Geol.* 96, p. 1827-1853.
- Johnson NE, Craig JR, Rimstidt JD (1986) Compositional trends in tetrahedrite. *Can Mineral* 24, p. 385-397.
- Ihle, T., Petersen, S., Herzig, P.M. and Hannington M.D. (2005) Siting of gold and characteristics of gold-bearing massive sulfides from the interior of the felsic-hosted PACMANUS massive sulfide deposit, eastern Manus basin (PGN). In: Mao J. and Bierlein F.P. (eds), *Mineral deposit research: Meeting the global challenge*. Springer, Berlin, p.623-626.
- Innocenti F., Manetti P., Peccerillo A., Poli G. (1981) South Aegean Volcanic Arc : Geochemical Variations and Geotectonic Implications. *Bull. Volcanol.*, Vol. 44-3, p. 377-391.
- Kalogeropoulos, S., Mitropoulos, P. (1983) Geochemistry of barytes from Milos Island Aegean Sea , Greece. *N. Jb. Miner. Mh.* 1, p.13–21.
- Kati M., Valsami-Jones E., Baltatzis E., Magganas A., (2003). Hydrothermal precipitates from the active submarine vents in Paleochori Bay, Milos Island, Greece. In SAAVA conference, Milos Greece, Abstract, p. 70.
- Katsouri S., Scott S.D., Gorton M.P., Magganas A., Valsami-Jones E., Baltatzis E. and Kati M. (2004). Hydrothermal sulfides forming in active shallow water systems: freshwater vs seawater. SEG 2002, International Conference, Perth Australia, p.220-223.
- Kelepertzis A., Charalambidis P.S. (1994) Tuffs of Vani area, Milos island, as a mineral deposit for the production of potash feldspar concentrates *Mineral Wealth* 88, p.7-8
- Kelepertzis A., Economou K., Skounakis S., Porfyris S. (1990) Mineral and chemical composition of kaolins from Milos island, Greece; procedure of kaolinite enrichment. *Applied clay science* 5, p. 277-293.
- Kesler, S.E., Campbell, I.H., Smith, C.N., Hall, C.M. and Allen, C.M. (2005) Age of the Pueblo Viejo gold-silver deposit and its significance to models for high-sulfidation epithermal mineralization. *Econ. Geol.* 100, p.253-272.
- Kilias S.P., Naden J., Cheliotis I., Shepherd T.J., Constandinidou H., Crossing J. and Simos I. (2001) Epithermal gold mineralisation in the active Aegean volcanic arc: the Profois Ilias deposit, Milos island, Greece, *Mineralium Deposita*, 36, p.32-44.
- Kim J., Lee I., Halbach P., Lee K.Y., Ko Y.T. and Kim K.H. (2006) Formation of hydrothermal vents in the North Fiji Basin: Sulfur and lead isotope constraints. *Chem. Geol.* (in press).
- Kiukkola K. & Wagner C. (1957) Measurements on galvanic cells involving solid electrolytes. *J. Electrochem. Soc.*, 104, p. 379-387.
- Kondopoulou D. and Pavlides S. (1990) Paleomagnetic and neotectonic evidence for different deformation patterns in the South Aegean volcanic arc: the case of Milos island. *Proceedings of the IESCA, Izmir*, vol. 1, p. 210– 223.

- Kornprobst, J., Kienast, J.R., Vilminot, J.C. (1979) "The high pressure assemblages at Milos, Greece. A contribution to the Petrological study of the basement of the Cyclades Archipelago". *Contr. Mineral. Petrol.* 69, p. 49 – 63.
- Koski R.A., Clague D.A., Oudin E. (1984) Mineralogy and chemistry of massive sulphide deposits from the Juan de Fuca ridge. *Geol. Soc. Am. Bull.* 95, p. 930-945.
- Kracek FC, Ksanda CJ, Cabri LJ. (1965) Phase relations in the silver-tellurium system. *Am Mineral.* 51, p.14-28.
- Krijgsman, W., Hilgen, F.J., Raffi, I., Sierro, F.J., Wilson, D.S. (1999) Chronology, causes and progression of the Messinian salinity crisis. *Nature* 400, p. 625– 655.
- Leitch C.H.B. (1980) Mineralogy and textures of the Lahanos and Kizilkaya massive sulphide deposits, northeastern Turkey, and their similarity to Kuroko ores. *Mineral Deposita.* 16, p.241-257.
- Leitch C.H.B. (1990) Ore textures in Turkish volcanogenic massive sulfide deposits in light of exhalative sulfide deposits from Axial Seamount and Explorer Ridge, north-eastern Pacific Ocean. *Can Mineral.* 28, p.51-54.
- Le Pichon, X., Angelier, J. (1979) The Hellenic arc and trench system: a key to the neotectonic evolution of the Eastern Mediterranean area. *Tectonophysics* 60, 1-42.
- Leycester E. M. (1852) Some account of the volcanic group of Milo, Antimilo, Kimolo, and Polino. *J. Royal. Geogr. Soc. London*, 22, p. 201-227, London.
- Liakopoulos A. (1987) Hydrothermalisme et mineralisations metaliferes de l'ile de Milos (Cyclades-Grece). *Mem. Sc. Terre Univ. Paris VI*, No. 87-36.
- Liakopoulos, A., Glasby, G.P., Papavassiliou, C.T. and Boulegue, J. (2001) Nature and origin of the Vani manganese deposit, Milos, Greece: an overview. *Ore Geol. Rev.* 18, p.181-209.
- Liatsikas N. (1949) The geology of Milos island. I.G.M.R Report n. 91, Athens.
- Liatsikas N. (1955) Geology of some useful minerals of Milos island. *Inst. Geol. Min. Res. (IGMR) Athens, Greece. Geol. Exped.* 20, p.1-30.
- Lyberis N., Angelier J., Huchon P. Le Pichon X., Renard V. (1981) La mer de Crete : Extension et Subsidence. In *Intern. Symp. On the Hell. Arc and Trench (H.E.A.T.)*, Athens-Greece, vol.1, p. 364-382.
- Magganas A., Baltatzis E., Valsami-Jones E., Kati M. (2003) Composition and formation of unusual sulphate efflorescences in Paleochori fumarolic field, Milos island, Greece. In *SAAVA conference, Milos Greece, Abstract*, p. 54.
- Makris J. (1977) Geophysical investigations of the Hellenides. *Hamburger Geophys. Einzelsch A*, 34, G.M.L. Wittemborg.
- Marinos G. (1955) Geological reconnaissance of the kaolinitic deposits of NW Milos. I.G.M.E. Report n. 404A, Athens.
- Marinos G. (1960) The volcano of Antimilos. *Bull. Soc. Geol. Greece*, vol. IV-1, p. 38-50.
- Makropoulos, K.C., Burton, P.W., (1984) Greek tectonics and seismicity. *Tectonophysics* 106, p. 275-304.
- Manetti P. (1997) Geology and volcanic history of the South Aegean volcanic arc, Greece. In : *Volcanism and archaeology in Mediterranean area*, p. 175-191.
- Marcoux E., Moëlo, Y., and Leistel J.M. (1996) Bismuth and cobalt minerals: indicators of stringer zones to massive-sulfide deposits, South Iberian Pyrite Belt. *Mineral. Deposita*, 31, p.1-26.
- Marques A.F.A., Barriga F., Chavagnac V., Fouquet Y. (2006) Mineralogy, geochemistry, and Nd isotope composition of the Rainbow hydrothermal field, Mid-Atlantic Ridge. *Mineral. Deposita* 41, p.52-67.

- Maskle J., Le Quellec P., and Leite O. (1981) Tectonic of the Active Hellenic Margin between Zakynthos and Karpathos. *Int. Symp. On Sedimentary basins of Mediterranean Margins*, Urbino, Italy.
- Maslennikov, V.V. and Maslennikova, S.P. (2005) Rare mineral assemblages in black and white smoker vent chimneys from Uralian VHMS deposits, Russia. In: Mao J. and Bierlein F.P. (eds), *Mineral deposit research: Meeting the global challenge*. Springer, Berlin, p.647-650.
- Mariolakos I.D. and Papanikolaou D.J.(1981) The Neogene basins of the Aegean arc from the paleogeographic and the geodynamic point of view, p.383-399
- McKenzie D. (1970) The plate tectonics of the Mediterranean region. *Nature*, 226, p.239-243.
- McKenzie D. P. (1972) Active tectonics of the Mediterranean region. *Geophys. J. Roy. Astr. Soc.* 30, p. 109-185.
- McKenzie, D. (1978a). Active tectonics of the Alpine - Himalayan belt: the Aegean Sea and surrounding regions. *Geophys. J. R. Astron. Soc.* 55, p.217–254.
- McPhie J., Doyle M., Allen R. (1993) *Volcanic Textures*. Centre for Ore Deposit and Exploration Studies (CODES), University of Tasmania, 198 pp.
- Meinert, D. L. (2000) Gold in skarns related to epizonal intrusions, in *Gold in 2000*, Hagemann, S. & Brown, Ph., *Reviews in Econ. Geol.*, 13, p.347-375.
- Mills KC (1974) *Thermodynamic data for inorganic sulfides, selenides and tellurides*. Butterworths, London, 925 pp
- Mitropoulos P., Tarney J., Saunders A.D., Marsh N.G. (1987) Paragenesis of Cenozoic volcanic rocks from the Aegean island arc. *J. Volcanol. Geotherm. Res.* 32, p. 177-193.
- Mitropoulos P. and Tarney J. (1992) Significance of mineral composition variations in the Aegean Island Arc. *J. Volcanol. Geotherm. Res.* 51, p. 283-303.
- Müller D., Kaminski K., Uhlig S., Graupner T., Herzig P.M. & Hunt S. (2002) The transition from porphyry- to epithermal-style gold mineralization at Ladolam, Lihir Island, Papua New Guinea: a reconnaissance study. *Mineral. Deposita*, 37, p. 61-74.
- Minniti M. and Bonavia FF.(1984) Copper-ore grade hydrothermal mineralization discovered in a seamount in the Tyrrhenian sea (Mediterranean): Is the mineralization related to porphyry coppers or to base metal lodes? *Marine Geology*, v.59, p.271-282.
- Muntean JL, Kesler SE, Russel N, Polanco J. (1990) Evolution of the Monte Negro acid-sulfate Au-Ag deposit, Pueblo Viejo, Dominican Republic. Important factors in grade development. *Econ Geol* 85, p. 1738-1758.
- Naden J., Kiliass S.P. & Liakopoulos A. (2003a) Land-based geothermal systems with entrained seawater as an alternative to the Broadlands epithermal-Au paradigm: the case for Milos island, Aegean sea, Greece. In: Eliopoulos D. et al. (eds.), *Mineral Exploration and Sustainable Development*, 1, p.507-510, Millpress, Rotterdam.
- Naden J., Kiliass S.P., Leng M.J., Cheliotis I. and Shepherd T.J. (2003b). Do fluid inclusions preserve a 18 O values of hydrothermal fluids in epithermal systems over geological time? Evidence from paleo- and modern geothermal systems, Milos island, Aegean Sea, *Chem. Geol.*, 197, p.143-159.
- Naden J., Kiliass S.P., Darbyshire D.P.F., Leng M.J., Dimou E. & Cheliotis I. (2002). Seawater and Low-sulphidation Epithermal Gold Mineralisation in the Modern Aegean Arc: Fluid inclusion, Isotopic and Mineralogical Evidence, *Transactions of the Institution of Mining and Metallurgy, Series B*, 110, p.230–231.
- Naden J, Kiliass S P, Darbyshire, DBF (2005) Active geothermal systems with entrained seawater as analogues for transitional continental magmato-hydrothermal and volcanic-

- hosted massive sulfide mineralization - the example of Milos Island, Greece. *Geology*, 33, p.541-544.
- Nagao K., Kita I., Matsuda J., and Mitropoulos P. (1991) Noble gas isotope geochemistry of volcanic gases from the Aegean Island Arc. *Bull. Geol. Soc. Greece* 25, p. 33-41.
- Normark W.R., Morton J.L., Koski R.A., Clague D.A. and Delaney J.R. (1983) Active hydrothermal vents and sulfide deposits on the southern Juan de Fuca Ridge. *Geology*, 11, p.158-163.
- Ohmoto, H. (1972) Systematics of sulfur and carbon isotopes in hydrothermal ore deposits. *Econ. Geol.* 67, p.551-578.
- Oudin E. and Constantinou G. (1984) Black smoker chimney fragments in Cyprus sulphide deposits. *Nature*, 308, p.349-353.
- Pals D.W. and Spry P.G. (2003) Telluride mineralogy of the low-sulfidation epithermal Emperor gold deposit, Vatukoula, Fiji, *Mineral. Petrol.*, 79, p. 285-307
- Papanikolaou D.J. and Dermitzakis M.D. (1981) Major changes from the last stage of the Hellenides to the actual Hellenic arc and trench system. In : Intern. Symp. on the Hell. Arc and Trench (H.E.A.T.), Athens-Greece, vol.2, p. 57-73.
- Papanikolaou D.J. (1986) *Geology of Greece*, Athens University, Dept. of Geol., Section of Tectonic Geology, 250 pp.
- Papanikolaou, D., Lykoussis, V., Chronis, G., Pavlakis, P. (1988) A comparative study of neotectonic basins across the Hellenic Arc: the Messiniakos, Argolikos and Southern Evoikos Gulfs. *Basin Res.* 1, p.167–176.
- Papanikolaou, D., Lekkas, E. and Syskakis, D. (1990) Tectonic analysis of the Milos geothermal field. *Bull. Geol. Soc. Greece*, 24, 27-46. In Greek with English Abstract .
- Parr J.M., Binns R.A. and Gemmell J.B. (1996) Sulfide chimneys from the Satanic Mills site in the PACMANUS hydrothermal field, eastern Manus basin, Papua New Guinea [abs]: EOS, American Geophysical Union Transactions, Western Pacific Geophysical Meeting Supplement, 77, W120.
- Pavlakis, P. (1993) The strike slip tectonic regime at southern Aegean as implied by combined marine geophysical survey. *Bull. Geol. Soc. Greece*, 28, 253-273.
- Papazachos B.C. (1973) *Geoph. J. R. Astron. Soc.*, 33, p. 421-430.
- Papazachos B.C and Komninakis P.E. (1971) Geophysical and tectonic features of the Aegean arc. *J. Geophys. Res.* 76, p. 8517-8533.
- Papazachos B.C., Panagiotopoulos D.G. (1993) Normal faults associated with volcanic activity and deep rupture zones in the southern Aegean volcanic arc. *Bull. Geol. Soc. Greece*, vol. XXVIII/3, p. 243-252.
- Papazachos C.B, Kiratzi A.A. (1996) A detailed study of the active crustal deformation in the Aegean and surrounding area. *Tectonophysics* 253, p.129-153.
- Papazachos, B.C., Karakostas, V.G., Papazachos, C.B., Scordilis, E.M. (2000) The geometry of the Wadati - Benioff zone and lithospheric kinematics in the Hellenic arc. *Tectonophysics* 319, p.275-300.
- Pe-Piper G.G. and Piper, D.J.W. (1972) Volcanism at subduction zones; The Aegean area. *Bull. Geol. Soc. Greece* 9.
- Pe-Piper, G., Hatzipanagiotou, K. (1997) The Pliocene volcanic rocks of Crommyonia, western Greece and their implications for the early evolution of the South Aegean arc. *Geol. Mag.* 134, p.55– 66.
- Peter J.M. and Scott S.D. (1988) Mineralogy, composition and fluid inclusion microthermometry of seafloor hydrothermal deposits in the southern trough of Guaymas Basin, Gulf of California, *Can. Mineral.* 26, p.567-587.

- Petersen S., Herzig P.M., Hannington M.D. (2000) Third dimension of a presently forming VMS deposit: TAG hydrothermal mound, Mid-Atlantic Ridge, 26°N. *Mineral. Deposita*, 35, p.233-259.
- Petersen S., Herzig, P.M., Schwarz-Schampera U., Hannington M.D., Jonasson, I.R. (2004) Hydrothermal precipitates associated with bimodal volcanism in the central Bransfield Strait, Antarctica. *Mineral. Deposita*, 39, p.358-379.
- Petersen S., Herzig P.M., Hannington M.D., Jonasson I.R., and Arribas A. (2002) Submarine gold mineralization near Lihir Island, New Ireland fore-arc, Papua New Guinea. *Econ. Geol.*, v.97, p.1795-1813.
- Petersen S., Kuhn, T., Herzig P.M. and Hannington M.D. (2005) Factors controlling precious and base-metal enrichments at the ultramafic-hosted Logatchev hydrothermal field, 14°45'N on the MAR: New insights from cruise M60/3. In: Mao J. and Bierlein F.P. (eds), *Mineral deposit research: Meeting the global challenge*. Springer, Berlin, p. 679-682.
- Pflumio, C., Boulegue, J., Liakopoulos, A., Briquieu, L. (1991) Oxygen, hydrogen, strontium isotopes in the present-day and past geothermal systems of Milos Island Aegean Arc. In: Pagel, M., Leroy, J.L. (eds), *Source, Transport and Deposition of Metals*. A.A. Balkema, Rotterdam, p. 107-112.
- Pichler, T., Giggenbach, W.F., McInnes, B.I.A., Buhl, D., and Duck, B. (1999) *Econ. Geol.* 94, p.281
- Pichler, T., Veizer, J., and G.E.M. Hall (1999a) *Marine Chemistry*, 64, p.229
- Pichler T., Veizer J. (2004) The precipitation of aragonite from shallow-water hydrothermal fluids in a coral reef, Tutum Bay, Ambitle Island, Papua New Guinea. *Chem. Geology*, 207, p.31-45.
- Pinto, A.M.M., Relvas, J.M.R.S., Barriga, F.J.A.S. and Munha, J. (2005) Gold mineralization in recent and ancient volcanic-hosted massive sulfides: The PACMANUS field and the Neves Corvo deposit. In: Mao J. and Bierlein F.P. (eds), *Mineral deposit research: Meeting the global challenge*. Springer, Berlin, p.683-686.
- Plimer, I. (2000) *Milos Geological History*. KOAN Publishing House, Athens, p.262
- Pouchou JL, Pichoir F (1991) Quantitative analysis of homogeneous or stratified microvolumes applying the model "PAP". In: Heinrich KFJ, Newbury DE (eds). *Electron Probe quantitation*. Plenum Press, New York, p 31-75.
- Reyes, A.G. (1990) Petrology of Philippine geothermal systems and the application of alteration mineralogy to their assessment. *Jour. of Volcan. and Geoth. Res.*, v. 43, p.279-309.
- Reyes, A.G., Giggenbach, W.F., Saleras, J.R.M., Salonga, N.D. and Vergara, M.C. (1993). Petrology and geochemistry of Alto Peak, a vapor-cored hydrothermal system, Leyte Province, Philippines. *Geothermics Vol.*, 22, p 479-520.
- Rouxel O., Fouquet Y., Ludden JN. (2004) Copper isotope systematics of the Lucky Strike, Rainbow and Logatchev sea-floor hydrothermal fields on the Mid-Atlantic Ridge. *Econ. Geol.* 99, p. 585-600
- Rucklidge J., Stumpfl EF. (1968) Changes in the composition of petzite (Ag₃AuTe₂) during analysis by electron microprobe. *N Jahrb Mineral Monatsh*, p.61-68
- Rye, R.O., Bethke, P.M. and Wasserman, M.D. (1992) The stable isotope geochemistry of acid sulfate alteration. *Econ. Geol.*, 87, p. 225-262.
- Sack, R.O. (2000) Internally consistent database for sulfides and sulfosalts in the system Ag₂S-Cu₂S-ZnS-FeS-Sb₂S₃-As₂S₃, *Geochim. Cosmochim. Acta*, 64, p.3803-3812.

- Sack, R.O. (2005) Internally consistent database for sulfides and sulfosalts in the system $\text{Ag}_2\text{S}-\text{Cu}_2\text{S}-\text{ZnS}-\text{FeS}-\text{Sb}_2\text{S}_3-\text{As}_2\text{S}_3$: Update. *Geoch. Cosmoch. Acta*, 69, p.1157-1164.
- Sakai H., Gamo T., and Shipboard Scientific Party (1991) Hydrothermal activity in the eastern Manus basin, Bismark Sea: A brief report of the Hakuho-Marukh Cruise KH-90-3, Leg 2:Ridge Events,v.2, p.39.
- Sarano, F., Murphy R.C., Houghton B.F., and Hedenquist J.W. (1989) Preliminary observations of submarine geothermal activity in the vicinity of White island Volcano,Taupo Volcanic Zone,New Zealand: *Journal of the Royal Society of New Zealand*,v.19, p.449-459.
- Savirage H. (1846) Description geologique de l'île de Milos. *Ann. De Mines*, t. X, Paris 1846, p. 97.
- Scotney P.M., Roberts S., Herrington R.J., Boyce A.J., Burgess R. (2005) The development of volcanic hosted massive sulphide and barite-gold orebodies on Wetar Island, Indonesia. *Min. Depos.* 40, p. 76-99.
- Sewell D.M. and Wheatley C.J.V. (1994) The Lerokis and Kali Kuning submarine exhalative gold-silver-barite deposits, Wetar island, Mauku, Indonesia, *Journ. Geochem. Explor.*, v.50, p. 351-370.
- Sharp, T.G., Buseck P.R. (1993) The distribution of Ag and Sb in galena: inclusions versus solid solution. *Amer. Mineral.* 78, p.85-95.
- Sievert S.M., Brinnkhoff T., Muyzer G., Ziebis W. and Kuever J. (1999) Spatial heterogeneity of bacterial populations along an environmental gradient at a shallow submarine hydrothermal vent near milos island (Greece). *Applied and Env. Microb.*, vol. 65, N. 9, p. 3834-3842.
- Sievert S.M., Kuever J. and Muyzer G. (2000) Identification of 16S Ribosomal DNA-Defined Bacterial Populations at a Shallow Submarine Hydrothermal Vent near Milos Island (Greece). *Applied and Env. Microb.*, vol. 66, N. 7, pp. 3102-3109.
- Simeakis, C. (1985) Neotectonic evolution of Milos island complex. IGME (unpublished report), 50 pp.
- Sillitoe H. R. (1985) Ore Related Breccias in Volcanoplutonic Arcs. *Econ. Geol.*,vol. 80, p. 1467-1514.
- Sillitoe, R.H. (1995) Exploration of porphyry copper lithocaps. In: Pacific RimCongress 95, 19-22 November 1995, Auckland, New Zealand, proceedings: Carlton South, The Australasian Institute of Mining and Metallurgy, p. 527-532.
- Sillitoe RH, Hannington MD, Thompson JFH (1996) High-sulfidation deposits in the volcanogenic massive sulfide environment. *Econ. Geol.* 91, p. 204-212
- Sillitoe, R.H. (1999) Styles of High-Sulphidation Gold, Silver and Copper Mineralisation in Porphyry and Epithermal Environments *in Pacrim '99 Proceedings*, Bali, Indonesia. The Australasian Institute of Mining and Metallurgy, Melbourne, p.29-45.
- Sillitoe, R.H., and Hedenquist, J.W. (2003) Linkages between volcanotectonic settings, ore-fluid compositions, and epithermal precious-metal deposits. In: Simmons, S.F, ed., *Understanding crustal fluids: Roles and witnesses of processes deep within the earth. Giggenbach memorial volume: Society of Economic Geologists and Geochemical Society*, Special Publication.
- Skarpelis N, Koutles Th. (2004) Geology of epithermal mineralization of the NW part of Milos island, Greece. 5th Int. Symp. Eastern Mediteranean Geology, 4pp.
- Sonder, R.A. (1924) Zur Geologie und Petrographie der Inselgruppe von Milos. *Zeitschrift Vulk.*, 8, p. 181-234.

- Solomon M., Gaspar O.C. (2001) Textures of the Hellyer volcanic-hosted massive sulphide deposit, Tasmania. The aging of sulphide sediment on the sea floor. *Econ. Geol.* 96, p.1513-1534.
- Spartali E. (1994) Current exploration for epithermal gold mineralisation in post-Tertiary volcanic rocks, Milos island, Greece. MSc. Thesis, University of London.
- Stoffregen, R. (1987) Genesis of acid sulfate alteration and Au-Cu-Ag mineralization at Summitville, Colorado. *Econ. Geol.*, v.82, p. 1575-1591.
- Stewart A.L. & McPhie J. (2003) Setting of epithermal Au deposits in a modern volcanic island arc setting, Milos, Greece: Implications for mineral exploration. In: Eliopoulos D. et al. (eds) *Mineral Exploration and Sustainable Development*, 1, p.533-536, Millpress, Rotterdam.
- Stewart A.L. & McPhie J. (2004) Facies architecture of the submarine to subaerial volcanic succession on Milos, Greece. 17 AGC Hobart- Tasmania. Abstracts, in p. 293.
- Stewart A.L. & McPhie J. (2005) Facies architecture and Late Pliocene-Pleistocene evolution of a felsic volcanic island, Milos, Greece. *Bull. Volcanol.*, 24p.
- Swarz-Schampera U., Herzig P.M., Hannington M.D. (2001) Shallow submarine epithermal style As-Sb-Hg-Au mineralization in the active Kermadec arc, New Zealand. In : Piestrzynski U., et al., (Eds.). *Mineral deposits at the Beginning of the 21st Century*. Balkema, Rotterdam, pp. 333-335.
- Thanassoulas K. (1983a) Geoelectrical reconnaissance survey in Western Milos. I.G.M.E.-Greece. Rep. 3777.
- Tivey M.K., Delaney J.R. (1986) Growth of large sulphide structures on the Endeavour Segment of the Juan de Fuca Ridge. *Earth Plan Sci Lett.* 77, p. 303-317.
- Tivey M.K., Humphris S.E., Thompson G., Hannington M.D. and Rona P.A. (1995) Deducing patterns of fluid flow and mixing within the TAG active hydrothermal mound using mineralogical and geochemical data. *J. Geophys. Res.* 100, p.12527-12555.
- Tomkins, A.G., and Mavrogenes J.A. (2002) Mobilization of gold as a polymetallic melt during pelite anatexis at the Challenger deposit, South Australia: a metamorphosed Archean gold deposit. *Econ. Geol.*, 97, p.1249-1271.
- Tsokas G. N. (1985) A geophysical study of Milos and Kimolos islands. Phd Thesis Univ. Thessaloniki, Greece.
- Tsokas G. N. (1996) Interpretation of the Bouguer anomaly of milos island (Greece). *Journal of volc. and Geoth. Res.* 1600, p. 1-19.
- Ulrich T., Golding S.D., Kamber B.S., Zaw K. and Taube A. (2002) Different mineralization styles in a volcanic-hosted ore deposit: the fluid and isotopic signatures of the Mt Morgan Au-Cu deposit, Australia. *Ore Geol. Rev.*, 22, p. 61-90.
- Valsami-Jones E., Baltatzis E., Magganas A., Bailey E.H., Alexander J.L., Ragnarsdottir K.V. and Kemp A.J. (1998). The geochemistry of hydrothermal vent waters from Milos Island, Hellenic Volcanic Arc. *Mineral. Magazine*, 62a, p. 1565-1566.
- Valsami-Jones E., Baltatzis E., Bailey E.H., Boyce A.J., Alexander J.L., Magganas A., Anderson L., Waldron S., Ragnarsdottir K.V. (2005) The geochemistry of fluids from an active shallow submarine hydrothermal system: Milos island, Hellenic Volcanic Arc. *J. Volc. Geother. Res* 148, p.130-151.
- Van Hinsbergen D.J.J., E. Snel, S.A. Garstman, M. Marunteanu, C.G. Langereis, M.J.R. Wortel, J.E. Meulenkaamp (2004) Vertical motions in the Aegean volcanic arc: evidence for rapid subsidence preceding volcanic activity on Milos and Aegina. *Marine Geology* 209, p. 329–345

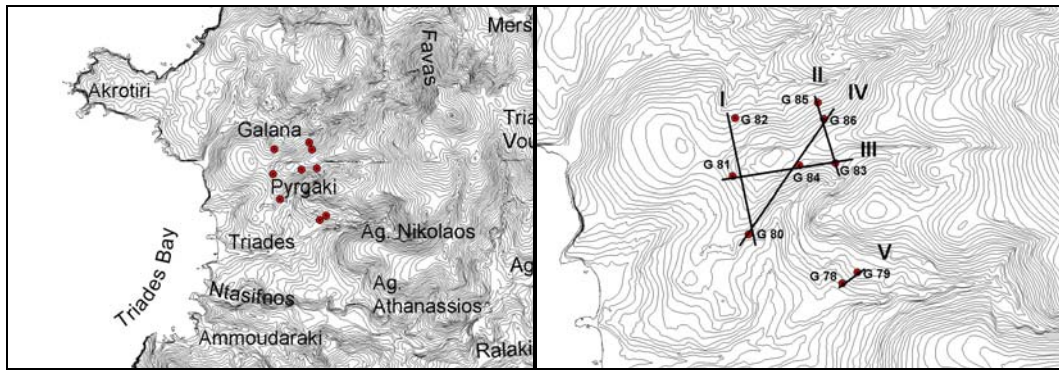
- Van Hinsbergen D.J.J., Langereis C.G., Meulenkamp J.E. (2005) Revision of the timing, magnitude and distribution of Neogene rotations in the western Aegean region. *Tectonophysics* 396, p.1-34.
- Vavelidis M. (1995) Framboidal Pyrite from the Kuroko-type barite Mineralization of the Katsimouti area, Milos Island, Greece. *Chem.Erde* 55, p.281-294.
- Vavelidis, M., V. Melfos. 1997. Two plumbian tetrahedrite-tennantite occurrences from Maronia area (Thrace) and Milos island (Aegean sea, Greece). *Eur. J. Mineral.*, 9, p.653-657.
- Vavelidis, M., Melfos, V. (1998) Fluid inclusion evidence for the origin of the barite silver-gold-bearing Pb-Zn mineralization of the Triades area, Milos Island, Greece. *Bull. Geol. Soc.Greece* 32 3, p.137-144.
- Vikentyev, I.V. (2006) Precious metal and telluride mineralogy of large volcanic-hosted massive sulphide deposits in the Urals. *Mineral. Petrol.*, 87, 305-326.
- Voreadis G. and Mourabas (1935) The silver-bearing ores of Milos. *Rep. Geol. Surv. Greece*, No. 22, 30pp.
- Voreadis G. (1956) The outcropping of kaolinite deposits at the area of Kondaros-Tria Pigadia on Milos. *Rep. Geol. Surv. Greece*, T, p. 157-180.
- Voudouris P. and Alfieris D. (2004) Ore mineralogy and evolution of Te-rich magmatic-hydrothermal systems in northeastern Greece. In: Cook N, Ciobanu CL (eds) *Au-Ag-telluride deposits of the Golden Quadrilateral, Apuseni Mts., Romania, IAGOD Guidebook Ser 12*, 256-259
- Voudouris, P. and Alfieris, D. (2005) New porphyry-Cu±Mo occurrences in northeastern Aegean/Greece: Ore mineralogy and transition to epithermal environment. In: Mao J. and Bierlein F.P. (eds), *Mineral deposit research: Meeting the global challenge*. Springer, Berlin, pp. 473-476.
- Voudouris, P. (2006) A comparative mineralogical study of Te-rich magmatic-hydrothermal systems in northeastern Greece, *Miner. Petrol.* 87, p.241-275.
- Yang K, Scott S.D. (1996) Possible contribution of a metal-rich magmatic fluid to a sea-floor hydrothermal system. *Nature* 383, p. 420-423.
- Yang K, Scott S.D. (2002) Magmatic degassing of volatiles and ore metals into a hydrothermal system on the modern sea-floor of the eastern Manus back-arc basin, western Pacific. *Econ Geol* 97, p. 1079-1100.
- Wetzenstein, W. (1969) Die bentonit lagestaetten im ostteil der insel Milos Griechenland und ihre mineralogische zusammensetzung. Stuttgart, Phd Thesis.
- Wetzenstein, W. (1975). Tektonik und Metallogeneese der Insel Milos Kykladen. *Bull. Geol. Soc. Greece* 12, 31-39.
- Stuben, D., Glasby, G.P. (1999) Geochemistry of shallow submarine hydrothermal fluids from Paleohori Bay, Milos, Aegean Sea. *Exploration and Mining Geology* 8, 273-287.
- White N.C. and Hedenquist J.W. (1995) Epithermal gold deposits: Styles, characteristics and exploration. *SEG Newsletter*, 23, p. 9-13.
- Williams, N.C., and Davinson G.J. (2004) Possible submarine advanced argillic alteration at the Basin Lake Prospect, western Tasmania, Australia. *Econ. Geol.* 99, p. 987-1002.
- Wright, R. (1978) Neogene paleobathymetry of the Mediterranean basen on benthic foraminifers from DSDP leg 42A. In: Hsu, L., Montadert, L., et al. (Eds.), *Initial Reports of the Deep Sea Drilling Project XLII*, p. 837- 846.
- Wright I.C., de Ronde C.E.J., Faure K., Gamble J.A. (1998) Discovery of hydrothermal sulfide mineralization from southern Kermadec arc volcanoes (SW Pacific). *Earth Plan. Sci. Lett.* 164, p. 335-343.

APPENDIXES

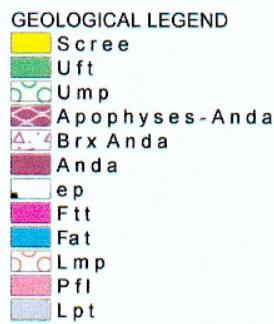
Appendix I	: Geological Sections	pp. 12
Appendix II	: Microprobe Analyses	pp. 7
Appendix III	: Equilibrium Constants Used for the Construction of the Phase Diagrams	pp. 2
Appendix IV	: Trace Elements Statistical Elaboration	pp. 45

APPENDIX I

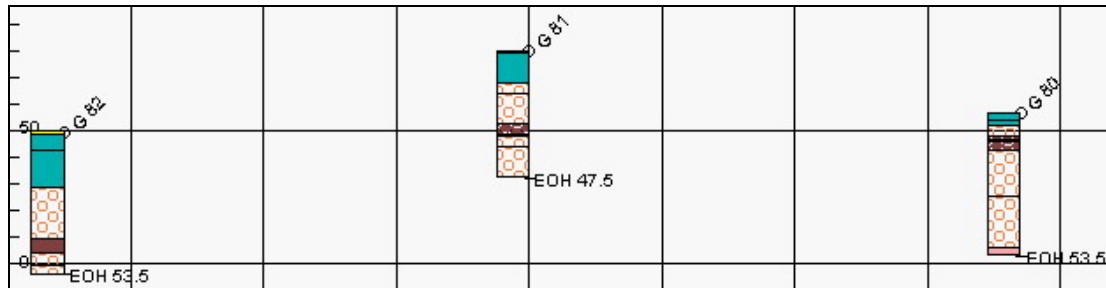
Triades - Pyrgaki - Ag. Nikolaos geological sections through drill holes data from 1972 drilling campaign.



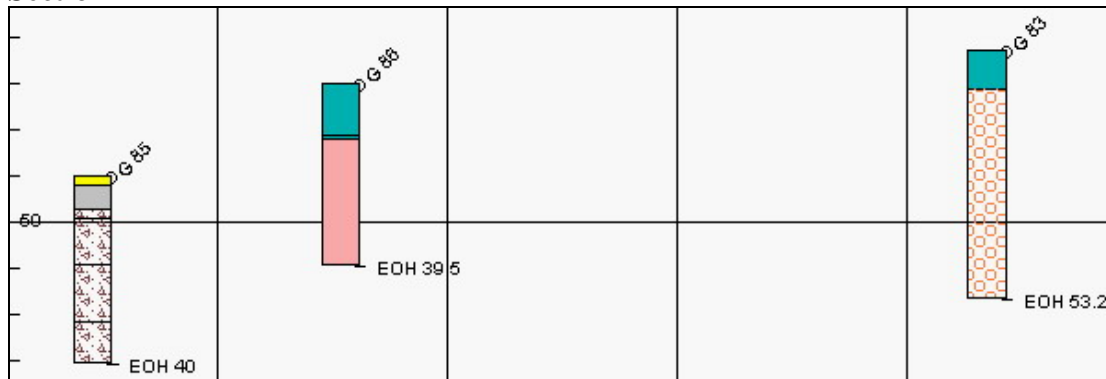
Location of the drill holes and geological sections through them at Triades-Pyrgaki-Ag. Nikolaos subareas.



Section I



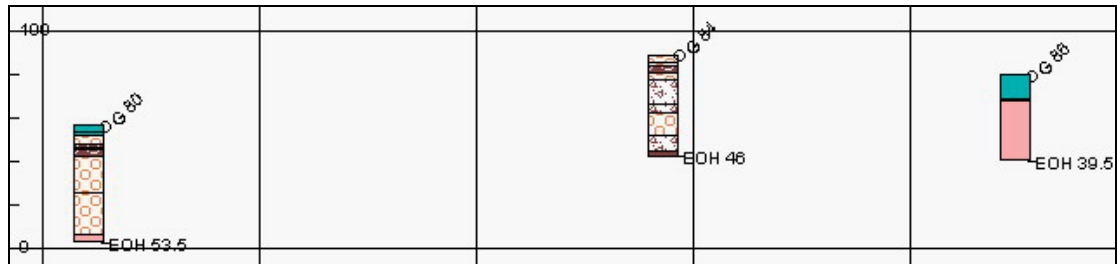
Section II



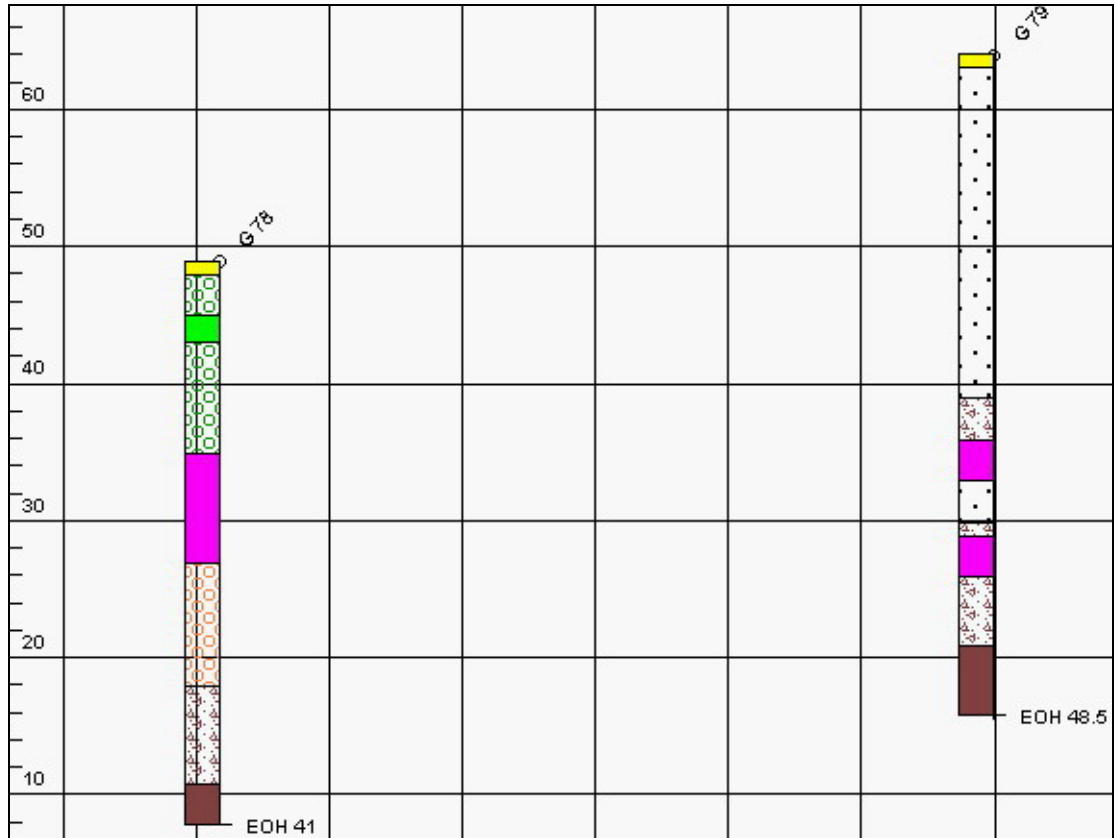
Section III



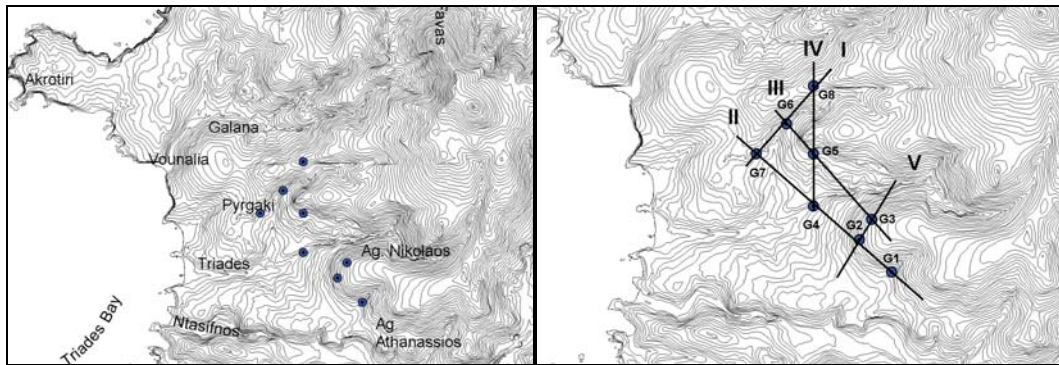
Section IV



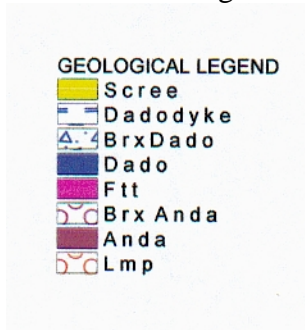
Section V



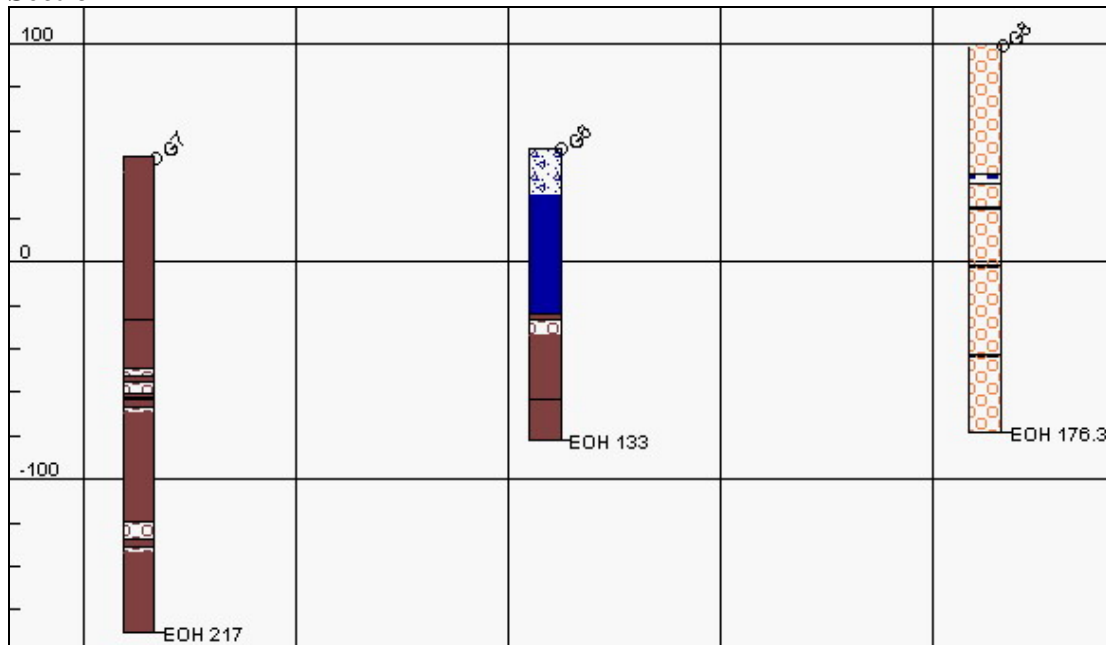
Triades – Ag. Athanassios - Ag. Nikolaos geological sections through drill holes data from 1992 drilling campaign.



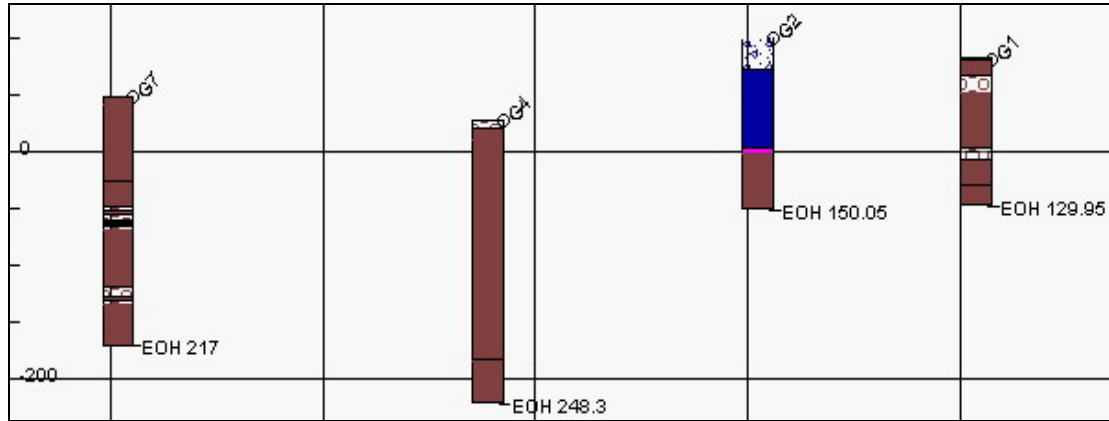
Location of the drill holes and geological sections through them at Triades-Ag. Athanassios-Ag. Nikolaos subareas.



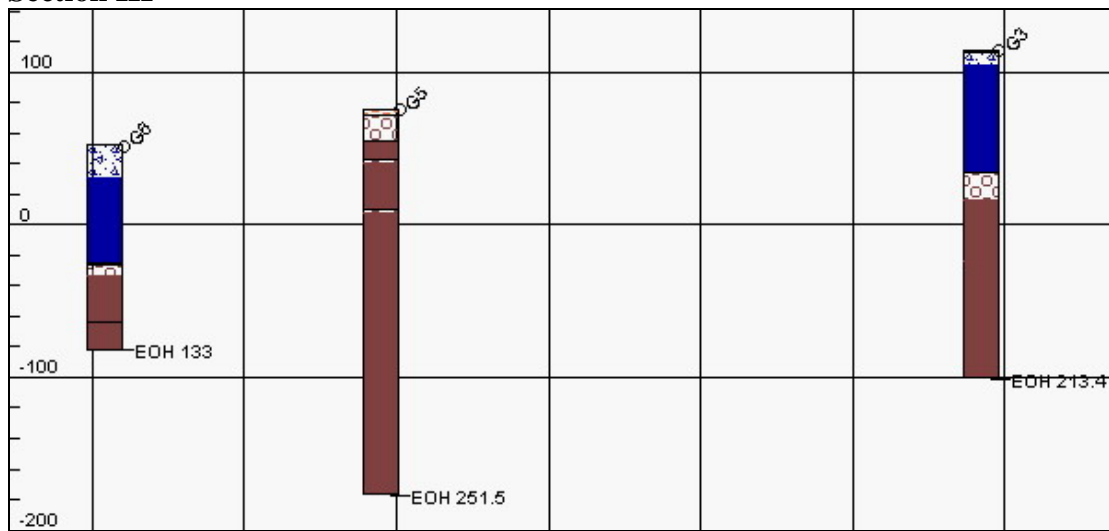
Section I



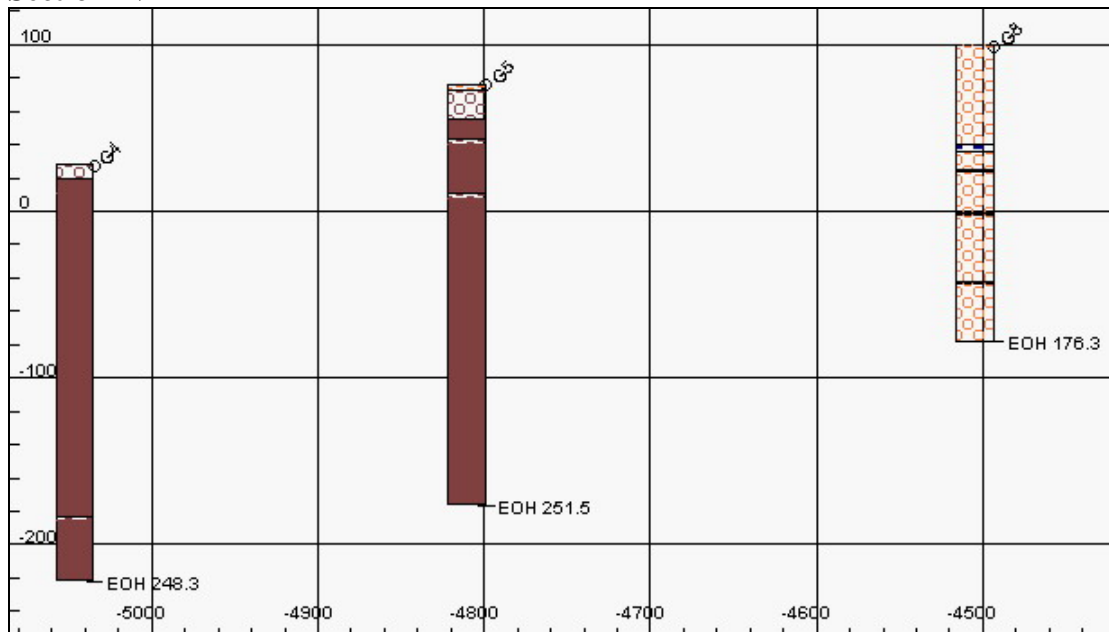
Section II



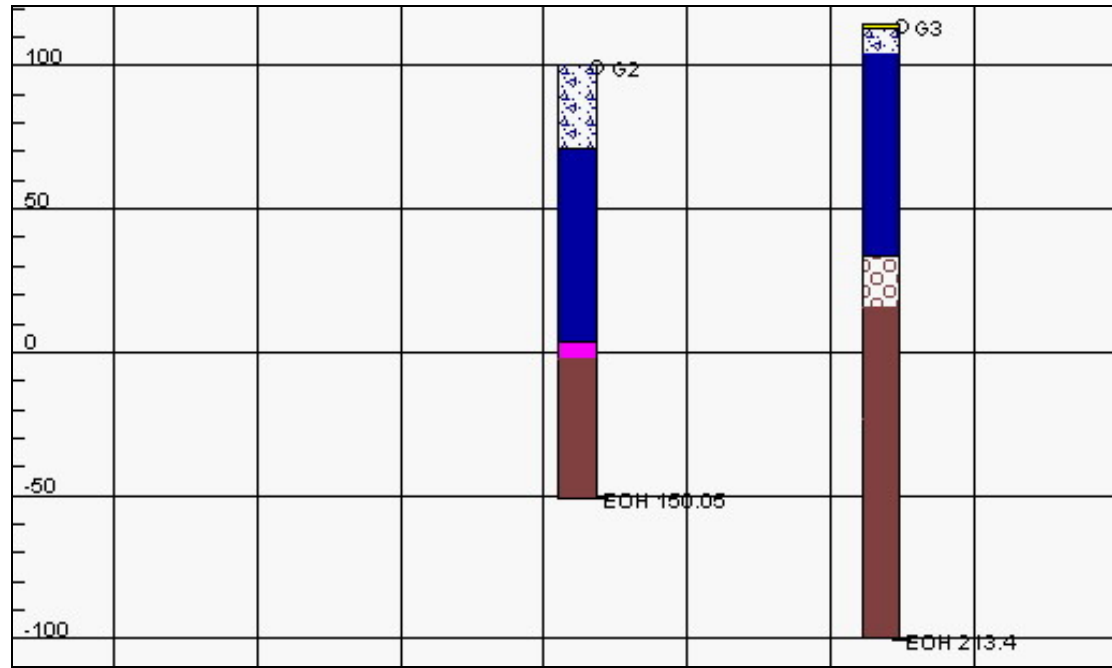
Section III



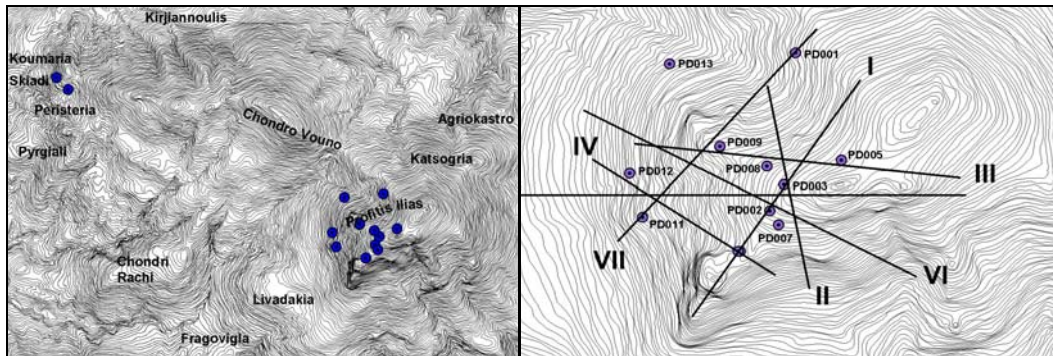
Section IV



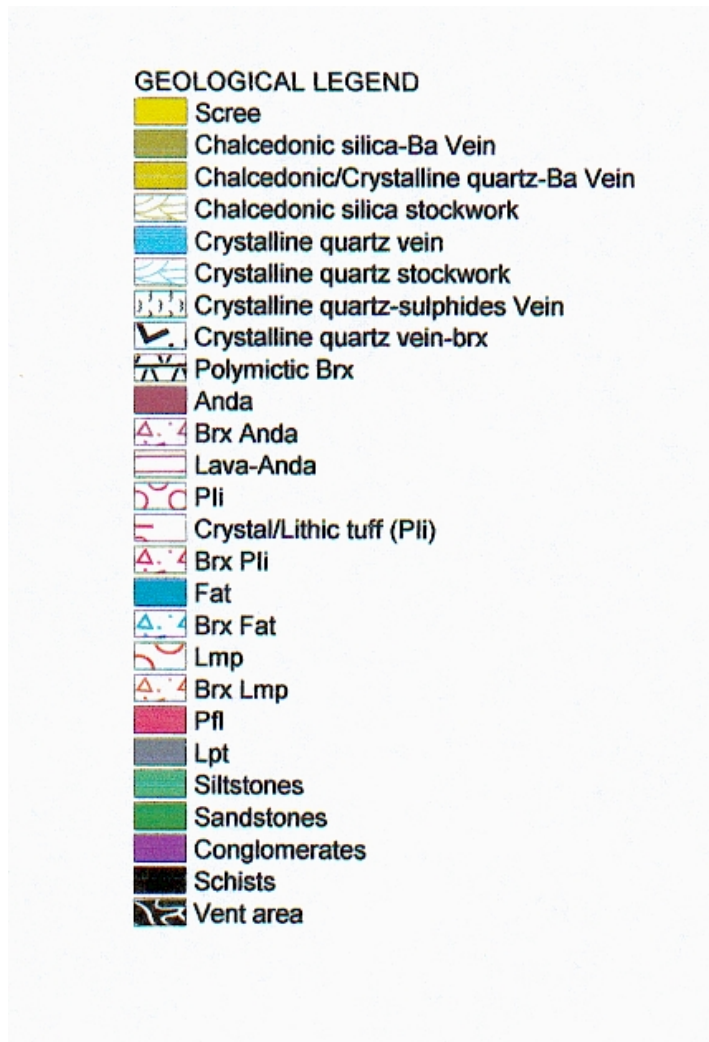
Section V



Profitis Ilias & Koumaria geological sections through diamond drill holes data from 1995 drilling campaign.

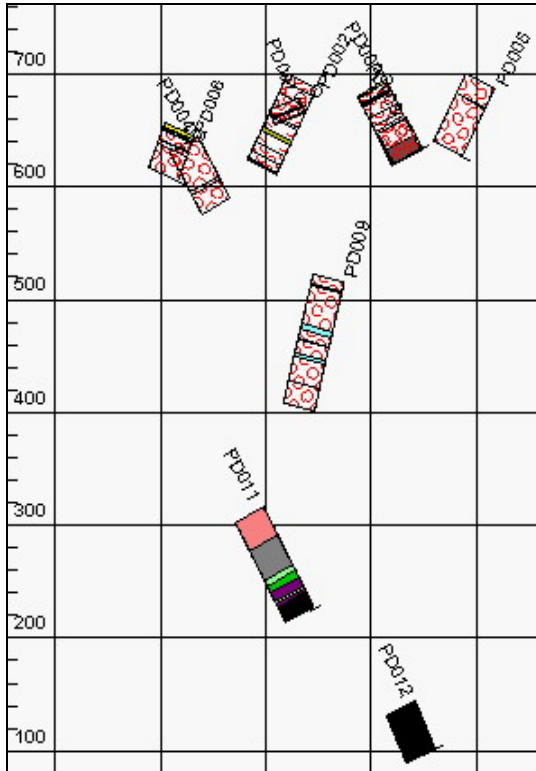


Location of the drill holes at Profitis Ilias and Koumaria, and geological sections through the Profitis Ilias subarea.

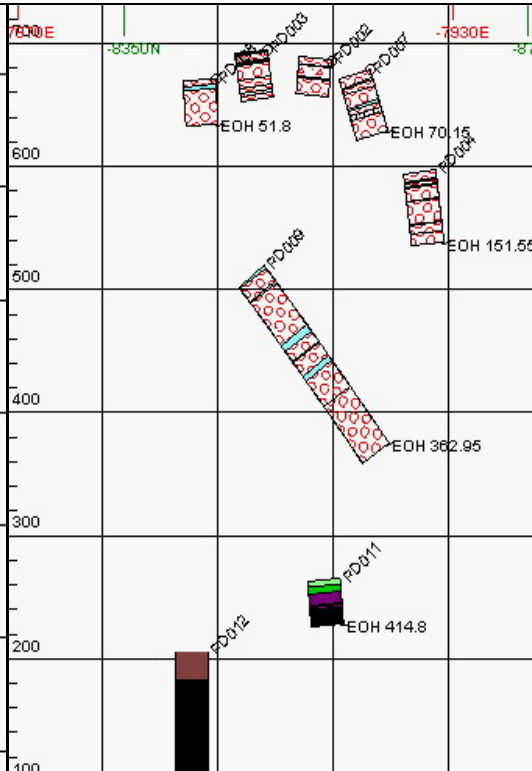


Profitis Ilias geological sections :

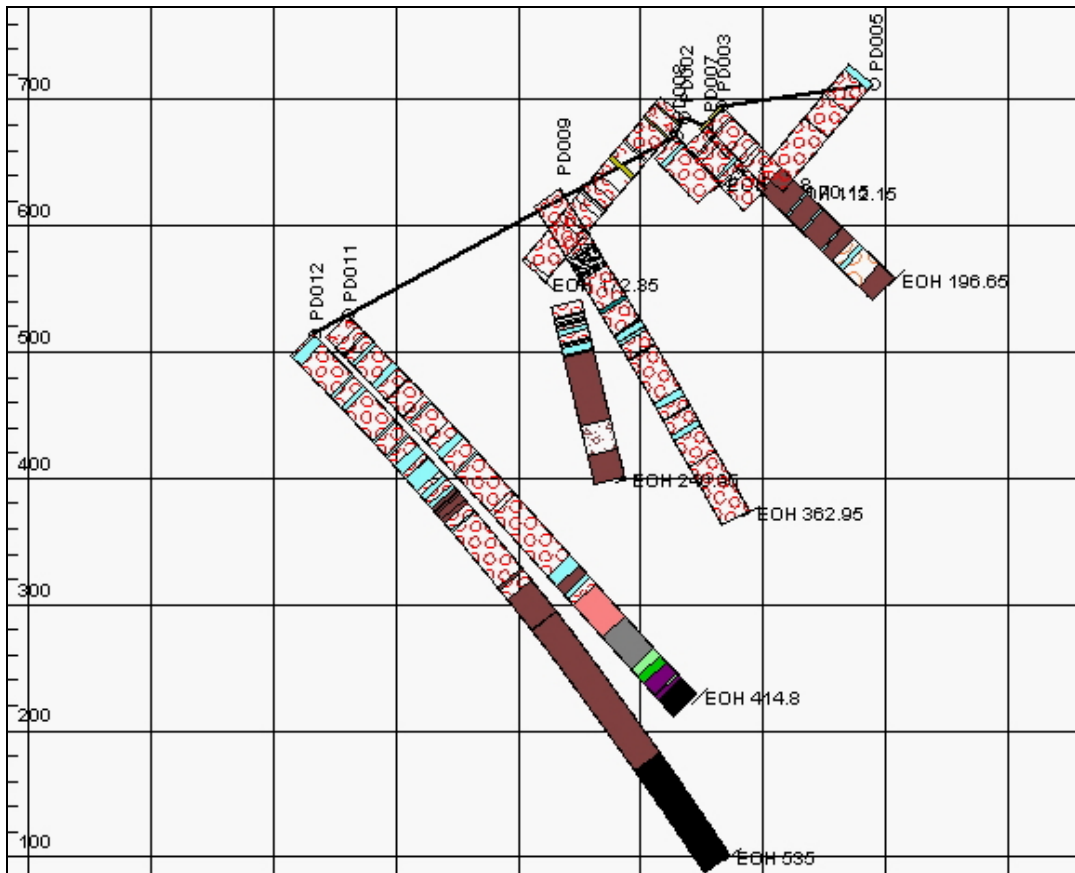
Section I



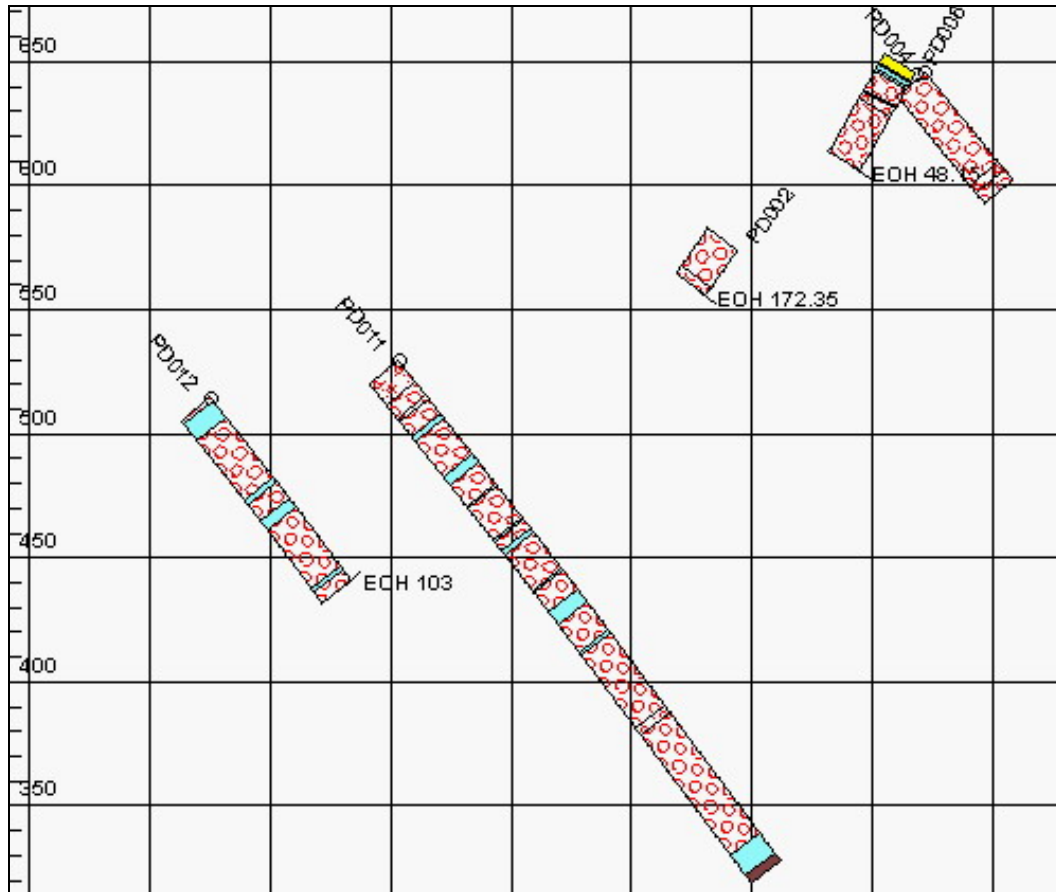
Section II



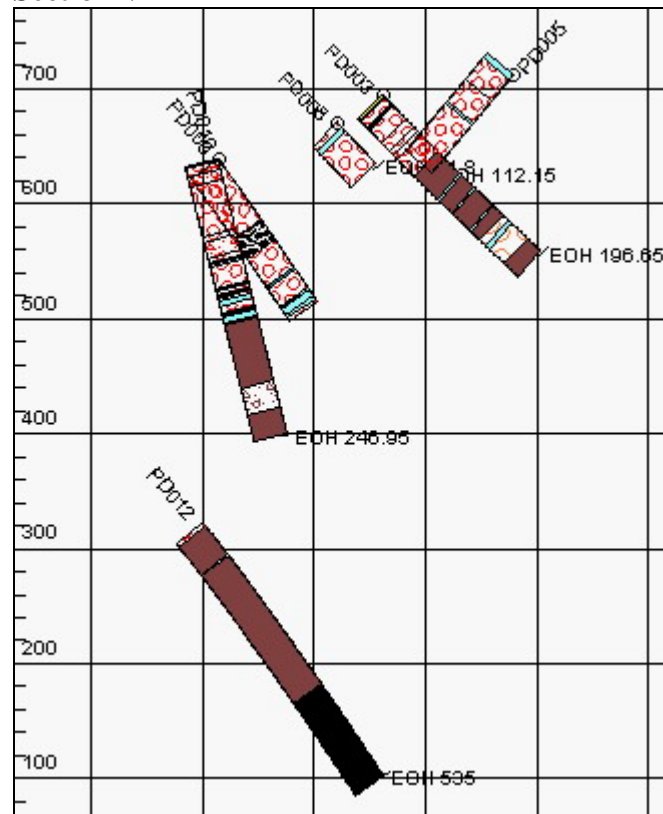
Section III



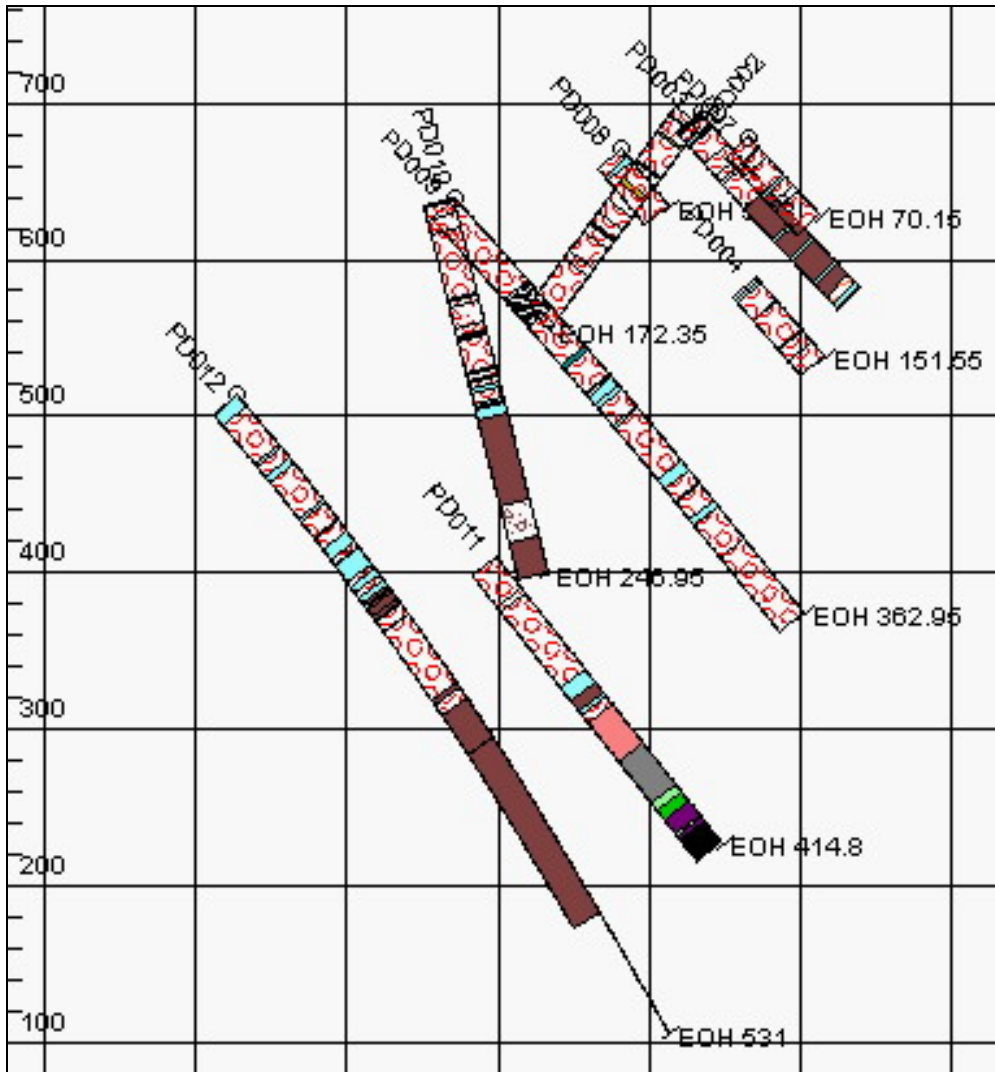
Section IV



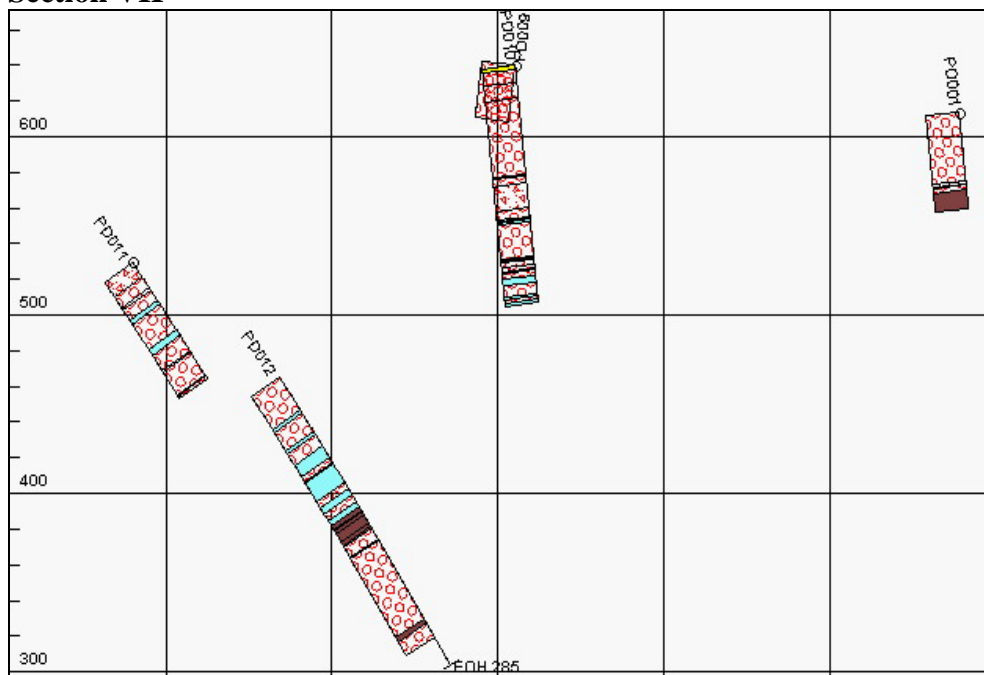
Section V



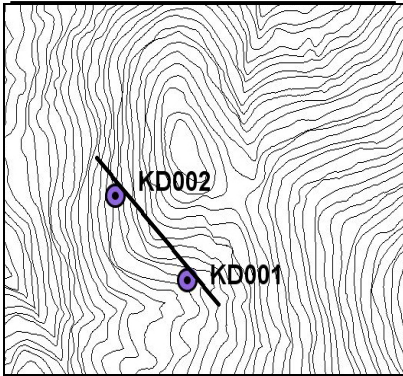
Section VI



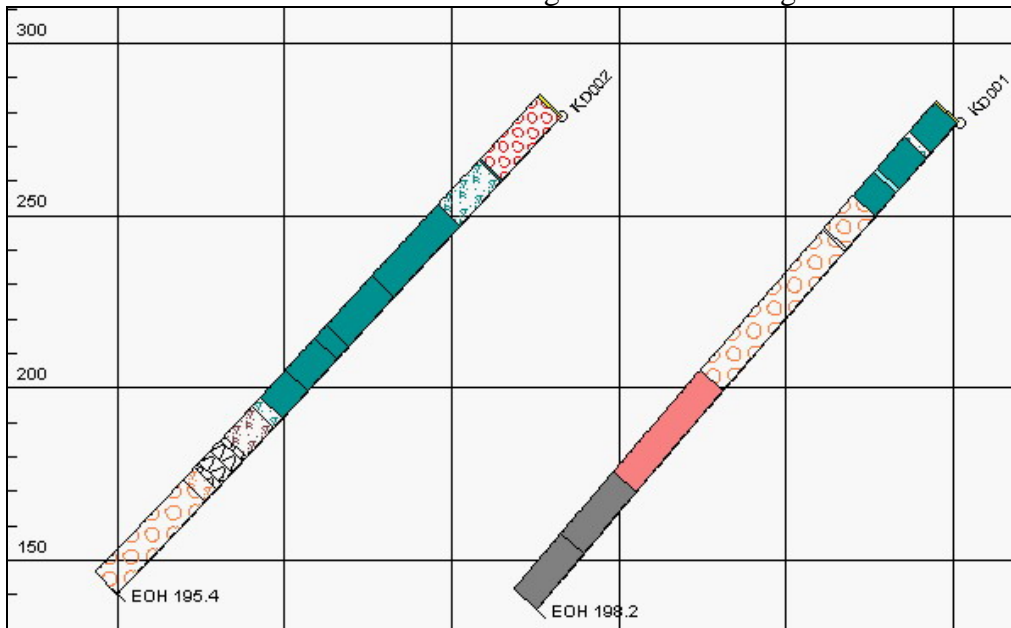
Section VII



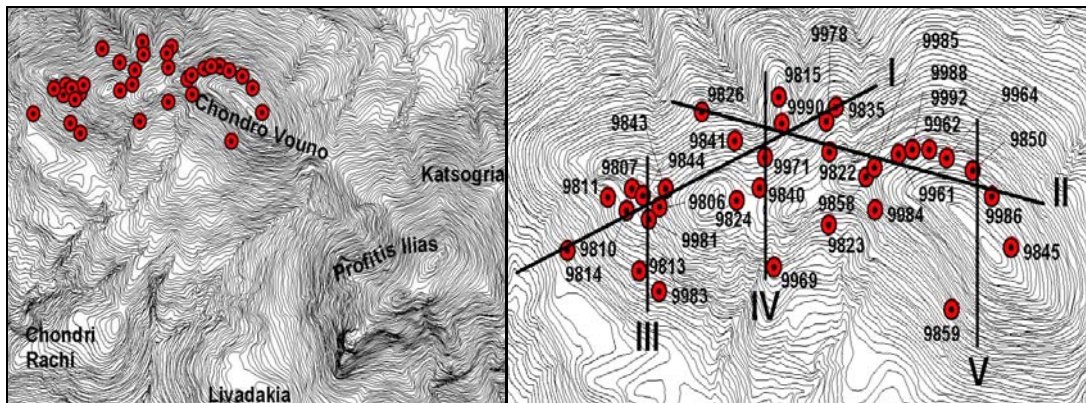
Koumaria geological sections :



: Geological section through Koumaria.



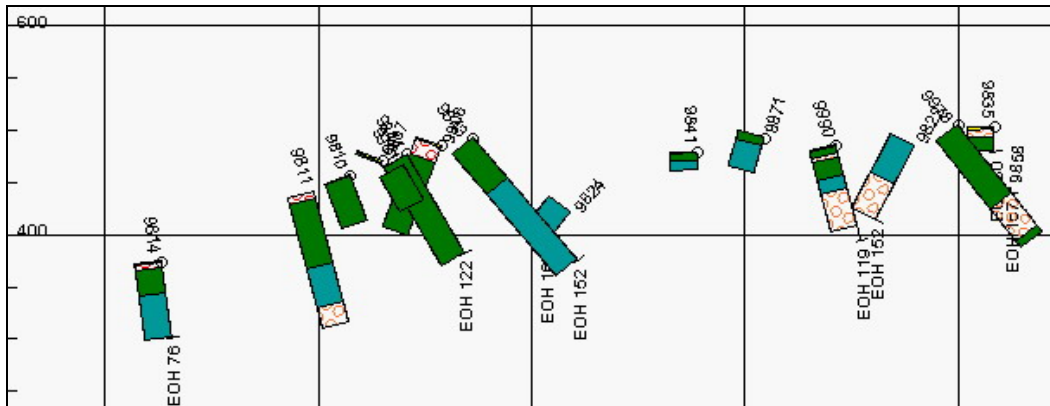
Chondro Vouno geological sections through RC drill holes data from 1998-2000 drilling campaign.



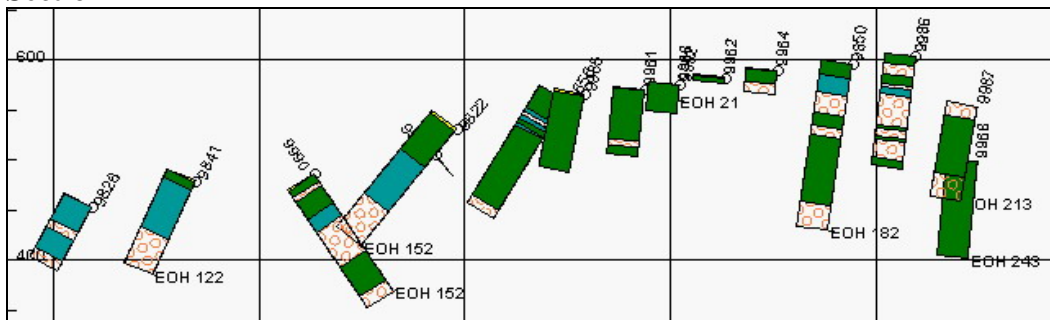
GEOLOGICAL LEGEND

- Scree
- Pli
- Fat
- Lmp
- Anda
- Rhyda

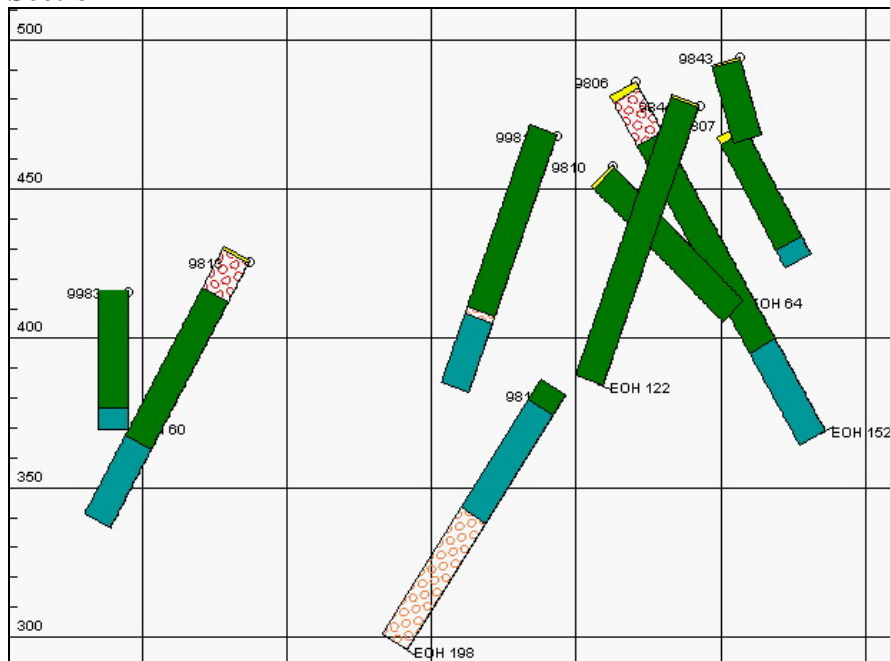
Section I



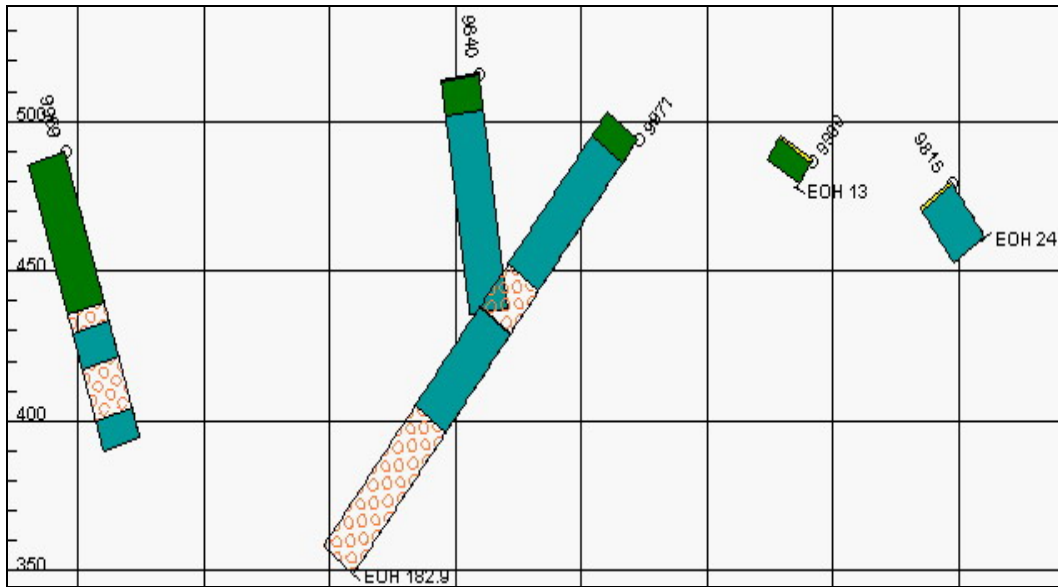
Section II



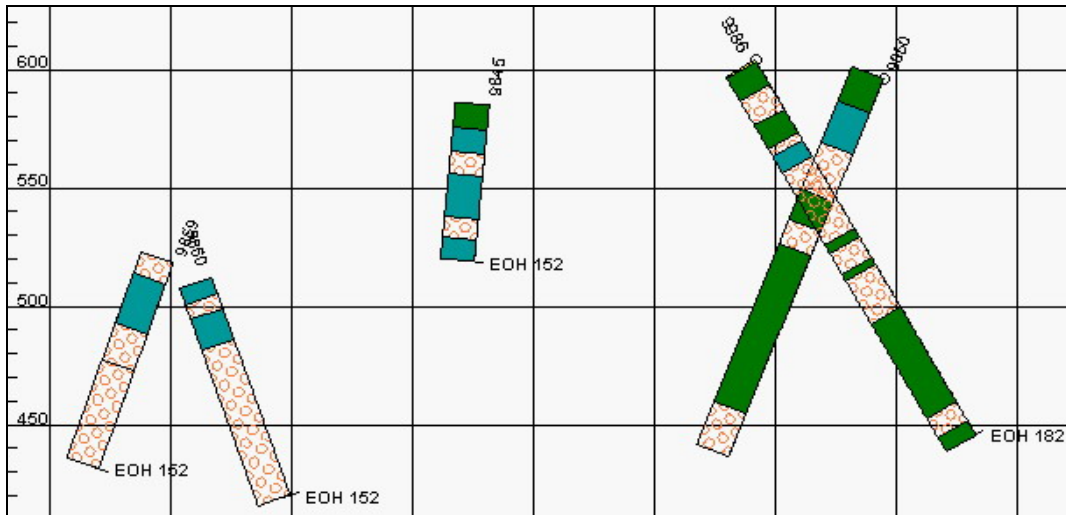
Section III



Section IV



Section V



The geological sections have been performed through using the Interdex software programme (developed by the Australian company Visidata Pty Ltd and now acquired by Gemcom software International Inc.-Canada). The location maps have been performed through using Arcview (v. 3.2) software (ESRI corporation) from USA.

APPENDIX II

Representative microprobe analyses of tetrahedrite-group
minerals from **Chondro Vouno-Profitis Ilias**

wt%	1	2	3	4	5	6
Cu	32.77	32.74	33.16	29.71	33.29	31.09
Ag	4.87	5.90	5.39	7.60	5.16	6.15
Fe	1.56	1.44	1.22	1.31	1.28	1.45
Zn	7.51	8.19	8.58	8.56	8.86	8.95
Sb	27.21	26.93	27.05	28.69	26.23	27.04
As	1.84	1.39	1.88	0.92	2.13	1.79
Hg	n.a.	n.a.	n.a.	n.a.	n.a.	n.a.
Pb	n.a.	n.a.	n.a.	n.a.	n.a.	n.a.
S	23.39	23.44	23.39	23.11	23.85	23.51
	99.14	100.04	100.66	99.91	100.83	99.98
atoms	29	29	29	29	29	29
Cu	8.897	8.831	8.894	8.161	8.848	8.404
Ag	0.777	0.937	0.853	1.230	0.806	0.980
Fe	0.481	0.444	0.371	0.409	0.386	0.447
Zn	1.984	2.149	2.239	2.288	2.288	2.352
Sb	3.857	3.790	3.787	4.112	3.637	3.814
As	0.423	0.319	0.426	0.215	0.479	0.409
Hg	n.a.	n.a.	n.a.	n.a.	n.a.	n.a.
Pb	n.a.	n.a.	n.a.	n.a.	n.a.	n.a.
S	12.583	12.531	12.432	12.583	12.557	12.592

1-6: Zincian tetrahedrite included in sphalerite.

Representative microprobe analyses of tetrahedrite-group minerals from **Triades**

wt%	1	2	3	4	5	6	7	8	9	10	11	12	13	14	15	16	17	18	19	20	21	
Cu	33.77	32.16	30.95	30.78	41.23	40.31	34.14	40.69	40.39	40.36	36.93	29.51	40.73	40.89	39.83	40.42	41.33	41.79	41.65	42.06	41.89	
Ag	5.63	7.19	7.52	7.34	1.40	1.35	5.57	0.86	1.10	0.64	2.65	9.98	0.91	0.79	0.72	0.47	0.50	0.34	0.64	0.38	0.33	
Fe	0.11	0.08	0.07	0.06	0.46	0.37	0.09	0.12	0.09	0.27	0.11	2.36	0.66	0.78	0.12	0.16	0.61	0.99	0.63	0.34	0.19	
Zn	7.20	6.87	6.32	6.33	8.57	8.89	7.14	8.14	8.82	10.89	10.37	8.26	7.60	6.94	10.33	8.37	8.17	8.03	8.28	8.31	8.62	
Sb	25.67	26.80	27.09	26.76	3.36	5.51	24.42	1.89	2.05	2.16	14.73	25.63	9.68	7.88	0.13	0.39	4.76	0.97	0.49	0.02	0.03	
As	2.89	1.94	1.32	1.47	18.53	16.85	3.52	19.26	19.09	19.63	10.50	2.23	14.34	15.44	20.81	20.73	17.69	20.40	20.48	20.86	21.09	
Hg	n.d.	n.d.	0.02	0.03	0.02	0.02	0.06	n.d.	n.d.	0.06	0.01	n.d.	0.13	0.29	n.d.	0.06	0.07	0.11	0.02	n.d.	n.d.	
Pb	n.d.	n.d.	n.d.	n.d.	n.d.	n.d.	n.d.	n.d.	n.d.	n.d.	n.d.	n.d.	n.d.	n.d.	n.d.	n.d.	n.d.	n.d.	n.d.	n.d.	0.02	n.d.
S	24.52	24.18	23.92	24.07	27.91	27.64	24.80	27.36	27.85	28.19	26.28	24.05	27.00	27.38	28.64	28.33	27.89	28.30	28.52	28.67	28.33	
	99.81	99.21	97.20	96.83	101.48	100.94	99.74	98.32	99.39	102.19	101.56	102.02	101.06	100.40	100.57	98.92	101.00	100.93	100.71	100.66	100.47	
atoms	29	29	29	29	29	29	29	29	29	29	29	29	29	29	29	29	29	29	29	29	29	29
Cu	9.012	8.740	8.608	8.563	9.667	9.573	9.053	9.770	9.587	9.341	9.124	7.848	9.828	9.837	9.248	9.532	9.740	9.707	9.666	9.736	9.739	
Ag	0.884	1.150	1.231	1.202	0.193	0.189	0.867	0.122	0.153	0.088	0.385	1.563	0.130	0.112	0.098	0.065	0.070	0.046	0.087	0.051	0.045	
Fe	0.034	0.025	0.022	0.020	0.122	0.099	0.027	0.033	0.026	0.072	0.030	0.714	0.182	0.214	0.031	0.044	0.163	0.261	0.167	0.090	0.050	
Zn	1.867	1.815	1.707	1.710	1.952	2.052	1.839	1.900	2.035	2.450	2.489	2.136	1.783	1.623	2.331	1.918	1.871	1.813	1.868	1.869	1.948	
Sb	3.578	3.801	3.932	3.885	0.412	0.683	3.379	0.237	0.254	0.260	1.899	3.557	1.219	0.990	0.016	0.048	0.585	0.117	0.059	0.002	0.004	
As	0.654	0.446	0.312	0.346	3.684	3.394	0.792	3.921	3.843	3.853	2.201	0.503	2.936	3.150	4.097	4.146	3.535	4.018	4.032	4.094	4.159	
Hg	0.000	0.000	0.002	0.003	0.002	0.002	0.005	0.000	0.000	0.004	0.001	0.000	0.010	0.022	0.000	0.005	0.005	0.008	0.002	0.000	0.000	
Pb	0.000	0.000	0.000	0.000	0.000	0.000	0.000	0.000	0.000	0.000	0.000	0.000	0.000	0.000	0.000	0.000	0.000	0.000	0.000	0.000	0.000	0.000
S	12.971	13.022	13.185	13.271	12.968	13.008	13.035	13.018	13.103	12.933	12.870	12.678	12.913	13.053	13.179	13.242	13.031	13.029	13.119	13.154	13.055	

1-7: (VA50); 8-12: (VA31); 13-21: (VA31/1).

Representative microprobe analyses of tetrahedrite-group minerals from **Galana**

wt%	1	2	3	4	5	6	7	8	9	10	11	12	13	14
Cu	42.08	42.42	40.90	41.16	41.32	41.45	41.63	41.71	36.64	35.51	35.89	33.71	35.49	35.08
Ag	0.06	0.04	0.06	0.04	0.05	0.03	0.06	0.08	2.09	2.24	2.29	2.75	1.87	1.81
Fe	0.35	0.36	0.27	0.32	0.28	1.40	1.01	1.52	0.62	0.41	0.04	0.33	0.19	1.32
Zn	7.96	8.18	7.80	7.68	7.77	8.63	9.16	8.24	7.24	6.94	8.57	10.23	10.94	7.29
Sb	1.45	1.56	1.66	3.18	1.85	0.00	0.02	0.00	23.55	25.94	28.56	25.22	24.57	20.99
As	19.66	19.88	19.58	18.67	19.30	20.84	20.92	20.71	4.48	2.85	1.64	3.36	3.03	7.19
Hg	0.03	0.04	0.05	n.d	0.07	n.d	n.d	0.03	n.d	n.d	n.d	n.d	n.d	n.d
Pb	n.d	n.d	n.d	n.d	n.d	n.d	n.d	n.d	n.d	n.d	n.d	n.d	n.d	n.d
S	28.12	27.94	28.02	27.93	27.98	28.10	28.46	28.11	25.61	25.04	23.71	24.35	24.38	25.53
	99.72	100.42	98.34	98.98	98.63	100.45	101.25	100.40	100.22	99.12	100.68	99.96	100.71	99.46
atoms	29	29	29	29	29	29	29	29	29	29	29	29	29	29
Cu	9.886	9.930	9.733	9.794	9.819	9.631	9.592	9.694	9.628	9.605	9.558	8.894	9.248	9.042
Ag	0.009	0.006	0.008	0.006	0.006	0.004	0.008	0.011	0.325	0.357	0.360	0.426	0.287	0.276
Fe	0.095	0.096	0.074	0.088	0.077	0.369	0.263	0.401	0.186	0.125	0.012	0.099	0.055	0.386
Zn	1.818	1.862	1.805	1.776	1.795	1.949	2.052	1.862	1.850	1.824	2.219	2.625	2.772	1.827
Sb	0.178	0.191	0.206	0.395	0.230	0.000	0.002	0.000	3.231	3.663	3.970	3.474	3.344	2.822
As	3.918	3.947	3.952	3.768	3.890	4.106	4.088	4.083	0.998	0.653	0.371	0.751	0.670	1.572
Hg	0.002	0.003	0.003	0.000	0.006	0.000	0.000	0.002	0.000	0.000	0.000	0.000	0.000	0.000
Pb	0.000	0.000	0.000	0.000	0.000	0.000	0.000	0.000	0.000	0.000	0.000	0.000	0.000	0.000
S	13.094	12.965	13.218	13.173	13.178	12.941	12.995	12.947	12.786	12.731	12.516	12.731	12.589	13.038

1-8: (VA51); 9-11: (GAL2); 12-14: (GAL1).

Representative microprobe analyses of tetrahedrite-group minerals from **Katsimoutis-Kondaros**

wt%	1	2	3	4	5	6	7	8	9	10	11	12	13	14	15
Cu	32.05	25.30	32.50	33.04	31.94	32.10	31.38	31.83	32.12	32.47	26.32	26.07	17.93	23.95	26.32
Ag	6.69	16.16	5.70	5.55	7.63	6.71	7.61	6.93	5.90	5.53	15.32	15.18	29.39	17.54	14.62
Fe	3.38	2.41	0.34	0.76	0.73	0.37	0.51	0.98	0.42	0.35	1.12	1.22	0.70	1.26	4.45
Zn	0.45	3.14	6.71	5.76	6.33	6.95	6.76	5.87	6.52	6.66	7.65	7.38	2.91	4.76	4.96
Sb	26.48	28.12	29.26	29.45	29.28	29.09	28.34	29.15	28.95	29.09	26.06	26.30	26.16	27.55	26.87
As	0.00	0.00	0.95	0.99	0.99	1.02	1.02	0.94	0.89	1.07	1.94	1.97	0.71	0.86	0.57
Hg	0.00	0.00	0.02	0.14	0.04	0.00	0.00	0.03	0.00	0.00	0.00	0.00	n.a.	n.a.	0.00
Pb	7.48	2.38	0.56	0.00	0.00	0.00	0.24	0.00	0.00	0.00	0.00	0.00	n.a.	n.a.	0.00
S	22.18	22.09	23.54	23.84	23.14	23.44	23.30	23.22	23.18	23.24	22.54	22.41	21.49	22.57	21.91
	99.18	99.51	99.58	99.73	100.14	99.69	99.19	98.93	97.98	98.49	101.02	100.52	99.29	98.48	99.71
atoms	29	29	29	29	29	29	29	29	29	29	29	29	29	29	29
Cu	9.213	7.357	8.918	9.012	8.783	8.804	8.673	8.811	8.937	8.986	7.339	7.314	5.434	6.933	7.427
Ag	1.134	2.770	0.922	0.892	1.237	1.085	1.240	1.129	0.967	0.901	2.516	2.506	5.245	2.991	2.430
Fe	1.262	0.797	0.105	0.236	0.231	0.113	0.160	0.308	0.133	0.110	0.357	0.389	0.240	0.414	1.430
Zn	0.128	0.887	1.790	1.525	1.692	1.852	1.815	1.579	1.762	1.792	2.072	2.012	0.857	1.339	1.363
Sb	3.973	4.269	4.191	4.191	4.204	4.164	4.088	4.212	4.204	4.202	3.793	3.851	4.138	4.163	3.959
As	0.000	0.000	0.220	0.229	0.230	0.238	0.240	0.220	0.211	0.252	0.459	0.468	0.182	0.210	0.136
Hg	0.000	nm	0.002	0.012	0.003	0.000	0.000	0.003	0.000	0.000	0.000	0.000	0.000	0.000	Nm
Pb	0.661	0.212	0.005	0.000	0.000	0.000	0.021	0.000	0.000	0.000	0.000	0.000	0.000	0.000	0.000
S	12.635	12.728	12.804	12.886	12.617	12.743	12.765	12.738	12.786	12.751	12.458	12.459	12.903	12.950	12.255

Katsimoutis : 1,2: (KAT1); 3-10: (Kat9); 11,12: (Kat1a); Kondaros : 13,14: (Kont13); 15: (KONT2).

Representative microprobe analyses of Enargite from Triades-Galana

	TRIADES				GALANA			
wt%	1	2	3	4	5	6	7	8
Cu	41.09	47.44	47.12	45.70	46.89	47.42	46.25	46.76
Ag	7.13	0.04	0.01	0.16	0.23	0.03	0.10	0.14
Fe	0.25	0.81	1.22	0.11	0.13	0.02	0.05	0.04
Zn	1.60	0.00	0.00	2.38	0.52	n.d.	1.02	0.04
Sb	5.34	0.12	0.34	0.34	0.03	n.d.	n.d.	n.d.
As	14.05	19.27	19.48	18.99	18.94	19.34	19.01	19.29
Hg	0.04	n.d.	n.d.	0.05	n.d.	0.04	0.07	0.01
S	29.85	32.67	32.95	31.91	32.77	33.28	32.75	32.56
	99.35	100.35	101.12	99.63	99.50	100.13	99.29	98.84
atoms	8	8	8	8	8	8	8	8
Cu	2.717	2.930	2.888	2.861	2.914	2.921	2.883	2.926
Ag	0.278	0.002	0.000	0.006	0.008	0.001	0.004	0.005
Fe	0.019	0.057	0.085	0.008	0.009	0.001	0.003	0.002
Zn	0.103	0.000	0.000	0.145	0.031	0.000	0.062	0.003
Sb	0.184	0.004	0.011	0.011	0.001	0.000	0.000	0.000
As	0.788	1.009	1.012	1.008	0.998	1.010	1.004	1.024
Hg	0.001	0.000	0.000	0.001	0.000	0.001	0.001	0.000
S	3.911	3.998	4.003	3.960	4.037	4.065	4.042	4.039

1: (VA50); 2-4 (VA31/1); 5- 8: (VA51).

Representative microprobe analyses of sphalerite from Triades

wt%	1	2	3	4	5	6	7	8	9	10	11	12
Zn	65.89	66.36	64.62	66.58	66.45	66.10	65.83	66.07	66.29	65.44	65.47	65.99
Fe	0.39	0.24	0.51	0.23	0.28	0.34	0.68	0.29	0.23	0.16	0.45	0.01
Mn	0.05	0.01	0.08	0.06	0.04	0.03	0.10	0.01	0.04	0.07	0.14	0.15
Cd	0.51	0.53	0.67	0.30	0.27	0.44	0.62	0.42	0.21	0.25	0.29	0.31
S	33.07	32.89	32.67	32.95	32.68	32.82	32.68	32.77	32.59	32.71	32.97	33.10
Total	99.91	100.02	98.54	100.11	99.73	99.73	99.90	99.56	99.36	98.61	99.34	99.57
atoms	2	2	2	2	2	2	2	2	2	2	2	2
Zn	0.982	0.990	0.977	0.992	0.994	0.988	0.984	0.990	0.995	0.987	0.980	0.986
Fe	0.007	0.004	0.009	0.004	0.005	0.006	0.012	0.005	0.004	0.003	0.008	0.003
Mn	0.001	0.000	0.001	0.001	0.001	0.001	0.002	0.000	0.001	0.001	0.003	0.003
Cd	0.004	0.005	0.006	0.003	0.002	0.004	0.005	0.004	0.002	0.002	0.003	0.003
S	1.006	1.001	1.007	1.001	0.997	1.001	0.997	1.001	0.998	1.007	1.007	1.009
mole%FeS	0.70	0.40	0.91	0.40	0.50	0.60	1.20	0.50	0.40	0.30	0.80	0.03

1, 2: (VA50); 3-10: (VA31); 11,12: (VA31/1).

Representative microprobe analyses of sphalerite from **Galana**

wt%	1	2	3	4	5	6	7	8
Zn	65.75	65.67	65.47	64.40	66.44	63.93	65.32	67.85
Fe	0.39	0.42	0.41	1.04	0.02	2.65	0.82	0.19
Mn	0.70	0.14	0.10	0.49	NM	NM	NM	0.00
Cd	0.39	0.32	0.32	0.31	0.20	0.30	0.49	0.09
S	32.69	32.65	32.49	32.63	32.35	32.33	32.05	33.82
Total	99.91	99.18	98.79	98.87	99.65	99.52	99.95	101.77
atoms	2	2	2	2	2	2	2	2
Zn	0.982	0.987	0.988	0.969	0.999	0.959	0.982	0.991
Fe	0.007	0.007	0.007	0.018	0.004	0.046	0.014	0.003
Mn	0.012	0.002	0.002	0.009	NM	NM	NM	0.000
Cd	0.003	0.003	0.003	0.003	0.002	0.003	0.004	0.001
S	0.995	1.001	1.000	1.001	0.992	0.989	0.982	1.006
mole%FeS	0.70	0.70	0.70	1.80	0.04	4.56	1.40	0.30

1-4: (VA51); 5-7: (GAL1); 8: (GAL2)

Representative microprobe analyses of sphalerite from **Katsimoutis-Kondaros and Chondro Vouno-Profitis Ilias**

wt%	1	2	3	4	5	6	7	8	9	10	11
Zn	64.32	67.36	65.77	65.43	65.60	66.46	66.57	67.73	67.30	66.08	64.85
Fe	2.47	0.79	1.79	1.31	0.68	0.22	0.28	0.48	0.28	0.52	0.38
Mn	0.11	0.13	0.18	0.04	0.03	0.02	0.01	0.06	0.00	0.37	0.44
Cd	0.20	0.77	0.81	0.08	0.09	0.15	0.79	0.23	0.21	0.24	0.47
S	31.89	32.05	31.02	32.97	33.08	32.68	33.31	33.18	31.50	32.86	31.34
Total	99.03	101.10	99.58	99.83	99.49	99.53	100.95	100.41	98.54	100.06	97.49
atoms	2	2	2	2	2	2	2	2	2	2	2
Zn	0.971	1.004	0.998	0.974	0.979	0.995	0.984	1.003	1.025	0.984	0.998
Fe	0.044	0.014	0.032	0.023	0.012	0.004	0.005	0.008	0.005	0.009	0.007
Mn	0.002	0.002	0.003	0.001	0.001	0.000	0.000	0.001	0.000	0.007	0.008
Cd	0.002	0.007	0.007	0.001	0.001	0.001	0.007	0.002	0.002	0.002	0.004
S	0.981	0.974	0.960	1.001	1.006	0.998	1.004	1.001	0.978	0.998	0.983
mole%FeS	4.32	1.36	3.08	2.30	1.21	0.40	0.50	0.79	0.48	0.90	0.71

Katsimoutis : 1: (KAT1); 4: (Kat1); 5,6: (Kat1b); Kondaros : 2,3: (KONT2); Chondro Vouno : 7,8: (CV); Profitis Ilias : 9: (PIL2); 10: (PI2-1b).

Representative microprobe analyses of polybasite (1-15), pearceite (16, 17) from **Kondaros-Katsimoutis**

	1	2	3	4	5	6	7	8	9	10	11	12	13	14	15	16	17
Ag	68.41	67.62	70.01	68.11	70.00	69.75	70.92	67.17	71.71	69.65	69.90	71.00	66.85	64.11	64.49	71.57	70.49
Cu	5.33	6.39	5.50	7.46	5.88	6.82	2.73	2.83	2.99	2.51	2.70	3.28	6.62	8.33	7.74	4.67	4.80
Sb	10.73	9.89	10.25	9.98	10.25	10.07	11.61	11.95	10.79	11.64	11.27	10.32	11.00	10.84	10.85	5.50	6.01
As	0.00	0.29	0.29	0.16	0.22	0.49	0.19	0.17	0.24	0.20	0.18	0.18	0.17	0.00	0.41	3.13	2.48
S	15.36	15.58	14.80	15.58	15.14	14.95	15.84	14.85	15.34	15.34	16.07	14.63	15.17	16.17	15.93	15.36	14.78
Total	99.83	99.77	100.85	101.29	101.49	102.08	101.30	97.00	101.07	99.41	100.19	99.48	99.83	99.45	99.42	100.24	98.69
Atoms	29	29	29	29	29	29	29	29	29	29	29	29	29	29	29	29	29
Ag	14.308	13.901	14.635	13.884	14.466	14.323	14.751	14.665	15.035	14.825	14.590	15.218	13.931	13.070	13.228	14.765	14.867
Cu	1.896	2.239	1.962	2.574	2.073	2.369	0.964	1.048	1.065	0.906	0.981	1.194	2.343	2.882	2.699	1.634	1.718
Sb	1.986	1.796	1.894	1.804	1.872	1.837	2.139	2.312	2.004	2.195	2.084	1.960	2.031	1.958	1.969	1.006	1.123
As	0.000	0.089	0.090	0.044	0.067	0.155	0.057	0.053	0.072	0.061	0.054	0.055	0.050	0.000	0.111	0.931	0.742
S	10.810	10.975	10.418	10.693	10.521	10.316	11.083	10.908	10.824	10.984	11.288	10.548	10.639	11.089	10.994	10.663	10.490

Kondaros : 1-3: (KONT4); 4-6: (KONT2); 7-12: (Kont13); Katsimoutis : 13: (kat9); 14,15: (KAT2); 16,17: (kat1a)

Representative microprobe analyses of hessite (1-4), petzite (5-10) and Native gold (11,12) from **Profitis Ilias**

	1	2	3	4	5	6	7	8	9	10	11	12
Au	0.05	n.a.	0.05	n.d.	26.17	24.84	18.35	24.99	25.45	24.68	85.15	81.08
Ag	62.86	66.27	64.86	63.75	44.02	41.31	47.97	42.41	40.95	41.35	13.79	14.37
Te	36.55	38.42	36.17	36.37	33.73	32.73	33.08	32.77	33.84	32.94	n.a.	5.07
	99.58	104.69	101.09	100.10	103.38	98.53	99.41	99.68	100.18	98.68	100.35	99.94
Atoms	3	3	3	3	6	6	6	6	6	6	1	1
Au	0.001	0.000	0.001	0.000	1.008	1.000	0.701	0.994	1.003	0.992	0.738	0.727
Ag	1.997	2.013	2.004	2.024	3.095	3.037	3.347	3.082	2.945	3.037	0.218	0.235
Te	0.982	0.987	0.945	0.976	2.005	2.034	1.952	2.013	2.057	2.045	0.000	0.070

1,2: (PI2-3); 3,4: (PI2b-1); 5-7: (PI2-3); 8: (PI2-1); 9: (PI2-1b); 10: (PI2-2); 11: (PI2b-1); 12 Gold (PI2-1b).

APPENDIX III

Thermodynamic Data for the construction of fO_2 – fS_2 Diagrams

Reaction		logK (225° C)	Source
Pyrite-Hematite-Magnetite-Pyrrhotite-Equilibrium			
1. $Fe_2O_3 + 2S_2(g)$	$= 2FeS_2 + 1.5 O_2 (g)$	-28.53	1
2. $3FeS_2 + 2O_2(g)$	$= Fe_3O_4 + 3S_2(g)$	34.52	1
3. $FeS + 0.5S_2(g)$	$= FeS_2$	6.37	1
4. $3FeS + 2O_2(g)$	$= Fe_3O_4 + 1.5S_2(g)$	53.63	1
5. $2Fe_3O_4 + 0.5O_2(g)$	$= 3Fe_2O_3$	16.53	1
Chalcopyrite-Covellite-Stability Fields			
6. $2CuS$	$= Cu_2S + 0.5S_2(g)$	-3.01	1
7. $4FeS_2 + Cu_5FeS_4$	$= 5CuFeS_2 + S_2(g)$	-7.63	2
8. $2Fe_2O_3 + Cu_5FeS_4 + 3S_2(g)$	$= 5CuFeS_2 + 3O_2(g)$	-64.69	1,2
9. $2Fe_3O_4 + 1.5Cu_5FeS_4 + 4.5S_2(g)$			
Tennantite –Enargite-Tetrahedrite-Famatinite-Limits			
10. $2/3Cu_{12}As_4S_{13} + S_2(g)$	$= 8/3Cu_3As_4S_4$	8.95	2
11. $2/3Cu_{12}Sb_4S_{13} + S_2(g)$	$= 8/3 Cu_3Sb_4S_4 + 3/2 O_2(g)$	7.87	2
Calcite – Anhydrite-Limits			
12. $CaSO_4 + CO_2(g)$	$= CaCO_3 + 1/2S_2(g) + 3/2 O_2 (g)$	-54.96	1
K-Feldspar/Sanidine-Muscovite-Kaolinite-Alunite-Stability Fields			
13. $KAl_3Si_3O_{10}(OH)_2 + 2H_2O(l) + S_2(g) + 3O_2(g)$	$= KAl_3(SO_4)_2(OH)_6$	98.54	1,3
14. $3KAlSi_3O_8 + 2H^+$	$= KAl_3Si_3O_{10}(OH)_2 + 6SiO_2(qtz) + 2K^+$	8.75a	1,3,4
15. $3KAlSi_3O_8 + 2H^+$	$= KAl_3Si_3O_{10}(OH)_2 + 6SiO_2(qtz) + 2K^+$	7.84b	1,3,4
16. $2KAl_3Si_3O_{10}(OH)_2 + 2H_2O(l) + 2H^+$	$= 3Al_2Si_2O_5(OH)_4 + 2K^+$	3.79	1,3,4

Reaction		logK (225° C)	Source
The Rest of the Reactions			
17. 2S(l)	= S2(g)	- 4.20	2
18. PbS + 2O2(g)	= PbSO4	59.84	1
19. FeS(sph) + 0.5 S2	= FeS2	logX = -6.74 - 0.5	5
H2S – SO2 - Concentration Lines			
20. SO2(g)	= O2(g) + 1/2 S2(g)	-30.80*	6
21. H2S (g) + 1/2O2(g)	= H2O(g) + 1/2S2(g)	14.68	1
pH - Lines			
22. 2HSO4- + 2 H+	= 2H2O(l) + S2(g) + 3O2(g)	-86.50	1,3,4,7
23. 4 H+ + 2 SO4=		-74.34	1,3,4,7
ΣS - Concentration Lines			
24. 2H2S(aq) + O2(g)	= 2H2O(l) + 2S2(g)	29.30	1,3,4,7
Sulfide – Sulfate – Domination			
25. H2S(aq) + 2O2(g)	= 2H+ + SO4=	51.82	1,4,7

1: Helgeson et al. (1978); 2: Barton & Skinner (1979); 3: Helgeson & Kirkham (1974a); 4: Helgeson et al. (1981);
5: Scott & Barnes (1971); 6: Robie et al. (1978); 7: Helgeson (1969).

* : interpolated

a : KAlSi3O8 = High – Sanidine

b : KAlSi3O8 = K-Feldspar

APPENDIX IV

Introduction

A series of parametric and non parametric statistical correlations have been applied to the trace elements referred to the various subareas of W. Milos aiming to better identifying the relationships between them.

Parametric Correlations

- The **Pearson correlation coefficient (r)**, gave for each subarea a correlation table which is a matrix of correlation coefficients expressing the extent to which values of the two variables are "proportional" to each other. This correlation matrix uses only the observations that have non missing values for all variables in the analyses.
- The **Pairwise (or Matched, or deletion of missing data) correlations** table, listed the correlations and the significant probabilities that were produced after the computation of all those observations (cases) that had non missing values, on those two variables. By using this methodology the matched 'partners' (observations) functioned as self controllers, thus lowering the level of unexplained variances or "errors".
- The **Inverse correlation** gave for each subarea a correlation table which contains the inverse of the correlation matrix. The diagonal elements of the inverse correlation matrix are a function of the extent to which the variables are linear combinations of other variables.
- The **Partial correlation** table showed a correlation between two variables that remained after controlling for (partialling out) one or more of the other existing variables.

Non Parametric Correlations

- **Spearman's Rho** is a variant of Pearson's r correlation coefficient which was used with the ranks of the data values instead of the values themselves.
- **Kendall's Tau** is a correlation for use with two ordinal variables or an ordinal and an interval variable. Under this correlation there was used a correction for those pairs of observations that had equal values of X or equal values of Y.
- **Hoeffding's D** is an independence test which has been used as a statistical scale. It ranges from -0.5 to 1. In this scale, large positive values indicated dependence.

Eigenvector Methods

In order to better identify and reveal any underlying structure/relation between the trace elements across a set of correlated variables (multivariate observations), it has been used the **Principal Components Analysis**. By using principal component analysis from one side it has been reduced the dimensionality of the set of the available data and from the other have been showed the most prominent directions of those data.

In the presented tables the n original variables were the eigenvectors (i.e., the trace elements) and the n principal components (eigenvalues) were the linear combinations of the standardized original variables (eigenvectors) that had the greatest possible variance (for the first principal component - only this parameter is enough) together with the

restriction that each successive component must be uncorrelated with all the previously defined components (i.e., for the second and so on - the rest of the components). In such a fashion the **Cum %** showed the cumulative percent of the variation of the eigenvalues, the **Percent** showed each eigenvalue as a percent of the total eigenvalues and the first row (**eigenvalue**) listed, from left to right, the first principal component, the second, and so on. Finally the columns of values of the **eigenvectors** in the reported tables, correspond to each of the principal component (in order from left to right).

All the statistical elaborations of the data have been performed by the **JMP**. The Statistical Discovery software program (A Business Unit of SAS - SAS Institute Inc.-USA).

The statistical description of the western Milos Subareas

Vani subarea

Parametric Correlations

Vani subarea Pearson's correlation

	Au ppm	Ag ppm	Cu ppm	Pb ppm	Zn ppm	As ppm	Sb ppm	Ba ppm	Hg ppm	Mn ppm
Au ppm	1	0,634677	-0,14279	-0,13204	-0,33723	-0,10228	-0,20477	-0,33143	-0,29541	-0,3933
Ag ppm	0,634677	1	-0,31832	-0,28384	-0,54932	-0,3255	-0,18947	-0,54636	-0,44087	-0,61962
Cu ppm	-0,14279	-0,31832	1	0,997772	0,794862	0,342853	-0,23291	0,722092	-0,32287	0,574764
Pb ppm	-0,13204	-0,28384	0,997772	1	0,799998	0,367666	-0,20568	0,722848	-0,31489	0,579784
Zn ppm	-0,33723	-0,54932	0,794862	0,799998	1	0,803852	-0,15568	0,984794	0,310825	0,952433
As ppm	-0,10228	-0,3255	0,342853	0,367666	0,803852	1	-0,01607	0,830432	0,701854	0,901722
Sb ppm	-0,20477	-0,18947	-0,23291	-0,20568	-0,15568	-0,01607	1	-0,27089	0,204601	-0,09332
Ba ppm	-0,33143	-0,54636	0,722092	0,722848	0,984794	0,830432	-0,27089	1	0,390371	0,969178
Hg ppm	-0,29541	-0,44087	-0,32287	-0,31489	0,310825	0,701854	0,204601	0,390371	1	0,583709
Mn ppm	-0,3933	-0,61962	0,574764	0,579784	0,952433	0,901722	-0,09332	0,969178	0,583709	1

Vani subarea Inverse correlation matrix

	Au ppm	Ag ppm	Cu ppm	Pb ppm	Zn ppm	As ppm	Sb ppm	Ba ppm	Hg ppm	Mn ppm
Au ppm	1,844424	-1,683314	-9,002036	9,070908	-0,404004	0	0	0	0	0
Ag ppm	-1,683314	4,842083	36,71326	-38,35384	3,59317	0	0	0	0	0
Cu ppm	-9,002036	36,71326	515,8202	-530,9384	31,87488	0	0	0	0	0
Pb ppm	9,070908	-38,35384	-530,9384	549,596	-35,66206	0	0	0	0	0
Zn ppm	-0,404004	3,59317	31,87488	-35,66206	6,030971	0	0	0	0	0
As ppm	0	0	0	0	0	0	0	0	0	0
Sb ppm	0	0	0	0	0	0	0	0	0	0
Ba ppm	0	0	0	0	0	0	0	0	0	0
Hg ppm	0	0	0	0	0	0	0	0	0	0
Mn ppm	0	0	0	0	0	0	0	0	0	0

Vani subarea Partial correlation matrix

	Au ppm	Ag ppm	Cu ppm	Pb ppm	Zn ppm	As ppm	Sb ppm	Ba ppm	Hg ppm	Mn ppm
Au ppm		0,563273	0,291851	-0,284904	0,121133					
Ag ppm	0,563273		-0,734611	0,743483	-0,664918					
Cu ppm	0,291851	-0,734611		0,997179	-0,571486					
Pb ppm	-0,284904	0,743483	0,997179		0,619428					
Zn ppm	0,121133	-0,664918	-0,571486	0,619428						
As ppm										
Sb ppm										
Ba ppm										
Hg ppm										
Mn ppm										

Vani subarea Pairwise correlations

Variable	by Variable	Correlation	Count	Signif Prob	Plot Corr
Ag ppm	Au ppm	0,6347	6	0,1758	
Cu ppm	Au ppm	-0,1428	6	0,7873	
Cu ppm	Ag ppm	-0,1289	57	0,3391	
Pb ppm	Au ppm	-0,1320	6	0,8031	
Pb ppm	Ag ppm	-0,0357	57	0,7922	
Pb ppm	Cu ppm	0,7414	71	0,0000	
Zn ppm	Au ppm	-0,3372	6	0,5133	
Zn ppm	Ag ppm	-0,0338	57	0,8026	
Zn ppm	Cu ppm	0,4565	71	0,0001	
Zn ppm	Pb ppm	0,3705	71	0,0015	
As ppm	Au ppm	-0,1023	6	0,8471	
As ppm	Ag ppm	-0,1901	57	0,1566	
As ppm	Cu ppm	0,2298	71	0,0538	
As ppm	Pb ppm	0,3345	71	0,0044	
As ppm	Zn ppm	0,2096	71	0,0793	
Sb ppm	Au ppm	-0,2048	6	0,6971	
Sb ppm	Ag ppm	-0,1630	57	0,2257	
Sb ppm	Cu ppm	0,1709	71	0,1541	
Sb ppm	Pb ppm	0,2541	71	0,0325	

Sb ppm	Zn ppm	-0,0078	71	0,9485	
Sb ppm	As ppm	0,3290	71	0,0051	
Ba ppm	Au ppm	-0,3314	6	0,5211	
Ba ppm	Ag ppm	-0,1653	57	0,2190	
Ba ppm	Cu ppm	0,5325	71	0,0000	
Hg ppm	Ag ppm	-0,1147	53	0,4136	
Hg ppm	Cu ppm	-0,0779	67	0,5310	
Hg ppm	Pb ppm	-0,0719	67	0,5629	
Hg ppm	Zn ppm	0,2588	67	0,0345	
Hg ppm	As ppm	0,1868	67	0,1302	
Hg ppm	Sb ppm	0,1052	67	0,3969	
Hg ppm	Ba ppm	0,2523	67	0,0394	
Mn ppm	Au ppm	-0,3933	6	0,4405	
Mn ppm	Ag ppm	-0,0570	56	0,6766	
Mn ppm	Cu ppm	0,3753	69	0,0015	
Mn ppm	Pb ppm	0,3657	69	0,0020	
Mn ppm	Zn ppm	0,5469	69	0,0000	
Mn ppm	As ppm	0,4660	69	0,0001	
Mn ppm	Sb ppm	0,2747	69	0,0224	
Mn ppm	Ba ppm	0,6604	69	0,0000	
Mn ppm	Hg ppm	0,3368	65	0,0061	

Non Parametric Correlations

Vani subarea Spearman's Rho correlation

Variable	by Variable	Spearman Rho	Prob> Rho	Plot
Ag ppm	Au ppm	0,3769	0,4615	
Cu ppm	Au ppm	0,5218	0,2883	
Cu ppm	Ag ppm	0,2335	0,0804	
Pb ppm	Au ppm	0,4928	0,3206	
Pb ppm	Ag ppm	0,3988	0,0021	
Pb ppm	Cu ppm	0,8004	<.0001	
Zn ppm	Au ppm	0,2029	0,6998	
Zn ppm	Ag ppm	-0,1579	0,2407	
Zn ppm	Cu ppm	0,4203	0,0003	
Zn ppm	Pb ppm	0,4071	0,0004	
As ppm	Au ppm	0,1160	0,8268	
As ppm	Ag ppm	-0,1346	0,3180	
As ppm	Cu ppm	0,3060	0,0095	
As ppm	Pb ppm	0,2476	0,0373	
As ppm	Zn ppm	0,4989	<.0001	
Sb ppm	Au ppm	-0,0290	0,9565	
Sb ppm	Ag ppm	-0,1109	0,4114	
Sb ppm	Cu ppm	0,0170	0,8878	
Sb ppm	Pb ppm	0,0126	0,9172	
Sb ppm	Zn ppm	0,1271	0,2908	
Sb ppm	As ppm	0,6328	<.0001	
Ba ppm	Au ppm	-0,1449	0,7841	
Ba ppm	Ag ppm	-0,1287	0,3399	
Ba ppm	Cu ppm	0,3093	0,0087	
Ba ppm	Pb ppm	0,2598	0,0287	
Ba ppm	Zn ppm	0,6316	<.0001	
Ba ppm	As ppm	0,4470	<.0001	
Ba ppm	Sb ppm	0,1764	0,1411	
Hg ppm	Au ppm	-0,0735	0,8899	
Hg ppm	Ag ppm	0,3297	0,0159	
Hg ppm	Cu ppm	0,1401	0,2581	
Hg ppm	Pb ppm	0,1025	0,4089	
Hg ppm	Zn ppm	0,3360	0,0054	
Hg ppm	As ppm	0,2552	0,0372	
Hg ppm	Sb ppm	0,1883	0,1270	
Hg ppm	Ba ppm	0,1841	0,1360	
Mn ppm	Au ppm	0,0441	0,9339	
Mn ppm	Ag ppm	-0,0854	0,5315	
Mn ppm	Cu ppm	0,3297	0,0057	
Mn ppm	Pb ppm	0,1531	0,2092	
Mn ppm	Zn ppm	0,7500	<.0001	
Mn ppm	As ppm	0,5128	<.0001	
Mn ppm	Sb ppm	0,2654	0,0275	
Mn ppm	Ba ppm	0,6962	<.0001	
Mn ppm	Hg ppm	0,3466	0,0047	

Vani subarea Kendall's Tau b correlation

Variable	by Variable	Kendall Tau b	Prob> Tau b	Plot
Ag ppm	Au ppm	0,2760	0,4442	
Cu ppm	Au ppm	0,4140	0,2511	
Cu ppm	Ag ppm	0,1371	0,1365	
Pb ppm	Au ppm	0,4140	0,2511	
Pb ppm	Ag ppm	0,2599	0,0045	
Pb ppm	Cu ppm	0,6098	<,0001	
Zn ppm	Au ppm	0,1380	0,7021	
Zn ppm	Ag ppm	-0,0954	0,2982	
Zn ppm	Cu ppm	0,2944	0,0003	
Zn ppm	Pb ppm	0,2712	0,0008	
As ppm	Au ppm	0,1380	0,7021	
As ppm	Ag ppm	-0,0872	0,3417	
As ppm	Cu ppm	0,2073	0,0113	
As ppm	Pb ppm	0,1775	0,0289	
As ppm	Zn ppm	0,3539	<,0001	
Sb ppm	Au ppm	0,0000	1,0000	
Sb ppm	Ag ppm	-0,0743	0,4266	
Sb ppm	Cu ppm	0,0037	0,9643	
Sb ppm	Pb ppm	0,0119	0,8853	
Sb ppm	Zn ppm	0,0834	0,3125	
Sb ppm	As ppm	0,4503	<,0001	
Ba ppm	Au ppm	-0,1380	0,7021	
Ba ppm	Ag ppm	-0,0721	0,4321	
Ba ppm	Cu ppm	0,2096	0,0105	
Ba ppm	Pb ppm	0,1442	0,0763	
Ba ppm	Zn ppm	0,4631	<,0001	
Ba ppm	As ppm	0,3133	0,0001	
Ba ppm	Sb ppm	0,1224	0,1381	
Hg ppm	Au ppm	-0,0714	0,8457	
Hg ppm	Ag ppm	0,2309	0,0308	
Hg ppm	Cu ppm	0,1253	0,1852	
Hg ppm	Pb ppm	0,0814	0,3863	
Hg ppm	Zn ppm	0,2527	0,0072	
Hg ppm	As ppm	0,2019	0,0318	
Hg ppm	Sb ppm	0,1480	0,1210	
Hg ppm	Ba ppm	0,1397	0,1375	
Mn ppm	Au ppm	-0,0714	0,8457	
Mn ppm	Ag ppm	-0,0572	0,5571	
Mn ppm	Cu ppm	0,2335	0,0073	
Mn ppm	Pb ppm	0,0888	0,3046	
Mn ppm	Zn ppm	0,5755	<,0001	
Mn ppm	As ppm	0,3705	<,0001	
Mn ppm	Sb ppm	0,1915	0,0292	
Mn ppm	Ba ppm	0,5092	<,0001	
Mn ppm	Hg ppm	0,2749	0,0061	

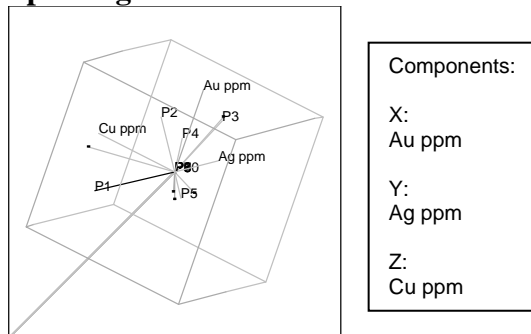
Vani subarea Hoeffding's D correlation

Variable	by Variable	Hoeffding D	Prob>D	Plot
Ag ppm	Au ppm	-0,1667	1,0000	
Cu ppm	Au ppm	-0,1250	0,9999	
Cu ppm	Ag ppm	0,0193	0,0365	
Pb ppm	Au ppm	0,1042	0,1121	
Pb ppm	Ag ppm	0,0450	0,0026	
Pb ppm	Cu ppm	0,2640	<,0001	
Zn ppm	Au ppm	0,0000	0,3643	
Zn ppm	Ag ppm	0,0131	0,0722	
Zn ppm	Cu ppm	0,0650	<,0001	
Zn ppm	Pb ppm	0,0404	0,0015	
As ppm	Au ppm	0,0000	0,3643	
As ppm	Ag ppm	0,0055	0,1787	
As ppm	Cu ppm	0,0259	0,0093	
As ppm	Pb ppm	0,0178	0,0265	
As ppm	Zn ppm	0,0831	<,0001	

Sb ppm	Au ppm	-0,1667	1,0000	
Sb ppm	Ag ppm	-0,0045	0,6651	
Sb ppm	Cu ppm	0,0014	0,2890	
Sb ppm	Pb ppm	-0,0064	0,9356	
Sb ppm	Zn ppm	0,0051	0,1586	
Sb ppm	As ppm	0,1301	<,0001	
Ba ppm	Au ppm	-0,0208	0,4688	
Ba ppm	Ag ppm	-0,0010	0,4150	
Ba ppm	Cu ppm	0,0595	0,0001	
Ba ppm	Pb ppm	0,0245	0,0111	
Ba ppm	Zn ppm	0,1822	<,0001	
Ba ppm	As ppm	0,0867	<,0001	
Ba ppm	Sb ppm	0,0129	0,0513	
Hg ppm	Au ppm	-0,1849	1,0000	
Hg ppm	Ag ppm	0,0089	0,1269	
Hg ppm	Cu ppm	0,0015	0,2890	
Hg ppm	Pb ppm	-0,0055	0,8298	
Hg ppm	Zn ppm	0,0150	0,0435	
Hg ppm	As ppm	0,0063	0,1402	
Hg ppm	Sb ppm	-0,0021	0,5128	
Hg ppm	Ba ppm	-0,0006	0,3981	
Mn ppm	Au ppm	-0,0182	0,4543	
Mn ppm	Ag ppm	-0,0067	0,8361	
Mn ppm	Cu ppm	0,0293	0,0067	
Mn ppm	Pb ppm	-0,0013	0,4535	
Mn ppm	Zn ppm	0,1916	<,0001	
Mn ppm	As ppm	0,0698	<,0001	
Mn ppm	Sb ppm	0,0264	0,0096	
Mn ppm	Ba ppm	0,1476	<,0001	
Mn ppm	Hg ppm	0,0118	0,0695	

Principal Components analysis

Spinning Plot for Vani subarea :



Vani subarea Principal components summary table :

Eigenvalue	5,394161	2,210998	1,301337	0,767668	0,325835	1,62E-15	5,39E-16	3,36E-16	-4,42E-17	-3,89E-16
Percent	53,94161	22,10998	13,01337	7,676685	3,258354	1,62E-14	5,39E-15	3,36E-15	-4,42E-16	-3,89E-15
Cum %	53,94161	76,05159	89,06496	96,74165	100	100	100	100	100	100
Eigenvectors :										
Au ppm	-0,178839	0,262437	0,573579	0,397505	-0,621274	0,057706	0,02227	-0,018709	0,041169	0,142432
Ag ppm	-0,275026	0,255726	0,421888	0,194424	0,757073	0,192666	0,040787	-0,008113	0,127839	0,121746
Cu ppm	0,317173	0,424968	-0,180319	0,140701	-0,040791	0,498621	-0,367473	-0,089585	0,25137	-0,45821
Pb ppm	0,317488	0,421698	-0,162539	0,191824	0,037843	-0,16026	0,69354	0,377957	-0,016511	-0,083178
Zn ppm	0,426862	0,070807	0,034868	0,064945	0,061117	0,046538	0,216976	-0,792723	-0,238796	0,262541
As ppm	0,347575	-0,1914	0,407081	0,237736	0,15963	-0,448185	-0,219851	0,048023	-0,281821	-0,51372
Sb ppm	-0,055022	-0,340652	-0,397971	0,822554	0,069851	0,069751	-0,07872	0,040329	-0,024425	0,1667
Ba ppm	0,424391	0,036653	0,121481	-0,087466	0,03596	0,291221	-0,298551	0,455791	-0,419594	0,48693
Hg ppm	0,170121	-0,577388	0,283066	-0,051124	-0,039758	0,554689	0,418146	0,080092	0,138369	-0,212781

Katsimoutis subarea

Parametric Correlations

Katsimoutis subarea Pearson's correlation

	Ag ppm	Cu ppm	Pb ppm	Zn ppm	As ppm	Sb ppm	Ba ppm	Hg ppm	Mn ppm
Ag ppm	1	0,725551	0,478639	0,909621	0,859216	0,097357	0,586843	0,759099	0,935468
Cu ppm	0,725551	1	0,565224	0,447997	0,543548	0,387519	0,400762	0,21074	0,516
Pb ppm	0,478639	0,565224	1	0,513013	0,609378	-0,4273	0,728428	0,527749	0,419021
Zn ppm	0,909621	0,447997	0,513013	1	0,951482	-0,29625	0,560716	0,897666	0,981665
As ppm	0,859216	0,543548	0,609378	0,951482	1	-0,37167	0,431626	0,756165	0,951899
Sb ppm	0,097357	0,387519	-0,4273	-0,29625	-0,37167	1	-0,11933	-0,37693	-0,17683
Ba ppm	0,586843	0,400762	0,728428	0,560716	0,431626	-0,11933	1	0,777271	0,43958
Hg ppm	0,759099	0,21074	0,527749	0,897666	0,756165	-0,37693	0,777271	1	0,807617
Mn ppm	0,935468	0,516	0,419021	0,981665	0,951899	-0,17683	0,43958	0,807617	1

Katsimoutis subarea Inverse correlation

	Ag ppm	Cu ppm	Pb ppm	Zn ppm	As ppm	Sb ppm	Ba ppm	Hg ppm	Mn ppm
Ag ppm	46,97349	-22,70731	9,571708	-37,46568	0	0	0	0	0
Cu ppm	-22,70731	12,52336	-5,330981	17,77949	0	0	0	0	0
Pb ppm	9,571708	-5,330981	3,628032	-8,179591	0	0	0	0	0
Zn ppm	-37,46568	17,77949	-8,179591	31,31065	0	0	0	0	0
As ppm	0	0	0	0	0	0	0	0	0
Sb ppm	0	0	0	0	0	0	0	0	0
Ba ppm	0	0	0	0	0	0	0	0	0
Hg ppm	0	0	0	0	0	0	0	0	0
Mn ppm	0	0	0	0	0	0	0	0	0

Katsimoutis subarea Partial correlation

	Ag ppm	Cu ppm	Pb ppm	Zn ppm	As ppm	Sb ppm	Ba ppm	Hg ppm	Mn ppm
Ag ppm		0,936222	-0,733208	0,976925					
Cu ppm	0,936222		0,790881	-0,897869					
Pb ppm	-0,733208	0,790881		0,76745					
Zn ppm	0,976925	-0,897869	0,76745						
As ppm									
Sb ppm									
Ba ppm									
Hg ppm									
Mn ppm									

Katsimoutis subarea Pairwise correlations

Variable	by Variable	Correlation	Count	Signif Prob	Plot Corr
Cu ppm	Ag ppm	0,7429	8	0,0347	
Pb ppm	Ag ppm	0,6006	8	0,1154	
Pb ppm	Cu ppm	0,7453	13	0,0035	
Zn ppm	Ag ppm	0,9261	8	0,0010	
Zn ppm	Cu ppm	0,5932	13	0,0326	
Zn ppm	Pb ppm	0,6607	13	0,0139	
As ppm	Ag ppm	0,8450	9	0,0041	
As ppm	Cu ppm	0,7980	13	0,0011	
As ppm	Pb ppm	0,7963	13	0,0011	
As ppm	Zn ppm	0,9050	13	0,0000	
Sb ppm	Ag ppm	0,2505	9	0,5156	
Sb ppm	Cu ppm	0,4980	13	0,0833	
Sb ppm	Pb ppm	-0,0144	13	0,9628	
Sb ppm	Zn ppm	0,0281	13	0,9275	
Sb ppm	As ppm	0,1164	14	0,6919	
Ba ppm	Ag ppm	0,6130	8	0,1061	
Ba ppm	Cu ppm	0,5772	13	0,0389	
Ba ppm	Pb ppm	0,6764	13	0,0111	
Ba ppm	Zn ppm	0,5618	13	0,0457	
Ba ppm	As ppm	0,6446	13	0,0174	
Ba ppm	Sb ppm	0,2570	13	0,3966	
Hg ppm	Ag ppm	0,7591	5	0,1367	
Hg ppm	Cu ppm	0,3944	6	0,4390	
Hg ppm	Pb ppm	0,5940	6	0,2138	
Hg ppm	Zn ppm	0,8992	6	0,0147	
Hg ppm	As ppm	0,7989	6	0,0566	
Hg ppm	Sb ppm	-0,2493	6	0,6338	
Hg ppm	Ba ppm	0,8064	6	0,0526	
Mn ppm	Ag ppm	0,9285	6	0,0075	

Variable	by Variable	Correlation	Count	Signif Prob	Plot Corr
Mn ppm	Cu ppm	0,5030	7	0,2498	
Mn ppm	Pb ppm	0,4648	7	0,2933	
Mn ppm	Zn ppm	0,9467	7	0,0012	
Mn ppm	As ppm	0,8579	7	0,0135	
Mn ppm	Sb ppm	-0,1271	7	0,7860	
Mn ppm	Ba ppm	0,4684	7	0,2892	
Mn ppm	Hg ppm	0,8076	5	0,0983	

Non parametric Correlations

Katsimoutis subarea Spearman's Rho correlation

Variable	by Variable	Spearman Rho	Prob> Rho	Plot
Ag ppm	Au ppm	0,0000	0,0000	
Cu ppm	Au ppm	0,0000	0,0000	
Cu ppm	Ag ppm	0,8144	0,0138	
Pb ppm	Au ppm	0,0000	0,0000	
Pb ppm	Ag ppm	0,6826	0,0621	
Pb ppm	Cu ppm	0,6905	0,0090	
Zn ppm	Au ppm	0,0000	0,0000	
Zn ppm	Ag ppm	0,6265	0,0965	
Zn ppm	Cu ppm	0,5255	0,0651	
Zn ppm	Pb ppm	0,8292	0,0005	
As ppm	Au ppm	0,0000	0,0000	
As ppm	Ag ppm	0,6276	0,0704	
As ppm	Cu ppm	0,7186	0,0056	
As ppm	Pb ppm	0,9256	<,0001	
As ppm	Zn ppm	0,7970	0,0011	
Sb ppm	Au ppm	0,0000	0,0000	
Sb ppm	Ag ppm	0,7764	0,0139	
Sb ppm	Cu ppm	0,3634	0,2223	
Sb ppm	Pb ppm	0,6898	0,0091	
Sb ppm	Zn ppm	0,6986	0,0079	
Sb ppm	As ppm	0,6386	0,0140	
Ba ppm	Au ppm	0,0000	0,0000	
Ba ppm	Ag ppm	0,7904	0,0195	
Ba ppm	Cu ppm	0,5530	0,0500	
Ba ppm	Pb ppm	0,8681	0,0001	
Ba ppm	Zn ppm	0,6446	0,0174	
Ba ppm	As ppm	0,7769	0,0018	
Ba ppm	Sb ppm	0,5900	0,0338	
Hg ppm	Au ppm	0,0000	0,0000	
Hg ppm	Ag ppm	0,6000	0,2848	
Hg ppm	Cu ppm	0,5508	0,2574	
Hg ppm	Pb ppm	0,7247	0,1032	
Hg ppm	Zn ppm	0,7353	0,0958	
Hg ppm	As ppm	0,3769	0,4615	
Hg ppm	Sb ppm	0,5294	0,2801	
Hg ppm	Ba ppm	0,9276	0,0077	
Mn ppm	Au ppm	0,0000	0,0000	
Mn ppm	Ag ppm	0,4857	0,3287	
Mn ppm	Cu ppm	0,3929	0,3833	
Mn ppm	Pb ppm	-0,2500	0,5887	
Mn ppm	Zn ppm	0,0721	0,8780	
Mn ppm	As ppm	0,1786	0,7017	
Mn ppm	Sb ppm	-0,2546	0,5817	
Mn ppm	Ba ppm	0,2500	0,5887	
Mn ppm	Hg ppm	0,2000	0,7471	

Katsimoutis subarea Kendall's Tau b

Variable	by Variable	Kendall Tau b	Prob> Tau b	Plot
Ag ppm	Au ppm	0,0000	0,0000	
Cu ppm	Au ppm	0,0000	0,0000	
Cu ppm	Ag ppm	0,6910	0,0178	
Pb ppm	Au ppm	0,0000	0,0000	
Pb ppm	Ag ppm	0,5455	0,0615	
Pb ppm	Cu ppm	0,5290	0,0122	
Zn ppm	Au ppm	0,0000	0,0000	
Zn ppm	Ag ppm	0,5185	0,0786	
Zn ppm	Cu ppm	0,3791	0,0752	
Zn ppm	Pb ppm	0,6754	0,0015	
As ppm	Au ppm	0,0000	0,0000	

Variable	by Variable	Kendall Tau b	Prob> Tau b	Plot
As ppm	Ag ppm	0,4789	0,0747	
As ppm	Cu ppm	0,5621	0,0083	
As ppm	Pb ppm	0,8053	0,0001	
As ppm	Zn ppm	0,6053	0,0047	
Sb ppm	Au ppm	0,0000	0,0000	
Sb ppm	Ag ppm	0,6667	0,0148	
Sb ppm	Cu ppm	0,2668	0,2167	
Sb ppm	Pb ppm	0,4903	0,0225	
Sb ppm	Zn ppm	0,4967	0,0220	
Sb ppm	As ppm	0,4686	0,0232	
Ba ppm	Au ppm	0,0000	0,0000	
Ba ppm	Ag ppm	0,6183	0,0340	
Ba ppm	Cu ppm	0,4516	0,0324	
Ba ppm	Pb ppm	0,7179	0,0006	
Ba ppm	Zn ppm	0,4416	0,0373	
Ba ppm	As ppm	0,6494	0,0022	
Ba ppm	Sb ppm	0,4373	0,0419	
Hg ppm	Au ppm	0,0000	0,0000	
Hg ppm	Ag ppm	0,4000	0,3272	
Hg ppm	Cu ppm	0,4140	0,2511	
Hg ppm	Pb ppm	0,5521	0,1260	
Hg ppm	Zn ppm	0,6429	0,0798	
Hg ppm	As ppm	0,2760	0,4442	
Hg ppm	Sb ppm	0,3571	0,3305	
Hg ppm	Ba ppm	0,8281	0,0217	
Mn ppm	Au ppm	0,0000	0,0000	
Mn ppm	Ag ppm	0,3333	0,3476	
Mn ppm	Cu ppm	0,3333	0,2931	
Mn ppm	Pb ppm	-0,2381	0,4527	
Mn ppm	Zn ppm	0,0000	1,0000	
Mn ppm	As ppm	0,1429	0,6523	
Mn ppm	Sb ppm	-0,1502	0,6447	
Mn ppm	Ba ppm	0,2381	0,4527	
Mn ppm	Hg ppm	0,2000	0,6242	

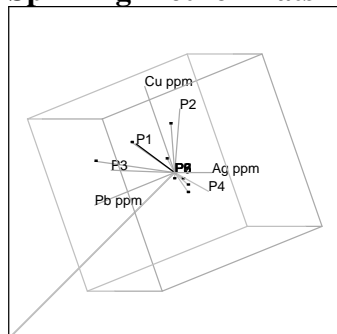
Katsimoutis subarea Hoeffding's D

Variable	by Variable	Hoeffding D	Prob>D	Plot
Ag ppm	Au ppm	0,0000	0,0000	
Cu ppm	Au ppm	0,0000	0,0000	
Cu ppm	Ag ppm	0,2098	0,0175	
Pb ppm	Au ppm	0,0000	0,0000	
Pb ppm	Ag ppm	0,1272	0,0529	
Pb ppm	Cu ppm	0,1416	0,0115	
Zn ppm	Au ppm	0,0000	0,0000	
Zn ppm	Ag ppm	0,0156	0,2805	
Zn ppm	Cu ppm	0,0634	0,0684	
Zn ppm	Pb ppm	0,4001	<.0001	
As ppm	Au ppm	0,0000	0,0000	
As ppm	Ag ppm	-0,0050	0,4010	
As ppm	Cu ppm	0,1842	0,0045	
As ppm	Pb ppm	0,6425	<.0001	
As ppm	Zn ppm	0,3272	0,0002	
Sb ppm	Au ppm	0,0000	0,0000	
Sb ppm	Ag ppm	0,2599	0,0057	
Sb ppm	Cu ppm	-0,0293	0,8130	
Sb ppm	Pb ppm	0,1411	0,0116	
Sb ppm	Zn ppm	0,2050	0,0029	
Sb ppm	As ppm	0,1495	0,0073	
Ba ppm	Au ppm	0,0000	0,0000	
Ba ppm	Ag ppm	0,0313	0,2175	
Ba ppm	Cu ppm	0,0929	0,0342	
Ba ppm	Pb ppm	0,4068	<.0001	
Ba ppm	Zn ppm	0,0538	0,0865	
Ba ppm	As ppm	0,2490	0,0011	
Ba ppm	Sb ppm	0,1007	0,0286	
Hg ppm	Au ppm	0,0000	0,0000	
Hg ppm	Ag ppm	-0,5000	.	
Hg ppm	Cu ppm	-0,2292	1,0000	
Hg ppm	Pb ppm	-0,0625	0,7543	
Hg ppm	Zn ppm	-0,0625	0,7543	
Hg ppm	As ppm	-0,3333	1,0000	
Hg ppm	Sb ppm	-0,1875	1,0000	

Variable	by Variable	Hoefding D	Prob>D	Plot
Hg ppm	Ba ppm	0,3750	0,0083	
Mn ppm	Au ppm	0,0000	0,0000	
Mn ppm	Ag ppm	0,0000	0,3643	
Mn ppm	Cu ppm	-0,1190	1,0000	
Mn ppm	Pb ppm	-0,1905	1,0000	
Mn ppm	Zn ppm	-0,0893	0,9917	
Mn ppm	As ppm	-0,1667	1,0000	
Mn ppm	Sb ppm	-0,0893	0,9917	
Mn ppm	Ba ppm	-0,0238	0,5147	
Mn ppm	Hg ppm	0,0000	.	

Principal Components analysis

Spinning Plot for Katsimoutis subarea



Components:	
X:	Ag ppm
Y:	Cu ppm
Z:	Pb ppm

Katsimoutis subarea Principal components summary table :

Eigenvalue	5,726212	1,560796	1,044594	0,668397	9,99E-17	1,79E-17	-1,27E-16	-1,85E-16	-1,18E-15
Percent	63,62458	17,34218	11,6066	7,426636	1,11E-15	1,99E-16	-1,41E-15	-2,05E-15	-1,31E-14
Cum %	63,62458	80,96676	92,57336	100	100	100	100	100	100
Eigenvectors :									
Ag ppm	0,387553	0,266238	-0,15311	0,084881	-0,02599	0,035982	0,440433	-0,673235	-0,314763
Cu ppm	0,252993	0,546199	0,256402	-0,38521	-0,341188	-0,278535	-0,456432	0,021771	-0,144005
Pb ppm	0,294311	-0,136002	0,612763	-0,352194	0,152591	0,558509	0,119274	-0,062035	0,205121
Zn ppm	0,401487	-0,061089	-0,258124	0,048239	0,669535	-0,000403	-0,549499	-0,124073	0,022387
As ppm	0,390715	-0,057419	-0,216296	-0,327816	0,040871	-0,45948	0,393373	0,191413	0,534438
Sb ppm	-0,105169	0,74199	-0,019812	0,339326	0,195451	0,25472	0,101366	0,150452	0,432275
Ba ppm	0,297534	-0,043084	0,536294	0,532803	0,174539	-0,381987	0,155953	0,285103	-0,236948
Hg ppm	0,368629	-0,224473	-0,051946	0,458345	-0,565665	0,149324	-0,281042	-0,14691	0,397623

Kondaros - Mersinia - Xerokampos subarea

Parametric correlations

Kondaros - Mersinia Xerokampos subarea Pearson's correlation

	Au ppm	Cu ppm	Pb ppm	Zn ppm	As ppm	Sb ppm	Ba ppm	Hg ppm
Au ppm	1	-0,152038	-0,149178	-0,474444	-0,333007	-0,323097	-0,409431	-0,0773
Cu ppm	-0,152038	1	0,332392	0,931695	0,930968	0,935569	0,552695	-0,311421
Pb ppm	-0,149178	0,332392	1	0,265915	0,040734	0,049254	-0,160312	-0,275486
Zn ppm	-0,474444	0,931695	0,265915	1	0,953825	0,952933	0,588263	-0,131534
As ppm	-0,333007	0,930968	0,040734	0,953825	1	0,999864	0,726482	-0,240018
Sb ppm	-0,323097	0,935569	0,049254	0,952933	0,999864	1	0,727178	-0,251764
Ba ppm	-0,409431	0,552695	-0,160312	0,588263	0,726482	0,727178	1	-0,65174
Hg ppm	-0,0773	-0,311421	-0,275486	-0,131534	-0,240018	-0,251764	-0,65174	1

Kondaros - Mersinia - Xerokampos subarea Inverse correlation

	Au ppm	Cu ppm	Pb ppm	Zn ppm	As ppm	Sb ppm	Ba ppm	Hg ppm
Au ppm	23,16141	-51,87521	4,323202	67,93282	0	0	0	0
Cu ppm	-51,87521	132,9207	-10,85378	-168,0649	0	0	0	0
Pb ppm	4,323202	-10,85378	1,946246	13,54735	0	0	0	0
Zn ppm	67,93282	-168,0649	13,54735	215,4393	0	0	0	0
As ppm	0	0	0	0	0	0	0	0
Sb ppm	0	0	0	0	0	0	0	0
Ba ppm	0	0	0	0	0	0	0	0
Hg ppm	0	0	0	0	0	0	0	0

Kondaros - Mersinia - Xerokampos subarea Partial correlation

Row	Au ppm	Cu ppm	Pb ppm	Zn ppm	As ppm	Sb ppm	Ba ppm	Hg ppm
Au ppm		0,934934	-0,643908	-0,961689				
Cu ppm	0,934934		0,674817	0,993158				
Pb ppm	-0,643908	0,674817		-0,661596				
Zn ppm	-0,961689	0,993158	-0,661596					
As ppm								
Sb ppm								
Ba ppm								
Hg ppm								

Kondaros - Mersinia - Xerokampos subarea Pairwise Correlations

Variable	by Variable	Correlation	Count	Signif Prob	Plot Corr
Cu ppm	Au ppm	-0,6517	8	0,0800	
Pb ppm	Au ppm	-0,2170	8	0,6058	
Pb ppm	Cu ppm	0,2915	8	0,4837	
Zn ppm	Au ppm	-0,8101	8	0,0148	
Zn ppm	Cu ppm	0,9673	8	0,0001	
Zn ppm	Pb ppm	0,2329	8	0,5788	
As ppm	Au ppm	-0,7257	8	0,0416	
As ppm	Cu ppm	0,9677	8	0,0001	
As ppm	Pb ppm	0,0785	8	0,8535	
As ppm	Zn ppm	0,9772	8	0,0000	
Sb ppm	Au ppm	-0,7209	8	0,0436	
Sb ppm	Cu ppm	0,9699	8	0,0001	
Sb ppm	Pb ppm	0,0845	8	0,8423	
Sb ppm	Zn ppm	0,9767	8	0,0000	
Sb ppm	As ppm	0,9999	8	0,0000	
Ba ppm	Au ppm	-0,6500	8	0,0810	
Ba ppm	Cu ppm	0,8780	8	0,0041	
Ba ppm	Pb ppm	-0,0010	8	0,9981	
Ba ppm	Zn ppm	0,8641	8	0,0056	
Ba ppm	As ppm	0,9306	8	0,0008	
Ba ppm	Sb ppm	0,9320	8	0,0007	
Hg ppm	Au ppm	0,1988	8	0,6370	
Hg ppm	Cu ppm	-0,6491	8	0,0816	
Hg ppm	Pb ppm	-0,3392	8	0,4111	
Hg ppm	Zn ppm	-0,5014	8	0,2056	
Hg ppm	As ppm	-0,5703	8	0,1399	
Hg ppm	Sb ppm	-0,5784	8	0,1331	
Hg ppm	Ba ppm	-0,7522	8	0,0313	

Non Parametric Correlations

Kondaros - Mersinia - Xerokampos subarea Spearman's Rho correlation

Variable	by Variable	Spearman Rho	Prob> Rho	Plot
Cu ppm	Au ppm	-0,5714	0,1390	
Pb ppm	Au ppm	-0,1429	0,7358	
Pb ppm	Cu ppm	0,5714	0,1390	
Zn ppm	Au ppm	-0,8571	0,0065	
Zn ppm	Cu ppm	0,7619	0,0280	
Zn ppm	Pb ppm	0,3810	0,3518	
As ppm	Au ppm	-0,7381	0,0366	

Variable	by Variable	Spearman Rho	Prob> Rho	Plot
As ppm	Cu ppm	0,7619	0,0280	
As ppm	Pb ppm	0,3095	0,4556	
As ppm	Zn ppm	0,9286	0,0009	
Sb ppm	Au ppm	-0,7143	0,0465	
Sb ppm	Cu ppm	0,8095	0,0149	
Sb ppm	Pb ppm	0,3333	0,4198	
Sb ppm	Zn ppm	0,9048	0,0020	
Sb ppm	As ppm	0,9762	<,0001	
Ba ppm	Au ppm	-0,8095	0,0149	
Ba ppm	Cu ppm	0,5952	0,1195	
Ba ppm	Pb ppm	0,0476	0,9108	
Ba ppm	Zn ppm	0,6429	0,0856	
Ba ppm	As ppm	0,7143	0,0465	
Ba ppm	Sb ppm	0,7381	0,0366	
Hg ppm	Au ppm	0,4048	0,3199	
Hg ppm	Cu ppm	-0,5238	0,1827	
Hg ppm	Pb ppm	-0,4048	0,3199	
Hg ppm	Zn ppm	-0,2143	0,6103	
Hg ppm	As ppm	-0,2857	0,4927	
Hg ppm	Sb ppm	-0,3095	0,4556	
Hg ppm	Ba ppm	-0,6429	0,0856	

Kondaros - Mersinia - Xerokampos subarea Kendall's Tau b correlation

Variable	by Variable	Kendall Tau b	Prob> Tau b	Plot
Cu ppm	Au ppm	-0,3571	0,2160	
Pb ppm	Au ppm	0,0000	1,0000	
Pb ppm	Cu ppm	0,5000	0,0833	
Zn ppm	Au ppm	-0,7857	0,0065	
Zn ppm	Cu ppm	0,5714	0,0478	
Zn ppm	Pb ppm	0,2143	0,4579	
As ppm	Au ppm	-0,6429	0,0260	
As ppm	Cu ppm	0,5714	0,0478	
As ppm	Pb ppm	0,0714	0,8046	
As ppm	Zn ppm	0,8571	0,0030	
Sb ppm	Au ppm	-0,5714	0,0478	
Sb ppm	Cu ppm	0,6429	0,0260	
Sb ppm	Pb ppm	0,1429	0,6207	
Sb ppm	Zn ppm	0,7857	0,0065	
Sb ppm	As ppm	0,9286	0,0013	
Ba ppm	Au ppm	-0,6429	0,0260	
Ba ppm	Cu ppm	0,4286	0,1376	
Ba ppm	Pb ppm	-0,0714	0,8046	
Ba ppm	Zn ppm	0,4286	0,1376	
Ba ppm	As ppm	0,5714	0,0478	
Ba ppm	Sb ppm	0,6429	0,0260	
Hg ppm	Au ppm	0,2143	0,4579	
Hg ppm	Cu ppm	-0,4286	0,1376	
Hg ppm	Pb ppm	-0,3571	0,2160	
Hg ppm	Zn ppm	0,0000	1,0000	
Hg ppm	As ppm	-0,1429	0,6207	
Hg ppm	Sb ppm	-0,2143	0,4579	
Hg ppm	Ba ppm	-0,5714	0,0478	

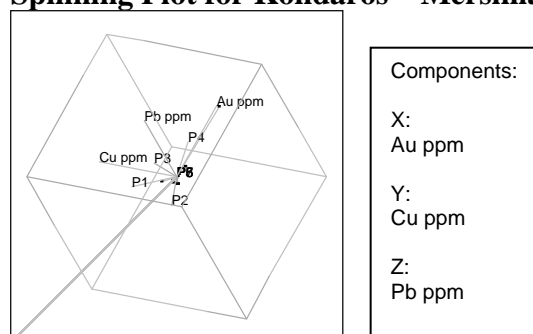
Kondaros - Mersinia - Xerokampos subarea Hoeffding's D correlation

Variable	by Variable	Hoeffding D	Prob>D	Plot
Cu ppm	Au ppm	0,1250	0,0545	
Pb ppm	Au ppm	-0,1071	1,0000	
Pb ppm	Cu ppm	0,1250	0,0545	
Zn ppm	Au ppm	0,4464	0,0009	
Zn ppm	Cu ppm	0,5000	0,0005	
Zn ppm	Pb ppm	-0,0536	0,8457	
As ppm	Au ppm	0,3393	0,0034	
As ppm	Cu ppm	0,4643	0,0007	
As ppm	Pb ppm	0,0179	0,2704	
As ppm	Zn ppm	0,8214	<,0001	
Sb ppm	Au ppm	0,3393	0,0034	
Sb ppm	Cu ppm	0,4643	0,0007	
Sb ppm	Pb ppm	0,0179	0,2704	
Sb ppm	Zn ppm	0,8214	<,0001	
Sb ppm	As ppm	1,0000	0,0000	

Variable	by Variable	Hoeffding D	Prob>D	Plot
Ba ppm	Au ppm	0,4643	0,0007	
Ba ppm	Cu ppm	0,0714	0,1172	
Ba ppm	Pb ppm	0,0000	0,3643	
Ba ppm	Zn ppm	0,3393	0,0034	
Ba ppm	As ppm	0,4464	0,0009	
Ba ppm	Sb ppm	0,4464	0,0009	
Hg ppm	Au ppm	-0,0893	0,9999	
Hg ppm	Cu ppm	-0,0179	0,4931	
Hg ppm	Pb ppm	0,0179	0,2704	
Hg ppm	Zn ppm	0,0714	0,1172	
Hg ppm	As ppm	0,0357	0,2026	
Hg ppm	Sb ppm	0,0357	0,2026	
Hg ppm	Ba ppm	0,1250	0,0545	

Principal Components analysis

Spinning Plot for Kondaros – Mersinia - Xerokampos subarea



Kondaros – Mersinia - Xerokampos subarea Principal components summary table :

Eigenvalue	4,659286	1,236295	1,179376	0,925044	2,47E-16	4,15E-17	-1,15E-16	-5,56E-16
Percent	58,24107	15,45369	14,7422	11,56305	3,09E-15	5,18E-16	-1,44E-15	-6,94E-15
Cum %	58,24107	73,69476	88,43695	100	100	100	100	100
Eigenvectors :								
Au ppm	-0,196738	-0,378633	-0,138037	0,818647	0,034555	0,292484	-0,058878	0,196181
Cu ppm	0,429511	-0,056568	0,183341	0,323582	0,074838	-0,768674	-0,223573	0,165999
Pb ppm	0,087827	-0,374058	0,808428	-0,148107	0,121482	0,217258	0,205719	0,269438
Zn ppm	0,441763	0,188696	0,190273	0,065769	-0,223601	0,445615	-0,674043	-0,16064
As ppm	0,451175	0,126206	-0,065221	0,170379	-0,631627	0,089336	0,576334	0,090203
Sb ppm	0,451767	0,112685	-0,062222	0,176469	0,665197	0,18581	0,326201	-0,405927
Ba ppm	0,365583	-0,182587	-0,458076	-0,309475	0,224016	0,169774	-0,091194	0,663386

Agathia - Larni subarea

Parametric Correlations

Agathia - Larni subarea Pearson's correlation

	Ag ppm	Cu ppm	Pb ppm	Zn ppm	As ppm	Sb ppm	Ba ppm	Hg ppm
Ag ppm	1	0,03747	0,074293	-0,026421	0,053552	-0,054268	0,00745	-0,036871
Cu ppm	0,03747	1	0,322615	0,586257	0,083425	-0,080758	0,095438	-0,094136
Pb ppm	0,074293	0,322615	1	-0,042051	0,041262	-0,145612	-0,334892	-0,076154
Zn ppm	-0,026421	0,586257	-0,042051	1	0,090649	0,083379	0,607071	0,040788
As ppm	0,053552	0,083425	0,041262	0,090649	1	0,811402	0,323654	0,818096
Sb ppm	-0,054268	-0,080758	-0,145612	0,083379	0,811402	1	0,496241	0,817186
Ba ppm	0,00745	0,095438	-0,334892	0,607071	0,323654	0,496241	1	0,456857
Hg ppm	-0,036871	-0,094136	-0,076154	0,040788	0,818096	0,817186	0,456857	1

Agathia - Larni subarea Inverse correlation

	Ag ppm	Cu ppm	Pb ppm	Zn ppm	As ppm	Sb ppm	Ba ppm	Hg ppm
Ag ppm	1,068942	-0,035259	-0,074623	0,240823	-0,466612	0,339969	-0,316387	0,269047
Cu ppm	-0,035259	2,12241	-0,490002	-1,571378	-0,594314	0,18947	0,545402	0,307476
Pb ppm	-0,074623	-0,490002	1,369988	0,014908	-0,17856	0,202447	0,553767	-0,217505
Zn ppm	0,240823	-1,571378	0,014908	3,278641	-0,452554	0,546782	-2,27855	0,692743
As ppm	-0,466612	-0,594314	-0,17856	-0,452554	4,798322	-2,478979	1,075968	-2,459557
Sb ppm	0,339969	0,18947	0,202447	0,546782	-2,478979	4,527991	-1,233673	-1,085069
Ba ppm	-0,316387	0,545402	0,553767	-2,27855	1,075968	-1,233673	3,342265	-1,224255
Hg ppm	0,269047	0,307476	-0,217505	0,692743	-2,459557	-1,085069	-1,224255	4,452212

Agathia - Larni subarea Partial correlation

	Ag ppm	Cu ppm	Pb ppm	Zn ppm	As ppm	Sb ppm	Ba ppm	Hg ppm
Ag ppm		0,023409	0,061665	-0,128639	0,206032	-0,154529	0,167387	-0,123328
Cu ppm	0,023409		0,287359	0,595688	0,186233	-0,061118	-0,204777	-0,100025
Pb ppm	0,061665	0,287359		-0,007034	0,069643	-0,081283	-0,25879	0,088069
Zn ppm	-0,128639	0,595688	-0,007034		0,114098	-0,14191	0,688321	-0,181316
As ppm	0,206032	0,186233	0,069643	0,114098		0,531833	-0,268679	0,532138
Sb ppm	-0,154529	-0,061118	-0,081283	-0,14191	0,531833		0,317122	0,241667
Ba ppm	0,167387	-0,204777	-0,25879	0,688321	-0,268679	0,317122		0,317368
Hg ppm	-0,123328	-0,100025	0,088069	-0,181316	0,532138	0,241667	0,317368	

Agathia - Larni subarea Pairwise correlations

Variable	by Variable	Correlation	Count	Signif Prob	Plot Corr
Ag ppm	Au ppm	.	0	.	
Cu ppm	Au ppm	.	0	.	
Cu ppm	Ag ppm	0,0471	38	0,7787	
Pb ppm	Au ppm	.	0	.	
Pb ppm	Ag ppm	0,0825	38	0,6224	
Pb ppm	Cu ppm	0,4117	71	0,0004	
Zn ppm	Au ppm	.	0	.	
Zn ppm	Ag ppm	-0,0226	38	0,8931	
Zn ppm	Cu ppm	0,5642	70	0,0000	
Zn ppm	Pb ppm	0,0398	73	0,7384	
As ppm	Au ppm	.	0	.	
As ppm	Ag ppm	0,1153	47	0,4404	
As ppm	Cu ppm	-0,1001	63	0,4352	
As ppm	Pb ppm	-0,0667	63	0,6035	
As ppm	Zn ppm	-0,0359	91	0,7354	
Sb ppm	Au ppm	.	0	.	
Sb ppm	Ag ppm	-0,0327	47	0,8271	
Sb ppm	Cu ppm	-0,1185	63	0,3551	
Sb ppm	Pb ppm	-0,0049	63	0,9697	
Sb ppm	Zn ppm	-0,0325	91	0,7595	
Sb ppm	As ppm	0,2266	102	0,0220	
Ba ppm	Au ppm	.	0	.	
Ba ppm	Ag ppm	-0,0370	39	0,8229	
Ba ppm	Cu ppm	-0,0109	70	0,9286	
Ba ppm	Pb ppm	-0,1274	73	0,2829	
Ba ppm	Zn ppm	0,0472	72	0,6937	
Ba ppm	As ppm	0,3451	64	0,0052	
Ba ppm	Sb ppm	0,0898	64	0,4803	
Hg ppm	Au ppm	.	0	.	
Hg ppm	Ag ppm	-0,0369	37	0,8285	
Hg ppm	Cu ppm	-0,1088	56	0,4249	
Hg ppm	Pb ppm	-0,0059	56	0,9655	
Hg ppm	Zn ppm	0,0270	56	0,8433	
Hg ppm	As ppm	0,8449	56	0,0000	
Hg ppm	Sb ppm	0,8030	56	0,0000	
Hg ppm	Ba ppm	0,3388	56	0,0106	
Mn ppm	Au ppm	.	0	.	
Mn ppm	Ag ppm	.	0	.	
Mn ppm	Cu ppm	0,9044	4	0,0956	
Mn ppm	Pb ppm	-0,7272	5	0,1639	
Mn ppm	Zn ppm	0,9282	5	0,0228	
Mn ppm	As ppm	.	0	.	
Mn ppm	Sb ppm	.	0	.	

Variable	by Variable	Correlation	Count	Signif Prob	Plot Corr
Mn ppm	Ba ppm	-0,2544	7	0,5820	
Mn ppm	Hg ppm	.	0	.	

Non Parametric Correlations

Agathia- Larni subarea Spearman's Rho correlation

Variable	by Variable	Spearman Rho	Prob> Rho	Plot
Ag ppm	Au ppm	0,0000	0,0000	
Cu ppm	Au ppm	0,0000	0,0000	
Cu ppm	Ag ppm	0,4904	0,0018	
Pb ppm	Au ppm	0,0000	0,0000	
Pb ppm	Ag ppm	0,3577	0,0275	
Pb ppm	Cu ppm	0,5276	<,0001	
Zn ppm	Au ppm	0,0000	0,0000	
Zn ppm	Ag ppm	0,2302	0,1643	
Zn ppm	Cu ppm	0,3285	0,0055	
Zn ppm	Pb ppm	0,5147	<,0001	
As ppm	Au ppm	0,0000	0,0000	
As ppm	Ag ppm	0,4229	0,0031	
As ppm	Cu ppm	-0,0653	0,6111	
As ppm	Pb ppm	-0,0199	0,8772	
As ppm	Zn ppm	-0,1493	0,1579	
Sb ppm	Au ppm	0,0000	0,0000	
Sb ppm	Ag ppm	0,0127	0,9326	
Sb ppm	Cu ppm	-0,3731	0,0026	
Sb ppm	Pb ppm	-0,1653	0,1955	
Sb ppm	Zn ppm	-0,2328	0,0264	
Sb ppm	As ppm	0,5952	<,0001	
Ba ppm	Au ppm	0,0000	0,0000	
Ba ppm	Ag ppm	-0,1403	0,3944	
Ba ppm	Cu ppm	-0,1492	0,2178	
Ba ppm	Pb ppm	-0,0869	0,4648	
Ba ppm	Zn ppm	-0,0329	0,7835	
Ba ppm	As ppm	0,1167	0,3585	
Ba ppm	Sb ppm	0,4743	<,0001	
Hg ppm	Au ppm	0,0000	0,0000	
Hg ppm	Ag ppm	0,1833	0,2775	
Hg ppm	Cu ppm	-0,1053	0,4400	
Hg ppm	Pb ppm	0,0318	0,8160	
Hg ppm	Zn ppm	0,1219	0,3708	
Hg ppm	As ppm	0,1858	0,1703	
Hg ppm	Sb ppm	0,1606	0,2370	
Hg ppm	Ba ppm	0,2211	0,1014	
Mn ppm	Au ppm	0,0000	0,0000	
Mn ppm	Ag ppm	.	.	
Mn ppm	Cu ppm	0,9487	0,0513	
Mn ppm	Pb ppm	-0,5643	0,3217	
Mn ppm	Zn ppm	0,5643	0,3217	
Mn ppm	As ppm	.	.	
Mn ppm	Sb ppm	.	.	
Mn ppm	Ba ppm	-0,4532	0,3072	
Mn ppm	Hg ppm	.	.	

Agathia- Larni subarea Kendall's Tau b

Variable	by Variable	Kendall Tau b	Prob> Tau b	Plot
Ag ppm	Au ppm	0,0000	0,0000	
Cu ppm	Au ppm	0,0000	0,0000	
Cu ppm	Ag ppm	0,3638	0,0016	
Pb ppm	Au ppm	0,0000	0,0000	
Pb ppm	Ag ppm	0,2345	0,0391	
Pb ppm	Cu ppm	0,3907	<,0001	
Zn ppm	Au ppm	0,0000	0,0000	
Zn ppm	Ag ppm	0,1396	0,2220	
Zn ppm	Cu ppm	0,2411	0,0038	
Zn ppm	Pb ppm	0,3650	<,0001	
As ppm	Au ppm	0,0000	0,0000	
As ppm	Ag ppm	0,2896	0,0044	
As ppm	Cu ppm	-0,0409	0,6428	
As ppm	Pb ppm	0,0021	0,9811	
As ppm	Zn ppm	-0,0992	0,1669	
Sb ppm	Au ppm	0,0000	0,0000	

Variable	by Variable	Kendall Tau b	Prob> Tau b	Plot
Sb ppm	Ag ppm	0,0141	0,8904	
Sb ppm	Cu ppm	-0,2663	0,0027	
Sb ppm	Pb ppm	-0,1147	0,1911	
Sb ppm	Zn ppm	-0,1550	0,0314	
Sb ppm	As ppm	0,4269	<,0001	
Ba ppm	Au ppm	0,0000	0,0000	
Ba ppm	Ag ppm	-0,1059	0,3451	
Ba ppm	Cu ppm	-0,0949	0,2531	
Ba ppm	Pb ppm	-0,0642	0,4235	
Ba ppm	Zn ppm	-0,0327	0,6864	
Ba ppm	As ppm	0,0759	0,3783	
Ba ppm	Sb ppm	0,3415	<,0001	
Hg ppm	Au ppm	0,0000	0,0000	
Hg ppm	Ag ppm	0,1479	0,2785	
Hg ppm	Cu ppm	-0,0870	0,4354	
Hg ppm	Pb ppm	0,0280	0,7992	
Hg ppm	Zn ppm	0,1001	0,3648	
Hg ppm	As ppm	0,1493	0,1766	
Hg ppm	Sb ppm	0,1317	0,2387	
Hg ppm	Ba ppm	0,1821	0,0983	
Mn ppm	Au ppm	0,0000	0,0000	
Mn ppm	Ag ppm	.	.	
Mn ppm	Cu ppm	0,9129	0,0710	
Mn ppm	Pb ppm	-0,5270	0,2065	
Mn ppm	Zn ppm	0,5270	0,2065	
Mn ppm	As ppm	.	.	
Mn ppm	Sb ppm	.	.	
Mn ppm	Ba ppm	-0,3944	0,2412	
Mn ppm	Hg ppm	.	.	

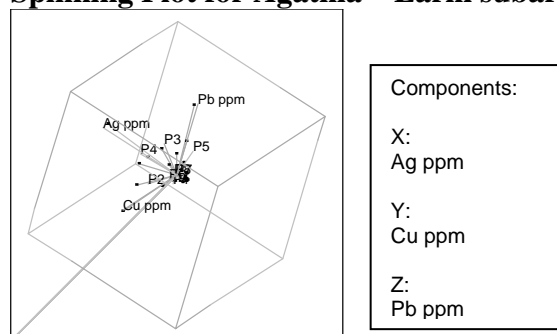
Agathia- Larni subarea Hoeffding's D

Variable	by Variable	Hoeffding D	Prob>D	Plot
Ag ppm	Au ppm	0,0000	0,0000	
Cu ppm	Au ppm	0,0000	0,0000	
Cu ppm	Ag ppm	0,0946	0,0005	
Pb ppm	Au ppm	0,0000	0,0000	
Pb ppm	Ag ppm	0,0145	0,1086	
Pb ppm	Cu ppm	0,1095	<,0001	
Zn ppm	Au ppm	0,0000	0,0000	
Zn ppm	Ag ppm	-0,0062	0,6327	
Zn ppm	Cu ppm	0,0338	0,0036	
Zn ppm	Pb ppm	0,0954	<,0001	
As ppm	Au ppm	0,0000	0,0000	
As ppm	Ag ppm	0,0443	0,0062	
As ppm	Cu ppm	-0,0013	0,4442	
As ppm	Pb ppm	-0,0065	0,8825	
As ppm	Zn ppm	0,0061	0,1056	
Sb ppm	Au ppm	0,0000	0,0000	
Sb ppm	Ag ppm	-0,0103	0,9548	
Sb ppm	Cu ppm	0,0425	0,0021	
Sb ppm	Pb ppm	0,0050	0,1766	
Sb ppm	Zn ppm	0,0098	0,0541	
Sb ppm	As ppm	0,1177	<,0001	
Ba ppm	Au ppm	0,0000	0,0000	
Ba ppm	Ag ppm	0,0020	0,3035	
Ba ppm	Cu ppm	0,0041	0,1878	
Ba ppm	Pb ppm	0,0066	0,1232	
Ba ppm	Zn ppm	-0,0076	0,9929	
Ba ppm	As ppm	-0,0052	0,7743	
Ba ppm	Sb ppm	0,0769	<,0001	
Hg ppm	Au ppm	0,0000	0,0000	
Hg ppm	Ag ppm	-0,0308	1,0000	
Hg ppm	Cu ppm	-0,0219	1,0000	
Hg ppm	Pb ppm	-0,0216	1,0000	
Hg ppm	Zn ppm	-0,0213	1,0000	
Hg ppm	As ppm	-0,0207	1,0000	
Hg ppm	Sb ppm	-0,0211	1,0000	
Hg ppm	Ba ppm	-0,0196	1,0000	
Mn ppm	Au ppm	0,0000	0,0000	
Mn ppm	Ag ppm	.	.	
Mn ppm	Cu ppm	.	.	
Mn ppm	Pb ppm	0,0000	.	

Variable	by Variable	Hoeffding D	Prob>D	Plot
Mn ppm	Zn ppm	0,0000	.	
Mn ppm	As ppm	.	.	
Mn ppm	Sb ppm	.	.	
Mn ppm	Ba ppm	-0,1190	1,0000	
Mn ppm	Hg ppm	.	.	

Principal Components Analysis

Spinning Plot for Agathia – Larni subarea



Agathia- Larni subarea Principal components summary table :

Eigenvalue	3,006151	1,761664	1,328135	0,988607	0,440779	0,185685	0,178263	0,110716
Percent	37,57689	22,0208	16,60169	12,35759	5,509739	2,321057	2,228282	1,383949
Cum %	37,57689	59,59769	76,19938	88,55697	94,06671	96,38777	98,61605	100
Eigenvectors :								
Ag ppm	-0,015117	0,040831	0,228712	0,967645	-0,023273	-0,00414	0,009277	0,093879
Cu ppm	0,030981	0,635821	0,285813	-0,103129	-0,533784	0,462624	0,054836	-0,022217
Pb ppm	-0,114611	0,164339	0,732674	-0,166052	0,62406	0,002427	0,075892	-0,01603
Zn ppm	0,188809	0,651671	-0,204619	-0,004988	0,127911	-0,605177	-0,127532	0,314512
As ppm	0,494881	-0,100879	0,321446	-0,011325	-0,267062	-0,423602	-0,083517	-0,619455
Sb ppm	0,525396	-0,163205	0,07987	-0,050982	-0,045454	0,00967	0,723059	0,404193
Ba ppm	0,404769	0,266707	-0,394789	0,142316	0,482837	0,408759	0,082971	-0,4264

Vromolimni – Akrotiri - Ampelakia subarea Multivariate Correlations

Parametric Correlations

Vromolimni – Akrotiri - Ampelakia subarea Pearson's correlation

	Ag ppm	Cu ppm	Pb ppm	Zn ppm	As ppm	Sb ppm	Ba ppm	Hg ppm
Ag ppm	1	0,969384	0,581125	-0,747219	-0,239933	-0,236426	-0,114288	-0,640701
Cu ppm	0,969384	1	0,418083	-0,81371	-0,365642	-0,3484	-0,354487	-0,453108
Pb ppm	0,581125	0,418083	1	-0,529734	-0,269108	-0,320632	0,545426	-0,971827
Zn ppm	-0,747219	-0,81371	-0,529734	1	0,824396	0,821374	0,421955	0,42362
As ppm	-0,239933	-0,365642	-0,269108	0,824396	1	0,997751	0,529493	0,063848
Sb ppm	-0,236426	-0,3484	-0,320632	0,821374	0,997751	1	0,471544	0,112773
Ba ppm	-0,114288	-0,354487	0,545426	0,421955	0,529493	0,471544	1	-0,621155
Hg ppm	-0,640701	-0,453108	-0,971827	0,42362	0,063848	0,112773	-0,621155	1

Vromolimni – Akrotiri - Ampelakia subarea Inverse correlation

	Ag ppm	Cu ppm	Pb ppm	Zn ppm	As ppm	Sb ppm	Ba ppm	Hg ppm
Ag ppm	43,81131	-38,56688	-9,33568	0	0	0	0	0
Cu ppm	-38,56688	35,16206	7,711512	0	0	0	0	0
Pb ppm	-9,33568	7,711512	3,201143	0	0	0	0	0
Zn ppm	0	0	0	0	0	0	0	0
As ppm	0	0	0	0	0	0	0	0
Sb ppm	0	0	0	0	0	0	0	0
Ba ppm	0	0	0	0	0	0	0	0
Hg ppm	0	0	0	0	0	0	0	0

Vromolimni – Akrotiri - Ampelakia subarea Partial correlation

	Ag ppm	Cu ppm	Pb ppm	Zn ppm	As ppm	Sb ppm	Ba ppm	Hg ppm
Ag ppm		0,982617	0,788316					
Cu ppm	0,982617		-0,726858					
Pb ppm	0,788316	-0,726858						
Zn ppm								
As ppm								
Sb ppm								
Ba ppm								
Hg ppm								

Vromolimni – Akrotiri - Ampelakia subarea Pairwise Correlations

Variable	by Variable	Correlation	Count	Signif Prob	Plot Corr
Ag ppm	Au ppm	.	1	.	
Cu ppm	Au ppm	.	2	.	
Cu ppm	Ag ppm	0,9694	4	0,0306	
Pb ppm	Au ppm	.	2	.	
Pb ppm	Ag ppm	0,5811	4	0,4189	
Pb ppm	Cu ppm	0,1134	54	0,4142	
Zn ppm	Au ppm	.	2	.	
Zn ppm	Ag ppm	-0,7472	4	0,2528	
Zn ppm	Cu ppm	0,2643	54	0,0535	
Zn ppm	Pb ppm	-0,0092	54	0,9473	
As ppm	Au ppm	.	2	.	
As ppm	Ag ppm	-0,2399	4	0,7601	
As ppm	Cu ppm	-0,0165	54	0,9060	
As ppm	Pb ppm	0,0605	54	0,6636	
As ppm	Zn ppm	-0,0016	54	0,9909	
Sb ppm	Au ppm	.	2	.	
Sb ppm	Ag ppm	-0,2364	4	0,7636	
Sb ppm	Cu ppm	-0,1500	48	0,3089	
Sb ppm	Pb ppm	0,1380	48	0,3496	
Sb ppm	Zn ppm	0,1698	48	0,2486	
Sb ppm	As ppm	0,7262	48	0,0000	
Ba ppm	Au ppm	.	2	.	
Ba ppm	Ag ppm	-0,1143	4	0,8857	
Ba ppm	Cu ppm	-0,1329	54	0,3381	
Ba ppm	Pb ppm	0,6864	54	0,0000	
Ba ppm	Zn ppm	-0,0840	54	0,5459	
Ba ppm	As ppm	-0,0196	54	0,8879	
Ba ppm	Sb ppm	0,2051	48	0,1620	
Hg ppm	Au ppm	.	1	.	
Hg ppm	Ag ppm	-0,6407	4	0,3593	
Hg ppm	Cu ppm	0,4059	20	0,0757	
Hg ppm	Pb ppm	-0,2231	20	0,3443	
Hg ppm	Zn ppm	0,4174	20	0,0671	
Hg ppm	As ppm	0,4553	20	0,0437	
Hg ppm	Sb ppm	0,0771	20	0,7465	
Hg ppm	Ba ppm	-0,1946	20	0,4111	
Mn ppm	Au ppm	.	0	.	
Mn ppm	Ag ppm	.	0	.	
Mn ppm	Cu ppm	.	0	.	
Mn ppm	Pb ppm	.	0	.	
Mn ppm	Zn ppm	.	0	.	
Mn ppm	As ppm	.	0	.	
Mn ppm	Sb ppm	.	0	.	

Variable	by Variable	Correlation	Count	Signif Prob	Plot Corr
Mn ppm	Ba ppm	.	0	.	
Mn ppm	Hg ppm	.	0	.	

Non Parametric Correlations

Vromolimni – Akrotiri - Ampelakia subarea Spearman's Rho

Variable	by Variable	Spearman Rho	Prob> Rho	Plot
Ag ppm	Au ppm	.	.	
Cu ppm	Au ppm	.	.	
Cu ppm	Ag ppm	0,4000	0,6000	
Pb ppm	Au ppm	.	.	
Pb ppm	Ag ppm	0,8000	0,2000	
Pb ppm	Cu ppm	0,0109	0,9377	
Zn ppm	Au ppm	.	.	
Zn ppm	Ag ppm	-0,8000	0,2000	
Zn ppm	Cu ppm	0,3712	0,0057	
Zn ppm	Pb ppm	0,1198	0,3884	
As ppm	Au ppm	.	.	
As ppm	Ag ppm	0,4000	0,6000	
As ppm	Cu ppm	-0,0329	0,8136	
As ppm	Pb ppm	0,7928	<,0001	
As ppm	Zn ppm	0,0469	0,7364	
Sb ppm	Au ppm	.	.	
Sb ppm	Ag ppm	0,4000	0,6000	
Sb ppm	Cu ppm	-0,2081	0,1558	
Sb ppm	Pb ppm	0,6685	<,0001	
Sb ppm	Zn ppm	-0,0283	0,8488	
Sb ppm	As ppm	0,7020	<,0001	
Ba ppm	Au ppm	.	.	
Ba ppm	Ag ppm	0,4000	0,6000	
Ba ppm	Cu ppm	-0,1547	0,2641	
Ba ppm	Pb ppm	0,7347	<,0001	
Ba ppm	Zn ppm	-0,0876	0,5286	
Ba ppm	As ppm	0,5212	<,0001	
Ba ppm	Sb ppm	0,4274	0,0024	
Hg ppm	Au ppm	.	.	
Hg ppm	Ag ppm	-0,8000	0,2000	
Hg ppm	Cu ppm	-0,1212	0,6106	
Hg ppm	Pb ppm	-0,1911	0,4196	
Hg ppm	Zn ppm	-0,0632	0,7913	
Hg ppm	As ppm	0,2679	0,2535	
Hg ppm	Sb ppm	0,0204	0,9321	
Hg ppm	Ba ppm	-0,1263	0,5957	
Mn ppm	Au ppm	0,0000	0,0000	
Mn ppm	Ag ppm	0,0000	0,0000	
Mn ppm	Cu ppm	0,0000	0,0000	
Mn ppm	Pb ppm	0,0000	0,0000	
Mn ppm	Zn ppm	0,0000	0,0000	
Mn ppm	As ppm	0,0000	0,0000	
Mn ppm	Sb ppm	0,0000	0,0000	
Mn ppm	Ba ppm	0,0000	0,0000	
Mn ppm	Hg ppm	0,0000	0,0000	

Vromolimni – Akrotiri - Ampelakia subarea Kendall's Tau b

Variable	by Variable	Kendall Tau b	Prob> Tau b	Plot
Ag ppm	Au ppm	.	.	
Cu ppm	Au ppm	.	0,0000	
Cu ppm	Ag ppm	0,3333	0,4969	
Pb ppm	Au ppm	.	0,0000	
Pb ppm	Ag ppm	0,6667	0,1742	
Pb ppm	Cu ppm	-0,0050	0,9582	
Zn ppm	Au ppm	.	0,0000	
Zn ppm	Ag ppm	-0,6667	0,1742	
Zn ppm	Cu ppm	0,2589	0,0066	
Zn ppm	Pb ppm	0,0769	0,4157	
As ppm	Au ppm	.	0,0000	
As ppm	Ag ppm	0,3333	0,4969	
As ppm	Cu ppm	-0,0384	0,6912	
As ppm	Pb ppm	0,6178	<,0001	
As ppm	Zn ppm	0,0264	0,7820	

Variable	by Variable	Kendall Tau b	Prob> Tau b	Plot
Sb ppm	Au ppm	.	0,0000	
Sb ppm	Ag ppm	0,3333	0,4969	
Sb ppm	Cu ppm	-0,1342	0,1921	
Sb ppm	Pb ppm	0,4912	<,0001	
Sb ppm	Zn ppm	-0,0262	0,7961	
Sb ppm	As ppm	0,5385	<,0001	
Ba ppm	Au ppm	.	0,0000	
Ba ppm	Ag ppm	0,3333	0,4969	
Ba ppm	Cu ppm	-0,0928	0,3308	
Ba ppm	Pb ppm	0,5634	<,0001	
Ba ppm	Zn ppm	-0,0534	0,5705	
Ba ppm	As ppm	0,3968	<,0001	
Ba ppm	Sb ppm	0,2922	0,0040	
Hg ppm	Au ppm	.	0,0000	
Hg ppm	Ag ppm	-0,6667	0,1742	
Hg ppm	Cu ppm	-0,1170	0,4744	
Hg ppm	Pb ppm	-0,1482	0,3631	
Hg ppm	Zn ppm	-0,0158	0,9224	
Hg ppm	As ppm	0,2011	0,2171	
Hg ppm	Sb ppm	0,0268	0,8706	
Hg ppm	Ba ppm	-0,0632	0,6970	
Mn ppm	Au ppm	0,0000	0,0000	
Mn ppm	Ag ppm	0,0000	0,0000	
Mn ppm	Cu ppm	0,0000	0,0000	
Mn ppm	Pb ppm	0,0000	0,0000	
Mn ppm	Zn ppm	0,0000	0,0000	
Mn ppm	As ppm	0,0000	0,0000	
Mn ppm	Sb ppm	0,0000	0,0000	
Mn ppm	Ba ppm	0,0000	0,0000	
Mn ppm	Hg ppm	0,0000	0,0000	

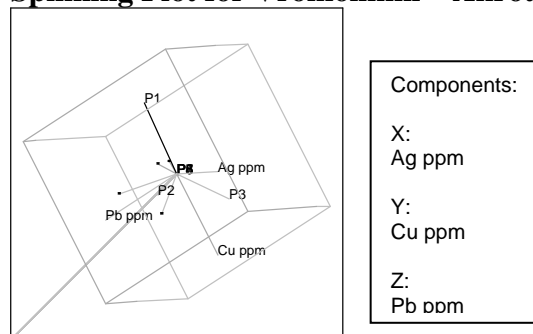
Vromolimni – Akrotiri - Ampelakia subarea Hoeffding's D

Variable	by Variable	Hoeffding D	Prob>D	Plot
Ag ppm	Au ppm	.	.	
Cu ppm	Au ppm	.	.	
Cu ppm	Ag ppm	.	.	
Pb ppm	Au ppm	.	.	
Pb ppm	Ag ppm	.	.	
Pb ppm	Cu ppm	0,0202	0,0371	
Zn ppm	Au ppm	.	.	
Zn ppm	Ag ppm	.	.	
Zn ppm	Cu ppm	0,0288	0,0157	
Zn ppm	Pb ppm	-0,0004	0,3832	
As ppm	Au ppm	.	.	
As ppm	Ag ppm	.	.	
As ppm	Cu ppm	0,0118	0,0901	
As ppm	Pb ppm	0,3177	<,0001	
As ppm	Zn ppm	-0,0042	0,6243	
Sb ppm	Au ppm	.	.	
Sb ppm	Ag ppm	.	.	
Sb ppm	Cu ppm	0,0102	0,1229	
Sb ppm	Pb ppm	0,1865	<,0001	
Sb ppm	Zn ppm	-0,0082	0,8570	
Sb ppm	As ppm	0,1809	<,0001	
Ba ppm	Au ppm	.	.	
Ba ppm	Ag ppm	.	.	
Ba ppm	Cu ppm	-0,0064	0,7954	
Ba ppm	Pb ppm	0,2195	<,0001	
Ba ppm	Zn ppm	-0,0094	0,9759	
Ba ppm	As ppm	0,1179	<,0001	
Ba ppm	Sb ppm	0,0440	0,0058	
Hg ppm	Au ppm	.	.	
Hg ppm	Ag ppm	.	.	
Hg ppm	Cu ppm	-0,0001	0,3652	
Hg ppm	Pb ppm	-0,0202	0,8576	
Hg ppm	Zn ppm	-0,0353	1,0000	
Hg ppm	As ppm	-0,0106	0,5920	
Hg ppm	Sb ppm	-0,0047	0,4523	
Hg ppm	Ba ppm	-0,0009	0,3797	
Mn ppm	Au ppm	0,0000	0,0000	
Mn ppm	Ag ppm	0,0000	0,0000	
Mn ppm	Cu ppm	0,0000	0,0000	

Variable	by Variable	Hoeffding D	Prob>D	Plot
Mn ppm	Pb ppm	0,0000	0,0000	
Mn ppm	Zn ppm	0,0000	0,0000	
Mn ppm	As ppm	0,0000	0,0000	
Mn ppm	Sb ppm	0,0000	0,0000	
Mn ppm	Ba ppm	0,0000	0,0000	
Mn ppm	Hg ppm	0,0000	0,0000	

Principal Components Analysis

Spinning Plot for Vromolimni – Akrotiri - Ampelakia subarea



Vromolimni - Akrotiri - Ampelakia subarea Principal components summary table :

Eigenvalue	4,284387	2,548255	1,167358	1,84E-15	4,53E-16	2,27E-16	5,03E-17	-5,36E-17
Percent	53,55483	31,85319	14,59198	2,3E-14	5,67E-15	2,84E-15	6,28E-16	-6,7E-16
Cum %	53,55483	85,40802	100	100	100	100	100	100
Eigenvectors :								
Ag ppm	-0,396805	0,170828	0,463737	0,562803	0,365134	-0,107197	0,328595	-0,169633
Cu ppm	-0,405335	0,018497	0,502886	-0,537967	-0,036112	0,311063	0,078537	0,434541
Pb ppm	-0,327444	0,416714	-0,289927	-0,014415	-0,095659	0,640274	-0,097482	-0,454159
Zn ppm	0,473067	0,127117	0,003119	-0,355403	0,345513	0,155964	0,667368	-0,211292
As ppm	0,35221	0,336835	0,392016	-0,115068	0,415354	0,004698	-0,636071	-0,135814
Sb ppm	0,355563	0,306054	0,433778	0,184554	-0,730398	0,043911	0,131396	-0,070765
Ba ppm	0,117298	0,572096	-0,302789	0,251349	0,131856	0,076333	0,075301	0,689353

Galana – Favas - Tria Vouna subarea

Parametric Correlations

Galana – Favas - Tria Vouna subarea Pearson's correlation

	Au ppm	Ag ppm	Cu ppm	Pb ppm	Zn ppm	As ppm	Sb ppm	Ba ppm	Hg ppm
Au ppm	1	0,842957	-0,288827	-0,151312	-0,482433	0,529989	-0,224736	0,24058	-0,570353
Ag ppm	0,842957	1	-0,200053	-0,13505	-0,293215	0,64811	-0,104419	-0,158724	-0,246766
Cu ppm	-0,288827	-0,200053	1	0,789071	0,726178	0,06395	0,918991	-0,242468	-0,080061
Pb ppm	-0,151312	-0,13505	0,789071	1	0,326823	0,011489	0,844187	-0,261685	-0,223619
Zn ppm	-0,482433	-0,293215	0,726178	0,326823	1	-0,253246	0,746449	-0,16526	0,13727
As ppm	0,529989	0,64811	0,06395	0,011489	-0,253246	1	-0,028389	-0,536378	-0,307286
Sb ppm	-0,224736	-0,104419	0,918991	0,844187	0,746449	-0,028389	1	-0,252556	-0,15461
Ba ppm	0,24058	-0,158724	-0,242468	-0,261685	-0,16526	-0,536378	-0,252556	1	-0,197925
Hg ppm	-0,570353	-0,246766	-0,080061	-0,223619	0,13727	-0,307286	-0,15461	-0,197925	1

Galana – Favas - Tria Vouna subarea Inverse correlation

	Au ppm	Ag ppm	Cu ppm	Pb ppm	Zn ppm	As ppm	Sb ppm	Ba ppm	Hg ppm
Au ppm	71,89958	-46,44844	77,09573	-127,8136	-100,039	-67,5137	105,2797	-64,87544	3,560162
Ag ppm	-46,44844	33,95356	-40,7987	77,01781	59,52484	36,58694	-68,84427	38,07017	-4,194422
Cu ppm	77,09573	-40,7987	179,1671	-267,7732	-223,4237	-138,9798	206,3301	-113,8425	-14,29972
Pb ppm	-127,8136	77,01781	-267,7732	441,6128	365,9589	214,3506	-366,1911	180,1601	18,09472
Zn ppm	-100,039	59,52484	-223,4237	365,9589	307,264	177,8508	-304,4029	147,6106	16,20423
As ppm	-67,5137	36,58694	-138,9798	214,3506	177,8508	113,3187	-168,7945	94,01517	10,2462
Sb ppm	105,2797	-68,84427	206,3301	-366,1911	-304,4029	-168,7945	321,3281	-143,9618	-11,20624
Ba ppm	-64,87544	38,07017	-113,8425	180,1601	147,6106	94,01517	-143,9618	81,87092	6,138902
Hg ppm	3,560162	-4,194422	-14,29972	18,09472	16,20423	10,2462	-11,20624	6,138902	5,303602

Galana – Favas - Tria Vouna subarea Partial correlation

	Au ppm	Ag ppm	Cu ppm	Pb ppm	Zn ppm	As ppm	Sb ppm	Ba ppm	Hg ppm
Au ppm		0,940081	-0,679263	0,717287	0,673054	0,747959	-0,692639	0,845575	-0,182314
Ag ppm	0,940081		0,523088	-0,628967	-0,582773	-0,589838	0,659099	-0,722067	0,312568
Cu ppm	-0,679263	0,523088		0,951957	0,952235	0,975375	-0,859922	0,939963	0,463888
Pb ppm	0,717287	-0,628967	0,951957		-0,993472	-0,958193	0,972104	-0,947486	-0,373892
Zn ppm	0,673054	-0,582773	0,952235	-0,993472		-0,953123	0,968765	-0,930672	-0,401409
As ppm	0,747959	-0,589838	0,975375	-0,958193	-0,953123		0,884572	-0,976073	-0,417952
Sb ppm	-0,692639	0,659099	-0,859922	0,972104	0,968765	0,884572		0,887581	0,271457
Ba ppm	0,845575	-0,722067	0,939963	-0,947486	-0,930672	-0,976073	0,887581		-0,294605
Hg ppm	-0,182314	0,312568	0,463888	-0,373892	-0,401409	-0,417952	0,271457	-0,294605	

Galana – Favas - Tria Vouna subarea Pairwise Correlations

Variable	by Variable	Correlation	Count	Signif Prob	Plot Corr
Ag ppm	Au ppm	0,4256	27	0,0269	
Cu ppm	Au ppm	0,1299	28	0,5102	
Cu ppm	Ag ppm	0,0447	31	0,8113	
Pb ppm	Au ppm	0,1907	28	0,3310	
Pb ppm	Ag ppm	0,0843	31	0,6521	
Pb ppm	Cu ppm	0,4098	216	0,0000	
Zn ppm	Au ppm	-0,0905	29	0,6407	
Zn ppm	Ag ppm	-0,0323	31	0,8631	
Zn ppm	Cu ppm	0,3707	216	0,0000	
Zn ppm	Pb ppm	0,0302	216	0,6589	
As ppm	Au ppm	0,3345	19	0,1615	
As ppm	Ag ppm	0,3474	21	0,1229	
As ppm	Cu ppm	0,0819	202	0,2465	
As ppm	Pb ppm	0,0494	202	0,4854	
As ppm	Zn ppm	0,0849	223	0,2067	
Sb ppm	Au ppm	0,2705	19	0,2628	
Sb ppm	Ag ppm	0,1204	21	0,6030	
Sb ppm	Cu ppm	0,2864	98	0,0042	
Sb ppm	Pb ppm	0,2816	98	0,0050	
Sb ppm	Zn ppm	0,0934	114	0,3230	
Sb ppm	As ppm	0,9318	114	0,0000	
Ba ppm	Au ppm	0,2741	18	0,2711	
Ba ppm	Ag ppm	-0,0531	21	0,8191	
Ba ppm	Cu ppm	0,1435	206	0,0396	
Ba ppm	Pb ppm	0,0740	206	0,2903	
Ba ppm	Zn ppm	0,0313	206	0,6551	
Ba ppm	As ppm	0,2729	202	0,0001	
Ba ppm	Sb ppm	0,2519	98	0,0123	
Hg ppm	Au ppm	-0,3880	12	0,2127	
Hg ppm	Ag ppm	-0,2176	17	0,4014	
Hg ppm	Cu ppm	0,1064	50	0,4621	
Hg ppm	Pb ppm	0,0316	50	0,8275	
Hg ppm	Zn ppm	0,0347	50	0,8107	
Hg ppm	As ppm	-0,0734	50	0,6125	
Hg ppm	Sb ppm	-0,0624	34	0,7259	
Hg ppm	Ba ppm	-0,0596	50	0,6808	

Non Parametric Correlations

Galana – Favas - Tria Vouna subarea Spearman's Rho correlation

Variable	by Variable	Spearman Rho	Prob> Rho	Plot
Ag ppm	Au ppm	0,6997	<,0001	
Cu ppm	Au ppm	0,5594	0,0020	
Cu ppm	Ag ppm	0,6868	<,0001	
Pb ppm	Au ppm	0,6403	0,0002	
Pb ppm	Ag ppm	0,6961	<,0001	
Pb ppm	Cu ppm	0,2887	<,0001	
Zn ppm	Au ppm	0,1047	0,5889	
Zn ppm	Ag ppm	0,4032	0,0245	
Zn ppm	Cu ppm	0,4110	<,0001	
Zn ppm	Pb ppm	0,2402	0,0004	
As ppm	Au ppm	0,6740	0,0016	
As ppm	Ag ppm	0,5582	0,0086	
As ppm	Cu ppm	0,1236	0,0797	
As ppm	Pb ppm	0,5287	<,0001	
As ppm	Zn ppm	0,0463	0,4911	
Sb ppm	Au ppm	0,7515	0,0002	
Sb ppm	Ag ppm	0,7206	0,0002	
Sb ppm	Cu ppm	0,2859	0,0043	
Sb ppm	Pb ppm	0,7117	<,0001	
Sb ppm	Zn ppm	0,1477	0,1167	
Sb ppm	As ppm	0,7074	<,0001	
Ba ppm	Au ppm	0,1012	0,6895	
Ba ppm	Ag ppm	-0,0845	0,7157	
Ba ppm	Cu ppm	-0,0775	0,2680	
Ba ppm	Pb ppm	0,2903	<,0001	
Ba ppm	Zn ppm	0,0105	0,8814	
Ba ppm	As ppm	0,2586	0,0002	
Ba ppm	Sb ppm	0,2507	0,0128	
Hg ppm	Au ppm	-0,3666	0,2411	
Hg ppm	Ag ppm	-0,4158	0,0969	
Hg ppm	Cu ppm	0,2729	0,0552	
Hg ppm	Pb ppm	0,1656	0,2503	
Hg ppm	Zn ppm	-0,0249	0,8635	
Hg ppm	As ppm	0,1648	0,2529	
Hg ppm	Sb ppm	0,2014	0,2534	
Hg ppm	Ba ppm	0,0245	0,8659	

Galana – Favas - Tria Vouna subarea Kendall's Tau b correlation

Variable	by Variable	Kendall Tau b	Prob> Tau b	Plot
Ag ppm	Au ppm	0,5452	<,0001	
Cu ppm	Au ppm	0,4085	0,0023	
Cu ppm	Ag ppm	0,5032	<,0001	
Pb ppm	Au ppm	0,4509	0,0008	
Pb ppm	Ag ppm	0,4973	<,0001	
Pb ppm	Cu ppm	0,1975	<,0001	
Zn ppm	Au ppm	0,0962	0,4644	
Zn ppm	Ag ppm	0,2657	0,0365	
Zn ppm	Cu ppm	0,3089	<,0001	
Zn ppm	Pb ppm	0,1673	0,0004	
As ppm	Au ppm	0,5161	0,0021	
As ppm	Ag ppm	0,4880	0,0020	
As ppm	Cu ppm	0,0749	0,1456	
As ppm	Pb ppm	0,4091	<,0001	
As ppm	Zn ppm	0,0337	0,4833	
Sb ppm	Au ppm	0,5471	0,0011	
Sb ppm	Ag ppm	0,5263	0,0009	
Sb ppm	Cu ppm	0,1941	0,0063	
Sb ppm	Pb ppm	0,5607	<,0001	
Sb ppm	Zn ppm	0,0994	0,1296	
Sb ppm	As ppm	0,5368	<,0001	
Ba ppm	Au ppm	0,1443	0,4043	
Ba ppm	Ag ppm	0,0192	0,9037	
Ba ppm	Cu ppm	-0,0643	0,1806	
Ba ppm	Pb ppm	0,2167	<,0001	
Ba ppm	Zn ppm	0,0054	0,9090	
Ba ppm	As ppm	0,2014	<,0001	

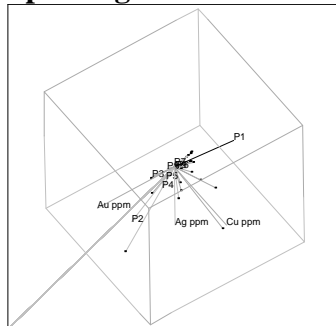
Variable	by Variable	Kendall Tau b	Prob> Tau b	Plot
Ba ppm	Sb ppm	0,1966	0,0054	
Hg ppm	Au ppm	-0,2543	0,2626	
Hg ppm	Ag ppm	-0,2944	0,1053	
Hg ppm	Cu ppm	0,1920	0,0537	
Hg ppm	Pb ppm	0,1099	0,2714	
Hg ppm	Zn ppm	-0,0241	0,8079	
Hg ppm	As ppm	0,0835	0,4108	
Hg ppm	Sb ppm	0,1413	0,2510	
Hg ppm	Ba ppm	0,0182	0,8537	

Galana – Favas - Tria Vouna subarea Hoeffding's D correlation

Variable	by Variable	Hoeffding D	Prob>D	Plot
Ag ppm	Au ppm	0,2149	<,0001	
Cu ppm	Au ppm	0,1287	0,0005	
Cu ppm	Ag ppm	0,2170	<,0001	
Pb ppm	Au ppm	0,1558	0,0001	
Pb ppm	Ag ppm	0,1666	<,0001	
Pb ppm	Cu ppm	0,0439	<,0001	
Zn ppm	Au ppm	0,0143	0,1448	
Zn ppm	Ag ppm	0,0981	0,0012	
Zn ppm	Cu ppm	0,0611	<,0001	
Zn ppm	Pb ppm	0,0176	0,0003	
As ppm	Au ppm	0,2234	0,0002	
As ppm	Ag ppm	0,1934	0,0002	
As ppm	Cu ppm	0,0205	0,0002	
As ppm	Pb ppm	0,1033	<,0001	
As ppm	Zn ppm	0,0069	0,0155	
Sb ppm	Au ppm	0,2122	0,0003	
Sb ppm	Ag ppm	0,1959	0,0002	
Sb ppm	Cu ppm	0,0377	0,0004	
Sb ppm	Pb ppm	0,2135	<,0001	
Sb ppm	Zn ppm	0,0082	0,0492	
Sb ppm	As ppm	0,1866	<,0001	
Ba ppm	Au ppm	0,0006	0,3561	
Ba ppm	Ag ppm	0,0034	0,3093	
Ba ppm	Cu ppm	0,0059	0,0280	
Ba ppm	Pb ppm	0,0356	<,0001	
Ba ppm	Zn ppm	-0,0005	0,4669	
Ba ppm	As ppm	0,0263	<,0001	
Ba ppm	Sb ppm	0,0430	0,0001	
Hg ppm	Au ppm	-0,0410	0,9366	
Hg ppm	Ag ppm	0,0346	0,1048	
Hg ppm	Cu ppm	0,0219	0,0370	
Hg ppm	Pb ppm	-0,0006	0,3895	
Hg ppm	Zn ppm	0,0001	0,3605	
Hg ppm	As ppm	-0,0045	0,6165	
Hg ppm	Sb ppm	0,0089	0,1840	
Hg ppm	Ba ppm	-0,0059	0,7224	

Principal Components Analysis

Spinning Plot for Galana - Favas - Tria Vouna subarea



Components:

X:
Au ppm

Y:
Ag ppm

Z:
Cu ppm

Galana - Favas - Tria Vouna subarea Principal components summary table :

Eigenvalue	3,608742	2,539351	1,409926	0,679813	0,476866	0,244293	0,023405	0,016912	0,000692
Percent	40,09713	28,21501	15,66585	7,553479	5,298507	2,714369	0,260058	0,187908	0,00769
Cum %	40,09713	68,31214	83,97799	91,53147	96,82997	99,54434	99,8044	99,99231	100
Eigenvectors :									
Au ppm	-0,339933	0,411912	0,262236	0,2176	0,168922	0,016971	-0,139215	0,723086	-0,166131
Ag ppm	-0,2677	0,447041	-0,107158	0,466537	0,310607	-0,273351	-0,12678	-0,549605	0,100077
Cu ppm	0,464975	0,230788	0,066402	0,081812	0,018602	0,519026	-0,557092	-0,162569	-0,336034
Pb ppm	0,385196	0,274929	0,147748	-0,419649	0,499228	-0,107438	-0,05394	0,099472	0,55184
Zn ppm	0,430607	-0,011175	0,001681	0,595773	-0,415775	-0,153246	-0,055878	0,224109	0,458043
As ppm	-0,148616	0,493178	-0,359153	-0,098403	-0,270832	0,557544	0,372238	-0,006934	0,270556
Sb ppm	0,46273	0,258692	0,125707	0,130448	0,1182	-0,163094	0,66029	-0,01645	-0,457511
Ba ppm	-0,144205	-0,230056	0,699521	0,240037	0,144914	0,448999	0,248668	-0,206704	0,228405

Triades – Ag. Nikolaos subarea

Triades – Ag. Nikolaos subarea Pearson's correlation

	Au ppm	Ag ppm	Cu ppm	Pb ppm	Zn ppm	As ppm	Sb ppm	Ba ppm	Hg ppm
Au ppm	1	0,347886	-0,348536	-0,204274	-0,108631	-0,278916	-0,116519	0,477704	0,329675
Ag ppm	0,347886	1	-0,179548	-0,095516	-0,040581	-0,200432	-0,064901	0,630093	0,637689
Cu ppm	-0,348536	-0,179548	1	0,273504	0,503068	0,372359	0,457771	0,04017	0,120422
Pb ppm	-0,204274	-0,095516	0,273504	1	-0,050545	-0,105468	-0,195809	-0,155473	-0,250526
Zn ppm	-0,108631	-0,040581	0,503068	-0,050545	1	-0,078067	-0,117291	0,10619	0,520717
As ppm	-0,278916	-0,200432	0,372359	-0,105468	-0,078067	1	0,831705	0,155688	-0,204665
Sb ppm	-0,116519	-0,064901	0,457771	-0,195809	-0,117291	0,831705	1	0,294779	-0,074356
Ba ppm	0,477704	0,630093	0,04017	-0,155473	0,10619	0,155688	0,294779	1	0,541191
Hg ppm	0,329675	0,637689	0,120422	-0,250526	0,520717	-0,204665	-0,074356	0,541191	1

Triades – Ag. Nikolaos subarea Inverse correlation

	Au ppm	Ag ppm	Cu ppm	Pb ppm	Zn ppm	As ppm	Sb ppm	Ba ppm	Hg ppm
Au ppm	1,927083	0,670289	0,503771	0,049241	0,436346	0,837311	-0,308932	-1,127359	-0,579776
Ag ppm	0,670289	3,432316	0,181964	-0,236172	1,562093	0,434305	0,284351	-1,577621	-2,340394
Cu ppm	0,503771	0,181964	3,812691	-1,556863	-2,115791	0,891045	-3,115221	0,419169	-0,305674
Pb ppm	0,049241	-0,236172	-1,556863	1,829773	0,730252	-0,317629	1,569323	-0,371707	0,652848
Zn ppm	0,436346	1,562093	-2,115791	0,730252	3,610996	-0,631635	2,299472	-0,823133	-2,095379
As ppm	0,837311	0,434305	0,891045	-0,317629	-0,631635	4,123007	-3,676381	-0,475527	0,416862
Sb ppm	-0,308932	0,284351	-3,115221	1,569323	2,299472	-3,676381	6,354434	-1,104073	-0,190982
Ba ppm	-1,127359	-1,577621	0,419169	-0,371707	-0,823133	-0,475527	-1,104073	3,029386	-0,156179
Hg ppm	-0,579776	-2,340394	-0,305674	0,652848	-2,095379	0,416862	-0,190982	-0,156179	4,130688

Triades – Ag. Nikolaos subarea Partial correlation

	Au ppm	Ag ppm	Cu ppm	Pb ppm	Zn ppm	As ppm	Sb ppm	Ba ppm	Hg ppm
Au ppm		-0,260626	-0,185852	-0,026223	-0,165412	-0,29705	0,088282	0,466589	0,205494
Ag ppm	-0,260626		-0,050301	0,09424	-0,443711	-0,11545	-0,060887	0,489251	0,621562
Cu ppm	-0,185852	-0,050301		0,589435	0,570221	-0,224738	0,632899	-0,123338	0,077025
Pb ppm	-0,026223	0,09424	0,589435		-0,284093	0,115642	-0,46023	0,157879	-0,237466
Zn ppm	-0,165412	-0,443711	0,570221	-0,284093		0,163699	-0,480039	0,248874	0,542548
As ppm	-0,29705	-0,11545	-0,224738	0,115642	0,163699		0,718249	0,134552	-0,101012
Sb ppm	0,088282	-0,060887	0,632899	-0,46023	-0,480039	0,718249		0,251641	0,037277
Ba ppm	0,466589	0,489251	-0,123338	0,157879	0,248874	0,134552	0,251641		0,04415
Hg ppm	0,205494	0,621562	0,077025	-0,237466	0,542548	-0,101012	0,037277	0,04415	

Triades – Ag. Nikolaos subarea Pairwise Correlations

Variable	by Variable	Correlation	Count	Signif Prob	Plot Corr
Ag ppm	Au ppm	0,6209	88	0,0000	
Cu ppm	Au ppm	0,2100	92	0,0446	
Cu ppm	Ag ppm	0,3480	87	0,0010	
Pb ppm	Au ppm	-0,1542	93	0,1400	
Pb ppm	Ag ppm	-0,1423	87	0,1885	
Pb ppm	Cu ppm	0,0568	171	0,4609	
Zn ppm	Au ppm	0,0262	94	0,8021	
Zn ppm	Ag ppm	0,1357	88	0,2075	
Zn ppm	Cu ppm	0,6662	171	0,0000	
Zn ppm	Pb ppm	-0,0192	172	0,8028	
As ppm	Au ppm	-0,0269	33	0,8820	

Variable	by Variable	Correlation	Count	Signif Prob	Plot Corr
As ppm	Ag ppm	0,3246	27	0,0986	
As ppm	Cu ppm	0,6892	109	0,0000	
As ppm	Pb ppm	0,8350	109	0,0000	
As ppm	Zn ppm	0,0355	110	0,7131	
Sb ppm	Au ppm	0,0242	33	0,8937	
Sb ppm	Ag ppm	0,2876	27	0,1458	
Sb ppm	Cu ppm	0,6860	100	0,0000	
Sb ppm	Pb ppm	0,6522	100	0,0000	
Sb ppm	Zn ppm	0,0098	101	0,9227	
Sb ppm	As ppm	0,8974	101	0,0000	
Ba ppm	Au ppm	0,5499	33	0,0009	
Ba ppm	Ag ppm	0,5658	27	0,0021	
Ba ppm	Cu ppm	0,3163	111	0,0007	
Ba ppm	Pb ppm	0,1942	111	0,0411	
Ba ppm	Zn ppm	0,0894	111	0,3507	
Ba ppm	As ppm	0,2056	109	0,0320	
Ba ppm	Sb ppm	0,2891	100	0,0035	
Hg ppm	Au ppm	0,4261	24	0,0379	
Hg ppm	Ag ppm	0,3963	25	0,0498	
Hg ppm	Cu ppm	0,3507	47	0,0157	
Hg ppm	Pb ppm	0,2656	47	0,0711	
Hg ppm	Zn ppm	0,2236	47	0,1309	
Hg ppm	As ppm	0,2909	47	0,0473	
Hg ppm	Sb ppm	0,2357	46	0,1148	
Hg ppm	Ba ppm	0,4371	47	0,0021	

Non parametric Correlations

Triades – Ag. Nikolaos subarea Spearman's Rho

Variable	by Variable	Spearman Rho	Prob> Rho	Plot
Ag ppm	Au ppm	0,7437	<,0001	
Cu ppm	Au ppm	0,6037	<,0001	
Cu ppm	Ag ppm	0,6472	<,0001	
Pb ppm	Au ppm	0,0791	0,4513	
Pb ppm	Ag ppm	-0,1329	0,2196	
Pb ppm	Cu ppm	0,5716	<,0001	
Zn ppm	Au ppm	0,4253	<,0001	
Zn ppm	Ag ppm	0,4594	<,0001	
Zn ppm	Cu ppm	0,6726	<,0001	
Zn ppm	Pb ppm	0,3421	<,0001	
As ppm	Au ppm	0,5594	0,0007	
As ppm	Ag ppm	0,1354	0,5008	
As ppm	Cu ppm	0,2410	0,0116	
As ppm	Pb ppm	0,7575	<,0001	
As ppm	Zn ppm	0,0667	0,4886	
Sb ppm	Au ppm	0,7195	<,0001	
Sb ppm	Ag ppm	0,5903	0,0012	
Sb ppm	Cu ppm	0,3293	0,0008	
Sb ppm	Pb ppm	0,7731	<,0001	
Sb ppm	Zn ppm	0,1007	0,3163	
Sb ppm	As ppm	0,8587	<,0001	
Ba ppm	Au ppm	0,6228	0,0001	
Ba ppm	Ag ppm	0,6558	0,0002	
Ba ppm	Cu ppm	0,3369	0,0003	
Ba ppm	Pb ppm	0,7298	<,0001	
Ba ppm	Zn ppm	0,1481	0,1208	
Ba ppm	As ppm	0,5853	<,0001	
Ba ppm	Sb ppm	0,6734	<,0001	
Hg ppm	Au ppm	0,3970	0,0548	
Hg ppm	Ag ppm	0,4302	0,0318	
Hg ppm	Cu ppm	0,2079	0,1608	
Hg ppm	Pb ppm	0,3468	0,0169	
Hg ppm	Zn ppm	0,2166	0,1436	
Hg ppm	As ppm	0,3837	0,0078	
Hg ppm	Sb ppm	0,4344	0,0026	
Hg ppm	Ba ppm	0,4224	0,0031	

Triades – Ag. Nikolaos subarea Kendall's Tau b

Variable	by Variable	Kendall Tau b	Prob> Tau b	Plot
Ag ppm	Au ppm	0,5679	<,0001	

Variable	by Variable	Kendall Tau b	Prob> Tau b	Plot
Cu ppm	Au ppm	0,4224	<,0001	
Cu ppm	Ag ppm	0,4652	<,0001	
Pb ppm	Au ppm	0,0502	0,4775	
Pb ppm	Ag ppm	-0,0876	0,2319	
Pb ppm	Cu ppm	0,3954	<,0001	
Zn ppm	Au ppm	0,2842	<,0001	
Zn ppm	Ag ppm	0,3078	<,0001	
Zn ppm	Cu ppm	0,4932	0,0000	
Zn ppm	Pb ppm	0,2488	<,0001	
As ppm	Au ppm	0,3755	0,0024	
As ppm	Ag ppm	0,0823	0,5567	
As ppm	Cu ppm	0,1451	0,0297	
As ppm	Pb ppm	0,5689	0,0000	
As ppm	Zn ppm	0,0375	0,5687	
Sb ppm	Au ppm	0,5092	<,0001	
Sb ppm	Ag ppm	0,4502	0,0013	
Sb ppm	Cu ppm	0,2064	0,0035	
Sb ppm	Pb ppm	0,5796	<,0001	
Sb ppm	Zn ppm	0,0708	0,3086	
Sb ppm	As ppm	0,6926	0,0000	
Ba ppm	Au ppm	0,4592	0,0002	
Ba ppm	Ag ppm	0,4749	0,0008	
Ba ppm	Cu ppm	0,2204	0,0008	
Ba ppm	Pb ppm	0,5315	<,0001	
Ba ppm	Zn ppm	0,0992	0,1261	
Ba ppm	As ppm	0,4138	<,0001	
Ba ppm	Sb ppm	0,5122	<,0001	
Hg ppm	Au ppm	0,2441	0,0962	
Hg ppm	Ag ppm	0,2898	0,0479	
Hg ppm	Cu ppm	0,1531	0,1340	
Hg ppm	Pb ppm	0,2408	0,0175	
Hg ppm	Zn ppm	0,1262	0,2122	
Hg ppm	As ppm	0,2490	0,0139	
Hg ppm	Sb ppm	0,2920	0,0047	
Hg ppm	Ba ppm	0,2909	0,0042	

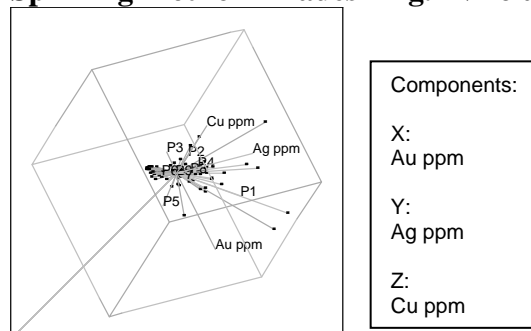
Triades – Ag. Nikolaos subarea Hoeffding's D

Variable	by Variable	Hoeffding D	Prob>D	Plot
Ag ppm	Au ppm	0,2610	<,0001	
Cu ppm	Au ppm	0,1197	<,0001	
Cu ppm	Ag ppm	0,1542	<,0001	
Pb ppm	Au ppm	0,0291	0,0020	
Pb ppm	Ag ppm	0,0199	0,0113	
Pb ppm	Cu ppm	0,1250	<,0001	
Zn ppm	Au ppm	0,0617	<,0001	
Zn ppm	Ag ppm	0,0619	<,0001	
Zn ppm	Cu ppm	0,1792	<,0001	
Zn ppm	Pb ppm	0,0631	<,0001	
As ppm	Au ppm	0,1176	0,0003	
As ppm	Ag ppm	-0,0075	0,5842	
As ppm	Cu ppm	0,0194	0,0055	
As ppm	Pb ppm	0,2500	<,0001	
As ppm	Zn ppm	0,0167	0,0091	
Sb ppm	Au ppm	0,2006	<,0001	
Sb ppm	Ag ppm	0,1242	0,0007	
Sb ppm	Cu ppm	0,0351	0,0005	
Sb ppm	Pb ppm	0,2474	<,0001	
Sb ppm	Zn ppm	0,0103	0,0401	
Sb ppm	As ppm	0,3670	<,0001	
Ba ppm	Au ppm	0,1359	0,0001	
Ba ppm	Ag ppm	0,1109	0,0014	
Ba ppm	Cu ppm	0,0284	0,0009	
Ba ppm	Pb ppm	0,2136	<,0001	
Ba ppm	Zn ppm	0,0089	0,0444	
Ba ppm	As ppm	0,1316	<,0001	
Ba ppm	Sb ppm	0,1947	<,0001	
Hg ppm	Au ppm	0,0182	0,1397	
Hg ppm	Ag ppm	0,0236	0,1018	
Hg ppm	Cu ppm	0,0112	0,1133	

Variable	by Variable	Hoeffding D	Prob>D	Plot
Hg ppm	Pb ppm	0,0204	0,0483	
Hg ppm	Zn ppm	-0,0006	0,3873	
Hg ppm	As ppm	0,0250	0,0319	
Hg ppm	Sb ppm	0,0415	0,0084	
Hg ppm	Ba ppm	0,0518	0,0033	

Principal Components Analysis

Spinning Plot for Triades - Ag. Nikolaos subarea



Triades – Ag. Nikolaos subarea Principal components summary table :

Eigenvalue	2,700485	2,271859	1,654722	1,013629	0,636108	0,303904	0,211531	0,127035	0,080729
Percent	30,00539	25,24287	18,3858	11,26254	7,067866	3,376712	2,350339	1,411495	0,896989
Cum %	30,00539	55,24826	73,63405	84,8966	91,96447	95,34118	97,69152	99,10301	100
Eigenvectors :									
Au ppm	0,419808	-0,074579	-0,241003	0,032763	0,774334	-0,214039	0,230723	0,244545	-0,024537
Ag ppm	0,487559	0,088283	-0,070454	0,317378	-0,52722	-0,193735	0,024465	0,565925	0,111517
Cu ppm	-0,191596	0,44726	0,417108	0,169046	0,168044	-0,498487	-0,306937	0,133307	-0,414711
Pb ppm	-0,18686	-0,118464	0,27525	0,834515	0,141739	0,156968	0,287362	-0,119025	0,19339
Zn ppm	0,107537	0,219174	0,636851	-0,312964	0,169471	0,380805	0,050895	0,338767	0,38182
As ppm	-0,25963	0,501299	-0,281177	-0,00991	-0,045004	0,355139	0,520286	0,247456	-0,376899
Sb ppm	-0,16014	0,556341	-0,312432	0,014329	0,048382	-0,278091	-0,016986	-0,178115	0,674783
Ba ppm	0,420072	0,343753	-0,150516	0,251382	0,115982	0,510535	-0,517796	-0,243631	-0,13401
Hg ppm	0,483058	0,213425	0,286887	-0,108457	-0,166069	-0,185495	0,477171	-0,56649	-0,128247

Ag. Stefanos- Ralaki – Ntasifnos - Spiritou Rema - Ammoudaraki subarea

Parametric Correlation

Ag. Stefanos- Ralaki - Ntasifnos - Spiritou Rema - Ammoudaraki subarea

Pearson's correlation

	Au ppm	Ag ppm	Cu ppm	Pb ppm	Zn ppm	As ppm	Sb ppm	Ba ppm	Hg ppm
Au ppm	1	0,619353	0,452164	-0,419088	-0,038432	-0,288477	0,43649	-0,536592	0,984411
Ag ppm	0,619353	1	0,234041	-0,497829	-0,264019	-0,281337	0,066873	-0,845081	0,573279
Cu ppm	0,452164	0,234041	1	0,405261	0,53265	0,608502	0,838403	0,004669	0,334255
Pb ppm	-0,419088	-0,497829	0,405261	1	0,564317	0,447171	0,2825	0,781242	-0,537418
Zn ppm	-0,038432	-0,264019	0,53265	0,564317	1	0,616321	0,819886	0,181209	-0,147684
As ppm	-0,288477	-0,281337	0,608502	0,447171	0,616321	1	0,624448	0,217089	-0,346938
Sb ppm	0,43649	0,066873	0,838403	0,2825	0,819886	0,624448	1	-0,093647	0,340938
Ba ppm	-0,536592	-0,845081	0,004669	0,781242	0,181209	0,217089	-0,093647	1	-0,550035
Hg ppm	0,984411	0,573279	0,334255	-0,537418	-0,147684	-0,346938	0,340938	-0,550035	1

Ag. Stefanos - Ralaki - Ntasifnos - Spiritou Rema – Ammoudaraki subarea

Inverse correlation

	Au ppm	Ag ppm	Cu ppm	Pb ppm	Zn ppm	As ppm	Sb ppm	Ba ppm	Hg ppm
Au ppm	2,88029	-0,46694	-1,909667	1,733764	0,026205	0	0	0	0
Ag ppm	-0,46694	2,117232	-0,939023	0,955627	0,501939	0	0	0	0
Cu ppm	-1,909667	-0,939023	3,457938	-2,125224	-0,963884	0	0	0	0
Pb ppm	1,733764	0,955627	-2,125224	3,293717	-0,407763	0	0	0	0
Zn ppm	0,026205	0,501939	-0,963884	-0,407763	1,877049	0	0	0	0
As ppm	0	0	0	0	0	0	0	0	0
Sb ppm	0	0	0	0	0	0	0	0	0
Ba ppm	0	0	0	0	0	0	0	0	0
Hg ppm	0	0	0	0	0	0	0	0	0

Ag. Stefanos- Ralaki – Ntasifnos - Spiritou Rema – Ammoudaraki subarea

Partial correlation

	Au ppm	Ag ppm	Cu ppm	Pb ppm	Zn ppm	As ppm	Sb ppm	Ba ppm	Hg ppm
Au ppm		0,189086	0,605105	-0,562897	-0,01127				
Ag ppm	0,189086		0,347043	-0,361877	-0,251785				
Cu ppm	0,605105	0,347043		0,629728	0,378337				
Pb ppm	-0,562897	-0,361877	0,629728		0,163994				
Zn ppm	-0,01127	-0,251785	0,378337	0,163994					
As ppm									
Sb ppm									
Ba ppm									
Hg ppm									

Ag. Stefanos- Ralaki – Ntasifnos - Spiritou Rema – Ammoudaraki subarea

Pairwise Correlations

Variable	by Variable	Correlation	Count	Signif Prob	Plot Corr
Ag ppm	Au ppm	0,0777	17	0,7669	
Cu ppm	Au ppm	0,2283	43	0,1409	
Cu ppm	Ag ppm	0,1918	12	0,5504	
Pb ppm	Au ppm	-0,0454	43	0,7726	
Pb ppm	Ag ppm	-0,0028	12	0,9932	
Pb ppm	Cu ppm	0,2046	108	0,0337	
Zn ppm	Au ppm	-0,0305	46	0,8407	
Zn ppm	Ag ppm	-0,2606	12	0,4133	
Zn ppm	Cu ppm	0,1366	108	0,1586	
Zn ppm	Pb ppm	0,2044	108	0,0338	
As ppm	Au ppm	-0,0843	43	0,5909	
As ppm	Ag ppm	-0,2290	11	0,4982	
As ppm	Cu ppm	0,2713	100	0,0063	
As ppm	Pb ppm	0,3444	100	0,0005	
As ppm	Zn ppm	0,1587	115	0,0903	
Sb ppm	Au ppm	0,0264	43	0,8667	
Sb ppm	Ag ppm	-0,3925	11	0,2325	
Sb ppm	Cu ppm	0,2958	99	0,0030	
Sb ppm	Pb ppm	0,1508	99	0,1362	
Sb ppm	Zn ppm	0,0845	111	0,3779	
Sb ppm	As ppm	0,8382	111	0,0000	
Ba ppm	Au ppm	-0,1828	41	0,2527	
Ba ppm	Ag ppm	-0,7276	11	0,0112	
Ba ppm	Cu ppm	0,2291	104	0,0193	
Ba ppm	Pb ppm	0,5788	104	0,0000	
Ba ppm	Zn ppm	0,2153	104	0,0281	
Ba ppm	As ppm	0,5080	100	0,0000	
Ba ppm	Sb ppm	0,4284	99	0,0000	
Hg ppm	Au ppm	0,1566	24	0,4649	
Hg ppm	Ag ppm	0,1303	10	0,7198	
Hg ppm	Cu ppm	-0,1139	53	0,4168	
Hg ppm	Pb ppm	0,0924	53	0,5103	
Hg ppm	Zn ppm	0,1136	53	0,4179	
Hg ppm	As ppm	0,0262	53	0,8524	
Hg ppm	Sb ppm	0,0172	53	0,9029	
Hg ppm	Ba ppm	-0,0756	53	0,5906	

Non Parametric Correlations

Ag. Stefanos- Ralaki – Ntasifnos - Spiritou Rema – Ammoudaraki subarea

Spearman's Rho correlation

Variable	by Variable	Spearman Rho	Prob> Rho	Plot
Ag ppm	Au ppm	0,4286	0,0861	
Cu ppm	Au ppm	0,1800	0,2480	
Cu ppm	Ag ppm	0,2228	0,4864	
Pb ppm	Au ppm	0,0834	0,5949	
Pb ppm	Ag ppm	0,0876	0,7867	
Pb ppm	Cu ppm	0,3660	<,0001	
Zn ppm	Au ppm	0,1204	0,4254	
Zn ppm	Ag ppm	-0,3853	0,2161	
Zn ppm	Cu ppm	0,4606	<,0001	
Zn ppm	Pb ppm	0,3677	<,0001	
As ppm	Au ppm	0,0595	0,7047	
As ppm	Ag ppm	-0,2096	0,5363	
As ppm	Cu ppm	0,2538	0,0109	
As ppm	Pb ppm	0,6584	<,0001	
As ppm	Zn ppm	0,2603	0,0050	
Sb ppm	Au ppm	0,0175	0,9111	
Sb ppm	Ag ppm	-0,4658	0,1488	
Sb ppm	Cu ppm	0,3279	0,0009	
Sb ppm	Pb ppm	0,4724	<,0001	
Sb ppm	Zn ppm	0,4281	<,0001	
Sb ppm	As ppm	0,6974	<,0001	
Ba ppm	Au ppm	-0,1332	0,4063	
Ba ppm	Ag ppm	-0,7443	0,0086	
Ba ppm	Cu ppm	0,3327	0,0006	
Ba ppm	Pb ppm	0,6545	<,0001	
Ba ppm	Zn ppm	0,2396	0,0143	
Ba ppm	As ppm	0,5013	<,0001	
Ba ppm	Sb ppm	0,3800	0,0001	
Hg ppm	Au ppm	0,1748	0,4141	
Hg ppm	Ag ppm	-0,0547	0,8807	
Hg ppm	Cu ppm	0,0700	0,6182	
Hg ppm	Pb ppm	0,1451	0,2999	
Hg ppm	Zn ppm	-0,0542	0,6997	
Hg ppm	As ppm	0,3564	0,0088	
Hg ppm	Sb ppm	0,0755	0,5911	
Hg ppm	Ba ppm	0,2408	0,0824	

Ag. Stefanos- Ralaki – Ntasifnos - Spiritou Rema – Ammoudaraki subarea

Kendall's Tau b correlation

Variable	by Variable	Kendall Tau b	Prob> Tau b	Plot
Ag ppm	Au ppm	0,2793	0,1250	
Cu ppm	Au ppm	0,1167	0,2962	
Cu ppm	Ag ppm	0,2462	0,2703	
Pb ppm	Au ppm	0,0496	0,6445	
Pb ppm	Ag ppm	-0,0153	0,9452	
Pb ppm	Cu ppm	0,2612	0,0002	
Zn ppm	Au ppm	0,0975	0,3474	
Zn ppm	Ag ppm	-0,2595	0,2426	
Zn ppm	Cu ppm	0,3501	<,0001	
Zn ppm	Pb ppm	0,2650	<,0001	
As ppm	Au ppm	0,0303	0,7772	
As ppm	Ag ppm	-0,0734	0,7548	
As ppm	Cu ppm	0,1823	0,0117	
As ppm	Pb ppm	0,4629	<,0001	
As ppm	Zn ppm	0,1760	0,0057	
Sb ppm	Au ppm	0,0056	0,9582	
Sb ppm	Ag ppm	-0,3519	0,1367	
Sb ppm	Cu ppm	0,2417	0,0009	
Sb ppm	Pb ppm	0,3351	<,0001	
Sb ppm	Zn ppm	0,3004	<,0001	
Sb ppm	As ppm	0,5241	<,0001	
Ba ppm	Au ppm	-0,1017	0,3560	
Ba ppm	Ag ppm	-0,5370	0,0231	
Ba ppm	Cu ppm	0,2479	0,0005	
Ba ppm	Pb ppm	0,4658	<,0001	

Variable	by Variable	Kendall Tau b	Prob> Tau b	Plot
Ba ppm	Zn ppm	0,1654	0,0138	
Ba ppm	As ppm	0,3632	<,0001	
Ba ppm	Sb ppm	0,2764	<,0001	
Hg ppm	Au ppm	0,1289	0,3838	
Hg ppm	Ag ppm	-0,0449	0,8575	
Hg ppm	Cu ppm	0,0501	0,6129	
Hg ppm	Pb ppm	0,0774	0,4198	
Hg ppm	Zn ppm	-0,0249	0,7941	
Hg ppm	As ppm	0,2403	0,0113	
Hg ppm	Sb ppm	0,0438	0,6452	
Hg ppm	Ba ppm	0,1452	0,1267	

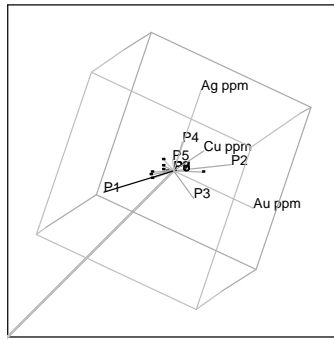
Ag. Stefanos- Ralaki – Ntasifnos - Spiritou Rema – Ammoudaraki subarea

Hoeffding's D correlation

Variable	by Variable	Hoeffding D	Prob>D	Plot
Ag ppm	Au ppm	0,0298	0,1230	
Cu ppm	Au ppm	-0,0023	0,4598	
Cu ppm	Ag ppm	-0,0066	0,4344	
Pb ppm	Au ppm	-0,0053	0,6191	
Pb ppm	Ag ppm	-0,0279	0,7465	
Pb ppm	Cu ppm	0,0355	0,0003	
Zn ppm	Au ppm	-0,0066	0,7308	
Zn ppm	Ag ppm	-0,0319	0,8111	
Zn ppm	Cu ppm	0,0689	<,0001	
Zn ppm	Pb ppm	0,0435	<,0001	
As ppm	Au ppm	-0,0096	0,8855	
As ppm	Ag ppm	-0,0106	0,4704	
As ppm	Cu ppm	0,0234	0,0037	
As ppm	Pb ppm	0,1471	<,0001	
As ppm	Zn ppm	0,0159	0,0092	
Sb ppm	Au ppm	-0,0071	0,7346	
Sb ppm	Ag ppm	-0,0227	0,6277	
Sb ppm	Cu ppm	0,0386	0,0003	
Sb ppm	Pb ppm	0,0656	<,0001	
Sb ppm	Zn ppm	0,0638	<,0001	
Sb ppm	As ppm	0,1782	<,0001	
Ba ppm	Au ppm	-0,0052	0,6004	
Ba ppm	Ag ppm	0,1948	0,0073	
Ba ppm	Cu ppm	0,0361	0,0003	
Ba ppm	Pb ppm	0,1502	<,0001	
Ba ppm	Zn ppm	0,0230	0,0034	
Ba ppm	As ppm	0,1012	<,0001	
Ba ppm	Sb ppm	0,0522	<,0001	
Hg ppm	Au ppm	0,0043	0,2877	
Hg ppm	Ag ppm	0,0134	0,2732	
Hg ppm	Cu ppm	-0,0070	0,8280	
Hg ppm	Pb ppm	-0,0037	0,5786	
Hg ppm	Zn ppm	-0,0048	0,6598	
Hg ppm	As ppm	0,0315	0,0128	
Hg ppm	Sb ppm	-0,0076	0,8702	
Hg ppm	Ba ppm	0,0089	0,1274	

Principal Components Analysis

Spinning Plot for Ag. Stefanos – Ralaki - Ntasifnos - Spiritou Rema - Ammoudaraki subarea



Components:

X:
Au ppm

Y:
Ag ppm

Z:
Cu ppm

Ag. Stefanos - Ralaki - Ntasifnos - Spiritou Rema - Ammoudaraki subarea

Principal components summary table :

Eigenvalue	3,892659	3,260109	0,88106	0,550542	0,415629	1,17E-15	4,16E-16	-1,13E-16	-2,14E-16
Percent	43,25177	36,22344	9,789553	6,117137	4,618103	1,3E-14	4,62E-15	-1,26E-15	-2,38E-15
Cum %	43,25177	79,47521	89,26476	95,3819	100	100	100	100	100
Eigenvectors :									
Au ppm	-0,376541	0,311691	0,38273	-0,059431	-0,029288	0,270479	0,46909	0,175631	-0,534923
Ag ppm	-0,403888	0,146843	-0,29515	0,558215	0,334146	0,448933	-0,027782	0,084922	0,308896
Cu ppm	0,058628	0,50994	0,09449	0,447757	-0,222754	-0,249785	-0,07703	-0,629318	-0,114554
Pb ppm	0,427227	0,127973	0,284512	0,433567	0,384037	-0,35864	0,082209	0,497891	-0,037575
Zn ppm	0,269512	0,38324	-0,118864	-0,426529	0,550205	0,081484	0,364993	-0,299104	0,228882
As ppm	0,308287	0,308217	-0,46001	0,047624	-0,564928	0,097719	0,368929	0,33354	0,14154
Sb ppm	0,074597	0,536423	-0,022808	-0,26781	0,026847	0,200614	-0,703795	0,272727	-0,154175
Ba ppm	0,417385	-0,106986	0,548357	0,099511	-0,184596	0,613974	-0,032276	-0,119696	0,278097
Hg ppm	-0,402093	0,252594	0,386749	-0,174864	-0,18363	-0,317627	0,028175	0,169076	0,656032

Plakota - Ag. Panteleimon - Petrovounia subarea

Parametric Correlations

Plakota - Ag. Panteleimon - Petrovounia subarea Pearson's correlation

	Ag ppm	Cu ppm	Pb ppm	Zn ppm	As ppm	Sb ppm	Ba ppm
Ag ppm	1	-0,03408	-0,188123	-0,376236	-0,203853	-0,283953	-0,225085
Cu ppm	-0,03408	1	0,960074	0,937207	0,412082	-0,144328	0,969346
Pb ppm	-0,188123	0,960074	1	0,949267	0,524268	-0,273726	0,926497
Zn ppm	-0,376236	0,937207	0,949267	1	0,480372	-0,03146	0,976834
As ppm	-0,203853	0,412082	0,524268	0,480372	1	-0,286548	0,352665
Sb ppm	-0,283953	-0,144328	-0,273726	-0,03146	-0,286548	1	0,007689
Ba ppm	-0,225085	0,969346	0,926497	0,976834	0,352665	0,007689	1

Plakota - Ag. Panteleimon - Petrovounia subarea Inverse correlation

	Ag ppm	Cu ppm	Pb ppm	Zn ppm	As ppm	Sb ppm	Ba ppm
Ag ppm	257,4064	-764,3217	133,2364	706,8581	-41,97051	0	0
Cu ppm	-764,3217	2285,885	-408,6345	-2102,821	126,59	0	0
Pb ppm	133,2364	-408,6345	90,08116	359,2384	-24,24339	0	0
Zn ppm	706,8581	-2102,821	359,2384	1952,187	-115,4845	0	0
As ppm	-41,97051	126,59	-24,24339	-115,4845	8,464338	0	0
Sb ppm	0	0	0	0	0	0	0
Ba ppm	0	0	0	0	0	0	0

Plakota - Ag. Panteleimon - Petrovounia subarea Partial correlation

	Ag ppm	Cu ppm	Pb ppm	Zn ppm	As ppm	Sb ppm	Ba ppm
Ag ppm		0,996413	-0,874976	-0,997153	0,899162		
Cu ppm	0,996413		0,900515	0,995438	-0,910072		
Pb ppm	-0,874976	0,900515		-0,856653	0,87797		
Zn ppm	-0,997153	0,995438	-0,856653		0,898393		
As ppm	0,899162	-0,910072	0,87797	0,898393			
Sb ppm							
Ba ppm							

Plakota - Ag. Panteleimon - Petrovounia subarea Partial correlation

Pairwise Correlations

Variable	by Variable	Correlation	Signif Prob	Plot Corr
Cu ppm	Ag ppm	-0,0341	0,9489	
Pb ppm	Ag ppm	-0,1881	0,7211	
Pb ppm	Cu ppm	0,9640	0,0000	
Zn ppm	Ag ppm	-0,3762	0,4623	
Zn ppm	Cu ppm	0,9427	0,0001	
Zn ppm	Pb ppm	0,9433	0,0000	
As ppm	Ag ppm	-0,2039	0,6985	
As ppm	Cu ppm	0,4121	0,4169	
As ppm	Pb ppm	0,5243	0,2856	
As ppm	Zn ppm	0,4804	0,3349	
Sb ppm	Ag ppm	-0,2840	0,5855	
Sb ppm	Cu ppm	-0,1443	0,7850	
Sb ppm	Pb ppm	-0,2737	0,5997	
Sb ppm	Zn ppm	-0,0315	0,9528	
Sb ppm	As ppm	-0,2865	0,5819	
Ba ppm	Ag ppm	-0,2251	0,6681	
Ba ppm	Cu ppm	0,9739	0,0000	
Ba ppm	Pb ppm	0,9371	0,0001	
Ba ppm	Zn ppm	0,9737	0,0000	
Ba ppm	As ppm	0,3527	0,4929	
Ba ppm	Sb ppm	0,0077	0,9885	

Non parametric correlations

Plakota - Ag. Panteleimon - Petrovounia subarea Spearman's Rho correlation

Variable	by Variable	Spearman Rho	Prob> Rho	Plot
Cu ppm	Ag ppm	0,4286	0,3965	
Pb ppm	Ag ppm	0,2571	0,6228	
Pb ppm	Cu ppm	0,7833	0,0125	
Zn ppm	Ag ppm	-0,2571	0,6228	
Zn ppm	Cu ppm	0,5333	0,1392	
Zn ppm	Pb ppm	0,8909	0,0005	
As ppm	Ag ppm	-0,0286	0,9572	
As ppm	Cu ppm	0,2571	0,6228	
As ppm	Pb ppm	0,6000	0,2080	
As ppm	Zn ppm	0,0857	0,8717	
Sb ppm	Ag ppm	-0,3769	0,4615	
Sb ppm	Cu ppm	-0,1449	0,7841	
Sb ppm	Pb ppm	-0,5798	0,2278	
Sb ppm	Zn ppm	-0,3189	0,5379	
Sb ppm	As ppm	-0,4638	0,3542	
Ba ppm	Ag ppm	0,1429	0,7872	
Ba ppm	Cu ppm	0,6000	0,0876	
Ba ppm	Pb ppm	0,7212	0,0186	
Ba ppm	Zn ppm	0,7697	0,0092	
Ba ppm	As ppm	-0,2000	0,7040	
Ba ppm	Sb ppm	0,1739	0,7417	

Plakota – Ag. Panteleimon - Petrovounia subarea Kendall's Tau b correlation

Variable	by Variable	Kendall Tau b	Prob> Tau b	Plot
Cu ppm	Ag ppm	0,4667	0,1885	
Pb ppm	Ag ppm	0,2000	0,5730	
Pb ppm	Cu ppm	0,6111	0,0218	

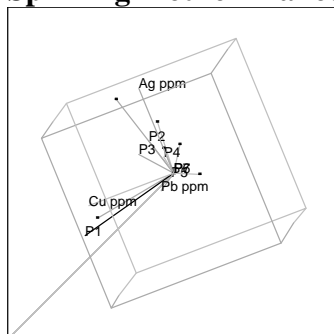
Variable	by Variable	Kendall Tau b	Prob> Tau b	Plot
Zn ppm	Ag ppm	-0,2000	0,5730	
Zn ppm	Cu ppm	0,4444	0,0953	
Zn ppm	Pb ppm	0,7778	0,0017	
As ppm	Ag ppm	-0,0667	0,8510	
As ppm	Cu ppm	0,2000	0,5730	
As ppm	Pb ppm	0,4667	0,1885	
As ppm	Zn ppm	0,0667	0,8510	
Sb ppm	Ag ppm	-0,4140	0,2511	
Sb ppm	Cu ppm	-0,1380	0,7021	
Sb ppm	Pb ppm	-0,4140	0,2511	
Sb ppm	Zn ppm	-0,2760	0,4442	
Sb ppm	As ppm	-0,2760	0,4442	
Ba ppm	Ag ppm	0,2000	0,5730	
Ba ppm	Cu ppm	0,4444	0,0953	
Ba ppm	Pb ppm	0,6000	0,0157	
Ba ppm	Zn ppm	0,6444	0,0095	
Ba ppm	As ppm	-0,0667	0,8510	
Ba ppm	Sb ppm	0,1380	0,7021	

Plakota – Ag. Panteleimon - Petrovounia subarea Hoeffding's D correlation

Variable	by Variable	Hoeffding D	Prob>D	Plot
Cu ppm	Ag ppm	0,1667	0,0592	
Pb ppm	Ag ppm	-0,3333	1,0000	
Pb ppm	Cu ppm	0,2460	0,0070	
Zn ppm	Ag ppm	-0,1667	1,0000	
Zn ppm	Cu ppm	-0,0040	0,3933	
Zn ppm	Pb ppm	0,5238	<,0001	
As ppm	Ag ppm	0,1667	0,0592	
As ppm	Cu ppm	-0,1667	1,0000	
As ppm	Pb ppm	-0,1667	1,0000	
As ppm	Zn ppm	-0,1667	1,0000	
Sb ppm	Ag ppm	0,1042	0,1121	
Sb ppm	Cu ppm	-0,0208	0,4688	
Sb ppm	Pb ppm	0,1042	0,1121	
Sb ppm	Zn ppm	-0,0208	0,4688	
Sb ppm	As ppm	-0,0417	0,6009	
Ba ppm	Ag ppm	0,0000	0,3643	
Ba ppm	Cu ppm	0,2302	0,0088	
Ba ppm	Pb ppm	0,2183	0,0071	
Ba ppm	Zn ppm	0,2500	0,0042	
Ba ppm	As ppm	0,0000	0,3643	
Ba ppm	Sb ppm	0,0000	0,3643	

Principal Components Analysis

Spinning Plot for Plakota - Ag. Panteleimon - Petrovounia subarea



Components:

X:
Ag ppm

Y:
Cu ppm

Z:
Pb ppm

Plakota – Ag. Panteleimon - Petrovounia subarea Principal components summary table:

Eigenvalue	4,195765	1,361415	0,935838	0,48154	0,025443	-6,7E-17	-4,33E-16
Percent	59,93949	19,44879	13,36911	6,879137	0,363465	-9,57E-16	-6,18E-15
Cum %	59,93949	79,38829	92,7574	99,63654	100	100	100
Eigenvectors :							
Ag ppm	-0,133503	0,616528	0,566302	0,472723	-0,016693	0,161238	0,177847
Cu ppm	0,467748	0,081944	0,275978	0,056696	0,044673	-0,154614	-0,818057
Pb ppm	0,479241	0,100127	0,040506	-0,109192	0,778647	-0,119401	0,355235
Zn ppm	0,48084	-0,135728	0,041484	-0,066102	-0,209225	0,830683	0,102326
As ppm	0,278417	0,189197	-0,670467	0,65275	-0,081784	-0,066063	0,005216
Sb ppm	-0,078883	-0,733376	0,295817	0,574293	0,193998	0,001767	0,031293
Ba ppm	0,46773	-0,105338	0,250485	-0,033631	-0,55076	-0,491363	0,401851

Koumaria – Kirjiannoulis – Skiadi subarea

Parametric Correlations

Koumaria - Kirjiannoulis - Skiadi subarea Pearson's correlation

	Au ppm	Ag ppm	Cu ppm	Pb ppm	Zn ppm	As ppm	Sb ppm	Ba ppm
Au ppm	1	0,201706	0,038959	0,38011	-0,145616	0,027873	0,279528	0,181732
Ag ppm	0,201706	1	0,207622	0,334317	-0,256208	0,802212	0,363953	0,033543
Cu ppm	0,038959	0,207622	1	0,199158	0,093984	0,353177	0,38013	0,027188
Pb ppm	0,38011	0,334317	0,199158	1	-0,188436	0,310385	0,588517	0,383535
Zn ppm	-0,145616	-0,256208	0,093984	-0,188436	1	-0,185454	-0,532307	-0,22449
As ppm	0,027873	0,802212	0,353177	0,310385	-0,185454	1	0,416304	0,140493
Sb ppm	0,279528	0,363953	0,38013	0,588517	-0,532307	0,416304	1	0,579177
Ba ppm	0,181732	0,033543	0,027188	0,383535	-0,22449	0,140493	0,579177	1

Koumaria - Kirjiannoulis - Skiadi subarea Inverse correlation

	Au ppm	Ag ppm	Cu ppm	Pb ppm	Zn ppm	As ppm	Sb ppm	Ba ppm
Au ppm	1,294476	-0,572114	-0,019193	-0,378121	-0,003521	0,613841	-0,135378	-0,079136
Ag ppm	-0,572114	3,450526	0,340439	-0,246444	0,275794	-2,777391	-0,122876	0,596778
Cu ppm	-0,019193	0,340439	1,651066	0,163405	-0,718543	-0,572145	-1,313462	0,564312
Pb ppm	-0,378121	-0,246444	0,163405	1,78709	-0,388905	-0,018558	-1,074005	-0,07553
Zn ppm	-0,003521	0,275794	-0,718543	-0,388905	1,833862	-0,141608	1,64784	-0,362729
As ppm	0,613841	-2,777391	-0,572145	-0,018558	-0,141608	3,559327	-0,276756	-0,367279
Sb ppm	-0,135378	-0,122876	-1,313462	-1,074005	1,64784	-0,276756	4,053287	-1,462411
Ba ppm	-0,079136	0,596778	0,564312	-0,07553	-0,362729	-0,367279	-1,462411	1,825156

Koumaria - Kirjiannoulis - Skiadi subarea Partial correlation

	Au ppm	Ag ppm	Cu ppm	Pb ppm	Zn ppm	As ppm	Sb ppm	Ba ppm
Au ppm		0,270703	0,013129	0,248605	0,002285	-0,285973	0,059101	0,051484
Ag ppm	0,270703		-0,142631	0,099243	-0,109637	0,79252	0,032856	-0,237804
Cu ppm	0,013129	-0,142631		-0,095129	0,41294	0,236015	0,507729	-0,325077
Pb ppm	0,248605	0,099243	-0,095129		0,214826	0,007358	0,399052	0,041821
Zn ppm	0,002285	-0,109637	0,41294	0,214826		0,055427	-0,604405	0,198266
As ppm	-0,285973	0,79252	0,236015	0,007358	0,055427		0,072863	0,144099
Sb ppm	0,059101	0,032856	0,507729	0,399052	-0,604405	0,072863		0,53767
Ba ppm	0,051484	-0,237804	-0,325077	0,041821	0,198266	0,144099	0,53767	

Koumaria - Kirjiannoulis - Skiadi subarea Pairwise Correlations

Variable	by Variable	Correlation	Signif Prob	Plot Corr
Ag ppm	Au ppm	0,2656	0,0000	
Cu ppm	Au ppm	0,0379	0,8163	
Cu ppm	Ag ppm	0,2076	0,2709	
Pb ppm	Au ppm	0,4445	0,0041	
Pb ppm	Ag ppm	0,3343	0,0710	
Pb ppm	Cu ppm	0,1811	0,2633	

Variable	by Variable	Correlation	Signif Prob	Plot Corr
Zn ppm	Au ppm	-0,2464	0,1254	
Zn ppm	Ag ppm	-0,2562	0,1717	
Zn ppm	Cu ppm	0,2786	0,0817	
Zn ppm	Pb ppm	-0,1879	0,2456	
As ppm	Au ppm	0,0782	0,6313	
As ppm	Ag ppm	0,8022	0,0000	
As ppm	Cu ppm	0,2440	0,1291	
As ppm	Pb ppm	0,3161	0,0469	
As ppm	Zn ppm	-0,2492	0,1210	
Sb ppm	Au ppm	0,3669	0,0199	
Sb ppm	Ag ppm	0,3640	0,0480	
Sb ppm	Cu ppm	0,2658	0,0973	
Sb ppm	Pb ppm	0,6244	0,0000	
Sb ppm	Zn ppm	-0,5191	0,0006	
Sb ppm	As ppm	0,4378	0,0047	
Ba ppm	Au ppm	0,1858	0,2509	
Ba ppm	Ag ppm	0,0335	0,8603	
Ba ppm	Cu ppm	-0,0307	0,8506	
Ba ppm	Pb ppm	0,3667	0,0200	
Ba ppm	Zn ppm	-0,2315	0,1507	
Ba ppm	As ppm	0,1344	0,4084	
Ba ppm	Sb ppm	0,5215	0,0006	

Non Parametric Correlations

Koumaria - Kirjiannoulis - Skiadi subarea Spearman's Rho correlation

Variable	by Variable	Spearman Rho	Prob> Rho	Plot
Ag ppm	Au ppm	0,4881	<,0001	
Cu ppm	Au ppm	0,1924	0,2342	
Cu ppm	Ag ppm	0,0644	0,7354	
Pb ppm	Au ppm	0,5504	0,0002	
Pb ppm	Ag ppm	0,4536	0,0118	
Pb ppm	Cu ppm	0,2185	0,1755	
Zn ppm	Au ppm	-0,4668	0,0024	
Zn ppm	Ag ppm	-0,7271	<,0001	
Zn ppm	Cu ppm	0,1334	0,4117	
Zn ppm	Pb ppm	-0,2265	0,1599	
As ppm	Au ppm	0,2190	0,1745	
As ppm	Ag ppm	0,5295	0,0026	
As ppm	Cu ppm	-0,0495	0,7616	
As ppm	Pb ppm	0,2382	0,1389	
As ppm	Zn ppm	-0,5180	0,0006	
Sb ppm	Au ppm	0,6819	<,0001	
Sb ppm	Ag ppm	0,7830	<,0001	
Sb ppm	Cu ppm	0,0202	0,9016	
Sb ppm	Pb ppm	0,6138	<,0001	
Sb ppm	Zn ppm	-0,7559	<,0001	
Sb ppm	As ppm	0,5663	0,0001	
Ba ppm	Au ppm	0,0996	0,5411	
Ba ppm	Ag ppm	0,3476	0,0598	
Ba ppm	Cu ppm	0,0100	0,9510	
Ba ppm	Pb ppm	0,2394	0,1368	
Ba ppm	Zn ppm	-0,2817	0,0782	
Ba ppm	As ppm	0,2122	0,1886	
Ba ppm	Sb ppm	0,4339	0,0052	

Koumaria - Kirjiannoulis - Skiadi subarea Kendall's Tau b correlation

Variable	by Variable	Kendall Tau b	Prob> Tau b	Plot
Ag ppm	Au ppm	0,3433	<,0001	
Cu ppm	Au ppm	0,1211	0,2731	
Cu ppm	Ag ppm	0,0209	0,8722	
Pb ppm	Au ppm	0,3753	0,0007	
Pb ppm	Ag ppm	0,3384	0,0091	
Pb ppm	Cu ppm	0,1440	0,1918	
Zn ppm	Au ppm	-0,3449	0,0018	
Zn ppm	Ag ppm	-0,5529	<,0001	
Zn ppm	Cu ppm	0,0875	0,4280	
Zn ppm	Pb ppm	-0,1463	0,1840	
As ppm	Au ppm	0,1514	0,1756	

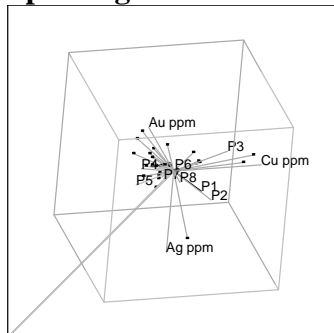
Variable	by Variable	Kendall Tau b	Prob> Tau b	Plot
As ppm	Ag ppm	0,3735	0,0046	
As ppm	Cu ppm	-0,0522	0,6404	
As ppm	Pb ppm	0,1589	0,1544	
As ppm	Zn ppm	-0,3703	0,0009	
Sb ppm	Au ppm	0,5311	<,0001	
Sb ppm	Ag ppm	0,5774	<,0001	
Sb ppm	Cu ppm	0,0311	0,7795	
Sb ppm	Pb ppm	0,4238	0,0001	
Sb ppm	Zn ppm	-0,5951	<,0001	
Sb ppm	As ppm	0,4081	0,0003	
Ba ppm	Au ppm	0,0771	0,4844	
Ba ppm	Ag ppm	0,2225	0,0864	
Ba ppm	Cu ppm	0,0026	0,9814	
Ba ppm	Zn ppm	0,1410	0,2000	
Ba ppm	Pb ppm	-0,1900	0,0846	
Ba ppm	As ppm	0,1615	0,1477	
Ba ppm	Sb ppm	0,3178	0,0041	

Koumaria - Kirjiannoulis - Skiadi subarea Hoeffding's D correlation

Variable	by Variable	Hoeffding D	Prob>D	Plot
Ag ppm	Au ppm	0,0870	<,0001	
Cu ppm	Au ppm	-0,0038	0,5234	
Cu ppm	Ag ppm	-0,0116	0,7892	
Pb ppm	Au ppm	0,0852	0,0006	
Pb ppm	Ag ppm	0,0663	0,0076	
Pb ppm	Cu ppm	0,0022	0,2955	
Zn ppm	Au ppm	0,0732	0,0014	
Zn ppm	Ag ppm	0,2309	<,0001	
Zn ppm	Cu ppm	-0,0077	0,7349	
Zn ppm	Pb ppm	0,0079	0,1782	
As ppm	Au ppm	0,0029	0,2770	
As ppm	Ag ppm	0,0794	0,0038	
As ppm	Cu ppm	0,0093	0,1580	
As ppm	Pb ppm	0,0013	0,3215	
As ppm	Zn ppm	0,0920	0,0004	
Sb ppm	Au ppm	0,2407	<,0001	
Sb ppm	Ag ppm	0,2329	<,0001	
Sb ppm	Cu ppm	0,0081	0,1744	
Sb ppm	Pb ppm	0,1268	<,0001	
Sb ppm	Zn ppm	0,2554	<,0001	
Sb ppm	As ppm	0,0887	0,0005	
Ba ppm	Au ppm	-0,0026	0,4671	
Ba ppm	Ag ppm	0,0260	0,0694	
Ba ppm	Cu ppm	-0,0118	0,9441	
Ba ppm	Pb ppm	0,0096	0,1541	
Ba ppm	Zn ppm	0,0416	0,0132	
Ba ppm	As ppm	0,0119	0,1268	
Ba ppm	Sb ppm	0,0965	0,0003	

Principal Components Analysis

Spinning Plot for Koumaria - Kirjiannoulis - Skiadi subarea



Components:

X:
Au ppm

Y:
Ag ppm

Z:
Cu ppm

Koumaria-Kirjiannoulis-Skiadi subarea Principal components summary table :

Eigenvalue	3,081173	1,442887	1,043019	0,940146	0,693072	0,489963	0,160462	0,149277
Percent	38,51466	18,03608	13,03774	11,75183	8,663404	6,124541	2,00578	1,865963
Cum %	38,51466	56,55075	69,58848	81,34031	90,00372	96,12826	98,13404	100
Eigenvectors :								
Au ppm	0,234341	-0,291201	0,160978	0,773894	-0,232567	0,397123	-0,072574	-0,135645
Ag ppm	0,390851	0,444273	-0,295705	0,249255	0,173186	0,0935	0,288263	0,615188
Cu ppm	0,231075	0,350097	0,619444	-0,253671	-0,502395	0,10707	-0,236605	0,236916
Pb ppm	0,407587	-0,182258	0,249283	0,2098	0,230295	-0,768026	-0,218581	0,061806
Zn ppm	-0,284944	0,256567	0,626882	0,182116	0,518579	0,081596	0,373056	-0,109909
As ppm	0,398086	0,496159	-0,155006	-0,040751	0,256302	0,152682	-0,326646	-0,611527
Sb ppm	0,493225	-0,201095	0,063481	-0,267384	-0,187205	-0,027182	0,714538	-0,307272
Ba ppm	0,299766	-0,457819	0,140548	-0,352525	0,490736	0,448904	-0,226814	0,250465

Ag. Ioannis - Voulismata subarea

There are available data only for Au and Ag, which show no correlations in the subarea.

	Au ppm	Ag ppm
Au ppm	1	0,072898
Ag ppm	0,072898	1

Chondro Vouno – Pyrgiali - Peristeria subarea**Parametric Correlations****Chondro Vouno - Pyrgiali - Peristeria subarea Pearson's correlation**

	Au ppm	Ag ppm	Cu ppm	Pb ppm	Zn ppm	As ppm	Sb ppm	Ba ppm
Au ppm	1	-0,090221	0,288503	-0,054459	-0,007204	-0,074404	-0,055568	-0,159443
Ag ppm	-0,090221	1	-0,109046	-0,032296	0,320619	0,026612	0,497229	0,170346
Cu ppm	0,288503	-0,109046	1	0,204057	0,437453	0,085642	-0,253022	-0,110361
Pb ppm	-0,054459	-0,032296	0,204057	1	0,032938	0,052477	0,040107	0,107524
Zn ppm	-0,007204	0,320619	0,437453	0,032938	1	-0,002501	0,099682	0,106154
As ppm	-0,074404	0,026612	0,085642	0,052477	-0,002501	1	0,292802	0,01139
Sb ppm	-0,055568	0,497229	-0,253022	0,040107	0,099682	0,292802	1	0,391176
Ba ppm	-0,159443	0,170346	-0,110361	0,107524	0,106154	0,01139	0,391176	1

Chondro Vouno - Pyrgiali - Peristeria subarea Inverse correlation

	Au ppm	Ag ppm	Cu ppm	Pb ppm	Zn ppm	As ppm	Sb ppm	Ba ppm
Au ppm	1,197393	0,081677	-0,524406	0,148399	0,214479	0,199645	-0,263422	0,181175
Ag ppm	0,081677	1,546068	0,156301	0,048517	-0,499867	0,172556	-0,77224	0,114869
Cu ppm	-0,524406	0,156301	1,799249	-0,366829	-0,885474	-0,340345	0,546361	0,011921
Pb ppm	0,148399	0,048517	-0,366829	1,095501	0,134318	0,02373	-0,131518	-0,105961
Zn ppm	0,214479	-0,499867	-0,885474	0,134318	1,569256	0,138901	-0,121714	-0,11337
As ppm	0,199645	0,172556	-0,340345	0,02373	0,138901	1,210945	-0,595391	0,16669
Sb ppm	-0,263422	-0,77224	0,546361	-0,131518	-0,121714	-0,595391	1,921493	-0,567955
Ba ppm	0,181175	0,114869	0,011921	-0,105961	-0,11337	0,16669	-0,567955	1,254335

Chondro Vouno - Pyrgiali - Peristeria subarea Partial correlation

	Au ppm	Ag ppm	Cu ppm	Pb ppm	Zn ppm	As ppm	Sb ppm	Ba ppm
Au ppm		-0,06003	0,357276	-0,129571	-0,156466	-0,165797	0,173666	-0,147834
Ag ppm	-0,06003		-0,093713	-0,037279	0,320917	-0,126111	0,448042	-0,082486
Cu ppm	0,357276	-0,093713		0,261283	0,526967	0,230575	-0,293842	-0,007935
Pb ppm	-0,129571	-0,037279	0,261283		-0,102442	-0,020603	0,090648	0,090393
Zn ppm	-0,156466	0,320917	0,526967	-0,102442		-0,100762	0,070093	0,080806
As ppm	-0,165797	-0,126111	0,230575	-0,020603	-0,100762		0,39032	-0,135251
Sb ppm	0,173666	0,448042	-0,293842	0,090648	0,070093	0,39032		0,365837
Ba ppm	-0,147834	-0,082486	-0,007935	0,090393	0,080806	-0,135251	0,365837	

Chondro Vouno - Pyrgiali - Peristeria subarea Pairwise Correlations

Variable	by Variable	Correlation	Signif Prob	Plot Corr
Ag ppm	Au ppm	-0,0665	0,3008	
Cu ppm	Au ppm	0,2885	0,0188	
Cu ppm	Ag ppm	-0,1092	0,3792	
Pb ppm	Au ppm	-0,0545	0,6641	
Pb ppm	Ag ppm	-0,0329	0,7913	
Pb ppm	Cu ppm	0,2041	0,0976	
Zn ppm	Au ppm	-0,0072	0,9542	
Zn ppm	Ag ppm	0,3343	0,0057	
Zn ppm	Cu ppm	0,4151	0,0005	
Zn ppm	Pb ppm	0,0290	0,8159	
As ppm	Au ppm	-0,0744	0,5527	
As ppm	Ag ppm	0,0286	0,8185	
As ppm	Cu ppm	0,0855	0,4916	
As ppm	Pb ppm	0,0523	0,6743	
As ppm	Zn ppm	0,0039	0,9747	
Sb ppm	Au ppm	-0,0556	0,6577	
Sb ppm	Ag ppm	0,5043	0,0000	
Sb ppm	Cu ppm	-0,2509	0,0406	
Sb ppm	Pb ppm	0,0383	0,7582	
Sb ppm	Zn ppm	0,1417	0,2526	
Sb ppm	As ppm	0,2924	0,0164	
Ba ppm	Au ppm	-0,1594	0,2010	
Ba ppm	Ag ppm	0,1857	0,1325	
Ba ppm	Cu ppm	-0,1096	0,3775	
Ba ppm	Pb ppm	0,1039	0,4027	
Ba ppm	Zn ppm	0,1577	0,2024	
Ba ppm	As ppm	0,0152	0,9025	
Ba ppm	Sb ppm	0,4097	0,0006	

Non Parametric Correlations

Chondro Vouno -Pyrgiali - Peristeria subarea Spearman's Rho

Variable	by Variable	Spearman Rho	Prob> Rho	Plot
Ag ppm	Au ppm	0,0274	0,6705	
Cu ppm	Au ppm	0,2413	0,0509	
Cu ppm	Ag ppm	-0,2078	0,0915	
Pb ppm	Au ppm	-0,0377	0,7639	
Pb ppm	Ag ppm	-0,0942	0,4483	
Pb ppm	Cu ppm	0,4862	<,0001	
Zn ppm	Au ppm	0,0623	0,6194	
Zn ppm	Ag ppm	-0,0234	0,8508	
Zn ppm	Cu ppm	0,5703	<,0001	
Zn ppm	Pb ppm	0,4408	0,0002	
As ppm	Au ppm	-0,0239	0,8489	
As ppm	Ag ppm	0,2177	0,0768	
As ppm	Cu ppm	0,1765	0,1532	
As ppm	Pb ppm	0,1300	0,2945	
As ppm	Zn ppm	0,1811	0,1425	
Sb ppm	Au ppm	0,1109	0,3753	
Sb ppm	Ag ppm	0,6407	<,0001	
Sb ppm	Cu ppm	-0,3286	0,0066	
Sb ppm	Pb ppm	-0,1850	0,1340	
Sb ppm	Zn ppm	-0,1106	0,3731	
Sb ppm	As ppm	0,2994	0,0138	
Ba ppm	Au ppm	-0,0928	0,4588	

Variable	by Variable	Spearman Rho	Prob> Rho	Plot
Ba ppm	Ag ppm	0,2896	0,0175	
Ba ppm	Cu ppm	-0,0832	0,5034	
Ba ppm	Pb ppm	-0,0373	0,7646	
Ba ppm	Zn ppm	0,0708	0,5690	
Ba ppm	As ppm	0,2306	0,0605	
Ba ppm	Sb ppm	0,3848	0,0013	

Chondro Vouno - Pyrgiali - Peristeria subarea Kendall's Tau b

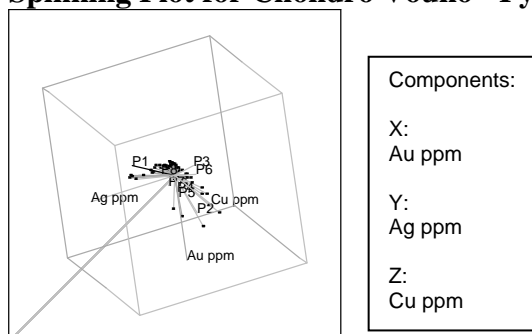
Variable	by Variable	Kendall Tau b	Prob> Tau b	Plot
Ag ppm	Au ppm	0,0179	0,6818	
Cu ppm	Au ppm	0,1530	0,0742	
Cu ppm	Ag ppm	-0,1381	0,1019	
Pb ppm	Au ppm	-0,0255	0,7648	
Pb ppm	Ag ppm	-0,0618	0,4616	
Pb ppm	Cu ppm	0,3437	<,0001	
Zn ppm	Au ppm	0,0477	0,5757	
Zn ppm	Ag ppm	-0,0105	0,9009	
Zn ppm	Cu ppm	0,4036	<,0001	
Zn ppm	Pb ppm	0,2880	0,0006	
As ppm	Au ppm	-0,0143	0,8678	
As ppm	Ag ppm	0,1583	0,0622	
As ppm	Cu ppm	0,1120	0,1877	
As ppm	Pb ppm	0,0902	0,2858	
As ppm	Zn ppm	0,1219	0,1495	
Sb ppm	Au ppm	0,0864	0,3105	
Sb ppm	Ag ppm	0,4674	<,0001	
Sb ppm	Cu ppm	-0,2373	0,0048	
Sb ppm	Pb ppm	-0,1263	0,1311	
Sb ppm	Zn ppm	-0,0734	0,3806	
Sb ppm	As ppm	0,2067	0,0145	
Ba ppm	Au ppm	-0,0564	0,5094	
Ba ppm	Ag ppm	0,2088	0,0131	
Ba ppm	Cu ppm	-0,0553	0,5122	
Ba ppm	Pb ppm	-0,0268	0,7494	
Ba ppm	Zn ppm	0,0527	0,5300	
Ba ppm	As ppm	0,1668	0,0491	
Ba ppm	Sb ppm	0,2702	0,0013	

Chondro Vouno - Pyrgiali - Peristeria subarea Hoeffding's D

Variable	by Variable	Hoeffding D	Prob>D	Plot
Ag ppm	Au ppm	0,0003	0,3147	
Cu ppm	Au ppm	0,0069	0,1314	
Cu ppm	Ag ppm	0,0038	0,2024	
Pb ppm	Au ppm	-0,0044	0,7115	
Pb ppm	Ag ppm	0,0021	0,2626	
Pb ppm	Cu ppm	0,0745	<,0001	
Zn ppm	Au ppm	0,0119	0,0669	
Zn ppm	Ag ppm	-0,0041	0,6918	
Zn ppm	Cu ppm	0,0992	<,0001	
Zn ppm	Pb ppm	0,0662	0,0001	
As ppm	Au ppm	-0,0052	0,7903	
As ppm	Ag ppm	0,0121	0,0635	
As ppm	Cu ppm	0,0002	0,3552	
As ppm	Pb ppm	-0,0058	0,8597	
As ppm	Zn ppm	0,0069	0,1292	
Sb ppm	Au ppm	0,0112	0,0731	
Sb ppm	Ag ppm	0,1536	<,0001	
Sb ppm	Cu ppm	0,0386	0,0025	
Sb ppm	Pb ppm	0,0112	0,0711	
Sb ppm	Zn ppm	0,0001	0,3560	
Sb ppm	As ppm	0,0201	0,0228	
Ba ppm	Au ppm	0,0014	0,2943	
Ba ppm	Ag ppm	0,0377	0,0028	
Ba ppm	Cu ppm	-0,0058	0,8527	
Ba ppm	Pb ppm	-0,0035	0,6350	
Ba ppm	Zn ppm	-0,0012	0,4443	
Ba ppm	As ppm	0,0168	0,0346	
Ba ppm	Sb ppm	0,0465	0,0010	

Principal Components Analysis

Spinning Plot for Chondro Vouno - Pyrgiali - Peristeria subarea



Chondro Vouno - Pyrgiali - Peristeria subarea Principal components summary table :

Eigenvalue	1,95192	1,574763	1,123557	1,039844	0,904884	0,747228	0,364223	0,29358
Percent	24,39901	19,68454	14,04446	12,99806	11,31105	9,340353	4,552785	3,669746
Cum %	24,39901	44,08355	58,12801	71,12606	82,43712	91,77747	96,33025	100
Eigenvectors :								
Au ppm	-0,246873	0,265884	-0,247287	0,425726	0,732702	-0,023818	-0,068454	0,289585
Ag ppm	0,506985	0,165888	-0,379583	0,015462	-0,054373	-0,471467	0,56443	0,165247
Cu ppm	-0,235755	0,672076	0,111238	0,0323	-0,046249	0,167695	0,384466	-0,548855
Pb ppm	0,03818	0,249253	0,671533	-0,340766	0,25961	-0,517663	-0,099428	0,155171
Zn ppm	0,176598	0,615837	-0,260012	-0,184799	-0,313561	0,131512	-0,522146	0,315515
As ppm	0,204618	0,093041	0,489106	0,690871	-0,310802	0,157654	0,108119	0,315919
Sb ppm	0,603167	-0,001165	0,016876	0,264315	0,242006	-0,080035	-0,412441	-0,575292
Ba ppm	0,433724	0,007781	0,155949	-0,346463	0,370363	0,657646	0,254164	0,182208

Profitis Ilias – Livadakia - Chontri Rachi subarea

Parametric Correlations

Profitis Ilias – Livadakia - Chontri Rachi subarea Pearson's correlation

	Au ppm	Ag ppm	Cu ppm	Pb ppm	Zn ppm	As ppm	Sb ppm	Ba ppm
Au ppm	1	0,021393	0,2325	0,21092	-0,018796	0,048503	-0,050251	-0,096225
Ag ppm	0,021393	1	0,088232	0,105267	0,08164	0,292708	0,310139	0,210719
Cu ppm	0,2325	0,088232	1	0,454492	0,170759	-0,004158	-0,044295	-0,119949
Pb ppm	0,21092	0,105267	0,454492	1	0,109219	0,318191	0,007901	0,081807
Zn ppm	-0,018796	0,08164	0,170759	0,109219	1	-0,117737	-0,108414	0,150675
As ppm	0,048503	0,292708	-0,004158	0,318191	-0,117737	1	0,174523	0,142364
Sb ppm	-0,050251	0,310139	-0,044295	0,007901	-0,108414	0,174523	1	-0,071041
Ba ppm	-0,096225	0,210719	-0,119949	0,081807	0,150675	0,142364	-0,071041	1

Profitis Ilias - Livadakia - Chontri Rachi subarea Inverse correlation

	Au ppm	Ag ppm	Cu ppm	Pb ppm	Zn ppm	As ppm	Sb ppm	Ba ppm
Au ppm	1,090059	-0,03816	-0,172496	-0,159314	0,061729	-0,012486	0,076431	0,10318
Ag ppm	-0,03816	1,284549	-0,174698	0,090173	-0,124116	-0,312707	-0,386602	-0,266928
Cu ppm	-0,172496	-0,174698	1,415694	-0,657353	-0,163012	0,207144	0,076948	0,244339
Pb ppm	-0,159314	0,090173	-0,657353	1,500915	-0,097716	-0,486344	-0,013529	-0,152965
Zn ppm	0,061729	-0,124116	-0,163012	-0,097716	1,11029	0,199309	0,108841	-0,167401
As ppm	-0,012486	-0,312707	0,207144	-0,486344	0,199309	1,30249	-0,102972	-0,093449
Sb ppm	0,076431	-0,386602	0,076948	-0,013529	0,108841	-0,102972	1,169852	0,180523
Ba ppm	0,10318	-0,266928	0,244339	-0,152965	-0,167401	-0,093449	0,180523	1,159348

Profitis Ilias – Livadakia - Chontri Rachi subarea Partial correlation

	Au ppm	Ag ppm	Cu ppm	Pb ppm	Zn ppm	As ppm	Sb ppm	Ba ppm
Au ppm		0,032248	0,138857	0,124552	-0,056111	0,010479	-0,067683	-0,091784
Ag ppm	0,032248		0,129547	-0,064942	0,103928	0,241754	0,315372	0,218731
Cu ppm	0,138857	0,129547		0,450958	0,130022	-0,152546	-0,059792	-0,190722
Pb ppm	0,124552	-0,064942	0,450958		0,075695	0,347839	0,01021	0,115959
Zn ppm	-0,056111	0,103928	0,130022	0,075695		-0,165738	-0,095501	0,147548
As ppm	0,010479	0,241754	-0,152546	0,347839	-0,165738		0,08342	0,076047
Sb ppm	-0,067683	0,315372	-0,059792	0,01021	-0,095501	0,08342		-0,15501
Ba ppm	-0,091784	0,218731	-0,190722	0,115959	0,147548	0,076047	-0,15501	

Profitis Ilias – Livadakia - Chontri Rachi subarea Pairwise Correlations

Variable	by Variable	Correlation	Signif Prob	Plot Corr
Ag ppm	Au ppm	0,1266	0,0020	
Cu ppm	Au ppm	0,2622	0,0050	
Cu ppm	Ag ppm	0,0643	0,4964	
Pb ppm	Au ppm	0,1883	0,0458	
Pb ppm	Ag ppm	0,1104	0,2421	
Pb ppm	Cu ppm	0,4019	0,0000	
Zn ppm	Au ppm	-0,0141	0,8820	
Zn ppm	Ag ppm	0,0528	0,5770	
Zn ppm	Cu ppm	0,2391	0,0101	
Zn ppm	Pb ppm	0,1494	0,1109	
As ppm	Au ppm	0,0492	0,6164	
As ppm	Ag ppm	0,2922	0,0023	
As ppm	Cu ppm	-0,0020	0,9840	
As ppm	Pb ppm	0,3205	0,0007	
As ppm	Zn ppm	-0,1163	0,2309	
Sb ppm	Au ppm	-0,0405	0,6700	
Sb ppm	Ag ppm	0,3108	0,0008	
Sb ppm	Cu ppm	-0,0946	0,3146	
Sb ppm	Pb ppm	-0,0204	0,8286	
Sb ppm	Zn ppm	-0,2172	0,0197	
Sb ppm	As ppm	0,1749	0,0703	
Ba ppm	Au ppm	-0,1040	0,2730	
Ba ppm	Ag ppm	0,1564	0,0966	
Ba ppm	Cu ppm	-0,1057	0,2607	
Ba ppm	Pb ppm	0,0667	0,4788	
Ba ppm	Zn ppm	0,1770	0,0584	
Ba ppm	As ppm	0,1374	0,1561	
Ba ppm	Sb ppm	-0,0928	0,3241	

Non Parametric Correlations

Profitis Ilias – Livadakia - Chontri Rachi subarea Spearman's Rho

Variable	by Variable	Spearman Rho	Prob> Rho	Plot
Ag ppm	Au ppm	0,1263	0,0021	
Cu ppm	Au ppm	0,3770	<,0001	
Cu ppm	Ag ppm	0,1503	0,1105	
Pb ppm	Au ppm	0,4704	<,0001	

Variable	by Variable	Spearman Rho	Prob> Rho	Plot
Pb ppm	Ag ppm	0,0933	0,3232	
Pb ppm	Cu ppm	0,4937	<,0001	
Zn ppm	Au ppm	0,2266	0,0158	
Zn ppm	Ag ppm	0,1249	0,1854	
Zn ppm	Cu ppm	0,5072	<,0001	
Zn ppm	Pb ppm	0,5380	<,0001	
As ppm	Au ppm	-0,1318	0,1781	
As ppm	Ag ppm	0,3966	<,0001	
As ppm	Cu ppm	0,1032	0,2877	
As ppm	Pb ppm	0,1367	0,1584	
As ppm	Zn ppm	-0,1382	0,1536	
Sb ppm	Au ppm	-0,1632	0,0841	
Sb ppm	Ag ppm	0,2844	0,0022	
Sb ppm	Cu ppm	-0,1607	0,0861	
Sb ppm	Pb ppm	-0,1024	0,2760	
Sb ppm	Zn ppm	-0,2891	0,0017	
Sb ppm	As ppm	0,1824	0,0588	
Ba ppm	Au ppm	-0,1831	0,0523	
Ba ppm	Ag ppm	0,3253	0,0004	
Ba ppm	Cu ppm	-0,0950	0,3126	
Ba ppm	Pb ppm	0,0524	0,5780	
Ba ppm	Zn ppm	0,1588	0,0901	
Ba ppm	As ppm	0,3139	0,0009	
Ba ppm	Sb ppm	0,0666	0,4794	

Profitis Ilias – Livadakia - Chontri Rachi subarea Kendall's Tau b

Variable	by Variable	Kendall Tau b	Prob> Tau b	Plot
Ag ppm	Au ppm	0,0876	0,0016	
Cu ppm	Au ppm	0,2582	<,0001	
Cu ppm	Ag ppm	0,1026	0,1080	
Pb ppm	Au ppm	0,3361	<,0001	
Pb ppm	Ag ppm	0,0557	0,3806	
Pb ppm	Cu ppm	0,3471	<,0001	
Zn ppm	Au ppm	0,1582	0,0138	
Zn ppm	Ag ppm	0,0867	0,1733	
Zn ppm	Cu ppm	0,3571	<,0001	
Zn ppm	Pb ppm	0,3810	<,0001	
As ppm	Au ppm	-0,0920	0,1684	
As ppm	Ag ppm	0,2749	<,0001	
As ppm	Cu ppm	0,0703	0,2878	
As ppm	Pb ppm	0,1023	0,1202	
As ppm	Zn ppm	-0,0777	0,2392	
Sb ppm	Au ppm	-0,1047	0,1043	
Sb ppm	Ag ppm	0,1900	0,0030	
Sb ppm	Cu ppm	-0,1110	0,0824	
Sb ppm	Pb ppm	-0,0661	0,2984	
Sb ppm	Zn ppm	-0,1932	0,0024	
Sb ppm	As ppm	0,1194	0,0712	
Ba ppm	Au ppm	-0,1311	0,0467	
Ba ppm	Ag ppm	0,2317	0,0004	
Ba ppm	Cu ppm	-0,0723	0,2686	
Ba ppm	Pb ppm	0,0382	0,5570	
Ba ppm	Zn ppm	0,1104	0,0903	
Ba ppm	As ppm	0,2167	0,0014	
Ba ppm	Sb ppm	0,0505	0,4406	

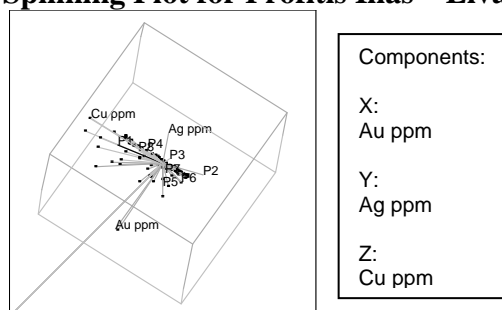
Profitis Ilias – Livadakia - Chontri Rachi subarea Hoeffding's D

Variable	by Variable	Hoeffding D	Prob>D	Plot
Ag ppm	Au ppm	0,0048	0,0015	
Cu ppm	Au ppm	0,0364	0,0002	
Cu ppm	Ag ppm	0,0018	0,2269	
Pb ppm	Au ppm	0,0785	<,0001	
Pb ppm	Ag ppm	-0,0013	0,5169	
Pb ppm	Cu ppm	0,0754	<,0001	
Zn ppm	Au ppm	0,0170	0,0079	
Zn ppm	Ag ppm	0,0054	0,0930	
Zn ppm	Cu ppm	0,0882	<,0001	
Zn ppm	Pb ppm	0,1005	<,0001	
As ppm	Au ppm	0,0079	0,0596	
As ppm	Ag ppm	0,0463	<,0001	

Variable	by Variable	Hoeffding D	Prob>D	Plot
As ppm	Cu ppm	0,0050	0,1091	
As ppm	Pb ppm	0,0115	0,0277	
As ppm	Zn ppm	0,0162	0,0108	
Sb ppm	Au ppm	0,0057	0,0874	
Sb ppm	Ag ppm	0,0202	0,0040	
Sb ppm	Cu ppm	0,0049	0,1041	
Sb ppm	Pb ppm	-0,0020	0,6354	
Sb ppm	Zn ppm	0,0216	0,0029	
Sb ppm	As ppm	0,0032	0,1644	
Ba ppm	Au ppm	0,0072	0,0623	
Ba ppm	Ag ppm	0,0375	0,0001	
Ba ppm	Cu ppm	0,0006	0,3093	
Ba ppm	Pb ppm	-0,0024	0,7006	
Ba ppm	Zn ppm	0,0029	0,1703	
Ba ppm	As ppm	0,0281	0,0011	
Ba ppm	Sb ppm	-0,0014	0,5422	

Principal Components Analysis

Spinning Plot for Profitis Ilias – Livadakia - Chontri Rachi subarea



Profitis Ilias – Livadakia - Chontri Rachi subarea Principal components summary table :

Eigenvalue	1,813942	1,512902	1,246083	0,98568	0,817884	0,633688	0,592081	0,397741
Percent	22,67427	18,91127	15,57603	12,32099	10,22355	7,921098	7,401018	4,971763
Cum %	22,67427	41,58555	57,16158	69,48258	79,70612	87,62722	95,02824	100
Eigenvectors :								
Au ppm	0,275359	-0,332233	-0,287657	-0,164683	0,80959	0,159919	0,147633	0,033565
Ag ppm	0,399829	0,424218	0,095393	0,311795	0,297258	-0,242495	-0,552386	-0,318691
Cu ppm	0,435494	-0,45064	-0,053473	0,256079	-0,213148	-0,430559	-0,132216	0,539015
Pb ppm	0,567539	-0,219394	-0,001985	-0,198944	-0,352407	-0,001056	0,295513	-0,615356
Zn ppm	0,144352	-0,212485	0,61364	0,451302	0,047825	0,589321	0,039329	0,051495
As ppm	0,422681	0,359213	-0,128079	-0,429722	-0,198972	0,485143	-0,23459	0,401566
Sb ppm	0,175543	0,452743	-0,352493	0,512895	-0,018069	0,044483	0,597418	0,132974
Ba ppm	0,149152	0,281584	0,622961	-0,345126	0,210655	-0,381573	0,393418	0,215684

Mavrovouni - Vathi Rema subarea

Parametric Correlations

There are available data only for Au and Ag, which show a slight correlation in the subarea.

Mavrovouni - Vathi Rema subarea Pearson's correlation

	Au ppm	Ag ppm
Au ppm	1	0,251472
Ag ppm	0,251472	1

Mavrovouni - Vathi Rema subarea Inverse correlation

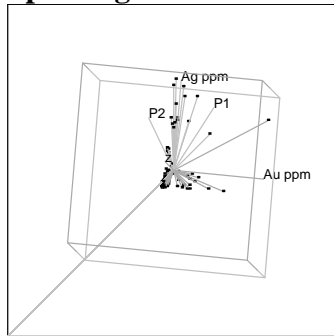
	Au ppm	Ag ppm
Au ppm	1,067507	-0,268448
Ag ppm	-0,268448	1,067507

Mavrovouni - Vathi Rema subarea Partial correlation

	Au ppm	Ag ppm
Au ppm		0,251472
Ag ppm	0,251472	

Principal Components Analysis

Spinning Plot for Mavrovouni - Vathi Rema subarea



Components:	
X:	Au ppm
Y:	Ag ppm

Mavrovouni - Vathi Rema subarea Principal components summary table :

Eigenvalue	1,251472	0,748528
Percent	62,57358	37,42642
Cum %	62,57358	100
Eigenvectors :		
Au ppm	0,707107	-0,707107
Ag ppm	0,707107	0,707107